The Effect of Fuel Formulation on the Exhaust Emissions of Spark Ignition Engines

ARTHUR BELL

Dissertation presented for the Degree of Doctor of Engineering at the University of Stellenbosch

Promoters : Dr A. B. TAYLOR & Prof. T.W. von BACKSTRÖM

April 2006

Declaration

I, the undersigned, hereby declare that the work contained in this dissertation is my own original work and that I have not previously in its entirety or in part submitted it at any university for a degree.

Signature:..... Date: .....

Synopsis

The research described in this dissertation examined the effects that fuel formulation can have on the regulated exhaust emissions produced by spark ignition engines in a South African context. Typical South African engine technology, and fuels representative of available fuels were investigated. To broaden the scope and provide information on as many fuel parameters as possible, fuel formulations other than typical retail fuels were also investigated. In order to gain insight into the mechanisms taking place, combustion analysis was performed on measured cylinder pressure traces. This type of analysis calculates the rate of combustion along with other useful parameters such as cylinder gas temperatures. A multivariate statistical analysis was then performed to enable the determination of the effects of the fuel formulation parameters of interest. This was done in such a way as to indicate the mechanisms through which the parameters influence the emissions.

An existing combustion analysis program was extensively modified as part of the research programme. The existing program consisted of a relatively simple single-zone combustion analysis while a two-zone combustion analysis model was added which splits the control volume into two distinct zones namely unburned reactants and burned products. An equilibrium reaction combustion model and routines for computing the gas properties of a mixture were incorporated. The extended Zeldovich NO formation model was also added to the combustion analysis routines to enable the investigation of some noteworthy statistical correlations identified in the research.

The experimental results attained, as well as the results of the combustion analysis, were shown to be repeatable and significant. The combustion analysis was found to be a useful tool which was successfully used to explain the combustion related mechanisms that affected the measured emissions. The statistical approach used was sufficiently able to predict the fuel properties and combustion analysis parameters that influenced the emissions and the fuel properties that influenced the combustion parameters. In this way the mechanisms by which the fuel properties effect the emissions were explained. Many of the effects of the relevant fuel formulation parameters agreed with the observations reported in the literature considered.

The hydrocarbon emissions were seen to be mostly affected by factors which influence the post combustion burn-up and stoichiometry. Post combustion burn-up is either influenced by the amount of hydrocarbon containing mixture that is precluded from taking part in the bulk gas combustion process by storage and release mechanisms or by factors which influence the rate of the post combustion reactions. The response to the stoichiometry effects are well understood.

The oxides of nitrogen (NO) were found to be mostly influenced by fuel parameters which influence the combustion rates and the overall combustion timing: the location of 50% burned parameter was found to have good correlation with the NO emissions. The NO formation process relies on non-equilibrium, rate controlled reactions which are highly temperature dependent and fuel properties which cause the combustion to be advanced will result in higher temperatures and thus increased NO emissions.

Carbon monoxide (CO) emissions are seen to be influenced by stoichiometry and equivalence ratio effects and effects linked to the rate of change of pressure. The response to the stoichiometry and equivalence ratio effects are well understood, but the physical mechanism of the influence of the fuel parameters on the equivalence ratio are not clear.

Opsomming

Die navorsing beskryf in hierdie verhandeling, ondersoek die moontlike gevolge van branstofformulasie op internasionaal gereguleerde uitlaatemissies van vonkontstekingenjins in ‘n Suid-Afrikaanse konteks. Tipiese Suid-Afrikaanse enjintegnologie en brandstowwe verteenwoordigend van brandstowwe beskikbaar in die handel, is ondersoek. Brandstofformulasies verskillend van tipiese beskikbare brandstowwe is ook ondersoek om die omvang van die projek te vergroot en soveel moontlik inligting ten opsigte van brandstofparameters beskikbaar te stel. Verbrandinganalise is op gemete verbrandingsdrukdata uitgevoer om die verbrandingsmeganismes wat voorkom, beter te verstaan. Die tempo van verbranding en verbrandingsruimgastemperatuur is van die uitsette wat bereken word met behulp van verbrandingsanalise. ‘n Multiveranderlike statistiese analise om die effek van branstofformulasieparameters te bepaal, is op so ‘n manier uitgevoer dat die meganismes waardeur hierdie parameters emissies beinvloed, aangetoon word.

Die oorspronklike program, ‘n relatief eenvoudige enkelsone-verbrandingsmodel, is omvattend gewysig om ‘n tweesone-verbrandingsanalisemodel daar te stel wat die verbrandingsvolume in twee sones - onverbrande reaktiewe en verbrande produkte -verdeel.’n Ekwilibriumreaksie-verbrandingsmodel en subroetines om die gaseienskappe van ‘n mengsel te bepaal, is ook geinkorporeer. Vir die bestudering van sekere interessante statistiese korrelasies wat gedurende die navorsing opgemerk is, is die uitgebreide Zeldovich stikstofmonoksied (NO) formasiemodel ook by die analiseroetine gevoeg.

Die eksperimentele resultate asook die resultate van die verbrandingsmodel is as herhaalbaar en beduidend aangetoon. Die verbrandingsanalise is ‘n bruikbare werktuig wat suksesvol aangewend is om te verduidelik hoe die meganismes wat verband hou met verbranding die gemete uitlaatgasemissies beinvloed. Die statistiese metodes kon aanvaarbare indikasies gee watter brandstofeienskappe en verbrandingsanalise-parameters emissies beinvloed en ook watter brandstofeienskappe verbrandingsparameters beinvloed. Op hierdie manier is die meganismes waardeur die brandstofeienskappe ‘n uitwerking op uitlaatgasemissies het, verduidelik. Die uitwerking van die relevante brandstofformulasieparameters stem grootliks ooreen met die waarnemings aangemeld in die bestudeerde literatuur.

Die analise het aangedui dat onverbrande koolwaterstofemissies die meeste beinvloed word deur faktore wat ‘n uitwerking het op stoichiometrie en na-verbrandingsoksidasie. Na-verbrandingsoksidasie word deur die volgende beinvloed: die hoeveelheid mengsel wat koolwaterstofverbindings bevat wat nie deelneem aan die hoofverbrandingsproses as gevolg van opgarings- en verspreidingsmeganismes nie of deur faktore wat ‘n uitwerking het op die tempo van na-verbrandingsreaksies. Die reaksie tot stoichiometriese effek is duidelik.

Daar is gevind dat stikstofmonoksied (NO) primer beinvloed word deur brandstofparameters wat op verbrandingsgastemperature inwerk. ‘n Toename in globale verbrandingsgastemperature lei tot ‘n vermindering in gevormde NO wat moontlik ‘n gevolg is van die toenemende NO ontbinding wat plaasvind omdat NO verbindings- en ontbindingsreaksies ‘n nie-ewewigtige, tempo-gereguleerde patroon volg.

Daar is gevind dat die stikstofmonokside (NO) hoofsaaklik beïnvloed word deur brandstofparameters wat ontbrandingstempo”s en algehele ontbrandingstydreëling beïnvloed: ‘n goeie korrelasie is gevind tussen die posisie van die 50% brandpunt en die NO uitlating. Die NO formasieproses is afhanklik van nie-ewewigtige,

tempogereguleerde reaksies wat hoogs temperaturafhanklik is. Brandstofeienskappe wat veroorsaak dat die ontbranding vroeër plaasvind, sal hoër temperature en dus verhoogde NO formasie tot gevolg hê.

Daar word gesien dat koolstofmonoksied (CO) emissies deur stoichiometrie en ekwivalensverhouding beinvloed word; asook deur oorsake gekoppel aan die tempo van verandering in verbrandingsdruk. Die reaksie op stiochiometrie en ekwivalensverhouding is duidelik, maar die fisiese meganismes van die invloed van brandstofparameters op ekwivalensverhouding is onduidelik.

.

Dedication

I dedicate this to my parents for all that they have done for me, to Janet, my ever patient wife, for all the love and support that I could wish for and to Jarryd, our son, who brightens every day.

Acknowledgements

Dr Andrew Taylor, for all the encouragement and guidance throughout this project.

Professor von Backström for always encouraging me to finish as well as his input in the final stages.

Sasol Oil, Research and Development, for financial and technical support including the supply and laboratory analysis of the test fuels.

The Technology and Human Resources for Industry Programme (THRIP) of the National Research Foundation (NRF) for financial support.

Toyota South Africa, for the donation of the engines used in the research.

Derek Moran for all the assistance with the programming, for making this seem like fun at times, and for his valued friendship.

Dr Randall, for the assistance with the statistical analysis.

Benn Vincent and the rest of the staff at the Centre for Automotive Engineering, for the assistance with the engine testing.

Table of Contents

Synopsis i
Opsomming ii
Dedication iv
Acknowledgements v
Table of Contents vi
List of Figures ix
List of Tables xii
List of Equations xv
Nomenclature and abbreviations xvi
1. INTRODUCTION 1
2. BACKGROUND TO AUTOMOTIVE EMISSIONS 3
2.1. Motivation 3
2.2. Air Quality, Photochemical Smog and Pollution Associated with Vehicle Emissions 5
2.2.1. Photochemical Smog in Cape Town 7
2.2.2. Holistic Approach to Air Quality Impact 10
2.3. Exhaust Gas Composition 11
2.3.1. Emissions Formation Mechanisms 12
2.4. Exhaust Emissions Measurement 16
2.4.1. Steady State Engine Operation 16
2.4.2. Chassis Dynamometer Driving Cycle Operation 17
2.4.3. Test Bench Driving Cycle Operation 19
2.4.4. Modal Analysis 20
3. LITERATURE REVIEW 21
3.1. Studies of the Effect of Fuel Formulation on Regulated Emissions. 21
3.1.1. The AQIRP Study. 21
3.1.2. The EPEFE Study. 25
3.2. Other Studies Investigating the Effects of Fuel Properties on Emissions. 29
3.2.1. Influence of Fuel Aromatic Content on Exhaust Emissions. 29
3.2.2. Aromatic Content and Volatility Effects on Exhaust Emissions. 30
3.2.3. Effect of Fuel Structure on Exhaust Emissions. 30
3.3. Specialised Studies 36
3.3.1. Oil Film Effects on Hydrocarbon Emissions 36
3.3.2. Role of Piston Crevice Volume on Hydrocarbon Emissions 37
3.3.3. Compression Ratio and Spark Timing effects on Hydrocarbon Emissions 37
4. RESEARCH OBJECTIVES AND METHODOLOGY 40
5. RESEARCH FUELS 44
5.1. Fuel Component Content 44
5.2. Fuel Volatility 46
5.3. Fuel Density and Octane Number 47
5.4. Fuel Carbon : Hydrogen : Oxygen : Nitrogen Ratio 47
5.4.1. Carbon : Hydrogen Ratio 48
5.4.2. Fuel Oxygen Molar Content 49
5.4.3. Fuel Nitrogen Molar Content 49
6. EXPERIMENTAL APPARATUS 50
6.1. Test Engines and Experimental Set-up 50
6.1.1. Toyota 4A-FE Engine Set-up 50
6.1.2. Toyota 4Y Engine Set-up 52
6.2. Cylinder Pressure Measurement 52
6.3. Engine-out Gas Analysis 55

6.4. Auxiliary Test Equipment 57
7. EXPERIMENTAL PROCEDURE 58
7.1. Test Sequence 58
7.2. Engine Load Point Determination 58
7.3. Preliminary Investigations 60
7.4. Test Procedure 60
7.5. Daily Calibration 61
8. HEAT RELEASE ANALYSIS 63
8.1. Heat Release Background and Results 63
8.1.1. Peak Rate of Heat Release 63
8.1.2. Cumulative Heat Released and Total Heat Released 63
8.1.3. Burn Angle and Induction Period 64
8.2. Single-Zone Heat Release Model 65
8.3. Two-Zone Heat Release Model 65
8.3.1. Detail of the Two-Zone Thermodynamic Model 66
8.3.2. Calculation of Gas Properties 68
8.3.3. Equilibrium Combustion Products Model 69
8.3.4. Heat Transfer Sub-Model 74
8.3.5. NO Formation Model 77
8.3.6. Detail of the Computer Code Written. 80
9. COMBUSTION ANALYSIS 83
9.1. Pressure Referencing 83
9.2. Program Inputs 86
9.2.1. Common Inputs 86
9.2.2. Single-Zone Analysis 96
9.2.3. Two-Zone Analysis 99
10. STATISTICAL ANALYSIS 102
10.1. Statistical modelling of Mixtures 102
10.2. Form of the variables 103
10.3. Selecting the Models 104
11. RESULTS 108
11.1. Test Repeatability and Significance 108
11.1.1. Repeatability of Load Points and Engine Operating Conditions 108
11.1.2. Repeatability and Significance of Emissions Test Results 109
11.1.3. Repeatability and Significance of Combustion Analysis Results 112
11.2. Presentation of Emissions Results 113
11.3. Validation of Two-Zone Model 114
11.4. Validation of Zeldovich NO model 118
11.5. Results of Statistical Analysis 121
11.5.1. Hydrocarbon Emissions Results 121
11.5.2. NO Emissions Results 129
11.5.3. CO Emissions Results 133
11.5.4. Combustion Analysis Results – Fuel Properties Correlation 137
11.6. Detailed Analysis of NO Formation 146
12. DISCUSSION OF RESULTS 155
12.1. Hydrocarbon Emissions 155
12.1.1. Fuel Component Concentrations 155
12.1.2. Oxygen Content 157
12.1.3. Volatility 158
12.1.4. Lead Content 159

12.2. NO Emissions 161
12.2.1. Fuel Component Concentrations 161
12.2.2. Volatility 162
12.2.3. Lead Content 163
12.3. CO Emissions 163
12.3.1. Volatility 163
12.3.2. Oxygen Content 164
12.3.3. Fuel Component Concentrations 164
12.4. Effects on Catalyst Efficiency 165
13. CONCLUSIONS 166
14. RECOMMENDATIONS 170
15. REFERENCES 171

APPENDIX A : ANALYSIS OF RESEARCH FUELS A1
APPENDIX B : DERIVATIONOF TWO ZONE HEAT RELEASE FORMULAS GIVEN BY KRIEGER AND BORMAN B1
APPENDIX C : DERIVATION OF HEAT TRANSFER COEFFICIENT EQUATION C1
APPENDIX D : TABULATED RESULTS D1
APPENDIX E :GRAPHICALLY PRESENTED EMISSIONS RESULTS E1
APPENDIX F : RESULTS OF STATISTICAL REGRESSION MODELLING F1

List of Figures

Figure 2-1 Effect of initial NOx and NMHC concentrations on ozone formed [7]. 6

Figure 2-2 (*a*) Routes for photochemical smog formation. (*b*) Nitric oxide photo oxidation rate, or reactivity of different hydrocarbon classes [5]. 7

Figure 2-3 Atmospheric pollutant concentrations for City Hall monitoring site, Cape Town for three consecutive days in June 1996 (graphs courtesy of Scientific Services Division of CMC). 9

Figure 2-4. Atmospheric pollutant concentrations for Goodwood monitoring site, Cape Town for two consecutive days in 1996 (graph courtesy of Scientific Services Division of CMC) 10

Figure 2-5 Mole fractions of combustion products as a function of equivalence ratio from basic stoichiometry and equilibrium calculations. 12

Figure 2-6 (*a*) Measured pressure P and calculated mass fraction burned, x as a function of crank angle. (*b*) Calculated temperature of burned gas T_b and unburned gas T_u as a function of crank angle for two elements that burn at different times. (*c*) NO mass fractions as function of crank angle for two elements that burn at different times (From Ferguson [16]) 15

Figure 2-7 An example of the equipment layout required for a chassis dynamometer driving cycle test [18]. 18

Figure 2-8 Driving cycle used for FTP 75 test procedure. The driving cycle is broken down into three distinct phases and these phases are sampled into separate storage bags. [18] 18

Figure 2-9 Driving cycle used for ECE R15-04 test procedure. [18] 19

Figure 3-1 Original and lozenge blending targets and actual fuel properties of test fuels used in the EPEFE study [20]. 26

Figure 4-1 Illustration of the triangular approach to the statistical analysis. 41

Figure 5-1 The simplex factor space showing the concentrations of the three components of the research fuels. 45

Figure 5-2 The simplex factor space showing the concentrations of the three components of the leaded and unleaded fuels only. 45

Figure 5-3 Volatility curves for the research fuels. 47

Figure 5-4 Hydrogen : Carbon Ratio for Fuel Component Classes according to Carbon Number (adapted from Goodger [32]). 48

Figure 6-1 Photograph showing the transducer housing sleeve entering cylinder No. 1 at an oblique angle. The water coolant pipes and signal cable are visible exiting the rear of the housing sleeve. 54

Figure 6-2 Photograph showing the access to the combustion chamber for the pressure transducer (dummy is in situ in this photograph). The non-flush face of the transducer is apparent, as is the small volume created to one side of the transducer face. 54

Figure 6-3 Photograph of the cabinet containing the gas analysers and the calibration gas bottles. The individual analysers from top to bottom are NO_2 – NO converter, hydrocarbons, NO, dual analyser with CO_2 and CO, O_2 and unused H_2 analyser. The chiller unit for sample water removal is seen at the bottom and the heated sample line is seen coiled on the floor. 56

Figure 8-1 Typical burn rate and cumulative heat released curves and definition of peak burn rate as calculated by Racer from data measured in the Toyota 4A-FE engine. 64

Figure 8-2 Definition of burn angle and induction period (5 to 95% given by way of example). 65

Figure 8-3 Schematic of the two-zone, mass transfer based combustion analysis model. 66

Figure 8-4 Flow chart of Racer 2 program structure. 82

Figure 9-1 Examples of cylinder pressure during the inlet portion of the cycle at the test points at which combustion analysis was performed. 84

Figure 9-2 Racers default Analysis Parameters dialog box. 87

Figure 9-3 Calculated polytropic exponent and ratio of specific heats during compression (3000 rev/min WOT). 90

Figure 9-4 Calculated polytropic exponent and ratio of specific heats during compression (3000 rev/min WOT). 91
Figure 9-5 Burn Rate (single-zone model) as predicted by Racer during compression (Fuel P14 at 3000 rev/min and WOT). 91
Figure 9-6 Average surface temperature as a function of engine speed (after Wentworth [53]). 92
Figure 9-7 Average surface temperature as a function of manifold absolute pressure (after Wentworth [53]).....93
Figure 9-8 Average surface temperature as a function of coolant type and temperature (Wentworth [53]).....93
Figure 9-9 Racers default dialog box for access to the single-zone models adjustable parameters. 96
Figure 9-10 Rate of heat release for three reference fuels at 60 km/hr load point indicating the suitability of Woschni heat transfer coefficients.....98
Figure 9-11 Rate of heat release for three reference fuels at 120 km/hr load point indicating the suitability of Woschni heat transfer coefficients.....98
Figure 9-12 Rate of heat release for three reference fuels at 3000 rev/min load point indicating the suitability of Woschni heat transfer coefficients.....99
Figure 9-13 Racers default dialog box for access to the two-zone models adjustable parameters. 100
Figure 11-1 Graph of Hydrocarbon emissions from fuels P1 through P11 as tested on the 4A-FE engine, illustrating reproducibility and significance of the results. 111
Figure 11-2 Graph of NO emissions from fuels P1 through P11 as tested on the 4A-FE engine, illustrating reproducibility and significance of the results. 111
Figure 11-3 Graph of CO emissions from fuels P1 through P11 as tested on the 4A-FE engine, illustrating reproducibility and significance of the results. 112
Figure 11-4 Examples of the rate of combustion and cumulative mass transferred results from the two-zone combustion analysis model.....115
Figure 11-5 Comparison of two-zone and single-zone maximum combustion rate predictions for two reference fuels at all of the load points. 115
Figure 11-6 Comparison of predicted CO_2 concentrations during the cycle and measured exhaust CO_2 concentrations for two reference fuels at all of the load points.....117
Figure 11-7 Comparison of predicted CO concentrations during the cycle and measured exhaust CO concentrations for two reference fuels at all of the load points.....117
Figure 11-8 Comparison of predicted O_2 concentrations during the cycle and measured exhaust O_2 concentrations for two reference fuels at all of the load points.....117
Figure 11-9 Comparison of predicted NO concentrations during the cycle and measured exhaust NO concentrations for two reference fuels at all of the load points.....118
Figure 11-10 Temperature and NO formation histories as a function of crank angle for three different combustion elements.....119
Figure 11-11 Comparison of modelled and measured NO emissions. 120
Figure 11-12 Modelled NO versus equivalence ratio. 120
Figure 11-13 Measured NO versus equivalence ratio. 121
Figure 11-14 Graph of the HC's as predicted by model 3 versus measured HC's. 124
Figure 11-15 Graphical presentation of the effects of the fuel component content on predicted HC's.....125
Figure 11-16 Graphical presentation of the effects of the aromatic and olefin content on predicted HC's with paraffins as the swing component. 126
Figure 11-17 Graph of the HC's as predicted by model 1 versus measured HC's. 129
Figure 11-18 Graph of the NO as predicted by model 2 versus measured NO. 131
Figure 11-19 Graph of the NO as predicted by model 4 versus measured NO. 133
Figure 11-20 Graph of the CO as predicted by model 8 versus measured CO. 135
Figure 11-21 Graph of the CO as predicted by model 1 versus measured CO. 137
Figure 11-22 Comparisons of the time histories for four burned gas elements for two fuels at their native equivalence ratios and at an equivalence ratio of 0.9. 148

Figure 11-23 Comparison of the time histories for four burned gas elements for a fuel at similar engine load conditions except for ignition timing. 149
Figure 11-24 Comparison of the time histories for four burned gas elements for four fuels at two similar engine load conditions except for ignition timing. 151
Figure 11-25 Comparison of burn angle and induction period for select data points. 152
Figure 11-26 NO emissions as a function of location of maximum bulk gas temperature (CATMAX). 152
Figure 11-27 Correlation between the location of 50% burned parameter and the burn angle and induction period parameters. 153
Figure 11-28 Correlation of the location of maximum bulk gas temperature (CATMAX) and the location of 50% burned. 154
Figure 11-29 Correlation of the measured and the modelled NO emissions and the location of 50% burned. 154

List of Tables

Table 3-1 Fuel Property Factorial Design Targets and Industry Average Fuel Properties for the AQIRP study....22
Table 3-2 Comparison of Fleet Properties and Technology Utilised for the vehicles used for the AQIRP study....23
Table 3-3 Chemical formula, MBT and Carbon mole Fraction at 0.9 Equivalence Ratio of test fuels used by Kaiser et. al. [24]....31
Table 3-4 Chemical formula and MBT of test fuels used by Kaiser et. al. [25]....34
Table 4-1 Fuel formulation parameters given by fuel analysis and used for the analysis....43
Table 5-1 Minimum, maximum and mean values for fuel component concentration of research fuels....45
Table 5-2 Maximum, minimum and mean values of benzene, phenols, nitrogen, oxygen, sulphur and lead content of research fuels....46
Table 5-3 Minimum, maximum and mean values of volatility measures for the research fuels....47
Table 5-4 Minimum, maximum and mean values of research fuel density, RON and MON....47
Table 6-1 Test Engine Specifications....52
Table 7-1 Table of Engine Speed, Torque, Ignition Timing and Fuel Pressure or Equivalence Ratio for the Load Points for the Toyota 4A-FE engine....59
Table 7-2 Table of Engine Speed and Torque for the Load Points for the Toyota 4Y engine....60
Table 8-1 Rate constants applied to the extended Zeldovich mechanism from three different sources....79
Table 9-1 Details of the two limiting cases used to define window to approximate the inlet charge temperature increase....85
Table 9-2 Test matrix used by Wentworth [53]....92
Table 9-3 Coolant, Oil, Inlet Charge and calculated Chamber Wall Temperatures for the three load points....96
Table 10-1 Classification variables used and their application....104
Table 10-2 SAS® program statements for first step of model building for HC emissions....105
Table 10-3 SAS® output file for the Cp analysis of Hydrocarbon Emissions, modified to list only the preferred models....106
Table 10-4 An example of the co-linearity check....107
Table 11-1 Comparisons of the bracket reference fuel emissions results indicating reproducibility....110
Table 11-2 Comparisons of the standard deviation of the fuel emissions results and the test reproducibility indicating significance of the data set....110
Table 11-3 Comparisons of the bracket reference fuel combustion analysis results indicating reproducibility of the single-zone model....112
Table 11-4 Comparisons of the bracket reference fuel combustion analysis results indicating reproducibility of the two-zone model....113
Table 11-5 Comparisons of the standard deviation of the combustion analysis results and the test reproducibility indicating significance of the data set for the single-zone model....113
Table 11-6 Comparisons of the standard deviation of the combustion analysis results and the test reproducibility indicating significance of the data set for the two-zone model....113
Table 11-7 Summary of Cp analysis for HC's – Fuel Properties Correlation....122
Table 11-8 Summary of co-linearity analysis, giving the co-linear variables and the variable coefficients for the HC's – Fuel Properties Correlation....123
Table 11-9 Tabulated results of the investigation of the fuel class content effects on predicted HC's....125
Table 11-10 Tabulated results of the investigation of aromatic and olefin content effects on predicted HC's with paraffins as the swing component....126
Table 11-11 Investigation of low- to mid-range volatility effects, by normalising the coefficients, on predicted HC's....127
Table 11-12 Summary of Cp analysis for HC's – Combustion Analysis Correlation....128

Table 11-13 Summary of co-linearity analysis, giving the co-linear variables and the variable coefficients for the HC's – Combustion Analysis Correlation. 129
Table 11-14 Summary of Cp analysis for NO – Fuel Properties Correlation 130
Table 11-15 Summary of co-linearity analysis, giving the co-linear variables and the variable coefficients for the NO – Fuel Properties Correlation. 130
Table 11-16 Summary of Cp analysis for NO – Combustion Analysis Correlation. 131
Table 11-17 Summary of co-linearity analysis, giving the co-linear variables and the variable coefficients for the NO – Combustion Analysis Correlation. 132
Table 11-18 Comparison of different burn angle variables as model variables for NO prediction, using model 4 as a base model. 132
Table 11-19 Summary of Cp analysis for CO – Fuel Properties Correlation 133
Table 11-20 Summary of co-linearity analysis, giving the co-linear variables and the variable coefficients for the CO – Fuel Properties Correlation. 134
Table 11-21 Investigation of low-range volatility effects, by normalising the coefficients, on predicted CO. 135
Table 11-22 Summary of Cp analysis for CO – Combustion Analysis Correlation. 136
Table 11-23 Summary of co-linearity analysis, giving the co-linear variables and the variable coefficients for the CO – Combustion Analysis Correlation. 137
Table 11-24 Summary of Cp analysis for DPMAX – Fuel Properties Correlation 138
Table 11-25 Summary of co-linearity analysis, giving the co-linear variables and the variable coefficients for the DPMAX – Fuel Properties Correlation. 138
Table 11-26 Summary of Cp analysis for TMAX – Fuel Properties Correlation 139
Table 11-27 Summary of co-linearity analysis, giving the co-linear variables and the variable coefficients for the TMAX – Fuel Properties Correlation. 139
Table 11-28 Investigation of low-range volatility effects, by normalising the coefficients, on predicted TMAX. 140
Table 11-29 Summary of Cp analysis for DHRMAX – Fuel Properties Correlation. 140
Table 11-30 Summary of co-linearity analysis, giving the co-linear variables and the variable coefficients for the DHRMAX – Fuel Properties Correlation. 141
Table 11-31 Investigation of low-range volatility effects, by normalising the coefficients, on predicted DHRMAX. 141
Table 11-32 Summary of Cp analysis for BA595 – Fuel Properties Correlation 141
Table 11-33 Summary of co-linearity analysis, giving the co-linear variables and the variable coefficients for the BA595 – Fuel Properties Correlation. 142
Table 11-34 Investigation of low-range volatility effects, by normalising the coefficients, on predicted BA595. 142
Table 11-35 Summary of Cp analysis for Z2BA298 – Fuel Properties Correlation 142
Table 11-36 Summary of co-linearity analysis, giving the co-linear variables and the variable coefficients for the Z2BA298 – Fuel Properties Correlation. 143
Table 11-37 Investigation of low-range volatility effects, by normalising the coefficients, on predicted Z2BA298. 144
Table 11-38 Investigation of high-range volatility effects, by normalising the coefficients, on predicted Z2BA298. 144
Table 11-39 Summary of Cp analysis for Equivalence Ratio – Fuel Properties Correlation 144
Table 11-40 Summary of co-linearity analysis, giving the co-linear variables and the variable coefficients for the Equivalence Ratio – Fuel Properties Correlation. 145
Table 11-41 Investigation of low-range volatility effects, by normalising the coefficients, on predicted Equivalence Raito. 146
Table 11-42 Investigation of high-range volatility effects, by normalising the coefficients, on predicted Equivalence Ratio. 146
Table 11-43 Details of load points used for the detailed NO formation analysis. 147

Table 11-44 Some relevant parameters derived from the results indicated in Figure 11-23.....150
Table 12-1 Summary comparison of results for the HC emissions as a function of fuel components for the AQIRP and EPEFE studies and this research. 156
Table 13-1 Summary of conclusions drawn for HC emissions. 167
Table 13-2 Summary of conclusions drawn for NO emissions. 168
Table 13-3 Summary of conclusions drawn for CO emissions. 169

List of Equations

Equation 5-1 Calculation of oxygen number from mass percent oxygen content of fuel. 49
Equation 8-1 Equations for the solving of the two-zone mass transfer based burn rate model (for derivation see Appendix B). 67
Equation 8-2 Calculation of adiabatic flame temperature. 67
Equation 8-3 Form of the algorithms proposed by Gordon and McBride [31] for the calculation of species gas properties. 68
Equation 8-4 Mixture gas property relations. 69
Equation 8-5 Equations for the calculation of the partial derivatives of the gas properties. 69
Equation 8-6 Chemical reaction equation of hydrocarbon fuel in air used by the equilibrium combustion products model. 70
Equation 8-7 Simplification of the left side of the reaction equation used by the equilibrium combustion products model. 70
Equation 8-8 Atom balances used by the equilibrium combustion products model. 71
Equation 8-9 Mole fraction identity. 71
Equation 8-10 Seven hypothetical equilibrium reactions used. 72
Equation 8-11 Details of Taylor expansion used to linearise the non-linear equations. 73
Equation 8-12 Differentiation of the four non-linear equations with respect to temperature. 73
Equation 8-13 Form of the heat transfer coefficient calculation proposed by Woschni. 75
Equation 8-14 Dimensionless group relationship for forced turbulent convective heat transfer across a flat plate. 75
Equation 8-15 Rate controlled reactions for the extended Zeldovich mechanism for the formation of NO. 78
Equation 8-16 Rate controlled formation of NO. 78
Equation 8-17 Rate controlled formation of atomic nitrogen. 78
Equation 8-18 Reduction of Equation 8-16 by substitution of the assumption in Equation 8-17. 78
Equation 8-19 Equations indicating that forward and reverse reactions occur at equivalent rates at equilibrium, and the simplified rate controlled equation for NO formation. 79
Equation 9-1 Equation of polytropic process of an ideal gas. 88
Equation 9-2 The equations for polytropic compression of an ideal gas. 89
Equation 9-3 Correlations for γ as given by Cheung and Heywood [42] for compression and a burned gas mass fraction of 8.5%. 89
Equation 9-4 Equation for the calculation of average surface temperature. 95
Equation 10-1 Common third order mixture model equation with reduced terms. 103

Nomenclature and Abbreviations

°CA	Degrees of Crank Angle Rotation
ACEA	Association des Constructeurs d'Automobiles (European association of automobile manufacturers
Alkane	Paraffin – an alternative name used by some authors
Alkene	Olefin – an alternative name used by some authors
Burn Angle	Number of degrees of crank shaft rotation required for combustion to proceed from a specified start point, to a specified end point.
Burn Rate	Rate of combustion in internal combustion engines
Catalyst Light Off	Time taken for the exhaust catalyst to warm sufficiently that efficient operation is achieved
CI	Compression Ignition (refers usually to diesel engines)
CO	Carbon Monoxide
CO_2	Carbon Dioxide
CVS	Constant Volume Sampler
DOHC	Double Overhead Camshaft
$E_{\#\#}$	Distillation Point: % of fuel vaporised at ## ℃, [%]
EMS	Engine Management System
Engine-out emissions	Pre-catalyst exhaust concentrations (if fitted, or else expected tail-pipe emissions if no catalyst fitted)
EPA	Environmental Protection Agency (North American regulatory body)
Equivalence Ratio	Operating fuel/air ratio divided by stoichiometric fuel/air ratio
ER (ϕ)	Equivalence Ratio Calculated as [operational fuel/air ratio]/[stoichiometric fuel/air ratio] (ER > 1 - rich, ER < 1 - lean)
ETA	Engine Test Automation – PC based data acquisition system developed in the Department of Mechanical Engineering, University of Stellenbosch
EUROPIA	European Petroleum Industry Association
EVO and EVC	Crank angle at the point of Exhaust valve opening and closure respectively
Flame Quench Distance	Minimum distance for a given geometry, through which a flame will propagate
FTP	Federal Test Procedure
Fugacity	Gas property used in real gas thermodynamic calculations
HC	Various Hydrocarbon Species
HFID	Heated Flame Ionisation Detector, gas analyser type for measuring hydrocarbons
IBP	Initial Boiling Point, [℃]
IVO and IVC	Crank angle at the point of Inlet valve opening and closure respectively
Lambda (λ)	Inverse of Equivalence Ratio (λ < 1 - rich, λ > 1 - lean)
Lambda Sensor	Exhaust Oxygen Sensor, intended to measure operational air/fuel ratio, or Lambda
MBT	Ignition timing to achieve Maximum Brake Torque

Modal Analysis	Measurement of instantaneous exhaust emissions during driving cycle test - allows the identification of which components or “modes” of the driving cycle correspond to peaks in emissions
MTBE	Methyl Tertiary Butyl Ether
NDIR	Non-Dispersive Infra Red, gas analyser type (can measure many gas species)
NMHC	Non-Methane Hydrocarbons, Various Hydrocarbon Species, excluding Methane (Methane occurs naturally and is relatively inactive in photochemical reactions, and is therefore often ignored)
NO_x	Oxides of Nitrogen
OE	Original Equipment
OEM	Original Equipment Manufacturer
Photochemical Reactions	Chemical reactions catalysed by ultra violet radiation
Racer	Rapid Acquisition of Combustion Engine Results - PC based high-speed cylinder pressure data acquisition and combustion analysis system developed in the Department of Mechanical Engineering, University of Stellenbosch
Regulated Emissions	CO, HC and NOx, exhaust gases covered by legislation in developed countries
SI	Spark Ignition (refers usually to petrol engines)
SOHC	Single Overhead Camshaft
Stoichiometric	Ideal fuel/air ratio, exactly sufficient fuel supplied to an engine that it combusts all the induced air to form only CO_2 and water
$T_{\#\#}$	Distillation Point: Temperature required to evaporate ##% of fuel, [°C]
Tail-pipe emissions	Post-catalyst exhaust emissions
TDC	Top Dead Centre
Vapour/Liquid Ratio (V/L Ratio)	Measure of volatility, directly related to vapour lock problems
VOC	Volatile Organic compound
WOT	Wide Open Throttle

1. INTRODUCTION

The importance of gaseous pollutants associated with automotive emissions has long been known and much research has been undertaken in an attempt to reduce the impact of these on air quality. Most developed countries have strict legislation limiting the emissions of certain gaseous compounds of new vehicles, and these limits are continuously being lowered as technology improvements allow engineers to produce lower emitting vehicles. While South Africa does not at present have any passenger vehicle gaseous emissions legislation, Cape Town and other cities are known to, at times, have poor air quality. The role of automotive related emissions in this poor air quality is undoubtedly important and the first steps in the implementation of vehicle emissions regulation have recently been taken. Legislation equivalent to ECER83.04 which is commonly referred to as Euro 2, comes into force for new vehicle homologations from 1 January 2006, and will be applied to all newly manufactured vehicles from 1 January 2008 [1]. It is intended that the legislation will gradually be tightened to bring it in line with the later ECE regulations. Vehicle emissions regulation is the most important mechanism to reduce vehicle emissions, and thus air pollution, however the effect of the fuel formulation may also be important. Furthermore, during the transition phase when most of the vehicles on the road were manufactured prior to the legislation enforcement dates, and are thus uncontrolled, any potential reductions in emission from these vehicles may have a significant impact on air quality. Thus it is prudent to investigate the potential for influencing emissions through alterations to the fuel formulation as these effects can be felt immediately. The objective was thus to investigate whether meaningful differences in exhaust emissions can be achieved through fuel reformulation.

Vehicles impact air quality predominantly through two sources of pollutant emission. The first source is exhaust emissions, which are gaseous or particulate emissions released as a result of the combustion of fuel by the engine in the vehicle. The second source is evaporative emissions, which is the gaseous release of hydrocarbon compounds evaporated from the fuel storage and supply system. This research is concerned with the first source of emission, the exhaust or tail pipe emissions. Hydrocarbon emissions, both exhaust and evaporative, and the oxides of nitrogen emitted in the exhaust are precursors to photochemical smog and ozone formation. This is one of the major sources of poor air quality associated with vehicles. As the hydrocarbons are emitted in both exhaust and evaporative emissions, they are obviously of great importance. It must therefore be stressed that any action taken to attempt to reduce the air quality impact of the passenger vehicle must consider both sources of vehicle related emissions. It is probable that the main source of hydrocarbons emitted by non-regulated vehicles such as those making up the majority of those on the South African roads is evaporative.

At the time of inception of this research, the introduction of unleaded fuel to the South African market was imminent and there was much speculation as to the potential impact of this on air quality. This had some bearing on the choice of the fuels, and their specific formulation, used in the research. The objectives of the research were to study the effect of the formulation of the fuel on spark ignition engine exhaust emissions. The entire scope of the related work included the study of the regulated emissions (hydrocarbons, oxides of nitrogen and carbon monoxide) and speciated aldehydes from a range of fuels. The fuels included many of the market fuels being produced at the time, as well as unleaded formulations that were proposed for introduction. A number of

fuels were also specifically formulated to investigate the effects of a variety of fuel parameters. In all, thirty-five fuels were included in this phase of the research. A related study also investigated the effect of a number of alcohol compounds as potential fuel blending components in varying concentrations. This dissertation is limited to the regulated emissions of the thirty-five leaded, un-leaded and specially formulated fuels. The objectives of the study were to attempt to identify the fuel formulation parameters that influence the emissions, and to gain some understanding of the mechanisms through which the effect is occurring.

Vehicle technology and engine design influence exhaust emissions to a great extent. In order to meet the strict vehicle emissions legislation it is necessary to utilise exhaust gas after treatment. Homogenous charge, spark ignition engines are the dominant technology in passenger car and light commercial vehicles and this technology requires the use of a three-way catalytic converter. The use of this device also places constraints on the engine technology and operating parameters. The majority of vehicles on the South African roads, and of new vehicles currently being sold, do not have this technology and therefore are not constrained in their engine design. For this reason some local engines utilise outdated technologies or a mix of current technology without being constrained to use engine calibrations necessary for exhaust catalytic converter operation. This is one of the main reasons why this research was necessary when so much research had been performed internationally, as the results achieved in these other programmes are often based on the newer technology engines. For this reason engines typical of the technologies predominantly in use in the country were chosen.

The approach taken in terms of the fuel formulation and fuel formulation parameters investigated was somewhat different to the typical approach. In most previous studies a small number of fuel formulation parameters are pre-selected and a full factorial experimental approach is followed. In this research a large number of fuels, spanning very many different levels of a large number of fuel formulation parameters of interest, were blended and tested. The highly complex and interdependent nature of the process of exhaust emissions formation implies that the determination and quantification of the important parameters would be difficult. For this reason, statistical methods utilising multivariate linear regression techniques were used. The statistical analysis was constructed so as to enable the identification of the mechanisms through which the fuel parameter influences the emissions produced.

One of the main objectives was to gain an understanding of the mechanisms through which the fuel properties were influencing the emissions produced. This would require knowledge of the physical processes taking place and the interaction of the fuel properties with these processes. Advanced combustion analysis was identified as being necessary to achieve this. Combustion analysis is the process whereby the rate of combustion is determined by measuring the cylinder pressure trace in an engine, and performing specialised thermodynamic analysis thereon. This information can then be used to compare the combustion characteristics of the different fuel formulations. Although an existing software program was available for this purpose, the thermodynamic analysis was thought to be too simplistic and therefore a more advanced analysis was required. This was added to the software and used, along with the original analysis, in the analysis of the results. A further major modification was made to the thermodynamic analysis in order to investigate the cause of a noteworthy finding from the initial statistical analysis showing an unexpected interaction between the fuel properties and the exhaust NO emissions. This analysis was able to provide valuable insight into the mechanism of NO formation and thus the anomalous finding.

2. BACKGROUND TO AUTOMOTIVE EMISSIONS

2.1. Motivation

The important influence of automobile exhaust emissions on air quality, and in particular on photochemical smog, has been known for many years. Two of the major precursors in the formation of photochemical smog are present in significant concentrations in the exhaust gas of Spark Ignition (SI) engines, namely the Oxides of Nitrogen (NO_x) and Hydrocarbons (HC). Photochemical smog is of great concern in some highly populated cities around the world, the best known example being Los Angeles (LA). Automobile exhaust emissions were discovered to be a major source of the pollutants causing this and for this reason legislation was introduced in the United States of America (USA) in the 1970's which limited the exhaust emissions of new vehicles. Since then, the USA and many other developed countries have introduced increasingly stricter legislation in an attempt to improve air quality. In South Africa, Cape Town too is thought to have a photochemical smog problem, which is exacerbated by a peculiar geographical and meteorological phenomenon, which results in temperature inversion. This results in warm ground air being trapped below a layer of cooler air which prevents dispersion of the pollutants, intensifying the formation of photochemical smog. Temperature inversion occurs in Cape Town mostly on wind-still autumn and winter days resulting in visible smog, often called brown haze. A limited study incorporating a source apportionment of the Cape Town Brown Haze was undertaken and the results indicate that the major contributor of the visibility degradation is diesel engine particulate emission [2]. However, studying detailed ambient pollutant concentration data monitored at various locations in Cape Town by the Air Pollution Control and Scientific Services divisions of the Cape Metropolitan Council (CMC) indicates significant photochemical activity associated with gaseous vehicle emissions [3]. Air quality and photochemical smog are discussed in more detail below in Section 2.2.

The strict legislation introduced internationally has forced vehicle manufacturers to seek means of reducing the tailpipe emissions from their automobiles. This has resulted in much research being done internationally in an attempt to learn more about the mechanisms of automobile emissions formation and the factors that influence them. The majority of this research has been done in the USA where legislation is of the strictest in the world. The result of much of this research has led to major modifications to the SI engine itself in the last few decades, the most significant being electronic management of fuel injection and ignition timing. This allowed improved control of air/fuel ratio which can have a substantial effect on the exhaust emissions produced by the engine. However, development of the engine itself for improved emissions could not meet the strict legislation. This then necessitated the addition of exhaust after-treatment methods, the most significant being catalytic converters, which reduce the pollutants to legislated levels. Advanced three way catalytic converters only operate efficiently over a narrow equivalence ratio band, which necessitated the development of improved closed-loop air/fuel ratio control. This improved control mechanism employs an oxygen sensor, often called a lambda sensor, placed in the exhaust which provides feedback to the electronic engine management system (EMS). As catalysts and lambda sensors are poisoned by the lead based additive used as an octane improver in conventional gasoline,

new unleaded gasoline blends had to be developed. Further recent developments have included the production of direct injection, stratified charge, engines usually referred to as Gasoline Direct Injection engines (GDI).

A significant body of research exists aimed at quantifying the effects of the fuels formulation on the exhaust composition. This has led to the implementation of legislation in the USA which requires Reformulated Gasoline (RFG) to be available in certain regions where certain air quality standards are not met. Furthermore, as legislation is expected to get ever stricter, improvements to conventional engine technology and after treatment need to be supplemented with improved fuels to meet these targets. This has also promoted international research into the effect of fuel formulation on gaseous emissions.

In South Africa, legislation which will enforce the use of catalytic converters will only come into force, in a phased approach, starting in January 2006 [1]. Therefore local vehicle manufacturers have, up until now, been able to utilise traditionally lower cost engine technologies that have become outdated internationally. Unleaded gasoline became available in March 1996, and leaded gasoline will only be removed from fuel supply in January 2006. This lack of availability of unleaded fuel prior to 1996 had forced the utilisation of predominantly open-loop control of air/fuel ratio, as the sensor required for closed loop control, the lambda sensor, is poisoned by the lead. It is also important to note that the South African vehicle fleet differs in another significant way from fleets in other developed countries in that, due to the lack of emissions legislation, there are no evaporative emission controls on many of the models. This, combined with two significant factors, make the level of hydrocarbon evaporative emissions very large from these vehicles. Firstly, the utilisation of modern fuel injection systems, on some vehicles, results in the fuel being pressurised to high pressures (up to and over 300 kPa) for injection accompanied by high levels of fuel circulation (100 litres/hr). This results in the fuel being heated to a larger extent than with older technology carburettor equipped vehicles, leading to increased evaporation. Secondly, the fuel specifications internationally have tended towards fuels with reduced vapour pressure to minimise the evaporative potential of the fuel. The specifications in South Africa have not followed this trend and appear to be similar to specifications in countries with much cooler climates. All of these factors result in the evaporative emissions of modern South African vehicles being much greater than that of vehicles fitted with the evaporative control devices and this has been shown by de Waal [4] and van der Westhuizen [5]. The raw fuel lost to evaporation will also take part in the photochemical reactions and may conceivably be more significant than the exhaust hydrocarbons.

South Africa is also in a unique situation as regards the range of gasoline formulations available. With the large difference in altitude between the coastal and inland regions, four different fuel octane grades are available, both regions having a high and low octane grade. Fuel is also produced locally in a number of different ways producing unique fuel formulations. Fuel from coal and natural gas is produced by Sasol, while PetroSA (formerly Mosgas) produces fuel only from natural gas, both companies utilising variations of the Fischer-Tropsch process. Crude based fuel however, remains predominant, being produced by a number of refineries around the country.

A further motivation for studying the effects of fuel formulation on emissions is that South Africa has a low turnover of new vehicles by international standards. This means that the average age of the vehicles on the road is considerably older than in developed countries. The implication of this is that any new vehicle technology

introduced will take considerably longer to filter down into the vehicle park. However, if any improvement in emissions can be achieved through an alteration in fuel formulation, an immediate benefit is possible.

All of the above factors imply that results achieved internationally may not be directly translatable to the local conditions. At the time of inception of this research project all the locally produced fuel contained lead-based additives, while the production of unleaded fuel was imminent. It was therefore decided that a study of the emissions implications of the local leaded fuel formulations and that of the possible unleaded formulations, operating in engines representative of those currently being manufactured locally, be undertaken.

An important aspect of the research was the intention to study and quantify the mechanisms through which the fuel formulation influenced the engine out emissions. This fundamental understanding of these mechanisms would provide a direct transference to new vehicle technologies as well as being relevant to fuels manufactured under different regulations (such as after lead phase out). Furthermore, the experimental study incorporated aspects intentionally designed to simulate the vehicle technologies associated with exhaust after treatment engine technologies.

2.2. Air Quality, Photochemical Smog and Pollution Associated with Vehicle Emissions

The major impact that automobile exhaust emissions have on air quality and pollution is in the form of photochemical smog. Smog is a term originating in England (about 1911) as a synonym for the mixture of fog and coal smoke. Smog is thought to arise from the formation of sulphur trioxide, which forms hygroscopic nuclei, which, after absorbing water, forms sulphuric acid. Smog occurs on cold, wet, winter days or nights with low ozone concentrations and low visibility. Photochemical smog, on the other hand, occurs on hot, dry, summer days with high ground level ozone concentrations, and reduces visibility to a lesser extent. The process of photochemical smog formation is known to rely on photochemical reactions. The most popular theory [6] is that particular mixtures of hydrocarbons and nitrogen oxides react in the presence of, and are catalysed by, ultraviolet radiation to form a variety of products including aldehydes and ozone, which is a powerful irritant. Caplan [7] theorises that the formation of photochemical smog is governed not only by the quantity of hydrocarbons but by their reactivity, which he defined in terms of the affinity to form smog when present with nitric oxide. His data has indicated that smog is always reduced by decreasing the concentrations of reactive hydrocarbons, and that for a given concentration of hydrocarbons, the formation of smog is at a maximum for one particular nitric oxide concentration. This implies that the reduction of nitric oxides in the atmosphere may conceivably increase smog formation. This is supported by Amann [8] who defines three separate scenarios: the NO_x inhibition region, the knee region and the HC saturation region as shown below in Figure 2-1. In the HC saturation region reduction in HC concentration has no effect on ozone formation. In the knee region decreases in either NO_x or HC will reduce the ozone formed. However, in the NO_x inhibition region decreasing the HC will reduce the ozone formed, but independently reducing NO_x may actually increase the formation of ozone. Thus the effect on ozone formation from reduced vehicle emissions is dependent on the initial composition of the local urban atmosphere. This peculiarity is due to the fact that in the group of chemical reactions that Caplan postulates to govern smog formation, as given below in Figure 2-2 (*a*), NO_2 plays two separate roles. In reaction 2 it promotes smog

formation in its role as a precursor to ozone formation and in reaction 11 it inhibits smog formation by reacting with oxyalkyl radicals and thus terminating the chain reaction.

Understanding of this interplay between the relative concentrations of NO_x and HC is very important. Using the situation in Cape Town as an example, it is possible that prior to the introduction of unleaded petrol, many vehicles had high compression ratio engines, but no exhaust after treatment. Such cars are likely to be relatively high emitters of NO_x. The introduction of unleaded petrol then enabled the introduction of vehicles with catalytic converters, and many up-market vehicles, fitted with these devices, have been sold locally even in the absence of legislation. These vehicles will be low overall emitters. The mix of vehicle technologies on the road has thus changed in the last ten years. It is therefore conceivable that previously Cape Town may have been sitting in the NO_x inhibition region (upper left of Figure 2-1) due to a relatively high number of high NO_x emitters being on the road, and that any reduction in emissions would move the relative mix of NO_x and HC. Reducing emissions from the NO_x inhibition region, either vertically down due to NO_x reduction only, or diagonally due to overall reductions, will have the tendency to initially worsen the situation as it enters the knee region. Improvements would only be seen once the HC saturation region is reached.

An indication of the differences in the reactivity of different hydrocarbon groups can be seen in Figure 2-2 (*b*) where it can be seen that substituted internal olefins are extremely reactive whereas the paraffin family and benzene ring compounds are much less reactive.

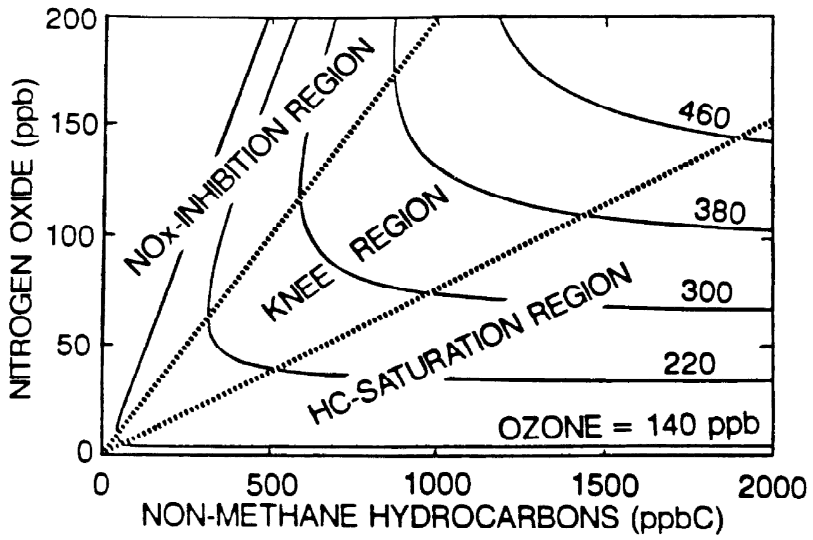

Figure 2-1 Effect of initial NOx and NMHC concentrations on ozone formed [8].

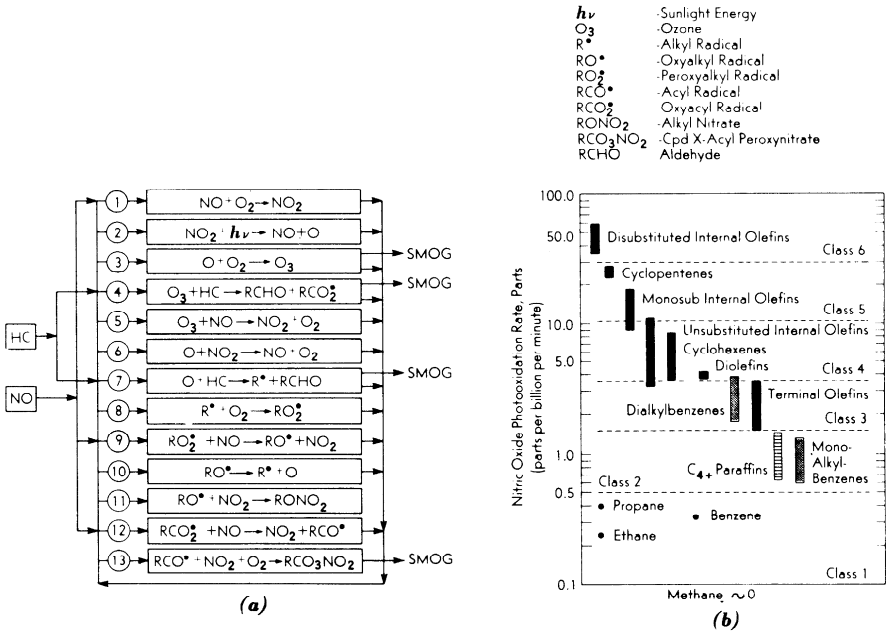

Figure 2-2 (*a*) Routes for photochemical smog formation. (*b*) Nitric oxide photo oxidation rate, or reactivity of different hydrocarbon classes [6].

Other undesirable compounds that may be linked to automobile exhaust emissions, and classified as pollutants, would include CO_2, CO, aldehydes, certain potential carcinogenic hydrocarbons, sulphur dioxide, particulates as well as compounds containing lead. CO_2 is classified as a "greenhouse gas" as CO_2 in the atmosphere is thought to block the radiation of heat away from the planet and thus, by trapping this heat, is causing a climatic change by increasing global average temperatures. The haemoglobin in the blood has a higher affinity for CO than oxygen, thus any CO inhaled bonds with the haemoglobin and is only slowly replaced by oxygen in the lungs. This reduces the ability of the body to exchange gases and causes drowsiness, impairs alertness, thinking and reflexes and can, in the extreme, be fatal. There are other compounds found in the exhaust that may be of interest due to their harmful nature. Aldehydes are irritants and some are thought to be carcinogenic while Benzene is a known carcinogen. Another carcinogenic compound that has received some attention lately is 1,3 Butadiene. Sulphur dioxide (SO_2) oxidises to form sulphur trioxide (SO_3) which combines with water vapour to form sulphuric acid (H_2SO_4). Sulphur dioxide is a strong irritant and sulphuric acid forms acid rain. Particulate matter can potentially adsorb carcinogenic hydrocarbons and carry these deep into the lungs where they can cause serious damage. Particulate matter is also known to reduce visibility and is a contributor to visible haze. The octane enhancing additive tetraethyl lead, used in gasoline since the 1920's, produces emissions of various compounds containing lead: these compounds are known neurotoxins and are thus undesirable.

2.2.1. Photochemical Smog in Cape Town

During episodes of temperature inversion, a meteorological phenomenon in which a layer of warm air is trapped below a layer of cooler air, there is a tendency for a haze to exist over parts of the Cape Peninsula

to the East of Cape Town. This "Brown Haze" is characterised by a white to brown mist which is trapped at a low level, mostly over the Cape Flats. A study, which focussed mainly on airborne particulate matter, has been performed by the Energy Research Institute of the University of Cape Town, comprising a source apportionment [2,9]. The pilot study [9] had indicated that particulate matter typically has higher light extinction factors than gaseous pollution, and thus the main study [2] focussed most of the effort on particulates. The conclusions drawn in the study were that the most important contributors to the visibility degradation were vehicles: 65% of the light extinction was directly attributed to traffic related causes. Diesel vehicle particulate emissions were found to be the major offender with 48%. Therefore, 17% of the visibility degradation was directly associated with petrol fuelled vehicles.

Visibility impairment by way of light extinction can be divided into four distinct categories:

- light scattering by particles
- light absorption by particles
- light scattering by gases
- light absorption by gases

The role of particles is indicated to be more important in direct visibility degradation than gases, however, NO_2 is known to be a gas which does produce significant visibility degradation and is a product of photochemical smog [9]. Elevated concentrations of NO_2 in ambient air are known to result in a brown discolouration.

Gaseous pollutant data are routinely monitored in and around Cape Town by the Scientific Services and the Air Pollution Control divisions of the Cape Metropolitan Council. Studying examples of data as given below in Figure 2-3 and Figure 2-4, the conclusion may be drawn that vehicle related photochemical activity is prevalent. As stated above, the combination of oxides of nitrogen and hydrocarbons in the presence of ultra violet light will, in certain circumstances, lead to the formation of photochemical smog. One of the products of this reaction is ozone. It is seen below in Figure 2-3 that on the three consecutive days (Wednesday 19th to Friday 21st June 1996) there are distinct trends of high NO and NMHC peaks at around 8am. There are also lower, but wider spread peaks in late afternoon or early evening. These trends are not consistent with industry or household activity but are consistent with commuter traffic patterns which indicate that these pollutants are probably dominated by passenger vehicles. Furthermore, on two of these days, the 19th and 21st, there is a distinct NO_2 peak after the morning's elevated NO levels. This is occurring as indicated by reaction 1 in Figure 2-2. This NO_2 may then, in the presence of ultra violet light, decompose and form NO and ozone as indicated by reactions 2 and 3. Furthermore, the presence of the NMHC provides the other reagent to promote the formation of photochemical smog. A typical photochemical smog episode is seen below in Figure 2-4, where on Sunday the 19th of May ozone levels are seen to be over the World Heath Organisation guideline. Again the morning and afternoon/evening peak in NO is seen, followed by NO_2 formation and the production of ozone. Therefore, it must be concluded that, in certain conditions, photochemical smog formation is occurring in the Cape

Town environs. It must be stressed, that the photochemical smog chain reaction will not always occur given, NO, NMHC and ultra violet light. In fact, there was no related ozone formation on the 21st June 1996 due to the extremely high NO levels, in which case extreme NO_x inhibition is occurring. However, it is apparent that there are occasions when the conditions favour this occurrence, and it appears that they are dominated by passenger vehicle emissions.

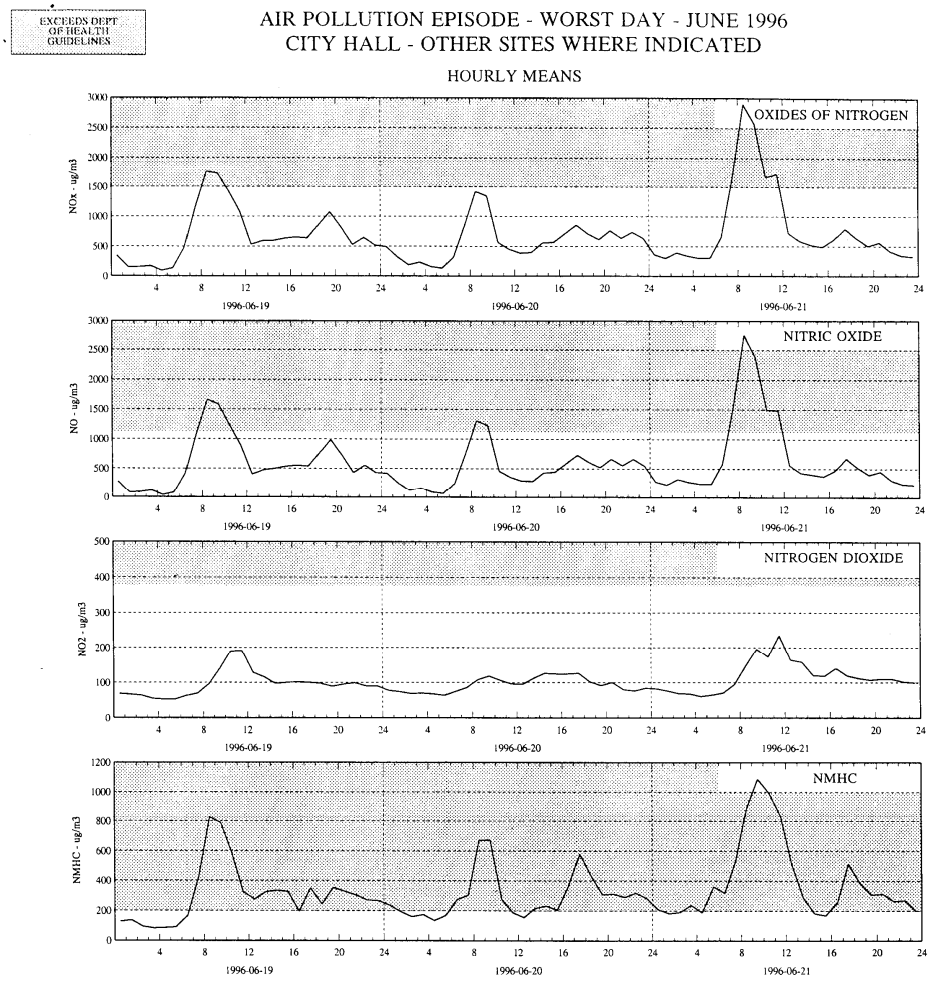

Figure 2-3 Atmospheric pollutant concentrations for City Hall monitoring site, Cape Town for three consecutive days in June 1996 (graphs courtesy of Scientific Services Division of CMC).

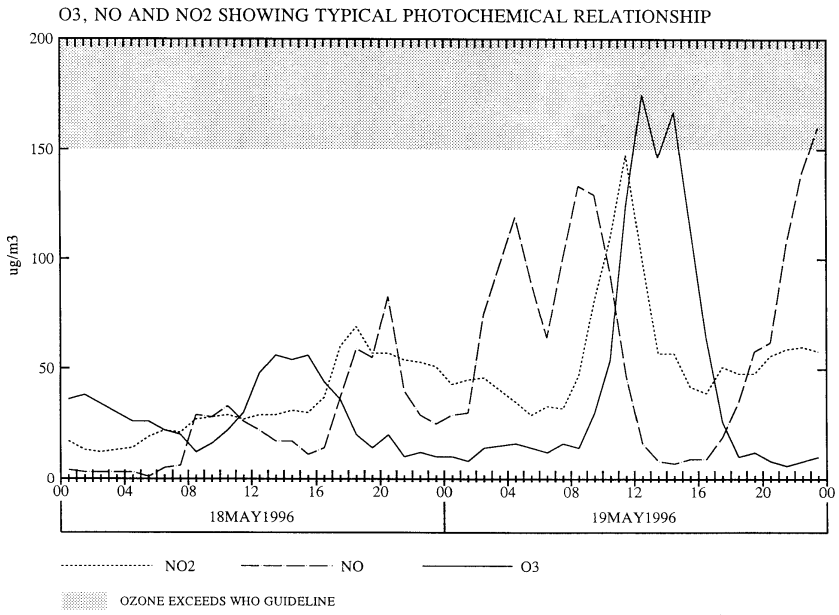

Figure 2-4. Atmospheric pollutant concentrations for Goodwood monitoring site, Cape Town for two consecutive days in 1996 (graph courtesy of Scientific Services Division of CMC).

2.2.2. Holistic Approach to Air Quality Impact

A holistic approach is required when considering the environmental, and specifically the air quality, impact of vehicle exhaust emissions. Firstly, the exhaust emissions are not the only vehicle related emissions that can influence air quality. Evaporative emissions and road dust [2, 9] are also known to play a role in ambient air quality. Secondly, it is vital to consider exhaust emissions in a rationalised way. In other words, emissions should be quantified in units that take into account influences on engine efficiency and other operating parameters. Exhaust emissions are usually measured in units of concentration of exhaust gas (% by volume or parts per million, ppm) but engines, especially SI engines, have highly variable mass throughput rates. Thus, using units of concentration may be misleading as far as actual air quality impact is concerned, and these results should be rationalised before reliable conclusions can be drawn.

Units of grams of pollutant per kilometre travelled (g/km) or grams of pollutant per kilowatt-hour of engine operation (g/kW.hr) are examples of appropriate rationalised units. By way of example, reducing the engine compression ratio may drastically reduce the NO_x concentrations in the exhaust stream, but there is an associated reduction in engine efficiency. In order for this engine to do a similar amount of work, it would have to consume more fuel and air. Thus the actual mass of pollutant emitted may actually be increased relative to the engine with the higher compression ratio and higher NO_x exhaust concentrations. Furthermore, the reduced compression ratio may have impacts on other pollutants emitted, which need to be considered.

When considering the influence of fuel formulation, it would also be important to consider the refining, or fuel manufacturing, required to produce the necessary reformulated fuels. If, for instance, complicated

processes requiring excessive energy are required, then the displaced emissions of this energy need to be considered. The overall cycle efficiency, or well-to-wheels efficiency, needs consideration too [10].

Another point that bears consideration is that there are many other ways of reducing the environmental impact of vehicles and transport [11] and the potential for reduced impact may be much larger than that achievable only from vehicle technology and fuel formulation. Reducing the number of vehicle kilometres travelled in a given zone will immediately reduce the release of pollutants. This can be achieved by encouraging the average vehicle occupancy to be raised by increasing the use of public transport services such as mini-bus taxis and commuter buses as well as car pooling which may be promoted by increasing parking fees and providing special allowances to high occupancy vehicles. Encouraging the use commuter rail as a convenient alternative could have a significant impact also. Improvements to traffic flow rates may at first seem to be desirable in that it would reduce the trip specific emissions. However, care must be taken as it has been reported that in areas where this has been achieved, the increased traffic efficiency has encouraged more vehicles to travel into the zone and thus actually increasing the release of pollutants [12].

2.3. Exhaust Gas Composition

The main constituents of an SI engine's exhaust gas are Nitrogen (N_2), Carbon Dioxide (CO_2), water (H_2O), Carbon Monoxide (CO), Oxygen (O_2), Unburned Hydrocarbons (HC's) and Oxides of Nitrogen (NO_x). Aldehydes and other partial oxidation compounds are released in much smaller concentrations. Sulphur dioxide is emitted from SI engines in extremely low concentrations due to the generally low concentration of sulphur in the parent fuel. Diesel engines do however release some SO_2 due to the often higher levels of sulphur in the diesel fuel. Particulates are also not emitted by conventional SI engines in significant quantities. The compounds of interest are CO_2, a greenhouse gas, CO a toxin and NO_x and HC's which are precursors to photochemical smog. The gases covered internationally by legislation for vehicles propelled by SI engines are NO_x, Hydrocarbons and CO, and this group of gases are referred to as the "regulated emissions". Particulates would be included in the definition of regulated emissions for diesel propelled vehicles.

The complete combustion of hydrocarbon based fuels produces only CO_2 and water. CO is produced if the combustion is not allowed to go to completion or if there is insufficient oxygen for complete combustion (a rich mixture). Hydrocarbons are present due either to combustion being incomplete or if some of the fuel or mixture does not take part in combustion, hence the term unburned hydrocarbons is often used. Excessive hydrocarbon emission is therefore often due to a rich mixture. Oxides of nitrogen are formed as a natural by-product due to the high temperatures and pressures associated with combustion in Internal Combustion Engines (ICE), promoting the dissociation of N_2 and the resulting formation of NO and other oxides of nitrogen.

The exhaust constituents of interest for this research are the regulated emissions. Exhaust aldehydes were measured and speciated alongside in a parallel project [13,14], but will not be dealt with here.

2.3.1. Emissions Formation Mechanisms

In order to understand the effect that engine or fuel properties may have on the emissions produced, it is necessary to understand the formation process and origin of the emissions. Thus the formation of each of the gases is discussed briefly below, along with the factors that may affect them.

Carbon Monoxide (CO)

An engine which is operating with an equivalence ratio richer than stoichiometric, will produce CO emissions due to the fact that there is insufficient oxygen available to convert all the carbon in the fuel to CO_2. The chemistry of the C-O-H system in SI engines is generally fast enough that local equilibrium may be assumed. It may therefore be assumed that lean running engines will produce no CO emission and the amount of CO produced by a rich running engine could easily be determined from a solution of the combustion equation or an equilibrium subroutine. However, once gas temperatures drop during expansion the C-O-H chemistry does become rate limited and therefore equilibrium can not be assumed [15]. Thus wall quenching and the lower temperatures occurring late in the expansion stroke will lead to the appearance of some CO in mixtures running lean of stoichiometric. The highly non-linear nature of CO formation as a function of equivalence ratio around the stoichiometric point, as evident from Figure 2-5 below, leads to a further significant source of CO emission. In a multi-cylinder engine, running with an overall equivalence ratio near stoichiometric, with some cylinders run lean and some cylinders run rich, the lean cylinders produce much less CO than the rich cylinders. The actual CO emissions would be higher than that predicted given the overall operating equivalence ratio. Therefore a multi-cylinder engine running near to stoichiometric but having even slightly uneven fuel distribution will produce disproportionately high CO emission. It thus apparent that the operating equivalence ratio is by far the most significant factor affecting CO formation and uneven fuel distribution will have a disproportionate effect on CO emissions.

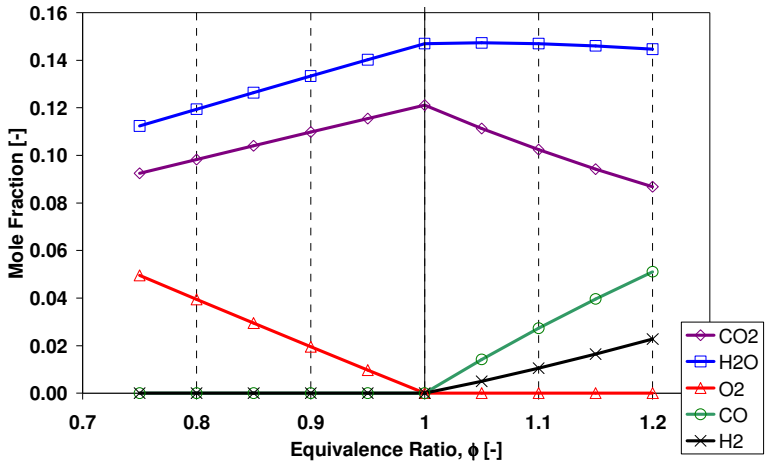

Figure 2-5 Mole fractions of combustion products as a function of equivalence ratio from basic stoichiometry and equilibrium calculations.

Hydrocarbons (HC's)

The specific hydrocarbons found in the exhaust gases comprise of both compounds found in the parent fuel and compounds not present in the fuel [15]. The latter may be derived from the fuel, the structure having been altered within the cylinder by chemical reactions which did not go to completion, or a small amount resulting from the hydrocarbon based lubricant. An engine running rich of stoichiometric would have unburned fuel present in the exhaust stream due to insufficient oxygen being available during combustion for complete combustion to take place. However, even stoichiometric and lean running engines have some hydrocarbons present in the exhaust. There are three important mechanisms which are believed to be responsible for the presence of these hydrocarbons in the exhaust stream:

1. misfire
2. storage and release of fuel by deposits and oil layers or flame quenching near the walls
3. flame quenching within crevice volumes.

Any form of misfire, whether total lack of combustion or partial combustion is usually associated with engines in a poor condition or operating under unusual conditions (for instance cold operation). Thus this mechanism for the presence of hydrocarbons is not of major concern in this research.

The remaining two mechanisms are closely linked and will be discussed together. In both cases the progressive flame is inhibited from reaching, and therefore burning, an amount of the inlet charge, which is then exhausted during blow-down. During compression, as the pressure increases, mixture is forced into the region between the top piston ring, piston and cylinder wall, called the top land crevice volume. Other crevice volumes are also subject to this filling procedure and they consist of the 'caves' formed by the rough nature of engine deposits and any other small gaps such as the protruding thread of the spark plug. The dimensions of these crevice volumes are smaller than the flame quenching distance and this prevents the passage of the flame into this region. Increased pressures during compression and combustion also promote the solubility of the fuel into the oil layer. During expansion, and when the exhaust valve opens and pressures begin to fall, the mixture in the crevice volumes and deposits expands and re-enters the cylinder while the fuel absorbed in the oil layer is also released. Some of this fuel may undergo combustion or partial combustion, but as these volumes of mixture are in close proximity to the cylinder surfaces and it is late in the cycle, their temperatures are not high enough to produce rapid reaction rates or combustion.

Some researchers [16] doubt the role of the oil layer absorption playing a role and argue that the flame is quenched as it approaches near to the relatively cold cylinder wall, therefore precluding a portion of the mixture from combustion. The exact mechanism taking place is not of major concern as both mechanisms are influenced by the same variables. The amount of fuel mixture involved in either mechanism is dependent on the same factors, they are both proportional to the surface area exposed and dependent on the cylinder pressure time history. Higher the cylinder pressures increase the density of the gas in the quench layer and thus there is a greater tendency for fuel absorption into the oil layer. However, if oil layer absorption is a valid mechanism then the specific fuel/oil solubility will influence the process.

Furthermore, the relative amount of fuel present in the gas which is forced into the crevices or is present in the quench layer, will be dependent on the equivalence ratio of the gas and in-cylinder mixing. Therefore the overall operational equivalence ratio, as well as mixing can influence this. It is possible that under certain conditions, possibly poor mixing or liquid fuel impingement on the cylinder surfaces, the equivalence ratio of the gas in these regions may differ from the bulk gas equivalence ratio.

It is important to note, too, that there is a considerable amount of burn-up occurring in the exhaust port. The bulk exhaust temperatures may still be high enough to promote some oxidation and the turbulence caused by the exhaust valve causes significant gas mixing. Thus the mixture that was precluded from combustion by contact with the relatively cold surfaces within the chamber becomes mixed with the hotter bulk gas, and some further combustion may take place.

Therefore the factors that effect the emissions of hydrocarbons include the equivalence ratio, crevice volumes, and flame quench area, cylinder pressure time history, the amount of post combustion burn-up and, to a lesser extent, fuel/oil solubility.

Oxides of Nitrogen (NO_x)

Oxides of Nitrogen are not a direct product of the combustion reaction, but are formed due to the high temperatures and pressures within the cylinder promoting the dissociation of N_2 to monatomic nitrogen. This nitrogen can then be oxidised by the oxygen present in the cylinder thus forming NO and, to a lesser degree higher oxides. Three distinct NO formation mechanisms can be identified, the thermal, prompt and nitrous oxide mechanisms (15, 17, 18).

For the thermal mechanism, the chemistry associated with the reactions involved in the formation of NO, in contrast with the C-O-H system, is not fast enough to be assumed to be in equilibrium, but is rate limited. In 1946, Zeldovich identified the most important reactions relevant to the thermal mechanism and thus this mechanism is often referred to as the Zeldovich mechanism (15, 17, 18). The rate of one of the important chemical reactions, that of the combining of monatomic nitrogen with oxygen forming NO and monatomic oxygen is highly temperature dependant. This implies that the actual concentrations lag behind the concentrations that would be predicted by equilibrium concentrations. This is demonstrated below in Figure 2-6. As can be seen from Figure 2-6 (*c*) the actual concentrations tend to equilibrate, if equilibrium concentrations are higher than actual concentrations then nitric oxides are being formed. If actual concentrations are higher, then the nitric oxides decompose. It is also important to realise that the chemical reaction rates become low enough at temperatures below 2000 K to assume that decomposition of nitric oxides is negligible and then the concentrations are assumed to be frozen. The net result is that the level of nitric oxides in the exhaust stream is higher than those predicted by equilibrium calculations. The Zeldovich mechanism for NO formation is presented in detail in Section 8.3.5 below.

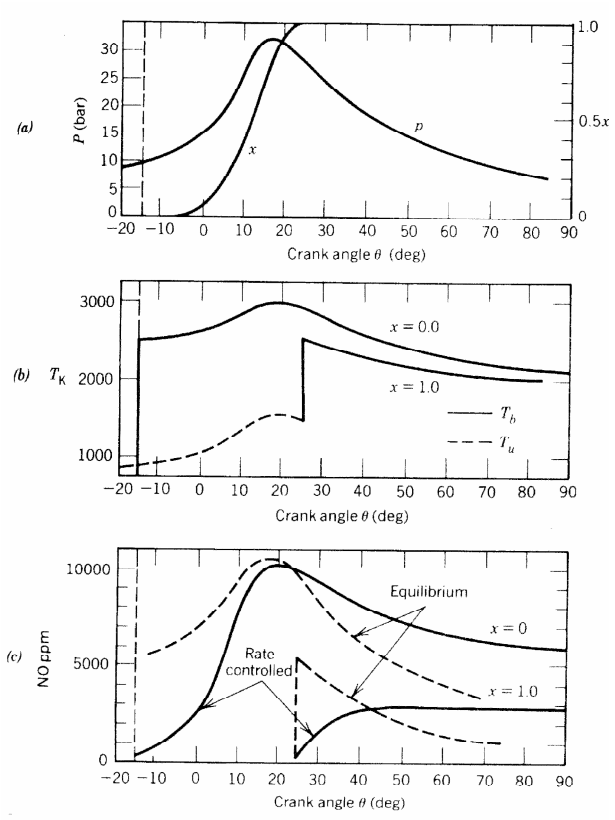

Figure 2-6 (*a*) Measured pressure *P* and calculated mass fraction burned, *x* as a function of crank angle. (*b*) Calculated temperature of burned gas T_b and unburned gas T_u as a function of crank angle for two elements that burn at different times. (*c*) NO mass fractions as function of crank angle for two elements that burn at different times (From Ferguson [17])

It can also be seen from Figure 2-6 (*b*) that the temperature histories of each element to burn are different. This occurs because each element to burn does so at a different time and is therefore at a different temperature at the time it burns (due to the continual compression ahead of the flame propagation). The element then burns to its adiabatic flame temperature and then tracks pressure as it is more or less isentropically compressed and expanded. As a result of this the first element to burn attains the highest temperatures as it is compressed after burning. Conversely, the last element to burn has the lowest temperature time history as it only expanded after burning. This also leads to different NO formation paths for elements burning at different times, as indicated in Figure 2-6 (c). It is apparent therefore that the thermal mechanism, due to low initial reaction rates, only forms NO in the hot burned gas.

NO is found to be present in the flame, and therefore can not have been formed through the thermal mechanism. The prompt mechanism is identified as being relevant here. The prompt mechanism relies on reactions in which N_2 and hydrocarbons react, liberating monatomic nitrogen which can then oxidise. The prompt mechanism is important if there is fuel bound nitrogen, and the resultant concentrations are much less than that associated with the thermal mechanism unless the burned gas temperatures are so low that the thermal mechanism is itself not significant. The nitrous oxide mechanism is significant for lean ($\phi < 0.65$) premixed laminar flames and is not thought to contribute significantly to IC engine emissions.

The thermal mechanism is most significant for spark ignition engines, while the prompt mechanism becomes important for compression ignition engines.

Engine operating conditions can influence the NO_x concentrations in the exhaust stream by way of affecting the temperature time histories of the cylinder charge. Equivalence ratio can influence in-cylinder gas temperatures as well as oxygen availability. Lean mixtures have more air for a given fuel mass induced, while rich mixtures have excess fuel. In both cases there is more mass to absorb heat per fuel energy content, thus resulting in lower charge temperatures than for stoichiometric conditions. In actual engines, however, maximum charge temperatures actually occur at equivalence ratios slightly rich of stoichiometric. This is due to the fact that imperfect charge mixing occurs, and it is difficult to burn, and release the energy of all of the fuel induced. Maximum NO_x emissions are actually usually found slightly lean of stoichiometric where temperatures are still high but there is now sufficient oxygen available for the reactions to progress effectively.

Ignition timing can significantly influence charge temperature histories. This is due to the direct effect that ignition timing has on cylinder pressure history. Ignition advanced from Maximum Brake Torque (MBT) will tend to produce higher maximum pressures because the energy release to the charge will raise the cylinder pressure, which is then compressed, further raising the pressure. Opposed to this, ignition retarded from MBT will tend to have lower maximum pressures because cylinder expansion will begin earlier in the heat release process. The corresponding charge temperatures will similarly be influenced, and in this way alter the formation of the rate limited reactions involved in the formation of NO_x.

Compression ratio too influences charge temperature histories. Higher compression ratios increase the cylinder pressures and temperatures throughout the cycle and would thus be expected to produce increased NO_x exhaust concentrations. The rate of combustion too can influence temperature time histories where increased burn speed would be expected to raise maximum temperatures.

2.4. Exhaust Emissions Measurement

Before continuing with a survey of studies previously undertaken, it is important to outline the methods used to measure exhaust composition. There are a number of ways to accomplish this, with varying degrees of sophistication and therefore effort required. These different methods also provide different qualities of information. These are outlined below. All of these methods rely on similar analysis equipment for the determination of the concentration of pollutants, but it is the method of gathering the exhaust sample for analysis that differs. Detail of the analysis equipment is therefore not included here.

2.4.1. Steady State Engine Operation

This is the simplest method of capturing an exhaust sample for analysis. An engine is operated on a bench dynamometer at a steady speed and load. A continuous sample of exhaust gas is drawn from the exhaust and passed to the analysis equipment. Once the engine and analysis equipment has stabilised, the concentrations of the constituents being monitored are recorded. As mentioned above, in order to

consider actual air quality impact, rationalised units are required. Thus the concentrations need to be converted to a rationalised mass based unit. This requires that the engine's total exhaust gas mass flow rate be determined. This is either estimated, or preferably measured (usually the sum of the air and fuel mass consumption rate). From this and the pollutant density, the mass rate of emission can be determined. If the engine load condition is equivalent to a specific vehicle velocity, then a properly rationalised term such as grams emitted per kilometre travelled can be determined.

The advantages of this type of procedure include the low cost and relative simplicity. Furthermore, the method lends itself to tight laboratory controls of most of the parameters that influence the emissions, thus leading to repeatable and reliable results. The disadvantages include the fact that this type of analysis is not always representative of an actual engine operating in an actual vehicle, especially as far as the transient nature of actual engine operation is concerned. This method does not lend itself to the testing of multiple engine types, as each engine needs to be installed on the test bench, a relatively time consuming activity.

This type of experimental procedure is well suited to research of a fundamental nature and was the method utilised in this research.

2.4.2. Chassis Dynamometer Driving Cycle Operation

This type of emissions measurement entails a complete vehicle being operated on a chassis dynamometer, commonly called a "rolling road". This allows the loading of an engine through the vehicle's drive train, while the vehicle is stationary in the laboratory. By simulating the vehicle's inertia and wind resistance, representative engine loads for the equivalent vehicle speed are achieved. This type of testing allows the vehicle to be driven through a driving cycle of continuously varying road speed, including gear changes, representative of vehicle operation on the road. This is usually achieved with a human driver following some type of "driver aid", a graphical based vehicle speed curve which the driver must follow within a certain error margin. This is the type of test used for vehicle certification and compliance for vehicle emissions regulation, where the test vehicle must, after being driven through a laid down driving cycle, produce emissions less than the legislated amounts.

The continuously varying engine load, and accompanying varying engine exhaust mass flow rate, coupled to uncertain gas analyser transient response, complicates the determination of representative rationalised emissions measurements. This is therefore achieved by diluting the exhaust gas with fresh air, sampling this mixture and storing it in a controlled manner. The apparatus used is called a Constant Volume Sampler (CVS). The principle of operation is simply that the total mass flow rate after mixing of the exhaust and dilution air is held constant, regardless of the instantaneous exhaust mass flow rate. A constant mass flow rate sample is then drawn from this diluted mixture into storage bags for later analysis: this set-up results in an "integration" of the emissions throughout the driving cycle. As long as the total mass flow rate is known and the mass flow rates of both total mass flow and sample mass flow remain constant, then the concentration of the diluted sample and the known densities of the pollutants can be

used to calculate the total mass of pollutant exhausted. This is then divided by the vehicle distance travelled, which is measured by the chassis dynamometer, to obtain the rationalised emission index.

The two most common test procedures used around the world are the Federal Test Procedure, FTP 75 (USA) and the ECE R15-04 (Europe). The experimental layout required is similar for the two and an example is given below in Figure 2-7. The driving cycle used for the FTP 75 procedure is given below in Figure 2-8. It can be seen that the driving cycle is divided into four blocks: the cold phase, stabilised phase, 10 minute break and hot phase. The three non stationary phases are sampled into separate bags and analysed separately. Note that the hot phase consists of a repeat of the cold phase driving cycle. The European driving cycle, ECE 15-04, consists of four repetitions of a relatively low-speed cycle, followed by a single high-speed cycle. The low-speed portions are referred to as the ECE portion while the high-speed portion as the EUDC or Extra-Urban Driving Cycle, which is intended to simulate highway driving conditions. These two distinct cycles are usually sampled into separate bags, while separate bags may also be used for each repetition of the ECE portion.

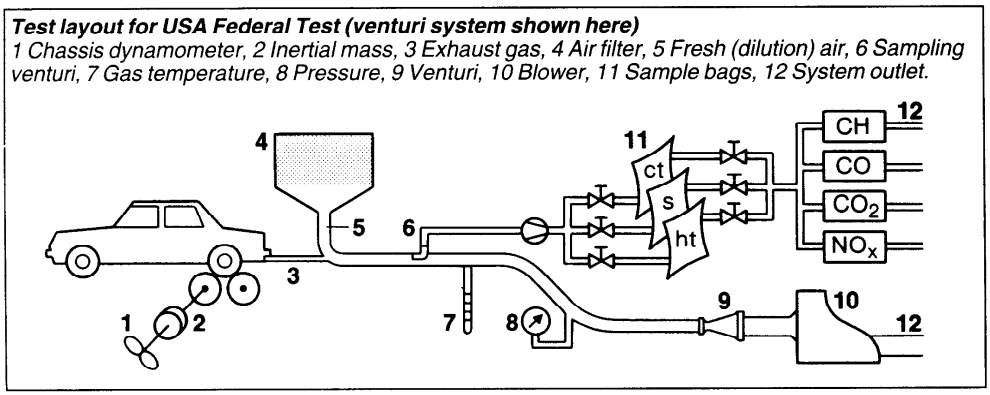

Figure 2-7 An example of the equipment layout required for a chassis dynamometer driving cycle test [19].

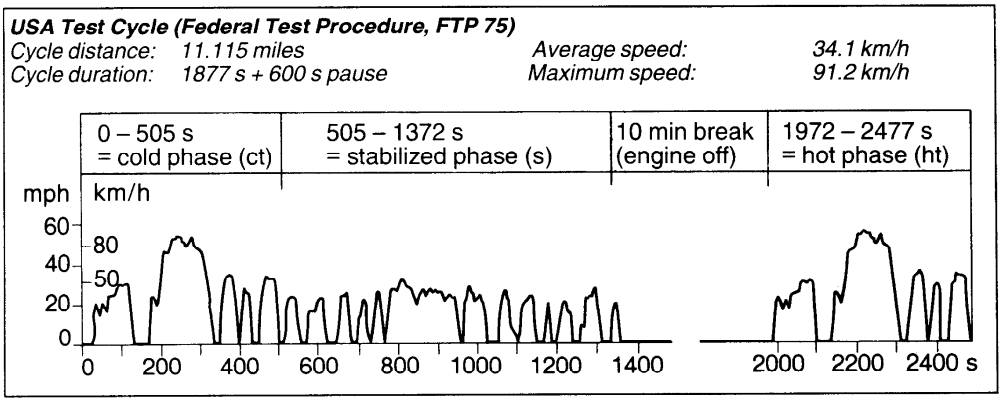

Figure 2-8 Driving cycle used for FTP 75 test procedure. The driving cycle is broken down into three distinct phases and these phases are sampled into separate storage bags. [19]

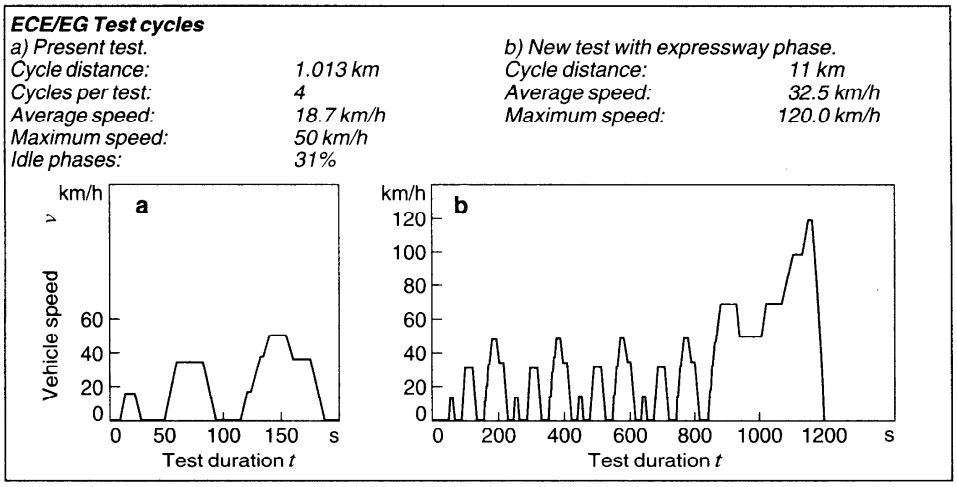

Figure 2-9 Driving cycle used for ECE R15-04 test procedure. [19]

The advantages of this type of emissions measurement procedure include the determination of results representative of on the road vehicle conditions. The overall turn-around time for a test is also relatively short, as the complete vehicle is prepared prior to the test, and installation onto the test apparatus is relatively simple. Disadvantages include the necessity to use human drivers, thus reducing the repeatability of results. Thus if the goal of the work is research and not certification, then large test matrices with many repeat tests may be required to reduce the statistical uncertainty. Furthermore, the results attained are for the entire driving cycle, or portion thereof, sampled into a discrete sample bag, thus the actual origin of the emissions is not well time resolved. In other words, a single portion of the driving cycle may be producing a significant portion of the overall emissions, but this can not be seen due to the integration over the entire portion of the driving cycle. Thus vital information as far as potential emissions reduction mechanisms is lost.

2.4.3. Test Bench Driving Cycle Operation

It is possible to operate an engine only on a transient capability test bench dynamometer, through a representative driving cycle. This entails utilising an electric dynamometer, which can both absorb engine power and drive the engine depending on the requirement. Advanced control software is required which uses closed loop dynamometer speed and engine torque (throttle position) control, and advanced vehicle and drive train simulation. Vehicle inertia, wind and rolling resistance, clutch assembly, gearbox, differential and drive shaft elasticity need to be simulated along with the human driver control inputs (accelerator and clutch interaction etc). This combination allows the engine to respond exactly as if a human driver were driving it on the road through the same vehicle speed/time profile. For the same reasons as for the chassis dynamometer driving cycle procedure, the exhaust gas needs to be sampled with a CVS system.

This procedure is a combination of the first two types of test mentioned above. It has the advantage of being more controllable in a laboratory manner, especially as no human driver is used and exactly

repeatable driving conditions can be achieved every time. Thus the repeatability is improved. However, the same disadvantage as far as testing different engines is concerned is seen, as changing engines on a test bench is time consuming. In contrast this is advantageous if the goal is development of the drive train. As this is a simulated system, changes to drive train parameters are achieved only in the software, and thus can be immediate. By use of the CVS as before, with the loss of time resolved information, vital information as to the origins of the pollutants is lost. This type of testing is invaluable during the preliminary design and optimisation of engines and drive trains.

2.4.4. Modal Analysis

To overcome the inability to time resolve the emissions a modal analysis may be performed. This may be utilised in conjunction with either the chassis or bench dynamometer driving cycles. In a coarse manner this may involve sampling over a short time interval into the sample bags of the CVS, and then analysing the bags separately. A higher order of time resolution may be achieved by directly sampling raw exhaust gas to the gas analysers during the driving cycle. The pollutant concentration/time profile may then be recorded. For this to be successful the gas sampling system and analyser time constants and transient response must be as short as possible and well known. The instantaneous engine exhaust mass flow rate must also be recorded if rationalised units are to be determined. These requirements make this type of analysis complicated and introduce uncertainties, however such analyses are extremely useful for the determination and understanding of the important effects taking place.

3. LITERATURE REVIEW

The literature review section is comprised of three sections: the first looks at two major studies which considered a broad range of fuel formulation effects on regulated emissions, the second includes a number of studies which present the effects that some specific fuel properties have on emissions, while the third section deals with specialised studies which considered in detail the mechanisms of formation of some of the emissions of interest.

3.1. Studies of the Effect of Fuel Formulation on Regulated Emissions.

A number of studies have been conducted internationally and two large-scale investigations that are relevant for discussion are summarised. The most extensive and relevant is the Auto/Oil Air Quality Improvement Research Program or AQIRP study [20, 1991]. This North American co-operative program was undertaken jointly by three automobile manufacturers and fourteen petroleum companies. A similar co-operative research program, The European Programme on Emissions, Fuels and Engine Technology or EPEFE [21, 1995] study, undertaken jointly by ACEA (Association des Constructeurs d'Automobiles) and EUROPIA (European Petroleum Industry Association), is also relevant.

The major differences between these two studies and the research undertaken in this study are summarised below:

1. The AQIRP and EPEFE studies targeted a select number of fuel properties for evaluation. This allowed a very structured experimental design to be used which facilitated the statistical and analytical examination of the results. The goal of the present study was to consider as many fuel formulation properties as were available, and to utilise statistical methods to identify, and quantify, the important properties.
2. Experimentation was done on complete vehicles according to the relevant legislated driving cycle in both of the above research projects. The majority of the vehicles tested were equipped with advanced emissions control devices, with only the AQIRP study including engine-out emissions measurements. This results in some experimental variation (complexity of complete vehicle on chassis dynamometer and human drivers), which necessitated the use of large test matrices. The scope of the present research only included the testing of engines on dynamometer test beds, at steady state conditions. This results in more repeatable results, but does not consider transient engine operation. No emissions control devices were fitted to the engines tested in this research.
3. A large number of vehicles of different makes, models and applications were investigated in these large scope research programmes. In the present study only two different engines employing two different levels of technology were tested.

3.1.1. The AQIRP Study.

The entire AQIRP research programme was an extensive study of many aspects of vehicle related emissions and resulted in many varied publications. One publication is of direct relevance and is

considered here. The title of the paper is: **The Effect of Aromatics, MTBE, Olefins and T_{90} on Mass Exhaust Emissions from Current and Older Vehicles - The Auto/Oil Air Quality Improvement Research Program** [20].

Experimental Design and Testing.

This phase of the AQIRP study utilised a total of eighteen fuels and thirty-four vehicles. Of the fuels, sixteen formed a full factorial experimental design, studying two levels of each of the four fuel parameters. The other two fuels tested were an industry average fuel and an emissions certification fuel used as a reference. The fuel parameters studied, and the factorial design target levels utilised are given in Table 3-1. The blends of fuels were achieved by increasing or reducing the paraffinic content of the fuel to achieve the desired component ratios.

Table 3-1 Fuel Property Factorial Design Targets and Industry Average Fuel Properties for the AQIRP study.

Parameter	Lower Level	Upper Level	Industry Average
Aromatics	20 vol%	45 vol%	32 vol%
MTBE†	0 vol%	15 vol%	0 vol%
Olefins	5 vol%	20 vol%	12 vol%
T_{90}‡	138-149 °C	177-182 °C	168 °C

† MTBE - Methyl Tertiary Butyl Ether
‡ Distillation Point: Temperature for 90% evaporation

The vehicles were divided into two fleets distinguished by the age of the vehicle (and therefore technology and mileage covered). The “current model” fleet consisted of twenty 1989 vehicles each having covered between 16 000 and 46 500 km while the “older model” fleet consisted of fourteen vehicles each having covered between 67 000 and 126 500 km. The vehicle fleets consisted of cars and light duty trucks spanning both American and “imported” makes and the specific models chosen represented the high selling models. Two of each vehicle model was procured for the study. The vehicle properties and technology levels of the two fleets are summarised below in Table 3-2.

The emissions testing was carried out using the Federal Test Procedure (FTP) for exhaust emissions along with some additional steps to avoid fuel carry over effects. Both tailpipe (post catalytic converter) and engine-out (pre catalytic converter) emissions results were gathered and compared. The FTP cycle is divided into three distinct stages, and the diluted exhaust sample from each stage is stored in a separate mixing bag for analysis. Thus the emissions from each stage can be considered separately. The first bag would be most representative of a cold operating engine, while the second and third bags represent a fully warmed engine. This allowed the determination of when and where a particular effect was occurring. The effect could thus be associated with cold or hot engine operation or a combustion chamber or catalytic

converter effect. The emissions measured were Hydrocarbons (HC), Non-Methane Hydrocarbons (NMHC), Carbon monoxide (CO) and Oxides of Nitrogen (NO_x).

Table 3-2 Comparison of Fleet Properties and Technology Utilised for the vehicles used for the AQIRP study.

	Current Fleet	Older Fleet
Vehicle Mileage	>16 000 km <46 500 km	>67 000 km <126 500 km
Number of Cars	20	14
Catalyst Type		
Three Way	20	10
Oxidation (Open Loop)	0	4
Fuel Metering		
Carburettor	2	12
Throttle Body Injection	4	2
Port Fuel injection	14	0
Adaptive Learning Controls	20	0

Results

The result of the factorial design experiment, consisting of sixteen fuels, was subjected to regression analyses using the SAS® computer program. The regression analyses examined the main effects and the two- and three-factor interactions of the fuel properties. The Industry Average fuel was tested a number of times throughout the test programme and indicated a time trend in NO_x results, and the results were corrected for this. A positive correlation was also found between NO_x and humidity even though the data had been corrected for humidity by the FTP method.

Tailpipe Hydrocarbon Response: Both vehicle fleets showed that increasing MTBE and reducing T_{90} reduced tail pipe HC emissions while reducing olefins increased the emission of HC's. Contradictory trends were seen with the response to aromatics where the current fleet showed a reduced HC emission with reduced aromatics while the older fleet indicated the opposite. For the current fleet two-factor interactions were seen between aromatics/MTBE, aromatics/T_{90} and olefins/T_{90} while the three factor interaction aromatics/MTBE/T_{90} was also seen. The older fleet showed two factor interactions between aromatics/olefins, aromatics/T_{90} and olefins/T_{90} while the three factor interaction aromatics/MTBE/olefins was seen.

Engine-Out Hydrocarbon Response: The current fleet indicated reduced HC emission for reductions in aromatics and T_{90} with reduced HC emissions from increased MTBE, while reduced olefins increased the HC emission. The older fleet showed similar responses to olefins and T_{90} but had no significant response to aromatics or MTBE. The current fleet indicated five two factor effects aromatics/MTBE, aromatics/T_{90},

MTBE/olefins, MTBE/T_{90} and olefins/T_{90}. The three factor interaction aromatics/MTBE/T_{90} was also significant. The older fleet did not indicate any significant interactions.

Discussion of Hydrocarbon Responses: For the current fleet, the impact of the fuel variables were seen in all three stages, or bags, of the FTP cycle. The effect of T_{90} was largest in bag 1 and smaller but still significant in bags 2 and 3, indicating that it effects a cold engine to a larger degree than a warm one. The effect of T_{90} was split between engine-out and tailpipe, which indicates that lowering T_{90} improves both combustion and catalyst efficiency.

For the older fleet lowering the T_{90} reduced the HC emissions in all three bags with the largest effect being seen in bag 1. Reducing aromatics had little effect on engine-out HC while it increased tailpipe HC indicating that catalyst efficiency is lower with lower fuel aromatics.

Tailpipe Non-Methane Hydrocarbon Response: Both fleets showed reductions in NMHC for increased MTBE and reduced T_{90}, while an increase in NMHC is seen from reduced olefins. Opposite trends were again seen for the response to aromatics of the two fleets. The current fleet showing reduced NMHC from reduced aromatics and the older fleet indicating the reverse. The same interaction groups were found to be significant for the NMHC as for HC emissions in the current fleet. The older fleet indicated similar significant groups as for HC with the exception that the aromatic/olefin and aromatic/MTBE/olefin were not seen to be significant for NMHC.

Engine-Out Non-Methane Hydrocarbon Response: Engine-out Non-Methane Hydrocarbons were not measured.

Discussion of Non-Methane Hydrocarbon Responses: The responses to the fuel variables was seen to be similar to the response seen for Hydrocarbons with some exceptions. The current fleet showed almost double the response of NMHC to aromatic reduction than HC response. This suggests that the increased paraffin content of the lower aromatic fuel produces increased methane emission. The older fleet indicated that the response of NMHC to aromatics and T_{90} were about 20 to 25% smaller, and to olefins was about 20% higher than the response of HC.

Tailpipe Carbon Monoxide Response: The current fleet only showed significant responses for CO to aromatics and MTBE with reductions seen for reduced aromatics and increased MTBE. The older fleet showed significant main effects for CO to MTBE and T_{90} only, with reduced CO from increased MTBE and increased CO from reduced T_{90}. The only significant interaction for the current fleet was aromatic/T_{90}. The older fleet indicated significant interactions for aromatic/T_{90} and olefin/T_{90}.

Engine-Out Carbon Monoxide Response: Both fleets indicated reduced CO emissions with reduced aromatics and T_{90} and increased MTBE. Olefins were not seen to have a significant effect. The current fleet indicated a significant interaction of aromatic/MTBE/olefin. The older fleet indicated significant interactions of aromatic/MTBE and olefin/T_{90}.

Discussion of Carbon Monoxide Response: For the current fleet the effect of MTBE was seen to be largest in Bag 2 although present in all three bags. It was about three times larger in tailpipe emissions

than in engine-out emission thus implying that the addition of fuel oxygen had a larger effect on catalyst efficiency than on the combustion process. The older fleet also indicated reduced CO for the addition of MTBE and the effect occurred in engine-out emissions. Thus no catalyst efficiency response to MTBE is seen. Reduced T_{90} reduced engine-out CO emissions but also reduced catalyst efficiency to the point of significant tailpipe CO increase.

Tailpipe Oxides of Nitrogen Response: In both fleets reducing olefins reduced NO_x and in the current fleet reduced T_{90} increased NO_x. The older fleet also indicated significant reduction in NO_x emission for reduced aromatics. The current fleet indicated a significant interaction between aromatic/MTBE while the older fleet had two significant three factor interactions, aromatic/MTBE/olefin and aromatic/MTBE/T_{90}.

Engine-Out Oxides of Nitrogen Response: Both fleets show that NO_x is reduced for reduced aromatic and olefin content, and increased with reduced T_{90}. The current fleet also shows reduced NO_x with increased MTBE. No significant interactions are seen with the older fleet while the current fleet has three significant interactions of aromatic/olefin, aromatic/T_{90} and olefin/T_{90}.

Discussion of Oxides of Nitrogen Response: The current fleet showed reduced engine-out NO_x emission with reduced aromatics but essentially unchanged tailpipe emissions, indicating reduced catalyst efficiency. The older fleet again saw reduced engine-out emissions with reduced aromatic but the reductions carried through the catalyst indicating no effect on catalyst efficiency. Both fleets indicated reduced engine-out NO_x emission from reduced olefins while catalyst efficiency was unaffected.

Discussion

The regression equations as determined for the above test fuel formulations were used to predict the expected emissions for the other two fuels tested (industry average and emissions certification fuels). These regressions were found to be within acceptable margins for the older fleet. However, the predictions for the current fleet were higher than the measured values. This effect is attributed to the fuel sulphur content. A separate part of AQIRP has found that fuel sulphur content can influence emissions. When this is accounted for the predictions are seen to be accurate.

It is seen that the response of the two fleets to olefins and MTBE were similar however the response to aromatics and T_{90} were different and sometimes opposite. It is noted that the technology utilised by the two fleets is quite different, as summarised in Table 3-2, and these differences may account for these inconsistent responses.

3.1.2. The EPEFE Study.

The European Programme on Emissions, Fuels and Engine Technologies (EPEFE) research program carried out between 1991 and 1993 culminated in a document entitled: **EPEFE Report** [21], and the relevant sections of that document are summarised below. The main aim of the study was to provide the European commission with the necessary information to enable it to propose a strategy for vehicles and

fuels for the future. For this reason the study focused on the relationship between what are referred to as ***advanced fuels*** and ***advanced vehicles/engine technologies***.

Experimental Design and Testing.

The test fuels used were developed in two matrices addressing the effects of

a) Aromatic content and E_{100} (Distillation Point: % evaporated at 100° C) - nine fuels

b) Sulphur content - four fuels.

The design of the matrices was orthogonal with only the study parameters varying, octane number, oxygenate and olefin content, E_{150} and RVP (Reid Vapour Pressure) were fixed. The vehicles chosen all satisfied the 1996 model year requirements (Directive 94/12/EEC, Euro 2) and spanned a broad range of engine capacity, power and technology. Most incorporated prototype emission components and calibrations, with several approaching assumed, emission levels for future years.

The original target levels set for the orthogonal fuel blend matrices were

a) Aromatics at three levels: 20, 35, 50 %vol

b) E_{100} at three levels: 35, 50, 65 % evaporated.

However, the bending of the fuel distillation curve about the E_{100} axis proved impossible with two of the fuels being physically unrealisable. Thus a ''lozenge'' design matrix was used as shown in Figure 3-1. The original target values as well as the actual fuels tested are also shown on this figure.

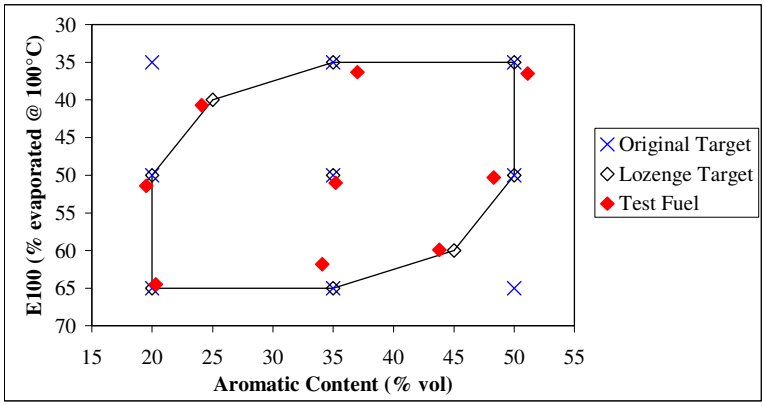

Figure 3-1 Original and lozenge blending targets and actual fuel properties of test fuels used in the EPEFE study [21].

The original target values for the Sulphur content investigation called for 4 Sulphur levels of 30, 100, 200 and 400 mg/kg, with the final attained values being 18, 95, 182 and 382 mg/kg. The base fuel chosen for the doping was one of the E_{100}/Aromatic matrix fuels with intersection occurring at the 100 mg/kg level.

The regulated type approval test procedure, incorporating the ECE-15 and EUDC (Extra Urban Driving Cycle) driving cycles or expressway phase, was slightly modified and used for all the testing. The

modification made was to begin engine cranking and exhaust sampling simultaneously, whereas the regulated procedure requires that sampling begins after the 11-second idle period. Results for the ECE and EUDC portions were measured separately and combined to give a composite result, however the ECE and EUDC portions results were also quoted and analysed separately.

Care was taken to reduce fuel carry-over effects, and back to back testing with bracketing using reference fuels was performed. A special procedure was undertaken to remove sulphur loading of the catalyst before each vehicle was tested on a new fuel. This procedure involved warming the vehicle and catalytic converter, and then performing a predetermined number of acceleration runs. The resulting rich operation resulted in the removal of sulphur by the formation of H_2S.

Results of the E100/Aromatics Investigation.

Hydrocarbons: A linear increase in HC emissions was found with increasing aromatics, however there was an interaction with E_{100} whereby the magnitude of the effect depends on the fuel E_{100}. Reducing aromatics from 50 to 20% for the two higher E_{100} (more volatile) fuels reduced HC emissions by 10%. A stronger effect was seen for the low volatility fuel where a 32% reduction was seen. However, it was noted that the two lowest volatility fuels suffered from poor driveability (poor driveability has been shown to contribute to increased HC emissions) and this is linked to their distillation curves. These two fuels had substantially different distillation curves than the other low volatility fuel due to the lozenge design matrix, and were substantially less volatile over the range E_{90} to E_{140}.

The effect of E_{100} on HC emissions was non-linear at all levels. HC emissions were seen to increase with reduced E_{100}, but increased sharply for the low E_{100} level fuels. Increasing E_{100} from 35% to 50% reduced HC emissions by 25% for 20% aromatics, 35% for 35% aromatics and 42% for 50% aromatics, with the effect being most strongly seen in the ECE portion of the cycle. Increasing E_{100} from 50% to 65% only had effects of the order of 1% reduction for composite and ECE and 10% reduction for EUDC.

Carbon Monoxide: Linear responses to aromatic content were seen for CO emissions and the E_{100} level had little effect. The composite and ECE portion showed increases of 17% for an increase in aromatics from 20% to 50%, while the EUDC indicated a larger relative effect of 44%. This large effect over the EUDC is surprising as CO is understood to almost solely depend on air/fuel ratio, which should be controlled to $\phi = 1$ when the engine is fully warmed up. It is possible, however, that variations in density and stoichiometry of the fuels could have effected air/fuel ratios during transient operation over the EUDC.

The response of CO to E_{100} was non-linear and an apparent minimum in CO emissions for the composite and ECE cycles was seen at an E_{100} of 50%. The effect of E_{100} did not change significantly with aromatic levels. Increasing E_{100} from 35% to 50% reduced CO emissions by 10% for both the composite and ECE, but increasing E_{100} from 50% to 65% increased emissions to almost the same level as at 35% E_{100}, with an overall reduction of less than 4%. The effect over the EUDC cycle was linear with reductions of CO emissions for increased E_{100}.

Oxides of Nitrogen: Aromatic content was seen to have an essentially linear effect on NO_x emissions, however there was an interaction between aromatics and E_{100} over the composite and ECE cycles. The ECE cycle produced 10%, 14% and 17% increases in NO_x emission for an increase in aromatics from 20% to 50% for E_{100} levels of 35%, 50% and 65% respectively. Interestingly, aromatics had directionally opposite effects on NO_x emissions for the ECE and EUDC cycles with the EUDC cycle producing reduced NO_x emissions for increased aromatics. The direction of the effect on the composite result was therefore dependant on the balance between the ECE and EUDC emissions. The different directional trends for the ECE and EUDC cycles are explained by the authors as follows: "*it is well known that engine peak flame temperature increases with increased aromatics leading to an increase in NO_x emissions*". Thus the increase during the ECE cycle is explained as much of the emission occurs prior to catalyst light-off. However, it has also been shown that catalyst conversion efficiency can be reduced in certain vehicles with low aromatic fuels. Thus, during the EUDC, when the catalyst is fully operative this reduced conversion efficiency would explain the increased NO_x emission.

A linear response was also seen for the effect of E_{100} on NO_x emissions. Increased E_{100} increased the NO_x emission over all parts of the driving cycle. However, the effect was dependent on aromatic content for the ECE and composite cycles. Increases of 7%, 11% and 15% were found for the ECE cycle with increases of E_{100} from 35% to 65% with aromatic contents of 20%, 35% and 50% respectively. The EUDC showed a consistent increase of 0.011 g/km for all levels of aromatics which related to relative increases of between 10% and 19%. The composite cycle emissions also varied according to aromatic content with 7%, 13% and 20% increases for an increase of E_{100} from 35% to 65% for 20%, 35% and 50% aromatics respectively.

Results of Sulphur Investigation.

HC, CO and NO_x emissions were all seen to be reduced with reduced sulphur content. Only the CO emissions were affected by sulphur content during the ECE portion of the cycle. The ECE portion of the cycle is dominated by the portion of the cycle before catalyst light-off has occurred, which takes place during the first ECE sub-cycle. This indicates that the sulphur content has little effect on engine out emissions. Close scrutiny of a modal analysis conducted during the testing shows that there was some increase in catalyst light off time due to increased sulphur, and that over the ECE 2, 3 and 4 cycles and the EUDC there was an increase in all the regulated emissions with increased sulphur. This indicates that the effect of fuel sulphur on exhaust emissions is solely as a result of reduced catalyst conversion efficiency. There is a significant increase of all the regulated emissions over the EUDC cycle due to increased sulphur, and this is again attributable to reduced catalyst conversion efficiency. Reductions for the composite cycle results (ECE and EUDC results combined) were of the order of 10% for all the regulated emissions for a reduction from 382 mg/kg to 18 mg/kg sulphur content.

The authors note that these results were seen to be similar as those found in the AQIRP sulphur study, except that smaller effects are seen here for HC and CO. The effects on NO_x are similar on a relative basis in both studies.

3.2. Other Studies Investigating the Effects of Fuel Properties on Emissions.

A number of other studies are found in the literature which have investigated the effects of individual, or a small number of properties on exhaust emissions. These will be briefly discussed here.

3.2.1. Influence of Fuel Aromatic Content on Exhaust Emissions.

A paper entitled: **The Effect of Gasoline Aromatics Content on Exhaust Emissions: A Co-operative Test Program** [22] is discussed below. This study focused on the direct effect that fuel aromatic content may have on exhaust NO_x emissions. Previous literature had shown conflicting trends of emissions response to aromatic content. The authors hypothesised here that these results were possibly confounded by fuel blends not being specifically blended for the study of aromatic content. For this reason the fuel blend design requirement was formulated specifically to change aromatics without changing the other fuel parameters (e.g. RVP, distillation, sulphur etc). Paraffins were the swing component with the olefin content held constant, and three specifically blended fuels with aromatics content 10, 20 and 30 % by volume were tested. Nine vehicles were utilised, all of which had three-way catalysts except one which had an oxidation catalyst. The FTP (1975) test cycle was used for the study.

A statistical analysis showed that a significant relationship between aromatics and NO_x existed only at the 88% confidence level and this indicated a 5% reduction in NO_x when comparing the 30% and 10% aromatic fuels. However, the effect is largely apparent in three of the vehicles and these three vehicles were the only carburetted vehicles in the fleet. The other regulated emissions do not show any significant changes due to fuel aromatic content.

Further, exhaust emission of Non-Methane Hydrocarbons were speciated and their respective ozone reactivities calculated according to the photochemical reactivity factors published by Carter [23]. No significant effect of aromatics content on reactivity is apparent. Reactivities calculated from compositional analyses of the liquid fuels of 10% and 30% aromatics showed that the 30% fuel had 25% higher reactivity. Thus indicating that fuel composition alone may not be an accurate predictor of emission reactivity. A comparison is made of a fuels content and exhaust emission of methane, alkanes, alkenes and aromatics and they are found to be dissimilar. Methane is absent in the fuel but present in a significant portion in the exhaust emissions, while alkenes are significantly enriched. Furthermore, the alkenes are components with relatively high photochemical reactivities, and this magnifies the effect. Conversely, the methane has low relative photochemical reactivity and thus its contribution to exhaust photochemical reactivity is negligible.

The exhaust aromatic content was seen to be very similar to the fuel aromatic content. However, the percentage of alkanes and alkenes were different with enrichment of alkenes and depletion of alkanes. The exhaust alkenes are predominantly ethene, propene and butenes, components which are absent or only trace elements in the fuels. Therefore the light alkenes that appear in the exhaust are mainly produced by combustion or in catalyst reactions, most likely from the cracking of larger alkanes.

Therefore, any reduction in aromatic content is accompanied by an increase in alkanes, resulting in an increase in exhaust alkenes, and thus photochemical reactivity.

3.2.2. Aromatic Content and Volatility Effects on Exhaust Emissions.

A paper entitled: **The Independent Effects of Fuel Aromatic Content and Mid-Range Volatility on Tailpipe Emissions from Current Technology European Vehicle Fleets** [24] is discussed below. Previous studies had indicated that mid-range volatility exerted an independent effect on emissions (as opposed to T_{90} as was studied in AQIRP). Furthermore, the authors pointed out that European studies following Phase 1 of the AQIRP study have shown that European vehicles follow most of the trends identified in AQIRP except for the effect of aromatics on NO_x. Significant increases were seen in catalyst equipped vehicles NO_x emissions for reduced aromatics, and to a larger degree than was seen for the AQIRP current fleet. This effect, coupled with mid-range volatility was the main focus of the EPEFE study, however the focus was on future technology vehicles.

The fuels for this study were blended with three levels of T_{50} (75, 95 and 115°C) and two levels of aromatics content (25 and 45 %vol) with a seventh fuel in the centre of the matrix (T95, 35 %vol aromatics). The subsidiary fuel parameters were fixed with T_{30} and T_{90} defining the distillation curve along with the blend target T_{50}. The vehicles utilised comprised twelve catalyst vehicles (three way) and eight non-catalyst vehicles. Testing was done according to the combined European test cycle (ECE 15.04 + EUDC). The statistical manipulation of the data, where possible, followed the methods used in the EPEFE programme.

For the non-catalyst vehicles no significant HC emissions response is seen to either aromatics or T_{50}. CO response to increasing aromatics is somewhat surprising with significant increase at the mid-volatility level and a significant reduction at the highest volatility tested. NO_x is seen to respond to increased aromatics with significant emission increase, whereas volatility had no significant effect.

The catalyst fleet shows directionally similar trends to the non-catalyst fleet, but in absolute terms the changes are much smaller, though more often statistically significant. This agrees with observations made in the AQIRP study. Decreasing aromatics and increasing mid-range volatility both result in reduced HC and CO emissions. The reverse trend is seen for NO_x with increased emissions with reduced aromatics, which is ascribed to a catalyst efficiency effect. The individual measurements taken from the three bags (bag one - first two 15.04, bag 2 - second two 15.04, third bag - EUDC) show distinctly the reversal of the effect as the catalyst warms up. Bag one, influenced strongly by cold start and pre-light off effects shows the trend of increasing NO_x with increasing aromatics. The second and third bags are seen to have the reversed trend where increasing aromatics reduce the NO_x emitted.

3.2.3. Effect of Fuel Structure on Exhaust Emissions.

Two papers, which describe different phases of a research programme, are included for discussion in this section. They are entitled**: Effect of Fuel Structure on Emissions from a Spark-Ignited Engine** [25]

and **Effect of Fuel Structure on Emission from a Spark-Ignited Engine. 2. Napthene and Aromatic Fuels** [26]. This study took a far more fundamental approach than the previously mentioned studies by studying single component fuels, or simple fuel blends made from single component fuels, in a single cylinder, production type engine.

The first paper reports the results from the following fuels: methane, ethane, propane, n-butane, isopentane, isooctane and toluene along with a multi-component tracer fuel. Testing was predominantly undertaken at constant IMEP (3.8 bar), speed (1500 rev/min) and equivalence ratio (0.9) while MBT was used for spark timing. Furthermore, each of the following variations were also investigated in turn while holding the other conditions as above: speed - 2500 rev/min, spark timing - MBT-12° CA and equivalence ratio - 1.15. The MBT timing required for the fuels is given in Table 3-3.

Table 3-3 Chemical formula, MBT and Carbon mole Fraction at 0.9 Equivalence Ratio of test fuels used by Kaiser et. al. [25].

Fuel	Formula	MBT [° CA BTDC]	Carbon Mole Fraction [ppm C_1 at ER = 0.9]
Methane	CH_4	19	86 000
Ethane	C_2H_6	15	102 000
Propane	C_3H_8	17	109 000
n-Butane	C_4H_{10}	18	113 000
Isopentane	C_5H_{12}	20	115 000
Isooctane	C_8H_{18}	23	119 000
Toluene	C_7H_8	19	144 000
Tracer	[blend]	22	[blend]

Total Hydrocarbon Emissions : Alkane Fuels

The total hydrocarbon emissions mole fraction is strongly affected by the fuel used. Ethane produced the lowest and toluene the highest HC emissions. Methane produces about 50% higher emissions than ethane and the emissions then increase monotonically as the carbon number of the alkane fuel increases. Toluene, despite having fewer carbon atoms than isooctane is always the highest emitter. As the testing was performed at a lean equivalence ratio incomplete combustion does not contribute significantly to the HC emissions. Therefore the mechanism of HC storage in crevices and oil layers is important. Furthermore the fuels with fewer than six carbon atoms have low solubility in oil so the effect of oil film absorption will be minimal. The fraction of the initial fuel charge stored in the crevices should be similar, as the fuel affects neither the volume nor the filling pattern of crevices. Therefore two critical differences caused by fuel structure must be important (C_1-C_5):

1. different amounts of total carbon are present in the intake charge for the same equivalence ratio because of different H/C ratios.

2. different degrees of burn-up of fuel molecules occur upon exiting the crevice volumes because of their different reactivity, diffusion rate, and flame temperature.

Assuming that storage and burn-up factors were identical, the carbon mole fractions as indicated in Table 3-3 would suggest that isopentane would emit 13% more carbon containing species than ethane, far less than the observed difference, and ethane would be expected to have 20% more than methane, opposite to the observed trends.

CO_2 was seen to increase linearly with total carbon intake charge while CO increases but has a step up between gaseous and liquid fuels. Thus it was hypothesised that mixing was playing a role. However a test with the injector placed further upstream and charge preheating showed no difference in HC or CO trends, thus suggesting that mixing is not a factor.

The above suggests that burn-up is the major factor affecting the emissions of HC's and therefore that the fuels may have different reactivities with respect to burn-up. Equilibrium calculations (equivalence ratio - 0.9, temperature - 1500 to 2800 K) show the hydroxyl radical to be present at approximately eight times the density of the next most abundant reactive species. It is therefore reasonable to assume that the chemical consumption rate of stored fuel is controlled by their OH reaction rate constants. However, estimates of the rate constants for these fuels predict an opposite trend to that observed.

The equilibrium concentration of the OH radical increases with increase in H/C ratio leading to increased burn-up. However the equilibrium OH density for isooctane is only 8% less than that for ethane, seemingly too small to influence HC emissions significantly.

Adiabatic flame temperatures do not indicate to being a factor as they are very similar. An additional aspect may be the molecular diffusion rate. Gas stored in the piston ring crevices is laid along the wall a few tenths of a millimetre thick as the piston descends, which is the order of the thickness of the thermal boundary layer characterised by a sharp temperature gradient, therefore reducing OH concentration. The time necessary for a molecule in the deposited layer to reach a region of high OH concentration is inversely proportional to it's molecular diffusion constant. Higher molecular weight hydrocarbon species have slower diffusion rates and therefore less burn-up would occur.

Gas chromatography of the exhaust showed that for propane fuel, hydrocarbon species in the exhaust with molecular weight higher than propane accounted for less than three percent of the total HC emissions. Thus for a properly running engine any contribution of burning oil to the total HC emissions seems negligible. For every fuel the major HC species is the fuel itself. However the fractional contribution of unburned fuel to the total varies substantially. For methane, unburned fuel constitutes 95% of exhausted hydrocarbons, falling to 51% for isooctane (ethane 67%, propane 56%, n-butane 61%, isopentane 48%). Under lean conditions the balance consists primarily of olefins formed by β-scission of alkyl radical C-C bonds for the higher molecular weight fuels. To a lesser extent, disproportionation reactions of methyl radicals may generate C_2H_4 from highly branched alkanes such as isooctane. H-atom elimination from alkyl radicals is also a probable source of olefins, particularly for the light fuels.

The HC emissions from toluene are of a substantially different character. They consist primarily of unburned fuel (83%) and have low olefin content (1%). The balance are aromatic fragmentation (benzene) or partial oxidation (benzaldehyde) products (note that aldehydes were not measured except for benzaldehyde). Of the alkane fuels only isooctane produces any measurable benzene (0.3%). The major exhaust HC species for the tracer fuel are those expected from the two principal components present in the mixture.

For retarded ignition timing and higher speed conditions the unburned fuel contribution becomes smaller though it remains a major component. During fuel rich operation methane and acetylene emissions contribute a larger fraction than under lean conditions, resulting primarily from incomplete combustion in the chamber during flame passage.

NO_x Emissions: Alkane Fuels

Methane produces the lowest NO_x emissions of the gaseous fuels reflecting the lower N_2 fraction in the mixture and lower adiabatic flame temperature. The remaining gaseous fuels show a small increase in NO_x as the number of carbon atoms increase, although the effect is not very great which is consistent with similar flame temperatures. Isopentane and isooctane emit 15% less than gaseous fuels, except methane, which may result from evaporative cooling effects.

Conclusions: Alkane Fuels

The results prove that total emissions and individual species concentrations are significantly influenced by the chemical structure of the fuel. Total HC emissions span a factor of four under the same operating conditions, with ethane producing the lowest and toluene the highest total HC emissions. In all cases unburned fuel constitutes a large fraction of the emitted HC's although the fractional contribution varies from 95% to 50% (for methane and isooctane). High engine speed or retarded spark timing reduces the unburned fuel contribution by a factor of 2 for some fuels. Olefins formed by C-C bond scission of alkyl radicals make up the bulk of the remainder of the emissions from alkane fuels. For the aromatic fuel, toluene, olefins are not observed in appreciable quantity but benzene and benzaldehyde are present. It is probable that the total and individual species are controlled by the post-combustion burn-up of stored fuel under fuel lean conditions. During fuel rich operation methane and acetylene, formed by incomplete combustion in the bulk gas, contribute a greater amount to the HC emissions for all fuels.

The mole fraction of CO_2 increases with decreasing H/C ratio of the fuel as expected, with toluene producing approximately 60% more CO_2 than methane for the same output power. NO_x emissions show a much smaller, but still significant (20%), variation with fuel structure. This latter observation can be explained in part by differences in adiabatic flame temperature and, in the case of liquid fuels, by evaporative cooling.

The second paper, which considers napthene (cycloparaffin) and aromatic fuels used similar test equipment and procedures. Two cycloparaffin fuels (cyclohexane and methylcyclohexane), an aromatic

blend (containing 69.5% m- and p-xylene, 10.8% o-xylene and 19.6% ethylbenzene) and a fully blended gasoline are studied (91 RON, T_{90} - 157°C, 69% saturates, 30 % aromatics and <1% Olefins). The same experimental set-up and test points were used as before. The chemical formula and MBT spark timing are given for the four test fuels in Table 3-4.

Table 3-4 Chemical formula and MBT of test fuels used by Kaiser et. al. [26].

Fuel	Formula	MBT [° CA BTDC]
Cyclohexane	C_6H_{12}	17
Methylcyclohexane	C_7H_{14}	18
Aromatic Blend	[blend]	20
Gasoline	[blend]	19

Total Hydrocarbon Emissions: Napthene and Aromatic Fuels

Similar trends are seen to those of the first part of the study [25] and the results are compared to those results in the discussion below. The highest total HC emissions are observed for the aromatic blend and the levels are similar to those of toluene. The gasoline emissions are lower than either isooctane or the aromatic blend. Cyclohexane and methylcyclohexane emissions are lower and close to those observed for isopentane. The fuel rich operation resulted in higher total HC emission with most of the increase as a result of increased concentrations of unburned fuel, methane and acetylene.

Both retarded spark and high-speed operation reduce the total HC emissions by 20-50% depending on the fuel. At these two engine conditions, the fractional contribution of the unburned fuel to the exhaust emissions is reduced, particularly for the napthenes. This effect is ascribed to an increase in post-combustion burn-up of crevice volume or oil-film stored fuel. Increased post-combustion burn-up is expected because these conditions produce hotter late-cycle cylinder and exhaust gas temperatures.

At all conditions the cylcohexane emissions are approximately 25% less than the methylcyclohexane emissions. Similar levels of NO_x emissions for these two fuels indicate that combustion temperatures are similar and therefore this is unlikely to be a cause of the difference. A similar mechanism as described in the first part of the study [25] is a likely explanation of the difference. The diffusion rate of the stored fuel out of the wall layer (post-combustion) is a function of molecular mass and the methylcyclohexane has a 17% higher molecular weight. However, the difference in diffusion rate is estimated at 8% and is therefore unlikely to account for the entire difference in HC emission. Differences in oil-solubility and OH reaction rate may also have an influence.

87% of the total HC emissions from the cyclohexane fuel were made up of seven species - cyclohexane, cyclohexene, benzene, 1,3-butadiene, propylene, ethylene and acetylene. The 1,3-butadiene emissions from cyclohexane are 3 to 5 times greater than those observed for gasoline during lean operation and 7

times larger at fuel rich operation. Thus the addition of cyclohexane to a fuel could significantly increase the exhaust butadiene emission, particularly during rich cold start conditions.

Many of the same characteristics are seen for the HC species in the exhaust for the methylcyclohexane fuel as for the cyclohexane fuel. Eight species account for 78% of the total HC emissions, methylcyclohexane, methylcyclohexene, benzene, cyclohexene, 1,3-butadiene, propylene, ethylene and acetylene. For both the cycloalkane fuels, aromatic species, primarily benzene, account for approximately 7% of the non-fuel exhaust species under lean conditions and 1,3-butadiene is a particularly important product. A substantial fraction of the increase in the total HC emission for the methylcyclohexane fuel relative to the cyclohexane fuel is as a result of an increase in the unburned fuel content.

For the aromatic blend, unburned fuel makes up 80% of the HC emissions, an identical proportion to that seen with toluene. Benzene and toluene, although absent from the fuel are both present in the emissions, and the sum of these two species (6% of total) is nearly equal to the benzene emissions from a toluene fuelled engine (8% of total). These results suggest that all substituted aromatic species can dealkylate to form less highly substituted aromatic species in the exhaust. This is supported by evidence from the gasoline fuelled engine testing which produces benzene enrichment by this process. The gasoline is low in benzene but high in toluene content (2% and 14% respectively) but the concentration of benzene relative to xylene in the exhaust is 2 to 4 times larger than in the initial fuel. However the xylene to toluene ratio in the fuel is very similar to that in the exhaust. Thus the high fuel toluene ratio masks the enrichment of toluene during combustion.

NOx emissions: Napthene and Aromatic Fuels

The NO_x emissions are not discussed by the authors but the results are included in the tables presented and a summary of these results is given here. There is little difference between the two cyclohexane fuels emissions of NO_x for all the load points tested. At the standard load point the cyclohexane fuels emit approximately 8% higher concentrations of NO_x than isooctane (this is the only load point at which isooctane results are presented). The aromatic blend fuel consistently produced the highest concentration of NO_x, followed by the gasoline, with the cyclohexane fuels producing the lowest concentrations. Fuel rich and retarded spark timing operation drastically reduced the production of NO_x while the increased engine speed produced a marginal increase.

Conclusions: Napthene and Aromatic Fuels

It is again apparent that the HC emissions, both total and species produced, are affected by fuel structure as was seen in the first study [25]. However, two aspects of the emissions from these cyclic alkanes are strikingly different from the other alkane fuels examined previously:

1. Aromatic species, particularly benzene, contribute significantly to the hydrocarbon emissions with up to 10 times larger emissions than from isooctane, even though the fuels are themselves non-aromatic.

2. The quantity of 1,3-butadiene emitted by both fuels is large, typically 12% of the total HC emissions. Butadiene emissions from these fuels are substantially larger than from the gasoline fuel and therefore caution should be exercised when adding these cyclohexanes as substantial constituents in gasoline.

The aromatic blend fuel shows similar HC emissions characteristics to those observed in the first study [25] for toluene:

1. The unburned fuel itself constitutes approximately 80% of the total emissions.
2. Olefinic exhaust species concentrations, which are large for aliphatic fuels, appear to be low for aromatic fuels.
3. Substituted benzene fuels emit both benzene and toluene, probably formed by dealkylation. This must be responsible for a significant portion of the enrichment of benzene observed in the engine-out emissions from certain gasoline-fuelled vehicles, and could also result in toluene enrichment.

3.3. Specialised Studies

There are a number of other publications that are of interest, which do not necessarily look directly at the effects of fuel formulation on the exhaust emissions produced. Their interest lies in either being able to aid the explanation of some of the phenomena seen or to aid in interpreting the observed effects as far as actual air quality is concerned.

3.3.1. Oil Film Effects on Hydrocarbon Emissions

A paper which considers a mechanism by which unburned fuel escapes combustion through absorption and desorption in the oil film is discussed below. The paper's title is: **Hydrocarbon Emissions of SI Engines as Influenced by Fuel Absorption-Desorption in Oil films** [27]. Engine tests were performed with couples of fuel/oil combinations having varying solubilities of the fuel in the oil. Unburned hydrocarbon levels in the exhaust were measured with single constituent fuels and lubricants, commercial gasoline and an oil free engine. Various engine operating conditions were investigated including varying lubricant and engine coolant temperatures and engine load. A study was made of the solubility of different hydrocarbons in different oils and it was found that the solubility of fuels is independent of commercial oil formulations. With the same number of carbon atoms, non-aromatic fuels are less soluble than aromatic fuels.

The conclusions that the authors were able to make included the following:

1. Fuel solubility in oil is strongly dependent on temperature and mainly influenced by the nature of the fuel/lubricant couple.
2. The nature of commercial lubricant has little influence on unburned hydrocarbon emissions.
3. During the engine cycle, absorption-desorption of the vaporised fuel in the oil films is an effective mechanism that contributes to unburned hydrocarbon formation.

4. This phenomenon is mainly governed by fuel solubility: lowering the solubility by a factor of 40 leads to an unburned hydrocarbon emission reduction of 30%.
5. When an engine is run with no oil on the liner the unburned hydrocarbon emissions are reduced. The extent of the effect is directly influenced by the fuel solubility in oil.
6. When fuelled with commercial gasolines, only 10% of the total unburned hydrocarbon emission can definitively be accredited to oil film absorption-desorption in SI engines (at 4 bar IMEP). This influence increases with engine load.

3.3.2. Role of Piston Crevice Volume on Hydrocarbon Emissions

The role of the crevice volume formed between the top piston ring, the piston land and the cylinder wall in the hydrocarbon emissions is discussed below. The title of the paper is: **The Piston Crevice Volume Effect on Exhaust Hydrocarbon Emission** [28]. Modified pistons, which effectively eliminated the top land crevice volume by reducing it to 3% that of an equivalent production engine, were tested at various engine loads and speeds. The exhaust hydrocarbon emissions and blowby rate were compared to the production engine.

Exhaust hydrocarbon emissions were seen to be reduced by between 47% and 74% by the modified pistons in relation to the production engine. Tabulated results showed that the percentage improvement was largest at WOT (Wide Open Throttle) and decreased for increased manifold depression. This further supports the assertion that unburned mixture is forced into the top land crevice volume as cylinder pressures increase during compression and combustion, and are then released as pressure drops during expansion. Furthermore, the author notes that in the production engine, blowby and top ring gap position had an appreciable effect on exhaust hydrocarbon concentration.

3.3.3. Compression Ratio and Spark Timing effects on Hydrocarbon Emissions

A paper entitled **Storage and Partial Oxidation of Unburned Hydrocarbons in Spark-Ignited Engines - Effect of Compression Ratio and Spark Timing** [29] is discussed below. A single cylinder CFR engine was used for this investigation with varying compression ratios between 5.8:1 and 11:1, equivalence ratios of 0.85, 1.05 and 1.25 and ignition timings of MBT+10° CA (advanced), MBT and MBT-20° CA (retarded). During comparative testing all other parameters were held constant. Exhaust gas hydrocarbon content was measured with a hot flame ionisation detector, and samples were drawn for gas chromatographic analysis (GC) for determination of individual hydrocarbon concentrations. Cylinder pressure was measured and a simulation program was used to give added insight.

Compression Ratio Results

An increase in the compression ratio tends to increase the concentration of unburned hydrocarbons in the exhaust. Two mechanisms cause this effect, firstly the higher cylinder pressures before combustion (due to increased compression) increases the storage of unburned mixture in the crevice volumes and oil films. Secondly, the increased efficiency and heat transfer tends to reduce temperatures late in the cycle and thus reduce the post combustion burn-up of the mixture as it is released from crevices and oil films.

GC results show that, for lean operation (ϕ = 0.85), the increased compression ratio produced a larger relative increase in unburned fuel emission than non-fuel emissions (e.g. propane fuel : exhaust propane increased by a factor of 3.6, non-fuel HC's increased by a factor of $\leq$1.9). This result is shown to be indicative that less post combustion burn-up is occurring due to the increased compression ratio. The reduced gas temperatures are however shown to have less of an effect than the concentration of radicals. Equilibrium calculations have shown that OH, H and O concentrations are increased by factors of 3-10 by increasing the temperature from 1900K to 2050 K (simulation predicted that the higher compression ratio would have approximately 150K lower temperatures after 32°CA ATDC). Therefore the reduced post combustion burn-up is due mostly to the reduced concentrations of radicals.

Equivalence Ratio Effects

The percentage increase in exhaust hydrocarbons resulting from increased compression ratio is much lower for rich operation (ϕ = 1.25) than lean (ϕ = 0.85). The GC analysis showed that there was a higher proportion of the concentrations of methane and acetylene with rich operation, which is due to partial oxidation in the bulk gas and not from storage. Therefore the effect of the changes in peak cylinder pressures will have a reduced influence on the exhaust hydrocarbons produced. Post combustion burn-up is hindered by the lack of oxygen available after rich mixture combustion.

Spark Timing Results

Exhaust hydrocarbon concentrations were seen to decrease rapidly with ignition retardation for lean (ϕ = 0.85) mixture and high and low compression ratio. The change in the unburned fuel fraction is most significant, while the non-fuel hydrocarbons change more slowly. The reduction in the primary product of combustion is indicative of increased post combustion burn-up. The cylinder pressures for MBT are higher than during retarded operation, causing increased mixture storage. With rich operation (ϕ = 1.25), retarding the ignition decreased the concentration of unburned fuel while increasing the concentrations of the non-fuel hydrocarbons. Overall hydrocarbon emissions therefore decrease more slowly under rich operation than lean. Detailed examination of the results show that this is consistent with increased post flame burn-up.

Summary and conclusions

From the discussion and conclusions presented in this reference, the following points are significant to this particular research.

1. Increasing the compression ratio increases the exhaust hydrocarbon emissions and increases the percentage contribution of unburned fuel to the total hydrocarbons.
2. Retarding the spark timing in the absence of EGR decreases the total hydrocarbon emissions and decreases the percentage contribution of the unburned fuel to the total hydrocarbons.

Three major factors influence the total hydrocarbon emissions and species distribution as the compression ratio and spark timing are varied:

1. The cylinder pressure just prior to flame arrival at a crevice or oil film location, which determines the mass of unburned hydrocarbons stored.
2. The temperature of the post-flame gases, which influences the percentage of stored material that is burned up within the cylinder and exhaust system during out-gassing after flame passage. Examination of the chemical kinetics of the oxidation process indicates that the ratio of non-fuel hydrocarbon to fuel hydrocarbon in the exhaust gas will increase as the extent of post-flame burn-up increase.
3. The fuel-air equivalence ratio, which controls the amount of oxygen in the post-flame gases and, therefore, affects the post-flame burn-up process

Thus under lean operating conditions:

1. As the compression ratio increases, the peak cylinder pressure increases and the average late cycle in-cylinder and exhaust gas temperatures decrease. This should increase the amount of stored material and decrease the extent of post-flame burn-up. The observed increase in total exhaust hydrocarbon emission and the increase in the percentage contribution of the fuel relative to non-fuel hydrocarbons, indicating less post-flame burn-up, are consistent with these predictions.
2. As the spark timing is retarded, the peak cylinder pressure decreases and the average late cycle in-cylinder and exhaust gas temperatures increase. This should reduce the amount of unburned hydrocarbons stored in crevices and increase the extent of post flame burn-up. The observed decrease in total exhaust hydrocarbon emission and the decrease in the percentage contribution of the fuel relative to non-fuel hydrocarbons are also consistent with the predicted changes.

4. RESEARCH OBJECTIVES AND METHODOLOGY

The broad objectives of this research were to investigate the effect of fuel formulation parameters on the engine out emissions of hydrocarbons, carbon monoxide and oxides of nitrogen, from spark ignition engines. The objective was to identify the fuel formulation parameters that were seen to have the dominant influence and attempt to quantify the effect. Furthermore, considerable effort was taken in an attempt to gain insight into the mechanisms by which the parameters were influencing the emissions, and thus gain understanding of the interaction between fuel properties and the emissions produced. This was to be done in a South African context as far as engine technology and fuel formulations were concerned.

The methodology chosen for the study was to undertake steady state testing of two different engines in controlled laboratory conditions (see Section 6.1), with as many different fuel formulations as was feasible. In all, thirty five different test fuels as well as a "reference" fuel (for bracketing testing) were used for the research (see Section 5). Engine load points were chosen so as to be representative of normal steady state driving and hard acceleration. In order to gain insight into the mechanisms taking place, one of the engines was fitted with cylinder pressure measurement equipment so that combustion analysis could be performed (see Section 6.2). Raw engine out exhaust gas was sampled directly to a bank of gas analysers to measure the HC, CO and NO concentrations, as well as CO_2 and O_2 concentrations which are important for the associated calculations (see Section 6.3). The results, along with the fuel formulation parameters, were subjected to multivariate linear regression analyses to identify possible correlations between fuel formulation parameters and emissions effects (see Section 10).

The approach regarding the fuel formulations, and the fuel formulation parameters studied, was somewhat different to the approach of most of the previous studies (see Section 3). Previous studies had typically pre-selected a small number of fuel formulation parameters and followed a full factorial experimental procedure utilising several different vehicles or engines. Thus large experimental matrices are used, made up of a small number of fuels and a relatively large number of vehicles or engines. The full factorial fuel design approach requires the researchers to try, within practical limitations, to alter only the parameters of interest. This ideal is clearly not attainable in practice. By way of example, assume that the researchers have identified low-range volatility as an important parameter, fuels with different distillation curves are formulated by blending different combinations of available hydrocarbon refinery streams and thus the fuel is made up of different combinations of hydrocarbon species. Usually, the researchers take care to ensure that other parameters such as octane and the ratios of the different hydrocarbon classes (paraffin, aromatic and olefin) remain reasonably similar. However, using different combinations of molecules must alter other formulation parameters such as density: there is an unavoidable cross correlation between fuel formulation parameters. The factorial experimental approach will ascribe any response to the intentionally varied parameter, even if the actual mechanism of the response is not directly ascribable to that parameter.

The approach taken in this research was to take a large number of different fuel formulations, which for the purposes of this research, can be thought to have been randomly formulated, spanning significant variations in a

large number of different fuel formulation parameters. These fuels were then tested in great detail in only two different engines, employing two different engine technologies. Thus a large experimental matrix was generated, but in this case it is a large number of fuels and a small number of engines. All of the measured fuel parameters were then included in a multivariate regression analysis technique in order to identify the formulation parameters which correlate with measured emissions responses.

The combustion analysis program used to analyse the recorded cylinder pressure, contained a relatively simple single-zone, fully mixed heat release model. A more advanced two-zone mass transfer based combustion analysis, similar to that proposed by Krieger and Borman [30] was added to the existing program. This additional model contains a gas properties computation subroutine similar to that described by Gordon and Mc Bride [31]. The gas properties computations require the gas constituents to be known. Therefore a subroutine which computes the concentrations of the more important species was required. An equilibrium model was used for this, based on the work of Olikara and Borman [32]. The details of the additions to the combustion analysis models and their application are discussed in Section 8.

A noteworthy observation regarding the NO emissions was made from the statistical analysis, which required further investigation. An extensive literature review regarding the NO formation mechanisms was unable to fully explain the observation. In order to further investigate this, an extension was made to the combustion analysis program to include a routine which simulated the formation mechanism according to the extended Zeldovich mechanism [15, 17, 18] (see Section 8.3.5).

In order to gain the most insight into the mechanisms by which fuel properties effect the exhaust emissions, a triangular approach was taken. First the emissions were correlated with fuel properties only. Then the emissions were correlated with the combustion analysis results. From the results of this analysis the combustion parameters of interest could then be correlated back to the fuel properties. This process is illustrated in Figure 4-1. In this way it would be possible to draw conclusions as to how a specific fuel property influences the emissions. For example, if increasing paraffin content is seen to influence NO emissions and if maximum heat release rate is also seen to influence NO, then it can be checked to see whether the changed heat release rate is as a result of the different paraffin content. If so, it can then be explained that the mechanism by which the paraffin content influences NO emissions is through its effect on combustion rate.

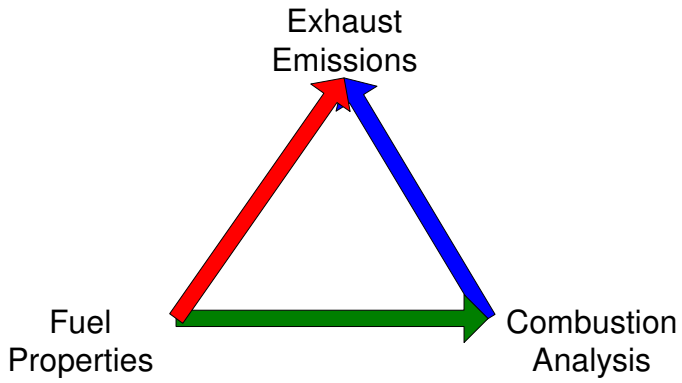

Figure 4-1 Illustration of the triangular approach to the statistical analysis.

In order to be representative of South African conditions the engines selected were chosen based on two main criteria: firstly, the two engines should employ different technologies representative of the two main technology classifications utilised in the country. These are the so-called older technology, carburettor based engines and current technology fuel injected, multi-valve engines. Secondly, the actual engines used should be common engines sold in large numbers in the country. Fuel formulations were also chosen based on the requirement of being representative of South African conditions. Eleven of the thirty five fuels were pump fuels available from different refineries at the time of initiation of the project, while eight fuels were formulations thought to be representative of the unleaded fuels expected to be produced by different refineries when unleaded fuel was made available (the experimental phase of this research took place just prior to the launch of unleaded gasoline in South Africa). A further sixteen fuels were specially blended so that properties outside of those spanned by the market fuels could be investigated.

Sasol Oil Research, provided technical support of this research and blended the special test fuels for the research. The fuel formulation parameters included in all analyses were those returned by the Sasol Oil laboratory analysis which included the parameters given in Table 4-1. Not all of the parameters measured in this type of routine fuel analysis have any bearing on fuel performance as far as combustion in an engine is concerned. These parameters are therefore not included in any analyses. Those parameters used are indicated in the table in the column labelled Short Name. A short name is required as the statistics package used for the analyses only allows single word variable names with a maximum character length of 8 characters. This short name is often used in tables, and sometimes in the text, throughout this document.

Table 4-1 Fuel formulation parameters given by fuel analysis and used for the analysis

Fuel Formulation Parameter	Unit	Short Name
Distillation Curve T_{xx} (10% steps + 5% and 95% evaporated)	° C	IBP, T10, T30, T50, T70, T90, FBP†
Recovery	vol %	-
Residual	vol %	-
Density	Kg/L	Dens
Copper Corrosion	-	-
Doctor Test	-	-
Volume/Liquid Ratio	℃	Vlratio
Vapour Pressure	KPa	VapPres
E_{70}	Vol%	E70
Volatility Index	-	Volind
Existing Gum	mg/100ml	-
Potential Gum	mg/100ml	-
Acid Number	MgKOH/g	-
Induction	Min	-
RON	-	RON
MON	-	MON
Sensitivity (RON - MON)	-	Sens
R100-Octane Number	-	-
Lead Content	MgPb/l	Lead
Aromatic Content	Vol%	Arom (A)
Olefin Content	Vol%	Olefin (O)
Paraffin Content	Vol%	Paraffin (P)
Sulphur Content	Mass%	Sulphur
Nitrogen Content	mg/l	Nitrogen
Oxygen Content	mass%	Oxygen
Benzene Content	mass%	Benzene
Phenol Content	mg/l	Phenols

† Only the distillation points listed here were used in the analysis, using all the points would have increased the number of variables unnecessarily.

5. RESEARCH FUELS

Sasol Oil, Research and Development formulated and supplied all of the sample fuels used for the investigation. The fuels can be broadly classified into three separate groups namely current commercial petrol (at time of project inception, all containing lead), proposed commercial unleaded petrol and reformulated unleaded petrol blends. The first grouping consisted of the available pump fuels of 93 or higher Octane (RON) from all of the petrol producing refineries in the country. This resulted in there being seven 93 Octane fuels (higher Octane inland fuels and lower Octane coastal fuels – see Section 2.1) and four 97 Octane fuels (higher Octane coastal fuels). The second grouping of fuels consisted of the proposed unleaded fuels from all the petrol producing refineries. Both of the proposed unleaded Octane grades were tested (91 Octane inland grade and 95 Octane coastal grade) resulting in eight fuels. The remaining sixteen fuels were unleaded blends utilising Sasol 91 Octane as the base fuel. The breakdown of the fuels is indicated below and the analyses of the fuels is given in Appendix A.

Commercial Leaded Fuels : P1 through P11 (11 fuels)

Commercial Unleaded Fuels : P12 through P19 (8 fuels)

Reformulated Unleaded Fuels : P20 through P35 (16 fuels)

Unforeseen difficulties resulted in the total consumption of reference fuel during the project being more than four times that initially catered for. It was thus necessary to use two reference fuels during the course of the project. The first reference fuel labelled Ref1 was used for the evaluation of the leaded fuels while a second reference fuel labelled Ref2 was used for the evaluation of the remaining fuels. However, back to back tests on the two reference fuels were carried out to measure the differences between their respective emissions to enable sensible data interpretation.

5.1. Fuel Component Content

The fuels were analysed for their compositions and this analysis is summarised for the three major classes of hydrocarbon content: aromatics, olefins and paraffins. As each of these hydrocarbon classes has specific properties the fuels can be broadly considered as three component mixtures. The maximum, minimum and mean values of the three components are tabulated in Table 5-1 The simplex factor space (or geometric description) of a three dimensional mixture is an equilateral triangle and this forms a convenient graphical tool for displaying the blends used. Shown in Figure 5-1 is the simplex factor space for the three components of the research fuels. As can be seen a large group of the fuels seem centred around 50% paraffin, and 25% each aromatic and olefin. However, when viewing the leaded and unleaded fuels only as in Figure 5-2 a good spread is seen. The clustered group of the fuels is due to the consistent base fuel used for the blending up of the reformulated fuels (base fuel has 45% paraffin, 28% aromatic and 27% olefin content).

Table 5-1 Minimum, maximum and mean values for fuel component concentration of research fuels.

	Aromatics	Olefins	Paraffins
	[vol %]	[vol %]	[vol %]
min	13	2	4
max	69	50	71
mean	33.5	25.2	41.3

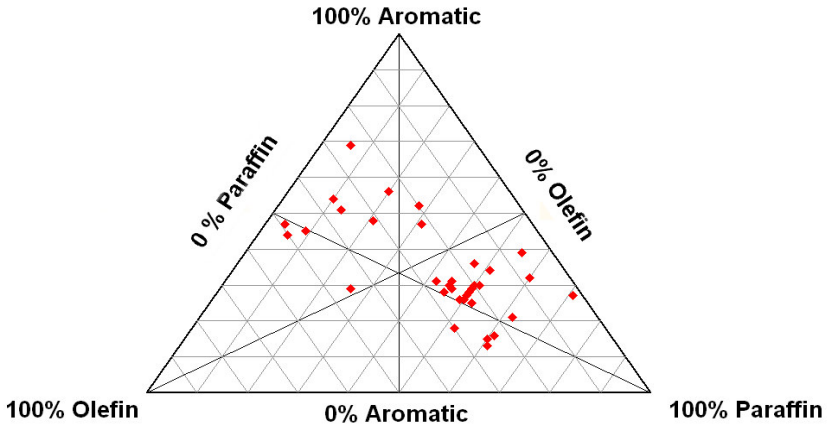

Figure 5-1 The simplex factor space showing the concentrations of the three components of the research fuels.

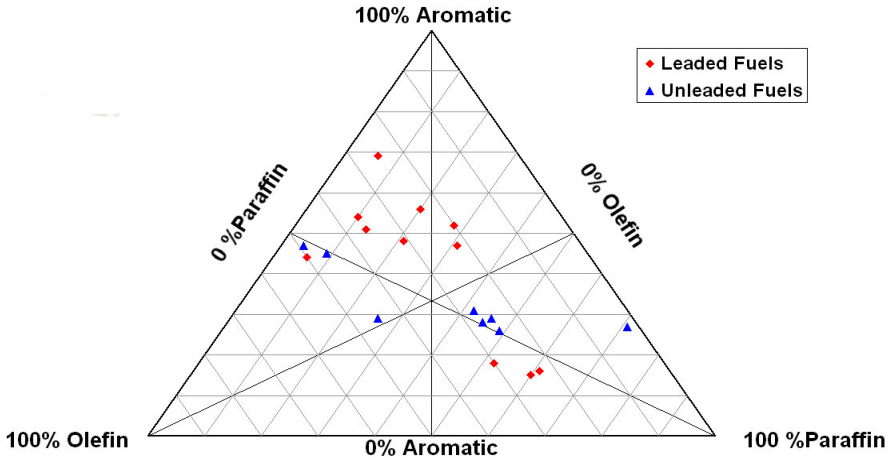

Figure 5-2 The simplex factor space showing the concentrations of the three components of the leaded and unleaded fuels only.

Other important fuel components are also given in the summary, including benzene, phenols, nitrogen, oxygen, sulphur and lead. The maximum, minimum and mean values of these are given below in Table 5-2.

Table 5-2 Maximum, minimum and mean values of benzene, phenols, nitrogen, oxygen, sulphur and lead content of research fuels.

	Benzene	Phenols	Nitrogen	Oxygen	Sulphur	Lead
	[mass %]	[mg/l]	[mg/l]	[mass %]	[mass %]	[mg Pb/l]
min	0.70	25.00	2.00	0.09	0.00	2.00
max	10.80	643.00	35.00	3.64	0.07	438.00
mean	2.50	133.73	16.12	1.92	0.02	139.16

5.2. Fuel Volatility

There are a number of ways of expressing a liquids volatility. The most complete description of volatility is the distillation curve which gives the temperature required to vaporise the fuel by percentage over the complete temperature range required to vaporise all of the liquid. However, when comparing fuels this would require either graphical comparison or the comparison of a series of numbers, neither of which is convenient. Certain regions of the distillation curve effect certain engine operating parameters (e.g. the lower end affects startability while the high end affects manifold fuel distribution, [33]) and therefore discrete values of specific interest are extracted. These values can be expressed in two different ways:

- the temperature required to evaporate a certain volume percent, expressed as T_{xx} where this refers to the temperature required to evaporate xx vol %
- the percentage volume evaporated at a given temperature, expressed as E_{xx} where this refers to the volume percent evaporated at xx °C.

Commonly used values include T_{90} and E_{70}.

Another measure of volatility commonly used is the vapour pressure which gives an indication of the extent of vapour loss likely to occur during storage in vented tanks, and the tendencies for vapour release and possible vapour lock in pipes. It is also an indication of the ease with which a vapour-air mixture can be produced for cold starting. The specific measure used is the Reid Vapour Pressure (RVP). A further volatility measure of direct interest in problems of vapour locking of fuel systems is the vapour/liquid (V/L) ratio measured against increasing temperature. Problems usually occur around the 36/1 V/L ratio and the temperature required to achieve this V/L ratio is usually quoted for comparison.

Another measure commonly used in the automotive fuels industry is the so called volatility index which is a composite quantity arrived at by summing the RVP and 0.7 times E70 (this measure has no units as it is a composite of two measures having different units).

The minimum, maximum and mean values of the above volatility measures are given below in Table 5-3 and the volatility curves are shown in Figure 5-3.

Table 5-3 Minimum, maximum and mean values of volatility measures for the research fuels.

	Vapour Pressure	V/L Ratio (36/1)	E70	Volatility Index
	[kPa]	[° C]	[vol %]	
min	50	55	12	58
max	76	71	39	96
mean	63.4	60.8	25.9	81.3

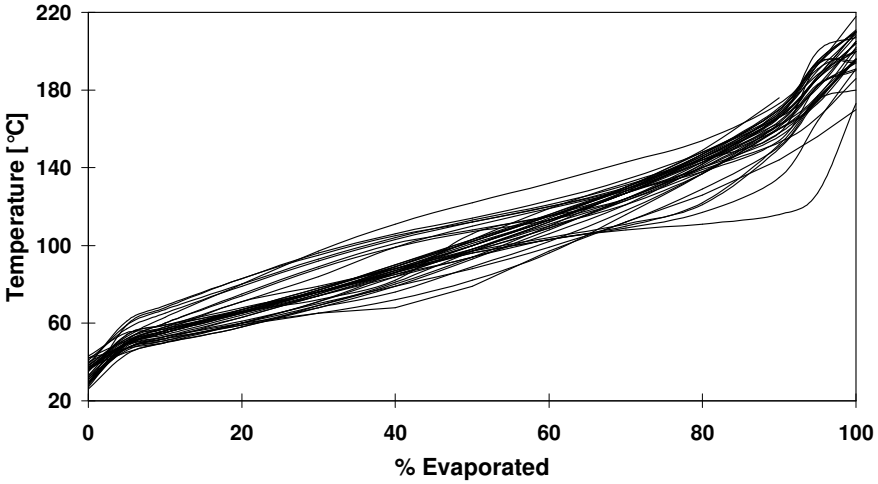

Figure 5-3 Volatility curves for the research fuels.

5.3. Fuel Density and Octane Number

The range of densities of the research fuels is indicated by the maximum, minimum and average values as listed below in Table 5-4. The range of Octane numbers was mostly dictated by the groups of commercially available leaded and unleaded fuels and the base fuel used for the blending of the reformulated fuels. The range of Octane numbers is also indicated in Table 5-4.

Table 5-4 Minimum, maximum and mean values of research fuel density, RON and MON.

	Density	RON	MON
	[mass %]	[mg/l]	[mg/l]
min	0.72	89.40	80.60
max	0.77	98.20	90.50
mean	0.74	93.85	84.23

5.4. Fuel Carbon : Hydrogen : Oxygen : Nitrogen Ratio

Many calculations used in automotive emissions work such as stoichiometry and equivalence ratio calculations rely on the known Carbon : Hydrogen : Oxygen : Nitrogen Ratio (C:H:O:N) of the fuel. This fuel property is not given by the fuel analysis (Appendix A) and must be calculated or estimated. The composition of the fuel based

on the ratios of the three basic fuel components (aromatics, olefins and paraffins) is given in the fuel analysis and this suggests that the C:H:O:N ratio could be calculated. However, the ratio is given in volume percent and only the three major fuel component classes are given along with mass percentage of oxygen and nitrogen. This precludes the direct calculation of C:H:O:N ratios and therefore some assumptions and estimations had to be made.

5.4.1. Carbon : Hydrogen Ratio

Goodger [33] indicates that the H:C ratio tends toward 2 (C_nH_{2n}) as the Carbon number (n) increases. This is indicated in Figure 5-4 where the C:H ratio is plotted for the more important fuel component classes. The graph is generated by considering the general formula for the major fuel component classes namely :

- Paraffins - C_nH_{2n+2}
- Olefins - C_nH_{2n}
- Cycloparaffins - C_nH_{2n}
- Acetylenes - C_nH_{2n-2}
- Alkylbenzene Aromatics (single ring Aromatics) - C_nH_{2n-6}
- Polynuclear Aromatics - (no generalised formula).

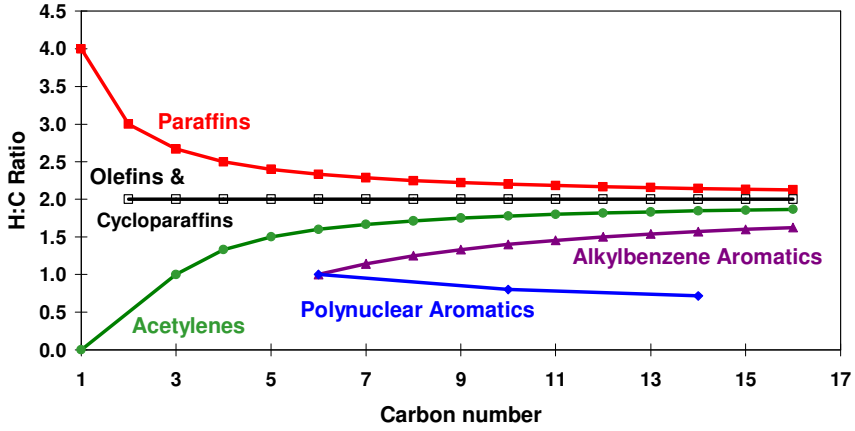

Figure 5-4 Hydrogen : Carbon Ratio for Fuel Component Classes according to Carbon Number (adapted from Goodger [33]).

As can be seen in Figure 5-4 the paraffins olefins and cyclic-paraffins tend to a H:C ratio of 2 while the alkylbenzene aromatics tend to 1.5 (for carbon numbers approaching 16 and it is assumed that gasoline does not contain molecules larger than C_{16} in significant quantities). It is only the polynuclear aromatics that deviate from the trend and these are also assumed to be in low concentrations in gasoline. So it can be deduced from the above that gasoline made up of mixtures of the above components would have a H:C ratio less than, but near to 2.

Some commonly used values for the H:C ratio found in the literature are given below:

- Heywood [15] - 1.87 typical, 1.8 - 2.0 range
- Ferguson [17] - 1.6 - 2.1
- Taylor [34] - 2.125 (C_8H_{17})
- Combustion Handbook [35] - 2
- Automotive Handbook, Bosch [19] - 1.95.

A value of 1.9 has been chosen as being typical of most gasolines. For most instances it is acceptable to use $C_1H_{1.9}$ as the representative fuel structure but in order to be more complete a Carbon number more typical of an actual fuels average molecule size is chosen. Taylor [34] indicates a carbon number of 8 and Ferguson [17] 7 while Heywood [15] suggests average molecular mass of 110 which translates to a carbon number of 7.9 (H:C ratio 1.87). Therefore a carbon number of 8 is chosen as being representative of a typical gasoline resulting in a Hydrogen number of 15.2 ($C_8H_{15.2}$).

5.4.2. Fuel Oxygen Molar Content

The fuel analysis provides the Oxygen content of the fuel by mass and thus a simple calculation is used to find the C:H:O ratio given the C:H ratio as discussed above. This calculation is given in Equation 5-1 below.

$$\text{Fuel structure - } C_nH_mO_r$$

$$mass\%O_2 = \frac{16.0r}{12.01n + 1.008m + 16.0r} \times 100$$

$$\therefore r = \frac{(12.01n + 1.008m)mass\%O_2}{16(100 - mass\%O_2)}$$

Equation 5-1 Calculation of oxygen number from mass percent oxygen content of fuel.

5.4.3. Fuel Nitrogen Molar Content

As nitrogen plays a role in the combustion of fuels in air, combustion equations often include fuel nitrogen content. The fuel analyses included Nitrogen content and the highest nitrogen content fuel had 35 mg/l which is 0.005 mass %, translating to a Nitrogen number of 0.0004 and is therefore assumed to be negligible.

6. EXPERIMENTAL APPARATUS

6.1. Test Engines and Experimental Set-up

In order for the results to be as representative of typical South African conditions as possible, engines utilising technology levels prevalent in vehicles on the roads of South Africa were selected. The use of carburettors for fuel delivery control is fast declining due to the clear advantages of fuel injection systems, which are rapidly becoming cost competitive. However, considering the low relative turnover of new vehicles into the national fleet, carburetted vehicles will remain in significant proportions in the vehicles on the road for some time into the future. For these reasons, two engines were selected, each being representative of one of the technology types, and the actual engines selected were of types sold in relatively large volumes into the local market. An electronically fuel injected engine, was chosen to be both representative of the existing and future new vehicle technology. A locally produced carburetted engine was chosen to represent the technology level of a large number of existing vehicles. Neither of the engines were new at the time of testing and thus were thought to be representative of engines in service.

Due to the fact that unleaded fuel was not available until 1996 in South Africa, engine management technology had lagged the trends in the rest of the world. Catalytic converters and exhaust lambda sensors are poisoned by the lead additive in leaded gasoline and were therefore excluded from use on all vehicles. Closed loop fuel injection control, which is essential for the effective operation of the catalytic converter, and relies on feedback from exhaust lambda sensors, has therefore not been possible. Ignition timing control was also most commonly open loop, although some local models in the high volume sector and most models in the low volume, high price end of the market used knock sensing and closed loop ignition control. Only recently has the fitment of catalytic converters become more common. Neither test engine had any knock sensing or exhaust gas after-treatment equipment fitted.

Both engines were extensively instrumented enabling measurement of numerous temperatures, pressures and other relevant information. A Personal Computer (PC) based data acquisition system called ETA (acronym for Engine Test Automation), enabled many channels of information to be conveniently displayed and stored to disk simultaneously including the exhaust gas analyser outputs. On line digital displays as well as time trend graphs are fully configurable and allow the convenient monitoring of the engine operating parameters.

6.1.1. Toyota 4A-FE Engine Set-up

The first of the two engines chosen for the investigation was a Toyota 4A-FE engine which is a multi-valve, fuel injected 1.6 litre engine. This engine type was installed was the most common of the fuel injected engines installed in the Toyota Corrolla and Conquest range of vehicles, which represents a large portion of the South African passenger vehicle fleet, recording record sales for many years. The engine was operated under conditions as close to standard as possible. The original equipment (OE) engine management system (EMS) was used. The system incorporated multi-point non-sequential injection,

utilising open loop ignition timing and fuel injection control. The system was not equipped with a lambda sensor or a knock sensor for feedback or closed loop control. Fuel injection and ignition timing were thus determined by a fixed "map" on the basis of manifold pressure and engine speed (with secondary maps allowing slight adjustment due to other factors such as engine temperature etc.). This fixed map, open loop strategy implies that the system was unable to detect and respond to changes in the fuel properties. As part of the investigation, the engine was also run at a constant equivalence ratio in order to simulate the response to closed loop fuel delivery control. Engine specifications are presented in Table 6-1.

Preliminary engine characterisation was carried out with the OE fuel pressure regulator fitted and with the engine set to the manufacturers ignition timing specifications. During these tests, fuel pressures and ignition timing at all relevant engine load points were recorded. The OE fuel pressure regulator was then replaced with an adjustable regulator, which enabled manual adjustment of the working pressure of the fuel injection system. This facilitated the variation of fuel delivery and hence the air/fuel ratio for the closed loop simulation test points. Although the variation in fuel pressure would also be responsible for changes in the atomisation and penetration of the fuel spray, not characteristic of normal engine operation, the effect was proved to be adequately small to have a negligible effect on the experiment. A precision adjustment mechanism was fitted to the ignition distributor to enable convenient and accurate adjustment of ignition timing without altering the OE EMS.

The dynamometer used for loading of the engine comprised of a large Direct Current motor controlled by sophisticated electronics. This dynamometer formed a regenerative system, which is capable of dynamic engine operation, although only steady state testing was used in this study. Load stability and repeatability was excellent with this system.

This engine was instrumented for in-cylinder pressure measurement, which is described separately in Section 6.2 below. However due to certain constraints, the engine was not instrumented from the beginning of the testing phase and the first eleven research fuels were tested without capturing pressure data. During this time a second, new cylinder head was instrumented with the pressure transducer housing sleeve. Unfortunately, it was found that significant differences existed between the performance of the new cylinder head and the previous one: it is thought that the cam shaft used was of a different specification. The new cylinder head was a standard component for this engine range and is therefore the correct one for the testing. This inconsistency of engine specification although significant, if taken into account in the analysis and discussion of the results, can be accounted for and should not influence any conclusions drawn. The sophisticated statistical analysis applied can allow for this by including the engine specification as a classification variable (see Section 10.2). Furthermore, only 11 of the total of 35 P series fuels (see Section 4) were tested with this engine configuration and this was the entire leaded fuel group. The thorough bracketing procedures with reference fuel, also allowed for this inconsistency to be accounted for.

6.1.2. Toyota 4Y Engine Set-up

The second engine used was a Toyota 4Y engine, which is a conventional 2 valve per cylinder, 2.2 litre engine. This engine is very commonly used in the light delivery and mini-bus sections of the national vehicle fleet. The engine is carburetted and utilises a conventional contact breaker type of ignition. For the primary investigation the engine was operated under conditions as close to standard as possible. No modifications were made to either the carburettor or ignition system as no closed loop simulation or ignition timing effects were to be investigated with this engine. Engine specifications are presented in Table 6-1. The engine was tested on the same dynamometer test stand as the Toyota 4A-FE described in Section 6.1.1.

Table 6-1 Test Engine Specifications.

Engine Model	Toyota 4A-FE	Toyota 4Y
Capacity	1.587 litre	2.237 litre
Bore/Stroke	81 / 77 mm	91 / 86 mm
Comp. Ratio	9.5 : 1	9.0 : 1
Cylinders	In-Line 4	In-Line 4
Valve Train	16 Valve DOHC	8 Valve SOHC
Ignition	Electronic / EMS	Contact Breaker
Fuel Injection	Non-Sequential - Multi-Point	Carburettor

6.2. Cylinder Pressure Measurement

Cylinder pressure measurement was performed with an AVL QH32C, water cooled pressure transducer which was mounted in the cylinder head. This type of in-cylinder pressure transducer contains a piezoelectric crystal, which responds to deformation caused by pressure, by developing an electrical charge. The QH32C is thermal shock compensated, having a quoted sensitivity of 0.02%/°C at 20 to 80°C. It also has a low sensitivity to acceleration with a quoted sensitivity of 0.02 bar/g. The type of electrical signal produced by the transducer requires very specific signal conditioning [36] and this was performed using an AVL 3057-AO1 charge amplifier, which provides a voltage output for use by any suitable recording device.

Two stainless steel sleeves were specially made to house and clamp the transducer in the cylinder head. They were designed in such a way as to allow the transducer to be easily removed and replaced with a stainless steel plug allowing the removal of the transducer whenever it was not necessary so as to protect it from unnecessary use and possible damage. The cylinder head was machined to accept the housing sleeve in such a way that minimal interference with ports, coolant jackets or auxiliary systems was achieved. The housing sleeve was mounted from the front of the engine at an oblique angle, and exposed the transducer to the gas pressure of cylinder number one, as indicated in Figure 6-1. This resulted in the transducer being placed in the end gas

region of the combustion bowl, and may be subjected to undesirable effects caused by the high gas velocities associated with the intentionally generated squish [15]. The transducer is also not flush with the cylinder head surface, as would be ideal. This is shown in Figure 6-2. Apparent in Figure 6-2 is the fact that, by not being flush mounted, a portion of the transducer protrudes into the chamber, while a small volume is created in front of another portion of the transducer. These factors indicate the possibility of some undesirable squish and turbulence effects bring induced onto the pressure trace.

Crank angle referencing was performed in a simple and unique way. A ferrous disk was machined and 120 holes were concentrically drilled through it (2 mm diameter holes on a 115 mm PCD). The holes were equidistant and therefore at three degree intervals. A single hole was also drilled (4 mm diameter, 100 mm PCD) to form a TDC reference. The disk was then rigidly fastened to the crankshaft pulley on the front of the engine. Thus crank angle was monitored at the nearest possible point to the cylinder in which pressure was measured to minimise any phase shift caused by crankshaft flexing. Two magnetic inductive sensors were then positioned to coincide with the PCD's of the holes drilled in the plate, one giving a pulse every three degrees and the other a single pulse for TDC reference. These two signals could then be fed into the data acquisition system alongside the pressure signal allowing the exact referencing of recorded pressure to crank position.

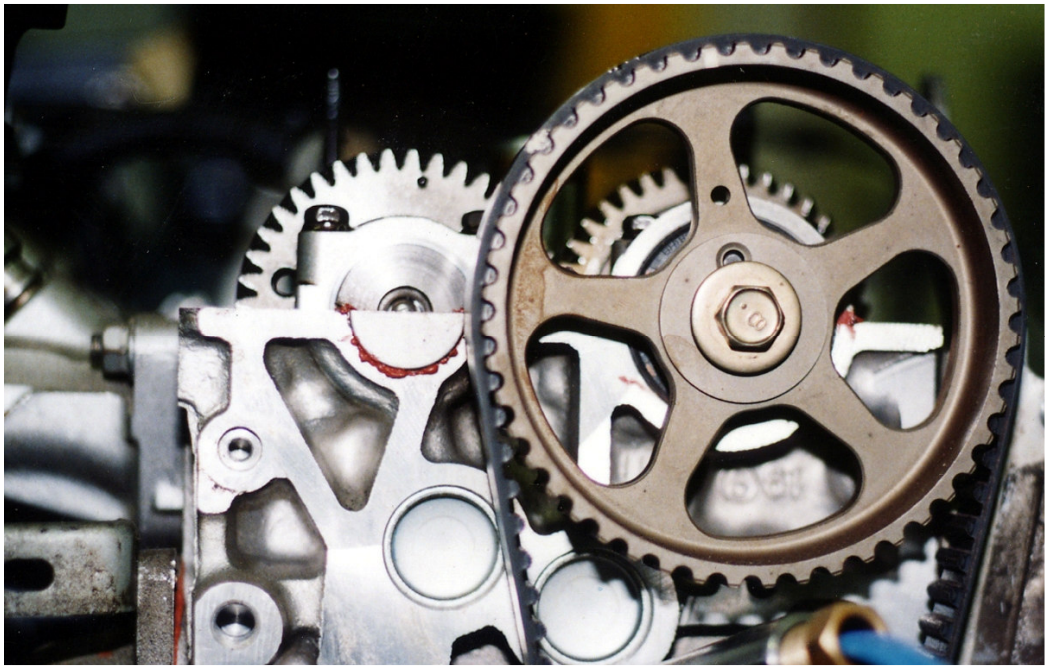

Figure 6-1 Photograph showing the transducer housing sleeve entering cylinder No. 1 at an oblique angle. The water coolant pipes and signal cable are visible exiting the rear of the housing sleeve.

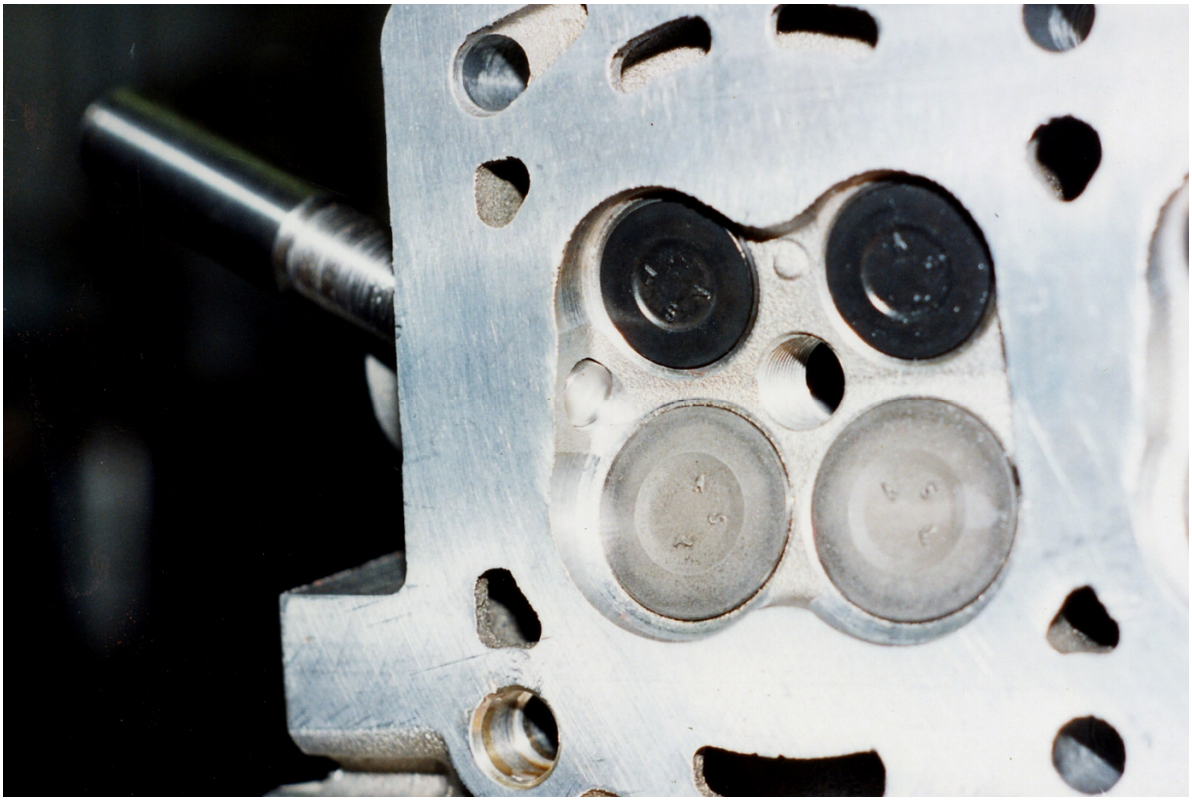

Figure 6-2 Photograph showing the access to the combustion chamber for the pressure transducer (dummy is in situ in this photograph). The non-flush face of the transducer is apparent, as is the small volume created to one side of the transducer face.

A Personal Computer based high speed data acquisition system called RACER (acronym for Rapid Acquisition of Combustion Engine Results) was used to record the cylinder pressure with exact reference to crankshaft position. The system was based around a high quality high speed data capture PC board (Eagle Electronics PC 30 DS 4) which allows sampling frequencies of up to 200 kHz (for a single channel). The board allows up to four channels to be simultaneously sampled (sample and hold). In the configuration used on this engine, only two channels need be sampled simultaneously. These two simultaneous sample channels monitor the crank angle and pressure signals, while the TDC signal is connected to the dedicated trigger input. This allowed a maximum sampling frequency of 100 kHz per channel which was more than adequate for all of the engine speeds to be tested.

The technique used by Racer to record pressure at the required crank angle resolution is to store pressure points at a fixed sampling frequency (burst sampling mode) and, from the simultaneously sampled crank angle pulses, to assign to each recorded pressure an accurate crank angle position. From this it then interpolates for the pressure at the required crank angles for storage to disk. Racer automatically averages all the pressure traces that it records during sampling and performs a number of functions on the measured data. Cylinder pressure was typically measured over at least 200 cycles to enable the determination of a representative average. Racer also calculates the standard deviation of recorded pressure throughout the cycle to give a representation of

cycle-to-cycle combustion variability or engine roughness. The averaged pressure trace is then subjected to an advanced digital filtering technique to remove any signal noise, which is generally amplified during heat release analysis due to it working with the differential of pressure. The technique used is known as Kaiser-Window filtering and has been shown to effectively remove the high frequency noise without distorting the signal in any way [37].

The filtered or smoothed profile was found to be highly repeatable for each test set of load, speed and fuel conditions. Racer stores arrays of the average pressure trace, standard deviation of pressure and smoothed pressure for every crank angle degree to disk. Racer can then either immediately, or during post processing carry out a heat release analysis (the analytical detail of which is described in detail in Section 8). The heat release analysis, in turn outputs for every crank angle degree a number of arrays of information including rate of heat release, cumulative heat release and gas temperatures. Certain parameters have been defined which attempt to describe the nature of combustion and these too are calculated, displayed and stored to disk. These parameters are also described in the section dealing with the analytical detail (Section 8.1).

6.3. Engine-out Gas Analysis

A specially designed probe was inserted in the exhaust system approximately 1.5 meters from the exhaust ports. The probe was designed such that it would enable the sampling of raw exhaust gas while minimising the potential of ingesting any particulate matter, such as engine deposit fragments, that might be in the exhaust stream. Furthermore the design was such that it ensured that a representative sample was taken by sampling from the centre of the exhaust diameter. The sample was fed to a bank of gas analysers via a sampling line maintained at 180 °C. This was to ensure that the water content of the exhaust remained in its vapour state due to the solubility of hydrocarbons in water, in this way the hydrocarbon concentration of the exhaust sample was affected as little as possible. This also reduced the likelihood of any of the hydrocarbon species themselves condensing and thus effecting the measurements.

A portion of the sample then passed through a Heated Flame Ionisation Detector (Seimens Fidamat K M52044) measuring unburned hydrocarbons, giving parts per million (ppm) on a methane scale. The detector uses Hydrogen and bottled air for combustion in the pilot flame. High quality gases were used to reduce the possibility of contamination (Hydrogen 5.0 and Zero Air were used respectively for these, both of these are international gas standards relating to contaminant concentrations). The remainder of the sample was then dried by passing through a chiller plant and water extraction unit before passing through the remaining analysers which are water sensitive. Therefore the results of the emissions other than HC's need to be corrected for the water removal which is done for all the results presented.

Nitrogen oxide (NO), carbon dioxide (CO_2) and carbon monoxide (CO) were measured by Seimens Ultramat 5E Non-Dispersive Infra Red (NDIR) analysers. The NO analyser recorded concentrations on the ppm scale and had an upper limit of 2000 ppm NO which proved to be slightly restrictive as concentrations exceeded this level at some of the engine load points investigated. The CO and CO_2 analysers measured percentage concentration by volume (% vol.). Engine-out oxygen concentration was also measured using a Seimens Oxymat 5E analyser,

which utilised a paramagnetic alternating pressure principle, recording percentage volume. The measurement of O_2, though not regulated or of direct interest, is required for many of the calculations used in the measurement of automotive emissions and is therefore of much value.

A catalytic converter using a carbon based catalyst, placed inline before the NO analyser, could convert Nitrogen Dioxide (NO_2) to NO thus allowing the concentration of NO + NO_2 to be measured. The quantity NO + NO_2 is generally referred to as NO_x (total oxides of nitrogen) as the concentrations of higher oxides of nitrogen are known to be insignificant. During preliminary investigations NO_2 concentrations in the raw engine out exhaust were found to be so low as to not necessitate the added complexity and uncertainty since the efficiency of the converter requires calibration and this was not possible at the time.

The cabinet which contained the bank of analysers can be seen below in Figure 6-3.

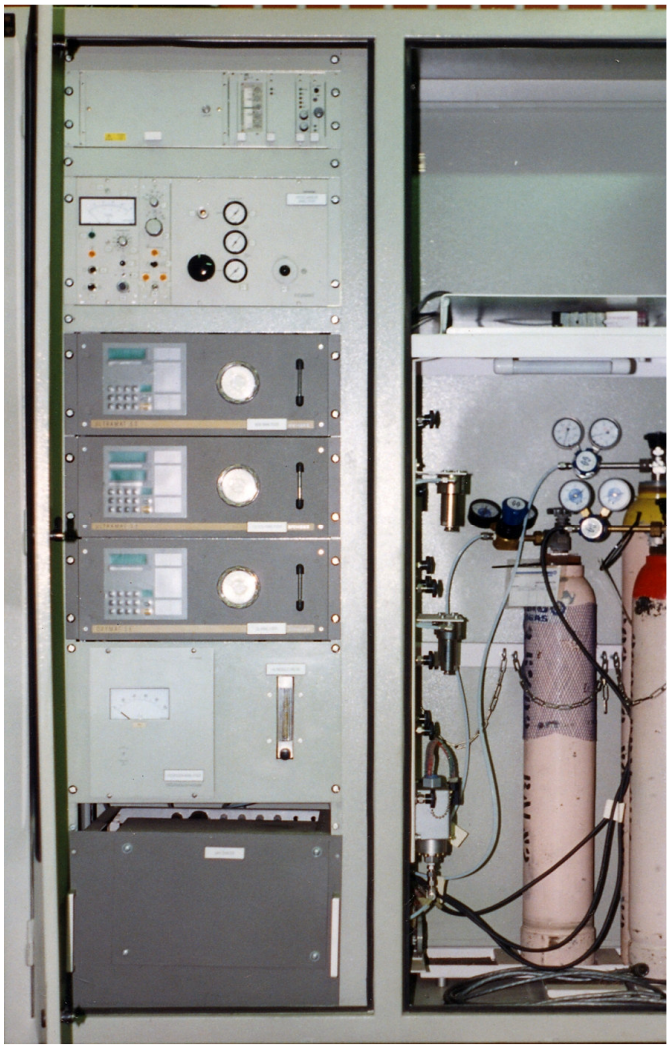

Figure 6-3 Photograph of the cabinet containing the gas analysers and the calibration gas bottles. The individual analysers from top to bottom are NO_2 – NO converter, hydrocarbons, NO, dual analyser with CO_2 and CO, O_2 and unused H_2 analyser. The chiller unit for sample water removal is seen at the bottom and the heated sample line is seen coiled on the floor.

All the analysers were calibrated before, and the calibrations were checked after, each test sequence, using standard gases having similar concentrations of the relevant compounds to that expected in the exhaust stream. Calibration gases were of a high quality being supplied with calibration certificates indicating the gas concentrations analysed along with tolerances and maximum contamination levels. Nitrogen gas (Nitrogen 5.0) was used as a zero reference for all the analysers. The analysers were coupled together in such a way as to conveniently allow switching over to the standard and zero gases for easy calibration. Electronic outputs of the analysers were connected directly to the engine data acquisition system to allow easy recording of the exhaust gas composition.

6.4. Auxiliary Test Equipment

Fuel consumption was measured using a gravimetric system in which fuel was drawn from, and returned to, a three-litre glass beaker standing on a precision electronic mass balance. As the engine consumes fuel, so the mass of fuel in the beaker continuously decreases. The continuously decreasing mass result was passed to ETA, which could calculate instantaneous fuel consumption on a mass flow rate basis, in units of kg/hr.

Air mass flow rate was monitored by connecting the engine's air inlet to the outlet of a large damping chamber ($1.38m^3$ volume) with a rubber diaphragm which suppresses the inherent pulsations within the inlet stream. The inlet to the chamber is through a bell mouth nozzle, and by measuring the depression in the mouth of the nozzle the air mass flow rate can easily be determined. A precision water manometer (Betz Water Manometer) or a calibrated pressure transducer was used to measure this depression.

Other parameters that were measured included inlet manifold air and fuel droplet temperature. As indicated by Moran [38], the measurement of the inlet manifold air temperature is complicated by the fact that manifold flow is inherently multi-phase so simple techniques may be misleading. A simple thermocouple placed in the inlet charge stream will reflect components of the air/vapour temperature, the droplet temperature and cooling due to fuel vaporisation from the probe itself. A unique probe described by Moran [38] was used to measure the inlet air/vapour temperature which prevents the wetting of the thermocouple measuring tip, and thus the effect of the liquid fuel temperature and evaporative effects are reduced. Moran further indicates that the degree of wetting of a bare thermocouple in the inlet stream is high and therefore a bare thermocouple would be a good indicator of fuel droplet temperature. Thus a bare thermocouple was also placed into the inlet manifold air stream. Type J thermocouples were used for these measurements.

Engine oil, fuel injection rail and inlet manifold pressures were measured with industrial quality pressure transducers. Engine coolant outlet and oil temperatures were measured with type J thermocouples while a type K thermocouple was used for exhaust temperature. The thermocouple signal conditioning modules used for the data acquisition system have on board cold junction compensation, so no cold junction was used. All the modules were calibrated using a dedicated micro-volt and thermocouple calibration source (Eurotherm 239), and checked at the ice and steam points.

7. EXPERIMENTAL PROCEDURE

7.1. Test Sequence

The Toyota 4A-FE engine testing on all the fuels was completed first, followed by the testing of the Toyota 4Y. Before the testing of the sample fuels could begin a large amount of preliminary work was required. This included tests to determine exactly the load points to be used for testing, this is discussed in detail below in Section 7.2. Furthermore, a large number of tests were performed using the reference fuel to establish the experimental procedures to be used. This process ensured that the test procedures used provided excellent repeatability. Further preliminary tests were undertaken to provide a data base of engine responses to certain variables that would aid the explanation of the results. These tests are described below in Section 7.3.

The fuels were tested in chronological order of their P series designation (see Section 4). A bracketing procedure using reference fuels was used such that any group of fuels testing had a complete reference fuel test at the beginning and end of the test series. Thus any outside effects that may influence the results could be detected and accounted for.

The 4A-FE testing was unavoidably interrupted and run in three consecutive groups or batches. The fuels in each group, and the order of testing was as follows:

1. 4A-FE - Fuels P1 through P11
2. 4A-FE - Fuels P12 through P24
3. 4A-FE - Fuels P25 through P35
4. 4Y - Fuels P1 through P35

There were no significant time delays during any given batch of fuels testing.

7.2. Engine Load Point Determination

It is well understood that to completely determine either an engine's or a fuel's true exhaust emissions characteristics, as they would effect air quality in service, it is necessary to measure exhaust gas composition from driving cycles. This, along with the advantages and disadvantages of the different exhaust emissions testing options is discussed in some detail in Section 2.4. As the objectives of this research were not only to quantify the differences in emissions caused by different fuel formulations, but also to establish the fundamental cause of these differences, steady state engine dynamometer testing, with all the advantages associated with this methodology, was chosen as the most appropriate approach.

A number of load points were chosen which together are thought to be adequately representative of actual driving conditions. Four vehicle speeds of 60, 80, 100 and 120 km/h were chosen to represent driving conditions ranging from town driving to highway cruising. Engine speeds were calculated from known gear ratios of a

typical vehicle in which the engine is fitted as standard. Torque was calculated by using data published by CAR Magazine [39] who, had measured fuel consumption at the steady speeds selected. An approximation was made through simple drag based calculations using realistic assumptions for vehicle drag coefficient and rolling resistance to determine a first estimate of engine torque at each test point. Then the engine was tested at the calculated load point and fuel consumption was measured. By comparing fuel consumption as reported during road testing (Car magazine) and that measured, it was possible to adjust the engine torque until exact agreement was attained. The torque values thus attained were then used for all further testing at these load points.

In order to gain some insight into the effects of acceleration and full throttle engine operation, testing was also carried out at an engine speed of 3000 rev/min and Wide Open Throttle (WOT). The simulation of closed loop fuel delivery control, as discussed in Section 6.1.1, was performed at the 60 km/hr load point on the Toyota 4A-FE engine only. Complete fuel loops and timing swings were performed for the first eleven fuels from which the equivalence ratio and ignition timing for minimum specific fuel consumption was determined for this engine. Running the engine at this predetermined equivalence ratio enabled the determination of the rest of the fuels responses to closed loop fuel management.

As mentioned in Section 6.1.1 the engine was run in its standard condition at all the relevant load points during initial engine characterisation. The fuel injection rail pressure and ignition timing were recorded, and for all subsequent testing these same values were attained with the adjustable equipment fitted to the engine. The engine speed, engine torque, ignition timing and fuel pressure for these load points for the Toyota 4A-FE engine are given below in Table 7-1, except for the closed loop simulation where the actual goal equivalence ratio is quoted in place of the fuel pressure.

Table 7-1 Table of Engine Speed, Torque, Ignition Timing and Fuel Pressure or Equivalence Ratio for the Load Points for the Toyota 4A-FE engine.

Load Point	Engine Speed [rev/min]	Engine Torque [Nm]	Ignition Timing [° BTDC]	Fuel Pressure / Equivalence Ratio
Acceleration Simulation	3000	WOT	18	3.10[bar]
120 km/hr	3760	72.0	22	2.82[bar]
100 km/hr	3130	55.0	26	2.71[bar]
80 km/hr	2500	48.8	24	2.69[bar]
60 km/hr	1880	35.9	20	2.72[bar]
Closed Loop Simulation	1880	35.9	25	0.90[ER]

The full matrix of six load points was only used for the first eleven fuels (unleaded market fuels), thereafter a reduced matrix excluding the 80 and 100 km/hr load points was used. The time taken for the full test sequence

was found to be too long to be practical and furthermore, the 80 and 100 km/hr results for the first eleven fuels were seen to be consistent with the other two part load test points.

A similar procedure was undertaken for the Toyota 4Y engine to determine the engine speed and torque for the relevant load points, these are given below in Table 7-2.

Table 7-2 Table of Engine Speed and Torque for the Load Points for the Toyota 4Y engine.

Load Point	Engine Speed [rev/min]	Engine Torque [Nm]
Acceleration Simulation	3000	WOT
120 km/hr	3760	109
60 km/hr	1880	39

7.3. Preliminary Investigations

Before the testing of the sample fuels began a series of tests were conducted, firstly to ensure that test reproducibility was of a high standard and to determine the response of the engine to the two engine operating parameters thought to have a primary influence on the exhaust emissions: ignition timing and equivalence ratio. Thus a comprehensive series of timing swings and fuel loops was undertaken. A timing swing consists of operating the engine at a given load condition and varying the ignition timing. Usually the timing is first retarded from the standard setting by approximately 10 °CA, and then advanced stepwise until the ignition is approximately 10 °CA advanced from standard. Thus the engines response to ignition timing can be determined and graphically represented as trends. Likewise, a fuel loop determines an engine's response to equivalence ratio. In this case, this was achieved by first reducing the fuel rail pressure, by means of the adjustable regulator, from the standard condition, and thus leaning out the fuel/air equivalence ratio. Then stepwise increases in fuel rail pressure produces a trend of engine response to progressively richer operation.

7.4. Test Procedure

The daily test procedure used was established during the exhaustive preliminary stage of the experimental phase of the project. The procedures were chosen so as to eliminate as much as possible any outside influences on the results and thus produce good experimental reproducibility. On any given day the engine was first warmed up using left over sample from the previous days testing or other fuel "slops". This was done to reduce wastage of research fuel sample. Any sample decanted from the supply drum and not used during testing was placed in a marked "slops" drum, and not returned to the supply drum. This precluded the contamination of the original fuel sample. Once the engine was warm, the fuel supply system was thoroughly flushed with the fuel sample to be tested. This was done to reduce any possible carry over effects. The flushing procedure used for the Toyota 4A-FE engine included a full flush of the fuel consumption apparatus and fuel injection system. The flush procedure

included first pumping the system as dry as possible by directing the fuel injection return to the slops drum, and running the fuel injection pump until the flow stopped. The glass beaker of the fuel consumption meter was then emptied and cleaned manually with a small amount of fresh fuel sample. A few litres of fuel sample was then introduced into the system and circulated for a time to create as much mixing as possible with any left over fuel. The system was then drained again as in the first step and the glass beaker again emptied and cleaned.

In the case of the Toyota 4Y which is a carburetted engine with no return to the fuel consumption measurement apparatus, the procedure was somewhat simpler. The beaker of the fuel consumption meter was first emptied and cleaned, thereafter the fresh fuel sample was introduced and the engine was allowed to run. Enough sample would be consumed in the time taken before recording was begun that the system would be well flushed of any previous fuel sample.

The load point testing order used for the testing consisted of first running the acceleration simulation (3000 rev/min, WOT) followed by the part load test points. A decreasing order of vehicle speeds was used (120, 100, 80, 60 km/hr) followed by the closed loop simulation. This test order was found to provide the best experimental reproducibility, especially for the measurement of exhaust aldehyde and ketone concentrations, which were being measured for a separate, but allied project. The engine was allowed to stabilise between load points by running at the new load point for at least four minutes. Engine stability was ensured by visually monitoring the time trend graph plotted by the engine monitoring and data acquisition system, ETA (see Section 6.1), and ensuring that engine coolant, oil and exhaust temperatures had fully stabilised. These parameters had the longest time constant and if they were all stable then the other parameters would also be fully stabilised. A number of data points were saved over a period of time (± 2 minutes) which when averaged would minimise any signal or experimental noise.

7.5. Daily Calibration

After warming the engine up for the first time on any given day of testing a dynamometer torque calibration was performed. Due to the fact that torque calibrations are regularly performed a calibration arm is permanently attached to the dynamometer. This makes the calibration procedure simpler and quicker by removing the necessity to counter balance the calibration arm to readjust to zero each time. Calibration was performed by setting the zero torque with the warm, stationary dynamometer. A known weight was then hung freely from the calibration arm a known distance from the dynamometer rotational axis and therefore the applied torque can easily be calculated. The dynamometer was then run up to engine idle speed and shut down. The vibration thus allowed the dynamometer flexure mountings and bearings to settle and reduced the effects of sticktion in the system. The load cell and bridge amplifier signal could then be scaled to the calculated torque.

The torque calibration was performed at the start of the project without the engine/dynamometer coupling shaft attached. Thus sticktion in the engine would not influence the zero calibration. The stability of the load cell and bridge amplifier electronics were such that the daily torque calibrations never required adjustment. A calibration check was also performed at the end of any days testing programme to check if any drift had occurred. On no occasion was significant drift encountered.

The gas analysers were continually left powered up, or were powered up at least 2 hours before testing commenced to ensure that stable operation had been attained. The analysers were calibrated before each fuel sample test and checked for drift after each test. Analyser drift did occur on a few occasions but was accounted for during data reduction.

8. HEAT RELEASE ANALYSIS

Heat release analysis was performed on measured cylinder pressure by the Racer computer program. This program, called Rapid Acquisition of Combustion Engine Results, was written by researchers within the research unit and was extensively modified as a prerequisite of this research project. Racer was originally equipped with a simple single-zone, zero dimensional, fully mixed, type of heat release analysis, as described by Gatowski, Balles, Chun, Nelson, Ekchian and Heywood [40] and Heywood [15]. This was not modified or altered significantly, but the results generated by it are used. The modifications undertaken specifically for this project included the addition of a two-zone model with equilibrium combustion products and gas property calculations. The detail of the two-zone model is given below in section 8.3.

8.1. Heat Release Background and Results

Heat release analysis is a broad description of any analysis which computes rate of combustion (or rate of heat release) from measured cylinder pressure / time histories [15]. The basis of such analyses is the accounting for cylinder pressure increase by considering cylinder volume, heat transfer, mass leakage and other known processes. Any measured pressure increase not accounted for must be due to heat addition from combustion. Any deviation in calculated volumes and heat transfer etc from that actually occurring in the engine will therefore manifest itself as apparent heat release or combustion. The basic analysis calculates a rate of combustion, which depending on the specific analysis is in units of rate of energy release or rate of mass combustion (e.g. Joules/sec, Joules/°CA or kg/sec etc.). From this, other useful quantities can be calculated which aid the description and comparisons of combustion processes. The term “burn rate” is often used when considering the rate of combustion and will be used in this context here. Some of the useful parameters used in this research work are discussed below.

8.1.1. Peak Rate of Heat Release

The peak, or maximum rate of heat released is a useful parameter, which indicates the maximum rate at which combustion occurs during the process. This term gives an indication of the speed of combustion but is restricted to the maximum rate only, so does not give any information about the entire process. The crank angle at which the peak rate occurs is also often of interest. A typical heat release, or burn rate curve is shown in Figure 8-1 and the peak burn rate is indicated.

8.1.2. Cumulative Heat Released and Total Heat Released

The step-wise integration of the heat release rate curve generates a parameter that is of interest and this is the “cumulative heat released”. Comparisons of this curve between different combustion processes gives insight into the relative time (or crank angle) taken for the combustion process to occur. The value of the

cumulative heat released after combustion has been completed gives the “total heat released”. A typical cumulative heat released curve is shown in Figure 8-1 and the total heat released is also indicated.

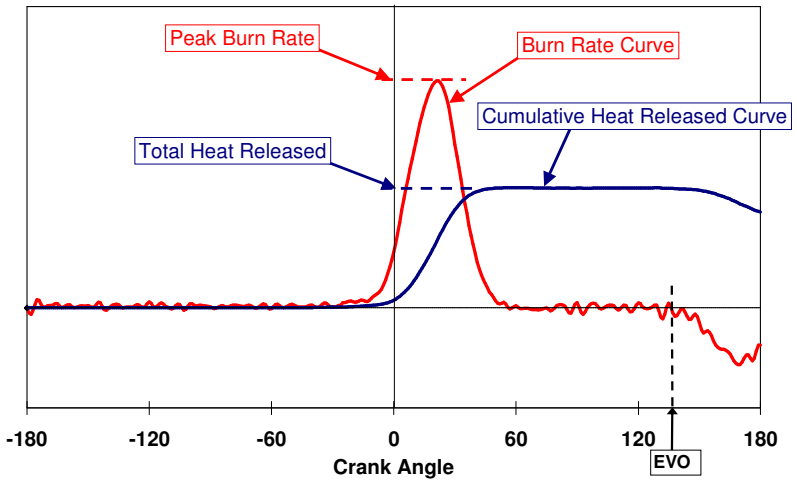

Figure 8-1 Typical burn rate and cumulative heat released curves and definition of peak burn rate as calculated by Racer from data measured in the Toyota 4A-FE engine.

8.1.3. Burn Angle and Induction Period

The cumulative heat released curve gives a graphical representation of the combustion process, but does not give quantifiable parameters that describe the combustion duration for the entire process. The complete duration required for combustion could be found by taking the difference between the crank angle at 100% burned and that at 0%. However, due to the asymptotic nature of the approach and departure to the horizontal, or near-zero heat release rate, of the curve at these points, the points are not well defined. This poor definition of these points would lead to large uncertainty in the results obtained. For this reason a more robust definition of a parameter to describe combustion duration is required. The term “burn angle” is used to describe the duration in crank angle degrees between two defined points on the cumulative heat released curve. Different groups of defined points are used including 2% to 98% burned, 5% to 95% burned and 10% to 90% burned. A further parameter can be extracted from the cumulative heat released curve if the point of initiation of combustion is known. In the case of spark ignition engines this is the crank angle at spark. The time required between initiation and the lower defined point (2%, 5% or 10% burned) is referred to as the “induction period” and is again usually measured in crank angle degrees. The definitions of both Burn Angle and Induction Period are illustrated in Figure 8-2 where, by way of example, 5% and 95% are taken as the defined points.

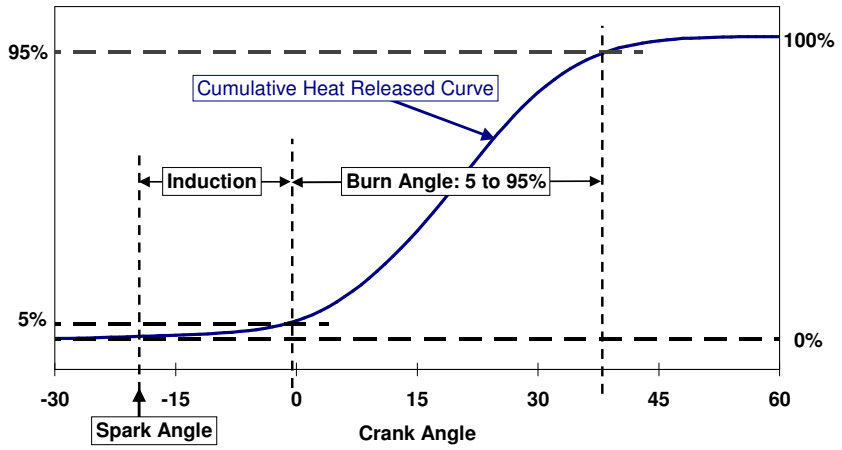

Figure 8-2 Definition of burn angle and induction period (5 to 95% given by way of example).

8.2. Single-Zone Heat Release Model

The workings of the single-zone model used by the Racer program was implemented as part of an undergraduate final year project [41] within the research group. As mentioned above, this was not altered significantly and will therefore not be described in detail. The single-zone model consists of a fully mixed heat release model, and is based on those described by Gatowski et al [40] and Heywood [15]. The model is a zero dimensional solution based on the first law of thermodynamics and assumed bulk properties, on the basis of gases being fully mixed. Sub models used included heat transfer and a model which allowed for a small portion of the cylinder gas to be passed into and then released from crevice volumes, and thus be excluded from the combustion process. The crevice gas is assumed to enter the crevices with the entropy of the bulk cylinder gas, but to be released at a lower temperature due to high heat transfer rates with the cylinder surfaces in the confined spaces of the crevice volumes. The model relies on empirically determined gas properties (ratio of specific heats) for the gas as determined by Cheung and Heywood [42].

8.3. Two-Zone Heat Release Model

The thermodynamic model used for the two-zone heat release analysis added to Racer was based on that proposed by Krieger and Borman [30]. This model requires certain gas properties, and their first derivative with respect to temperature and pressure, for both the burned and unburned gas mixtures. Algorithms given by Gordon and McBride [31] can be used to determine the gas properties for the individual species. In order then to compute the gas properties of the gas mixture, the species concentrations are needed, and for this, an equilibrium combustion products routine was used, based on that presented by Olikara and Borman [32]. The two-zone model is a more realistic representation of the actual spark ignition combustion process and does not rely on empirically determined gas properties as does the single-zone model.

8.3.1. Detail of the Two-Zone Thermodynamic Model

The two-zone model presented for use in spark ignition engines by Krieger and Borman [30] assumes that the chamber volume is divided into burned and unburned volumes separated by an infinitely thin flame front. The basis of this model is a mass transfer whereby the energy released due to combustion is related to the difference in the enthalpy of gas as it crosses the flame from the unburned zone into the burned zone. Therefore, the quantity that is determined is actually a rate of mass transfer and not an energy release rate as such. This is indicated in Figure 8-3 below.

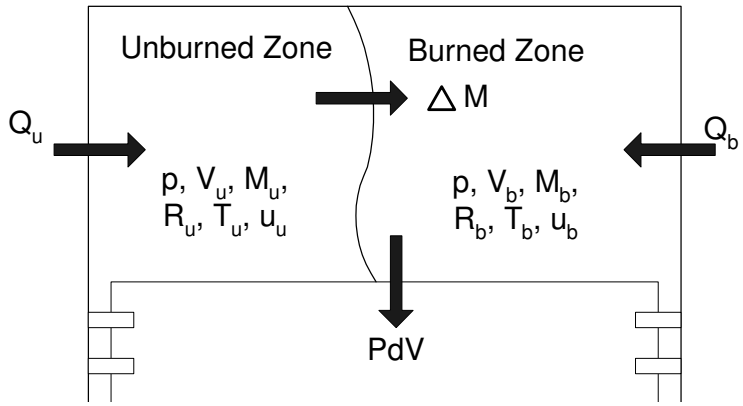

Figure 8-3 Schematic of the two-zone, mass transfer based combustion analysis model.

Each zone is treated as being in thermodynamic equilibrium (fully mixed) and both systems are assumed to be at the same pressure at any instant. The shape of the two systems is only important in so far as calculating the area of contact with the walls and each other, and therefore the relevant heat transfer rates. The equations forming the model are derived by considering the differential forms of both the equation of state and the energy equation (first law of thermodynamics) for the two zones, burned and unburned. The energy equation of the unburned zone is solved for the rate of change of the unburned gas temperature. The energy equation of the burned zone is then solved for the rate of mass transfer, or burn rate. The rate of change of the burned zone volume is simply found from the relationship of the burned and unburned volume and the total cylinder volume and the differential form of the equation of state for the unburned zone. The burned zone energy equation is then solved for the rate of change of the burned zone temperature. The resulting formulas are presented below in Equation 8-1. Before implementation of these equations was attempted, they were derived following the above procedure, and the derivations are given in Appendix B.

$$V = V_b + V_u$$

$$M = M_b + M_u$$

$$\therefore \dot{M}_b = -\dot{M}_u$$

$$\dot{T}_u = \frac{\left(T_u \frac{\dot{p}}{p} + \frac{\sum_i \dot{Q}_{ui}}{M_u R_u} \right)}{\frac{1}{R_u}\frac{\partial u_u}{\partial T_u} + 1}$$

$$\dot{M}_b = \frac{\left(M_u R_u \dot{T}_u - p\dot{V} \right)\left(\frac{1}{R_b}\frac{\partial u_u}{\partial T_b} + 1 \right) - \dot{p}V\left(\frac{1}{R_b}\frac{\partial u_b}{\partial T_b} + \frac{M_b}{V}\frac{\partial u_b}{\partial p} + \frac{V_u}{V} \right) + \sum_i \dot{Q}_{bi}}{\left(u_b - u_u \right) + \left(\frac{R_u T_u}{R_b} - T_b \right)\frac{\partial u_b}{\partial T_b}}$$

$$\dot{V}_b = V_u\left(\frac{\dot{M}_b}{M_u} - \frac{\dot{T}_b}{T_u} + \frac{\dot{p}}{p} \right) + \dot{V}$$

$$\dot{T}_b = \frac{-p\dot{V}_b + \sum_i \dot{Q}_{bi} + \dot{M}_b\left(h_u - u_b \right) - M_b \frac{\partial u_b}{\partial p}\dot{p}}{M_b \frac{\partial u_b}{\partial T_b}}$$

Equation 8-1 Equations for the solving of the two-zone mass transfer based burn rate model (for derivation see Appendix B).

The initial temperature of the burned gas is found from calculating the adiabatic flame temperature, which is found by equating the enthalpy before and after combustion. This is simply shown in Equation 8-2 below. Solving this requires an iterative procedure using the property calculation of the equilibrium combustion products model.

$$h_b\left(T_b \right) = h_u\left(T_u \right)$$

Equation 8-2 Calculation of adiabatic flame temperature.

For the consideration of the shape of the burned zone, the combustion chamber is assumed to be a flat disc having diameter equal to the bore and height calculated from the instantaneous volume. The burned zone is then assumed to be a cylinder, coaxial with the combustion chamber disc, having the same height as the combustion chamber and diameter calculated from the burned zone volume. Therefore, before combustion is completed, the burned zone is assumed to only have contact with the piston crown and cylinder head surface. The unburned zone is then assumed to occupy the remaining annular ring in the chamber.

The validation of the two-zone combustion rate model is presented below in Section 11.3.

8.3.2. Calculation of Gas Pr operties

The gas properties required by the two-zone heat release prediction model are internal energy (u), gas constant (R) and enthalpy (h) for both the burned and unburned zones. In order to do this the properties of the individual species are required, and the gas is then treated as an ideal gas mixture and the required gas properties can then be found using the appropriate relationships. The enthalpy for the individual species of the products is found by the algorithms given by Gordon and McBride [31] which are functional form reductions of data taken from the JANAF tables. Algorithms for the calculation of cp (specific heat at constant pressure) h, and s, (entropy) are also given using the same seven algorithm coefficients. The form of the equations is given below in Equation 8-3. Coefficients are given for two temperature ranges, 300-1000K and 1000-5000K.

$$\frac{c_p}{R} = a_1 + a_2 T + a_3 T^2 + a_4 T^3 + a_5 T^4$$

$$\frac{h}{RT} = a_1 + \frac{a_2}{2} T + \frac{a_3}{3} T^2 + \frac{a_4}{4} T^3 + \frac{a_5}{5} T^4 + \frac{a_6}{T}$$

$$\frac{s}{R} = a_1 \ln T + a_2 T + \frac{a_3}{2} T^2 + \frac{a_4}{3} T^3 + \frac{a_5}{4} T^4 + a_7$$

Equation 8-3 Form of the algorithms proposed by Gordon and McBride [31] for the calculation of species gas properties.

For the unburned zone, the gas is assumed to be an ideal gas mixture of air, fuel vapour and residual gas. The properties of the individual species with the exception of the vaporised fuel are found from the coefficients given by Gordon and McBride [31]. Ferguson [17] gives the coefficients for a number of different fuels and these are incorporated in the model.

The gas mixture molecular weight is needed for the property calculations and is found by a summation of the specie molar concentration, times the specie molecular weight. The gas constant is then simply, from its definition, the universal gas constant R_o divided by the gas molecular weight. The mixture enthalpy is determined similarly to the molecular weight with a weighted summation, but is divided by the mixture molecular weight. Finally the internal energy is found from its definition. These are presented by Olikara and Borman [32] and are given mathematically below in Equation 8-4.

$$M = \sum_i x_i M_i$$

$$R = \frac{R_o}{M}$$

$$h = \sum_i x_i h_i \Big/ M$$

$$u = h - RT$$

Equation 8-4 Mixture gas property relations.

The thermodynamic model also requires the partial derivatives of internal energy with respect to temperature, pressure and equivalence ratio. The equations used to determine these are also given by Olikara and Borman [32] and are given below in Equation 8-5.

$$\frac{\partial M}{\partial T} = \sum_i \frac{\partial x_i}{\partial T} M_i$$

$$\frac{\partial R}{\partial T} = -\frac{R_o}{M^2}\frac{\partial M}{\partial T} = -\frac{R}{M}\frac{\partial M}{\partial T}$$

$$\frac{\partial \mathrm{h}}{\partial T} = \frac{1}{M}\left[\sum_i \left(x_i \frac{\partial h_i}{\partial T} + \frac{\partial x_i}{\partial T} h_i \right) - \frac{\partial M}{\partial T} h\right]$$

$$\frac{\partial u}{\partial T} = \frac{\partial h}{\partial T} - R - \frac{\partial R}{\partial T} T$$

Note that $\frac{\partial h_i}{\partial T} = c_{pi}$

For the partial derivatives with respect to p and F (equivalence ratio),

replace $\partial/\partial T$ with $\partial/\partial p$ and $\partial/\partial F$

The exceptions being

$$\frac{\partial \mathrm{h}}{\partial p} = \frac{1}{M}\left[\sum_i \frac{\partial x_i}{\partial p} h_i - \frac{\partial M}{\partial p} h\right]$$

$$\frac{\partial u}{\partial p} = \frac{\partial h}{\partial p} - \frac{\partial R}{\partial p} T$$

$$\frac{\partial \mathrm{h}}{\partial F} = \frac{1}{M}\left[\sum_i \frac{\partial x_i}{\partial F} h_i - \frac{\partial M}{\partial \mathrm{F}} h\right]$$

$$\frac{\partial u}{\partial F} = \frac{\partial h}{\partial \mathrm{F}} - \frac{\partial R}{\partial \mathrm{F}} T$$

Equation 8-5 Equations for the calculation of the partial derivatives of the gas properties.

8.3.3. Equilibrium Combustion Products Model

The Equilibrium Combustion Products model described by Olikara and Borman [32], is adapted and presented by Ferguson [17], but Ferguson simplifies the development by not considering elemental Nitrogen or Argon. On inspection of the procedure required to perform the necessary calculations, it appears that the simplification does not lead to any significant reduction in the complexity of the calculations. Furthermore, the development given by the original authors is easier to follow and more

logically presented. Therefore the model used is based entirely on that presented by Olikara and Borman [32] and therefore includes all twelve product species including elemental Nitrogen and Argon. The model and solution technique is well dealt with by the authors and no detailed derivation of the model was undertaken as each step is well explained and easily followed. The important steps of the development of the model and solution technique are outlined below in Equation 8-6 to Equation 8-12.

The basis of the equilibrium combustion products model is a solution to the atom balance equations from the chemical reaction equation of fuel and air forming the twelve product species. This equation is given in Equation 8-6 where x_1 through x_{12} are mole fractions of the product species and x_{13} is the moles of fuel required to react with one mole of air. F is the reactant equivalence ratio.

$$x_{13}\left[C_nH_mO_lN_k + \frac{n+m/4-l/2}{F}\{O_2 + 3.7274N_2 + 0.0444AR\}\right] \rightarrow$$
$$x_1H + x_2O + x_3N + x_4H_2 + x_5OH + x_6CO + x_7NO +$$
$$x_8O_2 + x_9H_2O + x_{10}CO_2 + x_{11}N_2 + x_{12}Ar$$

Equation 8-6 Chemical reaction equation of hydrocarbon fuel in air used by the equilibrium combustion products model.

The five-element (C, H, O, N and Ar) atom balances plus the identity that the products mole fractions must add up to unity produces 6 equations. Simplifying the left side of Equation 8-6 gives:

$$x_{13}\left[nC + mH + rO_2 + r'N_2 + r''Ar\right]$$

where

$$r = \frac{l}{2} + r_O$$

$$r' = \frac{k}{2} + 3.7274r_O$$

$$r'' = 0.0444r_O$$

$$r_O = \left(n + \frac{m}{4} - \frac{l}{2}\right)\Big/F$$

Equation 8-7 Simplification of the left side of the reaction equation used by the equilibrium combustion products model.

The atom balances then become:

$$\text{C balance: } x_6 + x_{10} = nx_{13}$$
$$\text{H balance: } x_1 + 2x_4 + x_5 + 2x_9 = mx_{13}$$
$$\text{O balance: } x_2 + x_5 + x_6 + x_7 + 2x_8 + x_9 + 2x_{10} = 2rx_{13}$$
$$\text{N balance: } x_3 + x_7 + 2x_{11} = 2r' x_{13}$$
$$\text{Ar balance: } x_{12} = r'' x_{13}$$

Equation 8-8 Atom balances used by the equilibrium combustion products model.

The sixth equation is the simple identity that the sum of all the mole fractions must be unity, as given below:

$$\sum_{i=1}^{12} x_i = 1$$

Equation 8-9 Mole fraction identity.

The above give 6 equations in 13 unknowns, therefore 7 more equations are required. The 7 equations used are the equilibrium constant equations for 7 non-redundant hypothetical reactions. These equations are the equilibrium equations assuming ideal gas behaviour. It may be argued that at the high pressures and temperatures attained during combustion, deviations from ideal behaviour may be significant. This was investigated by Diab [43] and this is briefly considered here. The computational handling of real gas equilibrium entails the inclusion of terms containing gas fugacities. Fugacity is a gas property, which is a measure of deviation from ideal gas behaviour. The computation of fugacity is complex, and requires extra computational power. Olikara and Borman [32] developed this ideal gas based solution method in 1975 when the available computational power was far from the present state of the art. Therefore, if it is found that the deviation from ideal gas behaviour is significant, then the addition of these factors may be justified. However, Diab found that the addition of the fugacity term into these equilibrium equations, at temperatures and pressures typical of the maximum attained in a SI engine combustion chamber, had little effect on the results obtained. Therefore the simple partial pressure based equilibrium equations are used, and those equations used to generate the model are given below in Equation 8-10.

Reaction	Partial Pressure Equilibrium Constant
$\frac{1}{2}H_2 \Leftrightarrow H$	$K_1 = \frac{x_1 p^{\frac{1}{2}}}{x_4^{\frac{1}{2}}}$
$\frac{1}{2}O_2 \Leftrightarrow O$	$K_2 = \frac{x_2 p^{\frac{1}{2}}}{x_8^{\frac{1}{2}}}$
$\frac{1}{2}N_2 \Leftrightarrow N$	$K_3 = \frac{x_3 p^{\frac{1}{2}}}{x_{11}^{\frac{1}{2}}}$
$\frac{1}{2}H_2 + \frac{1}{2}O_2 \Leftrightarrow OH$	$K_5 = \frac{x_5}{x_4^{\frac{1}{2}} x_8^{\frac{1}{2}}}$
$\frac{1}{2}O_2 + \frac{1}{2}N_2 \Leftrightarrow NO$	$K_7 = \frac{x_7}{x_8^{\frac{1}{2}} x_{11}^{\frac{1}{2}}}$
$H_2 + \frac{1}{2}O_2 \Leftrightarrow H_2O$	$K_9 = \frac{x_9}{x_4 x_8^{\frac{1}{2}} p^{\frac{1}{2}}}$
$CO + \frac{1}{2}O_2 \Leftrightarrow CO_2$	$K_{10} = \frac{x_{10}}{x_6 x_8^{\frac{1}{2}} p^{\frac{1}{2}}}$

where p is the pressure in atmospheres.

Equation 8-10 Seven hypothetical equilibrium reactions used.

The above introduces the assumption that equilibrium conditions are achieved during combustion. The chemistry associated with all the products except NO are known to be fast enough that this assumption is valid ([15] and [17]). The reactions involved in the formation of NO are rate limited and thus should be dealt with in an appropriate manner. However, it is commonly ignored if the intended purpose is for the calculation of gas properties, as NO is produced in such small mole fractions (maximum mole fraction $\approx$ 0.01) that this introduces little error.

The equilibrium constants have been curve fitted from the JANAF Thermochemical Tables and can easily be calculated with an algorithm given the equilibrium gas temperature [32]. The carbon and argon atom balances given in Equation 8-8 are rearranged and used to eliminate x_{12} and x_{13} from the three remaining atom balances and the mole fraction identity. Furthermore, the equilibrium constant reactions given in Equation 8-10 can be rearranged such that x_1, x_2, x_3, x_5, x_7, x_9 and x_{10} can be written in terms of x_4, x_6, x_8 and x_{11}, K_1, K_2, K_3, K_5, K_7, K_9 and K_{10} and the gas pressure. Substituting these into the four remaining equations produces four non-linear equations in four unknowns. In order to solve these non-linear equations a Taylor series expansion is used as follows:

Let the four non - linear equations be symbolically represented by

$f_j(x_4, x_6, x_8, x_{11}) = 0, \quad j = 1, 2, 3, 4$

let the vector

$[x_4^{\,1}, x_6^{\,1}, x_8^{\,1}, x_{11}^{\,1}]$ be an approximation to the true solution vector

$[x_4^{\,*}, x_6^{\,*}, x_8^{\,*}, x_{11}^{\,*}]$, then

$\Delta x_i = x_i^{\,*} - x_i^{\,1}, \quad i = 4, 6, 8, 11$

neglecting the second order and higher partial derivatives this gives a set of linear equations for the four unknown corrections, Δx_i :

$$f_j + \frac{\partial f_j}{\partial x_4}\Delta x_4 + \frac{\partial f_j}{\partial x_6}\Delta x_6 + \frac{\partial f_j}{\partial x_8}\Delta x_8 + \frac{\partial f_j}{\partial x_{11}}\Delta x_{11} \cong 0, \quad j = 1, 2, 3, 4$$

where functions f_j are evaluated at the vector of the approximation to the solution.

Equation 8-11 Details of Taylor expansion used to linearise the non-linear equations.

This set of linear equations can then be solved for Δx_4, Δx_6, Δx_8 and Δx_{11} and an iterative procedure undertaken until the corrections are less than a specified tolerance. An initial estimate is required to get the iteration started. By making some further assumptions and simplifications, an acceptable starting point is found. If the products are assumed to consist only of H_2, CO, O_2, H_2O, CO_2, N_2 and Ar and the same simplification procedure is followed as before, a single equation with unknown mole fractions of x_8 and x_{13} is attained. x_{13} can be approximated by the mole fraction identity and the assumption that a lean or stoichiometric mixture will result in no CO and a rich mixture in no O_2 being produced. Thus a single equation in a single unknown, x_8, results, which can be solved by Newton's method. The remaining mole fractions are then easily found from the resulting rearranged equations.

The above results in the molar concentrations of the 12 product species, but the two-zone model for burn rate prediction requires the rates of change of certain gas properties with respect to temperature, pressure (and equivalence ratio if diesel combustion is to be studied). This requires the rates of change of species concentration with respect to these same variables. Differentiating the four non-linear equations given in Equation 8-11 with respect to temperature results in the differential equation given in Equation 8-12.

differentiating

$f_j(x_4, x_6, x_8, x_{11}) = 0, \quad j = 1,\ 2,\ 3,\ 4$

results in

$$\frac{\partial f_j}{\partial T} + \frac{\partial f_j}{\partial x_4}\frac{\partial x_4}{\partial T} + \frac{\partial f_j}{\partial x_6}\frac{\partial x_6}{\partial T} + \frac{\partial f_j}{\partial x_8}\frac{\partial x_8}{\partial T} + \frac{\partial f_j}{\partial x_{11}}\frac{\partial x_{11}}{\partial T} = 0 \qquad j = 1,\ 2,\ 3,\ 4$$

Equation 8-12 Differentiation of the four non-linear equations with respect to temperature.

It can be seen that the coefficient matrix is the same for this equation as that used to solve for the species concentrations as given in Equation 8-11. The partial derivatives with respect to pressure and equivalence ratio are identical except that p and F replace T. These similarities result in a simplified computational procedure, necessitating only the recalculation of the [B] vector for the matrix solution for each calculation as the [A] matrix is the same (matrix equation of the form [A][x]=[B]).

The validation of the equilibrium products model is presented below in Section 11.3

8.3.4. Heat Transfer Sub-Model

Heat transfer forms an important sub-model required by any detailed heat release analysis, for this project the heat release model used by the single-zone analysis was retained. The heat transfer model, originally proposed by Woschni [44] , but with modifications made by Heywood [15] had been used in the single-zone analysis. This has proven in the past to be a sufficiently accurate model, both by in-house use of the Racer program ([41] and [45]) and in literature where this type of model has been used ([15], [17], [30], [40], [41] and [44]). However, in studying the model some recommendations can be made as to possible improvements, and this will be discussed in detail here.

The original model - Woschni's Heat Transfer Coefficient

The single-zone heat release model incorporated in Racer is based on the development by Gatowski et al [40]. The actual model implementation is described in detail by Mc Laren [41]. The heat transfer sub-model used by Gatowski et al is the model proposed by Woschni [44], but Mc Laren improved on this by adding the effect of the swirl motion imparted to the inlet charge of some engines. The improved implementation follows that discussed by Heywood [15]. In studying the heat release analysis, it was seen that the development given in the original presentation of Woschni's formula [44], the author used mixed units, whereas the formula used by Gatowski et al [40] was consistently in SI units. However, the actual equation coefficient was not remarkably different (131 as compared to 126). In order to investigate this, and to gain a better understanding of the heat transfer model, an attempt was made to derive the formula. This required following the mathematical procedure described in the original presentation of the formula [44], but using consistent SI units. This was successfully accomplished and is given in Appendix C. For the purpose of this discussion the functional form of the equation is given here in Equation 8-13 and the function of the relevant parts discussed.

$$h = C_0 d^{-2} P^{0.8} T^{-0.53} \left[C_1 c_m + C_2 \frac{V_s T_1}{P_1 V_1} (P - P_0) \right]^{0.8}$$

h = heat transfer coefficient [watt/m^2.K]

d = characteristic length, bore is used [m]

P = cylinder pressure [atm]

P_0 = cylinder pressure for motored conditions [atm]

T = mean fluid temperature [K]

P_1, V_1, T_1 = cylinder pressure, volume and mean fluid temperature at some known reference condition

C_0 = equation coefficient

C_1, C_2 = calibration constants

c_m = mean piston speed

V_s = swept volume

Equation 8-13 Form of the heat transfer coefficient calculation proposed by Woschni.

The calculation of the heat transfer coefficient is based on forced turbulent convective heat transfer across a flat plate. The basis of the study of this type of heat transfer mechanism is that the dimensionless groups of the Nusselt, Reynolds and Prandtl numbers are related in the manner shown in Equation 8-14.

$$Nu = aRe^m Pr^n$$

Equation 8-14 Dimensionless group relationship for forced turbulent convective heat transfer across a flat plate.

The heat transfer coefficient calculation given in Equation 8-13, is a reduction of this equation making the assumption that, for the working fluid, the Prandtl number is constant and close to unity. Therefore the Prandtl number falls out of the equation since unity to any power remains unity. The group of factors outside the square brackets includes a coefficient, which derives from a composite of the coefficients used to calculate fluid properties from fluid temperature and pressure. The dimension term, *d*, derives directly from the characteristic dimension terms in the Nusselt and Reynolds numbers, while the pressure and temperature terms are again as a result of the calculation of fluid properties.

The term in the brackets is a term used to account for the relative velocity between the fluid and surface and originates from the velocity term in the Reynolds number. As there is no simple way of directly calculating an instantaneous fluid velocity within the chamber, a method of approximating this velocity is required. The assumption is made that the velocity is imparted onto the fluid by two mechanisms, the motion of the piston and the expansion of the burned gas due to combustion. Therefore, the velocity term is separated into two distinct parts to account for this. The velocity due to piston motion is considered in the first term, and the mean piston speed is used to approximate this. The coefficient C_1 is used to calibrate the engine speed velocity effects to a particular engine configuration. The second term accounts

for the added velocity caused by the combustion itself, and it too has a coefficient, C_2, for calibration to the specific engine configuration.

During the gas exchange process the relative velocities are high, and therefore a large C_1 is used (C_2 is zero as there is no combustion). During compression the gas velocity will decrease due to friction, therefore a smaller C_1 is employed (C_2 is still zero). The value of C_1 is held the same once combustion has begun and throughout expansion. However, during combustion, velocity is added to the gas due to the expansion from the energy addition in the form of heat. The burning gas expands drastically as heat is released, displacing unburned and burned gas away from the combustion zone. Thus an additional velocity is imparted to the gas which is nearly proportional to the rate of heat release, and decays after combustion due to fluid friction. Therefore a term having an appropriate velocity/time profile needs to be added to the velocity due to piston motion. Heat release rate information is not available at this point in the process for it to be used to determine this profile. Woschni indicates that the increase in pressure or temperature due to combustion have certain properties which are similar in nature to this profile: they are zero before combustion begins, increase as combustion takes place and then decay. The temperature increase is a measure of the change in internal energy of the working gas due to combustion only. The profile of this difference in gas temperatures is seen to rise sharply after combustion initiation, but to decay too slowly thereafter. The profiles for the difference between measured cylinder pressure and calculated cylinder pressure for a motored engine more closely approximates the desired profile. This term of measured pressure minus the motored pressure is therefore added to the equation with a group of terms that relate this pressure difference to the heat release rate. This follows from the ideal gas relation and the change in gas internal energy. The term $(P-P_0)$ is multiplied by the cylinder volume V_s and then divided by the cylinder charge mass (P_1V_1/T_1) and thus takes into account the dependence on the change in internal energy.

Woschni [44] did extensive testing to calibrate C_1 and C_2 to a specific engine configuration. Ideally the coefficients should be determined for each different engine configuration. However, in the absence of more detailed information, or without proceeding through an extensive experimental procedure similar to that employed by Woschni, these same coefficients are often used for all engine types investigated. An additional term may be added to account for additional velocity imparted to the inlet charge in the form of swirl as discussed by Heywood [15]. However, it must be realised that if the coefficient C_1 is calibrated for a specific engine configuration that has induced swirl, then this extra relative velocity has already been accounted for by the calibration coefficient.

A note needs to be added that Woschni's [44] equation and derivation appears not to take any radiation heat transfer into account. However, the author defends this in a closing discussion by stating that the effect of radiation is accounted for in the combustion related term. It is stated that, even though radiation heat transfer is proportional to the difference between the fourth power of the temperatures of the radiating bodies, in this case the gas and the chamber wall ($h_{rad} \propto (T^4_{gas} - T^4_{wall})$) the effect in the engine is somewhat simpler. The radiating gas is at the flame temperature, which is almost independent of parameters other than fuel type. Therefore the T_{gas} term becomes a constant and the rate of heat transfer

due to radiation becomes affected only by changes in the emissivity. The emissivity of the radiating body, the flame, is proportional to the mass of radiating gas and this is proportional to the rate of heat release. Therefore, the radiative component of the heat transfer has a similar effect to the velocity due to combustion and the two cannot be separated given the experimental procedure used to determine the constants and the radiative heat transfer is thus inherently accounted for.

The selection of, and validation of the coefficients chosen is presented below in Section 9.2.2.

Possible Improvements to the Heat Transfer Sub-Model.

The development of the heat transfer coefficient equation as given in Appendix C makes the assumption that air is the working fluid. In the absence of any empirical correlation's for air/fuel mixtures or combustion products mixtures, this is the best possible assumption to make. However, the two-zone heat release model utilised requires the calculation of equilibrium combustion products and this information may be used to calculate the gas properties required for the Nusselt, Reynolds and Prandtl numbers. This may be quite complicated as the calculation of the viscosity and conductivity of gas mixtures may not simply be a weighted summation like the other properties calculated in the gas property calculations already employed ([46] and [41]).

8.3.5. NO Formation Model

As discussed previously in Section 2.3.1, the formation of the oxides of Nitrogen in the combustion chamber is rate limited and thus the equilibrium predictions for NO are expected to be incorrect. This error is considered insignificant for the primary purpose of the equilibrium model, which is the prediction of the properties of the working fluid for use in the heat release modelling, as the NO concentrations are small. The statistical evaluation of the experimental results, as discussed below in Section 12.2, has indicated an unexpected correlation for the exhaust content of NO and gas temperature parameters. In order to evaluate this trend, further study of the formation mechanisms of NO was undertaken and a detailed NO formation model was added to the combustion rate program in order to investigate the experimental results further.

The formation mechanisms for NO in spark ignition engines is well covered in the literature [47, 15, 48, 49, 50, 18]. Three separate mechanisms are identified in the literature: the "thermal", the "prompt" and the "nitrous oxide" mechanisms. The thermal mechanism is the more important for spark ignition engines [18], while the prompt mechanism may contribute to the final NO content of the exhaust in fuel rich spark-ignition combustion [50]. The nitrous oxide mechanism is only appropriate for very lean mixtures and is thus inappropriate for spark-ignition engines. It is apparent that most NO modelling for spark-ignition engines only considers the thermal mechanism as it is by far the most significant [50].

The thermal mechanism was first proposed by Zeldovich and improved by Lavoie et al and these models are usually referred to as the extended Zeldovich mechanism [15, 17, 18]. The mechanism of formation relies on the thermal decomposition of the Nitrogen in the air charge, and Zeldovich proposed two rate-

controlled reactions involving both nitrogen and oxygen. Lavoie et al added a reaction involving OH. The reactions are given below in Equation 8-15

$$O + N_2 = NO + N \ldots\ldots\ldots\ldots \text{reaction } 1$$
$$N + O_2 = NO + O \ldots\ldots\ldots\ldots \text{reaction } 2$$
$$N + OH = NO + H \ldots\ldots\ldots\ldots \text{reaction } 3$$

Equation 8-15 Rate controlled reactions for the extended Zeldovich mechanism for the formation of NO.

Following the conventions of non-equilibrium chemistry, the rate of formation of NO is expressed in terms of the rate constants, in both the forward and reverse directions, and the species concentrations. This is indicated below in Equation 8-16.

$$\frac{d[NO]}{dt} = k_1^+[O][N_2] + k_2^+[N][O_2] + k_3^+[N][OH] - k_1^-[NO][N] - k_2^-[NO][O] - k_3^-[NO][H]$$

where :

k_n^+ is the forward rate constant for the nth reaction and k_n^- the reverse rate constant

[ ] denotes species concentrations in moles per cubic centimetre

Equation 8-16 Rate controlled formation of NO.

A similar equation is written for the formation of atomic nitrogen (Equation 8-17). The concentration of atomic nitrogen is low compared to the other species and thus a common simplifying assumption is made that the rate of change of atomic nitrogen is zero.

$$\frac{d[N]}{dt} = 0 = k_1^+[O][N_2] - k_2^+[N][O_2] - k_3^+[N][OH] - k_1^-[NO][N] + k_2^-[NO][O] + k_3^-[NO][H]$$

Equation 8-17 Rate controlled formation of atomic nitrogen.

This allows the reduction of Equation 8-16 as shown in Equation 8-18 below.

$$\frac{d[NO]}{dt} = 2k_1^+[O][N_2]\frac{1 - [NO]^2/(K[O_2][N_2])}{1 + k_1^-[NO]/(k_2^+[O_2] + k_3^+[OH])}$$
$$\text{where } K = (k_1^+/k_1^-)(k_2^+/k_2^-)$$

Equation 8-18 Reduction of Equation 8-16 by substitution of the assumption in Equation 8-17.

The concentrations of all the species in Equation 8-18, except NO, are assumed to be in equilibrium as the chemistry associated with them is very much faster than that associated with NO. The equilibrium concentrations of these species are determined from the normal equilibrium calculation described in Section 8.3.3 and these can be substituted into Equation 8-18. A further simplification can be made in

that, by definition, for equilibrium, the forward and reverse reactions are occuring at the same rate. This is indicated below in Equation 8-19 where the reduced form of the equation for the rate of change of NO is also presented.

$$R_1 = k_1^+[O]_e[N_2]_e = k_1^-[NO]_e[N]_e$$
$$R_2 = k_2^+[N]_e[O_2]_e = k_2^-[NO]_e[O]_e$$
$$R_3 = k_3^+[N]_e[OH]_e = k_3^-[NO]_e[H]_e$$

where $[\ ]_e$ refers to the equilibrium concentration

$$\frac{d[NO]}{dt} = \frac{2R_1\left(1-\alpha^2\right)}{1+\alpha R_1/\left(R_2+R_3\right)}$$

where $\alpha = \frac{[NO]}{[NO]_e}$ the fractioanl attainment of equilibrium

Equation 8-19 Equations indicating that forward and reverse reactions occur at equivalent rates at equilibrium, and the simplified rate controlled equation for NO formation.

Thus the rate of formation of NO can be determined from knowledge only of the reaction rates of three reactions, the equilibrium concentrations of five species and the actual current concentration of NO. As expected, when the NO concentration is less than equilibrium prediction, ($\alpha < 1$) then NO is formed $\left(\frac{d[NO]}{dt} > 0\right)$, and conversely, when NO concentrations are greater than equilibrium predictions, ($\alpha > 1$) then NO is decomposing $\left(\frac{d[NO]}{dt} < 0\right)$.

The rate constants for the three reactions have a strong temperature dependence. Typical values are given below in Table 8-1. There are a great variety of different rate constants presented in the literature, illustrating the difficulty in establishing these with certainty. Furthermore, these are typically determined in controlled experitments at temperatures and pressures far lower than are typical in internal combustion engines [18].

Table 8-1 Rate constants applied to the extended Zeldovich mechanism from three different sources.

Forward Rate Constant*	Heywood [15]	Ferguson [47]	Blumberg & Kummer [48]
k_1 [O+N_2=NO+N]	1.6 x 10^{13}	1.8 x 10^{11}exp(-38370/T)	1.32 x 10^{13}
k_2 [N+O_2=NO+O]	6.4 x 10^{9}Texp(-3150/T)	1.8 x 10^{7}exp(-4680/T)	1.81 x $10^{8}T^{1.5}$exp(-3000/T)
k_3 [N+OH=NO+H]	4.1 x 10^{13}	7.1 x 10^{10}exp(-450/T)	4.2 x 10^{13}

* Units cm^3/mol·sec except Ferguson where units are m^3/kmol·sec

From the strong temperature dependence and the fact that time is important from the rate controlled chemistry, it is apparent that it is necessary to handle the burned gas as a multi zone model [15, 50,18]. This is due to the strong temperature gradients that exist in the burned gas as a result of the post

combustion compression and expansion (as discussed in Section 2.3.1), as well as the temperature dependence of the equilibrium species concentrations.

The main combustion analysis model that is applied in Racer, dealt with only two discrete zones, the unburned and burned gas zones. The burned gas was treated as a fully mixed model which included the equilibrium model. Thus a entirely separate, un-mixed model is required to handle the Zeldovich mechanism calculations. This required setting up an entirely separate data structure to handle the discrete burned zone elements. This model had to incorporate its own, separate equilibrium model as the single burned zone model had to be left intact. The object oriented computing methodology allowed the incorporation of the original equilibrium model called from the new data structure, with the local zone gas temperatures. The NO model created is a multi-zoned, zero dimensional, adiabatic model similar to that described in the literature [47, 15, 48, 50, 18]. Specifically, the treatment by Blumberg and Kummer [48] is followed, as it provided the most appropriate equations in terms of the units employed.

The model creates a new burned zone element for each crank angle after ignition. For each new element, the model first computes the adiabatic flame temperature to deterine the starting point for that element. The equilibrium routine is then run for that element, and from the temperature and equilibrium species concentrations (converted from mole fraction to mol/cm^3), the rate of NO formation is then determined as per Equation 8-19. This is then converted back to units of mol fraction and integrated over the time per degree. For succesive time steps, the new temperature for this element is determined as the element is compressed or expanded by the change in cylinder pressure. Thus each zone, or element to burn, traces its own temperature time history and has different equilibrium species concentrations and thus different NO concentrations. Each element is tracked separately resulting in a fully unmixed model. There is no allowance for heat transfer between zones or with the cylinder walls. Raine et al [50] have shown that including heat transfer in the model would reduce the predicted NO concentrations to some degree. However, as the authors were predicting in-cylinder pressure from predetermined heat release curves (the opposite of what is being done in this study), the lack of heat transfer had a magnifying effect and the peak cylinder pressures were significantly higher for the adiabatic case versus the case with heat transfer. With a zero dimensional model, it is impossible to handle heat transfer without incorporating some arbitrary assumptions with regard to cylinder geometry, flame structure and gas motion.

The validation of the NO prediction model is presented in the discussion of the results in Section 11.4.

8.3.6. Dexcription of Computer Code

The Racer program, written in Borland Pascal for Windows (version 7.0) was upgraded to include the two-zone heat release prediction model and is now called Racer 2. The program is written in a structured, unit based style and therefore the working code for the additions was added in three separate units. The two-zone heat release prediction code was added in the unit called “brmodel2.pas” which independently accesses the unit that returns to it the various gas properties as required. This unit is called “gasprops.pas” which in turn has independent access to the unit that calculates the equilibrium species

concentrations, which is called “eqbm.pas”. The user interface was also updated to include the inputs and switches necessary to operate the two-zone model. Racer has a useful graphics interface that plots the more important results, and this was also updated to include the pertinent two-zone results. The original single-zone model was left intact, as it is a reliable, user friendly, and fast heat release analysis tool in itself.

The heat transfer sub-model used by the two-zone heat release prediction is based on the same model as for the single-zone heat transfer. The original single-zone code included the heat transfer coefficient calculation in the heat release unit itself, and therefore the two-zone unit would not have access to these routines. Therefore a fourth unit was written, based on the same calculation routines. However the new heat transfer coefficient calculation unit, called “rwoschni.pas”, allows for different heat transfer coefficients in the two distinct zones. The velocities are assumed to be the same in the two zones as the velocity component added by combustion is due to expansion in the combustion zone (flame), which compresses and displaces both the burned and unburned zones. The pressure is also the same in both of the zones as there is assumed to be no pressure gradient in the chamber, but the temperature, and therefore the gas properties, are different. Thus two different heat transfer coefficients are predicted for the two zones. At present there is no heat transfer coefficient predicted for energy transfer between the zones.

Furthermore, the rwoschni.pas unit also computes the actual rate of heat transfer between the two zones and the cylinder surfaces. In order to do this it also needs to compute the areas of contact and the temperature difference. It computes the area of contact for the two distinct zones based on the assumption as described in Section 8.3.1. The wall temperatures are assumed to be constant throughout the combustion chamber.

The structure of the Racer 2 program, including the data capture and single-zone is given below in Figure 8-4.

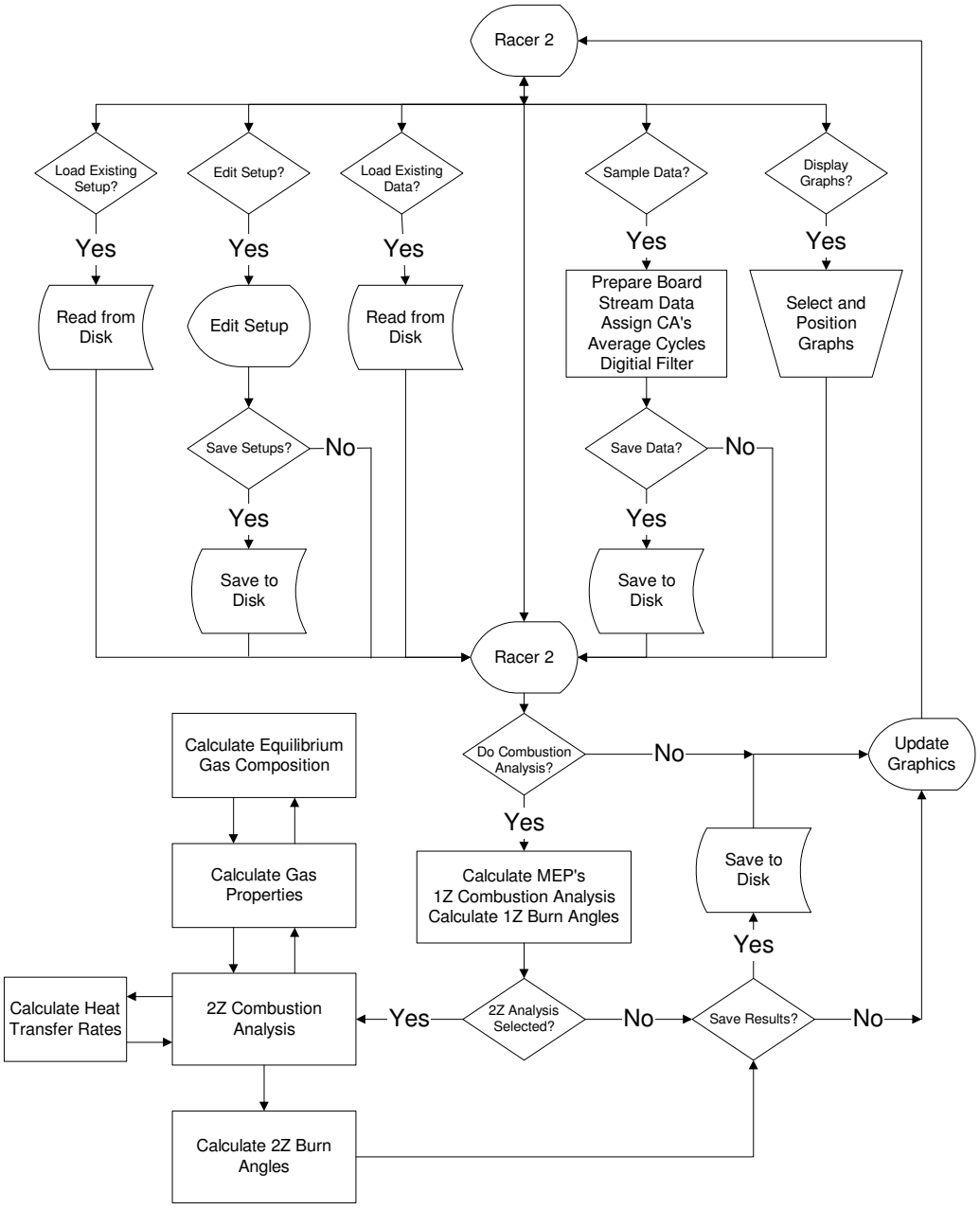

Figure 8-4 Flow chart of Racer 2 program structure.

Due to the unitised nature of the two pieces if code, gasprop.pas and eqbm.pas, they have been successfully and independently included into an engine simulation model. This was done as part of a Masters level research project conducted within the research group [51]. Furthermore, the development and understanding of the two-zone burn rate prediction model has been used to assist the development of the two-zone engine simulation model. This engine simulation model includes advanced mass flow modelling of the intake and exhaust processes using the method of characteristics, and is thus a very powerful engine development tool.

9. COMBUSTION ANALYSIS

Combustion analysis is a powerful tool to extract meaningful information from recorded cylinder pressure versus crank angle data, however there are a number of aspects that require careful attention in order to produce reliable results. The combustion analysis models require that the raw recorded pressure data be correctly scaled and that other model input parameters be correctly set, otherwise misleading results may be generated. The selection of the methods used for selecting these parameters, as well as the detailed description of the most important parameters of the combustion analysis routines used in this research are presented in this section.

9.1. Pressure Referencing

Piezoelectric pressure transducers used for dynamic cylinder pressure measurement do not record absolute pressure and therefore the pressure/crank angle curve needs to be referenced or scaled to provide absolute pressures [52]. Although referencing was performed during the data capture with Racer by inputting the inlet manifold absolute pressure as read from the engine steady state recording system (ETA), it was decided to re-scale the curve during data processing. This is necessary as scaling at the time of data capture is based on an assumed inlet valve closure and absolute inlet manifold pressure, which assumes that there is no inlet charge flow at this point, and therefore there is no pressure drop across the valve.

The re-scaling of the pressure data was investigated using the measured inlet manifold pressure, inlet manifold air/vapour temperature and charge mass as calculated from measured air and fuel consumption and inlet valve closure (IVC). The inlet manifold air temperature was measured in an inlet ram pipe in the manifold itself (as described in Section 6). However, the actual charge temperature at the point of inlet valve closure will be affected by heat transfer to the gas in the inlet port and evaporative cooling of the fuel, the magnitude of neither effect being easily determined. Static inlet valve closure was measured to be approximately 135° CA BTDC. A further complicating factor is the dynamic nature of the inlet manifold ram pipes, which can be seen by the oscillatory nature of the cylinder pressure during the inlet phase as shown in Figure 9-1.

Lancaster et al [52] made the assumption that the cylinder pressure at BDC was equal to the mean intake manifold pressure. This was justified by noting that at this point in the cycle the piston is stopped, the exhaust valve is closed, and the partially open intake valve sees little flow or pressure drop. However, the authors do point out that this procedure may be inaccurate due to pressure pulse effects in the inlet manifold. In the case of a petrol engine such as the one under investigation here, pressure pulse effects in the inlet tract become important. In fact engines such as this rely on manifold ramming effects to obtain the high specific engine power developed by modern engines. Therefore a modification is required to such a procedure.

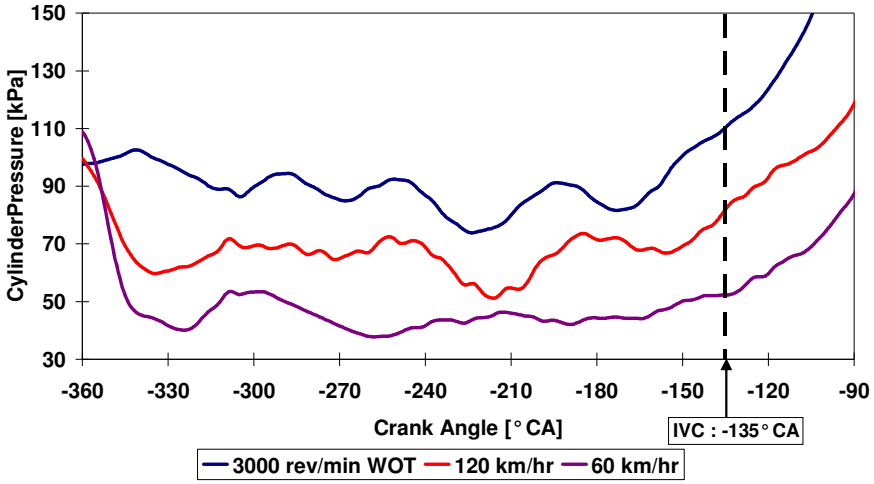

Figure 9-1 Examples of cylinder pressure during the inlet portion of the cycle at the test points at which combustion analysis was performed.

Some assumption will be required in order to calculate the cylinder pressure at some known point, given the charge mass induced, as insufficient information is available in that two independent thermodynamic properties are required. Two limiting cases were thus identified and investigated:

- Case 1: the assumption was made that the cylinder pressure at IVC was equal to the mean manifold pressure, and the charge temperature was calculated from the ideal gas law. This case assumes that there is no pressure drop across the valves, and overestimates the heat transfer to the inlet charge.
- Case 2: the assumption was made that no heat transfer takes place to the inlet charge, and the cylinder pressure was calculated at IVC from the ideal gas law. This case assumes that there is no heat transfer to the inlet charge or evaporative cooling, and overestimates the pressure drop across the valve.

The actual situation obviously lies somewhere between these two limiting cases. Calculations were performed, respectively assuming both of these limiting cases, for several tests at each load point. These calculated results were then averaged to reduce experimental scatter. The results are shown in Table 9-1. The standard deviations of the differences are shown to indicate the consistency of the data.

Table 9-1 Details of the two limiting cases used to define window to approximate the inlet charge temperature increase.

	Case 1			
Load Point	Manifold Air Temperature [measured] [℃]	Cylinder Charge Temperature [calculated] [℃]	Temperature Increase [calculated] [℃]	Standard Deviation [of difference] [℃]
3000 rev/min	28.2	44.8	16.6	1.9
120 km/hr	34.4	78.9	44.5	1.6
60 km/hr	54.2	99.6	45.4	4.3

	Case 2			
Load Point	Manifold Pressure [measured] [kPa]	Cylinder Pressure [calculated] [kPa]	Pressure Difference [calculated] [kPa]	Standard Deviation [of difference] [kPa]
3000 rev/min	99.3	94.1	-5.2	0.59
120 km/hr	68.7	60.0	-8.7	0.29
60 km/hr	49.6	43.6	-6.0	0.48

Considering Case 1, it can be seen that the two throttled load points indicate similar temperature increases while the WOT conditions indicates a much lower temperature increase. Heat transfer in the manifold and cylinder during intake will be a strong function of the relative gas velocity, which is directly proportional to engine speed. The 120 km/hr load point has the highest engine speed (3760 rev/min) while the 60 km/hr load point has the lowest (1880 rev/min). However, charge temperature increase will be reduced, for a given heat transfer rate, with increased engine speed due to there being less time for heat exchange. This will tend to reduce the effect of the increased heat transfer rate due to the increased gas velocities. Furthermore, the temperature increase will be affected by a number of other factors including manifold air temperature and density, and surface temperatures. Manifold air temperatures are seen to be highest for the 60 km/hr load point and lowest at 3000 rev/min. Charge densities are highest for the 3000 rev/min load point and lowest for the 60 km/hr load point (as seen by the manifold pressures shown in Table 9-1). As for surface temperatures, it is seen that the oil temperature is highest for the 120 km/hr load point and lowest for the 60 km/hr load point (110, 107 and 90 ℃ for 120 km/hr, 3000 rev/min and 60 km/hr respectively). Engine coolant temperatures were similar for all the load points.

Another process, called reversion, is also occurring. Reversion is the process whereby, at the point of inlet valve opening, the cylinder contents are both at a higher pressure and temperature than the inlet manifold, and thus a portion of the cylinder contents expand up into the inlet manifold. This gas will then be re-induced into the cylinder and mixed with the cooler fresh charge. This will further raise the average temperature of the inlet charge.

Thus it is seen that the process of heat addition to the inlet charge in the manifold and port, along with reversion, is complex and can not easily be assumed or approximated.

Considering case 2, it can be seen that assuming there is no heat addition to the inlet charge between the inlet manifold and the cylinder at IVC, then ramming effects do not recover all the pressure loss due to friction. In other words, volumetric efficiency is still less than 100% for the load points under consideration. Any heat transfer and reversion that would occur will further reduce this volumetric efficiency.

It is thought that there is significant heat transfer in the inlet port and within the cylinder (before IVC) and therefore the magnitude of the temperature increase will be similar to that calculated in Case 1. A value of approximately two thirds of the calculated temperature increase was assumed to be a good approximation. Thus the temperature increase due to heat transfer was assumed to be 10°C for the 3000 rev/min load point and 30°C for the other two load points. The procedure of pressure re-referencing was then the following:

- calculate charge temperature as measured manifold temperature plus temperature increase due to heat transfer,
- calculate charge pressure at IVC from the ideal gas law with measured charge mass, charge temperature and cylinder volume at IVC,
- compare the calculated cylinder pressure with the measured manifold pressure, and check that calculated difference is not larger than the difference found for case 2 above.

9.2. Program Inputs

The analyses require certain parameters to perform the necessary calculations and these are input into the Racer program via menu item dialogue boxes. Certain of the parameters are common for both the single-zone and two-zone models; these are parameters such as engine specifications, operating speed and ignition timing. Some of the parameters are universal to the process of combustion analysis and are thus used by both the single zone and two-zone analysis routines. These "common inputs" are discussed below in Section 9.2.1 Due to the fundamentally different nature of the two types of analysis there are some inputs which are specific to each type. The parameters used for specifically for the single-zone analysis are discussed in Section 9.2.2 and those for the two-zone analysis in Section 9.2.3

9.2.1. Common Inputs

Figure 9-2 below shows the input menu item which contains the inputs used generically by both combustion analysis routines. The engine specifications, or *Engine Setup Geometry*, which are required are bore, stroke, connecting rod length, compression ratio, number of cylinders and crank angle at inlet valve closure. These parameters are required to calculate instantaneous cylinder volume and for calculations pertaining to the cylinder charge mass induced. The bore, stroke, connecting rod length and compression ratio were obtained from OEM specifications and service literature for the engine. The IVC value used was the static angle for valve opening, determined on the engine by measuring the relative crank angle at which the cam follower begins to rock, which for this engine was measured as –135° CA.

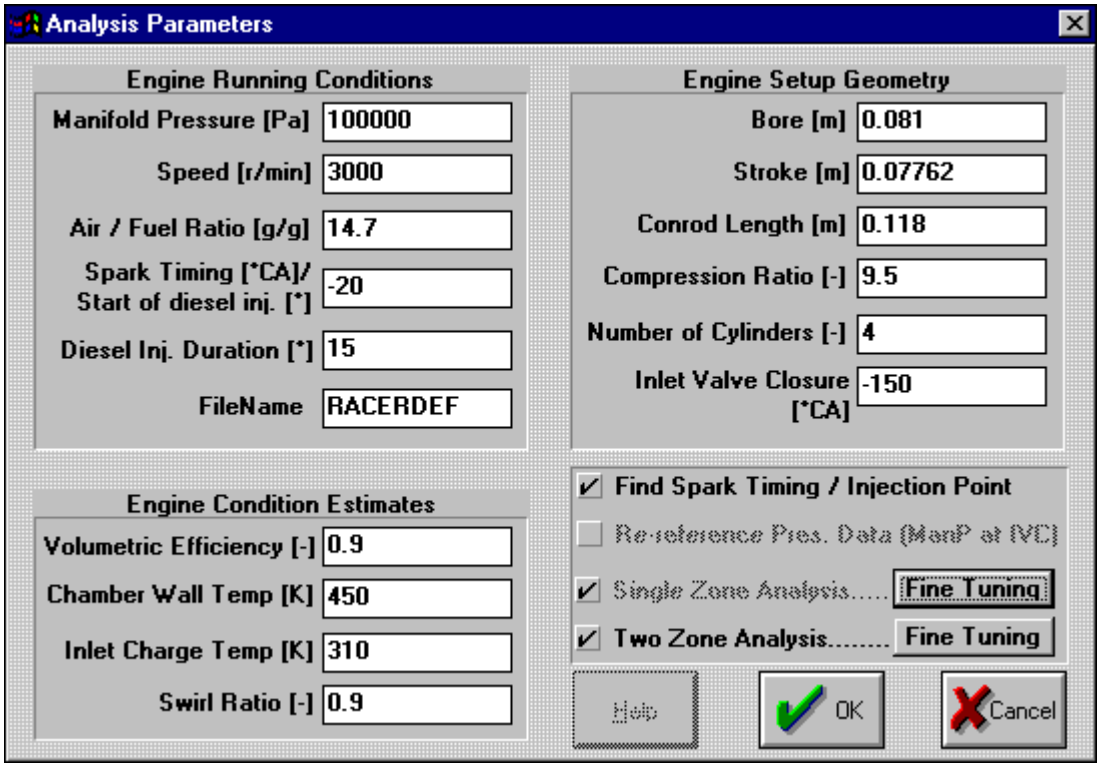

Figure 9-2 Racers default Analysis Parameters dialog box.

A number of switches are available in the block below the *Engine Setup Geometry* block. The switch *Find Spark Timing / Injection Point* instructs Racer to search data captured on a supplementary channel, to determine the relative crank angle of ignition (defined as spark timing for SI engines or injection timing for CI engines). This option was not used for this research as spark timing was manually measured and therefore this button was left unchecked. The second switch down is inactive. The last two switches select which analyses are to be conducted. The *Single-zone Analysis* is always performed (and therefore the check box is always checked and the switch is inactive), and if the *Two-Zone Analysis* is to be conducted then this check box should be checked. Next to both of these check box labels are buttons labelled *Fine Tuning*, these buttons call up dialogue boxes which contain the input fields required to manipulate the analyses. The parameters in these dialogue boxes are discussed in detail below in Sections 9.2.2 and 9.2.3.

Parameters relating to the engine load point, or *Engine Running Conditions*, include manifold pressure, engine speed, air/fuel ratio and spark timing. Engine Speed and spark timing are input directly from measurements taken during engine testing. The value used for the air fuel ratio is that calculated from the exhaust gas analysis, and verified by the measured air and fuel mass flow rates. Racer uses the manifold pressure and volumetric efficiency (under *Engine Condition Estimates*) to calculate the engine mass consumption by assuming that the cylinder pressure at IVC is equal to the manifold pressure times the volumetric efficiency. This enables the fast analysis of results during testing with assumed volumetric efficiencies. However, for more accurate analyses such as that required for this research, it is preferable to use a volumetric efficiency of 1.0 and to use the calculated cylinder pressure at IVC as used in the re-

referencing procedure described above in Section 9.1. The Diesel Injection Duration parameter is used only by the two-zone analysis for the calculation of instantaneous fuel injection rate directly into the cylinder as in a diesel engine and is therefore not relevant to this analysis.

A number of other parameters, which are not usually directly measurable, but which describe the engine condition at the specific load point, are required for combustion analysis. These include chamber wall temperature, inlet charge temperature and swirl ratio and these are input via the *Engine Condition Estimates* block.

Chamber wall temperatures vary with engine speed and load as well as with other factors including coolant and lubricant temperatures. The coolant temperature is thermostatically controlled (standard OEM thermostat fitted) while oil temperature is uncontrolled but was found to be repeatable from test to test for each load point (a cooling fan was used to cool the oil sump at the two higher load test points). Average values for the coolant and oil temperatures are given in Table 9-3. As can be seen the oil temperature varies by 20 °C between its lowest and highest value, indicating that the chamber wall temperature may vary quite considerably between the load points. A method of calculating the chamber wall temperature from measured pressure data is used to find reliable values for each load point. Chamber wall temperatures should only be load point dependant and not vary considerably from test to test, therefore the calculation was performed for a few tests at each of the three load points. A discussion of the method follows and the values used for the three load points are given in Table 9-3.

An attempt was made to calculate chamber wall temperatures based on the comparison of the instantaneous polytropic exponent during compression and the ratio of specific heats of the gas mixture. For any polytropic process the relationship between pressure and volume is given in Equation 9-1 where k is the polytropic exponent. This approach is somewhat similar to that used by Swartz and Yates [53] who were attempting to infer heat transfer rates and not wall temperatures.

$$PV^k = \text{constant}$$

Equation 9-1 Equation of polytropic process of an ideal gas.

Assuming that the inlet charge temperature is lower than the wall temperature, at some point during compression the gas temperature must be equal to the wall temperature. Therefore the heat transfer at that instant is zero, and the process becomes temporarily adiabatic (and therefore isentropic). Before this point, the wall temperatures are higher than the gas temperature and heat is being added to the gas whereas after this point the heat transfer is from the gas to the wall. Considering Equation 9-2, it can be seen that the polytropic exponent becomes the negative of the gradient of the $log(p)$ vs $log(V)$ curve. This forms a convenient way of finding the instantaneous polytropic exponent. Furthermore, it becomes obvious from the equation that if heat is added to the gas, pressure will rise more quickly than in the adiabatic case, and the gradient will be steeper. Thus k will be bigger (more negative) when heat is added. The opposite becomes true when heat is removed from the process. At the point where adiabatic

conditions occur, the process becomes truly isentropic and the polytropic exponent becomes equal to the ratio of specific heats, γ.

$$pV^k = \text{constant}$$
$$\log(p) + k\log(V) = \text{constant}$$
$$\log(p) = -k\log(V) + \text{constant}$$
$$\text{differentiating}$$
$$-k = \frac{d\{\log(p)\}}{d\{\log(V)\}}$$

Equation 9-2 The equations for polytropic compression of an ideal gas.

Therefore, by plotting the slope of the $log(p)$ vs $log(V)$ graph against crank angle, it is possible to see the crank angle at which the polytropic exponent is equal to γ. From this, the gas temperature at this crank angle can be found and therefore the chamber wall temperature. All that remains is to determine the correct γ for a fuel air mixture. Cheung and Heywood [42] give correlations for a number of different single and dual component fuels at different equivalence ratios and burned gas mass fraction. Different correlations are given for compression, combustion and expansion. The correlations given for iso-octane and indolene are very similar and would also be the most representative of a blend gasoline. The other fuels given are propane and methanol which are lighter molecules and would not be representative of commercial gasoline. The correlation for iso-octane is given below in Equation 9-3. These correlations were then used for the wall temperature determination.

$$\phi = 0.9 \qquad \gamma = 1.403 - 1.493 \times 10^{-4} T$$
$$\phi = 1.0 \qquad \gamma = 1.400 - 1.540 \times 10^{-4} T$$
$$\phi = 1.1 \qquad \gamma = 1.398 - 1.583 \times 10^{-4} T$$

Equation 9-3 Correlations for γ as given by Cheung and Heywood [42] for compression and a burned gas mass fraction of 8.5%.

Before the gas temperature at any point in the cycle can be calculated, the inlet charge temperature needs to be known as a starting point for compression. This was discussed in some detail in Section 9.1 when considering the absolute referencing of the measured pressure. The result of that process is used here and is given in Table 9-3.

Swartz and Yates [53] found that taking small crank angle windows to calculate instantaneous values of k resulted in instability of the computed k value due to digitisation errors since their data was not smoothed or filtered in any way, and it is assumed they were working with single recorded pressure traces. They found that increasing the window to 10, 20, 30 or 40° CA effectively smoothed the data and provided good estimations of the instantaneous polytropic coefficient.

In this research pressure traces were averaged over 200 or more cycles, and data smoothing was applied during the initial recording. An example of the determination of instantaneous k values from two randomly selected pressure traces, with a crank angle window of 2° CA, is displayed graphically in Figure 9-3. The portion of the cycle between inlet valve closure and TDC is displayed. Good agreement is seen between the results of the two pressure traces, and some instability early in the process (before about 90° CA) is noted. This instability early in the process, in contrast to that noted by Swartz and Yates, is probably due to pressure pulses occurring in the cylinder due to the inlet process. Swartz and Yates were working with a low engine speed, large bore CFR Octane Engine which is unlikely to have large pressure fluctuations within the inlet system like the engine under evaluation in this research. The pressure fluctuations inherent at the high engine speeds used in this research are likely to propagate into the combustion chamber and be relatively long lived. The sharp downturn after -30° CA is due to combustion. The line labelled "Gamma" is the ratio of specific heats as given by the correlations of Cheung and Heywood [42].

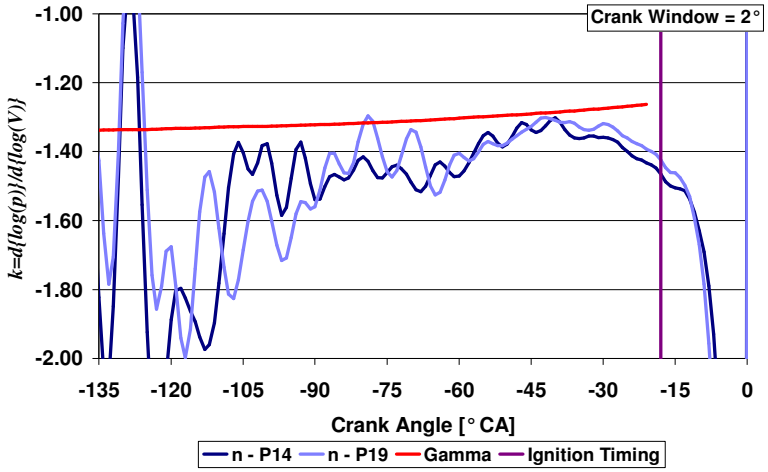

Figure 9-3 Calculated polytropic exponent and ratio of specific heats during compression (3000 rev/min WOT).

Wider crank windows of 10, 20 and 40° CA were investigated to reduce the pressure fluctuation effects and the results are seen in Figure 9-4. The desired result is the crank angle at the intersection of the instantaneous polytropic coefficient and the plot of gamma. However it can be seen that the two lines do not intersect, with the calculated polytropic coefficient always being larger than the ratio of specific heats. This is consistent with a trend observed in the burn rate results produced by combustion analysis while generating this data. Considering Figure 9-5 which shows the portion of the burn rate curve coinciding with that of Figure 9-3 and Figure 9-4, and it can be seen that the combustion analysis is predicting a small amount of heat release during compression where there is no combustion taking place. This is thought to be due to the placement of the pressure transducer which results in it being subjected to squish effects. The effect of this is that the transducer measures cylinder pressures increasingly elevated above the pure compression pressure as the piston ascends, resulting in the prediction of some apparent heat release, and larger values for k.

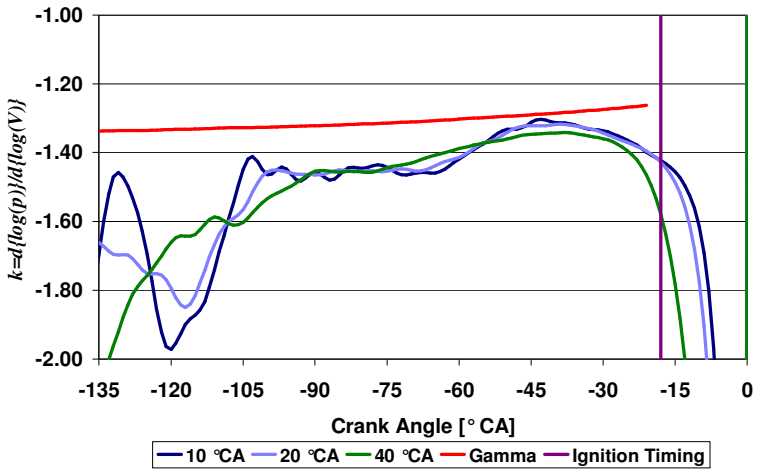

Figure 9-4 Calculated polytropic exponent and ratio of specific heats during compression (3000 rev/min WOT).

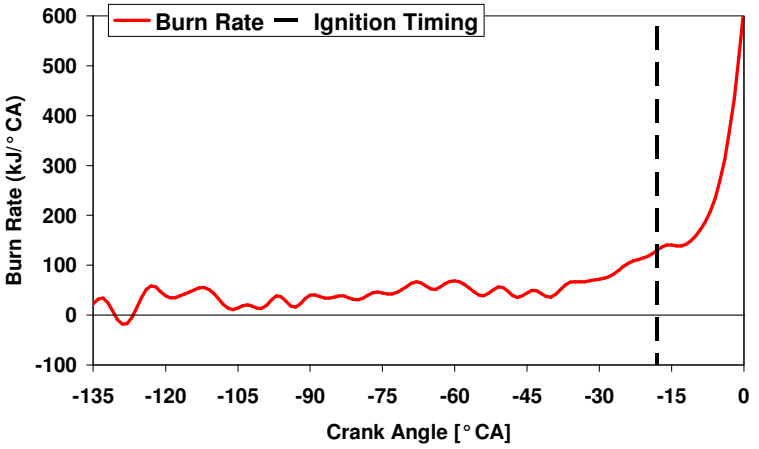

Figure 9-5 Burn Rate (single-zone model) as predicted by Racer during compression (Fuel P14 at 3000 rev/min and WOT).

Due to the failure of the method described above, an alternative method of determining wall temperatures must be sought. Valuable insight into the phenomenon was gained by studying the work of Wentworth [54]. In that study, surface temperatures were measured using purpose designed probes and correlated with exhaust hydrocarbon emission. The experimental procedures employed included the testing at various engine speeds and manifold pressures as well as different coolant types and temperatures. Thus using the results reported allows the trends of the dependence of surface temperature on these variables to be studied.

A number of factors have to be considered however. Firstly, the engine used had a grey cast iron cylinder head and cylinder block and measurements were in the cylinder head, just above the head gasket. Secondly, the engine had a relatively low compression ratio of 8.5:1. Thirdly, engine oil temperatures were controlled to be equal to the coolant temperature. The Toyota 4A-FE engine has an aluminium cylinder head, a compression ratio of 9.5:1 and oil temperatures between 1 and 20°C higher than the coolant

temperature. All of these factors are expected to make the average surface temperatures measured by Wentworth considerably different to those expected in the test engine. However, the effect of the variables mentioned above on surface temperature should have similar trends regardless of the above differences in engine specification.

The tests performed by Wentworth were with an engine speed/manifold pressure matrix as shown below in Table 9-2. Most testing was performed with a coolant temperature of 82°C, but coolant temperatures ranging from 38 to 104°C were investigated. Testing was also performed with coolants of 100% water, 100% ethylene glycol and a 50-50 water-glycol mixture. The positioning of the probes, although in the cylinder head, would provide results more representative of the top of the cylinder liner, or bore.

Table 9-2 Test matrix used by Wentworth [54].

Manifold Pressure [kPa]	Engine Speed [rev/min]			
	800	1200	1600	2000
100		✓		✓
80		✓		✓
60	✓	✓	✓	✓
40		✓		✓

The first consideration is the dependence of average surface temperatures on engine speed. Within the range of the test points, an essentially linear response is seen with increasing average surface temperature with increasing engine speed. This is demonstrated below in Figure 9-6. The dashed line represents a least squares linear fit to the test points. However, the obvious curvature displayed by the 60 kPa MAP test points indicates that extrapolation of this data is not easily possible.

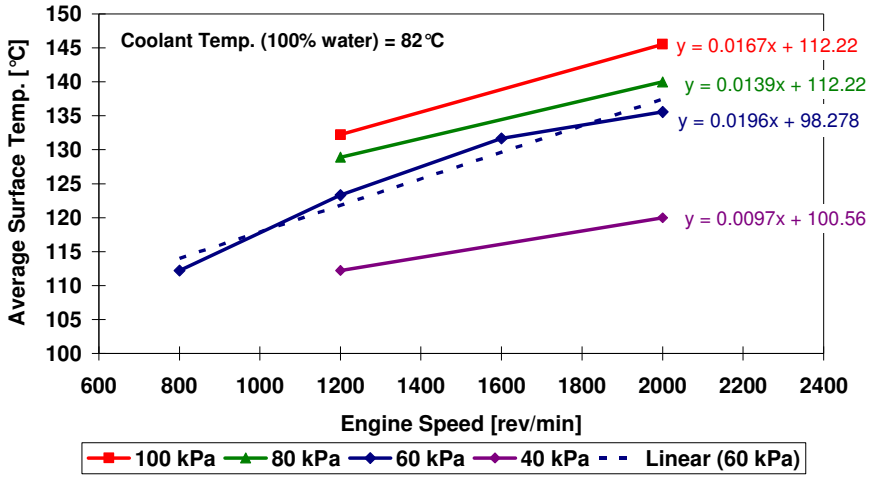

Figure 9-6 Average surface temperature as a function of engine speed (after Wentworth [54]).

Considering the effect of MAP on average surface temperature, it is again apparent that an essentially linear response can be seen. This is more directly useful as no extrapolation is necessary as in the engine speed case as the full engine operating envelope is represented (40 kPa - very light load too 100 kPa - WOT).

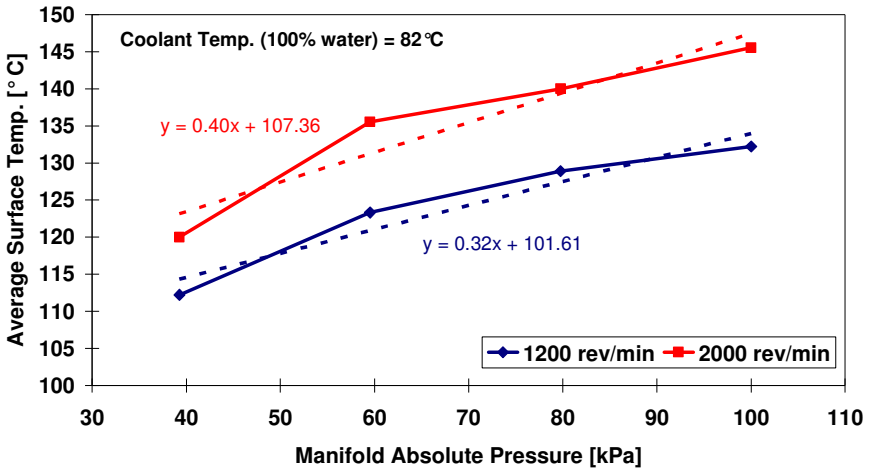

Figure 9-7 Average surface temperature as a function of manifold absolute pressure (after Wentworth [54]).

The effect of coolant type and temperature is displayed below in Figure 9-8. The effect of coolant temperature on the average surface temperature is linear, as expected. It must be noted that these results do not reflect the effects on piston temperatures which may not be as directly effected by coolant temperatures, but possibly have a higher dependence on oil temperatures. It can be seen that surface temperatures may be as much as 36°C higher when using 100% ethylene glycol than when using 100% water. This is due to the reduced thermal capacity of the glycol compared to water. The Toyota 4A-FE test engine used a 40:60 glycol:water mix as coolant.

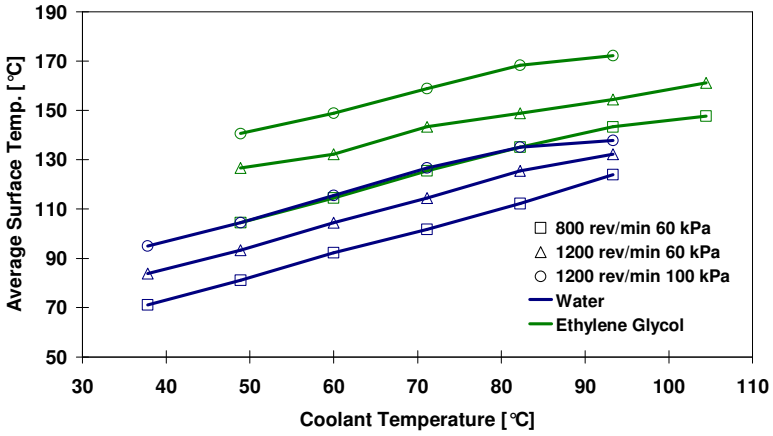

Figure 9-8 Average surface temperature as a function of coolant type and temperature (Wentworth [54]).

Heywood [15] discusses, by means of a literature review, surface temperature in the chapter dedicated to heat transfer, and from this an estimate of the surface temperature for this specific engine can be made. With the above treatment of the variables effecting surface temperature, the different load conditions can be accounted for. Considering cylinder head temperatures, measurements were made on an SI engine head, in both aluminium and cast iron, at various locations [55]. The load point given was 2000 rev/min, WOT and coolant temperature of 95°C. Temperatures on the cylinder head within the combustion chamber varied from 110 to 170°C for aluminium and 135 and 225°C for cast iron. This implies that aluminium cylinder head temperatures will be between 25 and 55°C lower than cast iron. Piston temperatures are given for an SI engine at 4600 rev/min and WOT [56]. Piston crown surface temperatures of between 252 and 285°C are given.

Taking the median cylinder head temperature, as given above, for aluminium of 140°C (median of 110 and 170°C) at 2000 rev/min WOT and considering Figure 9-6 it is necessary to increase this value for 3000 rev/min WOT. As noted, extrapolation will not be entirely reliable but in the absence of better information is the only route available. The slopes of the 1200 to 2000 rev/min points are all similar, indicating that MAP has little effect on the trend, so it is sufficient to use the 60 kPa line as it contains more information. Taking the slope of 1600 to 2000 rev/min portion of the line and then extending to 3000 rev/min gives an increase in surface temperature of 9.7°C. This is an upper estimate due to the obvious curvature. Attempts to use other curve fitting to include this curvature produced results that were obviously erroneous. A value of 149°C is therefore used for the head temperature.

For the 120 km/hr load point (engine speed - 3760 rev/min, MAP - 68.7kPa), using a similar argument as above for the engine speed dependence produces a cylinder head temperature of 157°C. To account for the MAP, consider Figure 9-7, using the 2000 rev/min curve a reduction of 12°C which translates to 145°C. Likewise for the 60 km/hr load point (engine speed – 1880 rev/min, MAP 49.6 kPa), the lower engine speed translates to 139°C and the low MAP reduces this further to 119°C. Due to the fact that coolant temperatures were controlled at close to 90°C for all the load points, no compensation to the cylinder head temperatures is necessary.

Piston crown surface temperatures will be affected, in a similar manner as are the cylinder head surface temperatures, by speed and load, and the identical arguments as above are used. However, the oil temperatures were uncontrolled and, as mentioned, vary from load point to load point. In the engine, a significant portion of the heat transfer away from the piston is via the crank case oil, although the majority is expected to be via the ring pack and ring belt zone. Therefore oil temperatures and coolant temperatures will influence the piston temperature in a similar manner as that indicated in Figure 9-8. In the absence of more detailed information a 50% dependence on oil temperature is assumed. Starting with a piston temperature, as given above, of 268°C (median of 252 and 285°C) for a load point of 4600 rev/min and WOT and assuming that the oil temperature for this experiment was 120°C, the temperatures for the three load points can be calculated. The results are as follows 246°C for the 3000rev/min, WOT load point, 243°C for the 120 km/hr load point and 207°C for the 60 km/hr load point.

For the cylinder liner temperature, the actual values given by Wentworth [54] can reliably be used as a starting point for the top of the liner temperatures. This is due to the positioning of his measurement probes and that the Toyota 4A-FE engine block is also cast iron. One of the experiments conducted by Wentworth included a 50:50 mixture of glycol - water (which is assumed to have properties close enough to a 40:60 mixture) at varying coolant temperatures and 2000 rev/min, WOT. At 93°C coolant temperature, an average surface temperature of 163°C was measured. Adjusting this for engine speed increases it to 172°C for the 3000 rev/min, WOT load point.

For the other load points, it is convenient to again take the above measured temperatures as a starting point and to adjust for speed and MAP. Doing so leads to 168°C and 142°C for the 120 and 60 km/hr load points respectively.

These liner temperatures coincide with the top of the liner, however it is well known that temperatures vary considerably down the liner [15]. As an approximation to this the average liner temperature is calculated by assuming that the length of the liner is equal to the stroke and that the bottom of the liner is at the oil temperature. The temperature distribution is assumed linear and the average temperature calculated for the mid point. Therefore the calculated liner temperatures are 140°C for both the 3000 rev/min and 120 km/hr load points and 116°C for the 60 km/hr load point.

Having ascertained, for each load point, average surface temperatures for the three main surface areas within the combustion chamber, namely the cylinder head, piston crown and liner, it is now necessary to find a single representative average overall surface temperature. This is done by a weighted average according to exposed surface areas and taking mid stroke, the weightings and their determination are shown below in Equation 9-4. The final values are shown tabulated in Table 9-3.

$$\text{Bore}: b = 0.081$$

$$\text{Stroke}: s = 0.0776$$

$$\text{Area of head and piston}: A_h = A_p = \left(\frac{\pi b^2}{4}\right) = 0.00515$$

$$\text{Area of liner}: A_l = \left(\frac{\pi b \times s}{2}\right) = 0.00988$$

$$\text{Total area} = A_T = A_p + A_h + A_l = 0.02018$$

$$\text{Temperature of head}: T_h \text{ etc}$$

$$\text{Average Temperature} = \left(\frac{A_h}{A_T} \times T_h\right) + \left(\frac{A_p}{A_T} \times T_p\right) + \left(\frac{A_l}{A_T} \times T_l\right)$$

$$= (0.255 \times T_h) + (0.255 \times T_p) + (0.490 \times T_l)$$

Equation 9-4 Equation for the calculation of average surface temperature.

Table 9-3 Coolant, Oil, Inlet Charge and calculated Chamber Wall Temperatures for the three load points.

Load Point	Coolant Temperature [° C]	Oil Temperature [° C]	Inlet Charge Temperature [MAT≡ Inlet manifold air temperature] [°C]	Combustion Chamber Wall Temperature [° C]
3000 rev/min, WOT	92	107	MAT + 10	169
120 km/hr	90	110	MAT + 30	168
60 km/hr	89	90	MAT + 30	140

Swirl Ratio is input into Racer as a parameter for the Woschni [44] type heat transfer coefficient calculation. It is used as an indication of charge motion induced during the intake process. The Toyota 4A-FE engine is a 4 valve per cylinder, pent-roof chamber design. This type of design usually incorporates the introduction of tumble, or transverse swirl, to the incoming charge, rather than the more traditional swirl. Therefore the actual number used will have no physical significance, but will add a component of charge motion imparted to the induced charge during intake. Mc Laren [41] had used a number of 0.9 for this value when modelling this engine, and this value is used here for convenience.

9.2.2. Single-Zone Analysis

The dialogue box used for the inputs for the single-zone model is shown below in Figure 9-9.

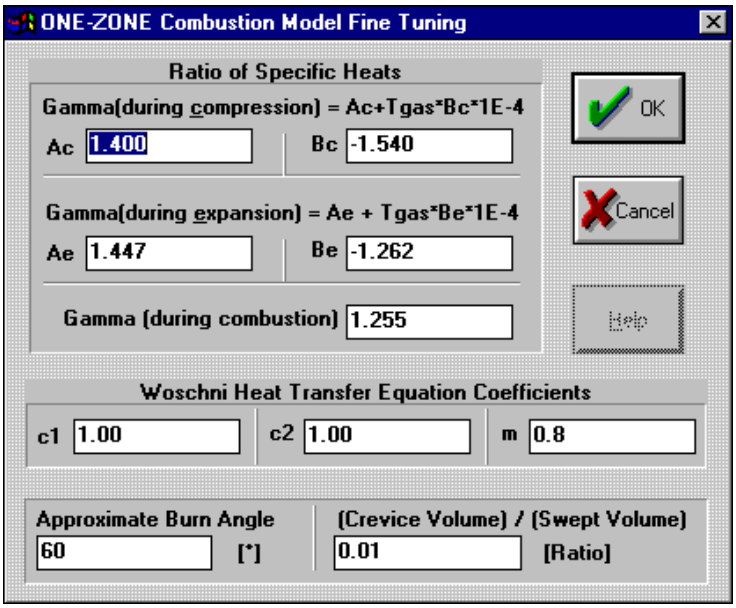

Figure 9-9 Racers default dialog box for access to the single-zone models adjustable parameters.

The single-zone analysis routines require the coefficients for the empirically determined ratio of specific heats for the gas and these are input under *Ratio of Specific Heats*. The format of the coefficients required

are those as given by Cheung and Heywood [42] and the values used during the processing of the various load points are taken from this source. Three distinct periods of the engine cycle are identified using different coefficients for the determination of the gas properties: compression, combustion, and expansion. Cheung and Heywood provide coefficients for various fuels (iso-octane, propane, indolene, methanol and methanol-indolene mixtures), equivalence ratios (0.7, 0.9, 1.0, 1.1, 1.2 and 1.3) and residual gas mass fraction (8.5, 22 and 37%). The coefficients chosen were for indolene and a residual gas mass fraction of 8.5% while the nearest equivalence ratio quoted was used.

The *Woschni Heat Transfer Equation Coefficients* allow the setting of the two coefficients used to account for the relative gas velocities (C_1 and C_2) and the exponent, m, as discussed in Section 8.3.4. For accurate determination of C_1 and C_2, extensive engine testing, requiring mechanical engine modifications and specialised testing equipment would be required. This is seldom done, and the coefficients as determined by Woschni [44] are often used without modification. In cases such as this, where the heat transfer model is being used for the purpose of combustion analysis, it is possible to deduce from the results if the heat transfer model is behaving correctly and the coefficients are therefore appropriate. If it can be assumed that all of the mathematical models used in conjunction with the heat transfer model, such as the calculation of specific heats and mass loss due to blowby, are working correctly, then the shape of the heat release curve should have certain characteristics. Deviation from these characteristics will indicate that the heat transfer model is incorrectly calibrated. Prior to combustion initiation in the early to mid compression stroke, the heat release rate is known to be zero and if the model predicts heat release (positive or negative), then the heat transfer model is not functioning correctly by over-predicting or under-predicting the heat transfer rate. Similarly, after combustion is known to have been completed during the mid to late expansion stroke, a similar argument can be made. The form of the equation (Equation 8-13, Section 8.3.4) shows that C_1 affects the relative gas velocities throughout the cycle as it calibrates the velocity due to piston motion. C_2 affects the velocity only after combustion has begun as it calibrates the velocity due to combustion. Thus modifying C_1 alters the predicted heat transfer before combustion, while C_1 and C_2 affect it after combustion has been initiated. Therefore C_1 can be set to achieve zero heat release before the initiation of combustion, and then C_2 can be set to achieve zero heat release after combustion. It should be noted that these coefficients should be engine specific and not differ between different engine load points. If the coefficients do not produce acceptable data for different load points then the Reynolds number power, m can be adjusted slightly to achieve this. Racer has the original Woschni coefficients C_1 and C_2 embedded in it and the input fields are only multipliers and therefore the default value is 1.

The values were chosen by performing a preliminary study using three sets of Reference fuel data at the three load points. Acceptable results were obtained with the original coefficients except for the 3000 rev/min load point. Here, the model was under-predicting heat release during the expansion stroke. Attempts were made to reduce this by increasing C_2. However, unrealistically large values of C_2 were required (≈5) and this was rejected. Changing m from 0.8 to 0.75 was found to have the desired effect without significant impact on the results achieved for the other two load points. Thus the coefficients chosen for the heat transfer equations are C_1=1.0, C_2=1.0 and m=0.75. The burn rate curves are shown

below in Figure 9-10, Figure 9-11 and Figure 9-12. Note that in all three of the load points there is a distinct sudden increase in heat release during the compression stroke. This is thought to be due to a squish effect caused by the specific mounting of the pressure transducer in this engine as indicated in Section 6.2 and discussed in Section 9.2.1. It is thought that due to the position of the transducer the gas in the squish zone is compressed and the localised pressure near the transducer becomes raised above the cylinder mean pressure as the piston nears the top of its stroke. The burn rate model can not account for this and therefore this pressure rise results in the prediction of some heat release. This effect should be consistent for all the fuels at a given load point and therefore should not influence the results significantly.

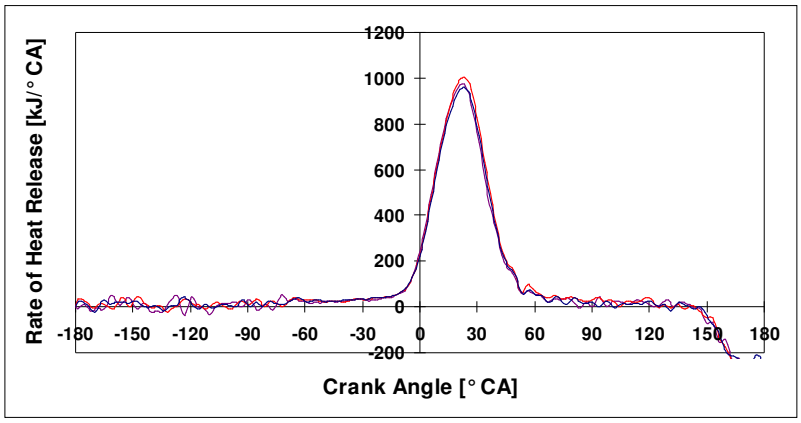

Figure 9-10 Rate of heat release for three reference fuels at 60 km/hr load point indicating the suitability of Woschni heat transfer coefficients.

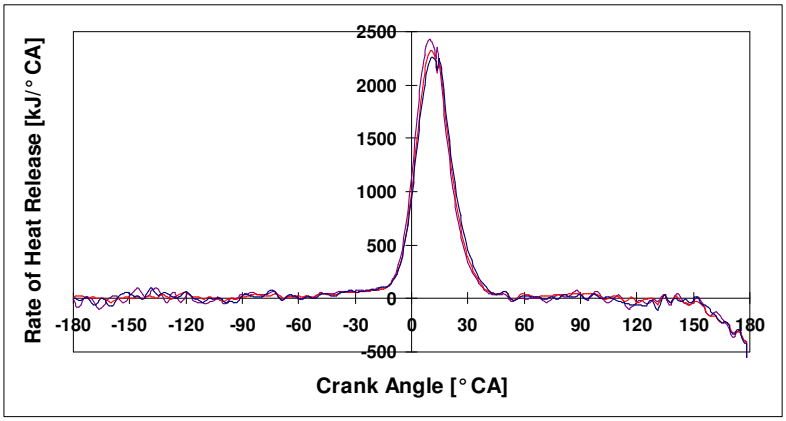

Figure 9-11 Rate of heat release for three reference fuels at 120 km/hr load point indicating the suitability of Woschni heat transfer coefficients.

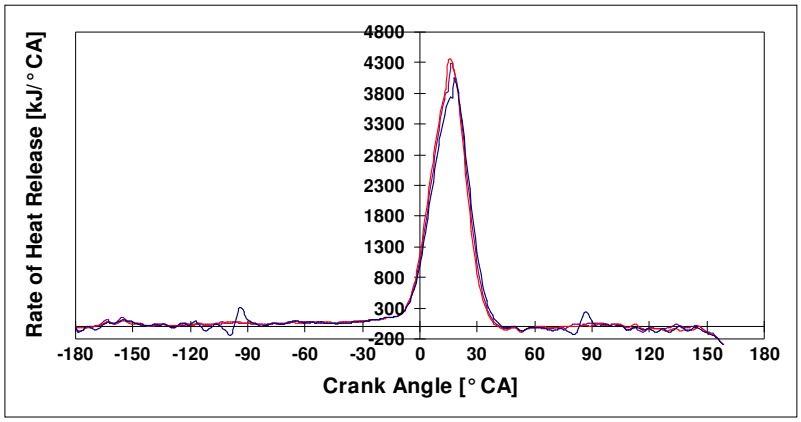

Figure 9-12 Rate of heat release for three reference fuels at 3000 rev/min load point indicating the suitability of Woschni heat transfer coefficients.

The remaining two adjustable parameters are *Approximate Burn Angle* and *(Crevice Volume)/(Swept Volume)*. The first is used by the program in determining when to apply which coefficients for the specific heat calculation (as described above). The coefficients for "compression" are used until the defined combustion initiation (Spark Timing), where after the "combustion" coefficients are used for the duration of the defined approximate burn angle. After this, the coefficients for "expansion" are applied. The values used were chosen by inspecting the results for each of the three load points as shown in Figure 9-10, Figure 9-11 and Figure 9-12. From this an approximate burn angle can be determined. The values used are 80°, 67° and 63° for the 60 km/hr, 120 km/hr and 3000 rev/min load points respectively.

As for the crevice volume to swept volume ratio, this is used by the combustion analysis model to account for the change in enthalpy of the gas forced into, and then released from the crevice volumes. The gas is assumed to enter the crevice volumes with temperature equal to the mean gas temperature, it is then in confined contact with the chamber surface and will efficiently exchange heat with the surface. Therefore it is assumed to exit the crevice region with a temperature equal to the chamber surface temperature. The value chosen is the same as that used by Mc Laren [41] when analysing this same engine and is 0.01, which implies that the crevice volume is approximately 1% of the swept volume.

9.2.3. Two-Zone Analysis

The dialogue box for the input of the adjustable parameters used for the two-zone combustion analysis is shown below in Figure 9-13.

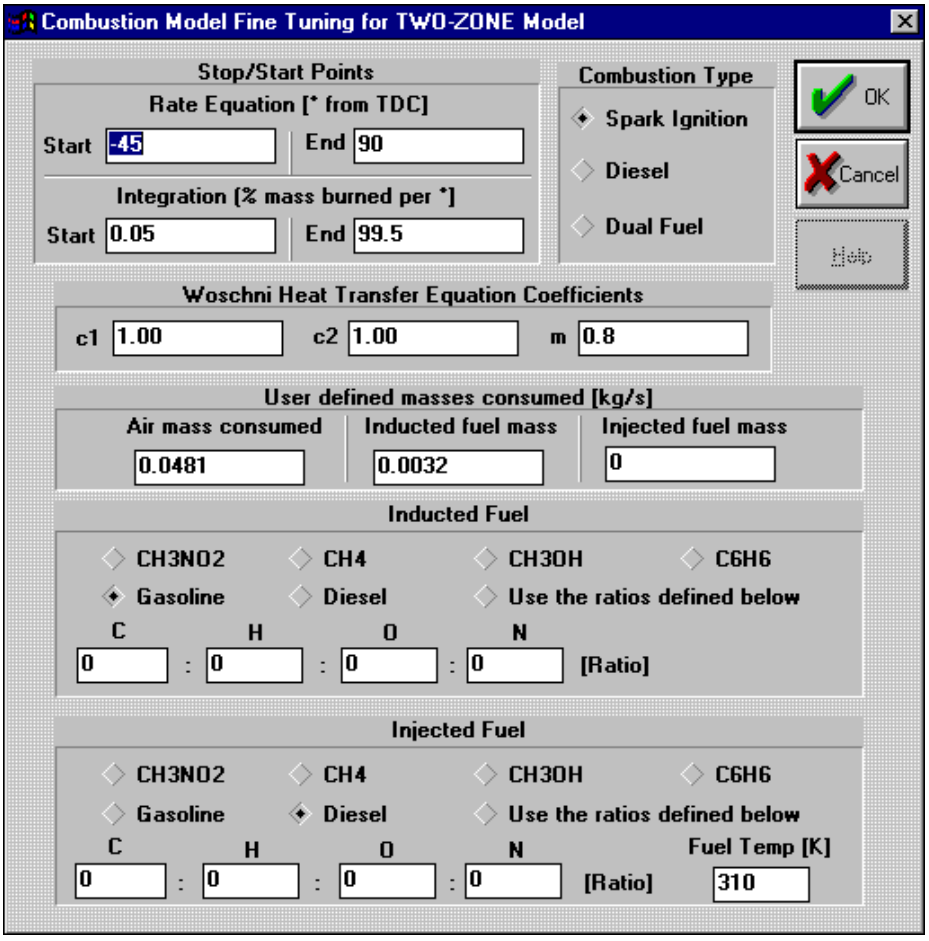

Figure 9-13 Racers default dialog box for access to the two-zone models adjustable parameters.

The parameters under *Stop/Start Points* control the criteria on which the calculation defines what phase the cycle is in and thus which calculations to perform. The *Rate Equation* parameters define the crank angle window in which the model performs the complicated calculations to determine the combustion rate. There is generally no need to perform these calculations when it is known that combustion is not occurring (early in compression and late in expansion). The *Integration* parameters define the point at which the model defines combustion to have initiated and ceased. The start of integration parameter (*Start*) is given in percentage of total charge mass transferred per degree (rate of mass transfer or rate of combustion). As soon as the model detects a rate of combustion greater than this value, combustion is defined to have begun and the model begins integrating the mass transferred. The *End* parameter is given in percentage of total charge mass, and once this percentage of the charge has been burned, combustion is defined to have ceased and the model stops computing the rate of combustion. Thus the values used here can drastically effect computational time. In order to get the model to return reliable burn angles it is necessary to carefully select these parameters, and this is usually done by visual inspection of the combustion rate and cumulative combustion curves.

The switches in the block labelled *Combustion Type* define the type of engine being analysed. For this present analysis the switch for Spark Ignition is always selected. The *Diesel* and *Dual Fuel* boxes merely

alter the way in which the charge mass is handled. These allow the respective fuel masses to be “injected” directly into the cylinder. The *Woschni Heat Transfer Coefficients* set the relevant parameters used by the heat transfer calculations for the two-zone analysis as described in Section 8.3.4. The values were chosen in a similar manner to that described above in Section 9.2.2 for the single-zone analysis and similar argument is made but a value of 0.7 is chosen for the exponent m.

The block labelled *User Defined Masses Consumed [kg/s]* give the input fields for the input of the measured or assumed mass of air, inducted fuel (fuel introduced upstream of the combustion chamber) and injected fuel (fuel introduced directly into the combustion chamber) consumed by the engine. The two-zone model is inherently a mass transfer model, and thus the initial masses are required for the calculations to proceed. It is necessary for these values to be reasonably well determined for reliable results to be obtained. For this exercise the measured values of air and inducted fuel are input into the respective fields. The last two blocks, *Inducted Fuel* and *Injected Fuel*, allow the specification of the respective fuel types. Six predefined selectable fuels are given as well as the option of defining the fuels Carbon:Hydrogem:Oxygen:Nitrogen ratio. This last option is used here and each fuels C:H:O:N ratio, as calculated in Section 5.4, is input into the respective fields in the *Inducted Fuel* box.

10. STATISTICAL ANALYSIS

The objectives of the research, as stated in Section 4 were to investigate the effect of fuel formulation on the engine out emissions of SI engines, attempt to quantify the effects, and most importantly to gain an understanding of the mechanisms through which these effects occur. The aim of the research was not to build statistically reliable predictor models of emissions as a function of fuel formulation parameters. Sound statistical techniques and procedures were employed in a logical manner that is believed to firstly identify the important fuel parameters influencing each of the regulated exhaust emissions, secondly to provide indication of the order of magnitude of the effects and thirdly to provide insight into the mechanisms driving the effects. All the statistical analyses were executed with the regression modelling procedures of SAS®, a professional PC based data manipulation and statistics package, a product of the SAS Institute Inc.

As indicated in Section 4, a triangular approach was taken whereby first the exhaust emissions were correlated with fuel formulation parameters. Then, the exhaust emissions were correlated to combustion parameters determined from the combustion analysis. Finally, the important combustion parameters were correlated back to fuel formulation parameters. This allowed the tracing of the combustion related mechanisms. The basic statistical methodology followed was to study multivariate regression predictor models, utilising the minimum number of variables and then to use these basic models to study the effects that the fuel variables may have on the prediction of the exhaust emissions. The primary reason for this was twofold:

- to eliminate the effects of confounding variables that may effect exhaust emissions (e.g. engine and ambient effects)
- to be able to incorporate as large a portion of the data set as possible in order to reduce the effect of any experimental noise.

It is, however, important to note that the statistics is not able to prove causality, that is to say that if the regression suggests that a certain variable has a certain effect, it may not actually be a physically real phenomenon. However, the results of the statistical analysis can then assist the physical explanation of the causality of the effect. Furthermore, there is no one correct predictor model, a large number of models can be found that adequately predict the variable of interest. However, from the set of possible models, the variables that occur most frequently can be concentrated on and investigated.

10.1. Statistical modelling of Mixtures

Before discussing the detail of the statistical analyses used, it is important to consider the special case when the variables (or some of the variables) are the proportions of components making up a mixture. This topic is well dealt with by Cornell [57] and the following discussion is based on this presentation of the subject. In this case the variables sum to one (or 100%) and are thus linearly dependant. For example, in a three component mixture any one component can be found by subtracting the other two components proportions from one. This reduces the model mathematically as certain terms become redundant, and also removes the intercept. If an intercept is

included in the model then the linear dependency precludes the inclusion of all the mixture terms. For example the common mixture model used is a third order model and the reduction of terms produces a model equation as shown in Equation 10-1 where the model is built for a three component mixture of components a, b and c. If this were not a mixture then a third order model would have to include terms of the form a^2 and a^2b etc., and an intercept which would require an additional ten terms.

$$y = c_a a + c_b b + c_c c + c_{ab} ab + c_{ac} ac + c_{bc} bc + c_{abc} abc$$

Equation 10-1 Common third order mixture model equation with reduced terms.

10.2. Form of the variables

The statistical modelling was performed with the dependent variables (exhaust emissions) expressed in the rationalised terms of grams per kilowatt-hour (g/kW.hr). This has three desirable consequences:

- g/kW.hr is a more useful unit in terms of comparing, in absolute terms, different vehicles and engines,
- g/kW.hr goes some way to rationalise the differences between the load points tested, thus making the statistical analysis more reliable,
- it allows as much of the experimental data to be statistically analysed together as possible.

Although the rationalised term grams per kilometre (g/km) has the first two advantages, and is a more useful term in quantifying actual air quality impact, it would preclude the addition of the 3000 rev/min load point data, as there is no meaningful way of expressing these results in g/km. This load point was chosen to simulate acceleration and does not have a corresponding steady vehicle speed.

A group of classification variables were added to account for the different engine configurations and load points. This was done in the standard way as shown below in Table 10-1. These classification variables should account for all of the variation due to the different load points, including engine operating conditions such as equivalence ratio, ignition timing, water and oil temperatures etc. However, these variables were still included in the statistical analyses due to possible differences between these operating conditions form test to test. For example, the engine calibration produces an operating equivalence ratio of approximately 0.9 and 1.1 for the 60 km/hr and 3000 rev/min load points respectively. The classification variables should account for this macro difference. However, test to test variation in operating equivalence ratio is seen between different tests at the same load point, and by including the variable in the analyses, effects due to this test to test variability will be accounted for without confounding the fuel property effects. Therefore it is possible that the macro effect due to some engine operating conditions will not be predicted by the statistical analysis as would be expected, as it has been accounted for in the classification variables. The engine operating conditions that were included in the statistical analyses were equivalence ratio, ignition timing, coolant temperatures, exhaust temperature, inlet manifold pressure, barometric pressure, cell dry bulb temperature and specific humidity.

Table 10-1 Classification variables used and their application.

$3\times$ Engine Configurations (E1 - E3)

(4A - FE $\times$ 2 Cylinder Heads and 4Y)

$6\times$ Vehicle Driving Condition Load Points (L1 - L6)

(60, 80, 100 and 120 km/hr, SFC, 3000 rev/min)

Load Point Matrix

4A - FE (Cyl. Head 1) - 60, 80, 100, 120 km/hr, 3000 rev/min (E1L1 - E1L4, E1L6)

4A - FE (Cyl. Head 2) - 60, 120 km/hr, SFC, 3000 rev/min (E2L1, E2L4, E2L5, E2L6)

4Y - 60, 120 km/hr, 3000 rev/min (E3L1, E3L4, E3L6)

Total = 12 discreet load point/engine combinations

$\therefore$ 11 Classification Variables Required (C1 - C11)

	C1	C2	C3	C4	C5	C6	C7	C8	C9	C10	C11
E1L1	0	0	0	0	0	0	0	0	0	0	0
E1L2	1	0	0	0	0	0	0	0	0	0	0
E1L3	0	1	0	0	0	0	0	0	0	0	0
E1L4	0	0	1	0	0	0	0	0	0	0	0
E1L6	0	0	0	1	0	0	0	0	0	0	0
E2L1	0	0	0	0	1	0	0	0	0	0	0
E2L4	0	0	0	0	0	1	0	0	0	0	0
E2L5	0	0	0	0	0	0	1	0	0	0	0
E2L6	0	0	0	0	0	0	0	1	0	0	0
E3L1	0	0	0	0	0	0	0	0	1	0	0
E3L4	0	0	0	0	0	0	0	0	0	1	0
E3L6	0	0	0	0	0	0	0	0	0	0	1

Thus the model responds as shown below :

model for first case $+ 0\beta_{C1} + 0\beta_{C2} + 0\beta_{C3} + ...$

model for first case $+ 1\beta_{C1} + 0\beta_{C2} + 0\beta_{C3} + ...$

model for first case $+ 0\beta_{C1} + 1\beta_{C2} + 0\beta_{C3} + ...$

etc where $\beta_{c\#}$ is the coefficient for the $\#^{th}$ classification variable

10.3. Selecting the Models

The regression models to be used were selected by performing a Cp analysis. Cp is a statistical quantity which, when compared to the number of variables in the model, p, indicates whether there are sufficient variables present for adequate prediction. If Cp is similar in magnitude to, or preferably less than, p, then the model contains a sufficient number of variables. If Cp is much less than p, then there are usually more variables present than necessary and therefore it is possible that one or more variables may produce misleading

information. SAS® performs a Cp analysis, listing all the possible models and their Cp and p values, in ascending order of Cp. In other words, the model at the top of the list has the lowest Cp and probably has more variables than necessary. The list can then be studied to find the possible models with similar Cp and p values. Of these models, the models with the least number of variables can be considered as good candidates. An example of the program steps required for this type of analysis is given below in Table 10-2.

Table 10-2 SAS® program statements for first step of model building for HC emissions.

```
proc reg;

 model HCgkWhr = C1 C2 C3 C4 C5 C6 C7 C8 C9 C10 C11
                 A O P AO AP OP AOP ER Vlratio DryB SpecHum
                 Benzene Sulphur IgnTim ManP Oxygen WaterT
                 ExhT Dens VapPres Volind Lead Nitrogen Phenols
                 IBP T10 T30 T50 T70 T90 FBP OilT RON MON Sens E70
               / noint selection=cp include=11 ;
*  ManT DropT;

run;
quit;
```

The "proc reg;" statement at the top of the program file instructs SAS® that regression procedure routines are to be used, these are linear routines. The data set, which is loaded prior to performing any analyses, sequentially loads all the variables from each observation (or test point) in the required order to associate them with the appropriate variable name. The variable names used are restricted to 8 characters and the variable names are listed in Appendix F. Then, the next statement instructs the program to, in this example, model the variable called HCgkWhr (HC emissions measured in g/kW.hr) and to use combinations of the variables in the next block. The "run;" and "quit;" commands are needed to instruct SAS® to perform the analysis and then to exit the regression procedure routines.

The "noint" statement informs the program not to include an intercept in the model. This is necessary as the model contains a mixture model as described above in Section 10.1. The "include=11" statement forces the first 11 variables listed into the base model, these are the classification variables and are necessary given the previous discussion. In a Cp analysis a full model is generated using all the variables listed and the reduced models are compared to this model to calculate the Cp value. Thus it is assumed that all the necessary variables are present in the variable set. Therefore, if any of the observations have missing data in one of the variables, that observation cannot be used for creating the full model. Therefore, some variables may have limiting effects on the data set size and therefore on the model generated. For this reason some of the variables are not considered from the outset. In this example, manifold and droplet temperature (ManT and DropT) were left out by using the syntax "* ManT DropT;" (SAS® ignores statements between a star and semi-colon). The variables A, O and P are abbreviations for Aromatics, Olefins and Paraffins respectively, while AO, AP, OP and AOP are the interaction variables. If an interaction is to be used in a model it requires what is known as "full support". This means that all the main variables in the interaction must also be present in the model. In other

words if the interaction AO is to be included then both A and O also need to be included, AO and OP require A, O and P etc. SAS® builds models without accounting for this requirement (it has no way of knowing that AO is an interaction between A and O, AO is seen as just another variable). Therefore models that SAS® suggests, but that do not have full support, were ignored.

A portion of a SAS® output file is given below in Table 10-3 (the complete file is very large), which has been modified to list only the preferred models. The raw output file lists all the models tested in ascending order of Cp value. In this modified output, the models having the least p value and sufficiently low Cp value are extracted and placed at the top of the list. Groups of models with the same p are assembled in ascending order of Cp. During this manual process of extracting the best models, insight is easily gained as to whether the same variables are appearing frequently. Therefore, in some circumstances only a few models need to be extracted for confidence to be gained that all the necessary variables are being considered. In other cases a number of models need to be considered. In some instances as many as 14 models were extracted, while in others as few as 4 were considered.

Table 10-3 SAS® output file for the Cp analysis of Hydrocarbon Emissions, modified to list only the preferred models.

N = 195 Regression Models for Dependent Variable: HCGKWH

C(p)	R-square	In	Variables in Model
2881	0.88235775	11	C1 C2 C3 C4 C5 C6 C7 C8 C9 C10 C11
NOTE: The above variables are included in all models to follow.			
18.47068	0.99354934	23	A O P AO AP ER DRYB IBP T30 T50 LEAD PHENOLS
17.79053	0.99365257	24	A O P AO AP ER DRYB IBP T30 VLRATIO E70 LEAD SULPHUR
18.57239	0.99362246	24	A O P AO AP OP ER DRYB IBP T10 T50 LEAD PHENOLS
18.16013	0.99371537	25	A O P AO AP OP ER DRYB SPECHUM IBP T10 T50 LEAD PHENOLS
18.38904	0.99370656	25	A O P AO AP ER DRYB IBP T30 VLRATIO E70 SENS LEAD SULPHUR
18.42866	0.99370503	25	A O P AO AP ER DRYB IBP T30 T50 VLRATIO E70 LEAD SULPHUR
18.53679	0.99370087	25	A O P AO AP OP AOP ER DRYB IBP T10 T50 LEAD PHENOLS

The selected models are then checked for co-linearity using the "collin" command, an example of which is given in Table 10-4. The output generated by the "collin" command is a large file and is thus not shown here, but it enables the user to see model instability caused by independent variable co-linearity. The variables that indicate co-linearity can then be investigated as to whether to include them or not. This is done by an iterative procedure of eliminating one of the co-linear variables at a time and performing a modified Cp analysis to see if a sufficiently good model is possible without it, or with some other variable in it's place. Co-linearity may often be predicted between classification variables and between the mixture variables. The classification variables are essential

and therefore can not be removed from the models, while the mixture variable co-linearity is also unavoidable and the variables are therefore retained.

The co-linearity output also gives the variable coefficients that are required for prediction for that specific model. It is these coefficients which, ultimately, are of interest as they indicate the magnitude and direction of influence that each independent variable has on the predicted dependent variable.

Table 10-4 An example of the co-linearity check.

```
proc reg ;

model HCgkWhr = C1 C2 C3 C4 C5 C6 C7 C8 C9 C10 C11 ER DryB IBP T30 Vlratio
                  E70 Sens Lead A O AO Sulphur
                / noint collin  ;

run ;
quit ;
```

11. RESULTS

The following chapter presents the experimental results. The experimental procedure and the results are first shown to be repeatable by indicating that repeat tests on the same fuel produce results within the expected range for acceptable repeatability. The significance of the results is then shown by indicating that the different fuels produce results that show differences significantly greater than the test repeatability. The statistical analysis of the results is then presented. This chapter does not include detailed discussions of the results: this is left for the following chapter.

11.1. Test Repeatability and Significance

Before the significance of the exhaust emissions results can be considered, it is important to establish if the engine operating conditions were reproduced consistently, as any deviation in operating conditions can have an overriding influence on exhaust gas composition. It is also important when considering all of the results presented, to bear in mind that the cylinder head of the 4A-FE engine was changed after the first phase (fuels P1 through P11, plus reference fuels), as discussed in Section 6.1.1. This new cylinder head had significantly different performance and emissions characteristics and, therefore the results are considered to be from a completely different engine. Also, two different batches of reference fuel were used, however every batch of testing was bracketed by a reference fuel test on the same fuel so that test repeatability could be checked.

Furthermore, the repeatability and significance of the emissions measurement and combustion analysis results must be checked prior to performing any analyses on them. Experimental repeatability must be of a high standard and the magnitude of the effects being investigated must be greater than the test repeatability if the results are to be relied upon to be true reflections of the actual performance of the engine/fuel system. Therefore the repeatability and significance of the test results are discussed below.

11.1.1. Repeatability of Load Points and Engine Operating Conditions

The reproducibility of the dynamometer speed control set points was generally within ± 5 rev/min of the desired engine speed, while part load torque settings were generally achieved to within 1.5%. The testing on the 4A-FE engine required the manual setting of the fuel rail pressure and the reproducibility achieved was ± 3%. This led to a maximum deviation in equivalence ratio for the six reference tests of less than 0.4%. The ignition timing was also manually adjusted to the predetermined values and less than 1° CA deviation was recorded.

All of the WOT torque and power results were corrected using SABS 013 [58] correction factors to adjust for atmospheric variation. Corrected results for the reference tests were within 1% of each other for each test phase.

Engine coolant and oil temperatures were not actively controlled, however the engines were fitted with OEM coolant thermostats and the variation in coolant temperatures between tests was low, being less than

1° C for any given load point. Oil temperatures also varied within acceptable limits and this was aided by the use of a sump fan for certain of the load points. Variations in oil temperatures were less than 4° C for any given load point.

Thus it can be seen that the repeatability of the load points and engine operating conditions was excellent.

11.1.2. Repeatability and Significance of Emissions Test Results

Before any meaningful conclusions can be inferred from the data, it is important to establish whether the testing procedures produced results that were both reproducible and significant. The reproducibility of the testing is demonstrated by the difference between tests at the same engine conditions and with the same fuel type. Each batch of testing was bracketed by tests with a reference fuel. The difference between the results obtained with the reference fuels is indicative of the test reproducibility. As mentioned in Section 7.1, the testing of the 4A-FE engine was interrupted, and therefore broken into three distinct batches. Comparison between reference fuel results from different batches of testing is complicated by two factors. Firstly the engine configuration changed due to the new cylinder head being fitted as mentioned above and secondly the seasonal ambient condition changes. Therefore, comparisons should only be made between the reference fuel results of a given test group. The testing of the 4Y engine was performed in one continuous group and was bracketed before and after, making simple comparisons possible.

The results for HC's, NO and CO for all the bracket reference tests are tabulated below in Table 11-1. The "Difference" is calculated as the absolute value of the first reference minus the average of the two references ($|\ ref1-[(ref1+ref2)/2]|$). In other words it gives an indication of the variability of the measured results from the average and is considered to be indicative of the repeatability of measurement. It can be seen that in general the reproducibility of these results is within well 11%, with more than half of the measurements achieving better than 5% reproducibility. The exception is CO emissions for 60 km/hr in Group 3, in which the first test is considered an outlier, causing an apparent high percentage difference. This repeatability is considered to be acceptable given the nature of exhaust gas analysis. The "missing data" for the 4A-FE engine, 120 km/hr NO emissions is due to the analyser being saturated as indicated by the >2000 ppm reference results.

Table 11-1 Comparisons of the bracket reference fuel emissions results indicating reproducibility.

Hydrocarbon Emissions												
	60 km/hr				120 km/hr				3000 rev/min			
	4A-FE			4Y	4A-FE			4Y	4A-FE			4Y
	Group1[#]	Group2[#]	Group3[#]		Group1	Group2	Group3		Group1	Group2	Group3	
Ref Before	2323	1125	1113	2597	1605	1196	1150	2408	2052	1715	1743	2046
Ref After	2469	1087	1107	2149	1809	1071	1116	1924	2362	1529	1621	1823
Average	2396	1106	1110	2373	1707	1133	1133	2166	2207	1622	1682	1935
Difference	73	19	3	224	102	63	17	242	155	93	61	112
% Difference	3.1	1.7	0.3	9.4	6.0	5.5	1.5	11.2	7.0	5.7	3.6	5.8

NO Emissions												
	60 km/hr				120 km/hr				3000 rev/min			
	4A-FE			4Y	4A-FE			4Y	4A-FE			4Y
	Group1	Group2	Group3		Group1	Group2	Group3		Group1	Group2	Group3	
Ref Before	1782	1308	1236	1522	>2000	>2000	>2000	1485	1138	1652	1501	1338
Ref After	1840	1261	1269	1896	>2000	>2000	>2000	1808	1036	1811	1666	1452
Average	1811	1284	1252	1709	-	-	-	1646	1087	1732	1584	1395
Difference	29	24	17	187	-	-	-	162	51	79	82	57
% Difference	1.6	1.9	1.3	11.0	-	-	-	9.8	4.7	4.6	5.2	4.1

CO Emissions												
	60 km/hr				120 km/hr				3000 rev/min			
	4A-FE			4Y	4A-FE			4Y	4A-FE			4Y
	Group1	Group2	Group3		Group1	Group2	Group3		Group1	Group2	Group3	
Ref Before	0.83	0.14	*0.22*	1.31	1.62	0.68	0.64	3.38	4.96	3.47	3.54	3.84
Ref After	0.80	0.16	0.15	1.34	1.50	0.58	0.59	3.62	4.78	2.93	3.34	3.90
Average	0.82	0.15	*0.18*	1.32	1.56	0.63	0.62	3.50	4.87	3.20	3.44	3.87
Difference	0.02	0.01	*0.04*	0.02	0.06	0.05	0.02	0.12	0.09	0.27	0.10	0.03
% Difference	2.1	6.5	*19.5*	1.1	4.0	8.4	3.8	3.4	1.8	8.4	3.0	0.8

[#]Group1 – P1 to P11, Group2 – P12 to P24, Group3 – P25 to P35

If the effect that the fuel properties has on the emissions produced is small in relation to the experimental noise or reproducibility, then the data is not significant in that no meaningful conclusions can be drawn from it. To indicate the significance of the data the standard deviation of each group of results can be compared to the expected test repeatability. If the standard deviation is larger than the test reproducibility then the data set can be considered significant, and it can be assumed that the effects due to the fuel properties are larger than the experimental repeatability. This is tabulated below in Table 11-2. It can be seen that in most cases the data is significant. Although this is not a rigorous test of significance, it indicates that the data can be used to investigate the effects that fuel formulation has on exhaust emissions. Furthermore, this test should not lead to the rejection of any of the groups of data if that group does not indicate significance in this way. The "missing data" for the 4A-FE engine, 3000 rev/min is due to the low octane of these fuels precluding their being tested at this load point.

Table 11-2 Comparisons of the standard deviation of the fuel emissions results and the test reproducibility indicating significance of the data set.

Hydrocarbon Emissions												
	60 km/hr				120 km/hr				3000 rev/min			
	4A-FE			4Y	4A-FE			4Y	4A-FE			4Y
	Group1[#]	Group2[#]	Group3[#]		Group1	Group2	Group3		Group1	Group2	Group3	
Group Average	2396	1106	1110	2373	1707	1133	1133	2166	2207	1622	-	1935
Std Deviation	336	128	111	182	226	141	59	218	201	177	-	143
Reproducibility	73	19	3	224	102	63	17	242	155	93	-	112

NO Emissions												
	60 km/hr				120 km/hr				3000 rev/min			
	4A-FE			4Y	4A-FE			4Y	4A-FE			4Y
Group Average	1811	1284	1252	1709	-	-	-	1646	1087	1732	-	1395
Std Deviation	93	182	45	197	-	-	-	353	75	93	-	193
Reproducibility	29	24	17	187	-	-	-	162	51	79	-	57

CO Emissions												
	60 km/hr				120 km/hr				3000 rev/min			
	4A-FE			4Y	4A-FE			4Y	4A-FE			4Y
	Group1	Group2	Group3		Group1	Group2	Group3		Group1	Group2	Group3	
Group Average	0.82	0.15	0.18	1.32	1.56	0.63	0.62	3.50	4.87	3.20	-	3.87
Std Deviation	0.16	0.03	0.02	0.22	0.32	0.19	0.09	0.46	0.55	0.56	-	0.49
Reproducibility	0.02	0.01	0.04	0.02	0.06	0.05	0.02	0.12	0.09	0.27	-	0.03

[#]Group1 – P1 to P11, Group2 – P12 to P24, Group3 – P25 to P35

The significance of the data can better be judged from the graphical representation of the data as is given in Appendix E and the graphs for the first group of fuels tested on the 4A-FE engine (P1 through P11) are given below by way of illustration. Here the data is presented in bar graph form with error bars equivalent to the reproducibility as indicated above (Table 11-1 and Table 11-2). It can be seen in most cases that there are deviations between fuels significantly greater than the test reproducibility.

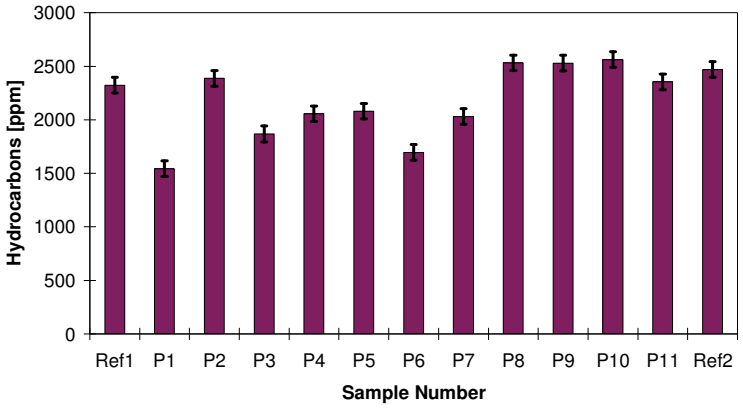

Figure 11-1 Graph of Hydrocarbon emissions from fuels P1 through P11 as tested on the 4A-FE engine, illustrating reproducibility and significance of the results.

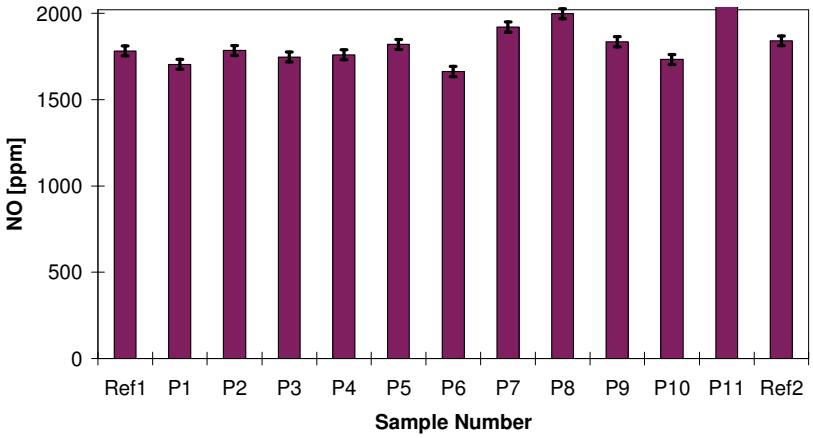

Figure 11-2 Graph of NO emissions from fuels P1 through P11 as tested on the 4A-FE engine, illustrating reproducibility and significance of the results.

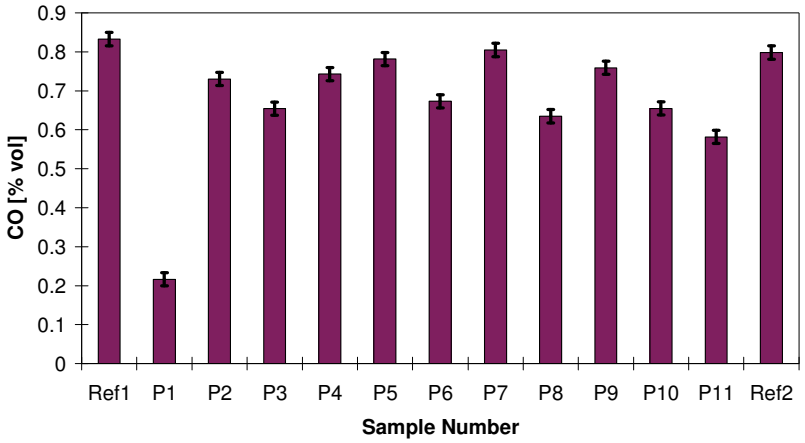

Figure 11-3 Graph of CO emissions from fuels P1 through P11 as tested on the 4A-FE engine, illustrating reproducibility and significance of the results.

11.1.3. Repeatability and Significance of Combustion Analysis Results

In a similar way as for the emissions results, the repeatability of the combustion analysis is shown in Table 11-3 and Table 11-4. Only the total heat released (mass transferred), maximum rate of heat release (maximum rate of mass transfer or combustion rate), induction period for 0 to 5% burned and burn angle for 5 to 95% are considered. These are thought to be representative of the performance of the models in general. It can be seen that the reproducibility is generally significantly better than 5%.

Table 11-3 Comparisons of the bracket reference fuel combustion analysis results indicating reproducibility of the single-zone model.

Single Zone Analysis												
	60 km/hr				120 km/hr				3000 rev/min			
	Total Heat Released		Maximum Release Rate		Total Heat Released		Maximum Release Rate		Total Heat Released		Maximum Release Rate	
	Group2	Group3	Group2	Group3	Group2	Group3	Group2	Group3	Group2	Group3	Group2	Group3
Ref Before	590	623	977	1002	1024	1008	2431	2324	1776	1784	4287	4353
Ref After	598	588	959	988	1011	944	2261	2366	1733	1622	4055	3808
Average	594	606	968	995	1017	976	2346	2345	1755	1703	4171	4081
Difference	4	18	9	7	6	32	85	21	21	81	116	272
% Difference	0.7	2.9	0.9	0.7	0.6	3.3	3.6	0.9	1.2	4.7	2.8	6.7

	60 km/hr				120 km/hr				3000 rev/min			
	Induction Period 5%		Burn Angle 5-95%		Induction Period 5%		Burn Angle 5-95%		Induction Period 5%		Burn Angle 5-95%	
	Group2	Group3	Group2	Group3	Group2	Group3	Group2	Group3	Group2	Group3	Group2	Group3
Ref Before	19.1	19.3	19.1	44.0	16.7	17.2	33.3	33.2	15.8	15.5	29.4	28.5
Ref After	19.0	18.9	19.0	43.6	17.1	17.1	34.5	33.3	15.8	15.6	30.2	29.6
Average	19.1	19.1	19.1	43.8	16.9	17.2	33.9	33.3	15.8	15.6	29.8	29.1
Difference	0.1	0.2	0.1	0.2	0.2	0.0	0.6	0.0	0.0	0.1	0.4	0.6
% Difference	0.3	1.0	0.3	0.5	1.2	0.3	1.8	0.2	0.0	0.3	1.3	1.9

Table 11-4 Comparisons of the bracket reference fuel combustion analysis results indicating reproducibility of the two-zone model

Two-Zone Analysis												
	60 km/hr				120 km/hr				3000 rev/min			
	% Total Mass Trans.		Maximum Transfer Rate		% Total Mass Trans.		Maximum Transfer Rate		% Total Mass Trans.		Maximum Transfer Rate	
	Group2	Group3	Group2	Group3	Group2	Group3	Group2	Group3	Group2	Group3	Group2	Group3
Ref Before	110.3	113.9	0.410	0.398	119.3	117.0	0.897	0.851	116.5	116.5	1.282	1.304
Ref After	111.6	112.8	0.372	0.400	119.7	117.2	0.832	0.866	116.9	114.7	1.233	1.227
Average	111.0	113.4	0.391	0.399	119.5	117.1	0.865	0.859	116.7	115.6	1.258	1.265
Difference	0.7	0.6	0.019	0.001	0.2	0.1	0.032	0.007	0.2	0.9	0.025	0.038
% Difference	0.6	0.5	4.9	0.2	0.2	0.1	3.8	0.9	0.2	0.8	2.0	3.0

Two-Zone Analysis												
	60 km/hr				120 km/hr				3000 rev/min			
	Induction Period 5%		Burn Angle 5-95%		Induction Period 5%		Burn Angle 5-95%		Induction Period 5%		Burn Angle 5-95%	
	Group2	Group3	Group2	Group3	Group2	Group3	Group2	Group3	Group2	Group3	Group2	Group3
Ref Before	20.1	19.9	43.8	43.7	17.3	17.8	28.7	29.3	16.7	16.4	30.0	29.2
Ref After	19.4	19.6	43.7	45.1	17.7	17.5	30.0	-	16.8	16.8	31.1	-
Average	19.8	19.8	43.8	44.4	17.5	17.7	29.4	29.3	16.8	16.6	30.6	29.2
Difference	0.4	0.1	0.0	0.7	0.2	0.1	0.7	-	0.1	0.2	0.6	-
% Difference	1.8	0.8	0.1	1.6	1.1	0.8	2.2	-	0.3	1.2	1.8	-

To investigate the significance of the combustion analysis results to the effects of fuel properties, as for the emissions above, the standard deviation of each group of results is compared to the indicated repeatability. This is tabulated below in Table 11-5 and Table 11-6. In general the data indicates that the test methods and mathematical models are sufficiently sensitive to be able to detect differences due to fuel formulation. This is especially evident with the induction period and burn angles, while it can also be seen that the two-zone model appears to be more sensitive and reliable than the single-zone model.

Table 11-5 Comparisons of the standard deviation of the combustion analysis results and the test reproducibility indicating significance of the data set for the single-zone model.

Single Zone Analysis												
	60 km/hr				120 km/hr				3000 rev/min			
	Total Heat Released		Maximum Release Rate		Total Heat Released		Maximum Release Rate		Total Heat Released		Maximum Release Rate	
	Group1	Group3	Group2	Group3	Group2	Group3	Group2	Group3	Group2	Group3	Group2	Group3
Group Average	605	606	970	1005	1011	984	2351	2352	1762	-	4149	-
Std Deviation	22	16	49	19	9	23	93	72	15	-	127	-
Reproducibility	4	18	9	7	6	32	85	21	21	-	116	-

Single Zone Analysis												
	60 km/hr				120 km/hr				3000 rev/min			
	Induction Period 5%		Burn Angle 5-95%		Induction Period 5%		Burn Angle 5-95%		Induction Period 5%		Burn Angle 5-95%	
	Group2	Group3	Group2	Group3	Group2	Group3	Group2	Group3	Group2	Group3	Group2	Group3
Group Average	19.1	18.9	19.1	43.3	17.2	17.2	33.7	33.3	15.7	-	30.4	-
Std Deviation	0.3	0.3	0.3	1.8	0.3	0.2	1.0	1.4	0.2	-	1.1	-
Reproducibility	0.1	0.2	0.1	0.2	0.2	0.0	0.6	0.0	0.0	-	0.4	-

Table 11-6 Comparisons of the standard deviation of the combustion analysis results and the test reproducibility indicating significance of the data set for the two-zone model.

Two-Zone Analysis												
	60 km/hr				120 km/hr				3000 rev/min			
	% Total Mass Trans.		Maximum Transfer Rate		% Total Mass Trans.		Maximum Transfer Rate		% Total Mass Trans.		Maximum Transfer Rate	
	Group2	Group3	Group2	Group3	Group2	Group3	Group2	Group3	Group2	Group3	Group2	Group3
Group Average	115.3	114.0	0.387	0.397	119.5	118.3	1.216	0.860	117.9	-	1.258	-
Std Deviation	4.3	1.6	0.019	0.013	1.4	1.3	1.308	0.027	3.2	-	0.025	-
Reproducibility	0.7	0.6	0.019	0.001	0.2	0.1	0.032	0.007	0.2	-	0.025	-

Two-Zone Analysis												
	60 km/hr				120 km/hr				3000 rev/min			
	Induction Period 5%		Burn Angle 5-95%		Induction Period 5%		Burn Angle 5-95%		Induction Period 5%		Burn Angle 5-95%	
	Group2	Group3	Group2	Group3	Group2	Group3	Group2	Group3	Group2	Group3	Group2	Group3
Group Average	19.6	19.4	43.3	38.6	17.8	17.7	30.3	24.3	16.6	-	31.4	-
Std Deviation	0.4	0.3	2.5	11.7	0.3	0.2	0.8	11.4	0.3	-	2.7	-
Reproducibility	0.4	0.1	0.0	0.7	0.2	0.1	0.7	-	0.1	-	0.6	-

11.2. Presentation of Emissions Results

The tabulated results can be found in Appendix D and in graphical format in Appendix E. The graphs take the form of a bar graph for the raw exhaust gas concentration as measured, with error bars indicating the

repeatability (difference between measured and average) as calculated in Section 11.1.2. It is therefore possible to see from the graph the significance of the data. Added to the graphs are the emissions calculated as g/kW.hr and g/km (except for 3000 rev/min where g/km has no direct significance as the load point is an acceleration simulation and not equivalent to any steady vehicle speed). These are added as line graphs for ease of readability and should not be interpreted as trends. In general it can be seen that all three presentations of the data indicate similar patterns. This suggests that the differences in exhaust gas composition dominated the effects on the rationalised emission indexes and not the other factors such as exhaust mass flow rate, power developed etc.

11.3. Validation of Two-Zone Model

The single-zone model was unaltered and has been successfully used for a number of investigations and is known to be accurate and sensitive [41, 45], therefore it is not necessary to validate the results of the model here. A visual inspection of the graphical results of a combustion analysis can immediately indicate if a model is not behaving correctly. If normal spark ignition combustion is occurring then the shape of the heat release rate curve has known properties and deviation from this indicates either an incorrect model, or poor quality pressure data. This was discussed in some detail in Section 9.2.2 during the consideration of the determination of the heat transfer sub-model coefficients. The two-zone combustion analysis model is a mass based model and calculates rate of combustion as a rate of mass transfer between the independent unburned and burned zones. The shape of this curve should indicate near zero combustion rate before combustion initiation, followed by a smooth and progressive increase in combustion rate up to a peak, and then decrease back to zero combustion rate during expansion. Although this is not a quantitative check, nor does it provide proof that the model is behaving correctly, any significant deviation from this expected shape will immediately indicate that the model is not operating correctly.

The integration of this rate of mass transfer, or cumulative mass transferred, can then be calculated with the final value being the total mass transferred. Racer does so, displaying and saving this in terms of a percentage of the specified cylinder charge mass. If the model is correct then, the final integrated value should be near to 100% indicating that the model has exactly accounted for all of the available combustible mass. It is seen that the model appears to over-predict the mass transfer and in almost all cases the predicted total mass is between 110 and 120 percent. This over-prediction is seen to be very consistent having an average of 116.5 and a standard deviation of only 3.1. Figure 11-4 gives an example of typical combustion rates determined by the two-zone combustion analysis. It can be seen that the general shape of the rate of combustion curve has the expected shape. It is again possible to see the unexpected prediction of combustion starting before spark ignition (positive combustion rate before –30° CA) as mentioned before in Section 9.2.2. This is assumed to be as a result of the squish effect due to the transducer placement.

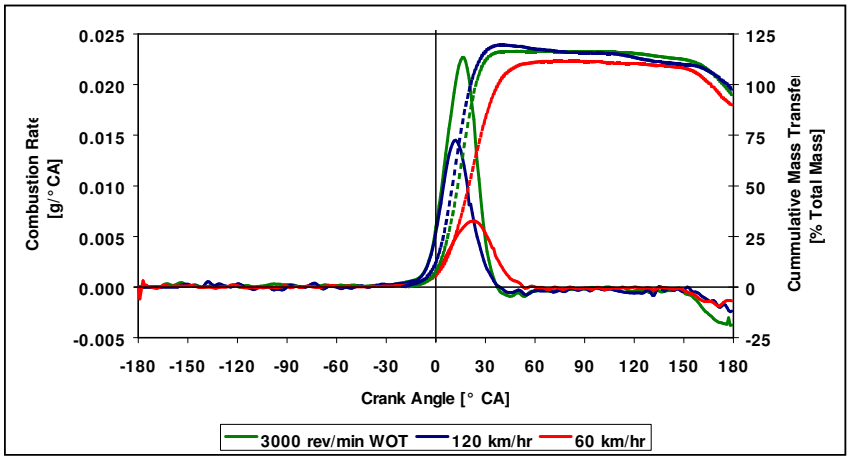

Figure 11-4 Examples of the rate of combustion and cumulative mass transferred results from the two-zone combustion analysis model.

To check that the model is sensitive to different conditions in as much as its prediction of combustion rates are concerned, the maximum predicted combustion rate was compared to the maximum burn rate as predicted by the single-zone model. This was done for two of the reference fuels data at all four load points at which pressure data was recorded. The results are shown below in Figure 11-5. Comparing the rate as computed in g/° CA with the single-zone combustion rate calculated in units of kJ/° CA results in a nearly straight line. This indicates that there is a nearly linear relationship between the two, but this still does not indicate whether good absolute agreement is seen. Once the two-zone results are converted to energy units by multiplying the gas mass transfer rate by it's specific energy content (mass rate x lower heating value x fuel/air ratio), a nearly straight line at 45° is achieved with good absolute value agreement.

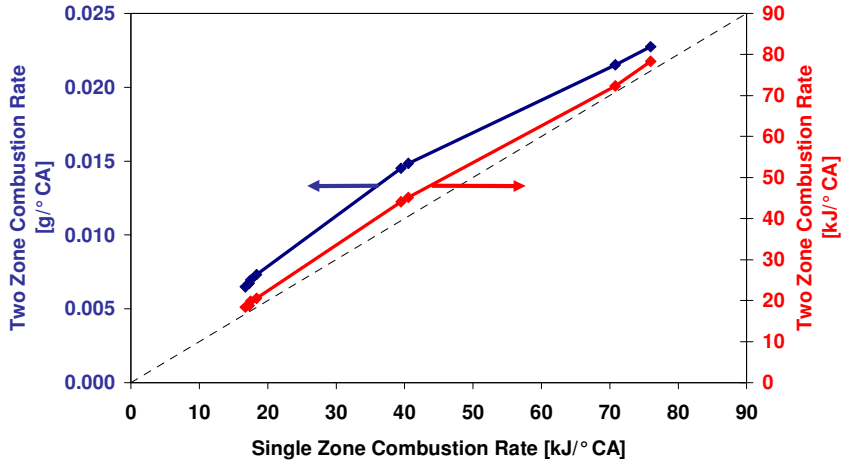

Figure 11-5 Comparison of two-zone and single-zone maximum combustion rate predictions for two reference fuels at all of the load points.

The two-zone model uses an equilibrium products model as an input into it's gas properties calculation routine as discussed in detail in Section 8.3.3. Although the purpose of this routine is not for emissions prediction, it would be instructive to compare the actual exhaust emissions measured and the predicted gas compositions at various

points in the cycle. A number of specific points were chosen during the cycle and the relevant species concentrations were extracted from the result files (for the same two reference fuels as above, at the four load points). The points of interest were the following:

- End of the cycle (180° CA)
- Exhaust valve opening, EVO (145° CA)
- End of combustion (calculated as spark timing + 2-98% induction + 2-98% burn angle + 2-98% induction)
- Maximum specie concentration (minimum concentration for O_2)
- NO concentration at 2000 K (burned gas temperature)
- NO concentration at maximum burned gas temperature
- Specie concentrations of C-O-H reacting system at 1800 K (burned gas temperature).

The reasons for these choices are as follows: the first is to see what the final prediction of the specie concentrations would be at the end of the cycle. However, this is not very useful as the model does not account for EVO and continues to make calculations based on the control mass and control volume as if the valve were closed. This can be seen by the negative combustion rate prediction after this event (at about 145° CA) in Figure 11-4. The result of this is a prediction of reactions in the reverse direction. Therefore, it would be more instructive to consider the concentrations at EVO or at some point near the end of combustion as is done in the next two choices. The maximum specie concentration was also extracted as a matter of interest. The last three choices pick out points based on the gas temperature of the burned gas. This is due to the fact that the NO formation chemistry is thought to become effectively frozen at below 2000 K, while the C-O-H system becomes rate limited at below 1800 K (as discussed in Section 2.3.1). The fact that the NO chemistry is known to be rate limited throughout (see Sections 2.3.1 and 8.3.5), it may also be interesting to find the NO concentration predicted by the equilibrium model at the maximum burned gas temperature. The results are presented below graphically in Figure 11-6, Figure 11-7, Figure 11-8 and Figure 11-9. It can be seen that the correlations are excellent with the exception of NO.

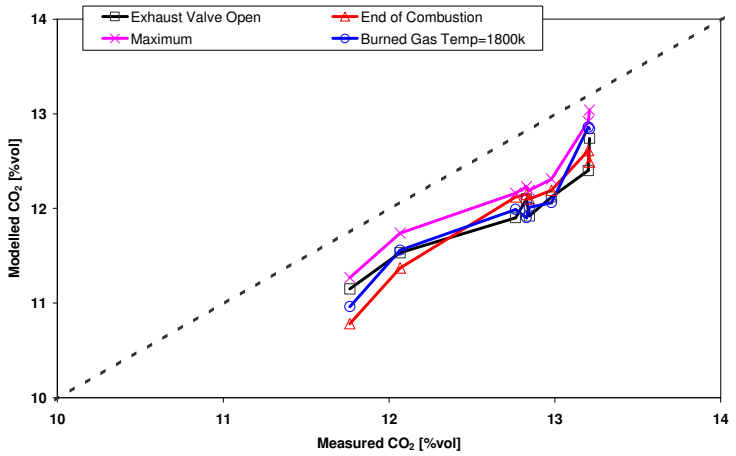

Figure 11-6 Comparison of predicted CO_2 concentrations during the cycle and measured exhaust CO_2 concentrations for two reference fuels at all of the load points.

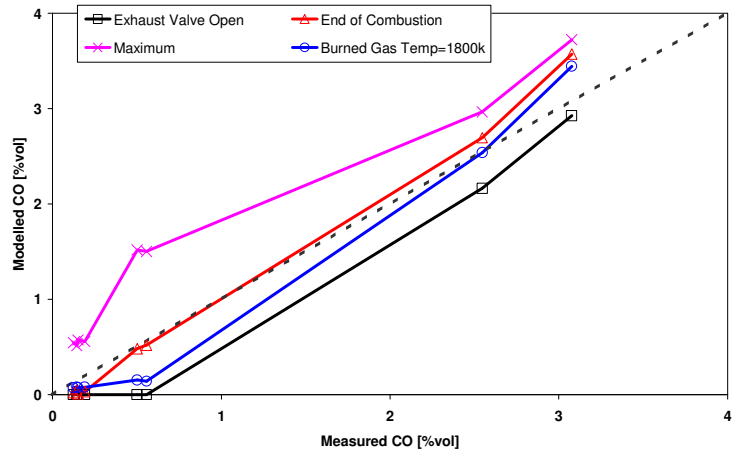

Figure 11-7 Comparison of predicted CO concentrations during the cycle and measured exhaust CO concentrations for two reference fuels at all of the load points.

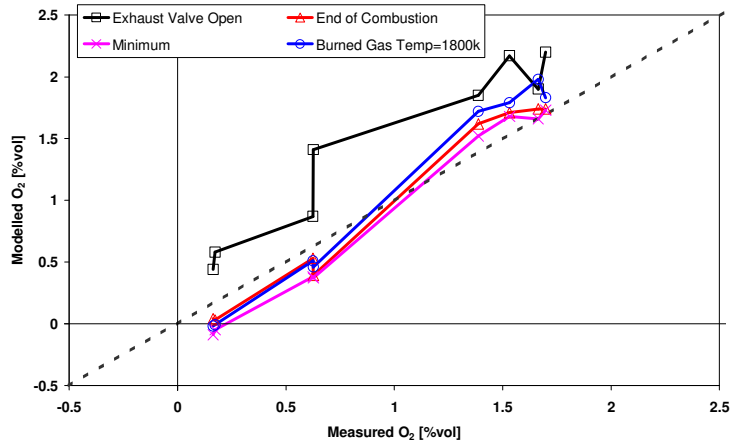

Figure 11-8 Comparison of predicted O_2 concentrations during the cycle and measured exhaust O_2 concentrations for two reference fuels at all of the load points.

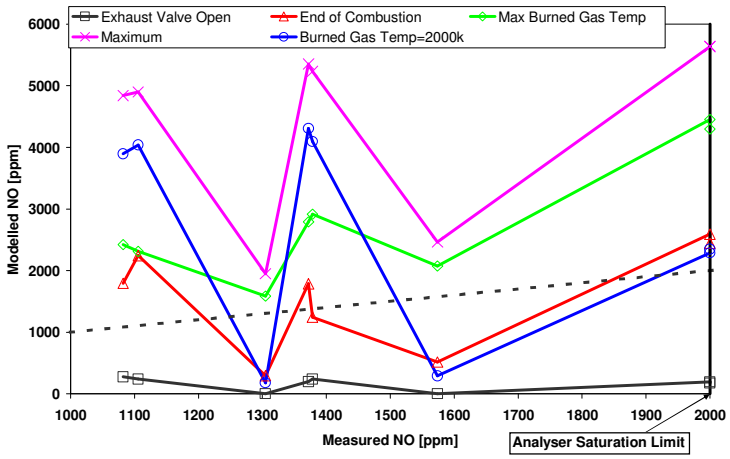

Figure 11-9 Comparison of predicted NO concentrations during the cycle and measured exhaust NO concentrations for two reference fuels at all of the load points.

The results for the CO emissions as displayed in Figure 11-7 are worth noting. As stated previously (Section 2.3.1) the CO concentrations emitted may be significantly higher than expected due to the non-linear response near to stoichiometric conditions, and slight uneven fuel distribution in multi-cylinder engines. This would tend to indicate that the equilibrium model should under-predict the CO emissions, and the good correlation seen is unexpected. However, due to the specific calibration of the engine under investigation, none of the operating points were near to an operating equivalence ratio of 1.0. Therefore this mechanism whereby higher than expected CO is measured will not be relevant and therefore the equilibrium routines would be expected to be applicable.

It can therefore be concluded that the equilibrium model appears to be behaving correctly. Although not intended to be an emissions predicting tool, the concentrations of the major species are similar to the measured emissions and the results of the model may be used as a predictor of the emissions of CO, CO_2 and O_2. Therefore the use of these specie concentrations for the prediction of gas properties is appropriate. Confidence can then be placed in the gas property calculations as used in the Racer2 program.

11.4. Validation of Zeldovich NO model

The extended Zeldovich NO model, as discussed above in Section 8.3.5 was added to the combustion analysis program Racer. The following discussion indicates the validation of the model.

Tracking the temperature and NO formation histories, as shown below in Figure 11-10, of an early, mid and late zone to burn indicates that the model is behaving as expected (by comparison with Figure 2-6, Section 2.3.1). In order to check whether the model is predicting actual NO values that correlate with measured values, the data at the simulated 60 km/hr vehicle speed (standard and closed loop simulation) was used. This is the only relevant data set available for the comparison as the NO analyser was saturated for all the simulated 120 km/hr load points and for most of the 3000 rev/min, WOT load points. The formation of NO is known to be highly sensitive to equivalence ratio. Initial attempts to correlate the model with the measured data did not produce encouraging results.

A detailed investigation was undertaken to investigate this, and it became evident that the there was some disparity between the equivalence ratio measurements for some of the data. Equivalence ratio was determined from measured fuel and air flow and fuel C:H:O ratios and separately from the measured exhaust emissions. It was noted that the data points which were indicating the poor correlation often corresponded with the data where there was uncertainty over the equivalence ratio. Thus the data points used for the correlation were reduced to only those where there was good agreement with regards to the equivalence ratios. This significantly improved the correlation.

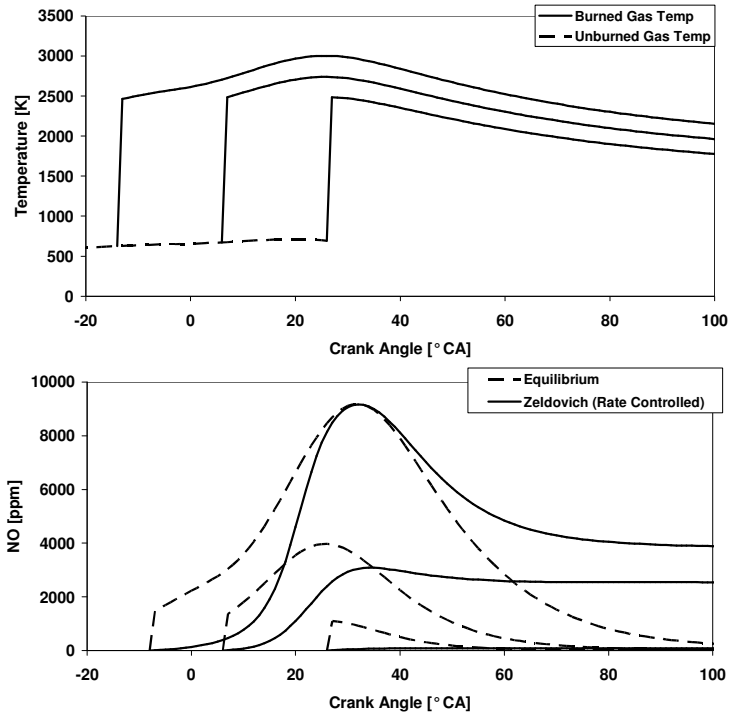

Figure 11-10 Temperature and NO formation histories as a function of crank angle for three different combustion elements.

The results of the correlation are indicated below in Figure 11-11. Excellent agreement is noted, in terms of the R^2 value (0.89), the slope of the correlation (0.96) and the absolute values. However, it is thought that the agreement in terms of absolute values is merely fortuitous. As indicated above, there is uncertainty regarding the appropriate values of the rate coefficients as these have not been accurately determined in conditions similar to that in real engines, and the model is unable to incorporate a number of salient factors such as heat transfer from the burned elements and inter-element mixing. Although there is insufficient data at the 3000 rev/min, WOT load point to perform a meaningful correlation, it was noted that at this load point the absolute values did not correlate as well with the measured values averaged at about 1750 ppm and the modelled values averaged at about 650 ppm.

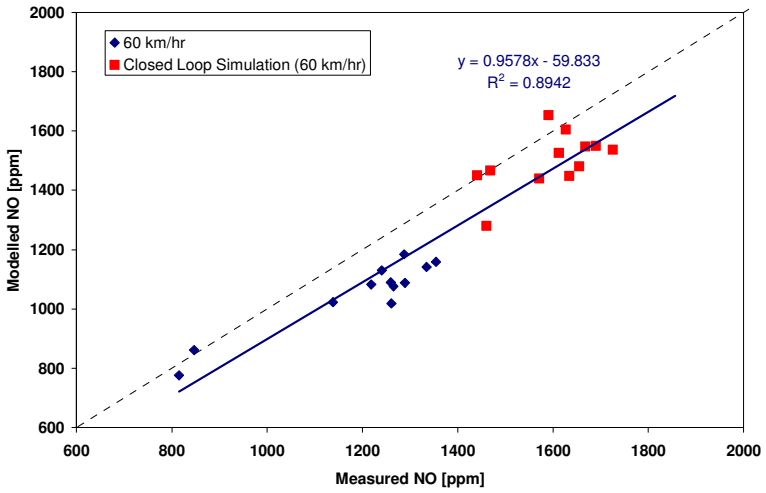

Figure 11-11 Comparison of modelled and measured NO emissions.

Considering further the response of the model and the measured NO, the NO was plotted as a function of equivalence ratio shown below in Figure 11-12 and Figure 11-13. This is done to see if the model is able to respond to factors other than equivalence ratio. It is quickly seen that equivalence ratio itself is unable to explain all the variation in NO, both modelled and measured. There is a distinct difference between the closed loop simulation and 60 km/hr vehicle speed simulation results. This is explained by the difference in ignition timing used for these two load points – with 20° advance used for the 60 km/hr load point and 25° used for the closed loop simulation. The model is therefore shown to be able to appropriately respond to the differing temperature histories of the burned gas elements caused by the difference in ignition timing. It is further evident from comparing the equivalence ratio graphs and the modelled versus measured graphs that, that the model is able to respond appropriately to differing temperature time histories within each subset of the data.

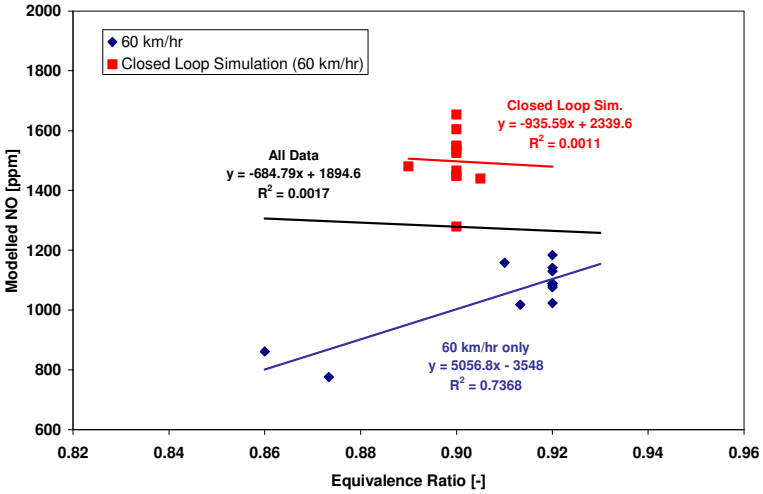

Figure 11-12 Modelled NO versus equivalence ratio.

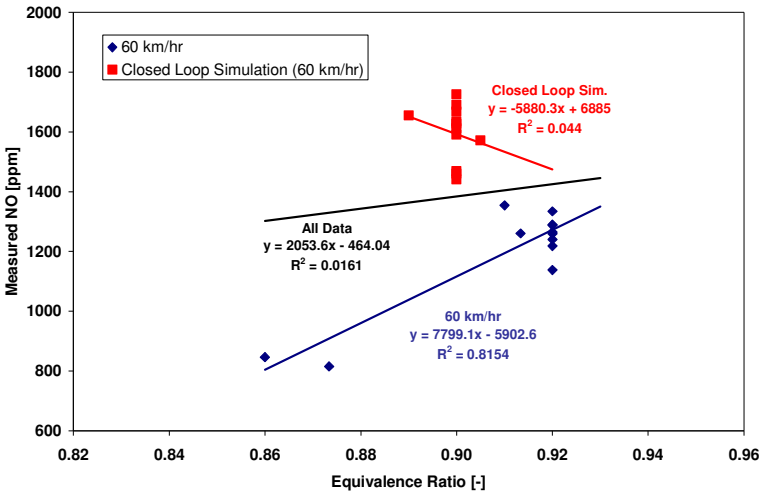

Figure 11-13 Measured NO versus equivalence ratio.

It can therefore be concluded that the model appears to be sensitive to both equivalence ratio and to the effects of temperature histories of the burned gas elements, both as a result of engine parameter differences, such as ignition timing, and fuel differences.

11.5. Results of Statistical Analysis

It is preferable in any statistical analysis, to utilise as large a data set as possible. By use of classification variables, as much of the collected data can be used in any given analysis as is possible. This is discussed in detail in Section 10.2. Certain engine operating conditions were also included so as to account for test to test variability, which is not accounted for by the classification variables. In the following discussion, the classification variables and their coefficients are not included, and the detail of these can be found in Appendix F.

11.5.1. Hydrocarbon Emissions Results

HC's – Fuel Properties Correlation

The results of the multivariate regressions, as derived from the Cp analysis technique detailed in Section 10.3, to find the fuel properties which indicate correlation with the hydrocarbon emissions are summarised in a convenient format below in Table 11-7. Eight different models, selected for having low p values, or total number of dependent variables, and having Cp values less than the p value, have been selected for evaluation. It can be seen that aromatics, olefins, paraffins, aromatic-olefin and aromatic-paraffin interactions, ER, DRYB, IBP and Lead all occur in at least 7 of the 8 models. It is therefore likely that they are the most important variables for prediction, and are thus strongly indicated as having correlation. Another interesting observation can be made – the importance of a group of variables, which are indicators of a fuels volatility characteristics. IBP, T10, T30, T50, VLRATIO and E70, of which at least three occur in every model proposed, indicates that low-end volatility is obviously important. All of the models have R^2

values of greater than 0.993, which indicates that the models are good predictors, accounting for most of the measured variation in hydrocarbon emissions. Two more variables are seen to occur in half of the models generated, they are sulphur and phenol content.

Table 11-7 Summary of Cp analysis for HC's – Fuel Properties Correlation

Model Nuimber	Cp	R^2	p	A	O	P	AO	AP	OP	AOP	ER	DRYB	SPECHUM	IBP	T10	T30	T50	DENS	VLRATIO	E70	SENS	LEAD	SULPHUR	PHENOLS	BENZENE
1	18.471	0.9935	23	✓	✓	✓	✓	✓			✓	✓		✓		✓	✓					✓		✓	
2	17.791	0.9937	24	✓	✓	✓	✓	✓			✓	✓		✓		✓			✓	✓		✓	✓		
3	18.572	0.9936	24	✓	✓	✓	✓	✓	✓		✓	✓		✓	✓		✓					✓		✓	
4	18.160	0.9937	25	✓	✓	✓	✓	✓	✓		✓	✓	✓	✓	✓		✓					✓		✓	
5	18.389	0.9937	25	✓	✓	✓	✓	✓			✓	✓		✓		✓			✓	✓	✓	✓	✓		
6	18.429	0.9937	25	✓	✓	✓	✓	✓			✓	✓		✓		✓	✓		✓	✓		✓	✓		
7	18.537	0.9937	25	✓	✓	✓	✓	✓	✓	✓	✓	✓		✓	✓		✓					✓		✓	
8	17.738	0.9937	25	✓	✓		✓				✓	✓		✓		✓		✓	✓	✓	✓	✓	✓		✓
Variable Occurrence Frequency				8	8	7	8	7	3	1	8	8	1	8	3	5	5	1	4	4	2	8	4	4	1

An investigation was made of the first three models, to check for co-linearity and to provide model coefficients. If co-linearities were predicted, reduced models were investigated by deleting each of the co-linear variables and checking for Cp and further co-linearities. A summarised table indicating co-linearities, R^2 values, Cp and p, the number of observations that were able to be used, along with the model coefficients and their uncertainties is presented in Table 11-8. The Cp and p values were included again in this table so that the new reduced models Cp and p values could be compared. The statistical uncertainty is the opposite of statistical significance and is given as a dimensionless fraction. As an example, a quoted uncertainty of 0.01 is the same as a 1% uncertainty, or a 99% significance. SAS® includes the predicted uncertainty in the output of the model coefficients and therefore it is used here for convenience. If an uncertainty greater than 0.05 (5%) is predicted then this is highlighted in the table by using *italics*. Variable coefficients with high uncertainties are usually not considered in the discussions of the results.

Table 11-8 Summary of co-linearity analysis, giving the co-linear variables and the variable coefficients for the HC's – Fuel Properties Correlation.

Model Number	Cp	R^2	P	Number of Observations Used	Colinearities		A	O	P	AO	AP	OP
1	18.47	0.9935	23	206	A/O/P/ER	Coefficient	-0.1416	-0.1286	-0.0865	0.0021	0.0007	
					T30/T50	Uncertainty	0.0001	0.0001	0.0001	0.0001	0.0001	
2	17.79	0.9937	24	238	A/O/P/ER	Coefficient	*-0.0490*	*-0.0350*	*-0.0037*	0.0019	0.0007	
					T30/T50	Uncertainty	*0.0709*	*0.2022*	*0.8950*	0.0001	0.0001	
2 Reduced	23.29	0.9927	23	238	A/O/P/ER	Coefficient	-0.0867	-0.0716	-0.0457	0.0018	0.0007	
						Uncertainty	0.0003	0.0037	0.0571	0.0001	0.0001	
3	18.57	0.9936	24	206	A/P/ER	Coefficient	-0.1212	-0.1255	-0.0625	0.0027	0.0008	*0.0003*
					O/AO/OP	Uncertainty	0.0001	0.0001	0.0012	0.0001	0.0001	*0.1198*
3 Reduced	19.34	0.9934	23	206	A/O/P/ER	Coefficient	-0.1063	-0.0911	-0.0589	0.0019	0.0007	
						Uncertainty	0.0001	0.0001	0.0021	0.0001	0.0001	

Model Number		ER	DRYB	IBP	T10	T30	T50	VLRATIO	E70	LEAD	SULPHUR	PHENOLS
1	Coefficient	11.0904	0.0759	0.0230		-0.0263	0.0295			0.0027		-0.0006
	Uncertainty	0.0001	0.0001	0.0241		0.0010	0.0001			0.0001		0.0365
2	Coefficient	8.8075	0.0866	0.0368		-0.0302		-0.0444	-0.0467	0.0027	-7.4081	
	Uncertainty	0.0001	0.0001	0.0003		0.0059		0.0002	0.0010	0.0001	0.0003	
2 Reduced	Coefficient	9.4934	0.0830	0.0349				-0.0395	*-0.0115*	0.0025	-6.0786	
	Uncertainty	0.0001	0.0001	0.0007				0.0011	*0.0651*	0.0001	0.0023	
3	Coefficient	8.8892	0.0788	0.0252	-0.0351		0.0223			0.0026		-0.0006
	Uncertainty	0.0001	0.0001	0.0145	0.0015		0.0001			0.0001		0.0264
3 Reduced	Coefficient	8.7396	0.0745	0.0242	-0.0353		0.0210			0.0026		-0.0006
	Uncertainty	0.0001	0.0001	0.0189	0.0014		0.0002			0.0001		0.0282

Good agreement is seen between the coefficient values having low uncertainty, for all the models. The reduced model 3, which appears to be the best of this selection by virtue of having only a single co-linearity, which appears in all the models, and a high R^2 value was selected for comparison with measured data. The co-linearity between the aromatic, olefin and paraffin contents and the equivalence ratio is considered to be a real, unavoidable co-linearity. As discussed in Section 5.4, it was not possible to determine exactly the C:H:O ratios of the various fuels. This ratio has a direct impact on the operating equivalence ratio. The test engines are both considered open loop and can not compensate for fuel variations. Fuel C:H ratios, as indicated in Figure 5-4, are directly related to the content of the various fuel component classes. Thus, there is a co-linearity between these variables. Had reliable C:H:O ratios been available, and thus been included in the statistical analysis, it is likely that the terms describing this ratio would have been significant and would have precluded the co-linearity. This predicted values from this model (model 3) were compared to the measured emissions and viewed graphically as shown in Figure 11-14. From this it can be seen that the model is a reliable predictor of HC emissions, and it is probable that the most important parameters have been captured.

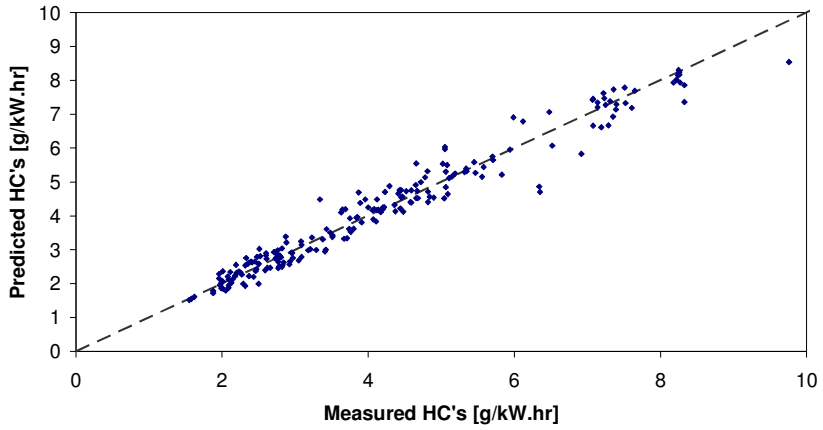

Figure 11-14 Graph of the HC's as predicted by model 3 versus measured HC's.

Before any discussion of the response to the fuel components can be given, it is important to note that co-linearity is predicted between aromatics, olefins, and paraffins in all the models. This may make any conclusions drawn from these variables inaccurate. Considering Table 11-8, it can be seen that aromatics and olefins indicate similar magnitude, negative coefficients (≈ -0.11) while paraffins indicate a somewhat smaller, though still negative coefficient (≈ -0.06). Fuel component interactions are also present in the prediction model. The coefficients of the two factor interactions AO and AP are positive, with AP being an order of magnitude smaller than AO, which is itself at least an order of magnitude smaller than any of the main effects. This greatly complicates any interpretation. It is relevant to note that the fuel composition is given in percentages and not fractions. Therefore, interaction variables are the multiplication of numbers larger than one, resulting in a larger number. It is therefore possible that the interactions may exert an overwhelming influence on the predicted emissions even though their coefficients are orders of magnitude smaller.

The order of magnitude disparity between the main and interaction variables was investigated using hypothetical fuel blends, spanning the range of fuel component concentrations, and by calculating the predicted emissions. The hypothetical fuel blends were constructed by taking the maximum and minimum concentrations of each fuel component class, as well as four intermediate concentrations (see Table 5-1). The concentrations of the remaining two components were then calculated to be in the same ratio as the "average fuel". This is in essence a process of increasing or decreasing only the concentration of the fuel component class being investigated. The effect of the individual fuel component classes could then be seen. The results of this analysis is tabulated and displayed graphically in Table 11-9 and Figure 11-15 respectively. In this investigation, none of the other parameters, or classification variables were included. Therefore, the values attained should merely be used for comparative purposes.

The non-linear effect of the interaction variables is plainly evident, especially when olefins or aromatics are varied. From this it would seem that the lowest predicted HC's may result from a highly aromatic or olefinic fuel (high negative coefficients), but one which has the lowest aromatic/olefinic interaction (high positive coefficient). The response of two more hypothetical fuels were calculated: Best Fuel 1 and Best Fuel 2, by

taking the maximum aromatics and olefins respectively, the minimum olefins and aromatics respectively and making the rest up with paraffins. The actual full range of possible aromatic or olefinic contents have obviously not been considered in this argument (merely the highest and lowest in the test fuels). Therefore this analysis should not be seen as differentiating between the two approaches (maximum aromatics/minimum olefins versus maximum olefins/minimum aromatics). Furthermore, this analysis does not take into account the interaction between the content of the various fuel components and the other fuel properties.

Table 11-9 Tabulated results of the investigation of the fuel class content effects on predicted HC's.

	Component Concentrations			Relative Contributions						Sum
	A	O	P		A	O	P	AO	AP	
	% vol	% vol	% vol	Coefficients	-0.12116	-0.12554	-0.06248	0.00270	0.00081	
Average Fuel	33.5	25.2	41.3		-4.059	-3.164	-2.581	2.282	1.114	-6.407
Maximum Aromatics	69.0	11.7	19.3		-8.360	-1.475	-1.203	2.191	1.069	-7.777
	57.8	16.0	26.2		-7.003	-2.008	-1.638	2.498	1.219	-6.930
	46.6	20.2	33.2		-5.646	-2.540	-2.072	2.549	1.244	-6.466
	35.4	24.5	40.1		-4.289	-3.073	-2.507	2.342	1.143	-6.383
	24.2	28.7	47.1		-2.932	-3.606	-2.941	1.879	0.917	-6.683
Minimum Aromatics	13.0	33	54.0		-1.575	-4.139	-3.376	1.158	0.565	-7.366
Maximum Olefins	22.4	50.0	27.6		-2.713	-6.277	-1.725	3.026	0.498	-7.191
	26.7	40.4	32.9		-3.234	-5.072	-2.056	2.915	0.707	-6.740
	31.0	30.8	38.2		-3.755	-3.867	-2.387	2.580	0.953	-6.476
	35.3	21.2	43.5		-4.276	-2.661	-2.719	2.022	1.236	-6.397
	39.6	11.6	48.8		-4.797	-1.456	-3.050	1.241	1.556	-6.506
Minimum Olefins	43.9	2.0	54.1		-5.318	-0.251	-3.381	0.237	1.912	-6.801
Maximum Paraffins	16.6	12.4	71		-2.005	-1.563	-4.436	0.557	0.946	-6.502
	24.2	18.2	58		-2.932	-2.285	-3.599	1.191	1.122	-6.503
	31.8	24.0	44		-3.858	-3.007	-2.762	2.062	1.133	-6.432
	39.5	29.7	31		-4.785	-3.729	-1.924	3.171	0.979	-6.288
	47.1	35.5	17		-5.711	-4.452	-1.087	4.518	0.660	-6.072
Minimum Paraffins	54.8	41.2	4		-6.638	-5.174	-0.250	6.103	0.176	-5.782
Best Fuel 1	69	2	29		-8.360	-0.251	-1.812	0.373	1.611	-8.439
Best Fuel 2	13	50	37		-1.575	-6.277	-2.312	1.757	0.387	-8.020

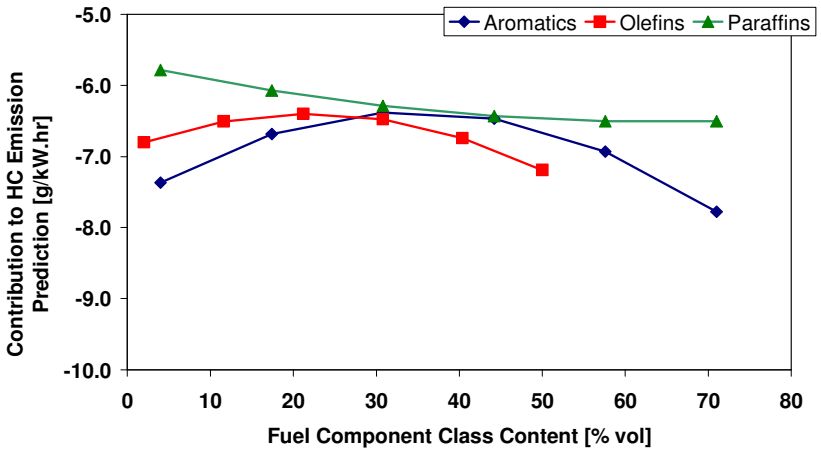

Figure 11-15 Graphical presentation of the effects of the fuel component content on predicted HC's.

The approach taken in much of the literature [20, 21 and 22] to fuel blending for the investigation of fuel component content on emissions has been that of using paraffins as a swing component. In other words,

if the effect of aromatics is being considered, then the olefin content is held constant, the desired aromatic content is then achieved by altering the paraffin content. This approach was also investigated by way of hypothetical fuels as above so as to be able to compare with the results presented in these publications. The results of this are presented in Table 11-10 and Figure 11-16. The response of the aromatics is much the same, however, the olefin response is quite different. The non-linear response seen for olefins before is not present. Here olefins are seen to have little influence on the hydrocarbon emissions.

Table 11-10 Tabulated results of the investigation of aromatic and olefin content effects on predicted HC's with paraffins as the swing component.

	Component Concentrations				Relative Contributions					Sum
	A	O	P		A	O	P	AO	AP	
	% vol	% vol	% vol	Coefficients	-0.12116	-0.12554	-0.06248	0.00270	0.00081	
Average Fuel	33.5	25.2	41.3		-4.059	-3.164	-2.581	2.282	1.114	-6.407
Maximum Aromatics	69.0	25.2	5.8		-8.360	-3.164	-0.362	4.700	0.322	-6.864
	57.8	25.2	17.0		-7.003	-3.164	-1.062	3.937	0.791	-6.501
	46.6	25.2	28.2		-5.646	-3.164	-1.762	3.174	1.058	-6.340
	35.4	25.2	39.4		-4.289	-3.164	-2.462	2.411	1.123	-6.380
	24.2	25.2	50.6		-2.932	-3.164	-3.162	1.648	0.986	-6.623
Minimum Aromatics	13.0	25.2	61.8		-1.575	-3.164	-3.861	0.886	0.647	-7.068
Maximum Olefins	33.5	50.0	16.5		-4.059	-6.277	-1.031	4.528	0.445	-6.394
	33.5	40.4	26.1		-4.059	-5.072	-1.631	3.658	0.704	-6.399
	33.5	30.8	35.7		-4.059	-3.867	-2.231	2.789	0.963	-6.404
	33.5	21.2	45.3		-4.059	-2.661	-2.830	1.920	1.222	-6.409
	33.5	11.6	54.9		-4.059	-1.456	-3.430	1.050	1.481	-6.415
Minimum Olefins	33.5	2.0	64.5		-4.059	-0.251	-4.030	0.181	1.739	-6.420

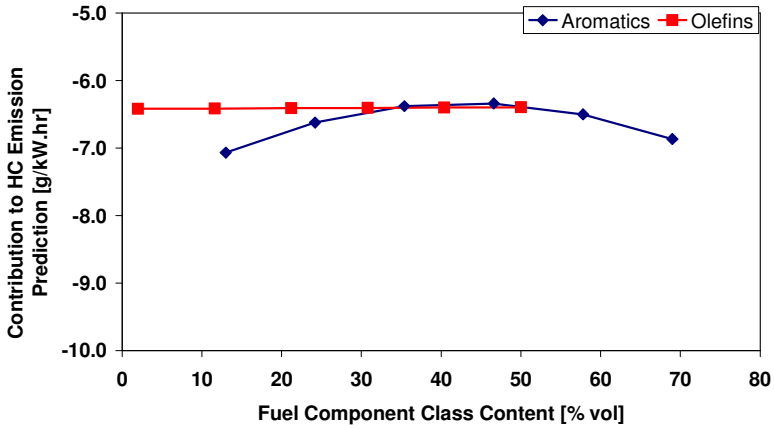

Figure 11-16 Graphical presentation of the effects of the aromatic and olefin content on predicted HC's with paraffins as the swing component.

The response to equivalence ratio, indicated by a positive coefficient, implies that richer operation would increase HC emission. This result is given with the lowest uncertainty that SAS® reports, 0.0001 (0.01%) and is thus highly significant. The indicated response to ambient variations shows an increased emission for higher engine test cell temperatures. The next group of six variables are all measures of fuel volatility characteristics. Initial boiling point (IBP), which appears in all the models, shows a positive coefficient indicating that the higher the temperature required to initiate vaporisation, the higher the HC emissions. The T_{10}, T_{30} and T_{50} responses seem to indicate contradictory trends, especially when considered with IBP. The two lower end volatility measures (T_{10} and T_{30}) indicate an opposite effect compared to IBP and

T_{50}. The co-linearities that are predicted between some of these volatility measures (T_{30} / T_{50} and T_{30} / E_{70}) indicate that their validity may be questionable. The vapour/liquid ratio (VLRATIO, the temperature required to obtain 36/1 vapour/liquid ratio under specified conditions) is a measure of volatility with a more volatile liquid having a lower vapour/liquid ratio temperature. Thus the negative coefficient implies that the models predict that less volatile liquids have reduced HC emissions. E_{70}, the percentage of a liquid vaporised at 70°C, indicates that the more fuel already vaporised at this temperature, the lower the HC emissions. IBP, T_{10}, T_{30}, T_{50}, vapour/liquid ratio and E_{70} are all measures of low- to mid-range volatility, and these seemingly contrary directional responses are difficult to interpret. IBP and E_{70} indicate, in some of the models, uncertainties greater than 0.01. These are still less than the 0.05 threshold, but are larger than the uncertainties of many of the other parameters.

Investigating the effects of volatility further, the average of these fuel properties was calculated for the entire sample fuel set, and this average multiplied with the respective variable coefficient. This in effect normalises the coefficients and thus the numerical value of this normalised coefficient is an indication of the magnitude of the effect of that particular variable. The results of this investigation are tabulated and presented in Table 11-11. Models which include both the distillation curve points (IBP and $T_{\#\#}$) and the other volatility measures are difficult to interpret. Considering the models with only the distillation curve points (models 1, 3 and 3 Reduced), a combined calculation is made and it is clear that increased low end volatility will lead to reduced HC emissions.

Table 11-11 Investigation of low- to mid-range volatility effects, by normalising the coefficients, on predicted HC's.

Model		IBP	T10	T30	T50	VLRATIO	E70	Combined[#]
	Fuel Property Average	34.5	56.5	77.5	100.2	60.8	26.3	
1	Model Coefficients	0.0230		-0.0263	0.0295			
2		0.0368		-0.0302		-0.0444	-0.0467	
2 Reduced		0.0349				-0.0395	-0.0115	
3		0.0252	-0.0351		0.0223			
3 Reduced		0.0242	-0.0353		0.0210			
1	Coefficient * Average	0.7942		-2.0382	2.9552			1.7111
2		1.2680		-2.3401		-2.6978	-1.2260	-
2 Reduced		1.2036				-2.4013	-0.3031	-
3		0.8667	-1.9812		2.2381			1.1236
3 Reduced		0.8339	-1.9907		2.0993			0.9424

[#] Combined = IBP + T10 + T30 + T50

The fuels lead content appears to influence the HC emissions with increased lead leading to increased HC emissions. Both fuel sulphur content and the concentration of phenols in the fuel is seen to reduce the HC emissions. The lead and sulphur results are seen to have low uncertainties of less than 0.5%, while the phenols response has relatively high uncertainties of greater than 2%.

HC's – Combustion Analysis Correlation

The tabulated summary of the Cp analysis for the HC – combustion analysis correlation is given in Table 11-12. This shows that the more important variables to consider are CADPMAX, DHRMAX, TMAX, Z2TOTG, Z2DGMAX, and Z2TUBMAX, all of which occur in all the models.

Table 11-12 Summary of Cp analysis for HC's – Combustion Analysis Correlation.

Model Nuimber	Cp	R^2	p	PMAX	CAPMAX	DPMAX	CADPMAX	TOTHR	DHRMAX	CADHRMAX	TMAX	CATMAX	IND5	BA595	Z2TOTG	Z2PERCNT	Z2DGMAX	Z2DGMXCA	Z2TUBMAX
1	7.541	0.9917	10				✓		✓		✓				✓		✓		✓
2	4.138	0.9923	11			✓	✓		✓		✓				✓		✓		✓
3	4.794	0.9923	11	✓			✓		✓		✓				✓		✓		✓
4	6.133	0.9921	11				✓		✓		✓				✓		✓	✓	✓
5	7.326	0.9920	11				✓		✓		✓			✓	✓		✓		✓
6	7.666	0.9919	11				✓		✓		✓				✓	✓	✓		✓
7	7.795	0.9919	11				✓		✓		✓	✓			✓		✓		✓
8	8.039	0.9919	11				✓		✓		✓		✓		✓		✓		✓
9	8.152	0.9919	11		✓		✓		✓		✓				✓		✓		✓
10	9.021	0.9918	11				✓	✓	✓		✓				✓		✓		✓
11	9.100	0.9918	11				✓		✓	✓	✓				✓		✓		✓
Variable Occurrence Frequency				1	1	1	11	1	11	1	11	1	1	1	11	1	11	1	11

Considering Table 11-13, the summarised results of the co-linearity checks, good agreement is again seen between the coefficients for all the models, with the possible exception of model 2. However, it can be seen that models 2, 5 and 8 each have 11 variables while model 1 has 10 (number of variables includes the classification variables not shown), but models 5 and 8 each have one variable which is not statistically significant. Therefore, model 2 has one more statistically significant variable and this will influence the coefficients. The predicted emissions from model 1 are plotted against measured emissions in Figure 11-17 and it can be seen that this model is a good predictor.

CADPMAX has a positive coefficient, which implies that the more retarded (later) that the maximum rate of change of pressure occurs, the higher the HC emissions. Likewise, the higher the maximum heat release rate (single-zone - DHRMAX), the higher the HC emissions. The negative coefficient of the TMAX variable indicates that the greater the maximum predicted gas temperature (single-zone), the lower the HC emissions. The positive coefficient for the total mass transferred (two-zone – Z2TOTG), indicates that increased HC emissions will be predicted for larger calculated cumulative mass transferred. The maximum combustion rate as computed by the two-zone model (Z2DGMAX) shows a contradictory trend as compared to that of the single-zone analysis. The negative coefficient implies that the greater the maximum combustion rate, the lower the HC emissions. Finally, higher predicted maximum unburned gas temperatures (two-zone model, Z2TUBMAX) suggest increased HC emissions. It is important however to note that a co-linearity is indicated between Z2DGMAX and Z2TUBMAX. The uncertainty of all of these variables is low, being generally less than 0.5%.

Table 11-13 Summary of co-linearity analysis, giving the co-linear variables and the variable coefficients for the HC's – Combustion Analysis Correlation.

Model Number	Cp	R^2	P	Number of Observations Used	Colinearities		DPMAX	CADPMAX	DHRMAX	TMAX	IND5	BA595	Z2TOTG	Z2DGMAX	Z2TUBMAX
1	7.54	0.9917	10	86	ZDGMAX / ZTUBMAX	Coefficient		0.0288	0.0032	-0.0014			13.5928	-8.3955	0.0077
						Uncertainty		0.0028	0.0001	0.0001			0.0018	0.0047	0.0054
2	4.14	0.9923	11	86	ZDGMAX / ZTUBMAX	Coefficient	0.0186	0.0327	0.0028	-0.0013			20.6718	-13.0570	0.0120
						Uncertainty	0.0171	0.0007	0.0001	0.0001			0.0001	0.0002	0.0003
5	7.33	0.9920	11	86	DHRMAX / ZDGMAX / ZTUBMAX	Coefficient		0.0278	0.0033	-0.0014		*-0.0348*	14.9756	-10.3971	0.0095
						Uncertainty		0.0038	0.0001	0.0001		*0.1312*	0.0008	0.0015	0.0017
8	8.04	0.9919	11	86	ZDGMAX / ZTUBMAX	Coefficient		0.0274	0.0033	-0.0015	*-0.1406*		14.3561	-9.2593	0.0085
						Uncertainty		0.0046	0.0001	0.0001	*0.2150*		0.0011	0.0025	0.0028

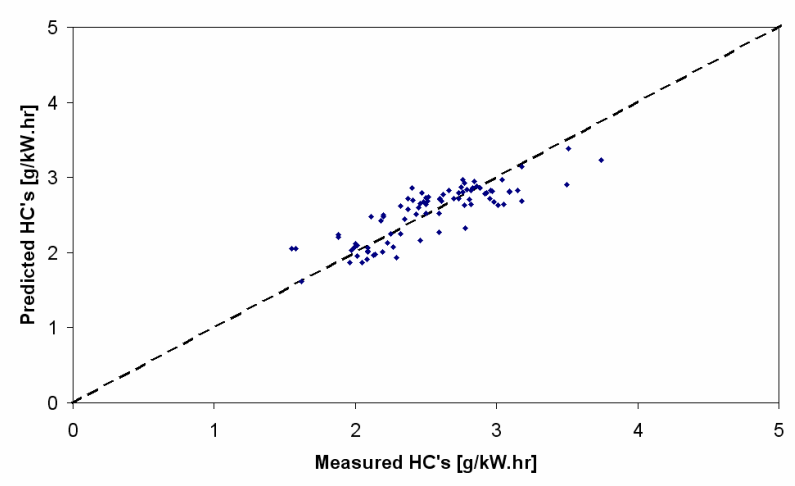

Figure 11-17 Graph of the HC's as predicted by model 1 versus measured HC's.

11.5.2. NO Emissions Results

NO – Fuel Properties Correlation

The summary for the Cp analysis for the NO emissions – fuel properties correlation is given in Table 11-14 from which it can be seen that OILT, MANP, BARO, DRYB, FBP and LEAD are all important variables.

Table 11-14 Summary of Cp analysis for NO – Fuel Properties Correlation

Model Nuimber	Cp	R^2	p	O	P	ER	IGNTIM	OILT	EXHT	MANP	BARO	DRYB	SPECHUM	T10	T70	FBP	SENS	LEAD	DENS	NITROGEN
1	7.089	0.9919	13				✓	✓		✓	✓	✓				✓		✓		
2	6.385	0.9921	14				✓	✓		✓	✓	✓				✓		✓		
3	6.901	0.9921	14					✓		✓	✓	✓				✓		✓		
4	6.934	0.9921	14	✓				✓		✓	✓	✓				✓		✓		
5	7.487	0.9920	14					✓		✓	✓	✓				✓	✓	✓		
6	7.532	0.9920	14					✓		✓	✓	✓	✓			✓		✓		
7	7.816	0.9920	14		✓			✓		✓	✓	✓				✓			✓	
8	7.872	0.9920	14		✓			✓		✓	✓	✓				✓		✓		
9	8.188	0.9920	14					✓		✓	✓	✓			✓	✓		✓		
10	8.249	0.9920	14				✓			✓	✓	✓			✓	✓		✓		
11	8.275	0.9920	14					✓		✓	✓	✓		✓		✓		✓		
12	8.402	0.9920	14					✓		✓	✓	✓				✓		✓		✓
13	8.446	0.9919	14					✓	✓	✓	✓	✓				✓		✓		
14	8.450	0.9919	14			✓		✓		✓	✓	✓				✓		✓		
Variable Occurrence Frequency				1	2	1	2	13	1	14	14	14	1	1	2	14	1	13	1	1

Considering the variable coefficients of selected models, as given in Table 11-15, it can be seen that the coefficient magnitudes are similar for all models shown (except where the variable has high statistical uncertainty). The NO emissions as predicted by model 2 are plotted against the measured emissions in Figure 11-18 and a fairly good capability of prediction is seen. Considering the sign of the variable coefficients, higher oil temperatures indicate increased NO emissions, however the uncertainty is relatively high at above 3%. Increased manifold pressures indicate reduced emissions while the opposite is seen for barometric pressure. The uncertainty of these is low at less than 0.05%. Manifold pressure data is recorded in kPa while barometric pressures are given in mBar, therefore the order of magnitude difference in the coefficients results in the magnitudes of the effects being of a similar order of magnitude. However, this relationship between manifold pressure and barometric pressure is confounded by a co-linearity between the two. Higher ambient dry bulb temperatures indicate increased NO emissions as indicated by the positive coefficient with uncertainties of between 0.5% and 5.5%. The only important fuel properties appear to be final boiling point and lead content. Higher FBP (reduced high-end volatility) indicates reduced NO emissions, while the higher lead content tends to imply increased emissions. Both of these parameters indicate coefficients with uncertainties of less than 1%.

Table 11-15 Summary of co-linearity analysis, giving the co-linear variables and the variable coefficients for the NO – Fuel Properties Correlation.

Model Number	Cp	R^2	P	Number of Observations Used	Colinearities		O	IGNTIM	OILT	MANP	BARO	DRYB	FBP	LEAD	BENZENE
1	7.09	0.9919	13	163	MANP / BARO	Coefficient			0.0653	-0.8751	0.0567	0.1582	-0.0321	0.0024	
						Uncertainty			0.0304	0.0003	0.0001	0.0287	0.0026	0.0037	
2	6.39	0.9921	14	159	MANP / BARO	Coefficient		*-0.5596*	0.0674	-0.8076	0.0627	0.2203	-0.0297	0.0020	
						Uncertainty		*0.1019*	0.0383	0.0009	0.0001	0.0041	0.0058	0.0141	
2 Reduced	13.75	0.9914	13	146	IGNTIM / BARO	Coefficient		-0.7337	0.0630		0.0276	*0.1447*	-0.0291	0.0018	
						Uncertainty		0.0367	0.0611		0.0005	*0.0545*	0.0088	0.0326	
3	6.90	0.9921	14	159	MANP / BARO	Coefficient			0.0671	-0.8533	0.0561	0.1645	-0.0378	0.0025	*0.0979*
						Uncertainty			0.0341	0.0004	0.0001	0.0247	0.0005	0.0022	*0.0999*
4	6.93	0.9921	14	163	MANP / BARO	Coefficient	0.0201		0.0589	-0.9617	0.0614	0.1674	-0.0352	0.0026	
						Uncertainty	0.0461		0.0499	0.0001	0.0001	0.0198	0.0010	0.0016	

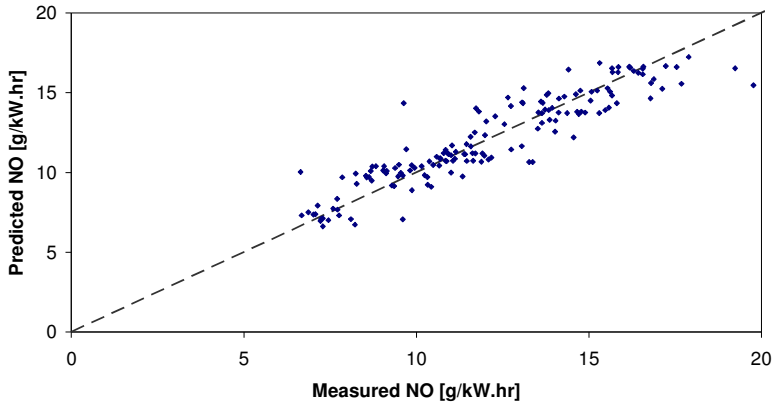

Figure 11-18 Graph of the NO as predicted by model 2 versus measured NO.

NO – Combustion Analysis Correlation

Considering Table 11-16, it can be seen that DPMAX, TMAX, and CATMAX are important variables, while TOTHR and BA595 can not be ignored, with each occurring in 7 of the selected 13 models.

Table 11-16 Summary of Cp analysis for NO – Combustion Analysis Correlation

Model Nuimber	Cp	R^2	p	STAB	PMAX	CAPMAX	DPMAX	TOTHR	TMAX	CATMAX	BA595	Z2TOTG	Z2PERCNT	Z2DGMAX	Z2DGMXCA	Z2TUBMAX	Z2TBMAX
1	8.475	0.9964	8				✓		✓	✓			✓	✓			
2	8.650	0.9964	8		✓		✓		✓	✓							✓
3	8.970	0.9964	8	✓			✓		✓	✓				✓			
4	9.052	0.9964	8				✓	✓	✓	✓	✓						
5	6.023	0.9968	9				✓	✓	✓	✓	✓					✓	
6	6.201	0.9967	9				✓	✓	✓	✓	✓						✓
7	7.132	0.9967	9				✓	✓	✓	✓	✓	✓					
8	7.897	0.9966	9		✓	✓	✓		✓	✓						✓	
9	8.040	0.9966	9		✓	✓	✓		✓	✓							✓
10	8.094	0.9966	9				✓	✓	✓	✓	✓			✓			
11	8.392	0.9966	9	✓			✓		✓	✓				✓	✓		
12	8.772	0.9966	9	✓			✓	✓	✓	✓	✓						
13	8.804	0.9966	9		✓			✓	✓	✓	✓					✓	
Variable Occurrence Frequency				3	4	2	12	7	13	13	7	1	1	4	1	3	3

Considering the first 5 models variable coefficients as displayed in Table 11-17, it can be seen that the higher the measured maximum rate of change of pressure, the lower the predicted NO emissions. The positive coefficient of the TOTHR variable implies that the higher the predicted total heat released (single-zone), the higher the predicted NO emissions. Maximum gas temperatures as predicted by the single-zone model, indicate that the NO emissions will be lower for higher temperatures. Furthermore, the crank angle at which this maximum gas temperature is calculated to have occurred is also important for prediction, with reduced emissions being predicted when maximum temperatures occur later in the cycle. The single-zone model burn angle of 5 to 95% indicates that the predicted emissions will be reduced for

longer burn angles (slower overall combustion). All of these coefficients show extremely low uncertainties of less than 0.5%.

Table 11-17 Summary of co-linearity analysis, giving the co-linear variables and the variable coefficients for the NO – Combustion Analysis Correlation.

Model Number	Cp	R^2	P	Number of Observations Used	Colinearities		STAB	PMAX	DPMAX	TOTHR	TMAX	CATMAX	BA595	Z2PERCNT	Z2DGMAX	Z2TUBMAX	Z2TBMAX
1	8.48	0.9964	8	58	Z2PERCNT / ZDGMAX	Coefficient			-0.2136		-0.0040	-0.5367		*-0.0708*	47.0499		
						Uncertainty			0.0001		0.0001	0.0001		*0.1202*	0.0001		
2	8.65	0.9964	8	58	-	Coefficient		0.0138	-0.2694		-0.0039	-0.5950					-0.0118
						Uncertainty		0.0003	0.0001		0.0013	0.0001					0.0178
3	8.97	0.9964	8	58	-	Coefficient	*0.1733*		-0.2072		-0.0040	-0.6109			42.3218		
						Uncertainty	*0.1645*		0.0001		0.0001	0.0001			0.0001		
4	9.05	0.9964	8	59	DPMAX/TMAX TOTHR/TMAX	Coefficient			-0.1417	0.0291	-0.0067	-0.5957	-0.3599				
						Uncertainty			0.0037	0.0001	0.0001	0.0001	0.0002				
5	6.02	0.9968	9	58	DPMAX/TMAX TOTHR/TMAX	Coefficient			-0.1522	0.0249	-0.0064	-0.5552	-0.3000			0.0356	
						Uncertainty			0.0015	0.0001	0.0001	0.0001	0.0016			0.0249	

The Cp analysis predicted that the single-zone 5 to 95% burn angle combustion rate descriptor was an important variable for prediction, however it would be instructive to see how the other burn angle variables compare. Thus models, based on model 4, were constructed using the other 5 burn angle descriptors and the results are given for comparison in Table 11-18. It can be seen that the models containing single-zone burn angle descriptors all appear similar. The models with burn angles derived from the two-zone combustion model have two of the other variables (DPMAX and TOTHR) displaying high statistical uncertainty. It should be noted, however, that this does not imply that the two-zone burn angle descriptors are not reliable model variables as the combination of variables used in these models are not necessarily the best possible combinations which include these specific burn angle variables. The coefficients for the 2 to 98% and 5 to 95% burn angles from the two-zone combustion model are directionally similar to the single-zone burn angle variables, although of somewhat different magnitude. The coefficient for the 10 to 90% burn angle (two-zone) is not statistically significant.

Table 11-18 Comparison of different burn angle variables as model variables for NO prediction, using model 4 as a base model.

Model Number	Cp	R^2	P	Number of Observations Used	Colinearities		DPMAX	TOTHR	TMAX	CATMAX	BA298	BA595	BA1090	Z2BA298	Z2BA595	Z2BA1090
4a	-	0.9960	8	59	DPMAX/TMAX	Coefficient	-0.1323	0.0289	-0.0066	-0.6471	-0.2816					
						Uncertainty	0.0093	0.0001	0.0001	0.0001	0.0044					
4	9.05	0.9964	8	59	DPMAX/TMAX TOTHR/TMAX	Coefficient	-0.1417	0.0291	-0.0067	-0.5957		-0.3599				
						Uncertainty	0.0037	0.0001	0.0001	0.0001		0.0002				
4b	-	0.9958	8	59	DPMAX/TMAX TOTHR/TMAX	Coefficient	-0.1214	0.0267	-0.0067	-0.5872			-0.3145			
						Uncertainty	0.0175	0.0002	0.0001	0.0001			0.0115			
4c	-	0.9964	8	56	-	Coefficient	*-0.0846*	*0.0080*	-0.0064	-0.6029				-0.0931		
						Uncertainty	*0.0842*	*0.2935*	0.0001	0.0001				0.0054		
4d	-	0.9963	8	56	-	Coefficient	*-0.0840*	*0.0081*	-0.0064	-0.5105					-0.2127	
						Uncertainty	*0.0927*	*0.3022*	0.0001	0.0007					0.0165	
4e	-	0.9959	8	56	-	Coefficient	*-0.0801*	*0.0076*	-0.0060	-0.5646						*-0.1711*
						Uncertainty	*0.1246*	*0.3529*	0.0001	0.0011						*0.2400*

The NO emissions as predicted by model 4 are graphically compared to measured emissions and this is displayed in Figure 11-19. Very good agreement can be seen between the predicted and measured emissions.

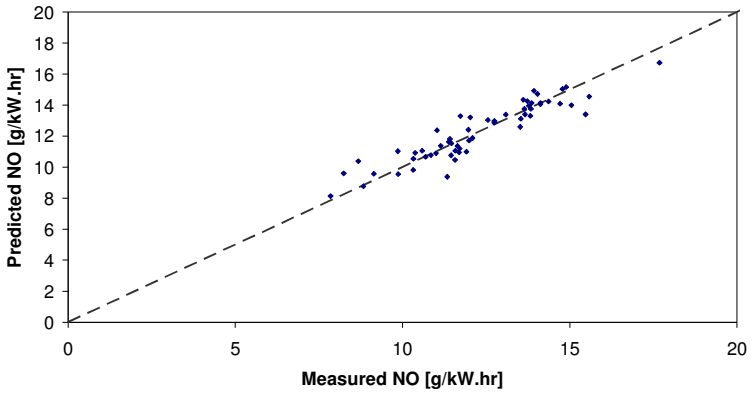

Figure 11-19 Graph of the NO as predicted by model 4 versus measured NO.

11.5.3. CO Emissions Results

CO – Fuel Properties Correlation

The results of the Cp analysis for CO emissions as a function of the fuel properties are summarised in Table 11-19. It can be seen that the important variables are aromatics, olefins, paraffins, ER, OILT, EXHT, MANP and E_{70}. As with the hydrocarbon emissions models (Section 11.5.1) the low-end volatility is important by virtue of IBP (2 models), T_{10} (2 models), T_{30} (8 models) and E_{70} (all models) occurring in various combinations.

Table 11-19 Summary of Cp analysis for CO – Fuel Properties Correlation

Model Nuimber	Cp	R^2	p	A	O	P	AP	ER	WATERT	OILT	EXHT	MANP	SPECHUM	IBP	T10	T30	E70	RON	SENS	LEAD	SULPHUR	PHENOLS
1	11.521	0.9957	22	✓	✓	✓		✓	✓	✓	✓	✓				✓	✓		✓			
2	12.620	0.9956	22	✓	✓	✓		✓	✓	✓	✓	✓					✓		✓			
3	12.902	0.9956	22	✓	✓	✓		✓	✓	✓	✓	✓				✓	✓			✓		
4	13.070	0.9956	22	✓	✓	✓		✓	✓	✓	✓	✓				✓	✓				✓	
5	13.177	0.9956	22	✓	✓	✓	✓	✓	✓	✓	✓	✓				✓	✓					
6	13.389	0.9956	22	✓	✓	✓		✓	✓	✓	✓	✓		✓		✓	✓					
7	13.458	0.9956	22	✓	✓	✓		✓	✓	✓	✓	✓				✓	✓					✓
8	13.894	0.9956	22	✓	✓	✓		✓	✓	✓	✓	✓		✓			✓		✓			
9	14.012	0.9956	22	✓	✓	✓		✓	✓	✓	✓	✓	✓			✓	✓					
10	14.131	0.9956	22	✓	✓	✓		✓	✓	✓	✓	✓			✓		✓				✓	
11	14.482	0.9956	22	✓	✓	✓		✓	✓	✓	✓	✓				✓	✓	✓				
Variable Occurrence Frequency				11	11	11	1	11	11	11	11	11	1	2	1	8	11	1	3	1	2	1

The coefficients for five of the more promising models are displayed in Table 11-20 in which some of the models have already been reduced to try to remove co-linearities. It can be seen that the coefficients for A, O and P are all similar. However 4 of the 5 models predict co-linearity between A, O and P. The fact that the coefficients are all of a similar magnitude results in the conclusion that the fuel components classes do not, in effect, influence the CO emissions. A very strong response is seen to ER with higher ER's (rich operation) indicating increased CO emissions, furthermore these coefficients have extremely

low uncertainties of 0.01%. Of the selected models WATERT only occurred twice, both occasions showing statistical uncertainty and co-linearity with other variables. Therefore, no conclusions can be drawn from this. OILT has a positive coefficient implying that higher oil temperatures would indicate an increased CO emission. The EXHT coefficient is negative meaning that higher exhaust temperatures would indicate a prediction of lower CO emission. The positive coefficient of the MANP variable indicates that increased manifold pressures would tend to predict increased CO emissions. The OILT, EXHT and MANP coefficients also all indicate extremely low uncertainties of 0.01%.

IBP, T_{10}, T_{30} and E_{70} are all measures of a fuels low-end volatility and need to be considered together. Some contradictory trends are again seen with these volatility measures. IBP has a positive coefficient and E_{70} a negative coefficient, indicating that reduced volatility will tend to cause increased CO production. In contrast, T_{10} and T_{30} have negative coefficients indicating the opposite trend. Normalising the coefficients, as was done for the HC emissions (Section 11.5.1) indicates that 4 of the 5 models show that reduced low end volatility (higher IBP, T_{10} and T_{30}, Lower E_{70}) will tend to reduce CO emissions. Model 8 reduced indicates the opposite trend. This is demonstrated in Table 11-21 by the dominant effect of T_{10} and T_{30} over E_{70} in models 1, 2, 2 reduced and 10 reduced and by the combined effect of IBP and E_{70} in model 8 reduced. All the volatility measures coefficients show uncertainties of between 1% and 4% except for E_{70}, which is considerably more significant with uncertainties of less than 0.05%.

Table 11-20 Summary of co-linearity analysis, giving the co-linear variables and the variable coefficients for the CO – Fuel Properties Correlation.

Model Number	Cp	R^2	P	Number of Observations Used	Colinearities		A	O	P	ER	WATERT
1	11.52	0.9957	22	259	A/O/P/WATERT T30/E70	Coefficient	-7.6237	-7.7149	-7.6931	554.1402	*1.0049*
						Uncertainty	0.0001	0.0001	0.0001	0.0001	*0.2567*
2	12.62	0.9956	22	259	A/O/P/WATERT	Coefficient	-6.6514	-6.7701	-6.7320	501.5805	*0.8915*
						Uncertainty	0.0001	0.0001	0.0001	0.0001	*0.3102*
2 Reduced	18.36	0.9954	21	259	A/O/P/MANP	Coefficient	-5.9802	-6.0984	-6.0592	501.7435	
						Uncertainty	0.0001	0.0001	0.0001	0.0001	
8 Reduced	21.08	0.9954	21	259	-	Coefficient	-7.2185	-7.3500	-7.3476	549.9446	
						Uncertainty	0.0001	0.0001	0.0001	0.0001	
10 Reduced	20.57	0.9954	21	259	A/O/P/MANP	Coefficient	-5.8040	-5.8415	-5.8614	472.7909	
						Uncertainty	0.0001	0.0001	0.0001	0.0001	

Model Number		OILT	EXHT	MANP	IBP	T10	T30	E70	SENS	SULPHUR
1	Coefficient	0.8627	-0.3226	5.7901			-0.3541	-0.7424	0.7345	
	Uncertainty	0.0001	0.0001	0.0001			0.0304	0.0004	0.0275	
2	Coefficient	0.9105	-0.3497	5.4554		-0.6366		-0.7553	0.8262	
	Uncertainty	0.0001	0.0001	0.0001		0.0151		0.0001	0.0132	
2 Reduced	Coefficient	0.9167	-0.3359	5.5330		-0.6228		-0.7478	0.8167	
	Uncertainty	0.0001	0.0001	0.0001		0.0173		0.0001	0.0142	
8 Reduced	Coefficient	0.8950	-0.3232	5.8749	0.3285			-0.2866	*0.6273*	
	Uncertainty	0.0001	0.0001	0.0001	0.0148			0.0005	*0.0617*	
10 Reduced	Coefficient	0.9464	-0.3269	5.5426		-0.5372		-0.6834		62.8491
	Uncertainty	0.0001	0.0001	0.0001		0.0402		0.0004		0.0289

Table 11-21 Investigation of low-range volatility effects, by normalising the coefficients, on predicted CO.

Model		IBP	T10	T30	E70
	Fuel Property Average	34.5	56.5	77.5	26.3
1	Model Coefficients			-0.354	-0.742
2			-0.637		-0.755
2 Reduced			-0.623		-0.748
8 Reduced		0.328			-0.287
10 Reduced			-0.537		-0.683
1	Coefficient * Average			-27.451	-19.504
2			-35.945		-19.842
2 Reduced			-35.163		-19.645
8 Reduced		11.319			-7.529
10 Reduced			-30.329		-17.953

The predicted emissions for model 8 reduced were plotted against the measured values as shown in Figure 11-20. This model was chosen, as it had no indicated co-linearities. It can be seen that a few of the predicted CO emissions are negative, which reduces confidence in the predictive capabilities of the model. On closer inspection of these respective test points, it was seen that these coincided with test results having inordinately low engine operating equivalence ratios. It is probable that these low reported equivalence ratios are as a result of some experimental uncertainty and may not be real effects. With the exception of these few points, the agreement between predicted and measured values is excellent.

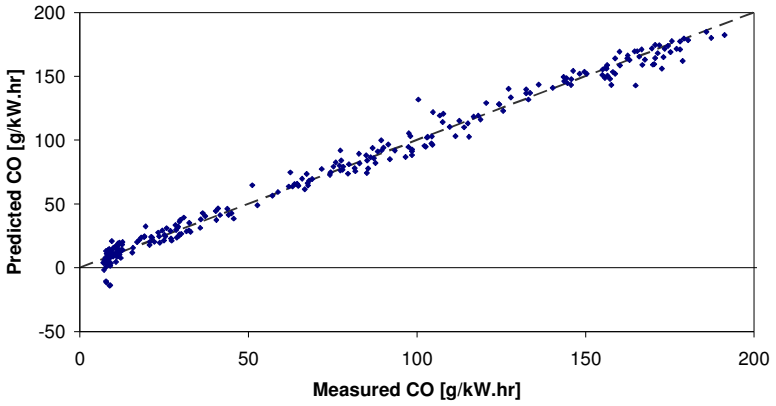

Figure 11-20 Graph of the CO as predicted by model 8 versus measured CO.

CO – Combustion Analysis Correlation

The summary table of the Cp analysis for the investigation of the CO emissions versus combustion analysis results is given below in Table 11-22. The important variables are DPMAX, Z2DGMAX and Z2DGMXCA.

Table 11-22 Summary of Cp analysis for CO – Combustion Analysis Correlation

Model Nuimber	Cp	R^2	p	PMAX	DPMAX	TOTHR	DHRMAX	TMAX	Z2DGMAX	Z2DGMXCA	Z2TUBMAX
1	4.850	0.9840	7		✓				✓	✓	
2	0.781	0.9853	8		✓		✓		✓	✓	
3	2.302	0.9850	8	✓	✓				✓	✓	
4	4.670	0.9845	8		✓	✓			✓	✓	
5	4.810	0.9845	8		✓			✓	✓	✓	
6	5.422	0.9843	8		✓		✓		✓		✓
Variable Occurrence Frequency				1	6	1	2	1	6	5	1

The results of the co-linearity investigations of these models are given in Table 11-23. Three of these models indicated no co-linearities and therefore the coefficients from these models, at least, can be considered further. It can be seen that the DPMAX coefficients are consistently positive, even though their magnitudes are not all similar. The disparity in the coefficient magnitudes is easily explained. The models with the smaller coefficient are all, except one, seen to include the DHRMAX (maximum rate of heat release) variable. These two variables are closely linked: the calculation of combustion rate is based on the rate of change of pressure. Therefore, this combination of variables is probably a response to the same physical mechanism taking place. Model 3 is seen to have a smaller DPMAX coefficient, but does not contain the DHRMAX variable, however, it does contain the PMAX (maximum pressure) variable and this can also be linked to rate of pressure rise. Thus it is indicated that increased rate of change of pressure, or some mechanism related to it, effects CO emission. An increased maximum rate of pressure rise and maximum combustion rate result in the prediction of increased CO emissions.

A similar pattern is seen for the maximum combustion rate as calculated by the two-zone model (Z2DGMAX), where a consistently negative coefficient is seen with different magnitudes. The negative coefficient implies that the higher the maximum combustion rate (as calculated by the two-zone combustion model), the lower the predicted CO emissions. Lastly, the crank angle at which the maximum combustion rate occurs is seen to have similar values for all the models. It can be seen that the more retarded that the maximum combustion rate occurs, the higher the predicted CO emissions.

The uncertainty of the DPMAX coefficients is extremely low at 0.01% while for the other important variables it is less than 2.7%, which is still low.

Table 11-23 Summary of co-linearity analysis, giving the co-linear variables and the variable coefficients for the CO – Combustion Analysis Correlation.

Model Number	Cp	R^2	P	Number of Observations Used	Colinearities		PMAX	DPMAX	TOTHR	DHRMAX	TMAX	IND5	Z2DGMAX	Z2DGMXCA	Z2TUBMAX
1	4.85	0.9840	7	86	-	Coefficient		1.0019					-71.7435	1.9713	
						Uncertainty		0.0001					0.0132	0.0159	
2	0.78	0.9853	8	86	DPMAX/Z2DGMAX /Z2DGMAXCA	Coefficient		0.9251		0.0262			-95.0452	2.6188	
						Uncertainty		0.0001		0.0116			0.0014	0.0018	
2 Altered	6.83	0.9840	8	86	-	Coefficient		0.5632		*0.0170*		*4.3851*	-2.7785		
						Uncertainty		0.0001		*0.0946*		*0.0677*	0.0257		
3	2.30	0.9850	8	86	DPMAX/Z2DGMAX /Z2DGMAXCA	Coefficient	0.0370	0.6599					-93.7241	2.5870	
						Uncertainty	0.0297	0.0054					0.0020	0.0025	
4	4.67	0.9845	8	86	DPMAX/TOTHR /Z2DGMAX /Z2DGMAXCA	Coefficient		1.0927	*0.0411*				-86.1019	2.3762	
						Uncertainty		0.0001	*0.1353*				0.0048	0.0058	
5	4.81	0.9845	8	86	DPMAX/Z2DGMAX /Z2DGMAXCA	Coefficient		1.0753			*0.0065*		-83.4633	2.3066	
						Uncertainty		0.0001			*0.1488*		0.0055	0.0066	
6	5.42	0.9843	8	86	Z2DGMAX/ ZTUBMAX	Coefficient		0.6401		0.0281			-125.1051		0.1145
						Uncertainty		0.0001		0.0151			0.0261		0.0289
6 Altered	7.06	0.9840	8	86	-	Coefficient		0.5609		*0.0167*		*4.3575*			-0.0025
						Uncertainty		0.0001		*0.1012*		*0.0697*			0.0293

The first model, chosen due to it's lack of co-linearities and having the least number of variables, was graphically compared with measured results. The graph is presented in Figure 11-21 where it can be seen that the models prediction abilities were good for low values of CO emission, but not as accurate for the higher emitting test data points. However, the spread of the data points, with the majority being between 5 and 35 g/kW.hr and a few between 80 and 120 g/kW.hr, is not ideal for the determination of a statistical model having good prediction abilities across the entire span of data points.

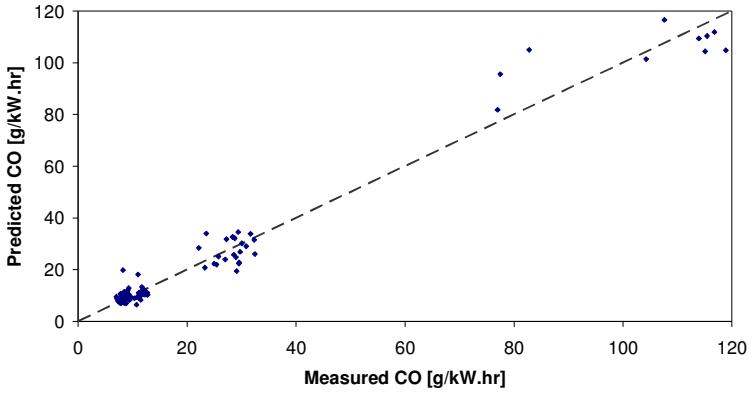

Figure 11-21 Graph of the CO as predicted by model 1 versus measured CO.

11.5.4. Combustion Analysis Results – Fuel Properties Correlation

As described at the beginning of this sub-section (Section 11.5), the combustion analysis results were statistically modelled against the fuel properties, as the third leg in the triangular approach. This was to give insight into the mechanism by which the fuel properties were influencing the emissions. Therefore, some of the more important combustion analysis parameters that were seen to be of the most relevance in the preceding sections were correlated against the fuel properties and the results are presented below.

Maximum Rate of Pressure Rise (DPMAX)

The summary of the Cp analysis for the maximum rate of pressure rise – fuel properties correlation is given in Table 11-24. The important variables are seen to be olefins, ER, IGNTIM, DRYB and both low- and high-end volatility (represented by T_{10} and T_{90} respectively).

Table 11-24 Summary of Cp analysis for DPMAX – Fuel Properties Correlation

Model Nuimber	Cp	R^2	p	A	O	ER	IGNTIM	DRYB	T10	T90	DENS	VOLIND	E70	SENS
1	3.061	0.9984	10		✓	✓	✓	✓		✓		✓		
2	3.254	0.9984	10		✓	✓	✓	✓	✓	✓				
3	3.359	0.9984	10	✓		✓	✓	✓	✓		✓			
4	1.439	0.9985	11		✓	✓	✓	✓	✓	✓			✓	
5	1.959	0.9985	11		✓	✓	✓	✓	✓	✓				✓
Variable Occurrence Frequency				1	4	5	5	5	4	4	1	1	1	1

Considering the coefficients of these variables as given in Table 11-25, only model 4 contains a co-linearity (T_{10} / E_{70}). It can be seen that increased olefin content will tend to predict an increase in the maximum rate of pressure rise. The predicted uncertainty of this response to olefin content is between 0.5% and 3.9%. The response to equivalence ratio and ignition timing are similar with higher equivalence ratio's (richer operation) and advanced ignition timing predicting increased maximum rate of pressure rise. The models indicated response to cell dry bulb temperature is a decreased maximum rate of pressure rise for hotter ambient test cell temperatures. The effect of low- and high-end volatility shows a consistent trend, with increased volatility (lower temperatures to achieve distillation point) predicting a higher maximum rate of pressure rise. The uncertainties for the coefficients for ER, IGNTIM, DRYB, T_{10} and T_{90} are generally less than 0.1%.

Table 11-25 Summary of co-linearity analysis, giving the co-linear variables and the variable coefficients for the DPMAX – Fuel Properties Correlation.

Model Number	Cp	R^2	P	Number of Observations Used	Colinearities		A	O	ER	IGNTIM	DRYB	T10	T90	DENS	VOLIND	E70	SENS
1	3.06	0.9984	10	87	-	Coefficient		0.1073	194.64	9.7569	-1.0959		-0.1899		0.2015		
						Uncertainty		0.0377	0.0001	0.0001	0.0008		0.0001		0.0008		
2	3.25	0.9984	10	87	-	Coefficient		0.1070	202.98	9.4432	-1.0795	-0.3352	-0.1600				
						Uncertainty		0.0386	0.0001	0.0001	0.0009	0.0008	0.0003				
3	3.36	0.9984	10	87	-	Coefficient	-0.2705		178.93	9.7069	-1.0336	-0.3436		235.11			
						Uncertainty	0.0101		0.0001	0.0001	0.0015	0.0002		0.0002			
4	1.44	0.9985	11	87	T10 / E70	Coefficient		0.1112	150.46	9.4612	-1.0678	-0.9283	-0.1767			-0.5181	
						Uncertainty		0.0285	0.0004	0.0001	0.0008	0.0027	0.0001			0.0401	
5	1.96	0.9985	11	87	-	Coefficient		0.1917	169.22	9.3258	-1.0902	-0.4160	-0.1700				*-1.0278*
						Uncertainty		0.0051	0.0001	0.0001	0.0007	0.0001	0.0001				*0.0569*

Maximum Gas Temperature – Single-Zone Model (TMAX)

The fuel properties required for the modelling of the maximum gas temperature as calculated by the single-zone model are given in the summary of the Cp analysis as indicated in Table 11-26. It is apparent that the important variables are IGNTIM, EXHT, low-end volatility (T_{10} and T_{30} / E_{70}) and LEAD.

Table 11-26 Summary of Cp analysis for TMAX – Fuel Properties Correlation

Model Nuimber	Cp	R^2	p	P	IGNTIM	OILT	EXHT	IBP	T10	T30	E70	LEAD
1	9.796	0.9987	9		✓		✓		✓		✓	✓
2	9.923	0.9986	9	✓			✓		✓		✓	✓
3	10.010	0.9986	9		✓		✓		✓	✓		✓
4	10.003	0.9987	10	✓	✓		✓		✓		✓	✓
5	10.035	0.9987	10		✓		✓	✓	✓	✓		✓
6	10.106	0.9987	10	✓		✓	✓		✓		✓	✓
7	10.159	0.9987	10		✓	✓	✓		✓		✓	✓
Variable Occurrence Frequency				3	5	2	7	1	7	2	5	7

The coefficients of the variables for the first four models are given in Table 11-27 where it can be seen that the ignition timing is not statistically significant in the selected models (the statistical uncertainty is large in each model in which ignition timing appears). It is important to note that the classification variables will account for the macro effect of ignition timing differences between the different test points, and that ignition timing is well controlled between test points. This result is therefore not surprising. The negative coefficient of the exhaust temperature variable indicates that the higher the exhaust temperature, the lower the predicted maximum gas temperature. The uncertainty given for the exhaust temperature coefficient is less than 1.1%. All the models indicate co-linearity between T_{10} and E_{70}, which is not surprising as they are both descriptors of low-end fuel volatility. Contradictory responses are seen for T_{10} and the T_{30} / E_{70} couple. T_{10} has a consistently negative coefficient indicating that increased low-end volatility tends to predict higher maximum gas temperatures. In contrast the T_{30} and E_{70} (which are descriptors of volatility at similar points in the distillation curve, and appear alternately in the models) responses tend to indicate the opposite trend. Normalising the coefficients by multiplying by the variable average as given in Table 11-28, shows clearly that the T_{10} variable dominates. Therefore, increased low-end volatility will predict higher maximum gas temperatures. Furthermore, the T_{10} coefficient shows lower uncertainty than the T_{30} / E_{70} couple, with less than 0.2% compared to between 1.5% and 3%. The predicted co-linearity between T_{10} and E_{70} may make this observation unreliable. The negative coefficient for the lead variable indicates that an increased fuel lead content will tend to produce the prediction of lower maximum gas temperatures. The lead coefficient is given with low uncertainty of less than 0.05%

Table 11-27 Summary of co-linearity analysis, giving the co-linear variables and the variable coefficients for the TMAX – Fuel Properties Correlation.

Model Number	Cp	R^2	P	Number of Observations Used	Colinearities		P	IGNTIM	EXHT	T10	T30	E70	LEAD
1	9.80	0.9987	9	87	T10 / E70	Coefficient		*-56.427*	-3.2095	-24.814		-12.978	-0.5270
						Uncertainty		*0.2075*	0.0089	0.0017		0.0271	0.0003
2	9.92	0.9986	9	87	T10 / E70	Coefficient	*-1.3949*		-3.0693	-27.365		-13.321	-0.5987
						Uncertainty	*0.2264*		0.0110	0.0012		0.0246	0.0001
3	10.01	0.9986	9	87	T10 / T30	Coefficient		*-72.993*	-3.6338	-23.249	8.3716		-0.5529
						Uncertainty		*0.1169*	0.0031	0.0016	0.0306		0.0002
4	10.00	0.9987	10	87	T10 / E70	Coefficient	*-1.5281*	*-61.429*	-3.4548	-28.777		-14.444	-0.5784
						Uncertainty	*0.1845*	*0.1698*	0.0053	0.0007		0.0155	0.0001

Table 11-28 Investigation of low-range volatility effects, by normalising the coefficients, on predicted TMAX.

Model		T10	T30	E70
	Fuel Property Average	6	77.5	26.3
1	Model Coefficients	-24.81		-12.98
2		-27.37		-13.32
3		-23.25	8.37	
4		-28.78		-14.44
1	Coefficients * Average	-1401		-341
2		-1545		-350
3		-1313	649	
4		-1625		-379

Maximum Rate of Heat Release – Single-Zone Model (DHRMAX)

The summary of the Cp analysis performed to find models for the maximum rate of heat release, single-zone model, as a function of fuel properties is given in Table 11-29. The important variables include IGNTIM, OILT, DRYB, T_{10}, E_{70} and SULPHUR.

Table 11-29 Summary of Cp analysis for DHRMAX – Fuel Properties Correlation

Model Nuimber	Cp	R^2	p	O	ER	IGNTIM	WATERT	OILT	EXHT	DRYB	T10	T50	T70	T90	VLRATIO	E70	VAPPRES	LEAD	SULPHUR
1	10.428	0.9991	11			✓		✓		✓	✓					✓		✓	✓
2	11.541	0.9991	11			✓		✓		✓	✓				✓	✓			✓
3	11.717	0.9991	11			✓	✓	✓			✓					✓		✓	✓
4	9.735	0.9992	12			✓		✓	✓	✓	✓					✓		✓	✓
5	9.763	0.9992	12	✓		✓		✓	✓	✓	✓		✓			✓			
6	10.462	0.9992	12			✓	✓	✓		✓	✓					✓		✓	✓
7	10.954	0.9992	12			✓		✓	✓	✓	✓				✓	✓			✓
8	11.091	0.9992	12	✓		✓		✓	✓	✓	✓	✓				✓			
9	11.261	0.9992	12	✓	✓	✓		✓	✓	✓				✓			✓		
Variable Occurrence Frequency				3	1	9	2	9	5	8	8	1	1	1	2	8	1	4	6

Of the nine potential models, models 1, 5 and 9 were chosen and investigated further for co-linearities and to determine the variable coefficients. The results of this are given in Table 11-30. The positive coefficients for IGNTIM and OILT imply that advanced timing and increased oil temperature lead to the prediction of higher maximum rates of heat release (single-zone). The response to ignition timing is given with low uncertainty of less than 1%, while that for oil temperature is higher, possibly as high as 2.4%. The negative coefficient for DRYB indicates that higher ambient temperatures cause the models to predict lower maximum heat release rates. However, the DRYB coefficient has relatively high uncertainty of between 2.5 and 4%. Again the low-end volatility variables, T_{10} and E_{70}, show co-linearity and the coefficients indicate inconsistent trends with negative coefficients for both variables. Normalising the coefficients, as shown in Table 11-31, shows that the T_{10} variable dominates and therefore that reduced volatility will reduce the maximum rate of heat release. These variables show uncertainties of less than 0.05%. The co-linearity, however, may make the observation unreliable. Increased fuel sulphur content is seen to increase the maximum rate of heat release, however the predicted uncertainty is relatively high at nearly 2%.

Table 11-30 Summary of co-linearity analysis, giving the co-linear variables and the variable coefficients for the DHRMAX – Fuel Properties Correlation.

Model Number	Cp	R^2	P	Number of Observations Used	Colinearities		O	ER	IGNTIM	OILT	EXHT	DRYB	T10	T70	T90	E70	VAPPRES	LEAD	SULPHUR
1	10.43	0.9991	11	87	T10 / E70	Coefficient			82.6210	11.6818		-11.144	-16.324			-11.565		-0.2451	1700.08
						Uncertainty			0.0009	0.0244		0.0383	0.0002			0.0003		0.0041	0.0192
5	9.76	0.9992	12	87	EXHT / OILT T10 / E70	Coefficient	2.1724		70.1104	24.5068	-2.5310	-12.127	-16.913	-2.9653		-12.182			
						Uncertainty	0.0116		0.0052	0.0061	0.0397	0.0239	0.0001	0.0142		0.0004			
9	11.26	0.9992	12	87	EXHT / OILT	Coefficient	1.8198	1095.08	72.2691	23.2101	*-2.2820*	-12.262			-1.6194		4.1183		
						Uncertainty	0.0251	0.0419	0.0047	0.0090	*0.0600*	0.0228			0.0235		0.0032		

Table 11-31 Investigation of low-range volatility effects, by normalising the coefficients, on predicted DHRMAX.

Model		T10	E70
	Fuel Property Average	6	26.3
1	Model Coefficients	-16.32	-11.56
5		-16.91	-12.18
1	Coefficient * Average	-922	-304
5		-955	-320

Burn Angle 5-95% - Single-Zone Model (BA595)

Table 11-32 lists the summarised results of the Cp analysis for the 5 to 95% burn angle (as calculated by the single-zone model) versus fuel properties. It can be seen that the important variables are OILT, DRYB, T_{10}, VLRATIO, E_{70} and SULPHUR.

Table 11-32 Summary of Cp analysis for BA595 – Fuel Properties Correlation

Model Nuimber	Cp	R^2	p	ER	IGNTIM	WATERT	OILT	EXHT	DRYB	T10	VLRATIO	E70	RON	LEAD	SULPHUR
1	9.688	0.9993	10				✓		✓	✓	✓	✓			✓
2	9.297	0.9993	11	✓					✓	✓		✓	✓	✓	✓
3	10.039	0.9993	11		✓		✓		✓	✓	✓	✓			✓
4	10.106	0.9993	11	✓			✓		✓	✓	✓	✓			✓
5	10.122	0.9993	11				✓	✓	✓	✓	✓	✓			✓
6	10.320	0.9993	11			✓	✓		✓	✓	✓	✓			✓
Variable Occurrence Frequency				2	1	1	5	1	6	6	5	6	1	1	6

The co-linearity checks for the first four models, the results of which are summarised in Table 11-33, predict T_{10} / E_{70} co-linearity for three of the four models. The significance of the oil temperature is marginal with only one model having a less than 5% uncertainty. The coefficients for oil temperature indicate that higher temperatures lead to predictions of reduced burn angle. Hotter ambient temperatures would cause the predicted burn angle to be increased. Volatility effects are considered by the three variables T_{10}, VLRATIO and E_{70}. The inconsistent results for volatility again require further investigation. Normalised coefficients as shown in Table 11-34 indicates that the T_{10} effect will dominate resulting in the prediction that increased low-end volatility will reduce the burn angle. The T_{10} / E_{70} co-linearity indicates that caution is required when considering this result. Increased fuel sulphur will tend to predict a shorter burn angle. All of the coefficients considered here have uncertainties of less than 0.5%, except for oil temperature as mentioned.

Table 11-33 Summary of co-linearity analysis, giving the co-linear variables and the variable coefficients for the BA595 – Fuel Properties Correlation.

Model Number	Cp	R^2	P	Number of Observations Used	Colinearities		ER	IGNTIM	OILT	DRYB	T10	VLRATIO	E70	RON	LEAD	SULPHUR
1	9.69	0.9993	10	87	T10 / E70	Coefficient			*-0.1614*	0.3278	0.3771	0.1318	0.2598			-46.618
						Uncertainty			*0.0597*	0.0004	0.0001	0.0001	0.0001			0.0001
2	9.30	0.9993	11	87	-	Coefficient	-23.675			0.2726	0.3988		0.2273	-0.1491	0.0072	-40.261
						Uncertainty	0.0467			0.0022	0.0001		0.0013	0.0361	0.0001	0.0014
3	10.04	0.9993	11	87	T10 / E70	Coefficient		*-0.5091*	-0.1710	0.3458	0.3676	0.1321	0.2492			-44.609
						Uncertainty		*0.2002*	0.0463	0.0002	0.0001	0.0001	0.0001			0.0002
4	10.11	0.9993	11	87	T10 / E70 / ER	Coefficient	*-14.410*		*-0.1581*	0.3298	0.3214	0.1300	0.2034			-40.218
						Uncertainty	*0.2096*		*0.0642*	0.0004	0.0001	0.0001	0.0033			0.0015

Table 11-34 Investigation of low-range volatility effects, by normalising the coefficients, on predicted BA595.

Model		T10	VLRATIO	E70
	Fuel Property Average	56.5	60.8	26.3
1	Model Coefficients	0.377	0.132	0.260
2		0.399		0.227
3		0.368	0.132	0.249
4		0.321	0.130	0.203
1	Coefficient * Average	21.29	8.01	6.82
2		22.52		5.97
3		20.75	8.03	6.55
4		18.15	7.90	5.34

Maximum Combustion Rate – Two-Zone Model (Z2DGMAX)

The Cp analysis for the maximum combustion rate (two-zone) did not find a model with high R^2 values. All models predicted had R^2 values of approximately 0.75 and therefore none of these models warrant further investigation.

Burn Angle 2-98% - Two-Zone (Z2BA298)

The fuel properties that are indicated as being important for the prediction of burn angle (2 to 98% as calculated by the two-zone analysis) are IGNTIM, EXHT, IBP, T_{10}, T_{70}, T_{90}, DENS, E_{70}, RON and SENS. This can be seen from the summarised results of the Cp analysis as given in Table 11-35.

Table 11-35 Summary of Cp analysis for Z2BA298 – Fuel Properties Correlation

Model Nuimber	Cp	R^2	p	A	O	P	OP	IGNTIM	OILT	EXHT	IBP	T10	T30	T50	T70	T90	DENS	VAPPRES	E70	VOLIND	RON	SENS	LEAD	SULPHUR	OXYGEN
1	16.951	0.9983	16	✓				✓	✓		✓	✓	✓		✓	✓	✓		✓				✓	✓	
2	17.012	0.9984	17					✓	✓		✓	✓			✓	✓	✓		✓	✓	✓	✓		✓	✓
3	17.391	0.9983	17					✓	✓		✓	✓		✓	✓	✓	✓	✓	✓	✓	✓	✓			
4	16.081	0.9984	18		✓	✓	✓	✓	✓	✓	✓	✓	✓	✓					✓		✓	✓	✓		
Variable Occurrence Frequency				1	1	1	1	4	4	1	4	4	2	2	3	3	3	1	4	2	3	3	2	2	1

The co-linearity analysis results are summarised in Table 11-36. The coefficients predicted for ignition timing indicate that advanced timing would result in the prediction of reduced burn angles. Increased oil temperatures too indicate a reduced burn angle. The uncertainties for both ignition timing and oil temperature are extremely low, being in general less than 0.02%.

IBP, T_{10} and E_{70} are all indicators of low-end volatility, however the coefficients show inconsistent trends and therefore more investigation is required. Table 11-37 shows the normalised coefficients of these three variables and it appears that in general T_{10} or the T_{10} / T_{30} combination dominate. This is apparent in all but one of the models (model 3). The positive coefficients of T_{10} and T_{30} indicate that increased low-end volatility will result in prediction of a reduced burn angle. T_{70} and T_{90} are indicators of high-end volatility and again this requires further investigation before conclusions can be drawn. Table 11-38 shows normalised coefficients for these parameters and from this it can be seen that models 2 and 3 indicate that high-end volatility is not very influential (normalised coefficients are of similar magnitude and opposite sign). For model 1, T_{70} has high statistical uncertainty (*italicised* to indicate this), however it is included as a similar result to models 2 and 3 is indicated when considered in combination with T_{90}. The uncertainties for the volatility measures considered are generally low, except for a few isolated cases where very high uncertainties are indicated. These high uncertainty coefficients are not included, except for model 1, T_{70} as discussed above, in any comparisons or discussions.

Negative coefficients for fuel density indicate that a higher fuel density will reduce the predicted burn angle, however a wide range of uncertainties are predicted for the fuel density coefficient, ranging from a low 0.01% to a high 6.5%. The fuel octane effects indicate that higher RON fuels and fuels with higher sensitivity have longer burn angles. This is in agreement with work presented by Swartz et. al. 59 who indicate that this is consistent with the notion that molecules indicating a resistance to oxidation do so both in the flame zone (high temperatures) and in the end gas (low temperatures) as associated with knocking combustion and thus Octane numbers. The fuel octane descriptors coefficients show low uncertainty, with the highest being slightly over 1%.

Table 11-36 Summary of co-linearity analysis, giving the co-linear variables and the variable coefficients for the Z2BA298 – Fuel Properties Correlation.

Model Number	Cp	R^2	P	Number of Observations Used	Colinearities		A	O	P	OP	IGNTIM	OILT	EXHT	IBP	T10
1	16.95	0.9983	16	81	A / T90 / DENS	Coefficient	*0.2111*				-7.4739	-0.8136		*-0.1475*	0.7121
						Uncertainty	*0.0747*				0.0001	0.0001		*0.1722*	0.0026
2	17.01	0.9984	17	81	-	Coefficient					-7.2389	-0.8387		-0.2971	1.2652
						Uncertainty					0.0001	0.0001		0.0164	0.0001
3	17.39	0.9983	17	81	VOLIND / E70 / VAPPRES	Coefficient					-7.4165	-0.7625		-0.3443	0.7046
						Uncertainty					0.0001	0.0002		0.0093	0.0175
4	16.08	0.9984	18	81	T10 / E70 / ER	Coefficient		-1.4443	-1.0449	0.0269	-7.2738	-1.0697	*0.0430*	-0.4982	0.9434
						Uncertainty		0.0002	0.0008	0.0002	0.0001	0.0012	*0.3391*	0.0007	0.0006

Model Number		T30	T50	T70	T90	DENS	VAPPRES	E70	VOLIND	RON	SENS	LEAD	SULPHUR	OXYGEN
1	Coefficient	0.4083		*0.0880*	-0.1866	-188.48		0.9368				0.0147	-131.47	
	Uncertainty	0.0036		*0.2863*	0.0163	0.0370		0.0001				0.0021	0.0010	
2	Coefficient			0.3622	-0.2097	*-123.14*		1.3892	-0.2137	0.7333	-1.1958		-167.26	-1.9519
	Uncertainty			0.0010	0.0031	*0.0649*		0.0001	0.0132	0.0001	0.0102		0.0142	0.0319
3	Coefficient		*0.1986*	0.3845	-0.2820	-237.27	1.6963	2.0479	-1.9367	0.5208	-1.4873			
	Uncertainty		*0.1827*	0.0020	0.0004	0.0001	0.0334	0.0002	0.0207	0.0080	0.0008			
4	Coefficient	0.5893	0.3389					1.4799		2.0326	-4.1741	*-0.0200*		
	Uncertainty	0.0020	0.0053					0.0001		0.0004	0.0010	*0.0513*		

Table 11-37 Investigation of low-range volatility effects, by normalising the coefficients, on predicted Z2BA298.

Model		IBP	T10	T30	E70
	Fuel Property Average	34.5	56.5	77.5	26.3
1	Model Coefficients		0.712	0.408	0.937
2		-0.297	1.265		1.389
3		-0.344	0.705		2.048
4		-0.498	0.943	0.589	1.480
1	Coefficient * Average		40.2	31.6	24.6
2		-10.3	71.4		36.5
3		-11.9	39.8		53.8
4		-17.2	53.3	45.7	38.9

Table 11-38 Investigation of high-range volatility effects, by normalising the coefficients, on predicted Z2BA298.

Model		T70	T90
	Fuel Property Average	124.4	160.6
1	Model Coefficients	*0.088*	-0.187
2		0.362	-0.210
3		0.384	-0.282
1	Coefficient * Average	*10.9*	-30.0
2		45.1	-33.7
3		47.8	-45.3

Equivalence Ratio (ER)

Although equivalence ratio is not a combustion analysis result, but an engine operating parameter, it is also considered due to the strong influence that it has on exhaust emissions. Furthermore, it is possible that fuel formulation can influence the ER, and in turn the emissions, and due to the inclusion of ER in the fuel properties correlation modelling, this may mask the identification of important variables. Table 11-39 is a summary of the Cp analysis performed for equivalence ratio. The important variables include the fuel component main effects (A, O and P) and the two-factor interaction between aromatics and olefins (AO). MANP, DRYB and OXYGEN are also important variables, while volatility is seen to have influence through T_{10}, T_{70}, T_{90}, FBP and E_{70}.

Table 11-39 Summary of Cp analysis for Equivalence Ratio – Fuel Properties Correlation

Model Nuimber	Cp	R^2	p	A	O	P	AO	AP	EXHT	MANP	BARO	DRYB	IBP	T10	T70	T90	FBP	VLRATIO	E70	NITROGEN	OXYGEN	BENZENE
1	22.559	0.9999	23	✓	✓	✓	✓			✓		✓		✓	✓	✓	✓		✓		✓	
2	21.724	0.9999	24	✓	✓	✓	✓			✓		✓		✓	✓	✓	✓	✓	✓		✓	
3	22.376	0.9999	24	✓	✓	✓	✓			✓	✓	✓		✓	✓	✓	✓		✓		✓	
4	22.664	0.9999	24	✓	✓	✓	✓		✓	✓		✓		✓	✓	✓	✓		✓		✓	
5	22.930	0.9999	24	✓	✓	✓	✓			✓		✓		✓	✓	✓	✓		✓	✓	✓	
6	23.020	0.9999	24	✓	✓	✓	✓			✓		✓		✓	✓	✓	✓		✓		✓	✓
7	23.243	0.9999	24	✓	✓	✓	✓			✓		✓	✓	✓	✓	✓	✓		✓		✓	
8	23.551	0.9999	24	✓	✓	✓	✓	✓		✓		✓		✓	✓	✓	✓		✓		✓	
Variable Occurrence Frequency				8	8	8	8	1	1	8	1	8	1	8	8	8	8	1	8	1	8	1

Considering the impact of the fuel classes on equivalence ratio, it can be seen that the two-factor interaction is three orders of magnitude smaller than the main effects. Therefore, it is not expected to

have a significant influence on prediction. Furthermore, the coefficients for aromatics and olefins are of a similar magnitude while the paraffin coefficient is somewhat smaller (approximately 8.5% less). All of these coefficients are positive. This implies that the paraffin content alone influences the equivalence ratio, and increasing its concentration would tend to reduce the equivalence ratio. The similar coefficients for the other two components implies that their relative concentrations would not influence the emissions if their combined concentration was unaltered or, in other words, if the paraffin content was unaltered. The main effects are seen to have extremely low uncertainty while the two-factor interaction still has a low uncertainty of less than 0.15%.

Higher manifold pressures are seen to predict reduced equivalence ratio, while increased ambient temperatures would result in increased equivalence ratio prediction, however the uncertainty of this result is relatively high at approximately 3%. Oxygen content is seen to influence the prediction of equivalence ratio with higher fuel oxygen concentration resulting in lower equivalence ratios. This result is given with extremely low uncertainty of 0.01%.

The volatility variables that are seen to be important can be classified into two groups: low-end volatility (T_{10} and E_{70}) and high-end volatility (T_{70}, T_{90} and FBP). Considering the low-end volatility first, Table 11-41 shows the normalised coefficients and it can be seen that T_{10} dominates. Thus reduced low-end volatility (higher T_{10}) would result in the prediction of reduced equivalence ratio. For the high-end volatility, T_{70} and FBP have negative coefficients while T_{90} has a positive coefficient. Considering the normalised coefficients in Table 11-42, it can be seen that the combined effect of T_{70} and FBP would outweigh the directionally opposite trend indicated by T_{90}. Therefore it can be concluded that reduced high-end volatility would lead to reduced equivalence ratio prediction. All the volatility measures return uncertainties of less than 0.1%.

Table 11-40 Summary of co-linearity analysis, giving the co-linear variables and the variable coefficients for the Equivalence Ratio – Fuel Properties Correlation.

Model Number	Cp	R^2	P	Number of Observations Used	Colinearities		A	O	P	AO	MANP	BARO
1	22.56	0.9999	23	238	A/O/P/MANP FBP/E70	Coefficient	0.0140	0.0143	0.0130	-0.00003	-0.0029	
						Uncertainty	0.0001	0.0001	0.0001	0.0005	0.0286	
3	22.38	0.9999	24	238	A/O/P/BARO	Coefficient	0.0140	0.0143	0.0129	-0.00003	-0.0029	*0.000006*
						Uncertainty	0.0001	0.0001	0.0001	0.0006	0.0372	*0.9759*
5	22.93	0.9999	24	206	A/O/P/MANP T10/FBP/E70	Coefficient	0.0149	0.0152	0.0136	-0.00004	-0.0046	
						Uncertainty	0.0001	0.0001	0.0001	0.0001	0.0021	
6	23.02	0.9999	24	233	A/O/P/MANP T10/FBP/E70	Coefficient	0.0138	0.0140	0.0128	-0.00003	-0.0030	
						Uncertainty	0.0001	0.0001	0.0001	0.0014	0.0237	

Model Number		DRYB	T10	T70	T90	FBP	E70	NITROGEN	OXYGEN	BENZENE
1	Coefficient	0.0015	-0.0019	-0.0006	0.0006	-0.0005	-0.0015		-0.0101	
	Uncertainty	0.0001	0.0001	0.0001	0.0001	0.0003	0.0001		0.0001	
3	Coefficient	0.0015	-0.0019	-0.0006	0.0006	-0.0005	-0.0015		-0.0101	
	Uncertainty	0.0001	0.0001	0.0001	0.0001	0.0003	0.0001		0.0001	
5	Coefficient	0.0023	-0.0019	-0.0008	0.0008	-0.0005	-0.0016	*-0.0001*	-0.0091	
	Uncertainty	0.0001	0.0001	0.0001	0.0001	0.0002	0.0001	*0.3323*	0.0001	
6	Coefficient	0.0013	-0.0016	-0.0007	0.0007	-0.0005	-0.0012		-0.0111	-0.0010
	Uncertainty	0.0008	0.0002	0.0001	0.0001	0.0007	0.0008		0.0001	0.0118

Table 11-41 Investigation of low-range volatility effects, by normalising the coefficients, on predicted Equivalence Raito.

Model		T10	E70
	Fuel Property Average	6	26.3
1	Model Coefficients	-0.0019	-0.0015
3		-0.0019	-0.0015
5		-0.0019	-0.0016
6		-0.0016	-0.0012
1	Coefficient * Average	-0.108	-0.039
3		-0.108	-0.039
5		-0.108	-0.041
6		-0.092	-0.031

Table 11-42 Investigation of high-range volatility effects, by normalising the coefficients, on predicted Equivalence Ratio.

Model		T70	T90	FBP
	Fuel Property Average	124.4	160.6	199.1
1	Model Coefficients	-0.00064	0.00065	-0.00054
3		-0.00064	0.00065	-0.00054
5		-0.00082	0.00077	-0.00055
6		-0.00072	0.00072	-0.00051
1	Coefficient * Average	-0.079	0.104	-0.108
3		-0.079	0.104	-0.108
5		-0.102	0.123	-0.108
6		-0.089	0.115	-0.101

11.6. Detailed Analysis of NO Formation

The statistical analysis of the NO emissions as a function of combustion analysis parameters yielded a somewhat unexpected correlation with respect to the bulk gas temperatures and the temperature time history. This is evident from Table 11-17 and the related discussion. The implication from the statistical analysis is that higher bulk gas temperatures would reduce the NO produced, a result which is somewhat counter intuitive given the formation mechanism which is thought to be taking place as discussed above in Section 2.3.1, where high gas temperatures are understood to promote the formation of NO. The correlation with the location of maximum bulk gas temperature was also identified as being important, with the implication that lower emissions are produced when the bulk gas temperature peak is later in the cycle. A detailed investigation of these noteworthy and unexpected results was thus undertaken. It was specifically for this purpose that the Extended Zeldovich NO formation model was added to the combustion analysis program, as discussed in detail in Sections 8.3.5 and 11.4 above.

The results of five of the load point / fuel couples used for the NO formation model validation were analysed in greater detail in an attempt to understand the NO formation process in order to explain the unexpected correlations. Four of the load points were chosen as the highest and lowest NO emitters each of the “60 km/hr” and the “closed loop simulation (60 km/hr)” groups of results, and the fifth was chosen in order to compare the same fuel operated with different engine load conditions. The difference in the load conditions is detailed in Table 7-1 in the discussion of the experimental procedure. The two load points simulate a steady vehicle speed of 60 km/hr, with the first using the standard engine settings simulating open loop fuel delivery control, and the second simulating closed loop ignition control at minimum specific fuel consumption (SFC). Importantly the

closed loop simulation had a more advanced ignition timing of 25° CA BTDC, corresponding to the best SFC condition, as opposed to only 20° CA BTDC for the standard condition. Thus the four load points will span differences in engine operating conditions both as a function of engine control and as a function of fuel property differences.

Modelling was done both with the native equivalence ratio and with a constant equivalence ratio of 0.9. This modified equivalence ratio will only effect the Zeldovich predictions by virtue of the direct equivalence ratio effect of the equilibrium NO formation "driver". As discussed in Sections 2.3.1 and 8.3.5, the local NO concentration at any time during the cycle is a function of the rate limited chemistry as the NO concentration tends towards the predicted equilibrium concentration for that element. The formation rates are strongly temperature dependant. The analysis with constant equivalence ratio will not correctly influence the temperature effect on the rate of NO formation as this is a factor of both the adiabatic flame temperature and the pressure time history. The small differences in the equivalence ratios from standard to the hypothetical constant equivalence ratio analyses result in small differences in adiabatic flame temperatures and less than 5K differences were noted. Thus for the purposes of this analysis, it can be assumed that the temperature time histories, and thus the temperature driver for NO formation is equivalent for each pair of analyses: native equivalence ratio versus constant equivalence ratio. This is a useful observation as it allows the effect of the temperature and the equivalence ratio drivers on the local equilibrium NO predictions to be differentiated from one another.

Table 11-43 below indicates the load points used for the analysis and includes both the measured and modelled NO concentrations.

Table 11-43 Details of load points used for the detailed NO formation analysis.

		60 kph			Closed Loop Simulation	
		Low Emitter	High Emitter	Comparison§	Low Emitter	High Emitter
	Fuel Sample :	P24	P35	P31	P29	P31
NO (Measured)	[ppm]	815	1287	1241	1460	1591
NO (Modelled)	[ppm]	776	1184	1130	1279	1653
Ignition Timing	[° CA BTDC]	20	20	20	25	25
Equiv Ratio	[-]	0.875	0.912	0.941	0.916	0.914
CATMAX†	[° CA ATDC]	48	40	40	39	35
TMAX‡	[K]	2837	3140	3052	2842	3159
IND5¥	[° CA]	20	19	18	21	20
BA595#	[° CA]	46	43	49	45	41
Equiv Ratio	[-]	0.90	0.90	0.90	0.90	0.90
NO (Modelled)	[ppm]	705	1247	1369	1371	1749

† - Crank angle for maximum bulk gas temperature
‡ - Maximum bulk gas temperature
¥ - Induction period: 0 - 5% burned fraction
- Burn Angle: 5 - 95 % burned fraction
§ - included for direct comparison with P31 - Closed Loop Simulation

In the following figures four elements of the cylinder charge are considered and compared. The elements labelled x_1 to x_4 were chosen in the following way. The bulk of combustion, occurring between 5% and 95% of the total was considered the most important. This was then divided equally into four, and the elements to burn at 5%, 27.5%, 50% and 72.5% were used. The element to burn at 95% was also initially considered, in order to maintain the symmetry, however this element always had insignificant NO concentrations and merely cluttered the graphs and hence was omitted.

Considering first the effect of equivalence ratio, the modelled results of two of the fuels were compared at their native equivalence ratio and at the equivalence ratio of 0.9. This is shown below in Figure 11-22. It can be seen that even the relatively small differences in equivalence ratio result in significant differences in the NO formation. This effect is not driven via any temperature effects, as discussed above, but is traceable purely to the direct effect on the equilibrium NO prediction. It is evident therefore that the equivalence ratio effect carries through the rate limited chemistry.

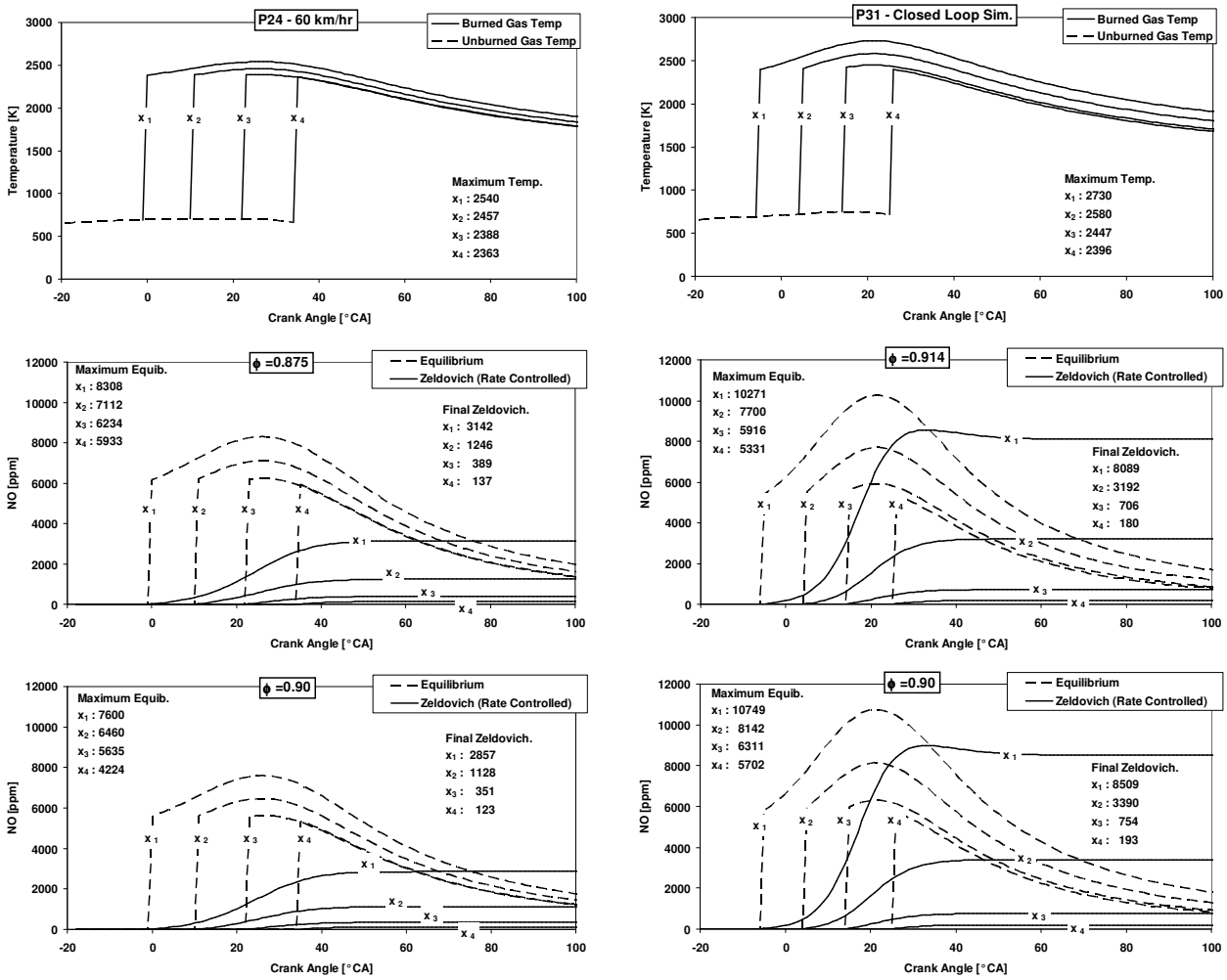

Figure 11-22 Comparisons of the time histories for four burned gas elements for two fuels at their native equivalence ratios and at an equivalence ratio of 0.9.

Considering further the effect of ignition timing, which naturally leads to a significant alteration in the temperature history of the burning elements, the results for the 60 km/hr and closed loop simulation on fuel P31 were compared. This was done with the Zeldovich model set to have the constant equivalence ratio of 0.9. This approach removes the influence of equivalence ratio, and it can be assumed that the fuels inherent combustion characteristics would be the same in both engine tests, hence only the effect of ignition timing on the temperature history remains. The results are graphed below in Figure 11-23 and some relevant parameters for this comparison have been extracted and listed in Table 11-44.

As expected, the earlier elements to burn result in higher maximum temperatures in the more advanced case: that of the closed loop simulation. This results in significantly higher equilibrium predictions for the maximum NO for these elements as indicated by the second and third rows in Table 11-44. The rate limited chemistry is strongly temperature dependent, and thus it is expected that higher rates of NO formation will result from the higher temperature elements in the advanced case. This is clearly seen in Figure 11-23 and in the fourth and fifth rows in Table 11-44. The last rows in the table have listed a parameter derived by dividing the final Zeldovich NO prediction by the maximum equilibrium NO predicted. This has been labelled the "Fractional Attainment" and is used here as an indicator for the extent to which the rate limited reactions have progressed: this parameter is not an exact measure nor does it have any real physical significance.

It is apparent that the extent to which the temperature influence on the rate controlled reactions is in itself insufficient to explain the overall increase in final Zeldovich NO: the difference between the fractional attainment for the two load points is much less than the ratio of final Zeldovich NO. This is simply due to the higher temperatures still prevailing at the latter stages of the combustion process, which promote the reverse reactions. This is clearly evident in the graphs by the negative gradient seen for the Zeldovich NO predictions for x_1 for the closed loop simulation, which does not occur in the 60 km/hr load point. It is therefore clear that the higher equilibrium NO prediction for the higher temperatures is playing a significant role, as well as the increased rate of formation. Thus temperature is a dual driver for the NO formation process by both promoting the rate of reactions, and thus fractional attainment, and by increasing the equilibrium NO to which the rate controlled chemistry approaches. However, the first of these effects is moderated to some extent by the reverse reactions also being promoted by the high temperatures.

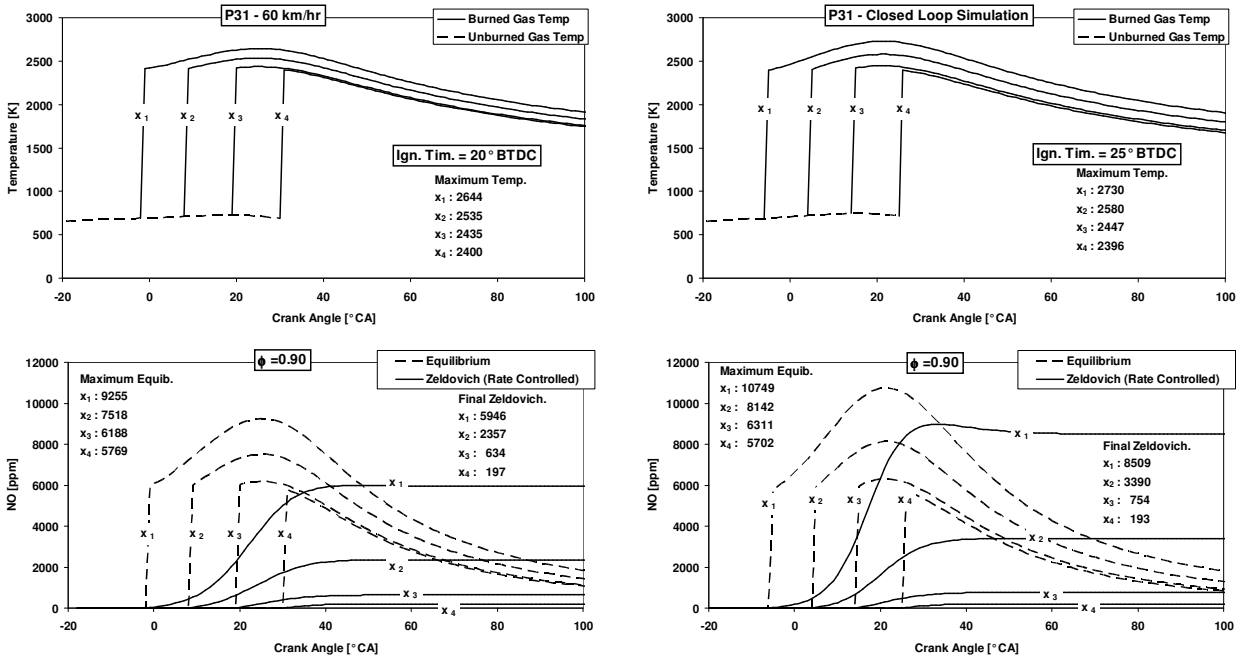

Figure 11-23 Comparison of the time histories for four burned gas elements for a fuel at similar engine load conditions except for ignition timing.

Table 11-44 Some relevant parameters derived from the results indicated in Figure 11-23

		Element :	x_1	x_2	x_3	x_4
Maximum Temperature Difference	**CLS† - 60‡**	**[K]**	85	45	12	-4
Maximum Equilibrium NO Difference	**CLS - 60**	**[ppm]**	1494	624	123	-67
Maximum Equilibrium NO Ratio	**CLS / 60**	**[-]**	1.16	1.08	1.02	0.99
Final Zeldovich NO Difference	**CLS - 60**	**[ppm]**	2563	1032	120	-4
Final Zeldovich NO Ratio	**CLS / 60**	**[-]**	1.43	1.44	1.19	0.98
Fractional Attainment¥	**60**	**[-]**	0.64	0.31	0.10	0.03
Fractional Attainment¥	**CLS**	**[-]**	0.79	0.42	0.12	0.03

† - Closed Loop Simulation
‡ - 60 km/hr
¥ - Final Zeldovich NO / Maximum Equilibrium NO

Considering now the fuel combustion characteristics themselves, the low and high emitter results for each of the load points were compared at constant equivalence ratio. This is indicated below in Figure 11-24 where the left hand graphs are for two different fuels at the 60 km/hr load point and the two right hand graphs are for two different fuels at the closed loop simulation load point. It is apparent that the fuels inherent combustion characteristics can play a significant role in the NO formation: significant differences exist in the NO traces for similar load points. This is directly traceable to the maximum burned gas temperatures for each element to burn: for both load conditions, the lower graph indicates the higher maximum temperatures and results in the highest final NO concentrations. This is exactly anomalous to the effect of ignition timing and thus indicates the possibility that faster burning fuels, which have the effect of advancing combustion, are resulting in the increased temperatures and thus NO.

Table 11-43 included parameters indicating burn speed: induction period and burn angles. It is seen that the high emitters both have shorter burn angles and induction periods than the low emitters, which supports this assertion, however this is based on very few data points. Burn angle was identified by the statistical analysis as correlating with NO emissions, but induction period was not, while the angle for maximum temperature of the bulk gas was indicated more strongly as being a predictor by occurring in every model considered, while burn angle only occurred in about half of the models. This is investigated in greater detail below.

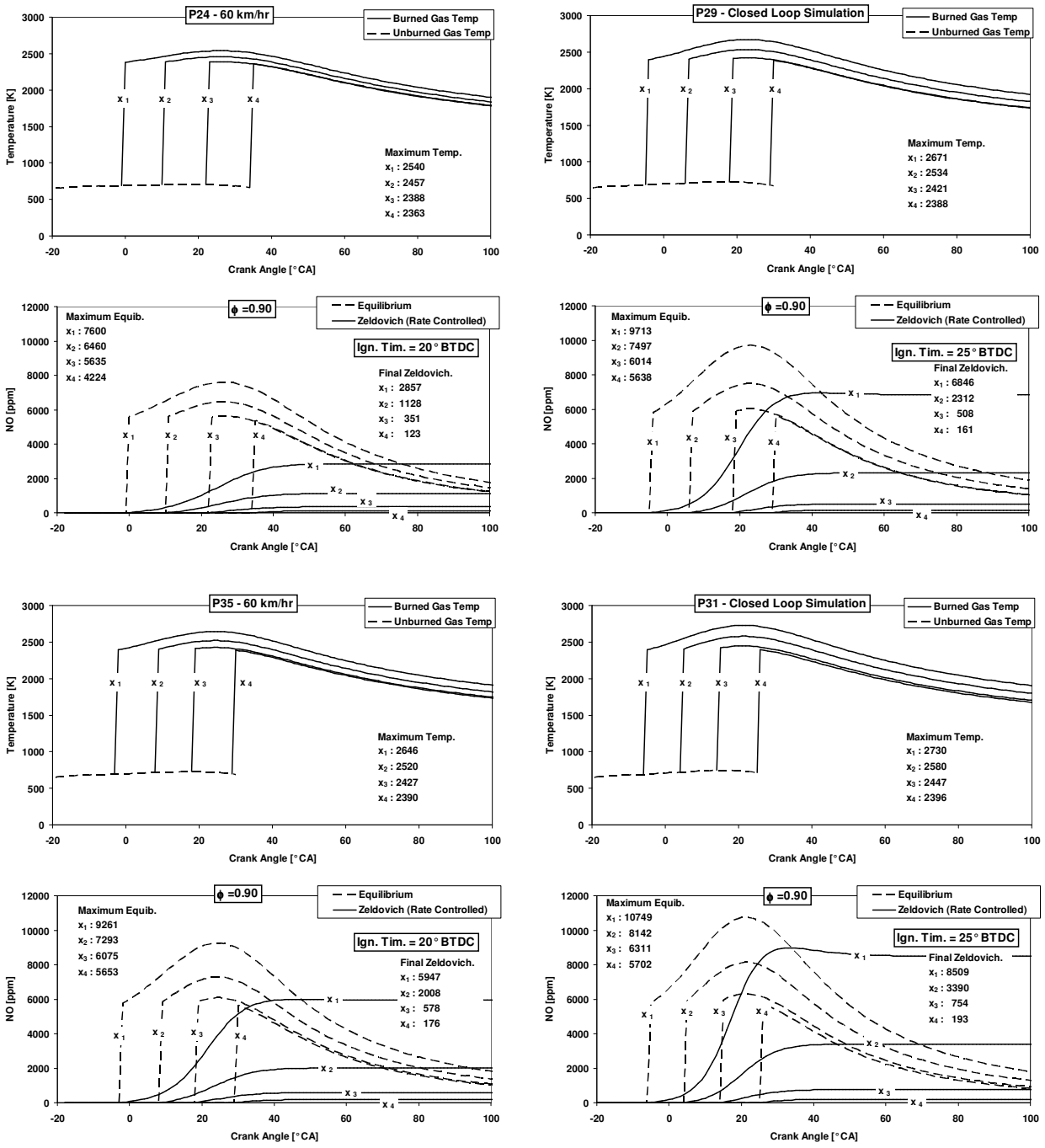

Figure 11-24 Comparison of the time histories for four burned gas elements for four fuels at two similar engine load conditions except for ignition timing.

It was first checked to see if fuels with short burn angle also had short induction periods, in other words to investigate if the concept of fast burning fuels was consistent throughout the entire combustion process. Figure 11-25 below indicates the correlation between induction period and burn angle for the data set. It is clear that there is some relationship between the two combustion parameters, although it is weak with low gradients and the correlations are not strong having very low R^2 values. Importantly, the difference between the two load points with different ignition timing is much stronger than the difference between the different fuels at a given load point.

It is thus apparent that not all “fast burning” fuels will have short induction periods and short burn angles. This is an important observation as it is clear that neither of these two parameters is an ideal measure of a fuels overall combustion characteristic in terms of speed of burn. This may explain why these parameters were not strongly identified in the statistical correlations.

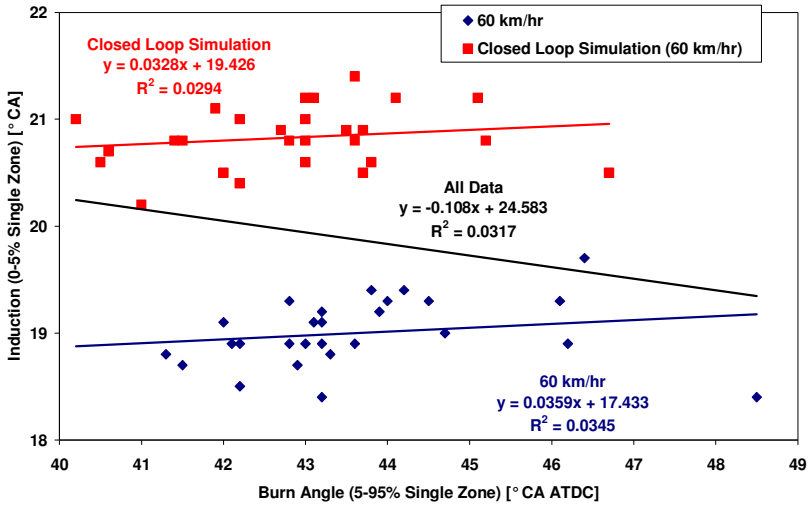

Figure 11-25 Comparison of burn angle and induction period for select data points.

The direct effect on the NO emissions of the location of maximum bulk gas temperature (CATMAX), being strongly identified as a correlation parameter for NO emissions, is plotted below in Figure 11-26. This supports the statistical correlation. The location of the maximum bulk gas temperature is obviously correlating with the overall combustion timing. A parameter indicating the centroid of the combustion process was then considered as a potential correlation parameter. The crank angle position for the point of 50% burned was manually extracted from this reduced data set and correlated with various parameters as indicated below in Figure 11-27. It is apparent from these figures that the location of 50% burned parameter captures information about both engine operating conditions such as ignition timing as well as burn speed of the fuels. It is also apparent that burn angle and induction period are insufficient to capture information about the entire process.

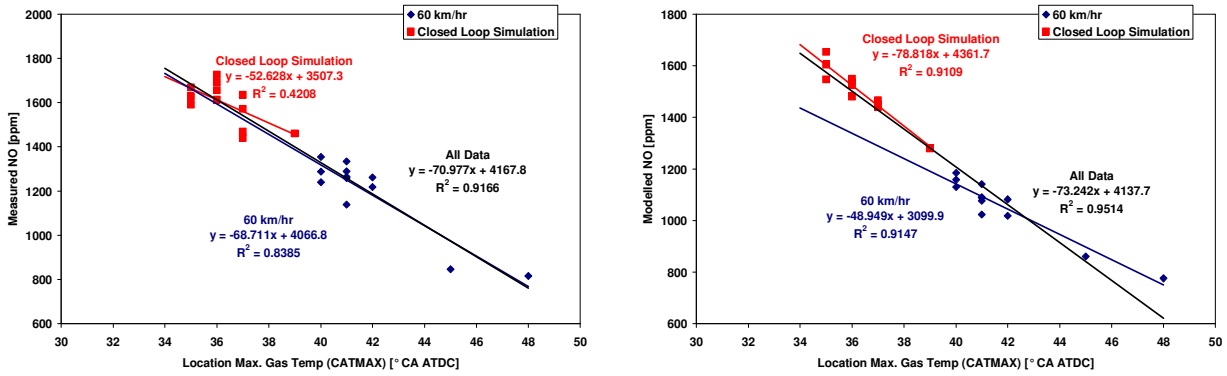

Figure 11-26 NO emissions as a function of location of maximum bulk gas temperature (CATMAX).

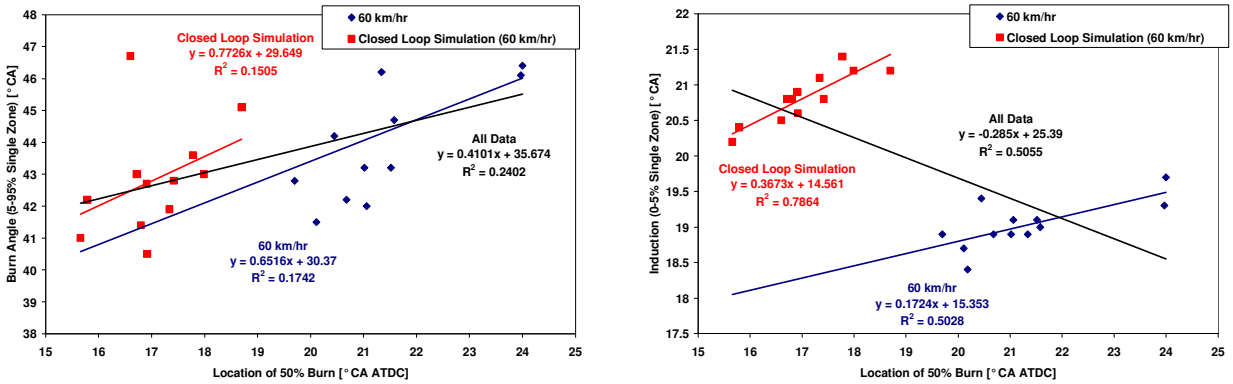

Figure 11-27 Correlation between the location of 50% burned parameter and the burn angle and induction period parameters.

Figure 11-28 below indicates the very strong relationship between the location of maximum bulk gas temperature and the location of 50% burned and Figure 11-29 indicates the correlation of NO emissions with this same parameter. Figure 11-26, Figure 11-28 and Figure 11-29 together indicate that the CATMAX parameter was merely identified in the statistical analysis as a surrogate for the location of 50% burned: unfortunately this parameter was not identified in the early phase of the research as being of interest and was thus not extracted during the initial automated data-processing and was thus unavailable during the statistical analysis. It is further thought that the indicated correlation with maximum bulk gas temperatures (TMAX), which has a trend which is directionally inconsistent with the understood mechanism of formation (reduced NO for higher temperatures), is acting in concert with the CATMAX parameter. Although no co-linearity between the two was indicated in the statistical analysis, it is obvious that the two parameters have an inherent relationship. It is therefore likely that the CATMAX parameter is almost fully accounting for the temperature/time history effect and that the TMAX parameter is merely correcting this in some way: the TMAX parameter as identified in the statistical analysis can not be considered a real direct driver for NO emissions. By comparing Figure 11-26 and Figure 11-29, it is apparent that the location of 50% burned parameter has a better correlation with NO emissions than the CATMAX parameter by itself. It is therefore possible that if this parameter had been included in the statistical analysis, it may have more correctly accounted for the temperature/time history effects and thus not indicated any correlation with TMAX.

The location of 50% burned parameter has a real, physical and easily understood mechanism of effect on NO emissions, whereas no such mechanism can be applied to the CATMAX parameter. The location of 50% burned, which is the centroid of the combustion process, fully describes the overall combustion process by combining the effects of ignition timing and burn speed. The impact of ignition timing was well described above where fuel burn speed effects were eliminated. The physical mechanism is identical: the location of 50% burned will be earlier for both advanced ignition timing and faster burning fuels, leading to increased emissions. This effect is traceable to the effect of temperature which both increases the equilibrium predicted NO as well as the rate of NO formation through the non-equilibrium, rate controlled reactions. Figure 11-24 again shows the somewhat moderating effect of the increased reverse reaction rate for the highest temperature case: P31 Closed Loop Simulation.

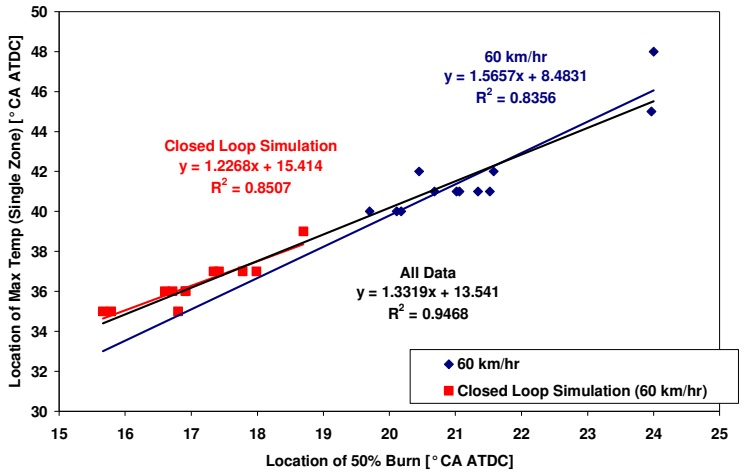

Figure 11-28 Correlation of the location of maximum bulk gas temperature (CATMAX) and the location of 50% burned.

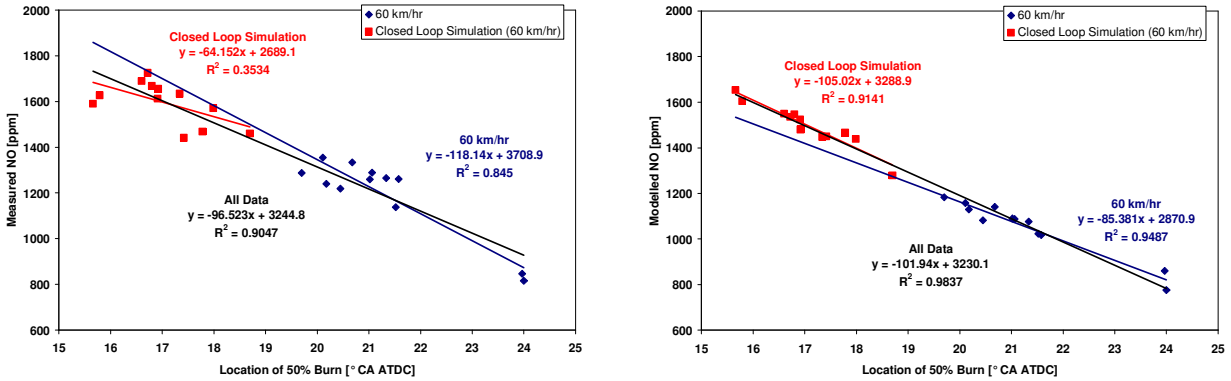

Figure 11-29 Correlation of the measured and the modelled NO emissions and the location of 50% burned.

It is therefore clear that a fuels burn speed is a significant driver for NO emissions, with in general, faster burning fuels leading to higher NO by virtue of advancing the entire combustion process. This is supported by the inclusion of burn angle as a predictor of NO emissions. Separating this effect from other effects leading to changes in combustion timing, such as ignition timing, are however difficult. The best parameter for correlating NO emissions is the location of 50% burned, which inherently incorporates both engine operating conditions such as ignition timing and fuel combustion characteristics such as burn speed.

12. DISCUSSION OF RESULTS

The aim in the following discussion of the results is to:

- explain the mechanisms by which the fuel properties effect the emissions,
- compare the results seen in this research with the results found by other researchers as described in Section 3.

The explanation of the mechanisms through which the emissions are influenced will include a discussion of the triangular approach undertaken for the statistical analysis, as described in Section 4. This will be supplemented by considering the principles of the formation of the emissions as described as background to this research (Section 2.3.1) and as discussed in the literature review (Section 3).

12.1. Hydrocarbon Emissions

12.1.1. Fuel Component Concentrations

Figure 11-15 indicated the effect of the fuel component concentrations on HC emissions. It can be seen that increasing paraffin content reduces the HC emissions, while non-linear responses are seen for olefin and aromatic content. Fuel component concentration effects are not seen to significantly influence those combustion analysis variables seen to influence HC emissions, and which were statistically modelled (DHRMAX and TMAX – see Section 11.5.4). Therefore, the mechanism by which the component concentrations influence HC's can not be traced to any of the combustion parameters considered.

Table 12-1 below summarises the responses found in the AQIRP [20] and the EPEFE [21] studies and the results found in this research. When considering each component non-linear responses are seen in this research for both aromatics and olefins, while the other research reports only linear responses. Factorial design experiments were used in both of the external studies, with paraffin as the swing component in an attempt to isolate a few pre-selected parameters, whereas in this research a large range of fuels with various levels of each parameter were studied. Even though the EPEFE study had a three level aromatic design, they still reported linear trends. There is excellent directional agreement between all three studies for aromatics, over the ranges of aromatics common to all the studies, especially when considering the "Paraffin Swing" results in this research. At high aromatic contents, this research has shown a decline in HC emissions. The comparison of results for olefins indicates opposite trends for olefin content.

Table 12-1 Summary comparison of results for the HC emissions as a function of fuel components for the AQIRP and EPEFE studies and this research.

Fuel Component	AQIRP		EPEFE		This Research				
	Levels‡ [vol %]	Effect [Direction]	Levels‡ [vol %]	Effect [Direction]	Levels [vol %]	Effect : Direct Parameter [Direction]		Effect : Paraffin Swing [Direction]	
Paraffins	Not Studied‡		Not Studied‡		Various: Range 4 - 71%	Near Linear	↓	Not Applicable	
Aromatics	20 and 45%	↑#	20, 35, 50%	↑†	Various: Range 13 - 69%	Non Linear	↑ over range 13 to 35% ↓ over range 35 to 69%	Non Linear	↑ over range 13 to 45% ↓ over range 45 to 69%
Olefins	5 and 20%	↓¥	Not Studied		Various: Range 2 - 50%	Non Linear	↑ over range 2 to 20% ↓ over range 20 to 50%	No Effect	

‡ - Paraffin swing used to generate blend
† - Linear relationship found even though 3 levels tested
# - "Current" fleet only, older fleet indicated no response
¥ - Both fleets

Section 3.2 presented a summary of a number of fundamental studies which considered the mechanisms by which exhaust emissions formation occurs. It is clear that an important mechanism, especially in lean operating engines, is the storage and release of hydrocarbons in crevices and oil layers, and the degree of post combustion burn-up of this stored fuel. The fuel components can influence the exhaust HC content via this mechanism in three important ways:

1. the solubility of the fuel in the oil layer
2. the post combustion concentration of radicals, especially OH, in the combustion chamber
3. the diffusion rate of the hydrocarbons through the thermal boundary layer and into the hot cylinder gas, with the presence of OH, after release from the crevices and oil layers.

Considering the first of these, Kaiser et. al. [25] indicate that molecules with less than six carbon atoms have low solubility in the oil, and Gatalier et. al. [27] indicate that aromatic fuel components are more soluble than non-aromatics. The OH radical concentrations as predicted by equilibrium analysis show that OH concentration increases with the fuel H:C ratio [25]. The aromatic fuels (general formula C_nH_{2n-6}) and olefinic fuels (general formula C_nH_{2n}) have lower H:C ratios than the paraffinic fuels (general formula C_nH_{2n+2}). As for diffusion rates, higher molecular weight molecules will have slower diffusion rates, resulting in less post combustion burn-up [25].

Aromatics have high solubility in oil by virtue of both their structure and the fact that they are high molecular mass (minimum carbon number is six), would result in low OH radical concentration in the bulk gas by virtue of the low H:C ratio and would have slow diffusion rates due to high molecular mass. All of these effects would tend to result in increased HC emissions. Thus the argument of storage and release in crevices and oil layers, and the factors influencing post combustion burn-up can explain the increase of HC's with increased aromatics. The non-linear effect at high aromatic concentrations can not be explained by this mechanism.

A similar argument can be made to explain the increase in HC emissions as olefins increase from 2 to 20 % by volume found in this research. Olefins too have lower H/C ratios than paraffins, although not as low as the aromatic family, and thus reducing the equilibrium OH radical concentrations after combustion. However, no distinct differences should exist for diffusion rate (molecules of similar size as paraffin family) and oil film loading (similar solubility in oil as paraffin family). However, the OH radical concentration may be the least significant of these drivers for HC emissions [25]. This may explain why no response was

seen when paraffins were the swing component as olefins and paraffins are similar in respect of the other two drivers. The non-linear response can also not be easily explained.

The reduction in HC emissions as paraffin content is increased is easily explained as exactly the opposite trend to the response of aromatics and olefins: paraffins have the lowest solubility in oil, have the highest H:C ratio, thus high OH radical concentrations and include low molecular mass components resulting in high diffusion rates through the thermal boundary layer. All these effects reduce HC emissions. A further effect may be traced through equivalence ratio effects. Hydrocarbon emissions are known to be sensitive to equivalence ratio (Section 2.3.1) and this is also indicated here by the occurrence of ER as a variable in the statistical analysis (Table 11-7). The positive coefficient for the ER variable (Table 11-8) indicates that, as expected, fuel rich operation leads to the prediction of increased HC's. Considering the effect of fuel properties on equivalence ratio as investigated above in Section 11.5.4, the fuel component concentrations were seen to have an influence. Increased concentration of paraffin components indicated a reduction in ER prediction (Table 11-40), and this will in turn lead to reduced HC emissions. The mechanism by which equivalence ratio influences HC emissions is well understood and discussed in detail in Section 2.3.1. The mechanism through which fuel components influence operating ER is uncertain.

An important aspect of the effect of fuel component content on HC emissions is the effect that the different fuel species have on the hydrocarbon species present in the exhaust. As described above in Section 2.2, Caplan [7] states that it is not only the quantity of hydrocarbons in the atmosphere which drives the formation of photochemical smog, but also the specific reactivity of the hydrocarbon species present. Kaiser et. al. ([25] and [26]) have shown that the exhaust hydrocarbons are made up of both species present in the parent fuel and species derived from partial combustion of the fuel. Therefore, the effect of fuel composition on the relative quantities of the more reactive species present in the exhaust stream should be determined before any fuel formulation changes are considered.

12.1.2. Oxygen Content

The fuel oxygen content was not identified as being an important variable in the prediction of HC emissions (Table 11-7), however its effect on equivalence ratio, and thus HC emissions is important. The manner in which the statistical models are built by SAS® results in this occurrence, the order of inclusion of the variables resulted in the effect being fully accounted for by the equivalence ratio, before the oxygen content is considered. The oxygen content is seen to have the expected response of reduced equivalence ratio for increased oxygen content (Table 11-40). This is purely a stoichiometry effect, the fuel C:H:O ratio is changed by the addition of oxygenated components, and as the engines are open loop fuel controlled, they cannot respond to the altered stoichiometric fuel / air ratio. The expected response to equivalence ratio is seen with a reduction in HC emissions for this reduced equivalence ratio (Table 11-8). This effect would not be seen with engines equipped with closed loop fuel delivery control.

The fuel MTBE content was studied as part of the AQIRP study [20] and the results are seen to agree with what is seen here. MTBE is an oxygen containing fuel component often used as an octane enhancer, and

is seen to reduce the engine out HC emissions from one of the two groups of vehicles tested (Section 3.1.1). However, the results seemingly contradict the assertion made above regarding the open and closed loop fuel delivery control effects. The "current fleet" studied in the AQIRP programme showed a response in engine-out HC emissions to MTBE content, while no statistically significant response was seen in the "older fleet". Studying the vehicle technology breakdown of the two fleets as given in Table 3-2, it can be seen that the "older fleet" used essentially open loop fuel delivery control technology, similar to the technology of the engines employed in this study. The "current fleet" vehicles were mostly closed loop controlled vehicles, and yet only this group had a statistically significant effect indicated for MTBE on HC emissions. Exhaust oxygen sensors (lambda sensor) require high operational temperatures before they become effective, and there is some delay upon start-up before these temperatures are reached. The AQIRP study utilised vehicle emissions tests including cold starts. Therefore, it is probable that the altered stoichiometry effects the HC emissions in the first few minutes of the test after start-up but before the closed loop fuel delivery control can begin to operate, influence the results of the entire test.

12.1.3. Volatility

Although no clear trend was found for the effect of fuel volatility on the HC emissions – fuel properties correlation, it is obviously very important. Fuel volatility can influence fuel mixing and preparation, evaporative cooling and other important factors. The investigation of the combustion analysis effects on HC's resulted in the identification of, amongst others, TMAX and DHRMAX being influential variables in the prediction of HC's (Table 11-12 and Table 11-13). These are in turn seen to be influenced by volatility effects (Table 11-26 and Table 11-29). Therefore it can be inferred that volatility can influence the hydrocarbon emissions through influences on the maximum bulk gas temperature and the maximum rate of heat release.

Increased low-end volatility will promote higher maximum temperatures (Table 11-28), which in turn will tend to reduce the HC emissions (Table 11-13). The influence of low-end volatility on maximum rate of heat release is also positive, with increased volatility tending to promote higher rates of heat release: the increased maximum temperatures and heat release rate are certainly directly linked. However, this increased heat release rate will tend to increase the emissions. These seemingly contradictory mechanisms may be explained by considering the impact of heat release rate on the pressure and temperature time histories. For a fixed ignition timing, any increase in combustion rate would tend to lead to a higher peak pressure, and higher cylinder pressures throughout the remainder of the cycle (until exhaust blow-down). This will in turn lead to higher bulk gas temperatures. However, these two effects have contrary effects on HC emissions. The higher peak pressures and associated higher late cycle pressures (before the flame front has reached any of the quench layers, oil films or crevice regions) will tend to increase the loading of fuel / air mixture into these regions. Furthermore, the increased late cycle pressures will further delay the release of this mixture from these regions, which will result in it's release at a time when conditions are, potentially, less conducive to promoting post combustion burn-up (less reactive species, less combustion related turbulence etc). This will tend to increase the tendency for fuel

to escape both combustion and post combustion burn-up, and thus result in increased hydrocarbon emissions. However, the increased bulk gas temperatures would actually promote the post combustion burn-up and thus tend to reduce the emissions. It may well be that these two contradictory trends have resulted in low end volatility not being detected as a primary driver for HC emissions.

The mechanism by which volatility influences combustion rate, and therefore gas temperatures is most likely to be through improved mixture preparation. The increased volatility will allow the fuel to be vaporised earlier and therefore better mixing and charge preparation can take place. This will in turn promote the speed at which combustion occurs. Laminar burning velocities are dependant on molecular structure, and it is typical for lower molecular mass hydrocarbon molecules to have higher flame speeds [18]. Low molecular mass hydrocarbons are typically high volatility components and hence there is also a direct link between molecular mass and volatility. It is also understood that laminar burning velocities, by themselves, do not have a strong influence on overall combustion rates in internal combustion engines [18]. It is therefore thought that the mixture preparation effect will dominate, although the effects are directionally consistent with increased volatility increasing combustion rates.

Volatility also influences the HC emissions via its influence on equivalence ratio. Considering Table 11-38 it can be seen that both low- and high-range volatility influences the equivalence ratio. Reduced volatility, both low- and high-range, is shown to be associated with the prediction of reduced equivalence ratio (Table 11-40 and Table 11-41). Therefore, reduced volatility can be linked to a reduction in HC emissions through the reduction in equivalence ratio. The mechanisms occurring which result in this correlation are uncertain.

When considering the volatility effects on HC emissions and the related air quality impact it is essential to consider vehicle evaporative emissions. No strong response to volatility is seen directly in this investigation, and therefore this implies that fuel volatility effects on evaporative emissions will dominate the influence on photochemical activity. However, the AQIRP study indicated that fuel volatility can influence the catalytic converter efficiency and therefore, if catalytic converters are prevalent in the target fleet, then the influence of fuel volatility on their performance should be accounted for. Furthermore, fuel volatility has large effects on vehicle startability and driveability, both of which can have overriding influences on HC emissions. This research studied only fully warm engine operation and steady state operating points.

12.1.4. Lead Content

Before discussing the influence of lead, it is important to consider the order of events during the testing phase. The order of the testing of the research fuels was performed with all the lead additised, commercial fuels followed by the unleaded fuels and then the reformulated fuels, which were based on an unleaded base fuel. In the case of the Toyota 4A-FE engine, the engine cylinder head was changed for a new one (with pressure transducer housing sleeve, see Section 6.1.1), after the leaded batch of fuels. Before the commencement of the testing of the unleaded and reformulated fuels the engine was run for

some time with lead additised fuels (in a related research project based on leaded fuels). The engine cylinder deposits, which are influenced by the lead additive, may therefore not have been the same in the two batches of tests. It was not the intention of this research to include the fuels impact on deposit formation, as this would require extensive engine operation on each fuel sample to achieve deposit level stabilisation. The classification variables used should however fully account for this step change in the deposit levels between the two batches of testing.

The testing of the Toyota 4Y engine was continuous, and thus there should be no such discontinuity in the deposit levels. This only leaves the possibility, with both engines, that a gradual reduction in lead based deposit may have occurred during the testing of the unleaded and reformulated fuels, as these fuels were all unleaded. With the exception of this last possible effect, it can be assumed that the influence of the lead on the emissions is through mechanisms other than the effect of the lead additive on deposit formation.

The fuel lead content correlates with HC emissions with an increase in fuel lead content leading to the prediction of increased emissions (Table 11-8). The correlation of lead content to the relevant combustion analysis results appears to only return significant correlation for TMAX. Increased lead is seen to correlate with reduced maximum bulk gas temperatures (Table 11-27), which in turn will tend to increase the HC emission (Table 11-13). Therefore, the mechanism by which the lead influences the HC emissions is possibly via the reduction of the potential for post combustion burn-up. Reduced gas temperatures would reduce the tendency for the gas which is discharged from the crevices, oil films and quench layers to react and be oxidised. The addition of the lead based additive, in such small quantities as between 2 and 438 mg/l (Table 5-2) is unlikely to have a significant impact on the thermal capacitance of the fuel / air mixture. Therefore, the mechanism by which it influences the gas temperatures must be through other factors. The mechanism by which lead improves octane rating is known to be through the reduction in pre-combustion reaction rates, and thus lengthening the time required under given conditions for localised auto-ignition to occur. Lead was not seen to be an important variable in any of the combustion analysis results that quantify combustion rate (DHRMAX, BA595, Z2IND2 or Z2BA298, Section 11.5.4). Therefore, it does not appear to influence the rate of combustion appreciably in the flame zone. The mechanism through which the lead content influences the gas temperatures is therefore unclear.

In general, the formulation of an un-leaded gasoline would be somewhat different from a leaded one in order to makeup the octane rating. Given the detailed fuel analyses results used in the correlations, it can be assumed that these formulation differences have been considered and it is therefore interesting that the lead content itself has been identified as an important variable. It is important to note that the fuel formulations for the unleaded reformulated fuels (P20 through P35) were not octane constrained: in other words the fuels were not specifically formulated to meet a minimum octane requirement.

12.2. NO Emissions

12.2.1. Fuel Component Concentrations

In the consideration of the effect of fuel properties on NO emissions, the fuel component concentrations were not identified as important variables (Table 11-14). This is in contrast to the findings of other researchers ([20], [21], [22] and [24], Section 3). In general these researchers indicate that increased aromatics will tend to increase the engine-out NO_x emissions. Only one of these research projects considered olefin content [20], and increased olefins were linked to increased NO_x emissions.

The mechanism identified in the EPEFE study [21] for the increase in NO_x for increased fuel aromatic content, is through the influence on the peak flame temperatures. The following statement is made, without reference, in the EPEFE report "*it is well known that engine peak flame temperature increases with increasing aromatics content, leading to higher engine-out NO_x emissions*". Flame temperatures were not determined in this project, but maximum bulk gas temperatures were recorded as an output of the combustion analysis. When correlated to fuel properties, the maximum bulk gas temperatures were not seen to be influenced by the fuel component concentrations (Table 11-26).

Although linked, flame temperatures and bulk gas temperatures are two distinct combustion characteristics, and their respective influences on NO emissions are independent. Considering the NO formation mechanism as described in Section 2.3.1 and demonstrated in Figure 2-6, the rate-limited reactions show a tendency to equilibrate. In other words, as each element burns, high temperatures accelerate the formation of NO. But as the element's temperature drops, and the equilibrium NO concentration drops below the actual gas NO concentration, higher relative temperatures will tend to accelerate the decomposition of NO, until the reactions essentially stop or "freeze".

The interaction between temperature and NO formation is discussed in detail above in Section 11.6, where it was concluded that faster burning fuels would tend to result in increased NO emissions by the combustion advancing nature of increased burn speed: strong correlation is indicated with the location of 50% burned parameter (which was not included in the statistical analysis). Burn angle and induction period are parameters which attempt to characterise burn speed and burn angle was identified as influencing NO emissions in the statistical analysis. The fuel components were not identified as having any direct influence on burn angle.

Olefin content is seen to influence one of the combustion analysis parameters identified as having an influence on NO emissions. The maximum rate of pressure rise (DPMAX) is seen to have a negative impact on NO emissions (Table 11-17). Higher olefin content fuels are seen to increase the maximum rate of pressure rise. This implies that increased olefin content would tend to reduce the NO emissions. This is in contrast to the reported effect of olefin content in the AQIRP [20] study.

12.2.2. Volatility

High-end volatility, by way of the final boiling point (FBP), influences the NO emissions with reduced volatility leading to a reduction in the prediction of NO (Table 11-15). High-end volatility is seen to influence the maximum rate of pressure rise (Table 11-24), a combustion analysis result which is seen to be of importance in the prediction of NO (Table 11-16). Reduced high-end volatility, through T_{90}, tends to reduce the maximum rate of pressure rise (Table 11-25). However, reduced maximum rates of pressure rise are shown to increase the NO produced (Table 11-17), an opposite trend to that predicted by the correlation of the fuel properties and NO emissions. Therefore, the mechanism through which the high-end volatility influences NO is not through its effect on the maximum rate of pressure rise. High-end volatility was seen to be an important variable in the prediction of the burn angle for 2 to 98 % burned (two-zone model) (Table 11-35), a combustion analysis variable which was shown to have an influence on NO emissions (Table 11-18). However, no clear trend was apparent for the effect of high-end volatility on this burn angle variable (Table 11-38), and therefore no conclusion can be drawn as to whether this is a valid mechanism through which NO emissions are effected.

Low-end volatility is not shown to be a fuel property which influences the NO emissions. However, it is seen to have some influence on a number of the combustion analysis results that are seen to effect the NO emissions (Table 11-17 and Table 11-18). IBP, T_{10}, T_{30}, E_{70} and V/L ratio, in different combinations, are seen to be important variables in the prediction of maximum rate of pressure rise (Table 11-24) and the burn angle variables: the burn angle from 5 to 95 % burned (as predicted by the single-zone model) (Table 11-32) and the burn angle from 2 to 98 % burned (as predicted by the two-zone model) (Table 11-35) were investigated. Increased low-end volatility results in the prediction of higher maximum rates of pressure rise (Table 11-25) which leads to a reduction in NO emissions (Table 11-17). A reduced burn angle (5 to 95 % burned, single-zone model) is predicted from increased low-end volatility (Table 11-34). However, this reduced burn angle will tend to increase the NO emissions (Table 11-17). The independent model generated with burn angle variables from the two-zone model supports the response to low-end volatility through combustion rate (burn angle). A reduced burn angle (2 to 98 % burned, two-zone model) is also predicted from an increase in low-end volatility (Table 11-37) which also leads to increased NO emissions (Table 11-18). These conflicting directional responses for low-end volatility probably resulted in low-end volatility not being picked out as an important variable when considering the effects of the fuel properties on NO emissions.

The low-end volatility effects on charge preparation are most likely the mechanism through which DPMAX and the burn angles are affected. Increased volatility will improve mixing of fuel and air and thus increase the combustion rate, and thus the rate of pressure rise.

The mechanism by which the rate of change of pressure influences the NO emissions is uncertain.

Comparing the above results with the literature discussed in Section 3 shows good agreement with the conclusions drawn above. The effect of high-end volatility was investigated in the AQIRP study (T_{90}) [20] and the same directional trend is seen, reduced NO_x emissions is reported for reduced volatility. The

EPEFE study [21] did not consider high-end volatility, but chose mid-range volatility (E_{100}) as the volatility variable. A similar directional response is again reported, with increased NO_x emissions from increased E_{100}. A third study intended to look specifically at mid-range volatility (and aromatic content) [24] reported no significant effect.

12.2.3. Lead Content

Fuel lead content is shown to have an effect on the NO emissions with higher lead content leading to an increase in NO emissions (Table 11-15). This can be traced through the effect on the maximum bulk gas temperature (TMAX). Lead is seen to influence the maximum bulk gas temperature with an increased lead content leading to reduced temperatures (Table 11-27) and a reduction in TMAX is shown to lead to an increase in NO emissions (Table 11-17). However, this statistically determined NO response to maximum bulk gas temperatures is contrary to the expected trend (Section 11.6), and it is thought that this parameter can not be isolated from the CATMAX parameter, and that their combined effect is accounting for the overall combustion timing, as may better be indicated by the location of 50% burned. Therefore, the mechanism by which lead influences the NO emissions is uncertain.

12.3. CO Emissions

12.3.1. Volatility

The only fuel property seen to affect the CO emissions was low-end volatility (T_{30} and E_{70}) (Table 11-19), with reduced low-end volatility linked to a reduction in CO emissions (Table 11-21). This can be linked to the effect of lower maximum rate of pressure rise and reduced equivalence ratio. Reduced low-end volatility is seen to reduce the maximum rate of pressure rise (Table 11-25), while a reduced maximum rate of pressure rise is shown to reduce the CO emissions (Table 11-23). A similar argument can be made for high-end volatility through it's effect on the maximum rate of pressure rise (through the variable T_{90}) (Table 11-25), even though high-end volatility was not identified as influencing CO emissions directly. The mechanics of this effect are uncertain.

The effect of volatility on equivalence ratio is seen to be a reduction in equivalence ratio for reduced volatility, either low- or high-end (T_{10} and T_{70} / FBP respectively) (Table 11-41 and Table 11-42). This reduced equivalence ratio will have the effect of reducing the CO emissions produced (Table 11-20), a well known and understood effect (Section 2.3.1). The mechanism by which the volatility influences the equivalence ratio is uncertain.

High-end volatility (T_{90}) was studied in the AQIRP [20] programme, and mid-range volatility (E_{100}) in the EPEFE study [21]. A trend contrary to what was found in this research was reported for engine-out CO emissions in the AQIRP results, with reduced emissions from increased volatility. Non-linear responses, and different responses were reported for different portions of the driving cycle in the EPEFE report (see Section 3.1.2). Considering the ECE portion of the cycle and the composite results, increasing the E_{100}

from 35% to 50% (increased volatility) reduced the CO emissions, while taking E_{100} from 50% to 65% increased the emissions. The EUDC portion of the cycle showed a linear response with reduced CO emissions for increased volatility. However, the EPEFE vehicle fleet incorporated advanced technologies and all the vehicles utilised closed loop fuel control. All results quoted in the EPEFE report are tailpipe emissions (post catalytic converter), and the AQIRP study indicated a reduction in catalyst efficiency for increased high-end volatility. It is thus difficult to directly compare these results with those found in this research.

12.3.2. Oxygen Content

Similarly to the hydrocarbon emissions, fuel oxygen content is not identified as an important variable for CO emissions prediction in the CO – fuel properties correlation (Table 11-19). This is again as a result of the order of the inclusion of the variables in the statistical modelling, as it is probably masked by the inclusion of equivalence ratio before oxygen content. The importance of the influence of oxygen content on the equivalence ratio is identified in Table 11-39. The reduction in equivalence ratio, which the engines do not respond to, caused by the increased oxygen content (Table 11-40) leads to a reduced CO emission (Table 11-20). The mechanism of this is again a pure stoichiometry effect as discussed above when considering the influence of oxygen content on the HC emissions (Section 12.1.2).

The results of the AQIRP study [20] confirm the response of CO emissions to oxygen content. The reported reduction in CO engine-out emissions for increased MTBE content supports the above assertion, however, the effect was seen in both the “current fleet” and the “older fleet”. This implies that the closed loop vehicles do not fully respond to fuel stoichiometry changes. This is due to the delayed functioning of the closed loop fuel delivery control at start-up, as discussed in detail in Section 12.1.2.

12.3.3. Fuel Component Concentrations

The correlation of CO emissions to the fuel properties did not result in the fuel component concentrations being identified as important variables. However, the effects of fuel component concentrations can be traced through their effect on maximum rate of pressure rise and equivalence ratio. The olefin content is seen to affect the maximum rate of pressure rise (DPMAX), with a higher DPMAX from an increased olefin content (Table 11-25). The effect of DPMAX on CO emissions is seen as an increase in emission for increased DPMAX (Table 11-23). Therefore the CO emissions may be increased for increased olefin content. The equivalence ratio is seen to be influenced by the paraffin content with increased paraffin content reducing the equivalence ratio (Table 11-40). This would then, in turn, reduce the CO emissions (Table 11-20). This effect may be viewed in another way, if either olefins or aromatics are added at the expense of paraffins then CO emissions will be increased through an increase in equivalence ratio. Therefore the addition of olefins has two directionally similar effects, through two separate mechanisms.

The results of the AQIRP study [20] corroborate this by reporting that increased aromatics tend to increase the engine-out CO. However, no significant response to olefin content was seen for CO emissions. CO

response to aromatic content was similarly reported in the EPEFE report [21] to be an increased emission for increased aromatic content. Aromatic content was reported to have no significant effect on CO emissions in a study that was purpose designed to test the fuel aromatic content effects on emissions [22]. Mc Donald et. al. [24] reported that increasing aromatic content had directionally opposite effects on CO emissions depending on the fuel mid-range volatility.

12.4. Effects on Catalyst Efficiency

Both the EPEFE [21] and AQIRP [20] research programmes, as well as other independent studies ([22] and [24]) have shown significant fuel property effects on catalyst efficiency. Aromatic content, fuel volatility and sulphur content have all been shown to influence either the catalyst conversion efficiency or their light off time. Exhaust after treatment was not a factor in the present research but these effects must be considered if the fuels are to be used on vehicles equipped with exhaust catalysts.

13. CONCLUSIONS

From the results and discussion thereof it can be concluded that:

- The repeatability of the load points and engine operating conditions was within acceptable limits;
- The emissions test results were sufficiently accurate and repeatable, and differences between the emissions for the different fuels were large enough for the data set to be significant;
- The combustion analysis produced results that were sufficiently repeatable and adequately sensitive to differences in combustion due to the fuel formulations and that significant results could be attained;
- The addition of the extended Zeldovich NO formation model to the combustion analysis program provided a reliable model which correlated well with the measured emissions, as well as providing valuable insight into the formation mechanisms of NO in the engine under test;
- The combustion analysis proved to be a useful tool which was successfully used to explain some of the combustion related mechanisms that affected the measured emissions;
- A statistical approach was used which was able to predict the fuel properties that influenced the regulated emissions, the combustion analysis parameters that influenced emissions and the fuel properties that, in turn, influenced the combustion analysis parameters. In this way the mechanisms by which the particular fuel properties affect the emissions were investigated, and in many cases the mechanisms were explained;
- Many of the effects of the relevant fuel formulation parameters were seen to agree with the observations reported in the literature considered;
- Although not included in the original statistical analysis, the location of 50% burned parameter is an important variable for the overall description of the burning process, and has a strong correlation with NO emissions.

The fuel properties found to influence the emissions, and a short description of the mechanism are tabulated below in Table 13-1, Table 13-2 and Table 13-3.

Table 13-1 Summary of conclusions drawn for HC emissions.

Fuel Property	Combustion Parameter Linked to Response	Emissions Response for Increase in Property	Description of Mechanism Linked to Emissions Response
Paraffin Content	None Traceable	Reduction	Equivalence Ratio is reduced for increased paraffin content, causes uncertain. Fuel structure influences diffusion rate through quench zone and OH radical concentration in bulk gas.
Aromatic Content	None Traceable	Non-linear, inconsistent direction	Effect on post-combustion burn-up. Fuel structure influences diffusion rate through quench zone and OH radical concentration in bulk gas. Oil solubility higher for aromatics than other hydrocarbon species.
Olefin Content	None Traceable	Non-linear, inconsistent direction	Effect on post-combustion burn-up. Fuel structure influences diffusion rate through quench zone and OH radical concentration in bulk gas.
Oxygen Content	None Traceable	Reduced	Equivalence Ratio reduced through stoichiometry
Volatility	a) TMAX b) DHRMAX	No apparent direct effect indicated	a) Increased late cycle temperatures increases the post combustion burn-up, reducing emissions. Increased volatility promotes charge preparation and thus combustion rates. b) Increased heat release rate increases, fuel loading of crevices and oil layers and delays release, increasing emissions. Increased volatility promotes charge preparation and thus combustion rates. Increased Equivalence Ratio from increased volatility and thus increased emission. Cause of volatility effect on ER uncertain.
Lead Content	TMAX	Increase	Reduced gas temperatures reduce the post combustion burn-up. Cause of reduced temperatures uncertain.

Table 13-2 Summary of conclusions drawn for NO emissions.

Fuel Property	Combustion Parameter Linked to Response	Emissions Response for Increase in Property	Description of Mechanism Linked to Emissions Response
Volatility, High-end	None Traceable	Increase	Cause uncertain.
Volatility, Low-end	a) DPMAX	No apparent direct effect indicated	a) Increased volatility leads to increased DPMAX, which reduces emissions. Volatility affects combustion rates, DPMAX, through improved charge preparation. Cause of emission effect from DPMAX uncertain.
	b) BA595 or Z2BA298		b) Increased volatility leads to reduced burn angles, which increases the emissions. Reduced burn angle from increased combustion rates due to improved charge preparation. Faster burning fuels essentially advance combustion leading to higher burned gas temperatures. Increased temperatures dual driver for NO formation, increasing reaction rates and equilibrium NO prediction.
Lead Content	TMAX	Increase	Cause uncertain
	Location of 50% burned		A strong correlation is found between NO and the location of 50% burned parameter. This parameter best accounts for the aspects of combustion timing effects on NO.

Table 13-3 Summary of conclusions drawn for CO emissions.

Fuel Property	Combustion Parameter Linked to Response	Emissions Response for Increase in Property	Description of Mechanism Linked to Emissions Response
Volatility, low-end	DPMAX	Increase	Increased volatility increases DPMAX which increases the emissions. Cause of increased emission is uncertain. Increased volatility increases Equivalence Ratio which increases emissions. Cause of volatility effect on ER is uncertain.
Oxygen Content	None Traceable	Reduction	Equivalence Ratio reduced through stoichiometry.
Paraffin Content	None Traceable	No apparent direct effect indicated	Increased paraffin content reduces the Equivalence Ratio, and thus should reduce emissions. Cause uncertain.
Olefin Content	DPMAX	No apparent direct effect indicated	Increased olefin content increases DPMAX and thus increases emissions. Cause uncertain. Increasing olefin content increases Equivalence Ratio and thus emissions. Cause uncertain.

14. RECOMMENDATIONS

The following recommendations can be made:

- This research has shown that the experimental approach whereby a large number of fuels with various formulations are tested and a wide range of fuel formulation parameters are included in the statistical analysis, is a valid methodology to investigate the effect of fuel formulation on exhaust emissions. This method can then be used, where suitable, in favour of the more traditional full factorial experimental approach which is usually constrained to a small number of fuel formulation parameters for practical reasons. As it is impossible to fully separate the various fuel parameters when blending test fuels, this methodology reduces the potential for inappropriately attributing observed responses to the initially targeted fuel properties which may actually be responses to other fuel formulation parameters. Even when full factorial experiments are undertaken, it is recommended that all the measured fuel parameters that are available be included in the statistical analysis.

- The statistical results generated are a useful tool and can be used for decisions related to fuel formulation parameters in order to minimise the emissions from spark ignition engine powered vehicles. This would have to be done simultaneously with the broader requirements for fuel formulation as required to meet specifications other than those related to exhaust emissions - for example gasoline octane number. Furthermore, South Africa is in the unique situation whereby local companies have developed fuel manufacturing technologies which have increased flexibility in terms of the fuel formulation parameters than traditional crude oil based refining techniques. In the coming years, as vehicle emissions and fuel formulation legislation develops, South African companies may be required to alter their plants in order to meet any new fuel formulation requirements. Thus, it is conceivable that the results and conclusions reported in this research can be applied in the design and operation of flexible fuel refining and manufacturing plants.

- The research has identified that fuel formulation parameters do influence engine out emissions. The research relied only on the results from two different engines. In order for meaningful air quality impacts to be attained, the specific results and conclusions of this research can be used in guiding the fuel formulation on a national or refinery specific basis only if one of two further steps is undertaken. The results should be validated on a larger cross section of engine technologies. Alternatively, fuel formulation parameters can be optimised where clear formation mechanisms have been identified and explained and these mechanisms can be considered relatively universal across engine technologies.

- The improved understanding of some of the emissions formation mechanisms, and especially the extended Zeldovich NO formation model, can be applied during engine development for the minimisation of engine out exhaust emissions.

15. REFERENCES

1 Government Gazette, No 27947, R 856, Withdrawal and Replacement of the Compulsory Specification for Motor Vehicles of Category M1, pp 49 – 64, 2 September 2005.

2 Wicking-Baird, M. C., de Villiers, M. G. and Dutkiewicz, R. K., *Cape Town Brown Haze Study*, ERI Report No. Gen 182, UCT, South Africa, September 1997.

3 Information courtesy of Grant Ravenscroft, Manager, Scientific Services Division of the Cape Metropolitan Council. Additional information from http://www.capetown.gov.za/airqual/

4 de Waal, P. N., *Verdampingsverliese van Petrol uit Motorvoertuie*, Unpublished Undergraduate B.Eng (Mech) Thesis Dissertation, University of Stellenbosch, South Africa, October 1997.

5 van der Westhuizen, H. J., *Evaporative Emissions and Fuel Loss in South Africa*, Unpublished Undergraduate B.Eng (Mech) Thesis Dissertation, University of Stellenbosch, South Africa, October 1997.

6 Obert, E. F., *Internal Combustion Engines and Air Pollution*. Harper CollinsNew York, 1973.

7 Caplan ,J., "Spotting the Culprits in Smog Formation." *SAE J.* pp. 62-65, December 1965.

8 Amann, C. A., "Future automotive fuels from a US standpoint.", *Int. J. of Vehicle Design*, vol. 13, nos 5/6, pp. 407-427, 1992.

9 de Villiers, M. G., *The Cape Town Brown Haze Pilot Study*, ERI Report No. Gen 157, UCT, South Africa, September 1993.

10 Thompson, N. D., Larive, J. F., "Regulations to Control Emissions and Fuel Implications", 2003-00717-01-E, Concawe, 2003.

11 Bell, A. J., "International Experience with Various Vehicle Emissions Reduction Schemes", Proceedings of the Annual Clean Air Conference, National Association for Clean Air, Cape Town, 1999.

12 Mills, R., "Strategies for Reducing Vehicle Emissions and their Impact on Urban Areas.", *Papers of 11th World Clean Air and Environment Congress*, vol 5, paper 13F-5, Durban, South Africa, September 1998.

13 de Goede, S., *Moniteering van die Emissies van Vonkontstekingsenjins Onder Verskillende Rykondisies en met Verskillende Brandstofformulerings*, Unpublished M.Sc (Chem) Thesis Dissertation, University of Stellenbosch, South Africa, 1997.

14 de Goede, S., Engelbrecht, W. J., van der Merwe, L., Bell, A. J. and Taylor, A. B., "Aldehyde Emissions Quantification with Primary and Secondary Alcohols in Spark-ignition Fuel Blends.", *Proceedings of the Eleventh International Symposium on Alcohol Fuels (ISAF)*, South Africa, vol 1, pp. 12-23, 1996.

15 Heywood, John B., *Internal Combustion Engine Fundamentals*. McGraw Hill International Editions, New York, 1988.

16 Daniel, W. A., "Why Engine Variables Affect Exhaust Hydrocarbon Emission.", SAE Paper 700108, *SAE Trans.,* vol. 79, 1970.

17 Ferguson, Colin R., *Internal Combustion Engines, Applied Thermosciences*. John Wiley and Sons, New York, 1986.

18 Stone, R. Introduction to Internal Combustion Engines, Third Edition, Society of Automotive Engineers No R-278, ISBN 0-7680-0495-0, 1999.

19 Bosch, *Automotive Handbook*, 3rd ed., Robert Bosch GmbH, Stuttgart, Germany, 1993.

20 Hochhouser, A. M., Benson, J. B., Burns, V., Gorse, R. A., Koehl, W. J., Painter, L.J., Rippon, B. H., Reuter, R. M. and Rutherford, J. A., "The Effect of Aromatics, MTBE, Olefins and T_{90} on Mass Exhaust Emissions from Current and Older Vehicles - The Auto/Oil Air Quality Improvement Research Program.", SAE Paper 912322, *SAE Trans*, vol 100, section 4, pp.748-788, 1991.

21 Palmer, F. *Epefe Report.*, Report Compiled on Behalf of ACEA and EUROPIA, CD-ROM December 1995.

22 Gething, J. A., Kent Hoekman, S., Guerrero, A. R. and Lyons, J. M., “The Effect of Gasoline Aromatics Content on Exhaust Emissions: A Co-operative Test Program.”, SAE Paper 902073, *SAE Trans*, vol 99, section 4, pp. 568-580, 1990.

23 Carter, W. P. L., “Development of Ozone Reactivity Scales for Volatile Organic Compounds”, submitted to Atmospheric Environment, May 1990.

24 McDonald, C.R., Morgan, T. D. B., Graupner, O. and Wilkinson, E., “The Independent Effects of Fuel Aromatic Content and Mid-Range Volatility on Tailpipe Emissions from Current Technology European Vehicle Fleets”, *SAE Paper 962026, Gasoline Performance and Deposit Control Additives* (SP-1214), 1996.

25 Kaiser, E. W., Siegl, W. O., Henig, Y. I., Anderson, R. W. and Trinker, F. H., ”Effect of Fuel Structure on Emissions from a Spark-Ignited Engine”, Environ. Sci. Technol., vol 25, No. 12, 1991.

26 Kaiser, E. W., Siegl, W. O., Cotton, D. F. and Anderson, R.W., ”Effect of Fuel Structure on Emissions from a Spark-Ignited Engine. 2. Napthene and Aromatic Fuels”, Environ. Sci. Technol., vol 26, No. 8, 1992.

27 Gatellier, B., Trapy, J., Herrier, D., Quelin, J. M. and Galliot, F., “Hydrocarbon Emissions of SI Engines as Influenced by Fuel Absorption-Desorption in Oil films.”, SAE paper 920095, *SAE Trans*, vol 101, section 4, pp. 31-42, 1992.

28 Wentworth, J. T., “The Piston Crevice Volume Effect on Exhaust Hydrocarbon Emission.”, Combustion Science and Technology, vol. 4, 1971.

29 Kaiser, E. W., Rothschild, W. G. and Lavoie, G. A., “Storage and Partial Oxidation of Unburned Hydrocarbons in Spark-Ignited Engines - Effect of Compression Ratio and Spark Timing.”, Combustion Science and Technology, vol. 36, 1984.

30 Krieger, R. B. and Borman, G. L., “The Computation of Apparent Heat Release for Internal Combustion Engines,” ASME paper 66-WA/DGP-4, 1966.

31 Gordon, S. and McBride, B. J., “Computer Program for the Calculation of Complex Chemical Equilibrium Composition, Rocket Performance, Incident and Reflected Shocks and Chapman-Jouquet Detonations,” NASA publication SP-273, 1971 (NTIS number N71-37775).

32 Olikara, C. and Borman, G. L., “A Computer Program for Calculating Properties of Equilibrium Combustion Products with some Applications to I. C. Engines,” SAE paper 750468, 1975.

33 Goodger, E. M., *Hydrocarbon Fuels, Production, Properties and Performance of Liquids and Gases*. The Macmillan Press Limited, London, 1975.

34 Taylor, C. F., *The Internal-Combustion Engine in Theory and Practice.* 2nd rev. ed., Cambridge, Mass., MIT Press, vol 2, 1985.

35 Reed, R. J., *North American Combustion Handbook*., Volume 1, 3rd edition, North American Mfg. Co., Cleveland, USA, 1986.

36 Wimmer A. and Glaser, J., *Engine Indicating User Handbook*, AVL, Graz, 2002.

37 Moran, D. P., Bell, A. J. and Williams, P. N. T., *Manual : RACER – Engine Combustion Data Acquisition and Burn-Rate Analysis System*., Unpublished In-house System Operations Manual, Centre for Automotive Engineering, University of Stellenbosch, September 1997.

38 Moran, D. P. and Taylor A. B., “An Evaporative and Engine Cycle Model for Fuel Octane Sensitivity Prediction.”, SAE Paper 952524, *Gasoline Additives and Performance (SP-1118)*, 1995.

39 Toyota Corolla 160i GLE, *CAR*, ISSN 0008-5995, Volume 38, No 9, October 1994.

40 Gatowski, J. A., Balles, E. N., Chun, K. M., Nelson, F. E., Ekchian, J. A. and Heywood, J. B., “Heat Release Analysis of Engine Pressure Data,” SAE paper 670931, *SAE Trans*., Vol. 77, 1967.

41 McLaren, M. R., *Heat Release Analysis of a Spark-Ignition Engine*., Unpublished Undergraduate B.Eng (Mech) Thesis Dissertation, University of Stellenbosch, South Africa, January 1994.

42 Cheung, H. M. and Heywood, J. B., “Evaluation of a One-Zone Burn-Rate Analysis Procedure Using Production SI Engine Pressure Data.”, SAE paper 932749, *SAE Trans*, vol 102, section 3, pp 2292-2303, 1993.

43 Diab, A., Research Note Comparing Equilibrium Calculations Assuming Ideal Gas and Calculations Accounting for Deviations from Ideal Gas Behaviour, part of M.Sc (Mech) research project, University of Stellenbosch, 1998.

44 Woschni, G., “A Universally Applicable Equation for the Instantaneous Heat Transfer Coefficient in the Internal Combustion Engine.” SAE paper 670931, *SAE Trans.*, vol. 76, 1967.

45 Taylor, A. B., Moran, D. P., Bell, A. J., Hodgson, N. G., Myburgh, I. S. and Botha, J. J., “Gasoline/Alcohol Blends: Exhaust Emissions, Performance and Burn Rate in a Multi-Valve Production Engine”, SAE paper 961988, *Topics in Alternative Fuels and Their Emissions* (SP-1208), 1996.

46 White, F. M., *Viscous Fluid Flow,* 2nd ed., McGraw-Hill, Inc., New York. 1991.

47 Ferguson, C. R., and Kirkpatrick, A. T., *Internal Combustion Engines, Applied Thermosciences,* 2nd ed, John Wiley and Sons, New York, 2001

48 Blumberg, P, Kummer, J. T., Prediction of NO Formation in Spark-Ignited Engines - An Analysis of Methods of Control, Combustion Science and Technology, Vol 4, pp 73-95, 1971

49 Komiyama, K., Heywood, J. B., Predicting NO_x Emissions and Effects of Exhaust Gas Recirculation in Spark Ignition Engines, SAE paper 730475, pp 1458-1476, 1973

50 Raine, R. R., Stone, C. R., Gould, J., Modelling Nitric Oxide Formatio in Spark Ignition Engines with a Multizone Burned Gas, Combustion and Flame, vol 102, pp 241-255, 1995

51 Williams, P. N. T., *Modelling of Internal Combustion Engine Thermodynamics, Valve Dynamics and Valve Flow*, Unpublished M.Sc. Eng (Mech) Thesis Dissertation, University of Stellenbosch, South Africa, November 2002.

52 Lancaster, D. R., Krieger, R. B. and Leinesch, J. H., “Measurement and Analysis of Engine Pressure Data,” SAE paper 750026, *SAE Trans.*, vol. 84, 1975.

53 Swarts, A. and Yates, A., “In-Cylinder Fuel Evaporation and Heat Transfer Information Inferred from the Polytropic Character of the Compression Stroke in a Spark-Ignition Engine”, SAE paper 2004-01-1856, 2005.

54 Wentworth, J. T., “Effect of Combustion Chamber Surface Temperature on Exhaust Hydrocarbon Concentration”, SAE paper 710587, *SAE Trans*, vol 80, section 3, pp 2003-2019, 1971.

55 Finlay, I. C., Harris, D., Boam, D. J. and Parks, B. I., “Factors Influencing Combustion Chamber Wall Temperatures in a Liquid Cooled, Automotive, Spark Ignition Engine.” Proc. Instn Mech Engrs, vol 199, no. D3, pp. 207-214, 1985.

56 Li, C-H, “Piston Thermal Deformation and Friction Considerations”, SAE paper 820086, 1982.

57 Cornell, John A., *Experiments with Mixtures. Designs, Models, and the Analysis of Mixture Data.* Second Edition. Wiley series in Probability and Statistics. John Wiley and Sons, Inc., New York, 1990.

58 SABS 013: Part I-1998, *The Determination of Performance (at net power) of Internal Combustion Engines. Part I: Road Vehicle Internal Combustion Engines at Sea Level*, South African Bureau of Standards, 1998.

59 Swarts, A., Viljoen, C. and Coetzer R., The Analysis of Observed Burn Rates in a Spark-Ignition Engine and the Relation to Fuel Properties, SAE Paper 2003-01-3125, 2003.

APPENDIX A : ANALYSIS OF TEST FUELS

Leaded Fuels

ANALYSIS	P1	P2	P3	P4	P5	P6	P7	P8	P9	P10	P11
ASTM DISTILLATION -IBP	31	43	32	29	30	29	28	31	29	27	26
- 5% ℃	49	55	47	47	47	49	48	46	47	51	44
- 10% ℃	53	57	53	52	51	54	53	51	52	60	50
- 20% ℃	60	71	63	59	60	64	61	60	63	74	60
- 30% ℃	65	79	74	68	69	75	70	71	74	88	71
- 40% ℃	68	88	85	76	80	89	79	84	86	99	86
- 50% ℃	79	98	97	89	94	103	88	98	100	107	103
- 60% ℃	97	110	109	102	110	116	99	112	113	113	119
- 70% ℃	112	121	123	118	128	129	112	127	127	124	132
- 80% ℃	126	137	140	137	146	145	129	144	143	142	144
- 90% ℃	144	160	162	161	170	166	151	163	162	167	158
- 95% ℃	156	174	183	182	191	200	175		182	194	193
- FBP ℃	170	200	191	205	200	207	180	196	194	194	195
- Recovery, vol %	97	99	96	98	97	96	96	95	96	96	95
- Residual, vol %	1.8	0.5	0.8	0.7	0.8	0.8	0.9	1	3.5	0.9	0.9
DENSITY,kg/L	0.7291	0.7191	0.7189	0.7208	0.7236	0.7216	0.7193	0.7374	0.7385	0.723	0.7358
COPPER COROSION	1a	1a	1a	1a	1a	1a	1a	1a	1a	1a	1a
DOCTOR TEST	Neg	Neg	Neg	Neg	Neg	Neg	Neg	Neg	Neg	Neg	Neg
V/L Ratio, ℃	59	59	60	59	58	59	57	58	60	59	55
VAPOUR PRESSURE,kPa	62	67	64	66	53	64	67	64	64	65	73
E70, vol%	44	23	29	33	34	30	34	31	30	20	33
VOLATILITY INDEX	93	83	84	89	77	85	91	85	86	79	96
EXISTING GUM,mg/100ml	<1	1	<1	<1	2	<1	<1	<1	2	<1	<1
POTENTIAL GUM,mg/100ml	1	2	1	2	6	<1	<1	<1	5	<1	<1
ACID NUMBERL,mgKOH/g	0.016	0.01	0.002	0.002	0.002	0.006	0.033	0.002	0.002	0.004	0.003
INDUCTION,min	>1440	>1440	1020	615	615	>1440	300	>1440	>1440	>1440	390
RON	95.1	93.3	93.6	94.4	93.9	93.8	94.8	97.4	97.2	97.4	98.2
MON	85	85	85.8	84.8	83.6	88.7	83.6	87.8	87.9	90.5	87.3
R100-octane number	92.1	84.8	84.3	86.3	86.4	83.7	88.5	85.5	84	86.4	89.1
LEAD CONTENT,mgPb/l	291	286	400	328	413	432	205	400	407	438	353
AROMATICS,vol%	16	15	18	56	52	69	48	44	54	51	47
OLEFINS,vol%	23	25	30	24	20	25	31	50	36	36	22
PARAFFINS,vol%	61	60	52	20	28	6	21	6	10	13	31
SULPHUR,mass%	0.0001	0.05	0.0001	0.049	0.069	0.005	0.033	0.033	0.003	0.002	0.017
NITROGEN,mg/l	29	11	12	18	22	6	12	14	10	7	10
OXYGEN, mass%	3.77	<1	<1	<1	<1	<1	<1	<1	<1	<1	<1
BENZENE mass%	1.68	1.65	1.64	1.96	1.56	3.36	4.81	3.25	0.7	3.1	1.86
PHENOLS,mg/l	53	48	28	326	643	25	166	215	217	<25	95
C	8	8	8	8	8	8	8	8	8	8	8
H	15.2	15.2	15.2	15.2	15.2	15.2	15.2	15.2	15.2	15.2	15.2
O	0.273	0.000	0.000	0.000	0.000	0.000	0.000	0.000	0.000	0.000	0.000

Unleaded Fuels

ANALYSIS	P12	P13	P14	P15	P16	P17	P18	P19
ASTM DISTILLATION -IBP	40	41	35	33	29	28	37	38
- 5% ℃	49	57	54	54	50	59	52	53
- 10% ℃	55	65	59	59	58	68	60	63
- 20% ℃	65	79	66	68	71	83	75	80
- 30% ℃	76	92	72	76	84	95	89	97
- 40% ℃	87	103	82	86	99	105	101	111
- 50% ℃	100	112	106	98	110	112	108	122
- 60% ℃	113	120	115	111	119	120	115	132
- 70% ℃	128	129	127	123	128	130	124	143
- 80% ℃	145	143	140	138	138	146	142	154
- 90% ℃	168	160	160	158	154	167	169	173
- 95% ℃	190	173	176	175	182	186	188	193
- FBP ℃	209	196	196	196	190	201	200	218
- Recovery, vol %	97	97	97	97	96	97	97	98
- Residual, vol %	1	1.1	1	0.9	0.7	0.8	0.7	0.8
DENSITY,kg/L	0.7319	0.7363	0.7408	0.7369	0.7661	0.7571	0.7322	0.746
COPPER COROSION	1a	1a	1a	1a	1a	1a	1a	1 a
DOCTOR TEST	Neg	Neg	Neg	Neg	Neg	Neg	Neg	Neg
V/L Ratio, ℃	64	64	63	63	60	63	62	59
VAPOUR PRESSURE,kPa	68	53	59	52	66	55	71	60
E70, vol%	27	15	27	24	22	14	19	17
VOLATILITY INDEX	87	64	78	69	81	65	84	72
EXISTING GUM,mg/100ml	<1	<1	1	<1	1	<1	<1	<1
POTENTIAL GUM,mg/100ml	<1	<1	1	1	2	<1	<1	<1
ACID NUMBERL,mgKOH/g	0.003	0.001	0.001	0.001	0.004	0.004	0.003	0.001
INDUCTION,min	>1440	>1440	>1440	>1440	840	>1440	>1440	390
RON	90.9	91	95.5	96.9	96.4	96.5	95.1	97.1
MON	81.6	81.8	83.3	85.1	85.2	86.1	88.2	84.1
R100-octane number	86.7	85	95.5	96.9	89.2	88.7	88.8	92.3
LEAD CONTENT,mgPb/l	7	3	<2	<2	5	16	3	3
AROMATICS,vol%	26	28	31	29	45	47	27	29
OLEFINS,vol%	25	27	27	25	46	49	2	45
PARAFFINS,vol%	49	45	42	46	9	4	71	26
SULPHUR,mass%	0.0189	0.0001	0.0001	0.0001	0.023	0.031	0.0004	0.0127
NITROGEN,mg/l	17	33	32	28	8	11	10	2
OXYGEN, mass%	<1	<0.01	3.14	3.64	<1	<1	<0.01	<1
BENZENE mass%		1.03	0.99	0.84	2.81	2.83	3.94	3.55
PHENOLS,mg/l	121	<25	45	<25	168	117	<25	60
C	8	8	8	8	8	8	8	8
H	15.2	15.2	15.2	15.2	15.2	15.2	15.2	15.2
O	0.000	0.000	0.226	0.263	0.000	0.000	0.000	0.000

Reformulated Fuels

ANALYSIS	P20	P21	P22	P23	P24	P25	P26	P27	P28	P29
ASTM DISTILLATION -IBP	31	36	36	37	36	36	32	42	38	39
- 5% ℃	49	49	49	49	47	49	50	51	52	59
- 10% ℃	55	56	56	55	52	56	56	57	58	67
- 20% ℃	66	67	66	65	59	66	66	66	67	80
- 30% ℃	76	77	77	75	65	77	76	76	76	93
- 40% ℃	88	90	90	87	72	89	88	86	85	104
- 50% ℃	101	103	102	100	82	102	100	97	94	113
- 60% ℃	113	115	116	114	96	115	113	109	106	121
- 70% ℃	127	130	130	130	116	129	127	124	121	131
- 80% ℃	145	148	147	149	137	147	145	143	141	144
- 90% ℃	166	168	170	176	163	171	166	166	164	162
- 95% ℃	187	193	195		186	195	187	186	186	177
- FBP ℃	210	211	210	207	204	210	210	208	204	202
- Recovery, vol %	98	97	97	95	97	97	98	98	97	98
- Residual, vol %	0.8	1.1	0.9	1	0.9	1.2	0.8	0.6	0.9	0.9
DENSITY,kg/L	0.7314	0.7311	0.731	0.7266	0.7327	0.7276	0.732	0.7388	0.7381	0.7369
COPPER COROSION	1a	1a	1a	1 a	1 a	1a	1a	1a	1a	1a
DOCTOR TEST	Neg	Neg	Neg	Neg	Neg	Neg	Neg	Neg	Neg	Neg
V/L Ratio, ℃	60	61	61	58	58	58	61	62	65	64
VAPOUR PRESSURE,kPa	69	68	67	63	62	76	69	65	61	52
E70, vol%	25	25	25	29	39	25	25	26	25	14
VOLATILITY INDEX	87	86	85	83	87	93	87	82	79	62
EXISTING GUM,mg/100ml	<1	4	2	1	1	1	1	<1	4	<1
POTENTIAL GUM,mg/100ml	<1	5	4	4	4	3	2	<1	4	<1
ACID NUMBERL,mgKOH/g	0.002	0.002	0.003	0.001	0.001	0.002	0.001	0.002	0.002	0.001
INDUCTION,min	>1440	>1440	>1440	>1440	>1440	>1440	>1440	>1440	>1440	>1440
RON	90.9	92.2	93.2	92.1	96.5	90.8	90.9	91.6	89.4	91
MON	81.3	82.2	82.7	82.2	84.9	81.8	81.4	81.8	80.6	81.8
R100-octane number	87.1	86.7	86.7	89.7	96.7	87	87.1	89.1	85.4	85.8
LEAD CONTENT,mgPb/l	<2	7	11	2	2	5	<2	5	2	5
AROMATICS,vol%	26	26	26	27	30	25	30	30	29	31
OLEFINS,vol%	24	24	25	23	20	23	19	25	21	24
PARAFFINS,vol%	50	50	49	50	50	52	51	45	50	45
SULPHUR,mass%	0.019	0.019	0.019	0.019	0.0174	0.019	0.019	0.031	0.031	0.0002
NITROGEN,mg/l	35	21	21	20	16	21	25	17	19	7
OXYGEN, mass%	<0.01	<0.01	<0.01	1.04	3.43	<0.01	<0.01	<0.01	<0.01	<0.01
BENZENE mass%	2.02	2.4	2.49	1.87	2.05	2.4	2.54	7.66	10.8	1.05
PHENOLS,mg/l	136	122	106	60	71	103	155	124	111	<25
C	8	8	8	8	8	8	8	8	8	8
H	15.2	15.2	15.2	15.2	15.2	15.2	15.2	15.2	15.2	15.2
O	0.000	0.000	0.000	0.073	0.247	0.000	0.000	0.000	0.000	0.000

Reformulated Fuels (Continued) and Reference Fuels

ANALYSIS	P30	P31	P32	P33	P34	P35	Ref 1	Ref 2
ASTM DISTILLATION -IBP	38	37	36	33	36	37	42	37
- 5% ℃	61	50	50	50	49	51	47	45
- 10% ℃	69	55	56	56	55	57	50	50
- 20% ℃	83	67	66	67	65	65	58	58
- 30% ℃	96	78	76	78	76	74	68	69
- 40% ℃	106	89	87	88	86	84	79	81
- 50% ℃	114	102	96	97	96	94	93	97
- 60% ℃	123	115	103	104	103	103	108	112
- 70% ℃	134	129	109	111	110	108	124	127
- 80% ℃	148	147	117	121	122	111	139	140
- 90% ℃	166	170	135	150	152	116	153	156
- 95% ℃	181	194	164	175	177	127	166	176
- FBP ℃	205	210	191	196	196	173	186	195
- Recovery, vol %	97	97	98	98	97	99	97	97
- Residual, vol %	1.1	0.9	0.5	0.8	0.1	0.5	1	1
DENSITY,kg/L	0.7415	0.7342	0.7628	0.7463	0.7263	0.771	0.7311	0.7429
COPPER COROSION	1a	1a	1a	1a	1a	1a		
DOCTOR TEST	Neg	Neg	Neg	Neg	Neg	Neg	Neg	Neg
V/L Ratio, ℃	67	59	61	61	58	59	63	71
VAPOUR PRESSURE,kPa	50	62	62	64	67	60	72	63
E70, vol%	12	25	26	24	27	27	34	33
VOLATILITY INDEX	58	80	80	81	86	79	96	86
EXISTING GUM,mg/100ml	<1	<1	<1	<1	<1	<1	<1	<1
POTENTIAL GUM,mg/100ml	<1	<1	<1	2	2	<1	1	1
ACID NUMBERL,mgKOH/g	0.001	0.004	0.001	0.001	0.001	0.002	0.001	0.001
INDUCTION,min	>1440	>1440	>1440	>1440	>1440	>1440	>300	>300
RON	90.9	90.6	91.8	91.9	92	92.9	97.7	97.5
MON	81.4	81	83.7	83.5	83.1	83.5	87.1	87
R100-octane number	82.5	86.5	85.1	87.5	90.7	84.6		
LEAD CONTENT,mgPb/l	3	5	3	2	3	3	361	335
AROMATICS,vol%	34	26	32	21	13	39	28	36
OLEFINS,vol%	15	25	8	17	26	6	22	17
PARAFFINS,vol%	51	49	60	62	61	55	50	47
SULPHUR,mass%	0.0076	0.02	0.0315	0.0233	0.0163	0.0463	0.038	0.0385
NITROGEN,mg/l	7	23	12	14	15	12		
OXYGEN, mass%	<0.01	<0.01	<0.01	0.09	0.16	<0.01	<0.01	<0.01
BENZENE mass%	1.19	2.37	1.45	1.13	1.09	1.62	1.5	2.14
PHENOLS,mg/l	<25	144	<25	40	31	<25		
C	8	8	8	8	8	8	8	8
H	15.2	15.2	15.2	15.2	15.2	15.2	15.2	15.2
O	0.000	0.000	0.000	0.006	0.011	0.000	0.000	0.000

APPENDIX B : DERIVATION OF TWO ZONE HEAT RELEASE FORMULAS GIVEN BY KRIEGER AND BORMAN

The following is a derivation of the equations presented by Kreiger and Borman [1] for a two-zone, mass transfer based combustion analysis model suitable for spark-ignition engine analyses.

Consider the schematic of an engine cylinder while combustion is occurring in an infinitely thin flame separating the burned zone from the unburned zone, as in Figure B-1.

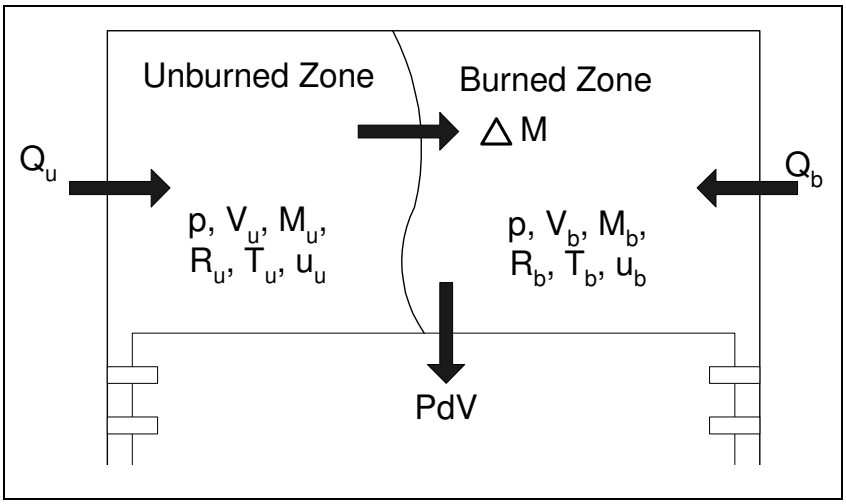

Figure B-1 Schematic of the two-zone, mass transfer based combustion analysis model.

Assumptions:

1. Pressure, p, in the burned and unburned zones is equal
2. The individual zones are in thermal equilibrium (there are no temperature gradients within the zones), this assumption leads to a "fully mixed model"
3. There is no heat transfer between the burned and unburned zones
4. No chemical reactions take place in the unburned zone (zone is said to be frozen)

   i.e. $\frac{\partial x}{\partial \mathrm{T}} = \frac{\partial x}{\partial \mathrm{p}} = 0 \Rightarrow \frac{\partial M}{\partial \mathrm{T}} = \frac{\partial R}{\partial \mathrm{T}} = \frac{\partial M}{\partial \mathrm{p}} = \frac{\partial R}{\partial \mathrm{p}} = \frac{\partial u}{\partial \mathrm{p}} = 0$ ..... Eqn B-1

5. The flame has zero volume or mass

   i.e. the total cylinder volume and mass is taken up by the burned and unburned volumes and masses only

   $\therefore\ V = V_u + V_b$ and $m = m_u + m_b$ ..... Eqn B-2

From Eqn B-2 we can write

$m_{u1} - \Delta m = m_{u2}$ and $m_{b1} + \Delta m = m_{b2}$ which leads to $-\dot{m}_u = \dot{m}_b$ ..... Eqn B-3

The ideal gas law states

$pV = mRT$ ..... Eqn B-4

from which we can write

$$p = \frac{m_b R_b T_b}{V_b} = \frac{m_u R_u T_u}{V_u} \quad \text{Eqn B-5}$$

Differentiating Eqn B-4 gives

$$pdV + Vdp = mRdT + mTdR + RTdm \quad \text{Eqn B-6}$$

Dividing by pV gives

$$\frac{dV}{V} + \frac{dp}{p} = \frac{mR}{pV}dT + \frac{mT}{pV}dR + \frac{RT}{pV}dm \quad \text{Eqn B-7}$$

Using Eqn B-4 gives

$$\frac{dV}{V} + \frac{dp}{p} = \frac{dT}{T} + \frac{dR}{R} + \frac{dm}{m} \quad \text{Eqn B-8}$$

Writing in reduced notation and applying to unburned and burned zones gives

$$\frac{\dot{p}}{p} = \frac{\dot{m}_b}{m_b} + \frac{\dot{R}_b}{R_b} + \frac{\dot{T}_b}{T_b} - \frac{\dot{V}_b}{V_b} = \frac{\dot{m}_u}{m_u} + \frac{\dot{R}_u}{R_u} + \frac{\dot{T}_u}{T_u} - \frac{\dot{V}_u}{V_u} \quad \text{Eqn B-9}$$

Writing the energy equation for the unburned zone gives

$$m_{u2}u_{u2} = m_{u1}u_{u1} - \Delta m h_u + Q_u - \int_1^2 pdV_u \quad \text{Eqn B-10}$$

$$m_{u2}u_{u2} - m_{u1}u_{u1} = -\Delta m h_u + Q_u - \int_1^2 pdV_u \quad \text{Eqn B-11}$$

writing in differential form

$$\dot{\overline{m_u u_u}} = \dot{m}_u h_u + \dot{Q}_u - pdV_u \quad \text{Eqn B-12}$$

$$\dot{m}_u u_u + m_u \dot{u}_u = \dot{m}_u h_u + \dot{Q}_u - p\dot{V}_u \quad \text{Eqn B-13}$$

Similarly, writing the energy equation for the burned zone gives

$$m_{b2}u_{b2} = m_{b1}u_{b1} + \Delta m h_u + Q_b - \int_1^2 pdV_b \quad \text{Eqn B-14}$$

$$m_{b2}u_{b2} - m_{b1}u_{b1} = \Delta m h_u + Q_b - \int_1^2 pdV_b \quad \text{Eqn B-15}$$

writing in differential form

$$\dot{\overline{m_b u_b}} = \dot{m}_b h_u + \dot{Q}_b - pdV_b \quad \text{Eqn B-16}$$

$$\dot{m}_b u_b + m_b \dot{u}_b = \dot{m}_b h_u + \dot{Q}_b - p\dot{V}_b \quad \text{Eqn B-17}$$

Solving for $\dot{T}_u$:

From Eqn B-13 we can write

$$\dot{m}_u\left(u_u - h_u\right) + m_u\left(\frac{\partial u_u}{\partial \mathrm{T}_u}\dot{T}_u + \frac{\partial u_u}{\partial \mathrm{p}}\dot{p}\right) = \dot{Q}_u - p\dot{V}_u \quad \text{Eqn B-18}$$

but from Eqn B-1 this simplifies to

$$\dot{m}_u\left(u_u - h_u\right) + m_u\frac{\partial u_u}{\partial \mathrm{T}_u}\dot{T}_u = \dot{Q}_u - p\dot{V}_u \quad \text{Eqn B-19}$$

From the definition of enthalpy [2] $h = u + RT \Rightarrow u - h = -RT$ Eqn B-20

$$-\dot{m}_u R_u T_u + m_u\frac{\partial u_u}{\partial \mathrm{T}_u}\dot{T}_u = \dot{Q}_u - p\dot{V}_u \quad \text{Eqn B-21}$$

$$\dot{m}_u R_u T_u - m_u\frac{\partial u_u}{\partial \mathrm{T}_u}\dot{T}_u = p\dot{V}_u - \dot{Q}_u \quad \text{Eqn B-22}$$

$$\dot{m}_u = m_u\frac{\partial u_u}{\partial \mathrm{T}_u}\frac{\dot{T}_u}{R_u T_u} + \frac{p\dot{V}_u}{R_u T_u} - \frac{\dot{Q}_u}{R_u T_u} \quad \text{Eqn B-23}$$

dividing by m_u

$$\frac{\dot{m}_u}{m_u} = \frac{\partial u_u}{\partial \mathrm{T}_u}\frac{\dot{T}_u}{R_u T_u} + \frac{p\dot{V}_u}{m_u R_u T_u} - \frac{\dot{Q}_u}{m_u R_u T_u} \quad \text{Eqn B-24}$$

From Eqn B-9 and Eqn B-1

$$\frac{\dot{p}}{p} = \frac{\dot{m}_u}{m_u} + \frac{\dot{T}_u}{T_u} - \frac{\dot{V}_u}{V_u} \quad \text{Eqn B-25}$$

Substituting Eqn B-24 into Eqn B-25

$$\frac{\dot{p}}{p} = \frac{\partial u_u}{\partial \mathrm{T}_u}\frac{\dot{T}_u}{R_u T_u} + \frac{p\dot{V}_u}{m_u R_u T_u} - \frac{\dot{Q}_u}{m_u R_u T_u} + \frac{\dot{T}_u}{T_u} - \frac{\dot{V}_u}{V_u} \quad \text{Eqn B-26}$$

$$\frac{\dot{T}_u}{T_u}\left(1 + \frac{\partial u_u}{\partial \mathrm{T}_u}\frac{\dot{T}_u}{R_u}\right) = \frac{\dot{p}}{p} - \frac{p\dot{V}_u}{m_u R_u T_u} + \frac{\dot{Q}_u}{m_u R_u T_u} + \frac{\dot{V}_u}{V_u} \quad \text{Eqn B-27}$$

However

$$\frac{\dot{V}_u}{V_u} - \frac{p\dot{V}_u}{m_u R_u T_u} = \frac{\dot{V}_u}{V_u}\left(1 - \frac{pV_u}{m_u R_u T_u}\right) = 0 \quad \text{Eqn B-28}$$

Therefore Eqn B-27 becomes

$$\frac{\dot{T}_u}{T_u}\left(1 + \frac{\partial u_u}{\partial \mathrm{T}_u}\frac{\dot{T}_u}{R_u}\right) = \frac{\dot{p}}{p} + \frac{\dot{Q}_u}{m_u R_u T_u} \quad \text{Eqn B-29}$$

$$\dot{T}_u\left(1+\frac{\partial u_u}{\partial \mathrm{T}_u}\frac{\dot{T}_u}{R_u}\right)=T_u\frac{\dot{p}}{p}+\frac{\dot{Q}_u}{m_u R_u} \quad \text{Eqn B-30}$$

$$\dot{T}_u=\left(\frac{T_u\frac{\dot{p}}{p}+\frac{\dot{Q}_u}{m_u R_u}}{1+\frac{\partial u_u}{\partial \mathrm{T}_u}\frac{\dot{T}_u}{R_u}}\right) \quad \text{Eqn B-31}$$

Solving for $\dot{m}_b$:

From Eqn B-17

$$\dot{m}_b\left(u_b-h_u\right)+m_b\left(\frac{\partial u_b}{\partial \mathrm{T}_b}\dot{T}_b+\frac{\partial u_b}{\partial \mathrm{p}}\dot{p}\right)=\dot{Q}_b-p\dot{V}_b \quad \text{Eqn B-32}$$

$$\dot{m}_b\left(u_b-\left(u_u+R_u T_u\right)\right)=\dot{Q}_b-p\dot{V}_b-m_b\left(\frac{\partial u_b}{\partial \mathrm{T}_b}\dot{T}_b+\frac{\partial u_b}{\partial \mathrm{p}}\dot{p}\right) \quad \text{Eqn B-33}$$

$$\dot{m}_b\left(\left(u_b-u_u\right)-R_u T_u\right)=\dot{Q}_b-p\dot{V}_b-\frac{\partial u_b}{\partial \mathrm{T}_b}\dot{T}_b m_b-\frac{\partial u_b}{\partial \mathrm{p}}\dot{p}m_b \quad \text{Eqn B-34}$$

From Eqn B-9

$$\frac{\dot{p}}{p}=\frac{\dot{m}_b}{m_b}+\frac{\dot{R}_b}{R_b}+\frac{\dot{T}_b}{T_b}-\frac{\dot{V}_b}{V_b} \quad \text{Eqn B-9}$$

However if the assumption that $\frac{\partial u_b}{\partial \mathrm{T}_b}=\frac{\partial u_b}{\partial p}=0$ is made (this is supported by numerical investigation according to the authors), then $\dot{R}_b=0$ and therefore

$$\dot{T}_b=T_b\left(\frac{\dot{p}}{p}-\frac{\dot{m}_b}{m_b}+\frac{\dot{V}_b}{V_b}\right) \quad \text{Eqn B-35}$$

Substituting Eqn B-35 into Eqn B-34 gives

$$\dot{m}_b\left(\left(u_b-u_u\right)-R_u T_u\right)=\dot{Q}_b-p\dot{V}_b - \frac{\partial u_b}{\partial \mathrm{T}_b}T_b m_b\left(\frac{\dot{p}}{p}-\frac{\dot{m}_b}{m_b}+\frac{\dot{V}_b}{V_b}\right)-\frac{\partial u_b}{\partial \mathrm{p}}\dot{p}m_b \quad \text{Eqn B-36}$$

$$\dot{m}_b\left(\left(u_b-u_u\right)-R_uT_u-\frac{\partial u_b}{\partial \mathrm{T}_b}T_b\right)=\dot{Q}_b-p\dot{V}_b$$
$$-\frac{\partial u_b}{\partial \mathrm{T}_b}T_bm_b\left(\frac{\dot{p}}{p}+\frac{\dot{V}_b}{V_b}\right)-\frac{\partial u_b}{\partial \mathrm{p}}\dot{p}\,m_b \quad \text{..... Eqn B-37}$$

$$\dot{m}_b\left(\left(u_b-u_u\right)-R_uT_u-\frac{\partial u_b}{\partial \mathrm{T}_b}T_b\right)=\dot{Q}_b-p\dot{V}_b\left(1+\frac{\partial u_b}{\partial \mathrm{T}_b}\frac{T_bm_b}{V_bp}\right)$$
$$-\dot{p}\left(\frac{\partial u_b}{\partial \mathrm{T}_b}\frac{T_bm_b}{p}+\frac{\partial u_b}{\partial \mathrm{p}}m_b\right) \quad \text{..... Eqn B-38}$$

$$\dot{m}_b\left(\left(u_b-u_u\right)-R_uT_u-\frac{\partial u_b}{\partial \mathrm{T}_b}T_b\right)=\dot{Q}_b-p\dot{V}_b\left(1+\frac{\partial u_b}{\partial \mathrm{T}_b}\frac{1}{R_b}\right)$$
$$-V_b\,\dot{p}\left(\frac{\partial u_b}{\partial \mathrm{T}_b}\frac{1}{R_b}+\frac{\partial u_b}{\partial \mathrm{p}}\frac{m_b}{V_b}\right) \quad \text{..... Eqn B-39}$$

From Eqn B-2 $V=V_b+V_u$ we get

$$\dot{V}=\dot{V}_b+\dot{V}_u \quad \text{..... Eqn B-40}$$

Substituting Eqn B-40 into Eqn B-39

$$\dot{m}_b\left(\left(u_b-u_u\right)-R_uT_u-\frac{\partial u_b}{\partial \mathrm{T}_b}T_b\right)=\dot{Q}_b-p\left(\dot{V}-\dot{V}_u\right)\left(1+\frac{\partial u_b}{\partial \mathrm{T}_b}\frac{1}{R_b}\right)$$
$$-\left(V-V_u\right)\dot{p}\left(\frac{\partial u_b}{\partial \mathrm{T}_b}\frac{1}{R_b}+\frac{\partial u_b}{\partial \mathrm{p}}\frac{m_b}{V_b}\right) \quad \text{..... Eqn B-41}$$

$$\dot{m}_b\left(\left(u_b-u_u\right)-R_uT_u-\frac{\partial u_b}{\partial \mathrm{T}_b}T_b\right)=\dot{Q}_b-\left(p\dot{V}-p\dot{V}_u\right)\left(1+\frac{\partial u_b}{\partial \mathrm{T}_b}\frac{1}{R_b}\right)$$
$$-\dot{p}V\left(\frac{\partial u_b}{\partial \mathrm{T}_b}\frac{1}{R_b}+\frac{\partial u_b}{\partial \mathrm{p}}\frac{m_b}{V_b}\right)+\dot{p}V_u\left(\frac{\partial u_b}{\partial \mathrm{T}_b}\frac{1}{R_b}+\frac{\partial u_b}{\partial \mathrm{p}}\frac{m_b}{V_b}\right) \quad \text{..... Eqn B-42}$$

From Eqn B-25 we can write

$$\dot{V}_u=V_u\left(\frac{\dot{m}_u}{m_u}+\frac{\dot{T}_u}{T_u}-\frac{\dot{p}}{p}\right) \quad \text{..... Eqn B-43}$$

Substituting Eqn B-43-into Eqn B-42

$$\dot{m}_b\left(\left(u_b-u_u\right)-R_uT_u-\frac{\partial u_b}{\partial \mathrm{T}_b}T_b\right)=\dot{Q}_b-$$

$$\left(p\dot{V}-pV_u\left(\frac{\dot{m}_u}{m_u}+\frac{\dot{T}_u}{T_u}-\frac{\dot{p}}{p}\right)\right)\left(1+\frac{\partial u_b}{\partial \mathrm{T}_b}\frac{1}{R_b}\right) \quad \text{.....Eqn B-44}$$

$$-\dot{p}V\left(\frac{\partial u_b}{\partial \mathrm{T}_b}\frac{1}{R_b}+\frac{\partial u_b}{\partial \mathrm{p}}\frac{m_b}{V_b}\right)+\dot{p}V_u\left(\frac{\partial u_b}{\partial \mathrm{T}_b}\frac{1}{R_b}+\frac{\partial u_b}{\partial \mathrm{p}}\frac{m_b}{V_b}\right)$$

$$\dot{m}_b\left(\left(u_b-u_u\right)-R_uT_u-\frac{\partial u_b}{\partial \mathrm{T}_b}T_b\right)=\dot{Q}_b-\left(p\dot{V}-m_uR_u\dot{T}_u\right)\left(1+\frac{\partial u_b}{\partial \mathrm{T}_b}\frac{1}{R_b}\right)$$

$$+\frac{pV_u\dot{m}_u}{m_u}\left(1+\frac{\partial u_b}{\partial \mathrm{T}_b}\frac{1}{R_b}\right)-V_u\dot{p}\left(1+\frac{\partial u_b}{\partial \mathrm{T}_b}\frac{1}{R_b}\right) \quad \text{.....Eqn B-45}$$

$$-\dot{p}V\left(\frac{\partial u_b}{\partial \mathrm{T}_b}\frac{1}{R_b}+\frac{\partial u_b}{\partial \mathrm{p}}\frac{m_b}{V_b}\right)+\dot{p}V_u\left(\frac{\partial u_b}{\partial \mathrm{T}_b}\frac{1}{R_b}+\frac{\partial u_b}{\partial \mathrm{p}}\frac{m_b}{V_b}\right)$$

Substituting Eqn B-3 into Eqn B-45

$$\dot{m}_b\left(\left(u_b-u_u\right)-R_uT_u-\frac{\partial u_b}{\partial \mathrm{T}_b}T_b+R_uT_u\left(1+\frac{\partial u_b}{\partial \mathrm{T}_b}\frac{1}{R_b}\right)\right)=\dot{Q}_b$$

$$+\left(m_uR_u\dot{T}_u-p\dot{V}\right)\left(1+\frac{\partial u_b}{\partial \mathrm{T}_b}\frac{1}{R_b}\right)$$

$$+V_u\dot{p}\left(-1-\frac{\partial u_b}{\partial \mathrm{T}_b}\frac{1}{R_b}+\frac{\partial u_b}{\partial \mathrm{T}_b}\frac{1}{R_b}+\frac{\partial u_b}{\partial \mathrm{p}}\frac{m_b}{V_b}\right) \quad \text{.....Eqn B-46}$$

$$-\dot{p}V\left(\frac{\partial u_b}{\partial \mathrm{T}_b}\frac{1}{R_b}+\frac{\partial u_b}{\partial \mathrm{p}}\frac{m_b}{V_b}\right)$$

$$\dot{m}_b\left(\left(u_b-u_u\right)+\left(\frac{R_uT_u}{R_b}-T_b\right)\frac{\partial u_b}{\partial \mathrm{T}_b}\right)=\dot{Q}_b+\left(m_uR_u\dot{T}_u-p\dot{V}\right)\left(1+\frac{\partial u_b}{\partial \mathrm{T}_b}\frac{1}{R_b}\right)$$

$$+V_u\dot{p}\left(\frac{\partial u_b}{\partial \mathrm{p}}\frac{m_b}{V_b}-1\right)-\dot{p}V\left(\frac{\partial u_b}{\partial \mathrm{T}_b}\frac{1}{R_b}+\frac{\partial u_b}{\partial \mathrm{p}}\frac{m_b}{V_b}\right) \quad \text{.....Eqn B-47}$$

Substituting a rearranged Eqn B-2, $V_u=V-V_b$ into Eqn B-47

$$\dot{m}_b\left(\left(u_b-u_u\right)+\left(\frac{R_uT_u}{R_b}-T_b\right)\frac{\partial u_b}{\partial \mathrm{T}_b}\right)=\dot{Q}_b+\left(m_uR_u\dot{T}_u-p\dot{V}\right)\left(1+\frac{\partial u_b}{\partial \mathrm{T}_b}\frac{1}{R_b}\right)$$

$$+\dot{p}\left(V-V_b\right)\left(\frac{\partial u_b}{\partial \mathrm{p}}\frac{m_b}{V_b}-1\right)-\dot{p}V\left(\frac{\partial u_b}{\partial \mathrm{T}_b}\frac{1}{R_b}+\frac{\partial u_b}{\partial \mathrm{p}}\frac{m_b}{V_b}\right) \quad \text{.....Eqn B-48}$$

$$\dot{m}_b\left(\left(u_b-u_u\right)+\left(\frac{R_uT_u}{R_b}-T_b\right)\frac{\partial u_b}{\partial \mathrm{T}_b}\right)=\dot{Q}_b+\left(m_uR_u\dot{T}_u-p\dot{V}\right)\left(1+\frac{\partial u_b}{\partial \mathrm{T}_b}\frac{1}{R_b}\right)$$
$$+\dot{p}V\left(\frac{\partial u_b}{\partial \mathrm{p}}\frac{m_b}{V_b}-1\right)-\dot{p}V_b\frac{\partial u_b}{\partial \mathrm{p}}\frac{m_b}{V_b}+\dot{p}V_b \quad \text{..... Eqn B-49}$$
$$-\dot{p}V\left(\frac{\partial u_b}{\partial \mathrm{T}_b}\frac{1}{R_b}+\frac{\partial u_b}{\partial \mathrm{p}}\frac{m_b}{V_b}\right)$$

$$\dot{m}_b\left(\left(u_b-u_u\right)+\left(\frac{R_uT_u}{R_b}-T_b\right)\frac{\partial u_b}{\partial \mathrm{T}_b}\right)=\dot{Q}_b+\left(m_uR_u\dot{T}_u-p\dot{V}\right)\left(1+\frac{\partial u_b}{\partial \mathrm{T}_b}\frac{1}{R_b}\right)$$
$$-\dot{p}\left(\frac{\partial u_b}{\partial \mathrm{p}}m_b+V_b\right)-\dot{p}V\left(\frac{\partial u_b}{\partial \mathrm{T}_b}\frac{1}{R_b}+\frac{\partial u_b}{\partial \mathrm{p}}\frac{m_b}{V_b}-\frac{\partial u_b}{\partial \mathrm{p}}\frac{m_b}{V_b}+1\right) \quad \text{..... Eqn B-50}$$

$$\dot{m}_b\left(\left(u_b-u_u\right)+\left(\frac{R_uT_u}{R_b}-T_b\right)\frac{\partial u_b}{\partial \mathrm{T}_b}\right)=\dot{Q}_b+\left(m_uR_u\dot{T}_u-p\dot{V}\right)\left(1+\frac{\partial u_b}{\partial \mathrm{T}_b}\frac{1}{R_b}\right)$$
$$-\dot{p}V\left(\frac{\partial u_b}{\partial \mathrm{T}_b}\frac{1}{R_b}+1+\frac{\partial u_b}{\partial \mathrm{p}}\frac{m_b}{V}-\frac{V_b}{V}\right) \quad \text{..... Eqn B-51}$$

From Eqn B-2, $V=V_u+V_b$ we can write

$$1=\frac{V_u}{V}+\frac{V_b}{V} \quad \text{..... Eqn B-52}$$

Substituting Eqn B-52 into Eqn B-51

$$\dot{m}_b\left(\left(u_b-u_u\right)+\left(\frac{R_uT_u}{R_b}-T_b\right)\frac{\partial u_b}{\partial \mathrm{T}_b}\right)=\dot{Q}_b+\left(m_uR_u\dot{T}_u-p\dot{V}\right)\left(1+\frac{\partial u_b}{\partial \mathrm{T}_b}\frac{1}{R_b}\right)$$
$$-\dot{p}V\left(\frac{\partial u_b}{\partial \mathrm{T}_b}\frac{1}{R_b}+\frac{\partial u_b}{\partial \mathrm{p}}\frac{m_b}{V}+\frac{V_u}{V}\right) \quad \text{..... Eqn B-53}$$

$$\dot{m}_b=\frac{\dot{Q}_b+\left(m_uR_u\dot{T}_u-p\dot{V}\right)\left(1+\frac{\partial u_b}{\partial \mathrm{T}_b}\frac{1}{R_b}\right)-\dot{p}V\left(\frac{\partial u_b}{\partial \mathrm{T}_b}\frac{1}{R_b}+\frac{\partial u_b}{\partial \mathrm{p}}\frac{m_b}{V}+\frac{V_u}{V}\right)}{\left(u_b-u_u\right)+\left(\frac{R_uT_u}{R_b}-T_b\right)\frac{\partial u_b}{\partial \mathrm{T}_b}} \quad \text{..... Eqn B-54}$$

Solving for $\dot{V}_b$:

Substituting Eqn B-3, $-\dot{m}_u=\dot{m}_b$ into Eqn B-43 gives

$$\dot{V}_u=V_u\left(\frac{-\dot{m}_b}{m_u}+\frac{\dot{T}_u}{T_u}-\frac{\dot{p}}{p}\right) \quad \text{..... Eqn B-55}$$

From Eqn B-40, $\dot{V}=\dot{V}_b+\dot{V}_u$ we can write

$$\dot{V} - \dot{V}_b = V_u \left(\frac{-\dot{m}_b}{m_u} + \frac{\dot{T}_u}{T_u} - \frac{\dot{p}}{p} \right) \quad \text{Eqn B-56}$$

$$\dot{V}_b = V_u \left(\frac{\dot{m}_b}{m_u} - \frac{\dot{T}_u}{T_u} + \frac{\dot{p}}{p} \right) + \dot{V} \quad \text{Eqn B-57}$$

The authors did not give an equation for the calculation of the burned gas temperature but one was derived using a similar methodology as above.

Again, starting with the energy equation for the burned gas Eqn B-17 and rearranging

$$\dot{m}_b u_b + m_b \left(\frac{\partial u_b}{\partial T_b} \dot{T}_b + \frac{\partial u_b}{\partial p} \dot{p} \right) = \dot{m}_b h_u + \dot{Q}_b - p \dot{V}_b \quad \text{Eqn B-58}$$

$$m_b \left(\frac{\partial u_b}{\partial T_b} \dot{T}_b + \frac{\partial u_b}{\partial p} \dot{p} \right) = \dot{m}_b \left(h_u - u_b \right) + \dot{Q}_b - p \dot{V}_b \quad \text{Eqn B-59}$$

$$m_b \frac{\partial u_b}{\partial T_b} \dot{T}_b = \dot{m}_b \left(h_u - u_b \right) + \dot{Q}_b - p \dot{V}_b - m_b \frac{\partial u_b}{\partial p} \dot{p} \quad \text{Eqn B-60}$$

$$\dot{T}_b = \frac{\dot{m}_b \left(h_u - u_b \right) + \dot{Q}_b - p \dot{V}_b - m_b \dfrac{\partial u_b}{\partial p} \dot{p}}{m_b \dfrac{\partial u_b}{\partial T_b}} \quad \text{Eqn B-61}$$

APPENDIX B REFERENCES

1 Krieger, R. B. and Borman, G. L., "The Computation of Apparent Heat Release for Internal Combustion Engines," ASME paper 66-WA/DGP-4, 1966.

2 Howell, J. R. and Buckius, R. O., *Fundamentals of Engineering Thermodynamics.* McGraw Hill, New York, 1987.

APPENDIX C : DERIVATION OF THE HEAT TRANSFER COEFFICIENT EQUATION

The Woschni [1] heat transfer equation is based on forced turbulent convective heat transfer, which is described by an equation of the form:

$$Nu = C\,\mathrm{Re}^{m}$$ ..... Eqn C-1

with C = 0.035 and m = 0.8.

Substituting $Nu = \frac{hx}{k}$ and $\mathrm{Re} = \frac{wx\rho}{\mu}$ [2] into the above equation gives :

$$\frac{hx}{k} = C\left(\frac{wx\rho}{\mu}\right)^{m}$$ ..... Eqn C-2

$$h = C\frac{k}{x}\left(\frac{wx\rho}{\mu}\right)^{m}$$ ..... Eqn C-3

$$h = Ckx^{m-1}w^{m}\rho^{m}\mu^{-m}$$ ..... Eqn C-4

Expressions for density, viscosity and conductivity, as functions of temperature and pressure (for air as the working fluid) can be found [3] and are as follows:

From Ideal Gas Law

$$\rho = \frac{P}{RT},\ R_{air} = 287\left[J/kg.K\right], P\left[Pa\right]$$ ..... Eqn C-5

From the viscosity Power Law $\mu = \mu_0\left(\frac{T}{T_0}\right)^{n}, \mu_{0air} = 1.716E^{-5}\left[N.s/m^2\right], n_{air} = 0.666, T_0 = 273\left[K\right]$ Eqn C-6

From the conductivity Power Law $k = k_0\left(\frac{T}{T_0}\right)^{n}, k_{0air} = 0.0241\left[W/m.K\right], n_{air} = 0.81, T_0 = 273\left[K\right]$ Eqn C-7

Substituting these into Equation Eqn C-4 yields

$$h = C\left(k_0\frac{T}{T_0}\right)^{0.81}x^{m-1}w^{m}\left(\frac{p}{RT}\right)^{m}\left(\mu_0\frac{T}{T_0}\right)^{-0.666m}$$ ..... Eqn C-8

$$h = C\left(\frac{k_0}{T_0}\right)^{0.81}R^{-m}\left(\frac{\mu_0}{T_0}\right)^{-0.666m}T^{0.81}x^{m-1}w^{m}\left(\frac{P}{T}\right)^{m}T^{-0.666m}$$ ..... Eqn C-9

Substituting the values of the constants from Eqn C-3, Eqn C-4 and Eqn C-5 into Eqn C-9 reveals the following equation:

$$h = 0.01249x^{m-1}P^{m}w^{m}T^{0.81-1.666m}$$ ..... Eqn C-10

Now if P is expressed in atm as opposed to Pa (and m=0.8) then it becomes:

$$h = 126.2x^{m-1}P^{m}w^{m}T^{0.81-1.666m}$$ ..... Eqn C-11

and including m=0.8 we get:

$$h = 126.2 x^{-0.2} P^{0.8} w^{0.8} T^{-0.52}$$ .....Eqn C-12

This is very similar to the form as givn by Gatowski et. al which is

$$h = 131 x^{-0.2} P^{0.8} w^{0.8} T^{-0.53}$$ .....Eqn C-13

The above development is limited in that it assumes air as the working fluid, and utilises simplified correlations for conductivity and viscosity. However it agrees well with the literature and shows consistency of units used. In the absence of more detail as to the nature of the correlations and working fluid assumed by Gatowski et. al and the fact that calibration constants need to be found for each individual engine the difference between the two is insignificant.

APPENDIX C REFERENCES

1 Woschni, G., "A Universally Applicable Equation for the Instantaneous Heat Transfer Coefficient in the Internal Combustion Engine." SAE paper 670931, *SAE Trans*., vol. 76, 1967.

2 Douglas, J. F., Gasiorek, J. M., and Swaffield, J. A., *Fluid Mechanics*, Second Edition. Longman Scientific and Technical, Harlow, 1985.

3 White, F. M., *Viscous Fluid Flow,* 2nd ed., McGraw-Hill, Inc., New York. 1991.

APPENDIX D : TABULATED RESULTS

Engine - 4A-FE, Load Point - 60 km/hr

Sample	Engine Operating Point			Engine Operating Conditions															
	Speed	Torque	Power	Fuel Flow Rate	Equivalence Ratio	Equivalence Ratio	Ignition Timing	BSFC	Water Temperature	Oil Temperature	Exhaust Temperature	Fuel Temperature	Fuel Pressure	Oil Pressure	Manifold Pressure	Manifold Temperature	Air Flow Rate	Air Flow Rate
	[rev/min]	[Nm]	[kW]	[kg/hr]	(calc) [-]	(meas) [-]	[° CA BTDC]	[kg/kW.hr]	[° C]	[° C]	[° C]	[° C]	[bar]	[bar]	[kPa]	[° C]	[mbar]	[kg/s]
Ref1	1881	36.2	7.1	2.5	1.01	1.05	20	0.347	88.7	85.7	487.9	13.1	2.6	3.7	49.8	53.8	0.10	0.010
P1	1880	36.2	7.1	2.5	0.94	0.95	20	0.350	89.1	86.3	492.6	7.8	2.6	3.8	51.3	53.9	0.12	0.011
P2	1880	35.8	7.1	2.4	1.00	0.93	20	0.337	89.2	89.1	499.1	19.9	2.6	3.8	50.4	57.3	0.12	0.010
P3	1881	36.3	7.1	2.5	0.99	0.94	20	0.345	89.4	87.5	500.8	19.5	2.6	3.8	50.3	56.7	0.12	0.011
P4	1881	36.1	7.1	2.5	1.00	0.93	20	0.349	89.2	87.7	500.7	22.2	2.6	3.8	50.4	57.6	0.13	0.011
P5	1878	36.2	7.1	2.5	1.00	0.89	20	0.345	89.3	88.4	500.2	25.1	2.6	3.7	50.5	58.0	0.14	0.011
P6	1881	35.9	7.1	2.5	0.99	0.88	21	0.349	89.7	88.9	501.2	20.7	2.6	3.7	50.6	58.7	0.14	0.012
P7	1880	35.8	7.1	2.4	1.00	0.91	20	0.345	88.9	87.6	496.5	20.9	2.6	3.8	49.9	56.2	0.13	0.011
P8	1878	36.0	7.1	2.5	1.00	0.89	20	0.346	89.1	88.6	502.6	27.0	2.6	3.7	50.3	57.8	0.14	0.011
P9	1881	35.9	7.1	2.5	1.00	0.90	20	0.352	89.4	88.5	503.8	24.4	2.6	3.7	50.4	57.3	0.14	0.011
P10	1882	36.1	7.1	2.5	1.00	0.94	20	0.348	89.3	88.5	503.0	19.5	2.6	3.8	50.6	57.2	0.12	0.011
P11	1880	35.9	7.1	2.5	0.99	0.84	21	0.349	90.0	90.5	503.3	35.0	2.6	3.7	50.7	59.9	0.16	0.012
Ref2	1883	36.0	7.1	2.5	1.00	0.97	20	0.350	89.2	89.7	502.7	28.1	2.6	3.8	50.9	57.2	0.12	0.010

Engine Out Emissions													Atmospheric Conditions			SABS Corrections		
Hydrocarbons			NO			CO2			CO			O2	Barometric Pressure	Dry Bulb Temperature	Wet Bulb Temperature	Correction Factor	Corrected Torque	Corrected Power
[ppm]	[g/kW.hr]	[g/km]	[ppm]	[g/kW.hr]	[g/km]	[% vol]	[g/kW.hr]	[g/km]	[% vol]	[g/kW.hr]	[g/km]	[% vol]	[mBar]	[° C]	[° C]	[-]	[Nm]	[kW]
2323	5.66	0.67	1782	14.41	1.71	14.6	1128.1	133.9	0.8	40.96	4.86	0.7	1003.5	18.0	11.0	0.98	35.4	7.0
1544	4.29	0.51	1704	15.68	1.86	13.9	1221.6	145.1	0.2	12.12	1.44	1.7	1012.9	18.5	14.0	0.98	35.7	7.0
2386	6.52	0.77	1785	16.17	1.90	14.1	1221.0	143.6	0.7	40.28	4.74	0.8	1009.1	21.0	15.5	0.99	35.6	7.0
1868	5.05	0.60	1747	15.67	1.86	14.5	1246.4	148.4	0.7	35.69	4.25	0.8	1007.4	19.0	14.5	0.99	35.9	7.1
2056	5.70	0.68	1759	16.18	1.92	14.4	1269.8	150.6	0.7	41.59	4.93	0.7	1010.9	21.0	15.5	0.98	36.1	7.1
2079	5.94	0.70	1820	17.23	2.05	14.4	1304.8	154.9	0.8	45.03	5.35	0.7	1006.2	21.5	16.0	0.99	36.2	7.1
1696	5.05	0.60	1663	16.43	1.93	14.2	1344.5	158.3	0.7	40.49	4.77	0.8	1005.1	22.0	18.0	1.00	35.7	7.0
2031	5.71	0.67	1921	17.89	2.10	14.3	1278.4	150.3	0.8	45.62	5.36	0.7	1013.5	19.0	12.5	0.97	34.8	6.9
2531	7.35	0.87	1998	19.24	2.27	14.3	1318.2	155.5	0.6	37.21	4.39	0.8	1004.4	20.0	14.5	0.99	35.6	7.0
2530	7.29	0.86	1835	17.54	2.07	14.4	1319.6	155.6	0.8	44.14	5.21	0.8	1002.8	21.0	16.0	0.99	35.5	7.0
2562	7.08	0.84	1732	15.86	1.88	14.2	1243.2	147.4	0.7	36.48	4.33	0.8	1007.6	20.0	15.0	0.99	35.7	7.0
2354	7.19	0.85	>2000	20.36	2.40	14.4	1397.3	164.8	0.6	35.83	4.23	0.9	1002.8	25.0	16.5	1.00	35.9	7.1
2469	6.70	0.79	1840	16.56	1.96	14.1	1212.8	143.7	0.8	43.71	5.18	0.8	1007.0	20.0	16.0	0.99	35.8	7.1

Sample	Engine Operating Point			Engine Operating Conditions															
	Speed	Torque	Power	Fuel Flow Rate	Equivalence Ratio	Equivalence Ratio	Ignition Timing	BSFC	Water Temperature	Oil Temperature	Exhaust Temperature	Fuel Pressure	Oil Pressure	Manifold Pressure	Manifold Temperature	Droplet Temperature	Air Flow Rate	Air Flow Rate
	[rev/min]	[Nm]	[kW]	[kg/hr]	(calc) [-]	(meas) [-]	[° CA BTDC]	[kg/kW.hr]	[° C]	[° C]	[° C]	[bar]	[bar]	[kPa]	[° C]	[° C]	[mbar]	[kg/s]
Ref3	1885	35.8	7.1	2.52	0.91	0.84	20	0.357	88.3	93.1	530.4	2.6	3.3	49.6	53.7	22.0	0.16	0.0123
P12	1879	36.1	7.1	2.49	0.91	0.92	20	0.353	87.7	94.4	531.8	3.3	2.6	49.2	52.7	20.8	0.13	0.0111
P13	1888	36.0	7.1	2.37	0.92	0.88	20	0.335	89.8	93.8	523.8	2.6	3.3	49.5	53.6	18.9	0.13	0.0111
P14	1882	35.4	6.9	2.54	0.86	0.94	20	0.367	90.0	89.3	498.8	2.6	3.5	50.3	51.4	11.9	0.13	0.0111
P15	1888	35.7	7.0	2.58	0.86	0.92	20	0.368	89.0	90.7	506.7	2.6	3.4	50.9	53.7	16.2	0.14	0.0114
P16	1884	36.3	7.1	2.55	0.92	0.95	20	0.359	88.9	88.3	494.1	2.6	3.6	49.6	53.6	16.6	0.13	0.0110
P17	1885	35.5	7.0	2.32	0.91	0.86	20	0.332	89.8	91.0	506.3	2.6	3.4	49.5	54.5	19.6	0.13	0.0110
P18	1884	35.5	7.0	2.23	0.92	0.83	20	0.320	90.2	90.7	503.3	3.4	2.6	49.4	55.4	25.4	0.13	0.0110
P19	1878	36.1	7.1	2.50	0.92	0.96	20	0.354	88.9	90.9	506.4	2.6	3.4	49.1	54.3	26.8	0.12	0.0106
P20	1882	36.3	7.1	2.48	0.92	0.92	20	0.350	90.3	90.9	505.8	2.6	3.4	49.4	54.5	26.6	0.13	0.0110
P21	1884	36.2	7.1	2.52	0.92	0.93	20	0.354	89.6	91.1	505.6	2.6	3.4	49.4	54.8	26.7	0.13	0.0110
P22	1877	36.4	7.1	2.47	0.92	0.95	20	0.347	89.1	90.4	504.0	2.6	3.4	49.2	54.8	24.4	0.12	0.0106
P23	1885	36.3	7.1	2.34	0.92	0.87	20	0.329	89.9	89.9	502.6	2.6	3.5	49.5	55.2	27.0	0.13	0.0110
P24	1879	35.9	7.0	2.58	0.87	0.92	20	0.368	89.8	89.9	507.5	2.6	3.4	50.9	54.5	24.5	0.14	0.0114
Ref4	1882	35.6	7.0	2.51	0.91	0.93	20	0.360	88.2	91.9	515.1	2.6	3.3	49.3	55.2	23.3	0.13	0.0110

Engine Out Emissions														
Hydrocarbons			NO			CO2			CO			O2	H2S	SO2
[ppm]	[g/kW.hr]	[g/km]	[ppm]	[g/kW.hr]	[g/km]	[% vol]	[g/kW.hr]	[g/km]	[% vol]	[g/kW.hr]	[g/km]	[% vol]	[ppm]	[ppm]
1125	3.51	0.41	1308	13.52	1.59	14.1	1396.5	164.4	0.14	9.01	1.06	1.8	-	-
1028	2.92	0.34	1354	12.75	1.50	14.1	1274.1	149.9	0.14	7.83	0.92	1.7	-	-
1051	2.97	0.35	1236	11.58	1.37	14.1	1267.2	149.5	0.17	9.51	1.12	1.6		2
855	2.51	0.29	846	8.24	0.95	13.3	1243.0	143.5	0.15	9.03	1.04	2.6	61	31
765	2.30	0.27	904	9.03	1.05	13.4	1276.3	149.0	0.13	7.90	0.92	2.5	54	95
1042	2.76	0.33	1240	10.88	1.29	15.2	1273.8	150.9	0.20	10.42	1.23	1.7	86	70
1100	3.09	0.36	1278	11.91	1.38	14.3	1279.0	148.5	0.20	11.15	1.29	1.7	116	189
967	2.79	0.32	1135	10.85	1.26	14.0	1278.9	148.4	0.20	11.49	1.33	1.6	54	96
1032	2.71	0.32	1365	11.88	1.40	14.9	1236.9	145.5	0.19	9.89	1.16	1.6	71	105
872	2.37	0.28	1265	11.42	1.35	14.8	1274.5	150.7	0.21	11.72	1.39	1.5	130	175
910	2.48	0.29	1259	11.39	1.35	14.7	1274.3	150.8	0.22	11.92	1.41	1.5	200	257
949	2.50	0.30	1334	11.64	1.38	14.7	1229.1	145.6	0.18	9.29	1.10	1.5	200	270
861	2.34	0.28	1236	11.12	1.32	14.7	1263.9	149.8	0.20	10.81	1.28	1.7	23	96
690	2.01	0.23	815	7.85	0.92	14.1	1296.1	151.4	0.13	7.81	0.91	2.4	89	132
1087	3.01	0.35	1261	11.57	1.34	14.6	1285.9	149.3	0.16	9.12	1.06	1.7	-	-

Atmospheric Conditions		
Barometric Pressure	Dry Bulb Temperature	Wet Bulb Temperature
[mBar]	[° C]	[° C]
1014.0	21.0	16.0
1013.0	18.5	13.5
1010.0	19.5	14.5
1007.0	17.0	12.0
1006.5	20.0	13.3
1001.2	19.0	14.0
1006.5	20.0	14.0
1007.1	20.5	14.5
1005.6	19.0	14.0
1005.6	21.0	15.0
1005.6	21.2	15.5
1005.8	18.5	13.0
1004.5	20.2	14.1
1003.8	20.0	15.5
1002.8	21.0	16.0

SABS Corrections		
Correction Factor	Corrected Torque	Corrected Power
[-]	[Nm]	[kW]
0.98	35.1	6.9
0.97	35.2	6.9
0.98	35.4	6.9
0.98	34.6	6.8
0.98	35.1	6.9
0.99	35.8	5.3
0.98	35.0	6.9
0.99	35.0	6.9
0.98	35.6	7.0
0.99	35.9	7.0
0.99	35.9	7.0
0.98	35.8	7.0
0.99	35.9	7.0
0.99	35.6	6.9
0.99	35.5	6.9

Sample	Engine Operating Point			Engine Operating Conditions							Racer Input Parameters				
	Speed	Torque	Racer File Name	Fuel Flow Rate	Equivalence Ratio	Ignition Timing	Manifold Pressure	Manifold Temperature	Droplet Temperature	Air Flow Rate	Charge Temperature	Cylinder Charge Mass	Re Reference Pressure	Air Fuel Ratio	Fuel Flow Rate
	[rev/min]	[Nm]	[-]	[kg/hr]	(calc) [-]	[° CA BTDC]	[kPa]	[° C]	[° C]	[kg/s]	[° C]	[kg]	[kPa]	[-]	[kg/s]
Ref3	1885	35.8	rf602106	*2.52*	0.91	20	49.6	53.7	22.0	0.01226	83.7	*0.0002062*	*52.55*	15.1	0.00070
P12	1879	36.1	P12-60	2.49	0.91	20	49.2	52.7	20.8	0.01108	82.7	0.0001879	47.76	15.1	0.00069
P13	1888	36.0	P13-60	2.37	0.92	20	49.5	53.6	18.9	0.01105	83.6	0.0001861	47.40	14.9	0.00066
P14	1882	35.4	P14-60	2.54	0.86	20	50.3	51.4	11.9	0.01107	81.4	0.0001877	47.53	15.9	0.00071
P15	1888	35.7	-	2.58	0.86	20	50.9	53.7	16.2	0.01144	83.7	0.0001931	49.22	15.9	0.00072
P16	1884	36.3	P1660	2.55	0.92	20	49.6	53.6	16.6	0.01101	83.6	0.0001866	47.54	14.9	0.00071
P17	1885	35.5	P17-60	2.32	0.91	20	49.5	54.5	19.6	0.01102	84.5	0.0001857	47.43	15.1	0.00064
P18	1884	35.5	P18-60	2.23	0.92	20	49.4	55.4	25.4	0.01102	85.4	0.0001854	47.46	14.9	0.00062
P19	1878	36.1	P19-60	2.50	0.92	20	49.1	54.3	26.8	0.01060	84.3	0.0001804	46.05	14.9	0.00069
P20	1882	36.3	P20-60	2.48	0.92	20	49.4	54.5	26.6	0.01100	84.5	0.0001864	47.60	14.9	0.00069
P21	1884	36.2	P21-60	2.52	0.92	20	49.4	54.8	26.7	0.01100	84.8	0.0001863	47.63	14.9	0.00070
P22	1877	36.4	P22-60	2.47	0.92	20	49.2	54.8	24.4	0.01061	84.8	0.0001805	46.15	14.9	0.00068
P23	1885	36.3	P23-60	2.34	0.92	20	49.5	55.2	27.0	0.01101	85.2	0.0001856	47.50	14.9	0.00065
P24	1879	35.9	P24-60	2.58	0.87	20	50.9	54.5	24.5	0.01143	84.5	0.0001938	49.50	15.7	0.00072
Ref4	1882	35.6	rf3-60	2.51	0.91	20	49.3	55.2	23.3	0.01099	85.2	0.0001863	47.66	15.0	0.00070

Sample	Pressure/CA results								Single Zone Model Results											
	IMEP	PMEP	IMEP(net)	Stability	Pressure		Rate of Pressure Rise		Heat Released			Gas Temperature		Induction Period			Burn Angle			
	[kPa]	[kPa]	[kPa]	[%]	Max [kPa]	CA [Max.] [° CA]	Max [kPa/°]	CA [Max.] [° CA]	Total [kJ]	Max. Rate [kJ/° CA]	CA [Max. Rate] [° CA]	Max [K]	CA [Max] [° CA]	2-98 [° CA]	5-95 [° CA]	10-90 [° CA]	2-98 [° CA]	5-95 [° CA]	10-90 [° CA]	
Ref3	474.39	-59.31	415.07	12.8	1607.2	25	29.5	10	590.19	976.92	22	2691.4	42	12.4	19.1	24	55.7	43.1	33.8	
P12	472.43	-59.45	412.98	11.4	1641.1	25	31.8	10	593.17	1007.43	21	2863.8	40	11.8	18.7	23.6	54.3	41.5	31.9	
P13	471.16	-59.52	411.64	11.3	1560.7	26	26.5	10	597.5	966.57	23	2853.4	43	12.3	19.3	24.4	57.6	44.5	32.8	
P14	459.88	-59.2	400.67	12.2	1477.9	26	22.8	10	593.87	899.49	25	2869.8	45	11.6	19.3	24.9	58.5	46.1	34.2	
P15	-	-	-	-	-	-	-	-	-	-	-	-	-	-	-	-	-	-	-	
P16	470.74	-57.62	413.12	10.2	1568.4	26	28	11	604.16	963.94	23	3018.7	42	12.2	19.3	24.5	57.6	42.8	33.1	
P17	469.2	-59.24	409.96	11.8	1535.9	26	26.5	11	597.05	957.18	23	2899.3	43	12.1	19.4	24.7	57.4	43.8	34.1	
P18	471.35	-58.26	413.08	11.8	1566.2	26	28.2	11	600.19	957.59	22	2905.1	43	12	19.2	24.4	57.2	43.9	34.5	
P19	475.24	-58.84	416.41	10.4	1602.3	25	29.9	10	612.57	993.29	22	3188.1	41	11.7	18.8	23.9	56.3	43.3	32.2	
P20	474.46	-57.87	416.59	9.7	1590.1	26	28.3	11	669.62	1056.71	24	3102.9	41	11.4	18.9	24.5	61.6	46.2	35.3	
P21	475.61	-58.24	417.38	11.7	1598.2	26	28.9	11	606.21	989.92	22	3005.7	41	12	18.9	24.1	58	43.2	33.8	
P22	478.63	-58.69	419.95	10.7	1618.6	26	30	10	610.42	1017.82	23	3094.5	41	12.1	18.9	24	56.6	42.2	32.8	
P23	475.7	-57.68	418.02	11.2	1612	26	30.2	11	607.86	1020.22	22	3067.7	41	12.1	19.2	24.3	57.9	43.2	32	
P24	464.32	-56.53	407.79	14.1	1461.2	26	22.9	-17	601.84	886.28	24	2837.1	48	12	19.7	25.3	60.7	46.4	36.2	
Ref4	465.92	-57.74	408.17	10.5	1554.9	26	27.5	11	598.36	959.01	23	3004.8	42	11.9	19	24.3	58	44.7	33.1	

Sample	Two Zone Model Results														Equilibrium Products Results - CO_2				
	Mass Transferred				Unburned Gas Temperature		Burned Gas Temperature		Induction Period			Burn Angle			End of Cycle	Exhaust Valve Open	End of Combustion	Maximum	Angle at Maximum
	Total [g]	Total % [%]	Max. Rate [g/° CA]	CA [Max. Rate] [° CA]	Max [K]	CA [Max] [° CA]	Max [K]	CA [Max] [° CA]	2-98 [° CA]	5-95 [° CA]	10-90 [° CA]	2-98 [° CA]	5-95 [° CA]	10-90 [° CA]	[% vol]	[% vol]	[% vol]	[% vol]	[° CA]
Ref3	0.228	110.32	0.410309	23	762.2	18.5	2432.06	15.5	14.1	20.1	24.9	56	43.8	32.7	9.6	11.6	11.6	11.7	81
P12	0.212	112.58	0.399015	21	718.05	18.5	2565.17	-17	12	19.1	24	53.7	40.1	30.8	11.1	13.4	13.5	13.7	81
P13	0.22	118.14	0.391567	23	714.34	18.5	2535.14	-17	12.5	19.6	24.8	56.2	42.4	33.1	11.2	13.5	13.7	13.8	82
P14	0.212	112.8	0.352597	24	705.61	18	2565.14	-17	11.9	19.7	25.3	60.6	46.5	34.1	11.0	13.4	13.5	13.6	82
P15	-	-	-	-	-	-	-	-	-	-	-	-	-	-	-	-	-	-	-
P16	0.256	136.99	9.598235	49	4578.74	49.5	361881.9	51	14.1	21.2	26.4				5.5	5.5	5.5	12.3	39
P17	0.225	121.07	0.39507	23	716.31	18.5	2514.25	-17	12.5	19.9	25.2	59.3	44.8	32.9	11.1	13.5	13.6	13.7	83
P18	0.231	124.41	0.40543	22	722.9	18.5	2493.24	-17	12.4	19.7	24.8	56.7	44.1	33.8	10.9	13.3	13.6	13.7	80
P19	0.201	111.67	0.78612	35	3649.9	35	2595.31	-17	11.7	18.9	24	52.6	39.9	29	11.7	13.7	14.1	14.1	62
P20	0.213	114.3	0.393778	23	720.1	19	2571.71	-17	12.4	19.6	24.8	55	41.3	30.1	11.1	13.6	13.9	13.9	76
P21	0.211	113.41	0.385781	22	718.6	18.5	2579.1	-17	12.3	19.3	24.4	56.3	41.5	32	11.3	13.7	13.9	14.0	84
P22	0.21	116.4	0.394611	23	719.31	18.5	2580	-17	12.1	19.2	24.3	52.9	40.3	30.7	11.6	14.1	14.4	14.5	85
P23	0.222	119.71	0.42115	22	727.62	18.5	2519.72	-17	12.5	19.6	24.7	57.9	41.8	31.1	11.2	13.3	13.6	13.7	84
P24	0.22	113.23	0.353325	24	706.88	18	2550.94	-17	12.5	20.2	25.8	65.3	48.1	35.7	10.6	13.1	13.3	13.4	85
Ref4	0.208	111.63	0.372078	23	717.14	18.5	2580.15	-17	12.2	19.4	24.7	56	43.7	31.6	11.1	13.5	13.7	13.8	83

Sample	Equilibrium Products Results - CO					Equilibrium Products Results - O_2					Equilibrium Products Results - NO							
	End of Cycle	Exhaust Valve Open	End of Combustion	Maximum	Angle at Maximum	End of Cycle	Exhaust Valve Open	End of Combustion	Minimum	Angle at Minimum	End of Cycle	Exhaust Valve Open	End of Combustion	Max Burned Gas Temp	Maximum	Angle at Maximum	Burned Gas Temp=2000k	Angle at Burned Gas Temp=2000k
	[% vol]	[% vol]	[% vol]	[% vol]	[° CA]	[% vol]	[% vol]	[% vol]	[% vol]	[° CA]	[% vol]	[% vol]	[% vol]	[% vol]	[% vol]	[° CA]	[% vol]	[° CA]
Ref3	0.0	0.0	0.0	0.3	28	4.4	0.8	0.7	0.6	80	0.001	0.026	0.251	0.255	0.518	33	0.279	58
P12	0.0	0.0	0.1	0.5	28	3.5	-0.1	-0.6	-0.6	64	0.000	0.020	0.272	0.003	0.547	32	0.252	60
P13	0.0	0.0	0.0	0.3	28	3.4	-0.3	-0.8	-0.8	65	0.001	0.025	0.274	0.003	0.587	34	0.317	59
P14	0.0	0.0	0.1	0.4	30	3.7	0.0	-0.3	-0.4	81	0.001	0.026	0.272	0.003	0.514	35	0.263	63
P15	-	-	-	-	-	-	-	-	-	-	-	-	-	-	-	-	-	-
P16	0.0	0.0	0.0	13.1	49	12.1	12.1	12.1	-4.3	49	0.000	0.000	0.000	1.626	4.934	49	#N/A	#N/A
P17	0.0	0.0	0.0	0.3	28	3.5	-0.3	-0.6	-0.7	82	0.001	0.028	0.304	0.003	0.609	34	0.350	58
P18	0.0	0.0	0.0	0.2	27	3.7	0.0	-0.7	-0.7	64	0.000	0.025	0.313	0.003	0.637	34	0.386	56
P19	0.0	0.0	0.0	1.0	35	2.5	-0.6	-1.2	-1.2	61	0.000	0.000	0.004	0.002	0.575	35	#N/A	#N/A
P20	0.0	0.0	0.0	0.6	29	3.4	-0.4	-1.0	-1.1	75	0.000	0.021	0.226	0.002	0.546	33	0.243	63
P21	0.0	0.0	0.1	0.6	29	3.2	-0.6	-1.1	-1.2	74	0.000	0.021	0.237	0.003	0.512	33	0.220	64
P22	0.0	0.0	0.1	0.7	29	2.6	-1.2	-1.9	-1.9	78	0.000	0.020	0.242	0.003	0.522	32	0.217	64
P23	0.0	0.0	0.0	0.3	27	3.4	0.0	-0.4	-0.5	84	0.000	0.016	0.234	0.003	0.644	32	0.334	54
P24	0.0	0.0	0.0	0.3	30	4.3	0.5	0.1	0.0	77	0.001	0.027	0.268	0.003	0.525	38	0.287	63
Ref4	0.0	0.0	0.0	0.7	38	3.4	-0.2	-0.8	-0.9	74	0.000	0.015	0.205	0.002	0.538	38	0.221	60

Sample	Engine Operating Point			Engine Operating Conditions															
	Speed	Torque	Power	Fuel Flow Rate	Equivalence Ratio	Equivalence Ratio	Ignition Timing	BSFC	Water Temperature	Oil Temperature	Exhaust Temperature	Fuel Pressure	Oil Pressure	Manifold Pressure	Manifold Temperature	Droplet Temperature	Air Flow Rate	Air Flow Rate
	[rev/min]	[Nm]	[kW]	[kg/hr]	(calc) [-]	(meas) [-]	[° CA BTDC]	[kg/kW.hr]	[° C]	[° C]	[° C]	[bar]	[bar]	[kPa]	[° C]	[° C]	[mbar]	[kg/s]
Ref5	1884	36.1	7.1	2.55	0.92	0.90	20	0.360	87.5	91.9	501.8	2.6	3.3	50.1	54.0	22.3	0.14	0.0116
P25	1879	35.9	7.0	2.51	0.93	0.90	20	0.358	87.6	90.2	491.1	2.6	3.4	49.2	55.1	28.4	0.14	0.0114
P26	1888	36.1	7.1	2.45	0.92	0.90	20	0.345	88.2	88.6	478.1	2.6	3.5	48.9	53.6	23.0	0.13	0.0111
P27	1879	36.0	7.0	2.35	0.92	0.87	20	0.334	89.1	88.4	480.5	2.6	3.5	49.2	55.0	23.6	0.13	0.0111
P28	1890	36.5	7.2	2.52	0.92	0.93	20	0.351	87.5	87.8	485.3	2.6	3.5	49.0	53.7	19.1	0.13	0.0110
P29	1879	36.1	7.0	2.44	0.92	0.94	20	0.346	87.5	87.8	484.1	2.6	3.5	48.9	52.9	17.4	0.12	0.0106
P30	1884	36.3	7.1	2.46	0.92	0.95	20	0.345	87.7	87.8	481.2	2.6	3.5	48.8	51.9	16.6	0.12	0.0106
P31	1884	36.4	7.1	2.47	0.92	0.95	20	0.346	88.6	88.3	484.2	2.6	3.5	48.9	51.6	17.7	0.12	0.0107
P32	1885	35.8	7.0	2.47	0.93	0.91	20	0.352	88.4	88.9	483.1	2.6	3.5	48.8	54.8	17.2	0.13	0.0110
P33	1885	36.4	7.1	2.46	0.93	0.91	20	0.344	89.2	89.0	484.5	2.6	3.6	49.3	55.2	18.7	0.13	0.0110
P34	1884	36.6	7.2	2.45	0.93	0.91	20	0.341	89.3	89.0	490.3	2.6	3.5	49.2	55.0	23.5	0.13	0.0110
P35	1881	35.8	7.0	2.50	0.92	0.93	20	0.356	89.4	89.1	490.4	2.6	3.5	48.9	54.5	13.9	0.13	0.0110
Ref6	1881	35.7	7.0	2.48	0.91	0.88	20	0.355	88.3	90.5	512.6	2.6	3.4	49.2	54.0	22.8	0.14	0.0115

Engine Out Emissions														
Hydrocarbons			NO			CO2			CO			O2	H2S	SO2
[ppm]	[g/kW.hr]	[g/km]	[ppm]	[g/kW.hr]	[g/km]	[% vol]	[g/kW.hr]	[g/km]	[% vol]	[g/kW.hr]	[g/km]	[% vol]	[ppm]	[ppm]
1113	3.18	0.37	1236	11.69	1.38	14.8	1341.7	158.3	0.22	12.52	1.48	1.6	-	-
912	2.60	0.30	1266	11.97	1.40	14.9	1343.7	157.0	0.22	12.66	1.48	1.4		
934	2.59	0.31	1273	11.71	1.38	14.6	1282.2	151.4	0.19	10.82	1.28	1.5		
906	2.50	0.29	1320	12.09	1.42	14.6	1282.5	150.4	0.20	11.29	1.32	1.6	17	
917	2.46	0.29	1289	11.46	1.37	14.9	1264.8	151.4	0.24	12.71	1.52	1.6		32
1005	2.62	0.31	1138	9.86	1.16	15.0	1242.6	145.9	0.21	11.20	1.31	1.6	195	215
1077	2.77	0.33	1218	10.38	1.23	15.1	1227.8	145.5	0.22	11.28	1.34	1.6		
1070	2.78	0.33	1241	10.69	1.27	14.9	1229.1	146.2	0.23	12.24	1.46	1.6	200	240
883	2.41	0.28	1220	11.03	1.29	15.1	1301.8	152.4	0.21	11.69	1.37	1.4	102	126
869	2.35	0.28	1242	11.14	1.33	14.8	1272.3	151.4	0.22	11.73	1.40	1.5	107	127
809	2.20	0.26	1220	11.00	1.31	14.6	1263.1	151.0	0.20	11.11	1.33	1.5	71	86
787	2.11	0.25	1287	11.45	1.34	15.3	1297.8	151.7	0.22	11.77	1.38	1.6	42	37
1107	3.15	0.37	1269	11.99	1.39	14.8	1335.0	155.3	0.15	8.43	0.98	1.8	-	-

Atmospheric Conditions		
Barometric Pressure	Dry Bulb Temperature	Wet Bulb Temperature
[mBar]	[° C]	[° C]
1017.7	21.0	14.5
1002.9	21.0	14.0
1013.7	18.0	12.0
1010.1	18.0	12.0
1005.2	18.0	12.0
1003.5	16.5	13.0
1002.2	18.0	14.0
1012.2	17.0	14.0
1007.0	19.0	15.0
1005.7	20.0	15.0
1003.0	19.5	14.5
1001.1	19.0	14.0
1008.9	20.0	14.0

SABS Corrections		
Correction Factor	Corrected Torque	Corrected Power
[-]	[Nm]	[kW]
0.97	35.1	6.9
0.99	35.6	6.9
0.97	35.1	6.8
0.97	34.9	6.8
0.98	35.8	7.0
0.98	35.4	6.9
0.99	35.8	7.0
0.97	35.3	6.9
0.99	35.3	6.9
0.99	36.0	7.1
0.99	36.3	7.1
0.99	35.5	6.9
0.98	34.9	6.8

Sample	Engine Operating Point			Engine Operating Conditions							Racer Input Parameters				
	Speed	Torque	Racer File Name	Fuel Flow Rate	Equivalence Ratio	Ignition Timing	Manifold Pressure	Manifold Temperature	Droplet Temperature	Air Flow Rate	Charge Temperature	Cylinder Charge Mass	Re Reference Pressure	Air Fuel Ratio	Fuel Flow Rate
	[rev/min]	[Nm]	[-]	[kg/hr]	(calc) [-]	[° CA BTDC]	[kPa]	[° C]	[° C]	[kg/s]	[° C]	[kg]	[kPa]	[-]	[kg/s]
Ref5	1884	36.1	rf460	*2.55*	0.92	20	50.1	54.0	22.3	0.01159	84.0	*0.0001958*	*49.93*	14.9	0.00071
P25	1879	35.9	P2560	2.51	0.93	20	49.2	55.1	28.4	0.01140	85.1	0.0001932	49.44	14.7	0.00070
P26	1888	36.1	P2660	2.45	0.92	20	48.9	53.6	23.0	0.01109	83.6	0.0001871	47.66	14.9	0.00068
P27	1879	36.0	P2760	2.35	0.92	20	49.2	55.0	23.6	0.01108	85.0	0.0001873	47.90	14.9	0.00065
P28	1890	36.5	P2860	2.52	0.92	20	49.0	53.7	19.1	0.01105	83.7	0.0001865	47.52	14.9	0.00070
P29	1879	36.1	P2960	2.44	0.92	20	48.9	52.9	17.4	0.01063	82.9	0.0001805	45.89	14.9	0.00068
P30	1884	36.3	P3060	2.46	0.92	20	48.8	51.9	16.6	0.01060	81.9	0.0001796	45.54	14.9	0.00068
P31	1884	36.4	P3160	2.47	0.92	20	48.9	51.6	17.7	0.01067	81.6	0.0001807	45.79	14.9	0.00069
P32	1885	35.8	P3260	2.47	0.93	20	48.8	54.8	17.2	0.01104	84.8	0.0001866	47.70	14.7	0.00069
P33	1885	36.4	P3360	2.46	0.93	20	49.3	55.2	18.7	0.01102	85.2	0.0001862	47.64	14.7	0.00068
P34	1884	36.6	P3460	2.45	0.93	20	49.2	55.0	23.5	0.01101	85.0	0.0001862	47.62	14.7	0.00068
P35	1881	35.8	P3560	2.50	0.92	20	48.9	54.5	13.9	0.01101	84.5	0.0001866	47.66	14.9	0.00069
Ref6	1881	35.7	rf560	2.48	0.91	20	49.2	54.0	22.8	0.01145	84.0	0.0001936	49.37	15.0	0.00069

Sample	Pressure/CA results								Single Zone Model Results											
	IMEP	PMEP	IMEP(net)	Stability	Pressure		Rate of Pressure Rise		Heat Released			Gas Temperature		Induction Period			Burn Angle			
	[kPa]	[kPa]	[kPa]	[%]	Max [kPa]	CA [Max.] [° CA]	Max [kPa/°]	CA [Max.] [° CA]	Total [kJ]	Max. Rate [kJ/° CA]	CA [Max. Rate] [° CA]	Max [K]	CA [Max] [° CA]	2-98 [° CA]	5-95 [° CA]	10-90 [° CA]	2-98 [° CA]	5-95 [° CA]	10-90 [° CA]
Ref5	486.52	-58.89	427.63	12.9	1605.2	26	28.1	10	623.21	1002.14	23	3063.7	42	12.1	19.3	24.5	57.1	44	32.7
P25	479.43	-57.96	421.48	12.6	1644.5	26	31.1	10	609.38	1022.49	22	3002.6	40	12.1	18.9	23.9	56.6	42.1	33
P26	473.71	-56.65	417.06	12.2	1647.7	25	31.9	10	605.9	1034.43	21	3103.7	40	12.1	18.9	23.9	56.9	43	31.6
P27	470.6	-56.32	414.28	9.9	1597.4	26	28.9	10	603.43	992.77	23	3018.4	41	12.1	19.1	24.2	56.7	42	32.3
P28	473.84	-57.36	416.48	11.3	1595.9	26	29.2	11	601.88	1004.94	22	2994.2	41	12.1	19.1	24.4	57.9	43.2	31.8
P29	460.93	-58.07	402.86	10.5	1528.7	26	27.8	12	578.38	959.22	22	2852.5	42	12.2	19.4	24.6	57.3	44.2	33
P30	465.16	-57.35	407.81	12.3	1574.6	25	30.9	9	647.33	996.56	21	3052	40	11.1	18.4	23.7	61.3	48.5	35.8
P31	470.23	-57.22	413.01	10.8	1611.4	25	30.8	10	605.13	997.78	21	3208.4	40	11.7	18.7	23.8	57.2	42.9	31.4
P32	474.47	-57.3	417.16	11.8	1676.5	24	34.9	9	595.44	1016.24	21	2950.1	39	11.9	18.5	23.3	55.4	42.2	30.8
P33	474.53	-55.98	418.56	11.2	1639.5	25	32	10	611.12	1022.89	24	3190.8	40	11.7	18.8	23.9	55.9	41.3	31.6
P34	473.07	-57.05	416.03	11	1639.6	25	32.8	10	606.18	1012.1	21	3139.9	40	12	18.9	23.8	55	42.8	31.5
P35	472.72	-58.45	414.27	13.2	1664.1	24	32.9	9	604.94	1014.56	20	3131.9	40	11.8	18.4	23.3	56.4	43.2	32.2
Ref6	468.69	-58.5	410.19	11.6	1621.4	25	32.9	10	588.07	987.58	21	2894.2	40	12.1	18.9	23.8	57.8	43.6	32.9

Sample	Two Zone Model Results														Equilibrium Products Results - CO_2				
	Mass Transferred				Unburned Gas Temperature		Burned Gas Temperature		Induction Period			Burn Angle			End of Cycle	Exhaust Valve Open	End of Combustion	Maximum	Angle at Maximum
	Total [g]	Total % [%]	Max. Rate [g/° CA]	CA [Max. Rate] [° CA]	Max [K]	CA [Max] [° CA]	Max [K]	CA [Max] [° CA]	2-98 [° CA]	5-95 [° CA]	10-90 [° CA]	2-98 [° CA]	5-95 [° CA]	10-90 [° CA]	[% vol]	[% vol]	[% vol]	[% vol]	[° CA]
Ref5	0.223	113.92	0.398374	23	722.5	19.5	2554.93	-17	12.8	19.9	25.1	60.3	43.7	33.5	10.9	13.4	13.4	13.6	96
P25	0.218	112.75	0.407087	22	725.28	18.5	2556.23	-17	12.6	19.5	24.4	54.9	40.1	30.5	10.8	13.1	13.4	13.5	80
P26	0.215	114.7	0.414658	21	727.76	19	2552.56	-17	12.5	19.4	24.3	53.8	40.8	30.5	11.0	13.3	13.7	13.7	82
P27	0.222	118.54	0.407455	23	724.78	18.5	2525.18	-17	12.5	19.6	24.6	53.8	41.4	30.5	10.7	13.1	13.5	13.6	78
P28	0.21	112.84	0.393006	22	717.97	19.5	2575.95	-17	12.3	19.5	24.7	56.2	41.4	32.1	11.2	13.6	13.8	13.9	83
P29	0.205	113.76	0.373375	22	709.55	19.5	2575.46	-17	12.4	19.7	25				11.6	14.0	13.9	14.2	120
P30	0.205	114.19	0.370842	20	720.31	18.5	2582.9	-17	12	19	24.1	64.8	45.7	31.8	11.7	14.0	14.0	14.2	101
P31	0.204	112.77	0.38603	21	723.06	18.5	2583.07	-17	11.9	19	24.1	52.7	40.6	29.8	11.4	13.8	14.1	14.2	82
P32	0.211	112.98	0.401891	21	726.21	18	2566.85	-17	12.2	18.9	23.7	52.4	40.6	30.4	11.1	13.5	13.7	13.7	83
P33	0.214	114.83	0.405488	22	729.96	18.5	2558.74	-17	12.1	19.2	24.3	52.5	40.3	29.5	10.9	13.3	13.7	13.8	63
P34	0.214	115.23	0.403622	21	728.93	18.5	2558.78	-17	12.5	19.4	24.3	55	40.6	30	11.0	13.4	13.7	13.8	83
P35	0.211	113.31	0.400465	21	729.08	18.5	2573.39	-17	12.3	19	23.8	57.4	41	30.4	11.1	13.5	13.6	13.8	87
Ref6	0.218	112.8	0.399992	21	726.6	18.5	2539.26	-17	12.9	19.6	24.5	68.5	45.1	32.7	10.8	13.0	13.0	13.3	103

Sample	Equilibrium Products Results - CO					Equilibrium Products Results - O_2					Equilibrium Products Results - NO							
	End of Cycle	Exhaust Valve Open	End of Combustion	Maximum	Angle at Maximum	End of Cycle	Exhaust Valve Open	End of Combustion	Minimum	Angle at Minimum	End of Cycle	Exhaust Valve Open	End of Combustion	Max Burned Gas Temp	Maximum	Angle at Maximum	Burned Gas Temp=2000k	Angle at Burned Gas Temp=2000k
	[% vol]	[% vol]	[% vol]	[% vol]	[° CA]	[% vol]	[% vol]	[% vol]	[% vol]	[° CA]	[% vol]	[% vol]	[% vol]	[% vol]	[% vol]	[° CA]	[% vol]	[° CA]
Ref5	0.0	0.0	0.0	0.4	29	3.8	-0.1	-0.4	-0.5	83	0.001	0.028	0.277	0.003	0.561	34	0.277	62
P25	0.0	0.0	0.0	0.5	28	3.9	0.3	-0.3	-0.3	65	0.000	0.021	0.266	0.003	0.573	32	0.266	61
P26	0.0	0.0	0.0	0.5	28	3.6	0.0	-0.7	-0.7	63	0.000	0.017	0.238	0.002	0.591	32	0.276	58
P27	0.0	0.0	0.0	0.3	28	4.0	0.3	-0.5	-0.5	63	0.000	0.022	0.300	0.003	0.623	33	0.335	58
P28	0.0	0.0	0.1	0.6	29	3.3	-0.5	-0.9	-1.0	74	0.000	0.022	0.232	0.003	0.521	33	0.232	63
P29	0.0	0.0	0.1	0.6	29	2.7	-1.0	-1.0	-1.3	120	0.001	0.024	0.227	0.002	0.491	33	0.213	64
P30	0.0	0.0	0.0	0.7	28	2.6	-1.1	-1.2	-1.5	101	0.001	0.020	0.196	0.002	0.495	31	0.211	62
P31	0.0	0.0	0.1	0.8	29	3.0	-0.7	-1.4	-1.4	63	0.000	0.017	0.220	0.003	0.498	32	0.197	64
P32	0.0	0.0	0.0	0.6	27	3.4	-0.2	-0.7	-0.7	65	0.000	0.019	0.248	0.003	0.555	31	0.248	60
P33	0.0	0.0	0.1	0.5	28	3.8	0.1	-0.8	-0.8	62	0.000	0.019	0.281	0.003	0.587	32	0.271	61
P34	0.0	0.0	0.1	0.5	28	3.6	-0.1	-0.8	-0.9	82	0.000	0.020	0.282	0.003	0.581	32	0.272	60
P35	0.0	0.0	0.1	0.6	27	3.5	-0.3	-0.7	-0.8	87	0.000	0.020	0.251	0.003	0.547	31	0.242	61
Ref6	0.0	0.0	0.0	0.4	27	4.0	0.5	0.4	0.1	103	0.001	0.025	0.256	0.003	0.575	32	0.284	59

Engine – 4Y, Load Point - 60 km/hr

Sample	Engine Operating Point			Engine Operating Conditions													
	Speed	Torque	Power	Fuel Flow Rate	Equivalence Ratio	Equivalence Ratio	Ignition Timing	BSFC	Water Temperature	Oil Temperature	Exhaust Temperature 1&4	Exhaust Temperature 2&3	Oil Pressure	Manifold Pressure	Air Flow Rate	Air Flow Rate
	[rev/min]	[Nm]	[kW]	[kg/hr]	(calc) [-]	(meas) [-]	[° CA BTDC]	[kg/kW.hr]	[° C]	[° C]	[° C]	[° C]	[bar]	[kPa]	[mbar]	[kg/s]
Ref1	1879	38.4	7.5	3.08	0.93	0.89	32.0	0.409	83.5	108.6	566.6	524.6	3.37	38.97	2.20	0.014
P1	1879	37.4	7.4	3.02	0.88	0.89	32.0	0.411	83.8	104.9	568.8	530.7	3.34	38.60	2.11	0.014
P2	1881	35.9	7.1	2.90	0.94	0.90	32.0	0.410	83.2	105.8	559.5	521.9	3.28	37.33	1.91	0.013
P3	1883	39.0	7.7	3.05	0.95	0.90	32.0	0.396	83.2	108.6	571.5	535.8	3.16	38.81	2.11	0.014
P4	1886	39.6	7.8	3.12	0.95	0.90	32.0	0.398	83.0	107.0	564.6	522.6	3.33	39.37	2.17	0.014
P5	1880	39.3	7.7	3.06	0.95	0.90	32.0	0.395	83.1	107.7	562.2	520.0	3.28	39.03	2.11	0.014
P6	1881	37.1	7.3	2.99	0.94	0.91	32.0	0.410	83.4	104.3	552.5	506.1	3.52	38.03	1.98	0.013
P7	1883	37.9	7.5	3.10	0.96	0.94	32.0	0.415	83.1	107.6	560.8	520.8	3.32	38.30	1.98	0.013
P8	1882	39.1	7.7	3.15	0.94	0.95	32.0	0.410	83.4	100.1	550.9	501.1	3.74	38.55	2.03	0.014
P9	1884	38.7	7.6	3.10	0.95	0.92	32.0	0.406	83.3	101.7	551.0	502.8	3.65	38.63	2.08	0.014
P10	1879	35.7	7.0	2.93	0.95	0.89	32.0	0.417	83.4	107.5	565.6	527.8	3.22	37.57	2.01	0.014
P11	1881	38.1	7.5	3.08	0.96	0.91	32.0	0.411	83.5	108.8	567.1	528.6	3.21	38.57	2.12	0.014
P12	1879	38.8	7.6	3.01	0.94	0.90	33.0	0.395	83.0	102.3	567.7	521.7	3.58	38.33	2.05	0.014
P13	1880	39.4	7.8	3.08	0.94	0.90	33.0	0.397	83.4	105.9	573.8	521.6	3.44	38.71	2.13	0.014
P14	1883	38.6	7.6	3.08	0.90	0.88	32.0	0.404	83.0	107.2	565.3	526.2	3.27	38.95	2.23	0.014
P15	1884	38.2	7.5	3.08	0.91	0.89	32.0	0.409	83.6	109.9	572.4	537.2	3.16	38.62	2.18	0.014
P16	1884	38.3	7.5	3.13	0.93	0.91	32.0	0.415	83.7	109.9	567.9	528.7	3.21	38.68	2.17	0.014
P17	1884	39.5	7.8	3.18	0.93	0.93	32.0	0.408	83.5	103.1	559.0	516.0	3.47	39.19	2.17	0.014
P18	1879	38.6	7.6	3.06	0.94	0.90	33.0	0.403	83.2	107.5	561.1	523.3	3.26	38.76	2.12	0.014
P19	1882	39.1	7.7	3.07	0.96	0.95	33.0	0.398	83.5	111.3	588.4	540.6	3.11	38.26	1.92	0.013
P20	1880	37.4	7.4	2.96	0.95	0.89	33.0	0.402	84.0	110.0	562.0	528.0	3.18	37.75	2.05	0.014
P21	1883	38.0	7.5	2.98	0.94	0.97	33.0	0.397	82.9	96.2	544.8	499.8	3.85	37.68	1.71	0.013
P22	1882	37.4	7.4	2.97	0.93	0.96	33.0	0.403	82.9	96.2	556.2	515.7	3.80	37.35	1.74	0.013
P23	1882	39.2	7.7	3.03	0.94	0.96	33.0	0.392	83.2	99.0	550.4	507.8	3.57	37.89	1.82	0.013
P24	1880	39.7	7.8	3.11	0.90	0.96	33.0	0.398	84.1	100.3	548.9	501.4	3.69	38.64	1.91	0.013
P25	1879	38.1	7.5	2.98	0.96	0.96	32.0	0.398	82.5	108.0	564.7	516.6	3.26	37.87	1.77	0.013
P26	1880	39.8	7.8	3.07	0.94	0.96	33.0	0.392	82.8	106.3	562.3	513.6	3.37	38.68	1.85	0.013
P27	1881	38.0	7.5	3.02	0.94	0.96	-	0.403	82.9	113.5	576.1	532.7	3.04	38.10	1.80	0.013
P28	1881	39.1	7.7	2.93	0.92	0.93	-	0.380	83.2	98.2	562.6	515.0	3.68	37.32	1.78	0.013
P29	1882	39.1	7.7	3.00	0.91	0.98	-	0.389	83.4	89.2	551.7	497.5	3.97	37.33	1.69	0.012
P30	1880	39.0	7.7	3.04	0.93	0.97	32.0	0.395	83.1	107.8	582.4	542.8	3.15	37.62	1.76	0.013
P31	1877	38.5	7.6	3.00	0.93	0.93	32.0	0.396	82.9	103.2	572.0	532.7	3.30	37.86	1.89	0.013
P32	1883	39.3	7.7	3.04	0.94	0.94	32.0	0.393	83.2	101.0	566.7	524.6	3.53	37.71	1.89	0.013
P33	1881	38.8	7.6	3.11	0.94	0.95	32.0	0.407	83.5	103.9	573.8	531.9	3.39	38.45	1.96	0.013
P34	1880	38.5	7.6	3.10	0.95	0.96	32.0	0.409	83.4	94.8	558.9	512.4	3.88	38.13	1.85	0.013
P35	1880	37.1	7.3	3.01	0.94	1.02	32.0	0.412	83.0	100.5	573.3	523.4	3.77	37.47	1.60	0.012
Ref2	1886	38.0	7.5	3.06	0.94	0.94	32.0	0.408	84.8	101.3	563.8	516.1	3.76	38.29	1.92	0.013

Sample	Engine Out Emissions													Atmospheric Conditions			SABS Corrections		
	Hydrocarbons			NO			CO2			CO			O2	Barometric Pressure	Dry Bulb Temperature	Wet Bulb Temperature	Correction Factor	Corrected Torque	Corrected Power
	[ppm]	[g/kW.hr]	[g/km]	[ppm]	[g/kW.hr]	[g/km]	[% vol]	[g/kW.hr]	[g/km]	[% vol]	[g/kW.hr]	[g/km]	[% vol]	[mBar]	[° C]	[° C]	[-]	[Nm]	[kW]
Ref1	2597	8.69	1.09	1522	16.88	2.12	13.2	1404.6	176.7	1.3	88.3	11.1	2.2	1002.3	30.0	22.0	1.02	39.2	7.7
P1	2146	7.40	0.91	1416	16.20	1.99	12.9	1411.1	173.0	0.8	52.7	6.5	2.7	1002.3	30.0	22.0	1.02	38.2	7.5
P2	2417	8.26	0.97	1351	15.31	1.81	12.9	1400.9	165.3	1.4	96.6	11.4	2.0	1006.0	29.5	21.0	1.01	36.4	7.2
P3	2068	9.76	1.25	1042	16.30	2.09	8.8	1312.8	168.3	0.9	90.1	11.5	1.2	1006.0	29.5	21.0	1.01	39.5	7.8
P4	2500	8.22	1.07	1571	17.13	2.23	13.0	1355.0	176.8	1.5	98.0	12.8	1.9	1006.0	29.5	21.0	1.01	40.2	7.9
P5	2517	8.25	1.06	1525	16.56	2.13	12.9	1339.9	172.7	1.6	103.2	13.3	2.0	1005.0	31.0	22.0	1.02	40.0	7.9
P6	2445	8.26	1.01	1413	15.84	1.93	12.9	1385.5	168.6	1.4	93.4	11.4	2.0	1005.9	29.5	21.5	1.01	37.6	7.4
P7	2495	8.24	1.03	1515	16.58	2.07	12.9	1351.9	168.4	1.7	111.4	13.9	1.8	1005.9	29.5	21.5	1.01	38.5	7.6
P8	2514	8.12	1.04	1564	16.75	2.15	13.2	1357.4	174.2	1.2	77.3	9.9	1.8	-	-	-	1.00	39.1	7.7
P9	2602	8.62	1.10	1516	16.65	2.12	13.1	1376.0	174.9	1.3	89.4	11.4	1.8	-	-	-	1.00	38.7	7.6
P10	2564	9.21	1.08	1366	16.27	1.91	12.7	1452.1	170.2	1.4	98.5	11.5	1.8	-	-	-	1.00	35.7	7.0
P11	2587	8.81	1.10	1679	18.97	2.37	13.0	1402.6	175.3	1.5	104.4	13.0	1.7	-	-	-	1.00	38.1	7.5
P12	2338	7.65	0.97	1350	14.66	1.86	12.9	1338.7	170.2	1.5	98.5	12.5	2.1	1001.2	28.0	20.5	1.02	39.4	7.7
P13	2285	7.51	0.97	1451	15.81	2.04	13.0	1353.4	174.8	1.4	91.5	11.8	2.0	1001.6	29.0	21.0	1.02	40.1	7.9
P14	2098	7.25	0.92	1105	12.65	1.60	13.0	1421.2	180.2	0.9	62.4	7.9	2.4	1005.1	27.5	20.0	1.01	38.9	7.7
P15	2146	7.39	0.93	1334	15.24	1.91	13.0	1419.9	178.5	1.0	71.7	9.0	2.3	1005.1	27.5	20.0	1.01	38.6	7.6
P16	2512	8.33	1.05	1412	15.54	1.95	13.4	1414.5	177.9	1.3	89.5	11.3	2.1	1005.1	27.5	20.0	1.01	38.6	7.6
P17	2551	8.18	1.06	1475	15.67	2.04	13.4	1363.8	177.2	1.3	86.8	11.3	2.1	1004.2	31.0	21.0	1.02	40.2	7.9
P18	2466	8.27	1.05	1315	14.62	1.85	12.8	1361.1	172.4	1.5	104.6	13.2	2.0	1004.2	31.0	21.0	1.02	39.3	7.7
P19	2487	7.81	1.00	1403	14.60	1.87	13.1	1304.1	167.3	1.5	97.6	12.5	1.8	-	-	-	1.00	39.1	7.7
P20	2352	8.03	0.99	1251	14.17	1.74	12.9	1402.3	172.1	1.5	102.6	12.6	1.8	-	-	-	1.00	37.4	7.4
P21	2348	7.23	0.90	1202	12.28	1.53	12.9	1261.0	157.6	1.4	87.2	10.9	2.0	1002.8	26.0	22.0	1.02	38.6	7.6
P22	2329	7.31	0.90	1135	11.81	1.45	13.0	1290.2	158.7	1.3	85.1	10.5	2.1	1002.8	26.0	22.0	1.02	38.0	7.5
P23	2703	8.33	1.07	1334	13.64	1.76	13.0	1267.5	163.3	1.4	86.2	11.1	2.0	1001.5	24.0	19.0	1.01	39.5	7.8
P24	2019	6.31	0.82	1253	12.99	1.69	12.9	1276.5	166.3	1.0	65.9	8.6	2.4	-	-	-	1.00	39.7	7.8
P25	2352	7.36	0.92	1453	15.08	1.88	12.9	1278.8	159.7	1.6	102.9	12.9	1.8	1002.7	27.5	20.5	1.01	38.6	7.6
P26	2317	7.07	0.92	1513	15.30	1.99	12.9	1244.3	162.2	1.6	97.5	12.7	2.0	1002.7	27.5	20.5	1.01	40.3	7.9
P27	2313	7.22	0.90	1517	15.69	1.96	12.9	1279.8	159.6	1.6	102.2	12.7	2.1	1002.7	27.5	20.5	1.01	38.5	7.6
P28	2078	6.12	0.79	1511	14.76	1.90	13.6	1269.0	163.0	1.2	68.8	8.8	2.2	1000.2	21.5	12.0	0.99	38.7	7.6
P29	2078	5.99	0.77	1644	15.71	2.02	13.6	1244.2	159.8	0.9	51.1	6.6	2.3	1000.2	21.5	12.0	0.99	38.7	7.6
P30	2203	6.48	0.83	1723	16.79	2.15	13.6	1265.6	162.2	1.3	75.8	9.7	2.2	1006.6	23.0	18.0	1.00	38.9	7.7
P31	2403	7.52	0.95	928	9.63	1.22	13.3	1320.7	166.7	1.3	81.5	10.3	2.1	1005.1	25.0	18.0	1.00	38.6	7.6
P32	2329	7.08	0.91	1300	13.11	1.69	13.3	1285.4	165.9	1.4	87.7	11.3	2.1	1004.8	27.0	19.0	1.01	39.5	7.8
P33	2244	7.14	0.91	1355	14.29	1.82	13.2	1330.1	169.5	1.4	91.9	11.7	1.9	1004.8	27.0	19.0	1.01	39.1	7.7
P34	2255	7.14	0.90	1245	13.07	1.65	13.0	1303.6	164.6	1.5	98.4	12.4	1.8	1004.8	27.0	19.0	1.01	38.7	7.6
P35	2593	7.61	0.93	1727	16.80	2.04	13.7	1274.5	155.2	1.3	79.8	9.7	2.0	1002.2	26.0	18.0	1.01	37.3	7.3
Ref2	2149	6.76	0.85	1896	19.77	2.47	13.6	1355.1	169.5	1.3	84.9	10.6	1.9	1002.2	28.0	19.0	1.01	38.4	7.6

Engine - 4A-FE, Load Point – Closed Loop Simulation

Sample	Engine Operating Point			Engine Operating Conditions															
	Speed	Torque	Power	Fuel Flow Rate	Equivalence Ratio	Equivalence Ratio	Ignition Timing	BSFC	Water Temperature	Oil Temperature	Exhaust Temperature	Fuel Pressure	Oil Pressure	Manifold Pressure	Manifold Temperature	Droplet Temperature	Air Flow Rate	Air Flow Rate
	[rev/min]	[Nm]	[kW]	[kg/hr]	(calc) [-]	(meas) [-]	[° CA BTDC]	[kg/kW.hr]	[° C]	[° C]	[° C]	[bar]	[bar]	[kPa]	[° C]	[° C]	[mbar]	[kg/s]
Ref3	1886	36.4	7.2	2.52	0.92	0.89	25	0.350	89.2	91.8	508.1	2.6	3.4	48.4	55.4	25.8	0.14	0.0115
P12	1882	36.2	7.1	2.40	0.89	0.92	25	0.338	89.1	92.6	510.2	3.3	2.5	48.8	53.8	22.8	0.12	0.0107
P13	1889	36.1	7.1	2.41	0.90	0.90	25	0.340	89.6	94.4	513.0	2.6	3.3	48.3	54.1	21.2	0.13	0.0109
P14	1883	35.6	7.0	2.48	0.90	0.95	25	0.355	88.9	90.2	487.1	2.8	3.4	47.8	53.0	15.6	0.12	0.0106
P15	1887	35.7	7.0	2.26	0.90	0.87	25	0.323	88.6	90.3	490.2	2.8	3.4	48.1	55.0	20.3	0.12	0.0106
P16	1885	36.3	7.1	2.47	0.90	0.92	25	0.347	88.2	88.4	480.1	2.5	3.6	48.6	53.7	17.7	0.13	0.0109
P17	1884	35.8	7.0	2.47	0.90	0.93	25	0.352	89.1	90.4	494.0	2.5	3.4	48.5	54.5	21.0	0.13	0.0109
P18	1886	36.0	7.1	2.42	0.90	0.93	25	0.342	89.8	90.9	494.2	3.4	2.5	48.8	55.5	26.6	0.12	0.0106
P19	1879	35.8	7.0	2.41	0.91	0.93	25	0.345	88.4	90.1	492.3	2.6	3.4	48.2	54.2	25.5	0.12	0.0106
P20	1882	35.7	7.0	2.39	0.90	0.92	25	0.342	89.3	90.6	490.6	2.5	3.4	48.3	54.7	27.6	0.12	0.0106
P21	1885	36.2	7.1	2.42	0.90	0.93	25	0.340	89.1	90.2	492.3	2.5	3.4	48.7	55.0	26.3	0.12	0.0106
P22	1878	35.7	7.0	2.40	0.90	0.92	25	0.343	88.6	89.5	489.4	2.5	3.4	48.1	54.4	27.3	0.12	0.0106
P23	1884	36.1	7.1	2.45	0.91	0.94	25	0.345	89.1	89.9	492.1	2.6	3.4	48.5	55.3	29.1	0.12	0.0106
P24	1880	35.7	7.0	2.49	0.90	0.95	25	0.357	89.2	89.9	493.0	2.7	3.4	48.5	55.0	25.1	0.12	0.0107
Ref4	1884	35.5	7.0	2.46	0.90	0.95	25	0.354	87.5	89.4	493.6	2.5	3.5	48.3	55.4	26.7	0.12	0.0106

Engine Out Emissions														
Hydrocarbons			NO			CO2			CO			O2	H2S	SO2
[ppm]	[g/kW.hr]	[g/km]	[ppm]	[g/kW.hr]	[g/km]	[% vol]	[g/kW.hr]	[g/km]	[% vol]	[g/kW.hr]	[g/km]	[% vol]	[ppm]	[ppm]
1302	3.74	0.45	1856	17.68	2.12	14.3	1305.8	156.4	0.16	9.27	1.11	1.5	-	-
1081	2.93	0.35	1655	14.89	1.76	13.9	1196.8	141.4	0.13	7.11	0.84	2.1		
1139	3.18	0.38	1690	15.62	1.85	14.0	1236.7	146.1	0.13	7.31	0.86	1.8		
986	2.76	0.32	1468	13.61	1.58	13.9	1230.3	143.1	0.19	10.72	1.25	1.9	189	85
995	2.77	0.32	1630	15.05	1.76	13.8	1216.8	142.0	0.14	7.87	0.92	1.9	108	137
1182	3.09	0.37	1627	14.12	1.67	15.0	1242.5	147.3	0.16	8.32	0.99	2.0	128	99
1192	3.29	0.39	1700	15.58	1.82	14.3	1249.3	146.2	0.18	9.85	1.15	1.9	157	220
1073	2.96	0.35	1514	13.84	1.63	13.8	1205.2	141.9	0.14	7.60	0.89	1.8	94	127
1089	2.88	0.34	1642	14.37	1.68	14.7	1230.1	143.4	0.16	8.70	1.01	1.9	84	88
948	2.52	0.29	1552	13.66	1.59	14.5	1222.4	142.3	0.16	8.57	1.00	1.9	151	185
989	2.60	0.31	1556	13.54	1.60	14.5	1207.5	142.9	0.16	8.29	0.98	1.9	67	103
1023	2.73	0.32	1668	14.78	1.72	14.5	1230.2	143.2	0.13	7.01	0.82	1.9		
954	2.51	0.30	1576	13.73	1.62	14.6	1217.4	143.6	0.18	9.37	1.11	1.8	8	66
875	2.40	0.28	1291	11.73	1.36	14.4	1251.9	145.7	0.15	8.10	0.94	1.9	153	200
1118	2.98	0.35	1563	13.82	1.60	14.5	1229.6	142.5	0.14	7.67	0.89	1.9	-	-

Atmospheric Conditions		
Barometric Pressure	Dry Bulb Temperature	Wet Bulb Temperature
[mBar]	[° C]	[° C]
1013.5	19.0	14.0
1013.0	17.0	14.0
1010.0	20.0	14.5
1007.0	17.5	12.5
1006.5	19.0	13.0
1001.2	18.5	14.0
1006.5	19.0	14.5
1007.1	19.0	14.0
1005.6	19.0	14.0
1005.8	21.0	15.0
1005.6	20.0	15.0
1005.8	18.0	13.0
1004.5	20.0	14.0
1003.8	20.0	15.0
1002.8	20.0	15.0

SABS Corrections		
Correction Factor	Corrected Torque	Corrected Power
[-]	[Nm]	[kW]
0.98	35.5	7.0
0.97	34.1	6.7
0.98	35.4	7.0
0.98	34.9	6.8
0.98	35.0	6.9
0.79	33.2	6.5
0.98	35.3	6.9
0.98	35.4	6.9
0.98	35.2	6.9
0.99	35.3	6.9
0.99	35.8	7.0
0.98	35.1	6.9
0.99	35.7	7.0
0.99	35.4	6.9
0.99	35.2	6.9

Sample	Engine Operating Point			Engine Operating Conditions							Racer Input Parameters				
	Speed	Torque	Racer File Name	Fuel Flow Rate	Equivalence Ratio	Ignition Timing	Manifold Pressure	Manifold Temperature	Droplet Temperature	Air Flow Rate	Charge Temperature	Cylinder Charge Mass	Re Reference Pressure	Air Fuel Ratio	Fuel Flow Rate
	[rev/min]	[Nm]	[-]	[kg/hr]	(calc) [-]	[° CA BTDC]	[kPa]	[° C]	[° C]	[kg/s]	[° C]	[kg]	[kPa]	[-]	[kg/s]
Ref3	1886	36.4	rf072106	*2.52*	0.92	25	48.4	55.4	25.8	0.01150	85.4	*0.0001940*	*49.66*	14.9	0.00070
P12	1882	36.2	P12-sfc3	2.40	0.89	25	48.8	53.8	22.8	0.01067	83.8	0.0001807	46.06	15.4	0.00067
P13	1889	36.1	P13-sfc	2.41	0.90	25	48.3	54.1	21.2	0.01090	84.1	0.0001838	46.88	15.2	0.00067
P14	1883	35.6	P14-sfc	2.48	0.90	25	47.8	53.0	15.6	0.01063	83.0	0.0001804	45.87	15.2	0.00069
P15	1887	35.7	P15-sfc	2.26	0.90	25	48.1	55.0	20.3	0.01061	85.0	0.0001786	45.67	15.2	0.00063
P16	1885	36.3	P16sfc	2.47	0.90	25	48.6	53.7	17.7	0.01091	83.7	0.0001846	47.05	15.2	0.00069
P17	1884	35.8	P17-sfc	2.47	0.90	25	48.5	54.5	21.0	0.01090	84.5	0.0001844	47.11	15.2	0.00069
P18	1886	36.0	P18-sfc	2.42	0.90	25	48.8	55.5	26.6	0.01061	85.5	0.0001795	45.96	15.2	0.00067
P19	1879	35.8	P19-sfc	2.41	0.91	25	48.2	54.2	25.5	0.01060	84.2	0.0001799	45.92	15.1	0.00067
P20	1882	35.7	P20-sfc	2.39	0.90	25	48.3	54.7	27.6	0.01057	84.7	0.0001791	45.78	15.2	0.00066
P21	1885	36.2	P21-sfc	2.42	0.90	25	48.7	55.0	26.3	0.01059	85.0	0.0001792	45.82	15.2	0.00067
P22	1878	35.7	P22-sfc	2.40	0.90	25	48.1	54.4	27.3	0.01062	84.4	0.0001802	46.02	15.2	0.00067
P23	1884	36.1	P23-sfc	2.45	0.91	25	48.5	55.3	29.1	0.01058	85.3	0.0001793	45.89	15.1	0.00068
P24	1880	35.7	P24-sfc	2.49	0.90	25	48.5	55.0	25.1	0.01072	85.0	0.0001821	46.58	15.2	0.00069
Ref4	1884	35.5	rf3-sfc	2.46	0.90	25	48.3	55.4	26.7	0.01057	85.4	0.0001793	45.90	15.2	0.00068

Sample	Pressure/CA results								Single Zone Model Results											
	IMEP	PMEP	IMEP(net)	Stability	Pressure		Rate of Pressure Rise		Heat Released			Gas Temperature		Induction Period			Burn Angle			
	[kPa]	[kPa]	[kPa]	[%]	Max [kPa]	CA [Max.] [° CA]	Max [kPa/°]	CA [Max.] [° CA]	Total [kJ]	Max. Rate [kJ/° CA]	CA [Max. Rate] [° CA]	Max [K]	CA [Max] [° CA]	2-98 [° CA]	5-95 [° CA]	10-90 [° CA]	2-98 [° CA]	5-95 [° CA]	10-90 [° CA]
Ref3	477.52	-58.09	419.44	11	1835.9	22	45.9	7	571.97	1049.67	17	2677.8	35	14.2	21	25.7	56.7	40.2	29.4
P12	472.24	-59.91	412.33	10.4	1784.6	23	41.2	7	584.84	1036.75	18	2964.5	36	12.8	20.6	25.8	56.8	40.5	30.7
P13	475.95	-60.51	415.43	11.3	1802.3	22	42.6	7	639.88	1081.27	18	2855.1	36	12.9	20.5	25.9	62.6	46.7	35.1
P14	468.06	-61.52	406.54	11.8	1714.8	23	38.1	9	575.22	1010.81	18	2854.3	37	13.7	21.4	26.6	57.8	43.6	30.5
P15	477.7	-61.95	415.75	10.7	1763.9	22	40.8	8	587.89	1017.85	18	2982.4	36	13.4	20.6	25.8	59.3	43.8	31.2
P16	476.35	-58.77	417.58	12	1850.4	21	47.1	7	589.24	1040.55	16	3020.1	35	13.3	20.4	25.3	58.3	42.2	31.5
P17	473.73	-59.82	413.9	10.7	1729.7	23	37.8	8	586.83	1008.25	19	2906.7	37	13.4	21.2	26.5	59.4	43.1	31.9
P18	478.42	-58.81	419.62	10.9	1764.5	23	39.2	8	597.19	1022.9	18	3018.2	37	13.5	20.9	26.2	57.6	43.5	32.5
P19	471.82	-59.94	411.88	13.2	1731.2	23	38	8	587.2	998.87	19	2958.3	37	13.6	21	26.2	59	43	32
P20	470.24	-58.9	411.34	10.9	1731.9	23	37.8	8	590.39	1008.77	19	3063	37	13.3	20.9	26.2	57.7	43.7	32.6
P21	477.35	-59.63	417.72	12.2	1756.8	23	39.7	8	599.26	1014.7	18	3112.3	36	13.4	20.8	26.1	59.2	45.2	32.5
P22	474.21	-58.83	415.38	10.7	1784.4	23	41.9	8	587.51	1035.72	18	3021.3	35	13.4	20.8	25.9	56.7	41.4	30.3
P23	474.34	-58.54	415.8	10.6	1744.1	23	38.3	8	594.4	1031.27	19	3111.1	36	13.2	21	26.2	58.2	42.2	31
P24	472.62	-59.67	412.95	10.3	1701.8	23	36.8	8	590.77	985.45	19	2991.7	38	13.5	21.2	26.5	60.5	44.1	33.1
Ref4	467.86	-58.08	409.79	11.8	1714.2	23	37.3	8	590.38	990.08	19	3091.7	37	13.2	20.8	26.3	58	43.6	32.1

Sample	Two Zone Model Results														Equilibrium Products Results - CO_2				
	Mass Transferred				Unburned Gas Temperature		Burned Gas Temperature		Induction Period			Burn Angle			End of Cycle	Exhaust Valve Open	End of Combustion	Maximum	Angle at Maximum
	Total [g]	Total % [%]	Max. Rate [g/° CA]	CA [Max. Rate] [° CA]	Max [K]	CA [Max] [° CA]	Max [K]	CA [Max] [° CA]	2-98 [° CA]	5-95 [° CA]	10-90 [° CA]	2-98 [° CA]	5-95 [° CA]	10-90 [° CA]	[% vol]	[% vol]	[% vol]	[% vol]	[° CA]
Ref3	0.213	109.97	0.42648	17	737.27	16.5	2516.71	13	14.6	21.5	26.2	53.8	39.8	28	10.8	12.9	13.0	13.1	76
P12	0.206	113.98	0.411365	18	734.08	16.5	2569.05	-17	15.5	21.8	26.6	48.6	37.7	28.1	11.4	13.7	13.9	13.9	67
P13	0.212	115.36	0.416653	17	736.14	16.5	2555.9	-22	13.6	21	26.1	55.2	40.6	30.3	11.5	13.7	13.8	13.8	79
P14	0.207	114.87	0.401398	18	727.01	17.5	2566.87	-22	13.7	21.6	26.9	58.3	40.6	29.3	11.7	13.9	13.9	14.0	84
P15	0.226	126.53	0.430426	18	743.67	16	2500.55	-22	13.9	21.1	26.3	60.9	42.8	30.7	11.8	14.0	14.0	14.1	107
P16	0.209	112.94	0.412887	16	742.85	15.5	2569.14	-22	13.7	20.8	25.7	58.5	39.5	28.7	11.5	13.7	13.7	13.9	107
P17	0.186	100.82	0.397138	19	1224.85	32.5	3006.83	33	12.6	20.6	26	42.6	0	0	12.2	12.1	9.9	12.3	33
P18	0.21	117.27	0.404564	18	734.92	16.5	2570.11	-22	13.4	21.1	26.4	56.5	41.8	31.5	11.7	14.0	14.3	14.4	72
P19	0.208	115.47	0.394053	19	731.69	16.5	2567.58	-22	13.6	21.2	26.5	58.3	42.6	30.5	11.6	13.9	14.1	14.2	79
P20	0.209	116.58	0.400937	19	736.2	16.5	2559.22	-22	13.5	21.2	26.5	54.7	40.3	30.5	11.5	13.8	14.1	14.2	76
P21	0.209	116.88	0.400667	18	737.77	16.5	2575.49	-22	13.5	21.1	26.4	57.8	41.7	31.2	11.8	14.1	14.3	14.4	83
P22	0.208	115.16	0.410442	18	737.22	16.5	2572.34	-22	13.6	21.1	26.2	54.7	39.7	28.7	11.6	13.8	14.0	14.1	81
P23	0.207	115.66	0.40548	19	736.13	16.5	2542.05	14	13.2	21.2	26.5	55.9	40.6	29.7	11.6	14.0	14.2	14.3	76
P24	0.212	116.44	0.392335	19	733.05	16.5	2559.2	-22	13.8	21.6	26.9	59.9	42.3	31.4	11.5	13.8	14.0	14.1	82
Ref4	0.203	113.44	0.386005	19	734.17	16.5	2577.04	-22	13.3	21	26.5	55.4	41.6	30.8	11.5	13.8	14.1	14.2	78

Sample	Equilibrium Products Results - CO					Equilibrium Products Results - O_2					Equilibrium Products Results - NO							
	End of Cycle	Exhaust Valve Open	End of Combustion	Maximum	Angle at Maximum	End of Cycle	Exhaust Valve Open	End of Combustion	Minimum	Angle at Minimum	End of Cycle	Exhaust Valve Open	End of Combustion	Max Burned Gas Temp	Maximum	Angle at Maximum	Burned Gas Temp=2000k	Angle at Burned Gas Temp=2000k
	[% vol]	[% vol]	[% vol]	[% vol]	[° CA]	[% vol]	[% vol]	[% vol]	[% vol]	[° CA]	[% vol]	[% vol]	[% vol]	[% vol]	[% vol]	[° CA]	[% vol]	[° CA]
Ref3	0.0	0.0	0.0	0.5	23	3.9	0.6	0.4	0.3	67	0.000	0.018	0.216	0.327	0.605	28	0.273	55
P12	0.0	0.0	0.0	0.6	24	2.9	-0.5	-1.0	-1.1	52	0.000	0.015	0.236	0.003	0.572	28	0.245	57
P13	0.0	0.0	0.0	0.5	23	2.9	-0.5	-0.9	-0.9	63	0.000	0.019	0.202	0.002	0.608	28	0.274	56
P14	0.0	0.0	0.0	0.6	25	2.7	-0.8	-0.9	-1.0	83	0.001	0.020	0.228	0.002	0.583	29	0.255	58
P15	0.0	0.0	0.0	0.3	23	2.6	-0.9	-1.0	-1.1	82	0.001	0.021	0.246	0.003	0.716	28	0.382	51
P16	0.0	0.0	0.0	0.7	23	2.9	-0.6	-0.8	-0.9	82	0.000	0.016	0.203	0.002	0.562	27	0.228	57
P17	0.0	0.2	2.3	4.1	36	1.7	1.5	2.0	1.4	33	0.061	0.256	0.969	0.203	1.608	36	0.867	67
P18	0.0	0.0	0.1	0.7	25	2.5	-1.1	-1.7	-1.8	71	0.000	0.017	0.236	0.002	0.568	28	0.245	59
P19	0.0	0.0	0.0	0.6	25	2.6	-0.9	-1.4	-1.4	79	0.000	0.018	0.212	0.002	0.552	29	0.237	59
P20	0.0	0.0	0.0	0.6	25	2.9	-0.7	-1.4	-1.4	63	0.000	0.017	0.241	0.002	0.584	29	0.185	67
P21	0.0	0.0	0.0	0.7	25	2.4	-1.2	-1.7	-1.7	74	0.000	0.017	0.217	0.002	0.566	28	0.174	67
P22	0.0	0.0	0.0	0.7	24	2.7	-0.8	-1.2	-1.3	81	0.000	0.016	0.228	0.002	0.578	28	0.237	58
P23	0.0	0.0	0.1	0.7	25	2.7	-1.0	-1.5	-1.5	76	0.000	0.018	0.229	0.308	0.569	29	0.176	67
P24	0.0	0.0	0.0	0.5	25	3.0	-0.6	-1.0	-1.0	82	0.001	0.021	0.234	0.002	0.598	30	0.271	59
Ref4	0.0	0.0	0.1	0.8	26	2.9	-0.8	-1.4	-1.4	63	0.000	0.016	0.213	0.002	0.523	29	0.206	61

Sample	Engine Operating Point			Engine Operating Conditions															
	Speed	Torque	Power	Fuel Flow Rate	Equivalence Ratio	Equivalence Ratio	Ignition Timing	BSFC	Water Temperature	Oil Temperature	Exhaust Temperature	Fuel Pressure	Oil Pressure	Manifold Pressure	Manifold Temperature	Droplet Temperature	Air Flow Rate	Air Flow Rate
	[rev/min]	[Nm]	[kW]	[kg/hr]	(calc) [-]	(meas) [-]	[° CA BTDC]	[kg/kW.hr]	[° C]	[° C]	[° C]	[bar]	[bar]	[kPa]	[° C]	[° C]	[mbar]	[kg/s]
Ref5	1884	36.4	7.1	2.48	0.91	0.91	25	0.348	86.3	87.9	473.1	2.5	3.5	49.5	54.4	22.1	0.13	0.0111
P25	1878	36.0	7.0	2.43	0.90	0.90	25	0.345	86.8	87.8	468.4	2.4	3.5	49.0	54.9	29.4	0.13	0.0110
P26	1887	36.3	7.1	2.41	0.90	0.90	25	0.338	87.9	88.3	469.3	2.5	3.5	48.6	53.8	23.1	0.13	0.0110
P27	1879	35.5	6.9	2.40	0.90	0.92	25	0.347	88.3	88.7	468.1	2.6	3.5	48.3	55.0	25.3	0.12	0.0106
P28	1887	36.8	7.2	2.42	0.90	0.91	25	0.334	87.1	87.7	471.0	2.5	3.5	48.4	53.9	19.7	0.12	0.0108
P29	1879	36.3	7.1	2.41	0.90	0.93	25	0.340	87.1	87.4	470.6	2.5	3.5	48.5	52.5	18.2	0.12	0.0106
P30	1883	35.7	7.0	2.39	0.90	0.96	25	0.341	87.7	87.6	470.0	2.5	3.5	48.0	52.2	17.3	0.11	0.0102
P31	1884	36.5	7.2	2.41	0.90	0.92	25	0.337	87.9	88.4	471.6	2.5	3.5	48.3	52.1	19.1	0.12	0.0107
P32	1886	35.8	7.0	2.42	0.90	0.90	25	0.344	88.2	88.5	473.9	2.5	3.5	48.4	54.5	17.6	0.13	0.0109
P33	1885	35.8	7.0	2.38	0.90	0.91	25	0.339	88.4	89.0	475.9	2.5	3.6	48.5	55.5	22.5	0.12	0.0107
P34	1882	36.4	7.1	2.35	0.90	0.87	25	0.330	88.6	89.1	477.1	2.5	3.5	48.5	54.9	26.6	0.13	0.0110
P35	1882	35.4	6.9	2.45	0.90	0.95	25	0.354	88.6	88.8	476.6	2.5	3.6	48.0	54.6	15.6	0.12	0.0106
Ref6	1882	35.9	7.0	2.38	0.90	0.90	25	0.339	87.7	89.0	490.6	2.5	3.5	48.3	54.9	24.7	0.12	0.0108

Engine Out Emissions														
Hydrocarbons			NO			CO2			CO			O2	H2S	SO2
[ppm]	[g/kW.hr]	[g/km]	[ppm]	[g/kW.hr]	[g/km]	[% vol]	[g/kW.hr]	[g/km]	[% vol]	[g/kW.hr]	[g/km]	[% vol]	[ppm]	[ppm]
1289	3.50	0.42	1571	14.13	1.68	14.6	1258.4	149.5	0.17	9.44	1.12	1.9	-	-
1005	2.75	0.32	1545	14.03	1.65	14.5	1262.1	148.0	0.14	7.74	0.91	1.9		
1043	2.83	0.34	1634	14.71	1.75	14.4	1238.9	147.2	0.14	7.85	0.93	1.9		
1039	2.81	0.32	1725	15.47	1.79	14.5	1243.0	143.5	0.16	8.73	1.01	1.9		
1025	2.66	0.32	1612	13.86	1.67	14.7	1205.9	145.1	0.20	10.29	1.24	1.9		
1094	2.84	0.34	1460	12.55	1.48	14.7	1212.8	143.3	0.16	8.37	0.99	2.0		
1124	2.82	0.33	1448	12.03	1.40	14.8	1179.2	137.6	0.17	8.42	0.98	2.0		
1178	3.05	0.36	1591	13.64	1.63	14.7	1205.0	143.6	0.19	9.65	1.15	1.9		
970	2.61	0.31	1465	13.09	1.53	14.7	1259.3	147.4	0.16	8.83	1.03	1.9	105	109
916	2.45	0.29	1441	12.74	1.49	14.6	1232.1	144.2	0.16	8.61	1.01	1.9	93	97
906	2.47	0.29	1539	13.93	1.65	14.4	1246.1	148.0	0.15	8.40	1.00	1.8	76	67
889	2.32	0.27	1592	13.78	1.59	15.0	1239.7	143.1	0.17	8.82	1.02	2.0	22	
1257	3.34	0.39	1673	14.75	1.73	14.7	1238.1	144.9	0.13	6.97	0.82	2.0	-	-

Atmospheric Conditions		
Barometric Pressure	Dry Bulb Temperature	Wet Bulb Temperature
[mBar]	[° C]	[° C]
1017.7	19.0	13.5
1002.9	20.0	13.5
1013.7	17.5	12.0
1010.0	18.0	12.0
1005.2	16.6	11.8
1003.5	16.0	13.0
1002.2	16.0	13.0
1012.2	17.0	14.0
1007.0	19.0	15.0
1005.7	19.5	15.0
1003.0	19.5	14.5
1001.1	19.0	14.0
1008.9	19.0	13.0

SABS Corrections		
Correction Factor	Corrected Torque	Corrected Power
[-]	[Nm]	[kW]
0.97	35.4	6.9
0.99	35.6	7.0
0.97	35.2	6.9
0.97	34.2	6.8
0.97	35.5	6.9
0.98	35.6	7.0
0.98	35.1	6.9
0.97	35.6	7.0
0.99	35.3	6.9
0.99	35.4	6.1
0.99	36.0	7.0
0.99	35.1	6.9
0.98	35.1	6.9

Sample	Engine Operating Point			Engine Operating Conditions							Racer Input Parameters				
	Speed	Torque	Racer File Name	Fuel Flow Rate	Equivalence Ratio	Ignition Timing	Manifold Pressure	Manifold Temperature	Droplet Temperature	Air Flow Rate	Charge Temperature	Cylinder Charge Mass	Re Reference Pressure	Air Fuel Ratio	Fuel Flow Rate
	[rev/min]	[Nm]	[-]	[kg/hr]	(calc) [-]	[° CA BTDC]	[kPa]	[° C]	[° C]	[kg/s]	[° C]	[kg]	[kPa]	[-]	[kg/s]
Ref5	1884	36.4	rf4sfc	*2.48*	0.91	25	49.5	54.4	22.1	0.01110	84.4	*0.0001878*	*47.94*	15.1	0.00069
P25	1878	36.0	P25sfc	2.43	0.90	25	49.0	54.9	29.4	0.01100	84.9	0.0001866	47.71	15.2	0.00067
P26	1887	36.3	P26sfc	2.41	0.90	25	48.6	53.8	23.1	0.01096	83.8	0.0001849	47.12	15.2	0.00067
P27	1879	35.5	P27sfc	2.40	0.90	25	48.3	55.0	25.3	0.01064	85.0	0.0001806	46.18	15.2	0.00067
P28	1887	36.8	P28sfc	2.42	0.90	25	48.4	53.9	19.7	0.01078	83.9	0.0001821	46.41	15.2	0.00067
P29	1879	36.3	P29sfc	2.41	0.90	25	48.5	52.5	18.2	0.01064	82.5	0.0001805	45.83	15.2	0.00067
P30	1883	35.7	P30sfc	2.39	0.90	25	48.0	52.2	17.3	0.01018	82.2	0.0001727	43.82	15.2	0.00066
P31	1884	36.5	P31sfc	2.41	0.90	25	48.3	52.1	19.1	0.01067	82.1	0.0001805	45.79	15.2	0.00067
P32	1886	35.8	P32sfc	2.42	0.90	25	48.4	54.5	17.6	0.01094	84.5	0.0001847	47.16	15.2	0.00067
P33	1885	35.8	P33sfc	2.38	0.90	25	48.5	55.5	22.5	0.01070	85.5	0.0001809	46.32	15.2	0.00066
P34	1882	36.4	P34sfc	2.35	0.90	25	48.5	54.9	26.6	0.01101	84.9	0.0001860	47.56	15.2	0.00065
P35	1882	35.4	P45sfc	2.45	0.90	25	48.0	54.6	15.6	0.01058	84.6	0.0001795	45.86	15.2	0.00068
Ref6	1882	35.9	rf5sfc	2.38	0.90	25	48.3	54.9	24.7	0.01077	84.9	0.0001821	46.56	15.2	0.00066

Sample	Pressure/CA results								Single Zone Model Results											
	IMEP	PMEP	IMEP(net)	Stability	Pressure		Rate of Pressure Rise		Heat Released			Gas Temperature		Induction Period			Burn Angle			
	[kPa]	[kPa]	[kPa]	[%]	Max [kPa]	CA [Max.] [° CA]	Max [kPa/°]	CA [Max.] [° CA]	Total [kJ]	Max. Rate [kJ/° CA]	CA [Max. Rate] [° CA]	Max [K]	CA [Max] [° CA]	2-98 [° CA]	5-95 [° CA]	10-90 [° CA]	2-98 [° CA]	5-95 [° CA]	10-90 [° CA]
Ref5	492.47	-59.87	432.6	10.4	1787	23	39.4	9	613.09	1052.34	18	3054.7	37	13.6	21.2	26.5	58.9	43	31.9
P25	480.03	-57.64	422.38	9.9	1813.3	22	42	8	598.45	1053.73	18	3017.4	36	13.3	20.8	25.9	57.1	41.5	30.1
P26	475.21	-56.83	418.39	12.1	1770.6	23	40.9	8	595.14	1014.75	18	3010.4	37	13.7	21.1	26.2	57.8	41.9	30.9
P27	473.12	-57.02	416.11	12.2	1790.3	22	42.5	8	593.51	1037.33	18	3102.7	36	13.4	20.8	25.9	58.5	43	31.9
P28	476.89	-58	418.89	10	1787.9	22	41.8	8	591.08	1040.82	18	3012.6	36	13.4	20.9	26	58.1	42.7	31.7
P29	461.95	-58.86	403.09	12.3	1638.4	23	34.7	7	570.69	939.29	19	2841.5	39	13.5	21.2	26.6	59.7	45.1	34
P30	464.91	-58.12	406.79	11.2	1726	22	40.4	7	577.57	987.8	17	3068.8	36	12.9	20.5	25.8	59.3	43.7	33.2
P31	475.68	-58.07	417.61	11.4	1843.3	21	46.5	7	592.9	1063.08	19	3158.5	35	12.9	20.2	25.2	56.3	41	29.9
P32	470.4	-57.9	412.5	12	1775	22	41.4	7	591.46	1020.66	17	3121.2	36	13	20.6	25.7	57	43	31.7
P33	466.6	-56.91	409.68	9.2	1731.8	23	38.7	8	593.21	999.55	18	3185.4	37	12.9	20.8	26.1	57.7	42.8	30.9
P34	475.5	-58.95	416.55	10.4	1844.1	22	46.1	8	590.13	1069.89	17	3092.3	34	13.4	20.7	25.6	57.1	40.6	29.7
P35	466.68	-59.68	407	9.6	1787.4	22	42.8	7	585.65	1015.08	18	3123.7	35	13.2	20.5	25.6	58.7	42	30.9
Ref6	-	-	-	-	-	-	-	-	-	-	-	-	-	-	-	-	-	-	-

Sample	Two Zone Model Results														Equilibrium Products Results - CO_2				
	Mass Transferred				Unburned Gas Temperature		Burned Gas Temperature		Induction Period			Burn Angle			End of Cycle	Exhaust Valve Open	End of Combustion	Maximum	Angle at Maximum
	Total [g]	Total % [%]	Max. Rate [g/° CA]	CA [Max. Rate] [° CA]	Max [K]	CA [Max] [° CA]	Max [K]	CA [Max] [° CA]	2-98 [° CA]	5-95 [° CA]	10-90 [° CA]	2-98 [° CA]	5-95 [° CA]	10-90 [° CA]	[% vol]	[% vol]	[% vol]	[% vol]	[° CA]
Ref5	0.219	116.87	0.419905	19	736.01	17	2562.25	-22	13.9	21.6	27	59.2	41.7	30.8	11.6	14.0	14.0	14.2	98
P25	0.216	115.93	0.426883	18	741.21	16.5	2551.2	-22	13.7	21.2	26.3	52.5	39.4	29.9	11.1	13.4	13.7	13.8	76
P26	0.214	115.85	0.408733	18	738.41	16.5	2552.76	-22	14	21.5	26.6	54.3	40.2	31	11.1	13.4	13.8	13.8	77
P27	0.208	115.1	0.412193	18	741.16	16.5	2568.06	-22	13.6	21.1	26.3	54	40.5	30.2	11.4	13.7	14.0	14.1	76
P28	0.211	115.89	0.416668	18	738.66	16.5	2562.14	-22	13.7	21.2	26.4	54.6	41.1	29.1	11.5	13.8	14.0	14.0	81
P29	0.207	114.72	0.371014	19	725.24	17	2567.42	-22	13.9	21.7	27.1	69.2	46.9	34.5	11.7	13.9	13.8	14.1	113
P30	0.201	116.12	0.385503	17	734.08	16	2586.18	-22	12.9	20.8	26.1	62.5	43.4	30.3	12.1	14.4	14.4	14.6	104
P31	0.207	114.82	0.42207	16	746.56	16	2564.69	-22	13.2	20.6	25.6	51.8	39.2	28.5	11.5	13.7	13.9	14.0	80
P32	0.211	114.13	0.411957	17	746.02	16.5	2547.39	-22	13.6	21.1	26.2	55.3	40.4	29.6	11.1	13.3	13.5	13.6	70
P33	0.209	115.58	0.401202	18	743.04	16.5	2554.78	-22	13.3	21.2	26.5	53.3	40.1	30.5	11.1	13.3	13.8	13.9	66
P34	0.219	118	0.444401	17	751.25	16.5	2524.21	-22	14.2	21.4	26.2	57.7	38.6	29.5	11.1	13.4	13.4	13.6	104
P35	0.202	112.68	0.397592	18	739.8	16	2582.75	-22	13.4	20.8	25.9	53.8	40.3	30.1	11.6	13.8	14.0	14.1	101
Ref6	-	-	-	-	-	-	-	-	-	-	-	-	-	-	-	-	-	-	-

Sample	Equilibrium Products Results - CO					Equilibrium Products Results - O_2					Equilibrium Products Results - NO							
	End of Cycle	Exhaust Valve Open	End of Combustion	Maximum	Angle at Maximum	End of Cycle	Exhaust Valve Open	End of Combustion	Minimum	Angle at Minimum	End of Cycle	Exhaust Valve Open	End of Combustion	Max Burned Gas Temp	Maximum	Angle at Maximum	Burned Gas Temp=2000k	Angle at Burned Gas Temp=2000k
	[% vol]	[% vol]	[% vol]	[% vol]	[° CA]	[% vol]	[% vol]	[% vol]	[% vol]	[° CA]	[% vol]	[% vol]	[% vol]	[% vol]	[% vol]	[° CA]	[% vol]	[° CA]
Ref5	0.0	0.0	0.0	0.6	25	2.7	-1.0	-1.2	-1.3	94	0.001	0.022	0.235	0.003	0.588	29	0.261	59
P25	0.0	0.0	0.0	0.5	24	3.4	-0.1	-0.8	-0.8	63	0.000	0.016	0.250	0.002	0.626	28	0.281	56
P26	0.0	0.0	0.0	0.5	24	3.4	-0.1	-0.8	-0.8	64	0.000	0.017	0.240	0.002	0.610	29	0.280	57
P27	0.0	0.0	0.0	0.7	24	3.0	-0.5	-1.3	-1.3	66	0.000	0.014	0.213	0.002	0.579	28	0.240	58
P28	0.0	0.0	0.0	0.6	24	2.8	-0.7	-1.1	-1.2	65	0.000	0.017	0.234	0.002	0.598	28	0.261	57
P29	0.0	0.0	0.0	0.6	26	2.6	-1.0	-0.9	-1.2	113	0.001	0.023	0.218	0.002	0.526	30	0.234	60
P30	0.0	0.0	0.1	0.8	25	1.9	-1.7	-1.8	-2.1	103	0.000	0.017	0.187	0.002	0.513	27	0.202	59
P31	0.0	0.0	0.0	0.7	23	2.8	-0.6	-1.1	-1.2	65	0.000	0.015	0.232	0.002	0.595	27	0.241	57
P32	0.0	0.0	0.0	0.5	24	3.5	0.1	-0.5	-0.5	69	0.000	0.017	0.260	0.003	0.610	28	0.278	56
P33	0.0	0.0	0.0	0.5	25	3.4	0.0	-1.0	-1.0	52	0.000	0.015	0.260	0.002	0.605	29	0.270	58
P34	0.0	0.0	0.0	0.4	22	3.4	0.0	-0.3	-0.4	81	0.000	0.020	0.262	0.003	0.684	27	0.319	54
P35	0.0	0.0	0.0	0.8	24	2.7	-0.8	-1.1	-1.2	85	0.000	0.015	0.188	0.002	0.534	27	0.210	58
Ref6	-	-	-	-	-	-	-	-	-	-	-	-	-	-	-	-	-	-

Engine - 4A-FE, Load Point - 80 km/hr

Sample	Engine Operating Point			Engine Operating Conditions														
	Speed	Torque	Power	Fuel Flow Rate	Equivalence Ratio	Equivalence Ratio	Ignition Timing	BSFC	Water Temperature	Oil Temperature	Exhaust Temperature	Fuel Temperature	Fuel Pressure	Oil Pressure	Manifold Pressure	Manifold Temperature	Air Flow Rate	Air Flow Rate
	[rev/min]	[Nm]	[kW]	[kg/hr]	(calc) [-]	(meas) [-]	[° CA BTDC]	[kg/kW.hr]	[° C]	[° C]	[° C]	[° C]	[bar]	[bar]	[kPa]	[° C]	[mbar]	[kg/s]
Ref1	2499	48.9	12.8	3.9	0.97	0.97	24	0.304	89.0	90.4	599.4	15.1	2.7	3.8	56.9	44.8	0.28	0.016
P1	2498	48.9	12.8	4.0	0.89	0.91	24	0.313	89.1	92.4	602.6	15.5	2.7	3.9	59.8	42.8	0.34	0.018
P2	2504	48.9	12.8	3.4	0.96	0.81	24	0.265	89.7	97.2	619.8	18.2	2.7	4.2	58.5	47.9	0.31	0.017
P3	2502	49.2	12.9	3.8	0.95	0.89	24	0.298	89.6	95.2	617.6	17.4	2.7	4.1	58.4	47.4	0.33	0.018
P4	2504	48.8	12.8	3.9	0.96	0.92	24	0.306	89.4	95.3	618.7	18.9	2.7	4.2	58.3	49.1	0.32	0.017
P5	2497	49.5	12.9	4.0	0.96	0.92	24	0.306	89.6	96.8	618.1	21.9	2.7	4.1	58.6	50.4	0.33	0.018
P6	2505	49.1	12.9	4.0	0.96	0.91	24	0.309	89.8	97.3	620.1	21.8	2.7	4.1	58.7	50.4	0.34	0.018
P7	2500	49.0	12.8	3.8	0.96	0.89	25	0.296	89.2	97.0	620.2	15.1	2.7	4.1	57.8	46.8	0.32	0.017
P8	2499	49.0	12.8	3.8	0.95	0.88	24	0.298	89.3	96.9	620.5	20.8	2.7	4.2	58.3	49.5	0.33	0.018
P9	2505	48.9	12.8	4.0	0.97	0.93	24	0.314	90.0	95.1	613.8	21.4	2.7	4.1	58.0	49.7	0.33	0.018
P10	2506	49.0	12.9	3.9	0.96	0.93	24	0.307	89.7	98.0	621.8	22.5	2.7	4.2	58.6	49.4	0.32	0.017
P11	2502	49.0	12.8	3.9	0.96	0.88	24	0.303	90.1	96.7	611.6	27.3	2.7	4.1	58.5	54.3	0.35	0.018
Ref2	2504	48.6	12.8	4.0	0.97	0.95	24	0.313	89.6	97.8	620.8	23.6	2.7	4.3	58.4	50.7	0.31	0.017

Engine Out Emissions												Atmospheric Conditions			SABS Corrections		
Hydrocarbons			NO			CO2			CO			O2	Barometric Pressure	Dry Bulb Temperature	Wet Bulb Temperature	Correction Factor	Corrected Torque	Corrected Power
[ppm]	[g/kW.hr]	[g/km]	[ppm]	[g/kW.hr]	[g/km]	[% vol]	[g/kW.hr]	[g/km]	[% vol]	[g/kW.hr]	[g/km]	[% vol]	[mBar]	[° C]	[° C]	[-]	[Nm]	[kW]
2004	4.60	0.74	>2000	15.23	2.44	14.4	1048.4	167.7	0.4	20.78	3.32	1.3	1003.5	18.0	11.0	0.98	47.9	12.5
1194	3.08	0.49	>2000	17.09	2.73	13.2	1082.2	173.1	0.2	8.79	1.41	2.6	1012.9	18.5	14.0	0.98	47.7	12.5
1916	4.68	0.75	>2000	16.19	2.59	13.8	1071.0	171.6	0.4	21.09	3.38	1.4	1009.1	21.0	15.5	0.99	48.2	12.6
1351	3.34	0.54	>2000	16.39	2.64	14.2	1114.1	179.5	0.3	15.53	2.50	1.5	1007.4	19.0	14.5	0.98	48.4	12.7
1656	4.08	0.65	>2000	16.35	2.61	14.2	1109.3	177.4	0.3	16.99	2.72	1.4	1010.9	21.0	15.5	0.98	48.0	12.6
1859	4.58	0.74	>2000	16.34	2.64	14.2	1111.4	179.7	0.4	21.39	3.46	1.3	1006.2	21.5	16.0	0.99	49.0	12.8
1989	5.04	0.81	>2000	16.80	2.70	14.0	1126.9	181.3	0.4	19.01	3.06	1.4	1005.1	22.0	18.0	1.00	49.0	12.8
1471	3.63	0.58	>2000	16.37	2.62	14.2	1110.7	177.9	0.4	20.71	3.32	1.3	1013.5	19.0	12.5	0.97	47.6	12.5
2130	5.32	0.85	>2000	16.58	2.66	14.0	1113.0	178.3	0.3	15.79	2.53	1.5	1004.4	20.0	14.5	0.99	48.4	12.7
2354	5.83	0.93	>2000	16.41	2.63	14.3	1120.1	179.4	0.5	25.13	4.03	1.3	1002.8	21.0	16.0	0.99	48.6	12.7
2068	5.11	0.82	>2000	16.39	2.64	14.0	1099.0	176.7	0.4	19.08	3.07	1.4	1007.6	20.0	15.0	0.99	48.3	12.7
2197	5.56	0.89	>2000	16.77	2.69	14.3	1143.6	183.5	0.4	18.17	2.91	1.3	1002.8	25.0	16.5	1.00	49.0	12.8
2123	5.25	0.84	>2000	16.38	2.61	13.9	1089.0	173.6	0.5	24.48	3.90	1.3	1007.0	20.0	16.0	0.99	48.1	12.6

Engine - 4A-FE, Load Point - 100 km/hr

Sample	Engine Operating Point			Engine Operating Conditions														
	Speed	Torque	Power	Fuel Flow Rate	Equivalence Ratio	Equivalence Ratio	Ignition Timing	BSFC	Water Temperature	Oil Temperature	Exhaust Temperature	Fuel Temperature	Fuel Pressure	Oil Pressure	Manifold Pressure	Manifold Temperature	Air Flow Rate	Air Flow Rate
	[rev/min]	[Nm]	[kW]	[kg/hr]	(calc) [-]	(meas) [-]	[° CA BTDC]	[kg/kW.hr]	[° C]	[° C]	[° C]	[° C]	[bar]	[bar]	[kPa]	[° C]	[mbar]	[kg/s]
Ref1	3128	54.8	18.0	5.6	1.05	1.07	26	0.311	88.5	99.0	664.2	11.4	2.7	4.1	60.6	37.4	0.49	0.021
P1	3131	55.7	18.2	5.5	0.97	1.00	26	0.303	88.9	100.6	676.5	12.9	2.7	4.4	62.2	33.6	0.54	0.023
P2	3132	55.4	18.2	5.2	1.04	0.96	26	0.288	88.9	101.7	679.9	15.1	2.7	4.4	62.1	38.5	0.53	0.022
P3	3128	55.3	18.1	5.5	1.04	1.01	26	0.303	88.9	102.5	674.7	14.1	2.7	4.4	61.5	37.9	0.53	0.022
P4	3130	55.1	18.1	5.5	1.04	1.00	26	0.302	88.9	102.7	677.6	12.7	2.7	4.4	61.7	41.6	0.53	0.022
P5	3131	54.8	18.0	5.6	1.04	1.01	26	0.311	88.9	102.6	678.2	14.6	2.7	4.4	61.5	40.7	0.55	0.023
P6	3131	55.4	18.2	5.6	1.03	1.00	26	0.308	89.3	102.9	686.3	16.8	2.7	4.4	62.5	41.6	0.57	0.023
P7	3132	55.3	18.2	5.6	1.04	1.04	26	0.306	88.4	101.8	677.7	11.0	2.7	4.4	61.4	37.7	0.51	0.022
P8	3131	55.4	18.2	5.5	1.04	0.99	26	0.303	89.0	102.3	685.9	14.1	2.7	4.3	61.9	39.9	0.55	0.023
P9	3129	55.2	18.1	5.5	1.04	1.00	26	0.306	88.9	102.2	684.6	14.5	2.7	4.4	62.0	41.2	0.55	0.023
P10	3132	55.2	18.1	5.7	1.05	1.03	27	0.314	89.0	102.5	680.1	16.9	2.8	4.4	62.0	41.0	0.54	0.022
P11	3130	55.2	18.1	5.7	1.04	1.01	27	0.315	89.1	104.9	686.5	20.7	2.7	4.3	62.5	45.5	0.58	0.023
Ref2	3130	55.7	18.3	5.8	1.04	1.06	26	0.316	88.6	103.5	685.2	13.4	2.7	4.3	62.6	40.2	0.53	0.022

Engine Out Emissions													Atmospheric Conditions			SABS Corrections		
Hydrocarbons			NO			CO2			CO			O2	Barometric Pressure	Dry Bulb Temperature	Wet Bulb Temperature	Correction Factor	Corrected Torque	Corrected Power
[ppm]	[g/kW.hr]	[g/km]	[ppm]	[g/kW.hr]	[g/km]	[% vol]	[g/kW.hr]	[g/km]	[% vol]	[g/kW.hr]	[g/km]	[% vol]	[mBar]	[° C]	[° C]	[-]	[Nm]	[kW]
2053	4.47	0.80	>2000	14.43	2.59	14.0	966.2	173.5	1.9	85.46	15.35	0.5	1003.5	18.0	11.0	0.98	53.7	17.6
1411	3.23	0.59	>2000	15.20	2.77	14.3	1037.8	189.4	0.4	19.45	3.55	1.0	1012.9	18.5	14.0	0.98	54.3	17.8
2236	5.09	0.92	>2000	15.08	2.74	13.7	986.5	179.1	1.6	75.20	13.65	0.5	1009.1	21.0	15.5	0.99	54.6	17.9
1724	3.87	0.70	>2000	14.88	2.70	14.1	1005.1	182.0	1.6	74.16	13.43	0.4	1007.4	19.0	14.5	0.98	54.4	17.8
1929	4.36	0.79	>2000	14.99	2.71	13.9	1000.0	180.8	1.7	77.87	14.07	0.5	1010.9	21.0	15.5	0.98	54.2	17.8
2022	4.66	0.84	>2000	15.30	2.75	13.9	1019.1	182.9	1.8	81.63	14.66	0.5	1006.2	21.5	16.0	0.99	54.3	17.8
2103	4.90	0.89	>2000	15.46	2.81	14.0	1033.5	187.8	1.4	67.20	12.21	0.5	1005.1	22.0	18.0	1.00	55.3	18.1
1996	4.44	0.81	>2000	14.74	2.68	13.9	979.8	177.8	1.8	79.48	14.43	0.5	1013.5	19.0	12.5	0.97	53.8	17.6
2216	5.08	0.92	>2000	15.20	2.76	13.9	1010.5	183.5	1.6	74.38	13.51	0.5	1004.4	20.0	14.5	0.99	54.7	17.9
2286	5.19	0.94	>2000	15.07	2.72	14.0	1012.0	182.9	1.7	77.31	13.97	0.6	1002.8	21.0	16.0	0.99	54.8	18.0
2324	5.35	0.97	>2000	15.27	2.77	13.7	999.6	181.1	1.8	85.20	15.44	0.5	1007.6	20.0	15.0	0.99	54.4	17.9
2347	5.47	0.99	>2000	15.46	2.79	14.0	1034.2	187.0	1.7	78.06	14.12	0.5	1002.8	25.0	16.5	1.00	55.2	18.1
2362	5.36	0.98	>2000	15.04	2.75	13.6	981.3	179.1	1.8	82.93	15.14	0.5	1007.0	20.0	16.0	0.99	55.0	18.0

Engine - 4A-FE, Load Point - 120 km/hr

Sample	Engine Operating Point			Engine Operating Conditions														
	Speed	Torque	Power	Fuel Flow Rate	Equivalence Ratio	Equivalence Ratio	Ignition Timing	BSFC	Water Temperature	Oil Temperature	Exhaust Temperature	Fuel Temperature	Fuel Pressure	Oil Pressure	Manifold Pressure	Manifold Temperature	Air Flow Rate	Air Flow Rate
	[rev/min]	[Nm]	[kW]	[kg/hr]	(calc) [-]	(meas) [-]	[° CA BTDC]	[kg/kW.hr]	[° C]	[° C]	[° C]	[° C]	[bar]	[bar]	[kPa]	[° C]	[mbar]	[kg/s]
Ref1	3761	71.9	28.3	8.2	1.04	1.04	22	0.289	88.8	108.9	755.5	12.7	2.8	4.2	71.9	30.5	1.11	0.032
P1	3762	72.3	28.5	8.2	0.97	1.01	22	0.286	89.2	107.9	765.1	12.8	2.8	4.3	73.0	27.7	1.14	0.033
P2	3756	72.4	28.5	8.0	1.03	1.00	22	0.281	89.4	111.0	769.5	16.3	2.8	4.2	73.1	31.4	1.13	0.033
P3	3758	72.0	28.3	8.0	1.03	1.02	22	0.284	89.2	110.0	761.4	15.4	2.8	4.2	72.2	29.9	1.11	0.032
P4	3760	72.8	28.7	8.0	1.03	1.01	22	0.281	89.1	110.1	763.9	13.9	2.8	4.2	72.9	31.2	1.13	0.033
P5	3758	72.4	28.5	8.1	1.04	1.01	22	0.285	88.6	110.3	766.1	15.1	2.8	4.3	72.8	32.3	1.15	0.033
P6	3758	72.2	28.4	8.2	1.03	1.00	22	0.287	88.7	110.3	771.8	17.1	2.8	4.3	73.4	33.4	1.19	0.033
P7	3758	72.6	28.6	8.1	1.04	1.02	22	0.282	88.7	109.7	762.8	12.1	2.8	4.3	72.1	27.4	1.11	0.032
P8	3759	72.5	28.5	8.2	1.03	1.02	22	0.286	88.8	109.9	773.6	14.6	2.8	4.3	72.7	31.2	1.15	0.033
P9	3760	72.1	28.4	8.2	1.03	1.02	22	0.288	89.1	110.3	772.3	15.3	2.8	4.3	72.8	32.0	1.16	0.033
P10	3762	72.2	28.4	8.1	1.03	1.01	22	0.285	89.1	110.6	772.8	17.7	2.8	4.2	73.1	32.1	1.15	0.033
P11	3764	72.1	28.4	8.2	1.03	1.02	22	0.290	89.8	112.3	778.2	17.6	2.8	4.3	73.5	36.0	1.19	0.033
Ref2	3756	72.2	28.4	8.2	1.03	1.02	22	0.289	89.2	111.0	774.3	14.6	2.8	4.1	73.5	31.9	1.15	0.033

Engine Out Emissions													Atmospheric Conditions			SABS Corrections		
Hydrocarbons			NO			CO2			CO			O2	Barometric Pressure	Dry Bulb Temperature	Wet Bulb Temperature	Correction Factor	Corrected Torque	Corrected Power
[ppm]	[g/kW.hr]	[g/km]	[ppm]	[g/kW.hr]	[g/km]	[% vol]	[g/kW.hr]	[g/km]	[% vol]	[g/kW.hr]	[g/km]	[% vol]	[mBar]	[° C]	[° C]	[-]	[Nm]	[kW]
1605	3.32	0.78	>2000	13.70	3.24	14.3	934.6	220.6	1.6	67.5	15.9	0.4	1003.5	18.0	11.0	0.98	70.5	27.8
1007	2.15	0.51	>2000	14.18	3.36	14.3	971.6	230.5	0.4	17.6	4.2	0.9	1012.9	18.5	14.0	0.98	70.5	27.8
1743	3.71	0.88	>2000	14.10	3.35	13.8	933.4	221.6	1.5	63.7	15.1	0.4	1009.1	21.0	15.5	0.99	71.4	28.1
1385	2.87	0.68	>2000	13.75	3.25	14.3	942.2	222.5	1.4	57.1	13.5	0.4	1007.4	19.0	14.5	0.98	70.8	27.9
1544	3.21	0.77	>2000	13.80	3.30	14.1	933.2	222.8	1.5	64.8	15.5	0.4	1010.9	21.0	15.5	0.98	71.6	28.2
1607	3.38	0.80	>2000	13.94	3.31	14.1	941.3	223.5	1.6	68.1	16.2	0.4	1006.2	21.5	16.0	0.99	71.8	28.2
1699	3.67	0.87	>2000	14.33	3.39	14.0	959.4	227.2	1.5	64.7	15.3	0.4	1005.1	22.0	18.0	1.00	72.0	28.4
1646	3.42	0.81	>2000	13.79	3.28	14.0	926.7	220.6	1.6	67.7	16.1	0.4	1013.5	19.0	12.5	0.97	70.6	27.8
1752	3.69	0.88	>2000	13.97	3.32	14.1	944.2	224.5	1.4	58.7	14.0	0.5	1004.4	20.0	14.5	0.99	71.6	28.2
1824	3.84	0.91	>2000	13.95	3.30	14.2	946.6	223.9	1.6	66.7	15.8	0.5	1002.8	21.0	16.0	0.99	71.7	28.2
1763	3.75	0.89	>2000	14.11	3.34	14.0	946.1	224.2	1.4	62.0	14.7	0.4	1007.6	20.0	15.0	0.99	71.1	28.0
1814	3.85	0.91	>2000	14.07	3.33	14.2	956.8	226.5	1.5	63.0	14.9	0.4	1002.8	25.0	16.5	1.00	72.1	28.4
1809	3.86	0.91	>2000	14.15	3.35	13.9	944.1	223.5	1.5	64.4	15.2	0.4	1007.0	20.0	16.0	0.99	71.4	28.1

Sample	Engine Operating Point			Engine Operating Conditions														
	Speed	Torque	Power	Fuel Flow Rate	Equivalence Ratio	Equivalence Ratio	Ignition Timing	BSFC	Water Temperature	Oil Temperature	Exhaust Temperature	Fuel Pressure	Oil Pressure	Manifold Pressure	Manifold Temperature	Droplet Temperature	Air Flow Rate	Air Flow Rate
	[rev/min]	[Nm]	[kW]	[kg/hr]	(calc) [-]	(meas) [-]	[° CA BTDC]	[kg/kW.hr]	[° C]	[° C]	[° C]	[bar]	[bar]	[kPa]	[° C]	[° C]	[mbar]	[kg/s]
Ref3	3762	73.6	29.0	8.01	0.98	1.00	22	0.277	89.7	110.4	740.8	2.8	4.4	69.6	34.1	12.3	1.14	0.033
P12	3761	71.4	27.9	7.81	0.98	1.01	22	0.280	89.2	107.4	729.8	4.3	2.8	67.6	31.8	10.4	1.05	0.032
P13	3764	71.9	28.1	7.92	0.99	1.02	22	0.281	89.9	111.4	744.5	2.8	3.9	68.2	34.0	15.9	1.07	0.032
P14	3759	73.0	28.5	8.07	0.93	1.01	22	0.283	89.3	109.1	733.0	2.8	4.3	69.5	30.8	10.5	1.13	0.033
P15	3762	72.9	28.5	8.23	0.94	1.03	22	0.288	89.6	110.5	740.3	2.8	4.4	69.7	32.6	13.0	1.14	0.033
P16	3760	72.6	28.4	8.12	0.98	1.03	22	0.286	89.8	109.9	743.6	2.8	4.2	68.7	33.8	14.4	1.11	0.032
P17	3758	73.7	28.8	8.17	0.98	1.03	22	0.284	89.7	110.7	744.9	2.8	4.3	69.6	35.1	16.3	1.13	0.032
P18	3758	72.6	28.4	7.98	0.99	1.02	22	0.281	90.8	111.2	738.4	4.4	2.8	69.0	36.8	14.4	1.11	0.032
P19	3765	72.8	28.5	8.05	0.99	1.03	22	0.282	90.2	109.7	737.4	2.9	4.3	68.6	35.8	16.5	1.10	0.032
P20	3761	71.6	28.0	7.88	0.98	1.02	22	0.281	90.0	108.5	734.5	2.8	4.2	68.0	34.6	12.3	1.08	0.032
P21	3759	71.6	28.0	7.89	0.97	1.01	22	0.282	89.4	108.1	735.9	2.8	4.2	68.2	34.3	12.0	1.09	0.032
P22	3759	71.8	28.1	7.93	0.99	1.03	22	0.282	89.7	109.1	733.6	2.8	4.1	67.7	34.8	11.9	1.06	0.031
P23	3758	71.7	28.0	7.85	0.98	1.01	22	0.280	90.0	110.2	739.2	2.8	4.2	68.1	36.5	12.1	1.08	0.032
P24	3760	72.6	28.4	8.36	0.93	1.05	22	0.295	89.8	108.7	731.4	2.8	4.4	69.7	34.9	10.1	1.15	0.033
Ref4	3762	72.2	28.2	7.88	0.98	1.00	22	0.279	89.6	108.4	736.6	2.8	4.3	68.6	35.2	12.9	1.11	0.032

Engine Out Emissions															Atmospheric Conditions			SABS Corrections		
Hydrocarbons			NO			CO2			CO			O2	H2S	SO2	Barometric Pressure	Dry Bulb Temperature	Wet Bulb Temperature	Correction Factor	Corrected Torque	Corrected Power
[ppm]	[g/kW.hr]	[g/km]	[ppm]	[g/kW.hr]	[g/km]	[% vol]	[g/kW.hr]	[g/km]	[% vol]	[g/kW.hr]	[g/km]	[% vol]	[ppm]	[ppm]	[mBar]	[° C]	[° C]	[-]	[Nm]	[kW]
1196	2.46	0.59	>2000	13.64	3.29	14.5	948.7	229.2	0.7	28.32	6.84	0.7	-	-	1014.0	18.0	15.5	0.98	72.1	28.3
1128	2.32	0.54	>2000	13.66	3.18	14.4	943.0	219.4	0.7	28.74	6.69	0.7	-	-	1014.3	18.0	13.4	0.97	67.4	26.4
1101	2.27	0.53	>2000	13.69	3.21	14.4	942.8	221.1	0.8	32.46	7.61	0.6	-	-	1010.2	21.0	14.9	0.99	70.6	27.6
753	1.59	0.38	>2000	14.00	3.33	14.1	946.4	225.0	0.3	11.08	2.63	1.4	-	-	1007.0	19.1	12.9	0.98	71.4	27.9
767	1.63	0.39	>2000	14.11	3.36	14.1	954.5	227.0	0.3	12.22	2.90	1.2	-	-	1006.5	21.6	14.0	0.99	71.8	28.1
1038	2.01	0.48	>2000	12.87	3.04	15.6	959.8	227.0	0.7	26.88	6.36	0.8	-	-	1001.2	19.9	14.1	0.94	67.8	28.2
1103	2.23	0.54	>2000	13.41	3.22	14.7	943.7	226.5	0.7	29.53	7.09	0.7	-	-	1006.5	22.3	14.3	0.99	71.4	28.4
1075	2.25	0.53	>2000	13.86	3.28	14.3	945.6	223.7	0.7	29.74	7.03	0.7	-	-	1007.1	21.9	14.9	0.99	71.8	27.5
1113	2.19	0.52	>2000	13.07	3.11	15.2	948.3	225.4	0.8	30.82	7.33	0.6	-	-	1005.6	22.0	14.0	0.99	72.0	28.2
1002	2.00	0.47	>2000	13.26	3.09	15.1	955.1	222.8	0.7	27.00	6.30	0.7	-	-	1005.8	22.9	15.2	0.99	71.0	27.8
976	1.96	0.46	>2000	13.33	3.11	15.0	958.9	223.6	0.6	23.70	5.53	0.8	-	-	1005.6	23.0	16.1	0.99	71.1	27.8
1048	2.08	0.49	>2000	13.15	3.08	15.0	944.8	221.1	0.7	28.58	6.69	0.7	-	-	1005.8	21.4	13.7	0.99	70.9	27.7
979	1.96	0.46	>2000	13.29	3.10	15.0	955.2	223.1	0.6	25.44	5.94	0.7	-	-	1004.5	23.1	14.9	0.99	71.2	27.8
759	1.57	0.37	>2000	13.68	3.23	14.8	970.0	229.4	0.2	8.26	1.95	1.3	-	-	1003.8	22.4	16.8	1.00	71.9	28.1
1071	2.14	0.50	>2000	13.26	3.12	15.2	960.8	226.1	0.6	23.24	5.47	0.7	-	-	1002.8	23.9	16.3	1.00	72.1	28.2

Sample	Engine Operating Point			Engine Operating Conditions							Racer Input Parameters				
	Speed	Torque	Racer File Name	Fuel Flow Rate	Equivalence Ratio	Ignition Timing	Manifold Pressure	Manifold Temperature	Droplet Temperature	Air Flow Rate	Charge Temperature	Cylinder Charge Mass	Re Reference Pressure	Air Fuel Ratio	Fuel Flow Rate
	[rev/min]	[Nm]	[-]	[kg/hr]	(calc) [-]	[° CA BTDC]	[kPa]	[° C]	[° C]	[kg/s]	[° C]	[kg]	[kPa]	[-]	[kg/s]
Ref3	3762	73.6	ra122106	*8.01*	0.98	22	69.6	34.1	12.3	0.03288	64.1	*0.0002799*	*67.41*	14.0	0.00223
P12	3761	71.4	P12-120	7.81	0.98	22	67.6	31.8	10.4	0.03150	61.8	0.0002686	64.23	14.0	0.00217
P13	3764	71.9	P13-120a	7.92	0.99	22	68.2	34.0	15.9	0.03170	64.0	0.0002702	65.04	13.8	0.00220
P14	3759	73.0	P14-120b	8.07	0.93	22	69.5	30.8	10.5	0.03260	60.8	0.0002780	66.29	14.7	0.00224
P15	3762	72.9	P15-120b	8.23	0.94	22	69.7	32.6	13.0	0.03263	62.6	0.0002785	66.77	14.6	0.00228
P16	3760	72.6	P16120b	8.12	0.98	22	68.7	33.8	14.4	0.03211	63.8	0.0002742	65.96	14.0	0.00226
P17	3758	73.7	P17-120b	8.17	0.98	22	69.6	35.1	16.3	0.03237	65.1	0.0002765	66.77	13.9	0.00227
P18	3758	72.6	P18-120c	7.98	0.99	22	69.0	36.8	14.4	0.03207	66.8	0.0002738	66.46	13.9	0.00222
P19	3765	72.8	P19-120	8.05	0.99	22	68.6	35.8	16.5	0.03201	65.8	0.0002728	66.04	13.9	0.00223
P20	3761	71.6	P20-120a	7.88	0.98	22	68.0	34.6	12.3	0.03167	64.6	0.0002700	65.13	14.0	0.00219
P21	3759	71.6	P21-120a	7.89	0.97	22	68.2	34.3	12.0	0.03179	64.3	0.0002712	65.35	14.1	0.00219
P22	3759	71.8	P22-120a	7.93	0.99	22	67.7	34.8	11.9	0.03140	64.8	0.0002681	64.71	13.9	0.00220
P23	3758	71.7	P23-120a	7.85	0.98	22	68.1	36.5	12.1	0.03164	66.5	0.0002700	65.48	14.0	0.00218
P24	3760	72.6	P24-120b	8.36	0.93	22	69.7	34.9	10.1	0.03264	64.9	0.0002789	67.33	14.7	0.00232
Ref4	3762	72.2	rf3-120a	7.88	0.98	22	68.6	35.2	12.9	0.03205	65.2	0.0002731	65.98	14.0	0.00219

Sample	Pressure/CA results								Single Zone Model Results									
	IMEP	PMEP	IMEP(net)	Stability	Pressure		Rate of Pressure Rise		Heat Released			Gas Temperature	Induction Period			Burn Angle		
	[kPa]	[kPa]	[kPa]	[%]	Max [kPa]	CA [Max.] [° CA]	Max [kPa/°]	CA [Max.] [° CA]	Total [kJ]	Max. Rate [kJ/° CA]	CA [Max. Rate] [° CA]	Max [K]	CA [Max] [° CA]	2-98 [° CA]	5-95 [° CA]	10-90 [° CA]	2-98 [° CA]	5-95 [° CA]	10-90 [° CA]
Ref3	898.86	-64.59	834.27	9.7	3710	18	151.7	7	1023.5	2431.27	10	3174.3	28	10.9	16.7	20.6	43.3	33.3	24
P12	866.44	-63.56	802.88	10.5	3624.2	18	149.9	7	1021.2	2577.14	12	3501.5	28	10.9	16.8	20.7	42.9	32	22.3
P13	873.27	-63.19	810.08	11.7	3546.2	18	140.6	8	1006.16	2353.25	11	3168	29	11.1	17.1	21.1	45.5	33.4	24.1
P14	868.66	-64.79	803.87	12.4	3435.8	19	129.4	8	998.25	2266.96	12	3127.3	31	11.2	17.4	21.6	45.9	33.7	24.4
P15	880.39	-65.77	814.62	11.2	3477.8	19	133.3	8	1004.28	2362.56	12	3073	30	11.3	17.7	21.9	47.5	33.4	24.2
P16	866.71	-68.8	797.91	11.5	3521.3	18	137.3	7	979.68	2312.22	11	2898.8	29	11.8	17.4	21.4	48	33.8	25.2
P17	870.67	-64.72	805.95	11.6	3479.1	19	133.6	8	1001.94	2301.9	11	3120	30	11.1	17.3	21.5	45.1	34.6	25
P18	880.17	-63.89	816.28	11.2	3526.3	19	139.5	8	1003.08	2360.07	11	3077.9	30	11.4	17.5	21.6	44.8	32.6	25.2
P19	881.63	-64.69	816.94	11.1	3580.6	18	143.5	7	1014.66	2349.36	10	3247.2	29	11.1	17	21	44.1	33.9	24.5
P20	877.05	-64.14	812.91	9.6	3523.6	19	136.3	8	1030.08	2458.47	14	3483	30	11	17.2	21.4	45.1	32.9	25.6
P21	877.01	-63.85	813.16	12.2	3494.5	19	135.3	7	1024.68	2374.65	14	3354.5	30	11.1	17.2	21.4	46.4	34.3	25.1
P22	873.69	-64.59	809.09	11.1	3515.6	19	139.2	7	1007.05	2315.27	11	3271.2	30	11.3	17.2	21.3	45.6	33.4	24
P23	873.15	-63.45	809.7	11.9	3486.1	19	135.2	7	1012.17	2284.25	11	3321.3	30	11.1	17.1	21.3	46.7	34.6	25.3
P24	875.99	-62.88	813.11	12.4	3461.3	19	129.6	8	1014.35	2241.61	11	3187.2	31	11	17.3	21.5	47.9	35.6	26.3
Ref4	871.94	-63.31	808.63	10.6	3471.5	19	131.3	8	1010.95	2261.49	11	3244.6	30	10.9	17.1	21.3	46.8	34.5	25.2

Sample	Two Zone Model Results														Equilibrium Products Results - CO_2				
	Mass Transferred				Unburned Gas Temperature		Burned Gas Temperature		Induction Period			Burn Angle			End of Cycle	Exhaust Valve Open	End of Combustion	Maximum	Angle at Maximum
	Total [g]	Total % [%]	Max. Rate [g/° CA]	CA [Max. Rate] [° CA]	Max [K]	CA [Max] [° CA]	Max [K]	CA [Max] [° CA]	2-98 [° CA]	5-95 [° CA]	10-90 [° CA]	2-98 [° CA]	5-95 [° CA]	10-90 [° CA]	[% vol]	[% vol]	[% vol]	[% vol]	[° CA]
Ref3	0.334	119.28	0.897045	10	787.03	14	2721.96	13	11.6	17.3	21.1	39.2	28.7	22.9	13.0	14.7	14.8	15.2	101
P12	0.325	120.9	0.878634	10	792.94	14	2732.94	13	11.6	17.4	21.2	37.7	29.8	21.4	12.7	14.4	14.9	15.1	61
P13	0.325	120.44	0.861774	11	779.5	14.5	2722.95	14	11.6	17.6	21.6	39.7	30.2	22.8	12.9	14.6	14.9	15.2	63
P14	0.329	118.39	0.843234	12	776.72	15.5	2691.59	14	12	18.1	22.2	41.7	31	23.5	12.7	14.5	14.7	15.0	93
P15																			
P16																			
P17	0.324	117.1	0.83767	12	775.61	15.5	2721.58	14	11.7	17.9	22	40.7	31.3	22.5	12.7	14.2	14.4	14.7	63
P18	0.328	119.79	0.861825	12	778	15	2719.74	14	11.9	18	22	41	30.6	21.6	13.0	14.6	14.9	15.2	67
P19	0.328	120.07	0.860123	11	784.3	14.5	2729.05	13	11.7	17.6	21.6	40.1	29.5	21.7	12.9	14.5	14.8	15.1	69
P20	0.328	121.28	0.858397	12	789.64	15	2726.77	14	11.6	17.8	21.9	39.6	29.7	21.8	12.9	14.6	15.0	15.3	67
P21																			
P22	0.323	120.31	0.845516	11	781.91	14.5	2727.57	14	11.9	17.8	21.7	39.7	30.5	21.6	12.9	14.6	14.8	15.1	91
P23	0.327	121.11	0.842266	11	787.91	15	2717.61	14	11.7	17.7	21.8	41	30.4	22.7	13.0	14.7	15.1	15.4	90
P24	0.327	117.11	0.821654	12	779.3	15.5	2713.87	14	11.6	17.9	22	42.2	31.5	24.3	12.7	14.4	14.7	15.1	92
Ref4	0.327	119.65	0.83213	12	782.37	15.5	2713.26	14	11.5	17.7	21.8	41.1	30	23.8	12.9	14.6	14.9	15.3	91

Sample	Equilibrium Products Results - CO					Equilibrium Products Results - O_2					Equilibrium Products Results - NO							
	End of Cycle	Exhaust Valve Open	End of Combustion	Maximum	Angle at Maximum	End of Cycle	Exhaust Valve Open	End of Combustion	Minimum	Angle at Minimum	End of Cycle	Exhaust Valve Open	End of Combustion	Max Burned Gas Temp	Maximum	Angle at Maximum	Burned Gas Temp=2000k	Angle at Burned Gas Temp=2000k
	[% vol]	[% vol]	[% vol]	[% vol]	[° CA]	[% vol]	[% vol]	[% vol]	[% vol]	[° CA]	[% vol]	[% vol]	[% vol]	[% vol]	[% vol]	[° CA]	[% vol]	[° CA]
Ref3	0.0	0.0	0.8	1.9	22	0.5	-2.1	-3.3	-3.3	41	0.002	0.014	0.308	0.514	0.649	22	0.102	69
P12	0.0	0.1	1.1	2.2	22	0.9	-1.8	-3.8	-3.8	40	0.000	0.000	0.274	0.494	0.617	21	0.047	69
P13	0.2	0.3	1.1	2.2	23	0.4	-2.3	-3.8	-3.9	43	0.000	0.000	0.211	0.464	0.564	22	0.027	71
P14	0.0	0.0	0.4	1.4	21	1.1	-1.6	-2.8	-2.8	51	0.003	0.025	0.369	0.522	0.693	24	0.170	69
P15																		
P16																		
P17	0.4	0.6	1.3	2.3	24	0.6	-2.1	-3.3	-3.3	44	0.000	0.000	0.169	0.402	0.505	21	0.016	70
P18	0.2	0.2	1.0	2.1	21	0.3	-2.3	-3.7	-3.7	44	0.000	0.000	0.219	0.450	0.566	21	0.034	71
P19	0.3	0.4	1.2	2.3	23	0.4	-2.3	-3.8	-3.8	42	0.000	0.000	0.213	0.431	0.558	22	0.022	71
P20	0.1	0.2	1.1	2.2	23	0.5	-2.2	-3.9	-4.0	42	0.000	0.000	0.234	0.469	0.585	23	0.036	72
P21																		
P22	0.4	0.6	1.3	2.5	20	0.2	-2.6	-3.9	-3.9	43	0.000	0.000	0.170	0.439	0.568	20	0.017	71
P23	0.0	0.0	0.8	1.9	23	0.5	-2.2	-3.7	-3.7	44	0.002	0.013	0.287	0.506	0.640	23	0.094	72
P24	0.0	0.0	0.7	2.0	22	1.1	-1.6	-2.9	-3.0	51	0.002	0.014	0.273	0.471	0.651	22	0.094	73
Ref4	0.0	0.0	0.8	1.9	23	0.6	-2.0	-3.5	-3.5	51	0.001	0.009	0.260	0.472	0.603	23	0.077	72

Sample	Engine Operating Point			Engine Operating Conditions															
	Speed	Torque	Power	Fuel Flow Rate	Equivalence Ratio	Equivalence Ratio	Ignition Timing	BSFC	Water Temperature	Oil Temperature	Exhaust Temperature	Fuel Pressure	Oil Pressure	Manifold Pressure	Manifold Temperature	Droplet Temperature	Air Flow Rate	Air Flow Rate
	[rev/min]	[Nm]	[kW]	[kg/hr]	(calc) [-]	(meas) [-]	[° CA BTDC]	[kg/kW.hr]	[° C]	[° C]	[° C]	[bar]	[bar]	[kPa]	[° C]	[° C]	[mbar]	[kg/s]
Ref5	3757	72.8	28.4	8.06	0.98	1.02	22	0.283	88.9	109.2	737.2	2.8	4.5	69.1	34.1	12.4	1.10	0.032
P25	3760	71.7	28.0	7.92	0.99	1.02	22	0.282	89.9	109.2	734.8	2.8	4.0	68.2	36.0	11.8	1.07	0.032
P26	3759	71.8	28.1	7.84	0.98	1.01	22	0.280	89.7	106.9	733.0	2.8	4.3	67.8	31.2	10.0	1.06	0.032
P27	3758	71.8	28.0	7.90	0.97	1.01	22	0.282	89.2	107.1	735.2	2.8	4.4	68.0	32.5	10.8	1.08	0.032
P28	3762	71.9	28.1	7.89	0.99	1.02	22	0.280	89.9	107.4	731.4	2.9	4.0	67.3	30.7	10.0	1.06	0.032
P29	3761	71.4	27.9	7.69	0.98	1.00	22	0.275	89.7	109.1	732.7	2.8	4.2	67.3	31.6	14.2	1.05	0.031
P30	3766	71.8	28.1	7.92	0.99	1.03	22	0.281	89.8	109.7	739.7	2.8	4.0	67.6	31.3	14.9	1.06	0.031
P31	3757	71.7	28.0	7.83	0.99	1.02	22	0.279	90.2	108.7	728.0	2.8	4.2	67.4	31.9	11.0	1.04	0.031
P32	3757	71.7	28.0	7.90	0.99	1.02	22	0.282	89.8	108.8	733.3	2.8	4.1	67.7	32.1	9.4	1.06	0.031
P33	3759	71.9	28.1	7.84	0.99	1.02	22	0.279	90.3	110.9	737.5	2.8	4.2	67.8	33.9	10.9	1.06	0.031
P34	3759	71.8	28.1	7.77	0.98	1.00	22	0.277	89.4	107.8	730.5	2.8	4.4	67.8	32.8	10.3	1.09	0.032
P35	3761	72.0	28.2	7.99	0.98	1.03	22	0.284	90.0	110.1	740.3	2.8	4.0	67.9	31.5	8.1	1.08	0.032
Ref6	3764	72.2	28.3	7.94	0.98	1.02	22	0.281	89.5	107.8	734.8	2.8	4.3	68.1	33.0	11.2	1.09	0.032

Engine Out Emissions														
Hydrocarbons			NO			CO2			CO			O2	H2S	SO2
[ppm]	[g/kW.hr]	[g/km]	[ppm]	[g/kW.hr]	[g/km]	[% vol]	[g/kW.hr]	[g/km]	[% vol]	[g/kW.hr]	[g/km]	[% vol]	[ppm]	[ppm]
1150	2.29	0.54	>2000	13.22	3.13	15.2	959.5	227.4	0.6	25.73	6.10	0.7	-	-
1051	2.09	0.49	>2000	13.20	3.08	15.1	950.8	222.1	0.7	28.96	6.77	0.7	-	-
1020	2.05	0.48	>2000	13.32	3.11	14.9	949.4	222.0	0.6	24.95	5.83	0.7	-	-
982	1.97	0.46	>2000	13.33	3.11	15.0	955.3	223.3	0.5	22.12	5.17	0.8	-	-
1061	2.09	0.49	>2000	13.03	3.06	15.2	945.5	221.8	0.8	30.03	7.04	0.7	-	-
1063	2.09	0.49	>2000	13.04	3.04	15.1	945.0	220.0	0.7	29.52	6.87	0.7	-	-
1038	2.01	0.47	>2000	12.85	3.01	15.4	948.2	222.3	0.7	29.10	6.82	0.7	-	-
1092	2.13	0.50	>2000	12.93	3.02	15.2	943.0	220.3	0.8	32.32	7.55	0.6	-	-
1027	2.01	0.47	>2000	13.01	3.04	15.3	952.6	222.4	0.8	31.63	7.39	0.6	-	-
1001	1.99	0.46	>2000	13.15	3.08	15.0	946.2	221.5	0.8	32.82	7.68	0.6	-	-
934	1.88	0.44	>2000	13.37	3.13	14.9	952.7	222.7	0.7	27.21	6.36	0.7	-	-
977	1.88	0.44	>2000	12.79	3.00	15.6	952.6	223.7	0.8	29.38	6.90	0.7	-	-
1116	2.20	0.52	>2000	13.06	3.08	15.2	951.9	224.3	0.6	23.54	5.55	0.8	-	-

Atmospheric Conditions		
Barometric Pressure	Dry Bulb Temperature	Wet Bulb Temperature
[mBar]	[° C]	[° C]
1017.7	20.8	14.5
1002.9	20.8	14.0
1013.7	19.3	12.8
1010.1	20.0	12.7
1005.2	19.4	12.0
1003.5	18.7	14.0
1002.2	18.0	14.0
1012.2	18.8	15.0
1007.0	20.6	15.6
1005.7	19.5	13.9
1003.0	21.8	15.0
1001.1	20.8	14.5
1008.9	21.7	14.0

SABS Corrections		
Correction Factor	Corrected Torque	Corrected Power
[-]	[Nm]	[kW]
0.98	70.6	27.6
0.98	70.9	27.7
0.97	69.6	27.2
0.98	70.1	27.4
0.98	70.3	27.5
0.99	70.4	27.5
0.99	70.7	27.7
0.97	78.0	30.5
0.99	70.9	27.7
0.99	70.7	27.7
0.99	71.3	27.9
0.99	71.4	27.9
0.98	70.8	27.7

Sample	Engine Operating Point			Engine Operating Conditions							Racer Input Parameters				
	Speed	Torque	Racer File Name	Fuel Flow Rate	Equivalence Ratio	Ignition Timing	Manifold Pressure	Manifold Temperature	Droplet Temperature	Air Flow Rate	Charge Temperature	Cylinder Charge Mass	Re Reference Pressure	Air Fuel Ratio	Fuel Flow Rate
	[rev/min]	[Nm]	[-]	[kg/hr]	(calc) [-]	[° CA BTDC]	[kPa]	[° C]	[° C]	[kg/s]	[° C]	[kg]	[kPa]	[-]	[kg/s]
Ref5	3757	72.8	rf4120b	*8.06*	0.98	22	69.1	34.1	12.4	0.03227	64.1	*0.0002756*	*66.35*	14.0	0.00224
P25	3760	71.7	P25120a	7.92	0.99	22	68.2	36.0	11.8	0.03155	66.0	0.0002693	65.22	13.9	0.00220
P26	3759	71.8	P26120a	7.84	0.98	22	67.8	31.2	10.0	0.03161	61.2	0.0002697	64.37	14.0	0.00218
P27	3758	71.8	P27120a	7.90	0.97	22	68.0	32.5	10.8	0.03178	62.5	0.0002712	65.00	14.1	0.00219
P28	3762	71.9	P28120b	7.89	0.99	22	67.3	30.7	10.0	0.03151	60.7	0.0002688	64.07	13.9	0.00219
P29	3761	71.4	P29120a	7.69	0.98	22	67.3	31.6	14.2	0.03133	61.6	0.0002670	63.80	13.9	0.00213
P30	3766	71.8	p30120a	7.92	0.99	22	67.6	31.3	14.9	0.03146	61.3	0.0002681	64.03	13.9	0.00220
P31	3757	71.7	P31120a	7.83	0.99	22	67.4	31.9	11.0	0.03125	61.9	0.0002669	63.85	13.8	0.00217
P32	3757	71.7	P32120a	7.90	0.99	22	67.7	32.1	9.4	0.03148	62.1	0.0002689	64.36	13.8	0.00219
P33	3759	71.9	P33120aa	7.84	0.99	22	67.8	33.9	10.9	0.03146	63.9	0.0002685	64.62	13.8	0.00218
P34	3759	71.8	P34120a	7.77	0.98	22	67.8	32.8	10.3	0.03173	62.8	0.0002705	64.88	14.0	0.00216
P35	3761	72.0	P35120a	7.99	0.98	22	67.9	31.5	8.1	0.03163	61.5	0.0002700	64.52	14.0	0.00222
Ref6	3764	72.2	rf5120b	7.94	0.98	22	68.1	33.0	11.2	0.03181	63.0	0.0002711	65.07	14.0	0.00220

Sample	Pressure/CA results								Single Zone Model Results											
	IMEP	PMEP	IMEP(net)	Stability	Pressure		Rate of Pressure Rise		Heat Released			Gas Temperature		Induction Period			Burn Angle			
	[kPa]	[kPa]	[kPa]	[%]	Max [kPa]	CA [Max.] [° CA]	Max [kPa/°]	CA [Max.] [° CA]	Total [kJ]	Max. Rate [kJ/° CA]	CA [Max. Rate] [° CA]	Max [K]	CA [Max] [° CA]	2-98 [° CA]	5-95 [° CA]	10-90 [° CA]	2-98 [° CA]	5-95 [° CA]	10-90 [° CA]
Ref5	874.4	-68.56	805.84	11.1	3562.7	18	138.9	7	1008.24	2323.57	11	3226.5	29	11.4	17.2	21.2	44.7	33.2	24.2
P25	867.03	-66.42	800.61	11.3	3541.5	18	138	7	1010.37	2351.76	14	3290.2	29	11.6	17.3	21.3	45.2	33.4	24.2
P26	857.71	-64.23	793.47	11.6	3496.7	18	135.5	7	1000.09	2296.79	11	3232.2	30	11.7	17.5	21.4	44.4	32.6	23.6
P27	868.65	-64.55	804.1	11.5	3586.8	18	142.9	7	999.63	2345.23	10	3138.4	29	11.4	17.2	21.1	45.2	33.8	24.7
P28	870.93	-64.93	806	11.2	3646.6	18	147.1	7	990.26	2374.1	10	3109.9	28	11.4	16.8	20.6	43.8	33	24.2
P29	835.84	-65.68	770.17	10.9	3405.7	18	134	7	945.24	2224.5	10	2965.2	29	11.5	17.1	21	47.8	34.3	24
P30	843.49	-65.97	777.53	11.3	3368.5	19	128.7	8	960.39	2237.41	11	2961.4	30	11.7	17.6	21.6	49.9	36.4	26.1
P31	847.06	-64.28	782.78	10.2	3580.3	18	147.1	7	974.2	2394.92	10	3143.5	28	11.2	17	20.9	43.5	31.3	24
P32	859.3	-63.63	795.67	9.9	3653.2	18	152.7	7	991.83	2441.11	10	3198.2	27	11.3	17	20.8	43.1	31.4	22.3
P33	879.12	-71.82	807.3	11.6	3606.4	18	145.4	7	973.64	2386.19	10	2753.8	28	12	17.4	21.2	48.5	34.2	24.3
P34	872.53	-66.51	806.02	10.5	3630.6	18	150.6	7	990.21	2427.37	10	2995	28	12	17.4	21.1	47.6	34.6	24.6
P35	875.48	-66.32	809.16	11.1	3684.5	17	153	7	993.92	2439.22	10	2997.4	28	11.9	17.2	20.9	46	31.9	23.4
Ref6	852.23	-67.87	784.36	10.5	3585.6	17	150.8	7	944.29	2365.54	9	2703.4	28	12	17.1	20.7	46.1	33.3	23.5

Sample	Two Zone Model Results														Equilibrium Products Results - CO_2				
	Mass Transferred				Unburned Gas Temperature		Burned Gas Temperature		Induction Period			Burn Angle			End of Cycle	Exhaust Valve Open	End of Combustion	Maximum	Angle at Maximum
	Total [g]	Total % [%]	Max. Rate [g/° CA]	CA [Max. Rate] [° CA]	Max [K]	CA [Max] [° CA]	Max [K]	CA [Max] [° CA]	2-98 [° CA]	5-95 [° CA]	10-90 [° CA]	2-98 [° CA]	5-95 [° CA]	10-90 [° CA]	[% vol]	[% vol]	[% vol]	[% vol]	[° CA]
Ref5	0.322	117.01	0.851205	11	780.8	14.5	2720.14	13	11.9	17.8	21.7	39.8	29.3	21.4	13.0	14.8	14.6	15.1	100
P25	0.322	119.41	0.84231	11	783.34	14.5	2722.93	13	12	17.8	21.7	39.7	29.2	21.3	13.1	14.7	14.8	15.1	70
P26	0.321	118.94	0.842377	11	777.42	15	2713.19	14	12.2	18	21.9	38.9	29.2	23.1	12.9	14.7	14.8	15.2	71
P27	0.323	119.05	0.861225	11	778.34	14.5	2716.58	13	11.8	17.7	21.6	38.3	28.5	22.2	13.1	14.8	14.9	15.3	99
P28	0.32	119.22	0.867129	10	777.16	14	2722.78	13	11.8	17.3	21	37.3	27.8	21.5	13.2	14.9	14.8	15.3	100
P29	0.31	116.1	0.820938	11	773.7	14.5	2704.53	13	12.1	17.6	21.5	41.595	31.361	23.595	13.1	14.9	14.6	15.3	101
P30	0.311	116.15	0.81482	12	766.4	15.5	2710.42	14	12.2	18.1	22.1				13.0	14.7	14.6	15.0	100
P31	0.316	118.49	0.876504	11	778.93	14.5	2723.59	13	11.7	17.5	21.4	37.3	29.3	22.4	12.8	14.4	14.6	15.0	65
P32	0.319	118.81	0.893905	10	781.76	14	2728.08	13	11.8	17.5	21.3	37.6	28.2	20.6	12.8	14.5	14.7	15.0	65
P33	0.319	118.77	0.873234	11	2366.18	179.5	2709.81	13	12	17.7	21.5	37.4	27.8	21.6	13.5	15.0	14.4	15.3	120
P34	0.324	119.66	0.893851	10	776.63	14	2711.41	13	12.3	17.8	21.5	37.7	28.5	20.9	13.3	15.2	15.2	15.6	101
P35	0.323	119.51	0.889005	10	772.18	14	2723.58	13	12.1	17.6	21.3	38.4	29.8	21.6	13.1	14.9	14.9	15.3	109
Ref6	0.318	117.16	0.865968	10	765.95	14	2714.15	12	12.3	17.5	21.2				13.4	15.2	14.6	15.4	119

Sample	Equilibrium Products Results - CO					Equilibrium Products Results - O_2					Equilibrium Products Results - NO							
	End of Cycle	Exhaust Valve Open	End of Combustion	Maximum	Angle at Maximum	End of Cycle	Exhaust Valve Open	End of Combustion	Minimum	Angle at Minimum	End of Cycle	Exhaust Valve Open	End of Combustion	Max Burned Gas Temp	Maximum	Angle at Maximum	Burned Gas Temp=2000k	Angle at Burned Gas Temp=2000k
	[% vol]	[% vol]	[% vol]	[% vol]	[° CA]	[% vol]	[% vol]	[% vol]	[% vol]	[° CA]	[% vol]	[% vol]	[% vol]	[% vol]	[% vol]	[° CA]	[% vol]	[° CA]
Ref5	0.2	0.3	1.0	2.1	23	0.2	-2.6	-3.2	-3.2	100	0.000	0.000	0.191	0.417	0.540	20	0.028	70
P25	0.3	0.5	1.1	2.3	23	0.1	-2.6	-3.7	-3.7	43	0.000	0.000	0.169	0.416	0.540	20	0.020	70
P26	0.1	0.1	0.9	2.0	21	0.6	-2.2	-3.5	-3.5	51	0.000	0.000	0.218	0.457	0.564	21	0.046	69
P27	0.1	0.1	0.9	2.0	22	0.3	-2.4	-3.5	-3.5	51	0.000	0.000	0.217	0.448	0.574	22	0.048	69
P28	0.3	0.4	1.1	2.2	22	0.0	-2.8	-3.6	-3.7	51	0.000	0.000	0.191	0.454	0.556	21	0.025	69
P29	0.0	0.0	0.5	1.8	21	0.3	-2.5	-2.8	-3.1	100	0.002	0.015	0.217	0.458	0.596	21	0.092	69
P30	0.4	0.6	1.0	2.2	22	0.1	-2.7	-3.1	-3.3	100	0.000	0.000	0.102	0.397	0.491	21	0.017	70
P31	0.2	0.3	1.1	2.2	22	0.6	-2.0	-3.4	-3.4	41	0.000	0.000	0.210	0.450	0.558	21	0.027	68
P32	0.3	0.4	1.1	2.3	21	0.5	-2.2	-3.5	-3.5	41	0.000	0.000	0.202	0.459	0.560	21	0.024	68
P33	0.2	0.3	1.2	2.3	26	-0.4	-2.9	-3.1	-3.4	114	0.000	0.010	0.251	0.437	0.616	25	0.040	97
P34	0.0	0.0	0.5	1.8	19	0.0	-2.9	-3.6	-3.6	70	0.002	0.014	0.216	0.498	0.625	19	0.097	69
P35	0.5	0.7	1.2	2.4	22	-0.1	-3.1	-3.8	-3.9	52	0.000	0.000	0.121	0.428	0.512	21	0.015	68
Ref6	0.2	0.2	0.7	2.0	20	-0.3	-3.1	-2.9	-3.5	119	0.000	0.000	0.142	0.421	0.543	20	0.035	68

Engine – 4Y, Load Point - 120 km/hr

Sample	Engine Operating Point			Engine Operating Conditions												
	Speed	Torque	Power	Fuel Flow Rate	Equivalence Ratio	Equivalence Ratio	Ignition Timing	BSFC	Water Temperature	Oil Temperature	Exhaust Temperature 1&4	Exhaust Temperature 2&3	Oil Pressure	Manifold Pressure	Air Flow Rate	Air Flow Rate
	[rev/min]	[Nm]	[kW]	[kg/hr]	(calc) [-]	(meas) [-]	[° CA BTDC]	[kg/kW.hr]	[° C]	[° C]	[° C]	[° C]	[bar]	[kPa]	[mbar]	[kg/s]
Ref1	3757	108.9	42.8	13.43	1.08	1.07	34.0	0.313	83.6	127.2	798.2	769.9	3.88	75.08	28.87	0.051
P1	3761	107.5	42.3	12.96	1.04	1.04	34.0	0.306	83.8	132.4	806.9	778.0	3.82	74.52	28.50	0.051
P2	3761	108.1	42.6	13.32	1.08	1.07	34.0	0.313	82.7	125.7	793.8	764.8	3.92	74.67	28.15	0.051
P3	3759	108.1	42.5	13.41	1.09	1.08	34.0	0.315	82.6	127.5	796.8	766.2	3.86	75.01	28.44	0.051
P4	3757	108.2	42.6	13.33	1.09	1.07	34.0	0.313	83.1	127.7	797.9	767.3	3.86	75.25	28.55	0.051
P5	3760	107.0	42.1	13.24	1.09	1.07	34.0	0.315	83.0	127.5	793.4	764.9	3.84	75.03	28.26	0.051
P6	3761	107.4	42.3	13.24	1.09	1.06	34.0	0.313	83.3	125.5	794.1	764.8	3.88	74.89	28.34	0.051
P7	3762	107.3	42.3	13.28	1.10	1.07	34.0	0.314	83.1	127.5	797.0	761.9	3.84	74.96	28.26	0.051
P8	3761	107.8	42.4	13.47	1.09	1.09	34.0	0.317	82.5	123.7	794.6	769.2	3.93	74.72	28.08	0.051
P9	3762	106.2	41.8	13.32	1.09	1.08	34.0	0.318	82.5	127.4	797.9	771.3	3.85	74.56	28.05	0.051
P10	3760	108.1	42.5	13.54	1.11	1.08	34.0	0.318	82.7	126.5	787.2	760.7	3.87	75.11	28.75	0.051
P11	3761	109.0	42.9	13.67	1.10	1.09	32.0	0.319	83.0	127.6	798.7	770.3	3.86	75.55	29.01	0.051
P12	3765	108.9	42.9	13.59	1.06	1.07	34.0	0.316	82.6	124.0	789.6	761.5	3.92	75.37	29.75	0.052
P13	3761	107.5	42.3	13.48	1.09	1.07	34.0	0.319	83.1	125.9	788.3	762.8	3.88	74.31	29.08	0.051
P14	3759	108.3	42.6	13.49	1.04	1.06	34.0	0.317	82.9	127.3	800.8	771.7	3.87	74.65	29.32	0.052
P15	3761	106.6	42.0	13.22	1.03	1.06	34.0	0.315	83.6	126.3	805.4	775.2	3.90	73.76	28.45	0.051
P16	3761	109.2	43.0	14.03	1.09	1.10	34.0	0.326	83.6	128.5	796.2	768.6	3.86	75.23	29.84	0.052
P17	3763	107.4	42.3	13.79	1.09	1.09	34.0	0.326	83.0	126.6	794.2	769.4	3.89	74.73	29.32	0.052
P18	3759	107.7	42.4	13.33	1.07	1.05	34.0	0.315	83.0	127.9	795.8	766.3	3.86	74.95	29.46	0.052
P19	3759	107.6	42.3	13.59	1.08	1.08	33.0	0.321	83.8	128.6	787.0	766.3	3.83	74.70	29.21	0.052
P20	3760	106.9	42.1	13.41	1.09	1.07	33.0	0.319	83.7	127.5	786.3	759.4	3.87	74.41	29.05	0.051
P21	3762	107.5	42.3	13.29	1.08	1.14	34.0	0.314	83.1	126.0	790.9	765.5	3.88	74.47	24.83	0.048
P22	3764	106.8	42.1	13.28	1.08	1.14	33.0	0.316	83.5	126.3	791.4	766.3	3.87	74.11	24.61	0.048
P23	3760	108.0	42.5	13.43	1.07	1.14	33.0	0.316	83.4	127.8	789.6	764.9	3.84	74.37	25.00	0.048
P24	3762	109.0	42.9	13.48	1.04	1.15	33.0	0.314	83.6	127.5	804.3	775.1	3.86	74.34	25.04	0.048
P25	3758	107.5	42.3	13.16	1.08	1.13	33.0	0.311	82.4	127.4	798.7	768.8	3.85	74.09	24.90	0.048
P26	3761	109.3	43.0	13.53	1.08	1.15	33.0	0.314	82.9	126.1	796.8	763.5	3.88	74.60	25.15	0.048
P27	3759	106.7	42.0	13.38	1.08	1.16	-	0.319	83.1	129.8	800.4	767.3	3.81	74.10	24.44	0.047
P28	3761	107.0	42.2	12.72	1.04	1.05	-	0.302	82.5	124.3	803.2	776.0	3.90	72.39	26.62	0.050
P29	3761	109.2	43.0	13.11	1.05	1.07	-	0.305	82.6	122.4	800.0	774.1	3.93	73.06	27.30	0.050
P30	3764	106.4	41.9	12.63	1.05	1.05	34.0	0.301	82.6	124.6	803.3	781.4	3.88	72.24	26.21	0.049
P31	3758	109.1	42.9	13.03	1.08	1.06	34.0	0.304	82.3	126.9	802.9	777.6	3.88	73.40	27.50	0.050
P32	3759	108.5	42.7	12.98	1.07	1.06	34.0	0.304	82.9	126.6	811.2	778.3	3.87	72.83	27.20	0.050
P33	3760	107.8	42.4	12.83	1.07	1.04	33.0	0.302	82.7	126.8	807.4	775.5	3.88	73.66	27.83	0.050
P34	3760	107.4	42.3	12.89	1.08	1.03	33.0	0.305	83.1	127.7	803.0	767.8	3.88	74.07	27.97	0.051
P35	3759	106.0	41.7	13.20	1.07	1.08	32.0	0.316	82.7	125.2	808.1	770.2	3.93	72.92	27.26	0.050
Ref2	3751	108.6	42.6	13.70	1.09	1.10	33.0	0.321	83.5	127.6	798.7	770.9	3.88	74.12	28.47	0.051

Sample	Engine Out Emissions													Atmospheric Conditions			SABS Corrections		
	Hydrocarbons			NO			CO2			CO			O2	Barometric Pressure	Dry Bulb Temperature	Wet Bulb Temperature	Correction Factor	Corrected Torque	Corrected Power
	[ppm]	[g/kW.hr]	[g/km]	[ppm]	[g/kW.hr]	[g/km]	[% vol]	[g/kW.hr]	[g/km]	[% vol]	[g/kW.hr]	[g/km]	[% vol]	[mBar]	[° C]	[° C]	[-]	[Nm]	[kW]
Ref1	2408	5.31	1.90	1485	10.85	3.87	12.8	894.7	319.4	3.4	150.3	53.7	0.7	1002.3	30.0	22.0	1.02	111.2	43.7
P1	2028	4.59	1.62	1938	14.56	5.14	13.1	939.4	331.5	2.4	107.7	38.0	0.8	1002.3	30.0	22.0	1.02	109.8	43.2
P2	2233	5.02	1.78	1434	10.69	3.79	12.4	886.3	314.4	3.4	156.5	55.5	0.6	1006.0	29.5	21.0	1.01	109.5	43.1
P3	2062	6.92	2.45	981	10.91	3.87	8.0	853.1	302.4	2.2	149.6	53.0	0.4	1006.0	29.5	21.0	1.01	109.5	43.1
P4	2238	5.06	1.79	1424	10.66	3.78	12.5	897.1	318.1	3.4	156.4	55.5	0.6	1006.0	29.5	21.0	1.01	109.6	43.1
P5	2402	5.45	1.91	1435	10.79	3.78	12.5	897.3	314.9	3.5	160.2	56.2	0.6	1005.0	31.0	22.0	1.02	109.0	42.9
P6	2042	4.66	1.64	1463	11.06	3.90	12.5	902.1	318.0	3.4	155.0	54.7	0.5	1005.9	29.5	21.5	1.01	109.0	42.9
P7	2461	5.58	1.97	1455	10.94	3.85	12.4	894.9	315.3	3.6	163.0	57.4	0.5	1005.9	29.5	21.5	1.01	108.9	42.9
P8	2198	4.89	1.73	1679	12.38	4.38	12.8	903.6	319.6	3.3	148.3	52.4	0.5	-	-	-	1.00	107.8	42.4
P9	2186	4.95	1.72	1712	12.85	4.48	12.8	922.3	321.5	3.2	146.3	51.0	0.4	-	-	-	1.00	106.2	41.8
P10	2318	5.37	1.90	1348	10.35	3.67	12.1	888.2	314.8	3.8	177.0	62.8	0.4	-	-	-	1.00	108.1	42.5
P11	2177	4.93	1.76	1561	11.72	4.19	12.5	900.8	322.1	3.5	158.8	56.8	0.5	-	-	-	1.00	109.0	42.9
P12	2491	5.80	2.07	1133	8.74	3.13	12.0	882.7	315.9	3.4	157.6	56.4	1.0	-	-	-	1.00	108.9	42.9
P13	2253	5.15	1.82	1312	9.95	3.51	12.3	891.9	314.5	3.7	169.9	59.9	0.7	1001.6	29.0	21.0	1.02	109.4	43.1
P14	2123	4.84	1.72	1455	11.00	3.90	12.9	933.3	331.3	2.7	124.3	44.1	0.9	1005.1	27.5	20.0	1.01	109.3	43.0
P15	1855	4.22	1.48	1770	13.37	4.67	13.1	946.1	330.9	2.5	112.6	39.4	0.9	1005.1	27.5	20.0	1.01	107.6	42.4
P16	2163	4.81	1.72	1159	8.54	3.06	12.6	887.4	318.0	4.0	178.8	64.1	0.8	1005.1	27.5	20.0	1.01	110.2	43.4
P17	2398	5.34	1.88	1284	9.49	3.35	12.7	900.9	317.6	3.8	170.3	60.0	0.8	1004.2	31.0	21.0	1.02	109.2	43.0
P18	2085	4.78	1.69	1335	10.15	3.58	12.4	901.4	318.3	3.4	157.2	55.5	0.8	1004.2	31.0	21.0	1.02	109.5	43.1
P19	2461	5.58	1.97	1199	9.02	3.18	12.5	898.3	317.0	3.6	166.8	58.9	0.8	-	-	-	1.00	107.6	42.3
P20	2363	5.45	1.91	1196	9.15	3.21	12.3	897.5	314.7	3.7	172.7	60.5	0.7	-	-	-	1.00	106.9	42.1
P21	2086	4.44	1.56	1325	9.35	3.30	12.6	848.6	299.3	3.3	143.5	50.6	0.7	1002.8	26.0	22.0	1.02	109.1	43.0
P22	2082	4.43	1.55	1288	9.09	3.19	12.5	847.0	296.9	3.4	145.8	51.1	0.7	1002.8	26.0	22.0	1.02	108.4	42.7
P23	2099	4.47	1.58	1233	8.71	3.08	12.5	845.3	299.5	3.4	144.7	51.2	0.8	1001.5	24.0	19.0	1.01	108.7	42.8
P24	1785	3.76	1.34	1691	11.79	4.22	13.0	870.2	311.4	2.5	104.7	37.5	0.8	-	-	-	1.00	109.0	42.9
P25	2372	5.06	1.78	1485	10.49	3.70	12.5	847.6	298.7	3.3	143.6	50.6	0.6	1002.7	27.5	20.5	1.01	108.9	42.9
P26	2293	4.82	1.73	1309	9.12	3.27	12.3	820.3	294.2	3.7	155.7	55.9	0.8	1002.7	27.5	20.5	1.01	110.8	43.6
P27	2206	4.65	1.63	1358	9.48	3.32	12.5	833.7	291.6	3.6	155.0	54.2	0.8	1002.7	27.5	20.5	1.01	108.1	42.5
P28	1939	4.07	1.43	2500			13.8	918.8	322.8	2.6	109.7	38.5	0.8	1000.2	21.5	12.0	0.99	106.0	41.7
P29	2003	4.20	1.50	2106			13.5	895.8	321.1	3.0	125.5	45.0	0.8	1000.2	21.5	12.0	0.99	108.1	42.6
P30	1979	4.14	1.45	2500			13.9	924.0	323.0	2.5	106.7	37.3	0.7	1006.6	23.0	18.0	1.00	106.1	41.8
P31	2954	6.35	2.27	932	6.64	2.37	13.3	908.5	325.0	2.9	127.2	45.5	0.5	1005.1	25.0	18.0	1.00	109.2	43.0
P32	2070	4.41	1.57	1375	9.71	3.46	13.5	911.5	324.4	2.8	120.5	42.9	0.5	1004.8	27.0	19.0	1.01	109.2	43.0
P33	2023	4.45	1.57	1596	11.63	4.11	13.2	920.4	325.6	2.9	127.9	45.2	0.5	1004.8	27.0	19.0	1.01	108.5	42.7
P34	2149	4.82	1.70	1635	12.17	4.29	12.9	918.1	323.5	3.0	136.1	47.9	0.5	1004.8	27.0	19.0	1.01	108.1	42.5
P35	2137	4.59	1.59	1970	14.02	4.87	13.7	930.4	323.5	3.1	133.1	46.3	0.5	1002.2	26.0	18.0	1.01	106.6	42.0
Ref2	1924	4.19	1.49	1808	13.05	4.64	13.1	906.1	322.0	3.6	158.8	56.4	0.4	1002.2	28.0	19.0	1.01	109.8	43.1

Engine - 4A-FE, Load Point - 3000 rev/min WOT

Sample	Engine Operating Point			Engine Operating Conditions															
	Speed	Torque	Power	Fuel Flow Rate	Equivalence Ratio	Equivalence Ratio	Ignition Timing	BSFC	Water Temperature	Oil Temperature	Exhaust Temperature	Fuel Temperature	Fuel Pressure	Oil Pressure	Manifold Pressure	Manifold Temperature	Air Flow Rate	Air Flow Rate
	[rev/min]	[Nm]	[kW]	[kg/hr]	(calc) [-]	(meas) [-]	[° CA BTDC]	[kg/kW.hr]	[° C]	[° C]	[° C]	[° C]	[bar]	[bar]	[kPa]	[° C]	[mbar]	[kg/s]
Ref1	3002	123.9	38.9	11.2	1.15	1.16	18	0.288	90.3	106.8	752.4	12.7	3.2	4.0	99.7	28.1	1.68	0.040
P1	3001	127.8	40.1	10.9	1.08	1.13	18	0.272	90.5	105.0	774.4	11.7	3.0	4.0	100.5	22.9	1.66	0.040
P2	2990	123.5	38.7	10.7	1.14	1.13	18	0.277	90.9	106.2	763.6	15.4	3.1	3.9	100.0	28.2	1.61	0.039
P3	3004	125.4	39.5	10.9	1.14	1.13	18	0.277	90.8	104.4	749.5	13.1	3.1	3.9	99.8	25.8	1.65	0.039
P4	3006	125.0	39.3	10.8	1.14	1.12	18	0.276	90.7	105.7	761.2	11.9	3.1	3.9	100.1	27.0	1.67	0.039
P5	3001	124.1	39.0	11.0	1.15	1.15	18	0.283	90.9	105.6	760.7	13.2	3.1	3.9	99.8	28.0	1.66	0.039
P6	2997	122.4	38.4	10.9	1.14	1.12	18	0.283	91.0	106.3	763.1	15.6	3.1	3.8	99.6	28.9	1.68	0.039
P7	3003	126.5	39.8	10.9	1.13	1.13	18	0.275	90.8	106.6	764.9	11.5	3.1	3.9	100.4	25.2	1.67	0.040
P8	3008	124.0	39.1	11.0	1.14	1.14	18	0.281	91.0	105.8	767.1	12.9	3.1	3.9	99.5	26.9	1.67	0.039
P9	2998	122.7	38.5	10.8	1.14	1.13	18	0.281	90.4	106.3	769.5	13.8	3.1	3.9	99.4	28.0	1.65	0.039
P10	2999	123.2	38.7	11.2	1.14	1.17	18	0.288	90.8	106.4	763.8	16.1	3.1	4.0	99.9	27.5	1.63	0.039
P11	3002	122.0	38.4	10.8	1.14	1.13	18	0.282	91.1	107.5	768.4	15.8	3.1	3.9	99.5	30.1	1.67	0.039
Ref2	3006	122.1	38.4	11.1	1.15	1.16	19	0.289	90.5	107.2	761.2	13.1	3.1	3.9	99.7	27.9	1.63	0.039

Engine Out Emissions													Atmospheric Conditions			SABS Corrections		
Hydrocarbons			NO			CO2			CO			O2	Barometric Pressure	Dry Bulb Temperature	Wet Bulb Temperature	Correction Factor	Corrected Torque	Corrected Power
[ppm]	[g/kW.hr]	[g/km]	[ppm]	[g/kW.hr]	[g/km]	[% vol]	[g/kW.hr]	[g/km]	[% vol]	[g/kW.hr]	[g/km]	[% vol]	[mBar]	[° C]	[° C]	[-]	[Nm]	[kW]
2052	3.93	-	1138	7.22	-	12.1	734.0	-	5.0	191.23	-	0.2	1003.5	18.0	11.0	0.98	121.4	38.2
1832	3.41	-	>2000	12.36	-	13.3	785.8	-	2.7	100.43	-	0.3	1012.9	18.5	14.0	0.98	124.6	39.2
2273	4.37	-	1142	7.29	-	12.0	732.3	-	4.4	170.64	-	0.3	1009.1	21.0	15.5	0.99	121.7	38.1
1944	3.65	-	1164	7.24	-	12.2	728.5	-	4.6	173.44	-	0.2	1007.4	19.0	14.5	0.98	123.4	38.8
2062	3.91	-	1185	7.45	-	12.2	735.1	-	4.5	171.92	-	0.2	1010.9	21.0	15.5	0.98	122.9	38.7
2189	4.17	-	1120	7.07	-	12.1	732.2	-	4.7	180.43	-	0.2	1006.2	21.5	16.0	0.99	123.0	38.7
2288	4.48	-	1059	6.87	-	12.0	747.8	-	4.5	178.03	-	0.3	1005.1	22.0	18.0	1.00	122.1	38.3
2015	3.80	-	1295	8.10	-	12.3	733.6	-	4.3	164.49	-	0.3	1013.5	19.0	12.5	0.97	123.0	38.7
2470	4.72	-	1225	7.76	-	12.1	735.6	-	4.5	175.22	-	0.3	1004.4	20.0	14.5	0.99	122.5	38.6
2454	4.67	-	1222	7.71	-	12.3	743.7	-	4.5	171.37	-	0.3	1002.8	21.0	16.0	0.99	122.1	38.3
2340	4.52	-	1094	7.01	-	12.1	738.8	-	4.5	174.43	-	0.2	1007.6	20.0	15.0	0.99	121.4	38.1
2319	4.45	-	1210	7.70	-	12.3	747.0	-	4.5	175.16	-	0.2	1002.8	25.0	16.5	1.00	122.1	38.4
2362	4.59	-	1036	6.67	-	11.9	730.7	-	4.8	187.27	-	0.3	1007.0	20.0	16.0	0.99	120.7	38.0

Sample	Engine Operating Point			Engine Operating Conditions															
	Speed	Torque	Power	Fuel Flow Rate	Equivalence Ratio	Equivalence Ratio	Ignition Timing	BSFC	Water Temperature	Oil Temperature	Exhaust Temperature	Fuel Pressure	Oil Pressure	Manifold Pressure	Manifold Temperature	Droplet Temperature	Air Flow Rate	Air Flow Rate
	[rev/min]	[Nm]	[kW]	[kg/hr]	(calc) [-]	(meas) [-]	[° CA BTDC]	[kg/kW.hr]	[° C]	[° C]	[° C]	[bar]	[bar]	[kPa]	[° C]	[° C]	[mbar]	[kg/s]
Ref3	3001	135.3	42.5		1.10		18		92.3	110.3	771.4	3.1	4.0	100.3	28.5	12.0	1.78	0.0411
P12																		
P13																		
P14	2998	133.5	41.6	11.25	1.05	1.13	15	0.270	92.4	107.8	789.2	3.1	3.9	99.6	25.1	10.7	1.76	0.0408
P15	3005	134.7	42.1	10.59	1.06	1.06	18	0.251	92.5	107.3	774.0	3.1	4.0	99.5	27.9	12.2	1.76	0.0407
P16	3000	133.4	41.6	11.38	1.09	1.14	18	0.273	91.7	104.0	764.9	3.1	3.9	98.8	29.0	14.4	1.75	0.0407
P17	3006	133.9	41.9	11.10	1.09	1.12	18	0.265	91.9	107.4	768.4	3.1	4.0	99.4	29.9	15.4	1.76	0.0406
P18	2999	134.5	42.0	11.11	1.10	1.12	18	0.265	93.0	107.8	759.7	3.9	3.1	99.5	28.0	13.6	1.76	0.0407
P19	3003	134.8	42.1	11.28	1.09	1.14	18	0.268	92.3	107.3	761.7	3.1	4.0	99.3	29.3	15.6	1.76	0.0406
P20																		
P21																		
P22																		
P23																		
P24	3002	133.9	41.8	11.04	1.06	1.11	18	0.264	92.6	107.0	772.3	3.1	4.1	99.1	27.4	12.0	1.77	0.0406
Ref4	2998	133.6	41.6	11.46	1.08	1.15	18	0.275	91.9	105.1	764.1	3.1	3.8	99.0	28.6	13.4	1.77	0.0406

Engine Out Emissions														Atmospheric Conditions			SABS Corrections		
Hydrocarbons			NO			CO2			CO			O2	H2S	SO2	Barometric Pressure	Dry Bulb Temperature	Wet Bulb Temperature	Correction Factor	Corrected Torque	Corrected Power
[ppm]	[g/kW.hr]	[g/km]	[ppm]	[g/kW.hr]	[g/km]	[% vol]	[g/kW.hr]	[g/km]	[% vol]	[g/kW.hr]	[g/km]	[% vol]	[ppm]	[ppm]	[mBar]	[° C]	[° C]	[-]	[Nm]	[kW]
1715	2.86	-	1652	9.14	-	13.0	690.2	-	3.47	116.79	-	0.3	-	-	1014.0	17.0	13.0	0.97	131.3	41.2
1307	2.43	-	>2000	12.30	-	13.6	800.1	-	2.06	76.98	-	0.3	-	-	1007.0	16.0	11.0	0.97	130.0	40.6
1291	2.37	-	>2000	12.16	-	13.4	781.1	-	2.24	82.76	-	0.3	-	-	1006.5	18.0	12.0	0.98	131.9	41.2
1606	2.76	-	1729	9.87	-	14.1	771.5	-	3.33	115.47	-	0.2	-	-	1001.2	13.9	10.5	0.74	115.5	36.0
1645	2.95	-	1910	11.34	-	13.3	756.7	-	3.15	113.91	-	0.2	-	-	1006.5	19.0	13.0	0.98	131.5	41.1
1481	2.73	-	1688	10.32	-	12.8	749.6	-	3.20	118.89	-	0.2	-	-	1007.1	19.0	13.0	0.98	132.0	41.2
1618	2.82	-	1788	10.33	-	13.7	755.9	-	3.27	115.08	-	0.2	-	-	1005.6	19.0	13.0	0.98	130.2	40.7
1224	2.18	-	>2000	11.83	-	14.1	799.2	-	2.15	77.47	-	0.2	-	-	1003.8	19.0	16.0	0.99	132.7	41.4
1529	2.70	-	1811	10.59	-	13.9	776.5	-	2.93	104.24	-	0.2	-	-	1002.8	21.0	15.0	0.99	132.6	41.3

Sample	Engine Operating Point			Engine Operating Conditions							Racer Input Parameters				
	Speed	Torque	Racer File Name	Fuel Flow Rate	Equivalence Ratio	Ignition Timing	Manifold Pressure	Manifold Temperature	Droplet Temperature	Air Flow Rate	Charge Temperature	Cylinder Charge Mass	Re Reference Pressure	Air Fuel Ratio	Fuel Flow Rate
	[rev/min]	[Nm]	[-]	[kg/hr]	(calc) [-]	[° CA BTDC]	[kPa]	[° C]	[° C]	[kg/s]	[° C]	[kg]	[kPa]	[-]	[kg/s]
Ref3	3001	135.3	rf302106	*11.46*	1.10	18	100.3	28.5	12.0	0.04112	38.5	*0.0004428*	*98.52*	12.5	0.00318
P12															
P13															
P14	2998	133.5	P14-3000	11.25	1.05	15	99.6	25.1	10.7	0.04077	35.1	0.0004392	96.68	13.0	0.00313
P15	3005	134.7	P15-3000	10.59	1.06	18	99.5	27.9	12.2	0.04072	37.9	0.0004358	96.81	12.9	0.00294
P16	3000	133.4	P163000	11.38	1.09	18	98.8	29.0	14.4	0.04067	39.0	0.0004382	97.69	12.6	0.00316
P17	3006	133.9	P17-3000	11.10	1.09	18	99.4	29.9	15.4	0.04058	39.9	0.0004358	97.40	12.6	0.00308
P18	2999	134.5	P18-3000	11.11	1.10	18	99.5	28.0	13.6	0.04067	38.0	0.0004377	97.24	12.5	0.00309
P19	3003	134.8	P19-3000	11.28	1.09	18	99.3	29.3	15.6	0.04056	39.3	0.0004366	97.40	12.6	0.00313
P20															
P21															
P22															
P23															
P24	3002	133.9	P24-3000	11.04	1.06	18	99.1	27.4	12.0	0.04064	37.4	0.0004369	96.87	13.0	0.00307
Ref4	2998	133.6	rf3-3000	11.46	1.08	18	99.0	28.6	13.4	0.04059	38.6	0.0004380	97.50	12.6	0.00318

Sample	Pressure/CA results								Single Zone Model Results											
	IMEP	PMEP	IMEP(net)	Stability	Pressure		Rate of Pressure Rise		Heat Released			Gas Temperature		Induction Period			Burn Angle			
	[kPa]	[kPa]	[kPa]	[%]	Max [kPa]	CA [Max.] [° CA]	Max [kPa/°]	CA [Max.] [° CA]	Total [kJ]	Max. Rate [kJ/° CA]	CA [Max. Rate] [° CA]	Max [K]	CA [Max] [° CA]	2-98 [° CA]	5-95 [° CA]	10-90 [° CA]	2-98 [° CA]	5-95 [° CA]	10-90 [° CA]
Ref3	1382.12	-48.12	1334.01	9.5	5183.2	23	165.2	11	1776.16	4286.93	16	3689.4	32	10.2	15.8	19.9	39.7	29.4	22.4
P12																			
P13																			
P14	1340.29	-43.08	1297.21	10.2	4587.6	26	124.8	13	1768.45	3889.67	19	3692.9	36	9.6	15.2	19.4	40.5	32.5	23.6
P15	1382.01	-42.13	1339.88	9.3	5109.2	23	158.9	11	1771.92	4201.16	16	3692.6	32	10.1	15.7	19.8	38.9	30.9	23.9
P16	1360.48	-45.14	1315.35	9.1	5125.3	23	161.9	11	1744.78	4200.7	16	3630	32	10.4	15.8	19.9	39.2	29.3	22.4
P17	1375.96	-44.84	1331.12	9.9	5152.3	23	161.7	10	1763.51	4227.49	16	3727.2	32	9.9	15.5	19.6	39.8	29.6	22.6
P18	1373.62	-45.39	1328.24	9.7	5072.3	23	156.3	11	1774.67	4174.21	16	3685	33	10.1	15.8	20	40.8	30.5	23.5
P19	1377.15	-43.57	1333.58	8.6	5138.8	23	157.6	11	1767.67	4258.26	17	3658.3	32	10	15.6	19.8	39.8	29.6	22.4
P20																			
P21																			
P22																			
P23																			
P24	1355.06	-39.95	1315.12	9.9	4921.6	24	143.2	11	1754.6	4050.57	17	3664.9	33	10.1	16	20.3	39.9	31.6	24.4
Ref4	1359.36	-40.56	1318.8	10.4	4981.8	23	149.2	11	1733.31	4055.13	18	3485.8	33	10.1	15.8	20.1	40.6	30.2	23.1

Sample	Two Zone Model Results														Equilibrium Products Results - CO_2				
	Mass Transferred				Unburned Gas Temperature		Burned Gas Temperature		Induction Period			Burn Angle			End of Cycle	Exhaust Valve Open	End of Combustion	Maximum	Angle at Maximum
	Total [g]	Total % [%]	Max. Rate [g/° CA]	CA [Max. Rate] [° CA]	Max [K]	CA [Max] [° CA]	Max [K]	CA [Max] [° CA]	2-98 [° CA]	5-95 [° CA]	10-90 [° CA]	2-98 [° CA]	5-95 [° CA]	10-90 [° CA]	[% vol]	[% vol]	[% vol]	[% vol]	[° CA]
Ref3	0.516	116.45	1.282342	17	742.36	19	2704.49	17	11.4	16.7	20.7	38.9	30	24	11.5	12.7	12.2	12.8	107
P12																			
P13																			
P14	0.555	126.28	1.219867	20	713.64	20.5	2661.9	-15	9.5	15.9	20.4	62.2	38.5	27.8	13.6	15.1	14.3	15.2	114
P15	0.513	117.71	1.290455	17	752.83	19	2709.6	18	11.2	16.5	20.6	38.7	30.2	22.6	12.5	14.8	14.5	15.3	105
P16	0.51	116.37	1.257856	17	741.41	19	2698.79	17	11.5	16.8	20.7	40.8	31.1	23.9	11.4	12.6	12.0	12.7	120
P17	0.512	117.46	1.268036	17	747.76	19	2713.66	17	11.1	16.4	20.5	39.1	30.1	23.9	11.8	13.1	12.8	13.3	107
P18	0.514	117.37	1.256422	17	741.98	19.5	2706.67	18	11.3	16.7	20.8	40.5	30.2	23.6	11.7	13.0	12.7	13.2	106
P19	0.514	117.79	1.280162	17	742.08	19.5	2703.86	18	11.1	16.5	20.6	39.1	29.8	23.2	11.6	12.8	12.4	12.9	106
P20																			
P21																			
P22																			
P23																			
P24	0.503	115.11	1.229661	18	742.16	20	2713.44	19	11.2	16.8	21	39.1	31.3	23.7	11.9	13.7	13.7	14.1	98
Ref4	0.512	116.91	1.232854	18	732.95	19.5	2686.09	18	11.3	16.8	20.9	41.3	31.1	24.7	11.4	12.4	11.9	12.5	107

Sample	Equilibrium Products Results - CO					Equilibrium Products Results - O_2				
	End of Cycle	Exhaust Valve Open	End of Combustion	Maximum	Angle at Maximum	End of Cycle	Exhaust Valve Open	End of Combustion	Minimum	Angle at Minimum
	[% vol]	[% vol]	[% vol]	[% vol]	[° CA]	[% vol]	[% vol]	[% vol]	[% vol]	[° CA]
Ref3	2.4	3.8	4.6	4.7	34	0.9	-2.8	-3.3	-3.4	51
P12										
P13										
P14	1.4	2.3	2.9	3.0	34	-1.4	-4.9	-4.5	-5.4	104
P15	0.0	0.0	1.2	1.9	27	1.4	-2.2	-3.2	-3.2	43
P16	2.3	3.8	4.8	4.8	35	1.1	-2.6	-3.2	-3.4	68
P17	2.0	3.2	4.0	4.1	32	0.8	-2.8	-3.5	-3.6	52
P18	2.0	3.2	4.0	4.2	33	0.9	-2.7	-3.5	-3.6	51
P19	2.3	3.7	4.6	4.7	34	0.9	-2.8	-3.6	-3.7	51
P20										
P21										
P22										
P23										
P24	1.0	1.5	2.2	2.7	30	1.6	-2.0	-3.0	-3.0	44
Ref4	2.6	4.1	5.1	5.2	36	1.0	-2.6	-3.4	-3.5	52

Sample	Equilibrium Products Results - NO							
	End of Cycle	Exhaust Valve Open	End of Combustion	Max Burned Gas Temp	Maximum	Angle at Maximum	Burned Gas Temp=2000k	Angle at Burned Gas Temp=2000k
	[% vol]	[% vol]	[% vol]	[% vol]	[% vol]	[° CA]	[% vol]	[° CA]
Ref3	0.000	0.000	0.039	0.148	0.183	23	0.002	67
P12								
P13								
P14	0.000	0.000	0.053	0.001	0.227	26	0.003	65
P15	0.000	0.001	0.329	0.428	0.555	27	0.048	76
P16	0.000	0.000	0.038	0.138	0.169	22	0.002	67
P17	0.000	0.000	0.057	0.185	0.228	23	0.002	68
P18	0.000	0.000	0.057	0.183	0.218	23	0.002	69
P19	0.000	0.000	0.049	0.161	0.191	25	0.002	68
P20								
P21								
P22								
P23								
P24	0.000	0.000	0.148	0.299	0.365	26	0.005	73
Ref4	0.000	0.000	0.034	0.125	0.149	23	0.002	67

Sample	Engine Operating Point			Engine Operating Conditions															
	Speed	Torque	Power	Fuel Flow Rate	Equivalence Ratio	Equivalence Ratio	Ignition Timing	BSFC	Water Temperature	Oil Temperature	Exhaust Temperature	Fuel Pressure	Oil Pressure	Manifold Pressure	Manifold Temperature	Droplet Temperature	Air Flow Rate	Air Flow Rate
	[rev/min]	[Nm]	[kW]	[kg/hr]	(calc) [-]	(meas) [-]	[° CA BTDC]	[kg/kW.hr]	[° C]	[° C]	[° C]	[bar]	[bar]	[kPa]	[° C]	[° C]	[mbar]	[kg/s]
Ref5	3004	136.6	42.7	11.31	1.11	1.12	18	0.265	92.2	107.6	758.1	3.1	3.9	100.6	28.8	12.8	1.78	0.0411
P25																		
P26																		
P27																		
P28																		
P29																		
P30																		
P31																		
P32																		
P33																		
P34																		
P35																		
Ref6	2999	136.1	42.5		1.10		18		92.5	106.2	763.6	3.1	3.8	99.7	28.0	12.1	1.76	0.0407

Engine Out Emissions														
Hydrocarbons			NO			CO2			CO			O2	H2S	SO2
[ppm]	[g/kW.hr]	[g/km]	[ppm]	[g/kW.hr]	[g/km]	[% vol]	[g/kW.hr]	[g/km]	[% vol]	[g/kW.hr]	[g/km]	[% vol]	[ppm]	[ppm]
1743	3.04	-	1501	8.68	-	13.5	748.5	-	3.54	124.47	-	0.2	-	-
1621	2.59	-	1666	8.83	-	13.8	697.5	-	3.34	107.61	-	0.2	-	-

Atmospheric Conditions		
Barometric Pressure	Dry Bulb Temperature	Wet Bulb Temperature
[mBar]	[° C]	[° C]
1017.7	18.0	13.5
1008.9	19.0	12.5

SABS Corrections		
Correction Factor	Corrected Torque	Corrected Power
[-]	[Nm]	[kW]
0.97	132.3	41.3
0.98	133.1	41.5

Sample	Engine Operating Point			Engine Operating Conditions							Racer Input Parameters				
	Speed	Torque	Racer File Name	Fuel Flow Rate	Equivalence Ratio	Ignition Timing	Manifold Pressure	Manifold Temperature	Droplet Temperature	Air Flow Rate	Charge Temperature	Cylinder Charge Mass	Re Reference Pressure	Air Fuel Ratio	Fuel Flow Rate
	[rev/min]	[Nm]	[-]	[kg/hr]	(calc) [-]	[° CA BTDC]	[kPa]	[° C]	[° C]	[kg/s]	[° C]	[kg]	[kPa]	[-]	[kg/s]
Ref5	3004	136.6	rf43000	*11.31*	1.11	18	100.6	28.8	12.8	0.04113	38.8	*0.0004422*	*98.49*	12.3	0.00314
P25															
P26															
P27															
P28															
P29															
P30															
P31															
P32															
P33															
P34															
P35															
Ref6	2999	136.1	rf53000	11.31	1.10	18	99.7	28.0	12.1	0.04071	38.0	0.0004386	97.43	12.5	0.00327

Sample	Pressure/CA results								Single Zone Model Results											
	IMEP	PMEP	IMEP(net)	Stability	Pressure		Rate of Pressure Rise		Heat Released			Gas Temperature		Induction Period			Burn Angle			
	[kPa]	[kPa]	[kPa]	[%]	Max [kPa]	CA [Max.] [° CA]	Max [kPa/°]	CA [Max.] [° CA]	Total [kJ]	Max. Rate [kJ/° CA]	CA [Max. Rate] [° CA]	Max [K]	CA [Max] [° CA]	2-98 [° CA]	5-95 [° CA]	10-90 [° CA]	2-98 [° CA]	5-95 [° CA]	10-90 [° CA]
Ref5	1388.28	-45.28	1343	9.6	5322.6	22	169	11	1783.82	4353.07	16	3656.6	31	10.2	15.5	19.5	38.5	28.5	21.6
P25																			
P26																			
P27																			
P28																			
P29																			
P30																			
P31																			
P32																			
P33																			
P34																			
P35																			
Ref6	1321.79	-50.51	1271.28	9.9	5003	22	167.9	10	1622.38	3808.23	18	3159.5	31	10.5	15.6	19.5	39.9	29.6	23.3

Sample	Two Zone Model Results														Equilibrium Products Results - CO_2				
	Mass Transferred				Unburned Gas Temperature		Burned Gas Temperature		Induction Period			Burn Angle			End of Cycle	Exhaust Valve Open	End of Combustion	Maximum	Angle at Maximum
	Total [g]	Total % [%]	Max. Rate [g/° CA]	CA [Max. Rate] [° CA]	Max [K]	CA [Max] [° CA]	Max [K]	CA [Max] [° CA]	2-98 [° CA]	5-95 [° CA]	10-90 [° CA]	2-98 [° CA]	5-95 [° CA]	10-90 [° CA]	[% vol]	[% vol]	[% vol]	[% vol]	[° CA]
Ref5	0.515	116.49	1.303552	16	746.07	18.5	2711.17	17	11.3	16.4	20.2	38	29.2	23	11.6	12.9	12.5	13.1	115
P25																			
P26																			
P27																			
P28																			
P29																			
P30																			
P31																			
P32																			
P33																			
P34																			
P35																			
Ref6	0.505	114.69	1.226895	16	728.9	18.5	2682.47	17	11.9	16.8	20.5	0	0	0	11.0	11.9	10.8	12.0	128

Sample	Equilibrium Products Results - CO					Equilibrium Products Results - O_2					Equilibrium Products Results - NO							
	End of Cycle	Exhaust Valve Open	End of Combustion	Maximum	Angle at Maximum	End of Cycle	Exhaust Valve Open	End of Combustion	Minimum	Angle at Minimum	End of Cycle	Exhaust Valve Open	End of Combustion	Max Burned Gas Temp	Maximum	Angle at Maximum	Burned Gas Temp=2000k	Angle at Burned Gas Temp=2000k
	[% vol]	[% vol]	[% vol]	[% vol]	[° CA]	[% vol]	[% vol]	[% vol]	[% vol]	[° CA]	[% vol]	[% vol]	[% vol]	[% vol]	[% vol]	[° CA]	[% vol]	[° CA]
Ref5	2.0	3.3	4.2	4.3	31	1.0	-2.6	-3.3	-3.4	51	0.000	0.000	0.054	0.176	0.212	22	0.002	67
P25																		
P26																		
P27																		
P28																		
P29																		
P30																		
P31																		
P32																		
P33																		
P34																		
P35																		
Ref6	3.2	4.8	5.7	5.7	38	0.9	-2.5	-2.2	-3.0	126	0.000	0.000	0.014	0.099	0.113	21	0.001	63

Engine – 4Y, Load Point - 3000 rev/min WOT

Sample	Engine Operating Point			Engine Operating Conditions													
	Speed	Torque	Power	Fuel Flow Rate	Equivalence Ratio	Equivalence Ratio	Ignition Timing	BSFC	Water Temperature	Oil Temperature	Exhaust Temperature 1&4	Exhaust Temperature 2&3	Oil Pressure	Manifold Pressure	Air Flow Rate	Air Flow Rate
	[rev/min]	[Nm]	[kW]	[kg/hr]	(calc) [-]	(meas) [-]	[° CA BTDC]	[kg/kW.hr]	[° C]	[° C]	[° C]	[° C]	[bar]	[kPa]	[mbar]	[kg/s]
Ref1	3011	160.2	50.5	15.04	1.08	1.11	22.0	0.298	83.7	125.9	773.5	769.2	3.76	94.66	34.00	0.056
P1	3002	161.9	50.9	14.89	1.04	1.09	22.0	0.293	84.2	121.4	776.0	760.1	3.86	94.77	34.16	0.056
P2	3003	163.2	51.3	14.92	1.09	1.10	22.0	0.291	82.9	124.3	762.6	759.0	3.77	95.08	33.89	0.056
P3	3006	163.0	51.3	15.01	1.11	1.10	22.0	0.293	83.0	123.8	762.5	759.5	3.77	95.08	33.93	0.056
P4	3004	162.4	51.1	14.89	1.10	1.09	22.0	0.292	83.1	123.4	765.0	762.5	3.77	95.03	33.85	0.056
P5	3004	162.1	51.0	15.14	1.12	1.12	22.0	0.297	83.3	123.4	757.2	756.0	3.76	94.97	33.68	0.055
P6	3001	161.7	50.8	14.86	1.10	1.09	22.0	0.293	83.5	121.9	762.3	759.5	3.79	94.99	33.79	0.055
P7	3003	163.3	51.4	15.01	1.11	1.10	22.0	0.292	83.2	122.1	761.8	759.3	3.79	95.03	33.88	0.056
P8	3008	162.0	51.0	15.34	1.12	1.13	22.0	0.301	83.0	121.0	759.7	761.2	3.80	95.19	33.92	0.056
P9	3002	162.8	51.2	15.18	1.11	1.12	23.0	0.297	83.0	119.1	762.2	760.2	3.84	95.10	33.84	0.055
P10	3001	162.0	50.9	15.19	1.13	1.11	23.0	0.299	82.8	120.4	752.2	753.2	3.81	94.98	34.03	0.056
P11	3002	162.1	51.0	15.34	1.12	1.13	23.0	0.301	83.3	123.8	760.8	762.9	3.74	94.96	33.81	0.055
P12	3003	164.9	51.9	15.09	1.08	1.09	23.0	0.291	82.7	106.9	753.3	749.3	4.09	94.54	34.82	0.056
P13																
P14	3005	162.5	51.1	15.10	1.05	1.09	22.0	0.295	83.2	123.7	770.6	765.2	3.76	94.62	34.92	0.057
P15	3005	162.6	51.2	15.24	1.06	1.10	22.0	0.298	83.7	123.7	769.2	765.7	3.75	94.72	34.90	0.057
P16	3001	162.2	51.0	15.39	1.09	1.12	22.0	0.302	83.9	125.3	764.8	765.2	3.72	94.85	34.66	0.056
P17	3000	161.9	50.9	15.28	1.09	1.11	22.0	0.300	83.3	124.0	762.6	766.9	3.74	94.76	34.68	0.056
P18	3001	162.3	51.0	14.87	1.09	1.08	22.0	0.292	83.3	124.7	761.4	761.0	3.74	94.79	34.79	0.056
P19	3000	164.9	51.8	14.89	1.08	1.09	22.0	0.287	83.1	116.2	782.1	782.4	3.92	94.85	34.32	0.056
P20	3001	163.8	51.5	15.09	1.11	1.09	22.0	0.293	83.9	123.4	758.2	759.4	3.76	94.82	34.87	0.056
P21																
P22	3002	166.8	52.4	14.98	1.08	1.16	22.0	0.286	83.2	101.1	752.3	752.2	4.23	94.83	30.42	0.053
P23	3003	166.8	52.4	15.09	1.07	1.16	22.0	0.288	83.4	107.8	757.0	755.0	4.10	94.70	30.38	0.053
P24	3000	165.6	52.0	15.08	1.04		22.0	0.290	83.7	124.1	777.8	774.0	3.74	94.44	30.36	
P25																
P26																
P27																
P28																
P29																
P30																
P31																
P32																
P33	3000	170.5	53.6	14.92	1.09	1.08	22.0	0.279	83.6	104.6	763.8	759.9	4.18	94.68	34.60	0.056
P34	3001	169.9	53.4	14.99	1.11	1.07	22.0	0.281	83.7	108.6	759.3	754.0	4.10	94.77	34.63	0.056
P35																
Ref2	3004	164.9	51.9	15.02	1.09	1.09	22.0	0.290	83.8	124.2	774.4	770.1	3.76	94.49	34.55	0.056

Sample	Engine Out Emissions									Atmospheric Conditions			SABS Corrections		
	Hydrocarbons		NO		CO2		CO		O2	Barometric Pressure	Dry Bulb Temperature	Wet Bulb Temperature	Correction Factor	Corrected Torque	Corrected Power
	[ppm]	[g/kW.hr]	[ppm]	[g/kW.hr]	[% vol]	[g/kW.hr]	[% vol]	[g/kW.hr]	[% vol]	[mBar]	[° C]	[° C]	[-]	[Nm]	[kW]
Ref1	2046	4.18	1338	9.06	12.4	800.2	3.8	158.1	0.9	1002.3	30.0	22.0	1.02	163.6	51.6
P1	1654	3.43	1930	13.27	12.6	829.8	2.8	118.2	1.0	1002.3	30.0	22.0	1.02	165.3	52.0
P2	1927	3.96	1502	10.24	12.1	786.6	3.9	162.4	0.7	1006.0	29.5	21.0	1.01	165.3	52.0
P3	2062	6.34	920	9.38	7.7	749.2	2.6	160.0	0.5	1006.0	29.5	21.0	1.01	165.2	52.0
P4	1943	4.00	1387	9.47	12.2	795.4	3.9	162.6	0.6	1006.0	29.5	21.0	1.01	164.5	51.7
P5	2053	4.23	1276	8.72	12.0	781.7	4.3	179.2	0.6	1005.0	31.0	22.0	1.02	165.1	51.9
P6	1979	4.12	1392	9.61	12.1	797.4	3.9	165.9	0.6	1005.9	29.5	21.5	1.01	164.1	51.6
P7	1898	3.89	1445	9.82	12.1	789.4	4.0	166.6	0.6	1005.9	29.5	21.5	1.01	165.7	52.1
P8	2067	4.25	1465	9.98	12.2	793.7	4.2	175.6	0.5	-	-	-	1.00	162.0	51.0
P9	2134	4.37	1515	10.29	12.3	800.3	4.0	165.3	0.5	-	-	-	1.00	162.8	51.2
P10	2081	4.40	1370	9.61	11.7	786.4	4.4	185.8	0.5	-	-	-	1.00	162.0	50.9
P11	2028	4.21	1396	9.60	12.0	791.8	4.3	178.1	0.5	-	-	-	1.00	162.1	51.0
P12	2003	4.11	1414	9.61	12.0	778.0	4.0	164.8	0.9	1001.2	28.0	20.5	1.02	167.5	52.7
P13															
P14	1670	3.48	1345	9.29	12.5	827.3	3.2	133.5	1.0	1005.1	27.5	20.0	1.01	164.0	51.6
P15	1679	3.51	1505	10.43	12.4	820.9	3.5	145.7	0.9	1005.1	27.5	20.0	1.01	164.1	51.6
P16	2039	4.12	1235	8.27	12.5	799.9	4.2	170.6	0.9	1005.1	27.5	20.0	1.01	163.7	51.4
P17	2074	4.20	1275	8.56	12.4	796.2	4.2	173.1	0.8	1004.2	31.0	21.0	1.02	164.7	51.7
P18	1952	4.06	1251	8.63	12.0	792.0	4.0	167.6	0.8	1004.2	31.0	21.0	1.02	165.1	51.9
P19	1922	3.87	1275	8.51	12.5	798.7	3.6	144.4	0.8	-	-	-	1.00	164.9	51.8
P20	1968	4.09	1040	7.16	12.1	797.1	4.1	169.7	0.6	-	-	-	1.00	163.8	51.5
P21															
P22	1967	3.74	1157	7.29	12.5	753.4	3.5	132.4	0.7	1002.8	26.0	22.0	1.02	169.4	53.2
P23	1838	3.51	1298	8.22	12.5	755.0	3.4	132.4	0.8	1001.5	24.0	19.0	1.01	167.9	52.8
P24	1619		1438		12.9	57.8	2.7		0.8	-	-	-	1.00	165.6	52.0
P25															
P26															
P27															
P28															
P29															
P30															
P31															
P32															
P33	1919	3.76	1168	7.59	12.7	792.4	3.5	140.3	0.5	1004.8	27.0	19.0	1.01	171.6	53.9
P34	1881	3.76	1078	7.14	12.3	782.1	3.9	155.9	0.4	1004.8	27.0	19.0	1.01	171.0	53.7
P35															
Ref2	1823	3.62	1452	9.55	12.6	794.5	3.9	156.2	0.8	1002.2	28.0	19.0	1.01	166.7	52.4

APPENDIX E : GRAPHICALLY PRESENTED EMISSIONS RESULTS

Carbon Monoxide Emissions

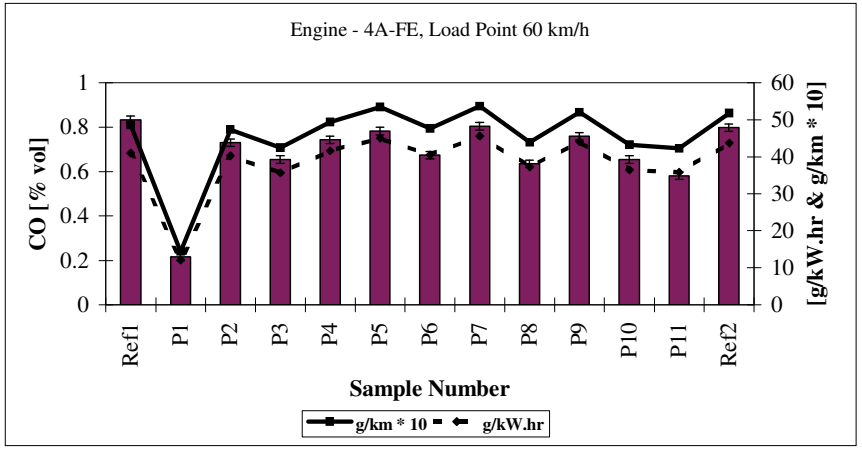

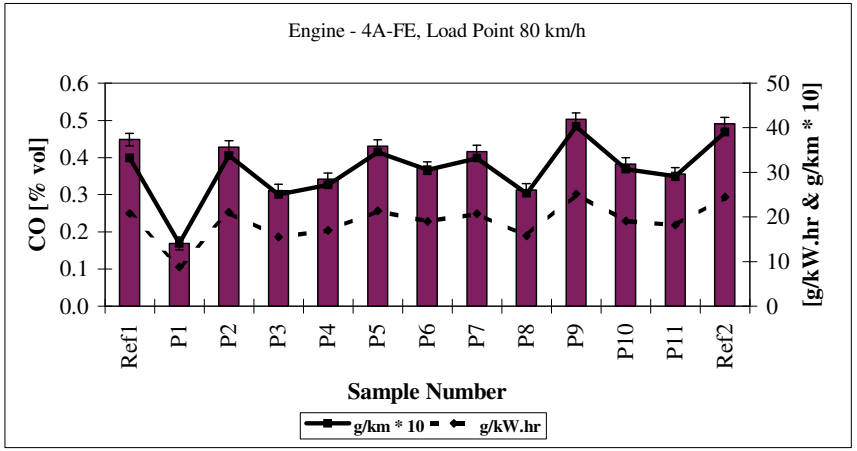

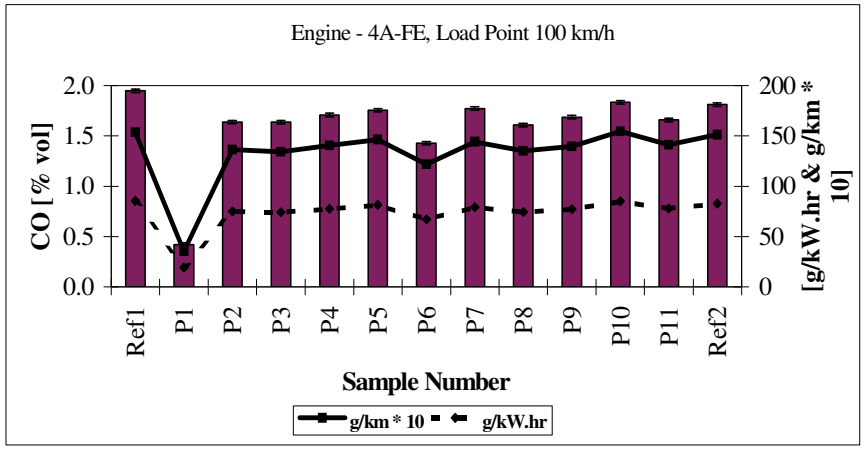

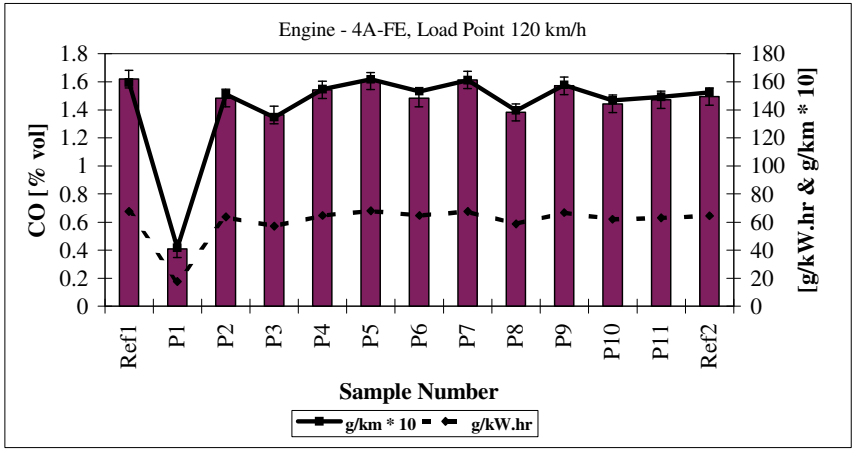

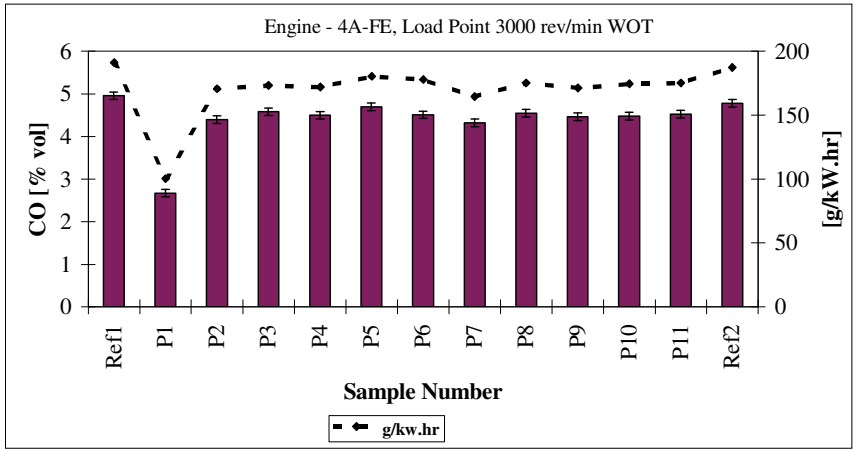
Engine - 4A-FE, Load Point 3000 rev/min WOT
CO [% vol]
[g/kW.hr]
Ref1 P1 P2 P3 P4 P5 P6 P7 P8 P9 P10 P11 Ref2
Sample Number
g/kw.hr

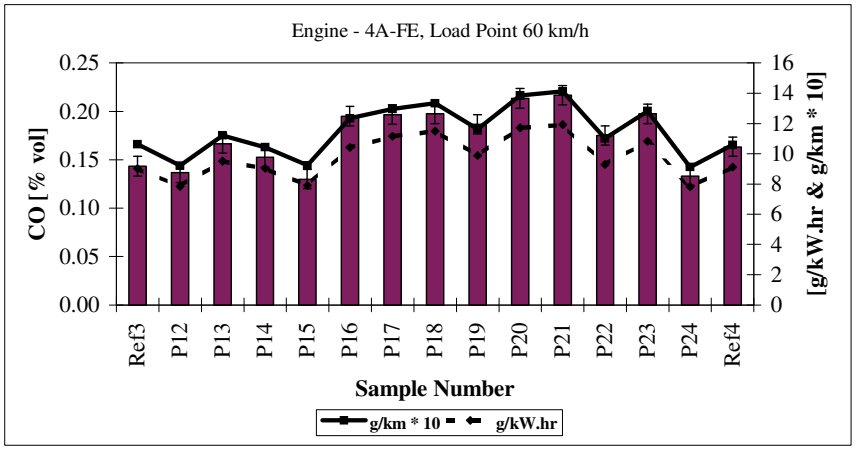
Engine - 4A-FE, Load Point 60 km/h
CO [% vol]
[g/kW.hr & g/km * 10]
Ref3 P12 P13 P14 P15 P16 P17 P18 P19 P20 P21 P22 P23 P24 Ref4
Sample Number
g/km * 10
g/kW.hr

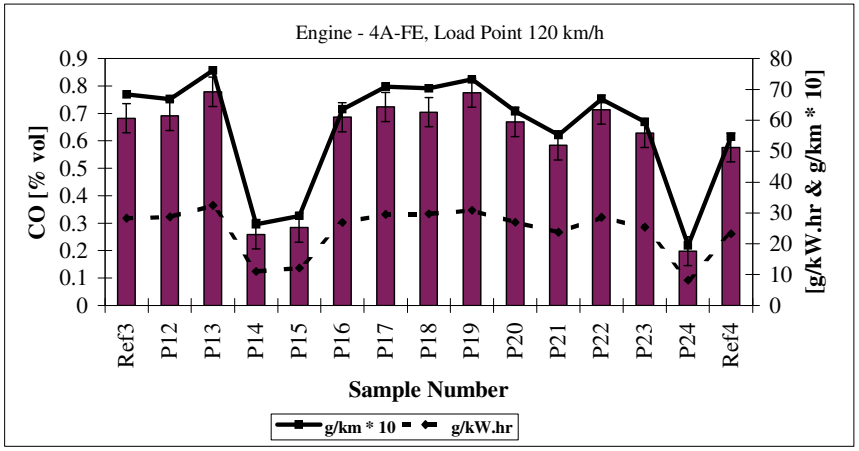
Engine - 4A-FE, Load Point 120 km/h
CO [% vol]
[g/kW.hr & g/km * 10]
Ref3 P12 P13 P14 P15 P16 P17 P18 P19 P20 P21 P22 P23 P24 Ref4
Sample Number
g/km * 10
g/kW.hr

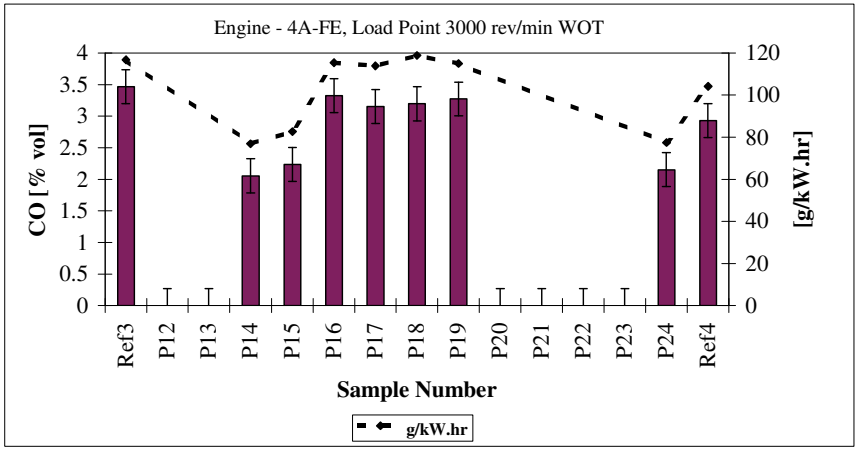
Engine - 4A-FE, Load Point 3000 rev/min WOT
CO [% vol]
[g/kW.hr]
Ref3 P12 P13 P14 P15 P16 P17 P18 P19 P20 P21 P22 P23 P24 Ref4
Sample Number
g/kW.hr

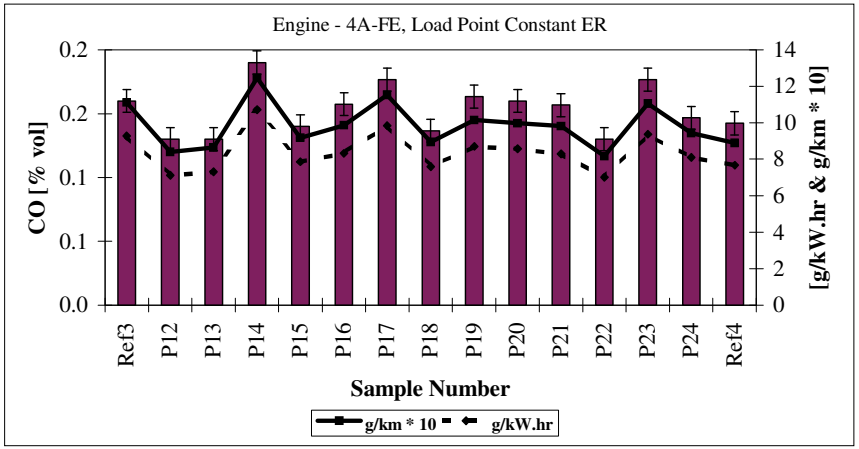
Engine - 4A-FE, Load Point Constant ER
CO [% vol]
[g/kW.hr & g/km * 10]
Ref3 P12 P13 P14 P15 P16 P17 P18 P19 P20 P21 P22 P23 P24 Ref4
Sample Number
g/km * 10
g/kW.hr

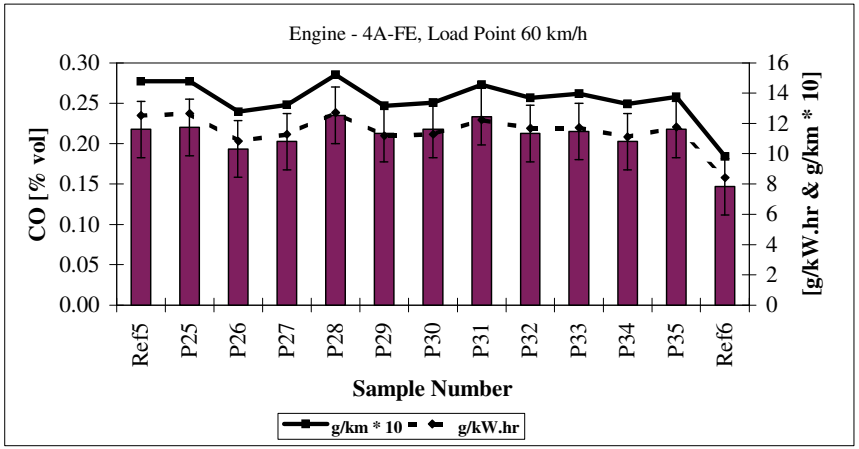
Engine - 4A-FE, Load Point 60 km/h
CO [% vol]
[g/kW.hr & g/km * 10]
Ref5 P25 P26 P27 P28 P29 P30 P31 P32 P33 P34 P35 Ref6
Sample Number
g/km * 10
g/kW.hr

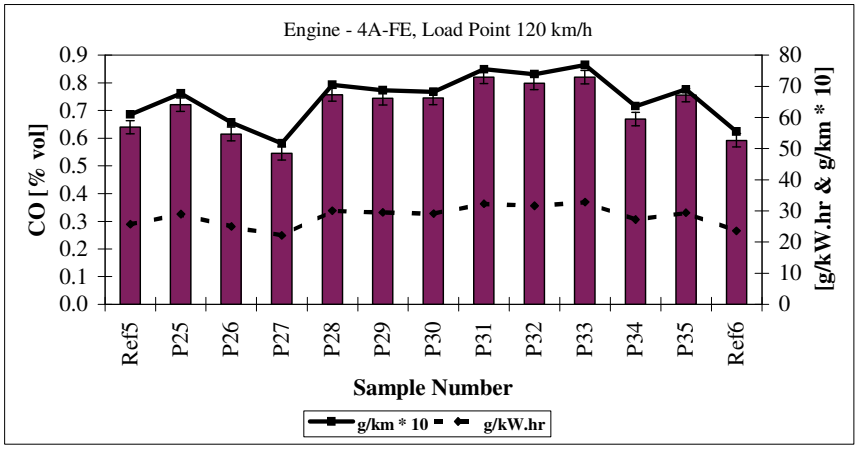
Engine - 4A-FE, Load Point 120 km/h
CO [% vol]
[g/kW.hr & g/km * 10]
Ref5 P25 P26 P27 P28 P29 P30 P31 P32 P33 P34 P35 Ref6
Sample Number
g/km * 10
g/kW.hr

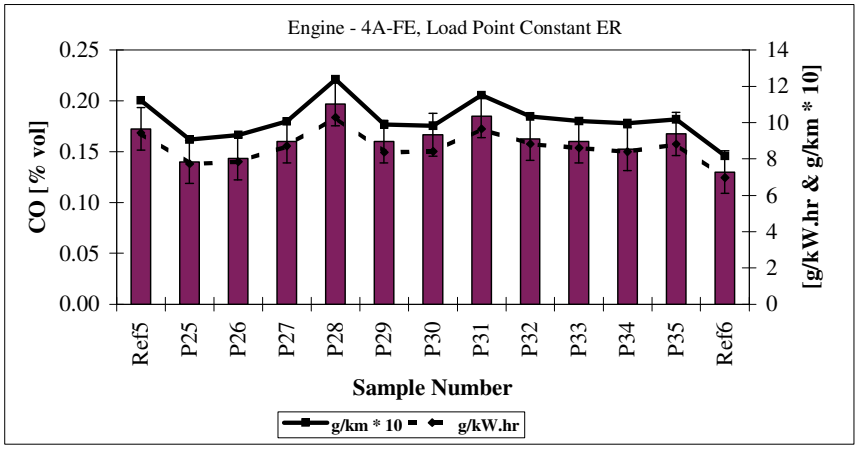
Engine - 4A-FE, Load Point Constant ER
CO [% vol]
[g/kW.hr & g/km * 10]
Ref5 P25 P26 P27 P28 P29 P30 P31 P32 P33 P34 P35 Ref6
Sample Number
g/km * 10
g/kW.hr

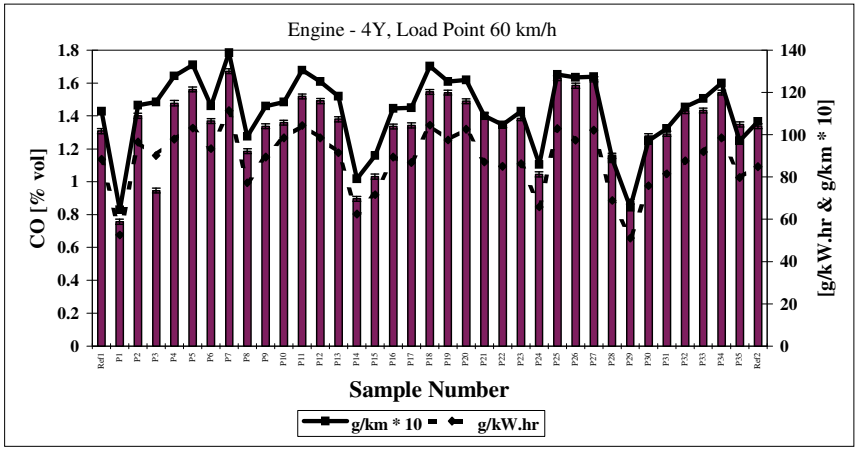
Engine - 4Y, Load Point 60 km/h
CO [% vol]
[g/kW.hr & g/km * 10]
Sample Number
g/km * 10
g/kW.hr

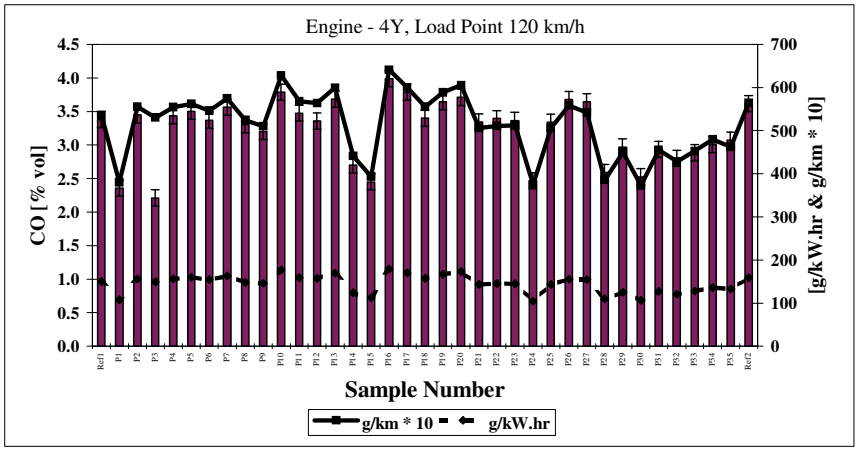
Engine - 4Y, Load Point 120 km/h
CO [% vol]
[g/kW.hr & g/km * 10]
Sample Number
g/km * 10
g/kW.hr

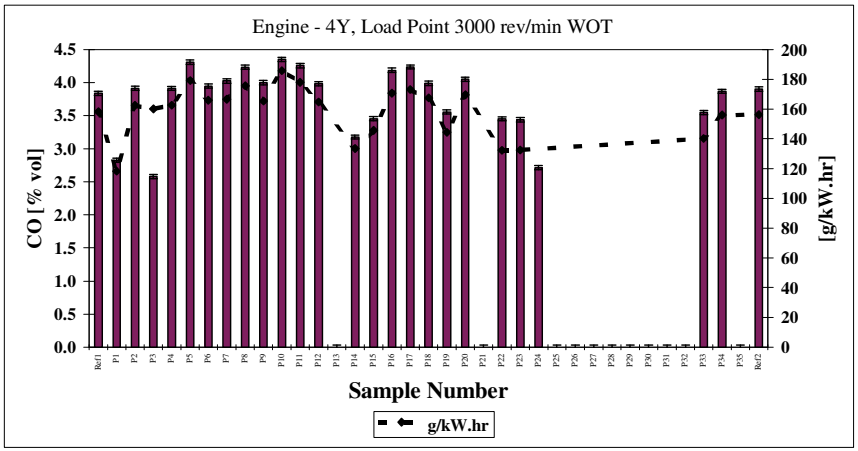
Engine - 4Y, Load Point 3000 rev/min WOT
CO [% vol]
[g/kW.hr]
Sample Number
g/kW.hr

Hydrocarbon Emissions

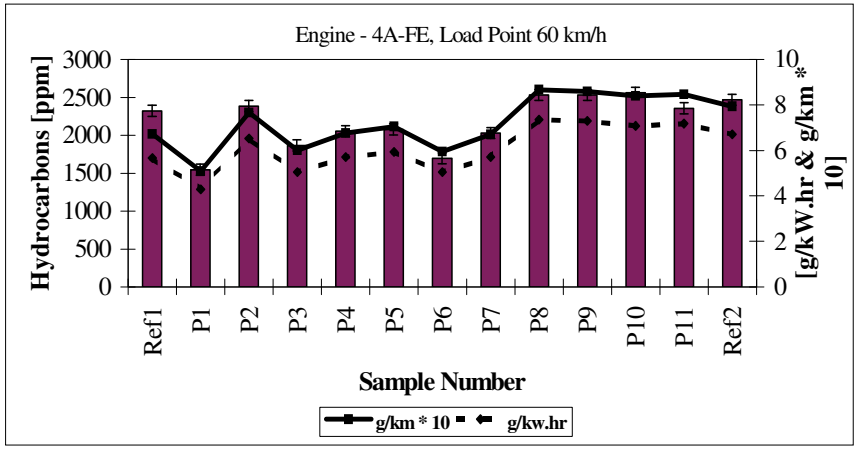

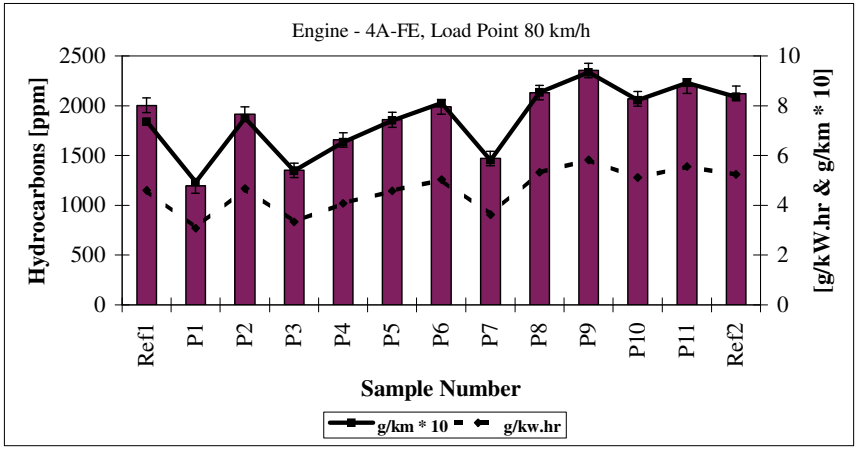

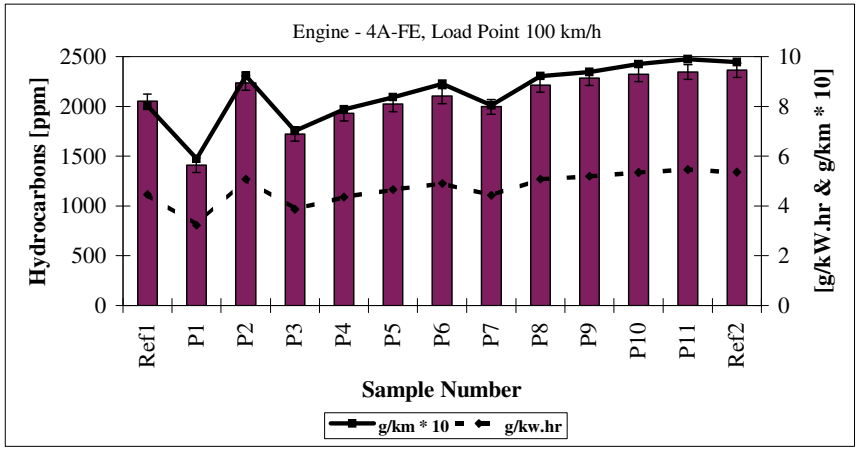

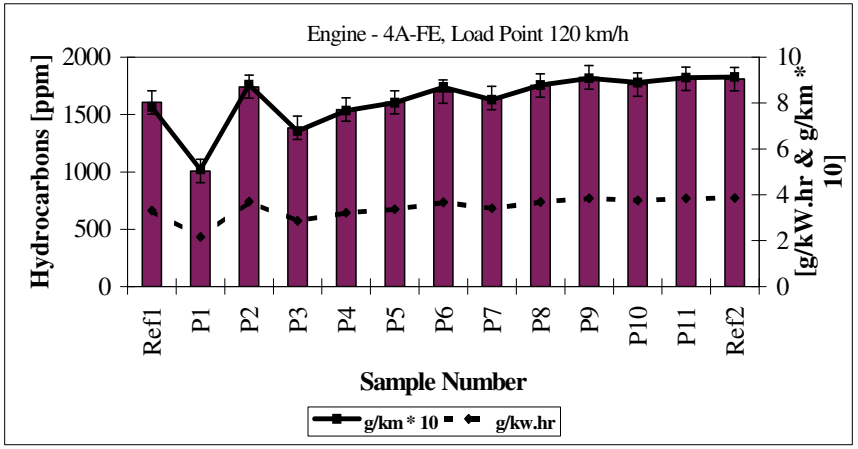

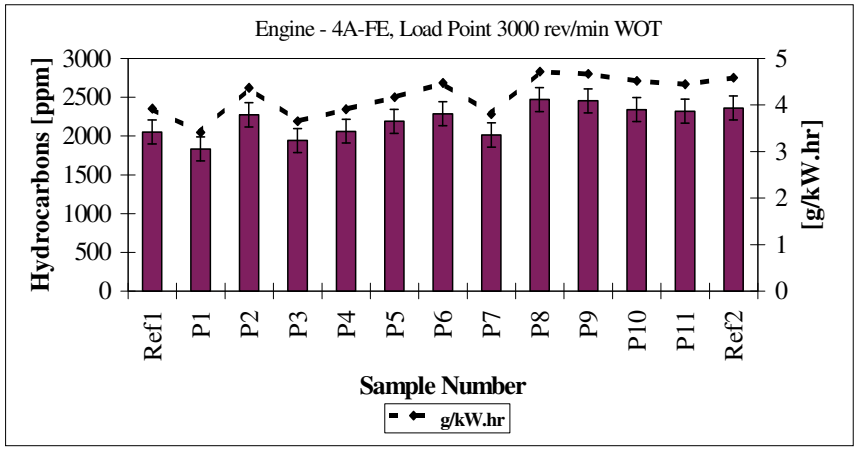
Engine - 4A-FE, Load Point 3000 rev/min WOT
Hydrocarbons [ppm]
[g/kW.hr]
Ref1 P1 P2 P3 P4 P5 P6 P7 P8 P9 P10 P11 Ref2
Sample Number
g/kW.hr

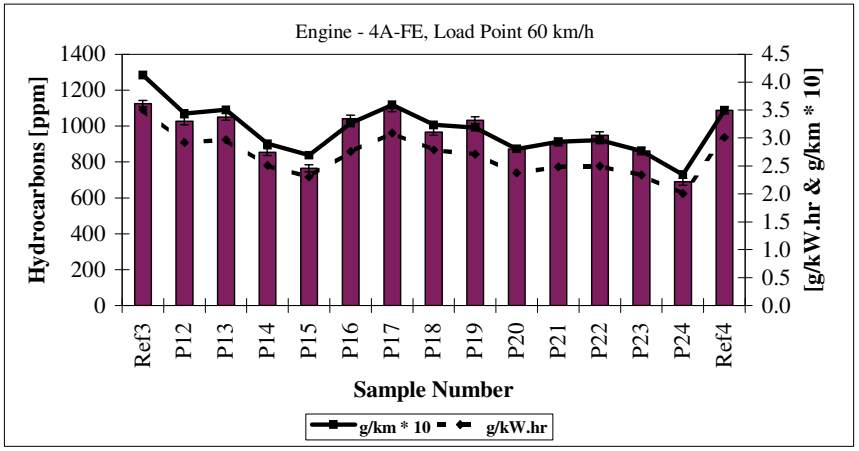
Engine - 4A-FE, Load Point 60 km/h
Hydrocarbons [ppm]
[g/kW.hr & g/km * 10]
Ref3 P12 P13 P14 P15 P16 P17 P18 P19 P20 P21 P22 P23 P24 Ref4
Sample Number
g/km * 10
g/kW.hr

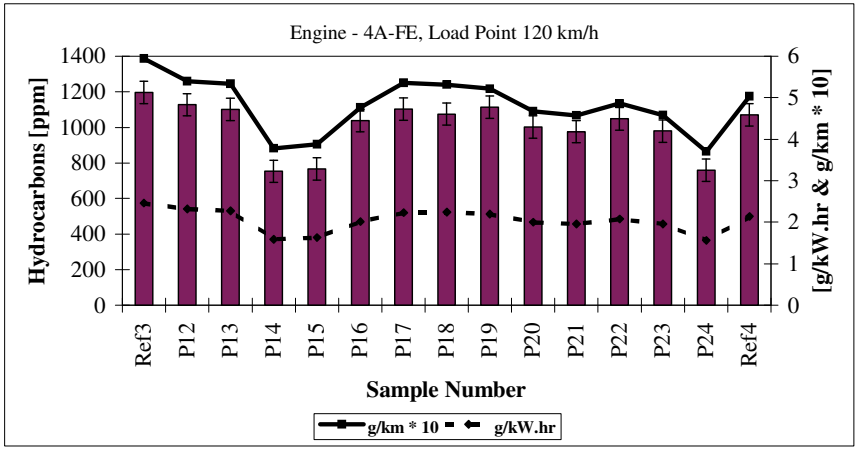
Engine - 4A-FE, Load Point 120 km/h
Hydrocarbons [ppm]
[g/kW.hr & g/km * 10]
Ref3 P12 P13 P14 P15 P16 P17 P18 P19 P20 P21 P22 P23 P24 Ref4
Sample Number
g/km * 10
g/kW.hr

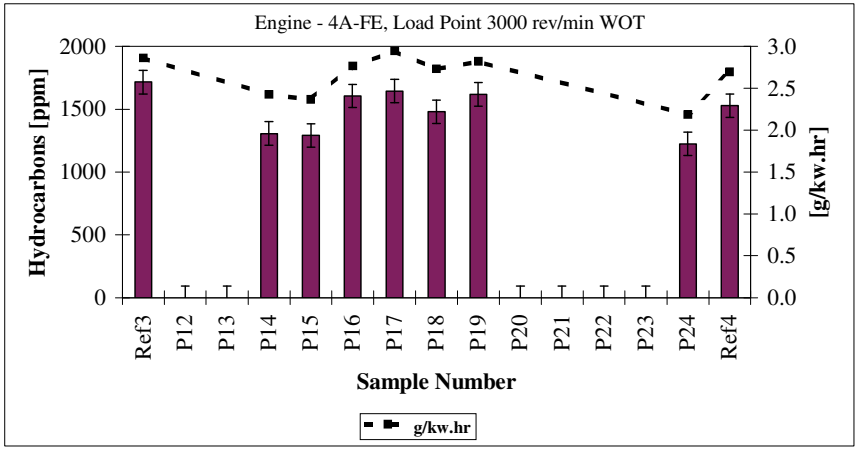
Engine - 4A-FE, Load Point 3000 rev/min WOT
Hydrocarbons [ppm]
[g/kw.hr]
Ref3 P12 P13 P14 P15 P16 P17 P18 P19 P20 P21 P22 P23 P24 Ref4
Sample Number
g/kw.hr

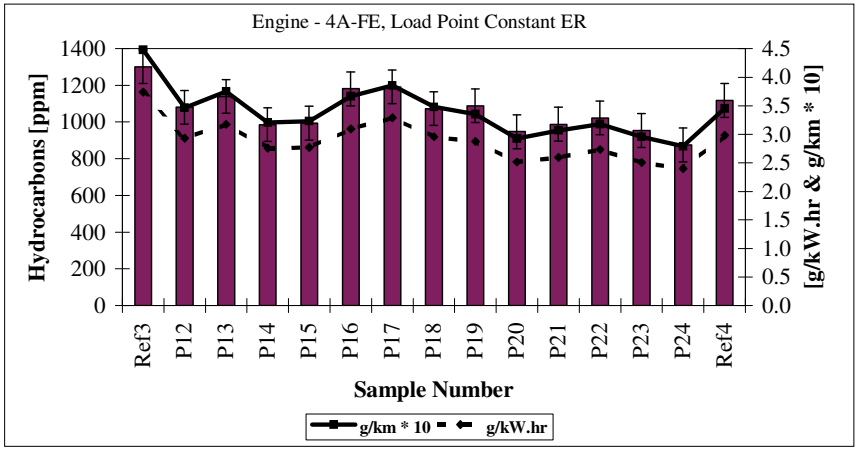
Engine - 4A-FE, Load Point Constant ER
Hydrocarbons [ppm]
[g/kW.hr & g/km * 10]
Ref3 P12 P13 P14 P15 P16 P17 P18 P19 P20 P21 P22 P23 P24 Ref4
Sample Number
g/km * 10
g/kW.hr

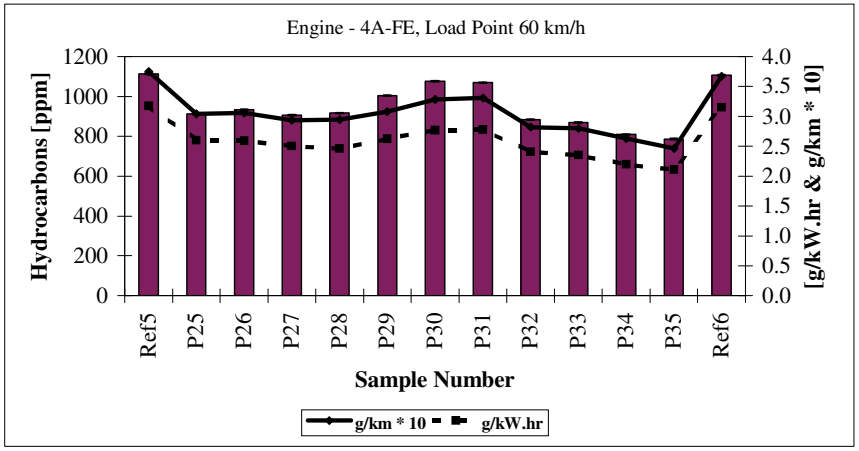
Engine - 4A-FE, Load Point 60 km/h
Hydrocarbons [ppm]
[g/kW.hr & g/km * 10]
Ref5 P25 P26 P27 P28 P29 P30 P31 P32 P33 P34 P35 Ref6
Sample Number
g/km * 10
g/kW.hr

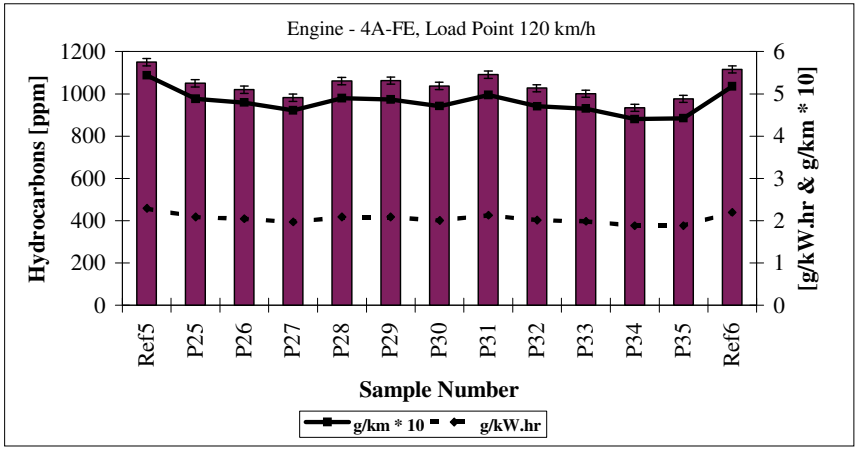
Engine - 4A-FE, Load Point 120 km/h
Hydrocarbons [ppm]
[g/kW.hr & g/km * 10]
Ref5 P25 P26 P27 P28 P29 P30 P31 P32 P33 P34 P35 Ref6
Sample Number
g/km * 10
g/kW.hr

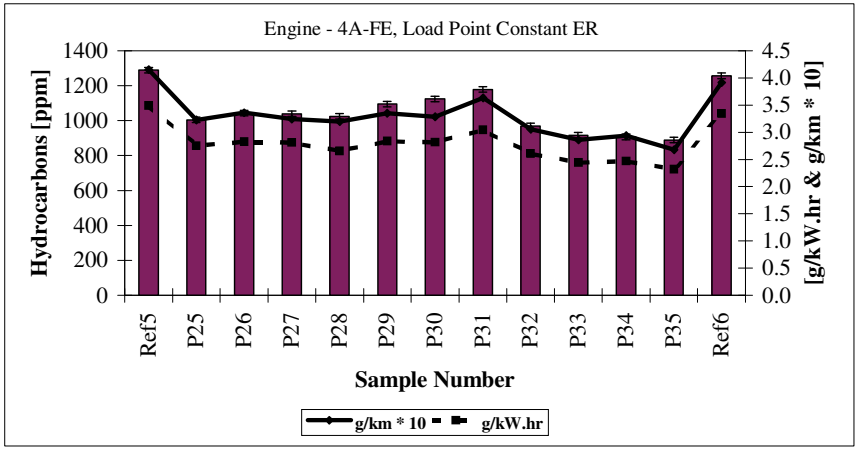
Engine - 4A-FE, Load Point Constant ER
Hydrocarbons [ppm]
[g/kW.hr & g/km * 10]
Ref5 P25 P26 P27 P28 P29 P30 P31 P32 P33 P34 P35 Ref6
Sample Number
g/km * 10
g/kW.hr

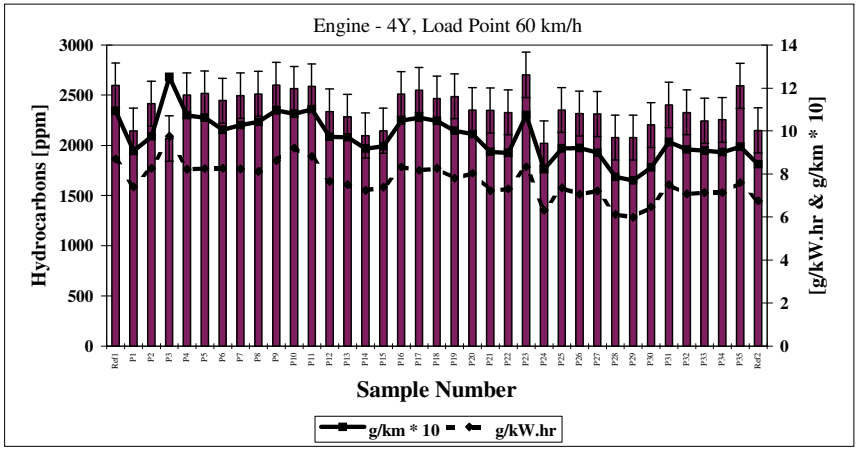
Engine - 4Y, Load Point 60 km/h
Hydrocarbons [ppm]
[g/kW.hr & g/km * 10]
Sample Number
g/km * 10
g/kW.hr

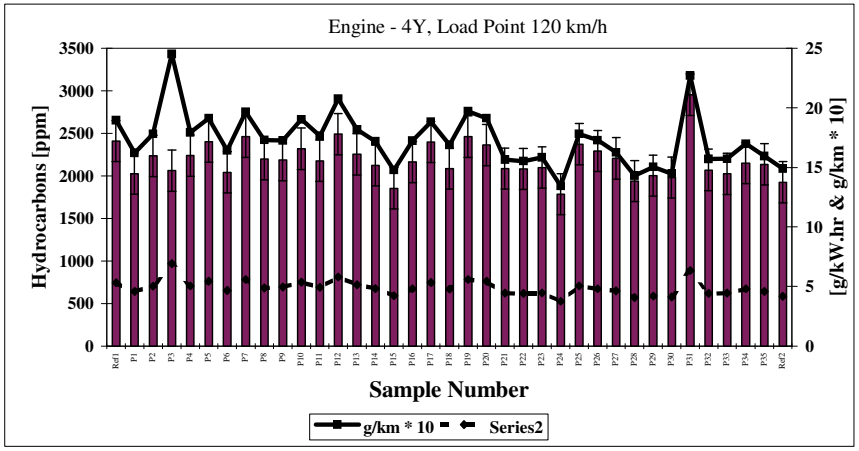
Engine - 4Y, Load Point 120 km/h
Hydrocarbons [ppm]
[g/kW.hr & g/km * 10]
Sample Number
g/km * 10
Series2

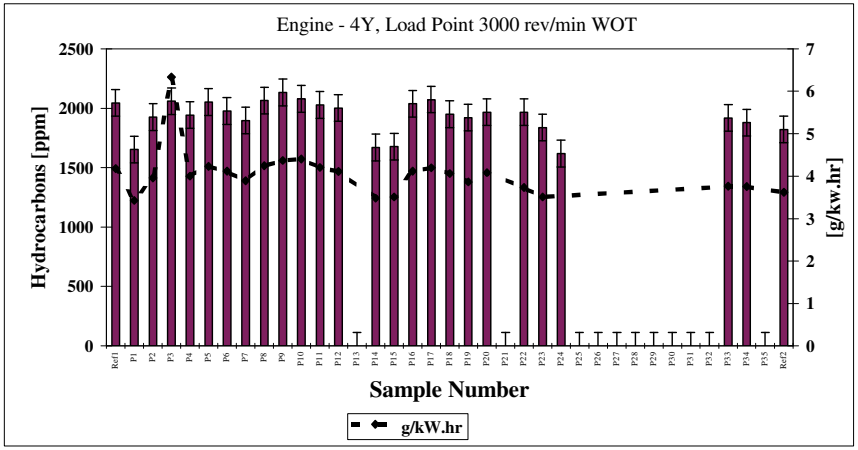
Engine - 4Y, Load Point 3000 rev/min WOT
Hydrocarbons [ppm]
[g/kw.hr]
Sample Number
g/kW.hr

NO Emissions

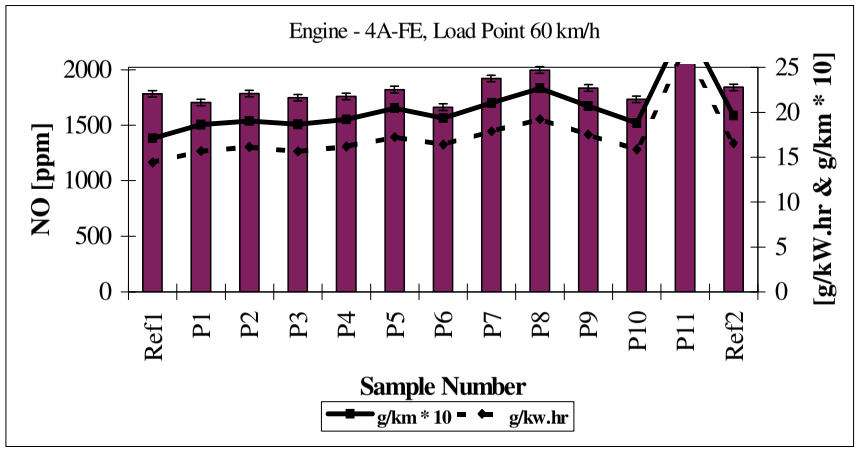

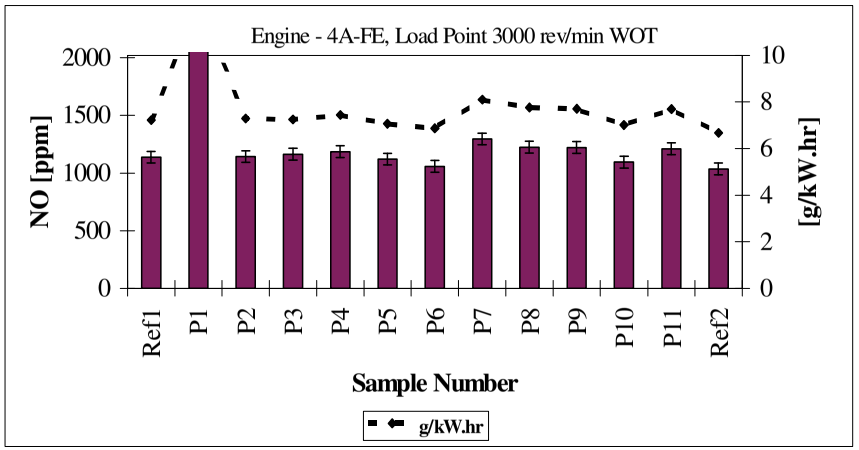

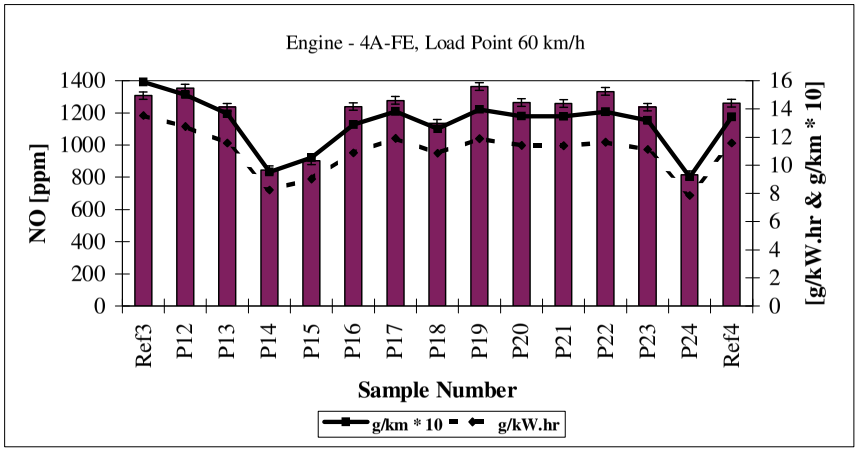

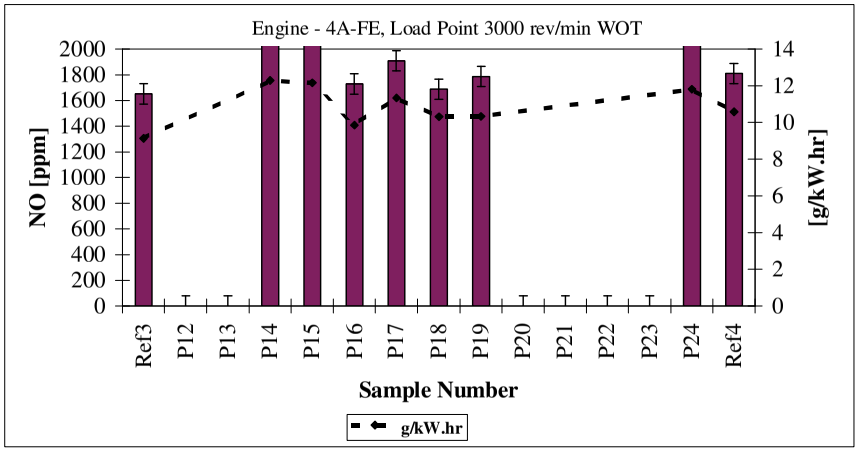

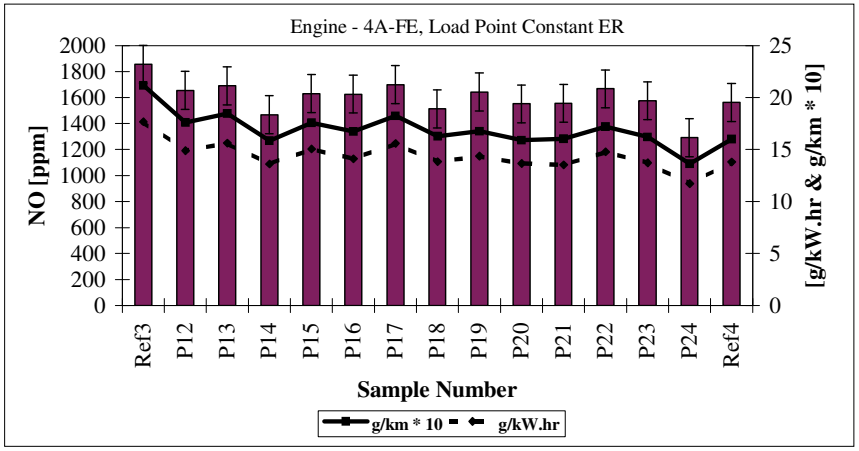
Engine - 4A-FE, Load Point Constant ER
NO [ppm]
[g/kW.hr & g/km * 10]
Ref3 P12 P13 P14 P15 P16 P17 P18 P19 P20 P21 P22 P23 P24 Ref4
Sample Number
g/km * 10
g/kW.hr

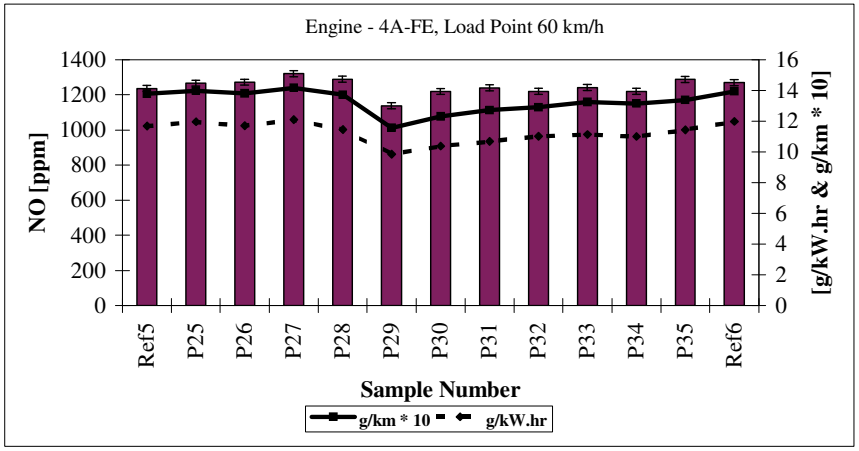
Engine - 4A-FE, Load Point 60 km/h
NO [ppm]
[g/kW.hr & g/km * 10]
Ref5 P25 P26 P27 P28 P29 P30 P31 P32 P33 P34 P35 Ref6
Sample Number
g/km * 10
g/kW.hr

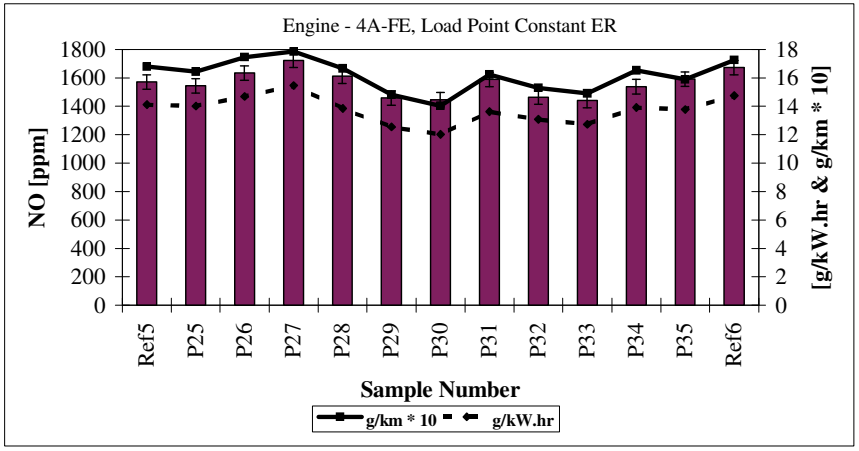
Engine - 4A-FE, Load Point Constant ER
NO [ppm]
[g/kW.hr & g/km * 10]
Ref5 P25 P26 P27 P28 P29 P30 P31 P32 P33 P34 P35 Ref6
Sample Number
g/km * 10
g/kW.hr

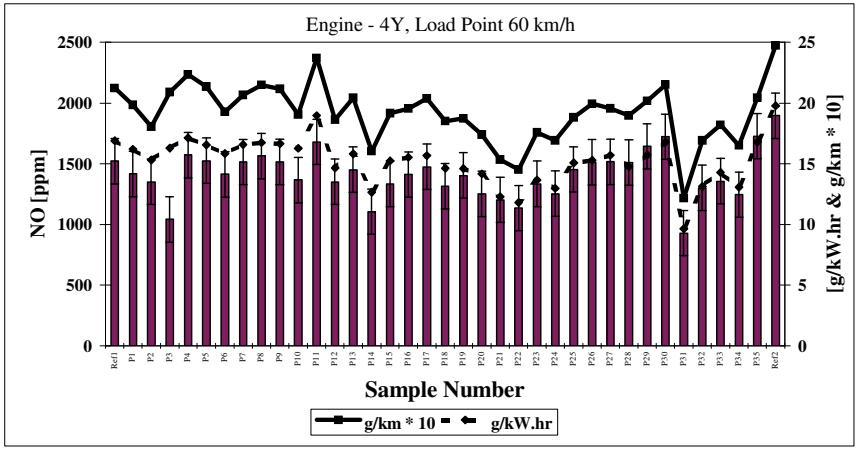
Engine - 4Y, Load Point 60 km/h
NO [ppm]
[g/kW.hr & g/km * 10]
Sample Number
g/km * 10
g/kW.hr

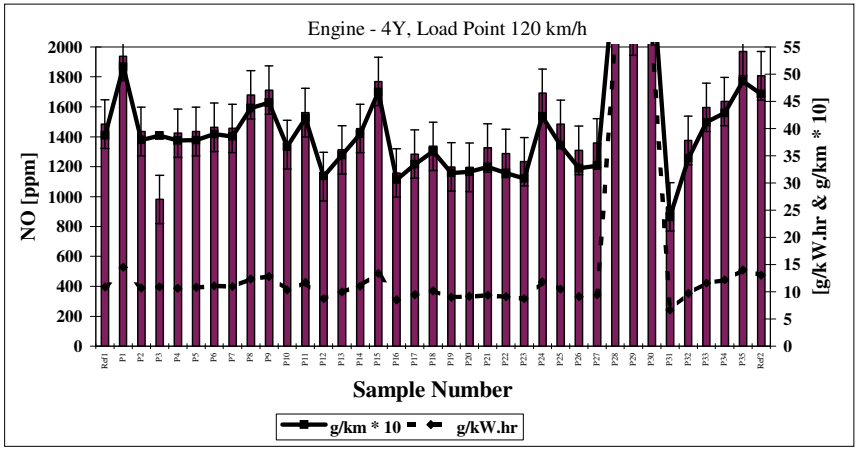
Engine - 4Y, Load Point 120 km/h
NO [ppm]
[g/kW.hr & g/km * 10]
Sample Number
g/km * 10
g/kW.hr

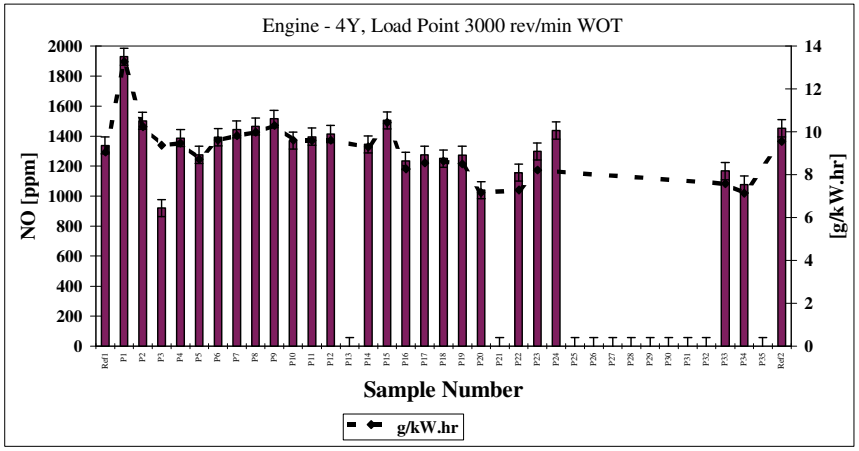
Engine - 4Y, Load Point 3000 rev/min WOT
NO [ppm]
[g/kW.hr]
Sample Number
g/kW.hr

APPENDIX F : RESULTS OF STATISTICAL REGRESSION MODELLING

Variable Labels

Fuel Properties & Engine Operating Conditions

HCGKWH..... HC emissions (g/kW.hr)
NOGKWH ..... NO emissions (g/kW.hr)
COGKWH ..... CO emissions (g/kW.hr)
HCGKM..... HC emissions (g/km)
NOGKM..... NO emissions (g/km)
COGKM..... CO emissions (g/km)
ER ..... Equivalence Ratio
IGNTIM..... Ignition Timing
WATERT..... Engine Coolant Temperature
OILT ..... Engine Oil Temperature
EXHT..... Engine Exhaust Temperature
MANP..... Manifold Absolute Pressure
MANT ..... Manifold Air Temperature
DROPT..... Fuel Droplet Temperature
BARO..... Barometric Pressure
DRYB ..... Cell Dry Bulb Temperature
SPECHUM ..... Cell Specific Humidity
IBP ..... Fuel Initial Boiling Point
T10..... Fuel Distillation Point T_{10}
T30..... Fuel Distillation Point T_{30}
T50..... Fuel Distillation Point T_{50}
T70..... Fuel Distillation Point T_{70}
T90..... Fuel Distillation Point T_{90}
FBP..... Fuel Final Boiling Point
DENS ..... Fuel Density
V/LRATIO..... Fuel Vapour/Liquid Ratio
VAPPRES ..... Fuel Vapour Pressure
E70..... Fuel Distillation Point E_{70}
VOLIND..... Fuel Volatility Index
RON ..... Fuel Research Octane Number
MON..... Fuel Motor Octane Number
SENS ..... Fuel Octane Sensitivity
LEAD..... Fuel Lead Content
A..... Fuel Aromatic Content
O ..... Fuel Olefin Content
P..... Fuel Paraffin Content
AO..... Aromatic/Olefin Interaction
AP ..... Aromatic/Paraffin Interaction
OP..... Olefin/Paraffin Interaction
AOP ..... Aromatic/Olefin/Paraffin Interaction
SULPHUR..... Fuel Sulphur Content
NITROGEN ..... Fuel Nitrogen Content
OXYGEN..... Fuel Oxygen Content
BENZENE ..... Fuel Benzene Content
PHENOLS..... Fuel Phenol Content

Combustion Analysis

IMEP ..... Indicated Mean Effective Pressure
PMEP..... Pumping Mean Effective Pressure
IMEPNET ..... Net Indicated Mean Effective Pressure
STAB..... Combustion Stability
PMAX..... Maximum Cylinder Pressure
CAPMAX..... Crank Angle at Maximum Cylinder Pressure
DPMAX ..... Maximum Rate of Pressure Rise
CADPMAX ..... Crank Angle at Maximum Rate of Pressure Rise
TOTHR..... Total Heat Released – Single Zone Model
DHRMAX..... Maximum Rate of Heat Released – Single Zone Model
CADHRMAX..... Crank Angle at Maximum Rate of Heat Release – Single Zone Model
TMAX ..... Maximum Bulk Gas Temperature – Single Zone Model
CATMAX ..... Crank Angle for Maximum Bulk Gas Temperature – Single Zone Model
IND2..... Induction Period to 2% Burned – Single Zone Model
IND5..... Induction Period to 5% Burned – Single Zone Model
IND10..... Induction Period to 10% Burned – Single Zone Model
BA298 ..... Burn Angle – 2 to 98% Burned – Single Zone Model
BA595 ..... Burn Angle – 5 to 95% Burned – Single Zone Model
BA1090 ..... Burn Angle – 10 to 90% Burned – Single Zone Model
2ZTOTG..... Total Mass Transferred – Two Zone Model
2ZPERCNT ..... Percentage of Total Mass Consumed Transferred – Two Zone model
2ZDGMAX..... Maximum Rate of Mass Transfer – Two Zone Model
2ZDGMXCA ..... Crank Angle at Maximum Rate of Mass Transfer – Two Zone Model
2ZTUBMAX..... Maximum Unburned Gas Temperature – Two Zone Model
2ZTBMAX..... Maximum Burned Gas Temperature – Two Zone Model
2ZIND2..... Induction Period to 2% Burned – Two Zone Model
2ZIND5..... Induction Period to 5% Burned – Two Zone Model
2ZIND10..... Induction Period to 10% Burned – Two Zone Model
2ZBA298..... Burn Angle 2 to 98% Burned – Two Zone Model
2ZBA595..... Burn Angle 5 to 95% Burned – Two Zone Model
2ZBA1090..... Burn Angle 10 to 90% Burned – Two Zone Model

Hydrocarbon Emissions

Fuel Properties Correlation

Model Number	Cp	R^2	P	Number of Observations Used	Colinearities		C1	C2	C3	C4	C5	C6	C7	C8	C9	C10	C11
1	18.47	0.9935	23	206	A/O/P/ER	Coefficient	-1.1046	-1.8756	-3.0768	-3.4938	-1.9197	-3.2825	-1.5189	-3.6865	2.16606	-2.0955	-3.2723
					T30/T50	Uncertainty	0.0001	0.0001	0.0001	0.0001	0.0001	0.0001	0.0001	0.0001	0.0001	0.0001	0.0001
2	17.79	0.9937	24	238	A/O/P/ER	Coefficient	-1.1559	-1.7551	-2.9758	-3.1725	-2.0089	-3.2901	-1.6367	-3.484	1.98088	-1.9935	-3.1172
					T30/T50	Uncertainty	0.0001	0.0001	0.0001	0.0001	0.0001	0.0001	0.0001	0.0001	0.0001	0.0001	0.0001
2 Reduced	23.29	0.9927	23	238	A/O/P/ER	Coefficient	-1.1295	-1.7836	-2.999	-3.2706	-1.9872	-3.3075	-1.6089	-3.6103	2.02724	-2.0422	-3.1728
						Uncertainty	0.0001	0.0001	0.0001	0.0001	0.0001	0.0001	0.0001	0.0001	0.0001	0.0001	0.0001
3	18.57	0.9936	24	206	A/P/ER	Coefficient	-1.1907	-1.7836	-3.0007	-3.1796	-2.0552	-3.2823	-1.6823	-3.4175	2.0531	-1.9017	-3.0475
					O/AO/OP	Uncertainty	0.0001	0.0001	0.0001	0.0001	0.0001	0.0001	0.0001	0.0001	0.0001	0.0001	0.0001
3 Reduced	19.34	0.9934	23	206	A/O/P/ER	Coefficient	-1.1965	-1.7773	-2.9955	-3.1583	-2.0761	-3.2869	-1.7075	-3.4503	2.07352	-1.8615	-3.0041
						Uncertainty	0.0001	0.0001	0.0001	0.0001	0.0001	0.0001	0.0001	0.0001	0.0001	0.0001	0.0001

Model Number		A	O	P	AO	AP	OP	ER	DRYB	IBP	T10	T30	T50	VLRATIO	E70	LEAD	SULPHUR	PHENOLS
1	Coefficient	-0.1416	-0.1286	-0.0865	0.00212	0.0007		11.0904	0.0759	0.02305		-0.0263	0.0295			0.00269		-0.0006
	Uncertainty	0.0001	0.0001	0.0001	0.0001	0.0001		0.0001	0.0001	0.0241		0.001	0.0001			0.0001		0.0365
2	Coefficient	*-0.049*	*-0.035*	*-0.0037*	0.00194	0.00075		8.80754	0.0866	0.0368		-0.0302		-0.0444	-0.0467	0.00272	-7.4081	
	Uncertainty	*0.0709*	*0.2022*	*0.895*	0.0001	0.0001		0.0001	0.0001	0.0003		0.0059		0.0002	0.001	0.0001	0.0003	
2 Reduced	Coefficient	-0.0867	-0.0716	-0.0457	0.00176	0.00074		9.49344	0.08302	0.03493				-0.0395	-0.0115	0.00254	-6.0786	
	Uncertainty	0.0003	0.0037	0.0571	0.0001	0.0001		0.0001	0.0001	0.0007				0.0011	0.0651	0.0001	0.0023	
3	Coefficient	-0.1212	-0.1255	-0.0625	0.0027	0.00081	*0.00034*	8.88925	0.07884	0.02515	-0.0351		0.02234			0.00263		-0.00064
	Uncertainty	0.0001	0.0001	0.0012	0.0001	0.0001	*0.1198*	0.0001	0.0001	0.0145	0.0015		0.0001			0.0001		0.0264
3 Reduced	Coefficient	-0.1063	-0.0911	-0.0589	0.00191	0.00074		8.73958	0.07447	0.0242	-0.0353		0.02095			0.00259		-0.000635
	Uncertainty	0.0001	0.0001	0.0021	0.0001	0.0001		0.0001	0.0001	0.0189	0.0014		0.0002			0.0001		0.0282

Combustion Analysis Results Correlation

Model Number	Cp	R^2	P	Number of Observations Used	Colinearities		C5	C6	C7	C8	DPMAX	CADPMAX	DHRMAX	TMAX	IND5	BA595	Z2TOTG	Z2DGMAX	Z2TUBMAX
1	7.54	0.9917	10	86	ZDGMAX /	Coefficient	*-1.7988*	-4.4172	*-1.5955*	-7.8764		0.0288	0.0032	-0.0014			13.5928	-8.3955	0.0077
					ZTUBMAX	Uncertainty	*0.2900*	0.0214	*0.3462*	0.0050		0.0028	0.0001	0.0001			0.0018	0.0047	0.0054
2	4.14	0.9923	11	86	ZDGMAX /	Coefficient	-5.1990	-8.3116	-5.1548	-10.8437	0.0186	0.0327	0.0028	-0.0013			20.6718	-13.0570	0.0120
					ZTUBMAX	Uncertainty	0.0180	0.0010	0.0211	0.0004	0.0171	0.0007	0.0001	0.0001			0.0001	0.0002	0.0003
5	7.33	0.9920	11	86	DHRMAX / ZDGMAX /	Coefficient	*-1.0195*	*-3.4526*	*-0.8392*	-6.5668		0.0278	0.0033	-0.0014		*-0.0348*	14.9756	-10.3971	0.0095
					ZTUBMAX	Uncertainty	*0.5619*	*0.0834*	*0.6311*	0.0233		0.0038	0.0001	0.0001		*0.1312*	0.0008	0.0015	0.0017
8	8.04	0.9919	11	86	ZDGMAX /	Coefficient	*0.7063*	*-2.0212*	*1.1692*	*-5.5898*		0.0274	0.0033	-0.0015	*-0.1406*		14.3561	-9.2593	0.0085
					ZTUBMAX	Uncertainty	*0.7879*	*0.4529*	*0.6747*	*0.0918*		0.0046	0.0001	0.0001	*0.2150*		0.0011	0.0025	0.0028

NO Emissions

Fuel Properties Correlation

Model Number	Cp	R^2	P	Number of Observations Used	Colinearities		C4	C5	C7	C8	C9	C10	C11	O	IGNTIM	OILT	MANP	BARO	DRYB	FBP	LEAD	BENZENE
1	7.09	0.9919	13	163	MANP / BARO	Coefficient	32.7826	-5.3050	-3.0459	35.9933	-13.3369	12.1219	28.8555			0.0653	-0.8751	0.0567	0.1582	-0.0321	0.0024	
						Uncertainty	0.0058	0.0001	0.0001	0.0026	0.0001	0.0335	0.0062			0.0304	0.0003	0.0001	0.0287	0.0026	0.0037	
2	6.39	0.9921	14	159	MANP / BARO	Coefficient	28.2641	-5.3442	*-0.1809*	31.5249	*-6.4139*	17.4907	26.3327		*-0.5596*	0.0674	-0.8076	0.0627	0.2203	-0.0297	0.0020	
						Uncertainty	0.0182	0.0001	*0.9230*	0.0087	*0.2488*	0.0117	0.0119		*0.1019*	0.0383	0.0009	0.0001	0.0041	0.0058	0.0141	
2 Reduced	13.75	0.9914	13	146	IGNTIM / BARO	Coefficient	-11.8462	-4.6384	*2.1144*	-8.5886	*6.0003*	*1.1367*	-8.5172		-0.7337	0.0630		0.0276	*0.1447*	-0.0291	0.0018	
						Uncertainty	0.0001	0.0001	*0.2430*	0.0001	*0.1662*	*0.8223*	0.0001		0.0367	0.0611		0.0005	*0.0545*	0.0088	0.0326	
3	6.90	0.9921	14	159	MANP / BARO	Coefficient	31.6829	-5.2736	-2.9815	34.9147	-13.1225	11.5332	27.7202			0.0671	-0.8533	0.0561	0.1645	-0.0378	0.0025	*0.0979*
						Uncertainty	0.0074	0.0001	0.0001	0.0032	0.0001	0.0419	0.0082			0.0341	0.0004	0.0001	0.0247	0.0005	0.0022	*0.0999*
4	6.93	0.9921	14	163	MANP / BARO	Coefficient	37.1823	-5.1646	-2.9862	40.4946	-14.1580	14.5632	32.9634	0.0201		0.0589	-0.9617	0.0614	0.1674	-0.0352	0.0026	
						Uncertainty	0.0020	0.0001	0.0001	0.0008	0.0001	0.0120	0.0020	0.0461		0.0499	0.0001	0.0001	0.0198	0.0010	0.0016	

Combustion Analysis Results Correlation

Model Number	Cp	R^2	P	Number of Observations Used	Colinearities		C5	C7	C8	STAB	PMAX	DPMAX	TOTHR	TMAX	CATMAX	BA595	Z2PERCNT	Z2DGMAX	Z2TUBMAX	Z2TBMAX
1	8.48	0.9964	8	58	Z2PERCNT / ZDGMAX	Coefficient	41.3767	43.2737	*24.6610*			-0.2136		-0.0040	-0.5367		*-0.0708*	47.0499		
						Uncertainty	0.0001	0.0001	*0.0802*			0.0001		0.0001	0.0001		*0.1202*	0.0001		
2	8.65	0.9964	8	58	-	Coefficient	63.7708	64.3365	47.7363		0.0138	-0.2694		-0.0039	-0.5950					-0.0118
						Uncertainty	0.0001	0.0001	0.0281		0.0003	0.0001		0.0013	0.0001					0.0178
3	8.97	0.9964	8	58	-	Coefficient	35.9195	37.4562	*21.9789*	*0.1733*		-0.2072		-0.0040	-0.6109			42.3218		
						Uncertainty	0.0001	0.0001	*0.1180*	*0.1645*		0.0001		0.0001	0.0001			0.0001		
4	9.05	0.9964	8	59	DPMAX/TMAX TOTHR/TMAX	Coefficient	58.0794	59.7591	35.5180			-0.1417	0.0291	-0.0067	-0.5957	-0.3599				
						Uncertainty	0.0001	0.0001	0.0138			0.0037	0.0001	0.0001	0.0001	0.0002				
5	6.02	0.9968	9	58	DPMAX/TMAX TOTHR/TMAX	Coefficient	30.1460	31.5430	*14.1665*			-0.1522	0.0249	-0.0064	-0.5552	-0.3000			0.0356	
						Uncertainty	0.0338	0.0270	*0.3754*			0.0015	0.0001	0.0001	0.0001	0.0016			0.0249	

CO Emissions

Fuel Properties Correlation

Model Number	Cp	R^2	P	Number of Observations Used	Colinearities		C1	C2	C3	C4	C5	C6	C7	C8	C9	C10	C11
1	11.52	0.9957	22	259	A/O/P/WATERT T30/E70	Coefficient	*-13.1864*	*-7.2185*	-58.2734	-165.2412	19.1689	-51.4027	25.5968	-202.9518	156.2111	*-13.8739*	-128.8619
						Uncertainty	*0.1700*	*0.6244*	0.0197	0.0004	0.0001	0.0118	0.0001	0.0001	0.0001	*0.6167*	0.0026
2	12.62	0.9956	22	259	A/O/P/WATERT	Coefficient	*-9.7495*	*2.9467*	*-42.7991*	-134.7409	14.9288	-40.3322	19.9735	-174.8912	149.2414	*3.9653*	-103.6830
						Uncertainty	*0.3073*	*0.8448*	*0.0894*	0.0041	0.0003	0.0480	0.0001	0.0002	0.0001	*0.8883*	0.0161
2 Reduced	18.36	0.9954	21	259	A/O/P/MANP	Coefficient	*-11.7534*	*-0.8640*	-48.5677	-141.0305	14.6071	-44.7117	19.5060	-179.8478	144.1729	*-7.6377*	-116.2618
						Uncertainty	*0.2087*	*0.9527*	0.0481	0.0025	0.0004	0.0251	0.0001	0.0001	0.0001	*0.7675*	0.0049
8 Reduced	21.08	0.9954	21	259	-	Coefficient	*-13.9036*	*-8.7374*	-60.7714	-167.7561	18.7182	-52.7463	24.7024	-204.1763	150.8631	-22.5495	-138.5312
						Uncertainty	*0.1369*	*0.5392*	0.0122	0.0003	0.0001	0.0078	0.0001	0.0001	0.0001	0.3725	0.0007
10 Reduced	20.57	0.9954	21	259	A/O/P/MANP	Coefficient	*-14.2116*	*-1.8041*	-50.8652	-140.2601	13.2538	-47.0728	17.9608	-179.0799	142.4616	*-8.4967*	-116.4826
						Uncertainty	*0.1309*	*0.9018*	0.0392	0.0027	0.0016	0.0189	0.0005	0.0001	0.0001	*0.7430*	0.0049

Model Number		A	O	P	ER	WATERT	OILT	EXHT	MANP	IBP	T10	T30	E70	SENS	SULPHUR
1	Coefficient	-7.6237	-7.7149	-7.6931	554.1402	*1.0049*	0.8627	-0.3226	5.7901			-0.3541	-0.7424	0.7345	
	Uncertainty	0.0001	0.0001	0.0001	0.0001	*0.2567*	0.0001	0.0001	0.0001			0.0304	0.0004	0.0275	
2	Coefficient	-6.6514	-6.7701	-6.7320	501.5805	*0.8915*	0.9105	-0.3497	5.4554		-0.6366		-0.7553	0.8262	
	Uncertainty	0.0001	0.0001	0.0001	0.0001	*0.3102*	0.0001	0.0001	0.0001		0.0151		0.0001	0.0132	
2 Reduced	Coefficient	-5.9802	-6.0984	-6.0592	501.7435		0.9167	-0.3359	5.5330		-0.6228		-0.7478	0.8167	
	Uncertainty	0.0001	0.0001	0.0001	0.0001		0.0001	0.0001	0.0001		0.0173		0.0001	0.0142	
8 Reduced	Coefficient	-7.2185	-7.3500	-7.3476	549.9446		0.8950	-0.3232	5.8749	0.3285			-0.2866	*0.6273*	
	Uncertainty	0.0001	0.0001	0.0001	0.0001		0.0001	0.0001	0.0001	0.0148			0.0005	*0.0617*	
10 Reduced	Coefficient	-5.8040	-5.8415	-5.8614	472.7909		0.9464	-0.3269	5.5426		-0.5372		-0.6834		62.8491
	Uncertainty	0.0001	0.0001	0.0001	0.0001		0.0001	0.0001	0.0001		0.0402		0.0004		0.0289

Combustion Analysis Results Correlation

Model Number	Cp	R^2	P	Number of Observations Used	Colinearities		C5	C6	C7	C8	PMAX	DPMAX	TOTHR	DHRMAX	TMAX	IND5	Z2DGMAX	Z2DGMXCA	Z2TUBMAX
1	4.85	0.9840	7	86	-	Coefficient	-34.2699	-74.7299	-38.4690	*4.8749*		1.0019					-71.7435	1.9713	
						Uncertainty	0.0037	0.0001	0.0002	*0.7388*		0.0001					0.0132	0.0159	
2	0.78	0.9853	8	86	DPMAX/Z2DGMAX	Coefficient	-63.0997	-112.6522	-64.2444	-73.3583		0.9251		0.0262			-95.0452	2.6188	
					/Z2DGMAXCA	Uncertainty	0.0001	0.0001	0.0001	0.0309		0.0001		0.0116			0.0014	0.0018	
2 Altered	6.83	0.9840	8	86	-	Coefficient	-104.8672	-165.6083	-122.0530	-118.4965		0.5632		*0.0170*		*4.3851*	-2.7785		
						Uncertainty	0.0282	0.0012	0.0203	0.0323		0.0001		*0.0946*		*0.0677*	0.0257		
3	2.30	0.9850	8	86	DPMAX/Z2DGMAX	Coefficient	-88.1697	-145.7077	-91.9870	-111.7424	0.0370	0.6599					-93.7241	2.5870	
					/Z2DGMAXCA	Uncertainty	0.0015	0.0001	0.0007	0.0438	0.0297	0.0054					0.0020	0.0025	
4	4.67	0.9845	8	86	DPMAX/TOTHR /Z2DGMAX	Coefficient	-65.1668	-120.6779	-67.8833	*-70.1674*		1.0927	*0.0411*				-86.1019	2.3762	
					/Z2DGMAXCA	Uncertainty	0.0067	0.0006	0.0025	*0.1793*		0.0001	*0.1353*				0.0048	0.0058	
5	4.81	0.9845	8	86	DPMAX/Z2DGMAX	Coefficient	-58.5389	-99.1097	-62.1778	*-20.9190*		1.0753			0.0065		-83.4633	2.3066	
					/Z2DGMAXCA	Uncertainty	0.0048	0.0001	0.0015	*0.3627*		0.0001			0.1488		0.0055	0.0066	
6	5.42	0.9843	8	86	Z2DGMAX/	Coefficient	-69.4864	-111.5959	-79.7675	*-38.2028*		0.6401		0.0281			-125.1051		0.1145
					ZTUBMAX	Uncertainty	0.0048	0.0001	0.0018	*0.2441*		0.0001		0.0151			0.0261		0.0289
6 Altered	7.06	0.9840	8	86	-	Coefficient	-103.2003	-164.4303	-120.3022	-117.9274		0.5609		*0.0167*		*4.3575*			-0.0025
						Uncertainty	0.0306	0.0013	0.0220	0.0333		0.0001		*0.1012*		*0.0697*			0.0293

Combustion Analysis Results – Fuel Properties Correlations

DPMAX

Model Number	Cp	R^2	P	Number of Observations Used	Colinearities		C5	C6	C7	C8	A	O	ER	IGNTIM	DRYB	T10	T90	DENS	VOLIND	E70	SENS
1	3.06	0.9984	10	87	-	Coefficient	-310.76	-229.59	-346.22	-196.61		0.1073	194.64	9.7569	-1.0959		-0.1899		0.2015		
						Uncertainty	0.0001	0.0001	0.0001	0.0001		0.0377	0.0001	0.0001	0.0008		0.0001		0.0008		
2	3.25	0.9984	10	87	-	Coefficient	-281.86	-200.73	-315.65	-170.21		0.1070	202.98	9.4432	-1.0795	-0.3352	-0.1600				
						Uncertainty	0.0001	0.0001	0.0001	0.0001		0.0386	0.0001	0.0001	0.0009	0.0008	0.0003				
3	3.36	0.9984	10	87	-	Coefficient	-454.63	-372.48	-490.03	-337.65	-0.2705		178.93	9.7069	-1.0336	-0.3436		235.11			
						Uncertainty	0.0001	0.0001	0.0001	0.0001	0.0101		0.0001	0.0001	0.0015	0.0002		0.0002			
4	1.44	0.9985	11	87	T10 / E70	Coefficient	-184.97	-100.49	-219.56	-63.99		0.1112	150.46	9.4612	-1.0678	-0.9283	-0.1767			-0.5181	
						Uncertainty	0.0024	0.1085	0.0006	0.3152		0.0285	0.0004	0.0001	0.0008	0.0027	0.0001			0.0401	
5	1.96	0.9985	11	87	-	Coefficient	-234.04	-150.34	-267.60	-116.21		0.1917	169.22	9.3258	-1.0902	-0.4160	-0.1700				*-1.0278*
						Uncertainty	0.0001	0.0020	0.0001	0.0157		0.0051	0.0001	0.0001	0.0007	0.0001	0.0001				*0.0569*

TMAX

Model Number	Cp	R^2	P	Number of Observations Used	Colinearities		C5	C6	C7	C8	P	IGNTIM	EXHT	T10	T30	E70	LEAD
1	9.80	0.9987	9	87	T10 / E70	Coefficient	7491.6	8538.0	7749.1	8886.7		*-56.427*	-3.2095	-24.814		-12.978	-0.5270
						Uncertainty	0.0001	0.0001	0.0001	0.0001		*0.2075*	0.0089	0.0017		0.0271	0.0003
2	9.92	0.9986	9	87	T10 / E70	Coefficient	6519.9	7418.7	6493.8	7995.7	*-1.3949*		-3.0693	-27.365		-13.321	-0.5987
						Uncertainty	0.0001	0.0001	0.0001	0.0001	*0.2264*		0.0110	0.0012		0.0246	0.0001
3	10.01	0.9986	9	87	T10 / T30	Coefficient	6967.8	8144.3	7299.6	8424.6		*-72.993*	-3.6338	-23.249	8.3716		-0.5529
						Uncertainty	0.0001	0.0001	0.0001	0.0001		*0.1169*	0.0031	0.0016	0.0306		0.0002
4	10.00	0.9987	10	87	T10 / E70	Coefficient	8055.1	9168.0	8330.6	9493.0	*-1.5281*	*-61.429*	-3.4548	-28.777		-14.444	-0.5784
						Uncertainty	0.0001	0.0001	0.0001	0.0001	*0.1845*	*0.1698*	0.0053	0.0007		0.0155	0.0001

DHRMAX

Model Number	Cp	R^2	P	Number of Observations Used	Colinearities		C5	C6	C7	C8	O	ER	IGNTIM	OILT	EXHT
1	10.43	0.9991	11	87	T10 / E70	Coefficient	*-302.61*	*694.15*	*-681.39*	2844.19			82.6210	11.6818	
						Uncertainty	*0.6872*	*0.4126*	*0.4185*	0.0004			0.0009	0.0244	
5	9.76	0.9992	12	87	EXHT / OILT	Coefficient	*468.42*	1847.43	*122.14*	4031.66	2.1724		70.1104	24.5068	-2.5310
					T10 / E70	Uncertainty	*0.5351*	0.0348	*0.8848*	0.0001	0.0116		0.0052	0.0061	0.0397
9	11.26	0.9992	12	87	EXHT / OILT	Coefficient	-2214.0	*-943.52*	-2553.6	*1117.19*	1.8198	1095.08	72.2691	23.2101	*-2.2820*
						Uncertainty	0.0042	*0.2961*	0.0026	*0.2135*	0.0251	0.0419	0.0047	0.0090	*0.0600*

Model Number		DRYB	T10	T70	T90	E70	VAPPRES	LEAD	SULPHUR
1	Coefficient	-11.144	-16.324			-11.565		-0.2451	1700.08
	Uncertainty	0.0383	0.0002			0.0003		0.0041	0.0192
5	Coefficient	-12.127	-16.913	-2.9653		-12.182			
	Uncertainty	0.0239	0.0001	0.0142		0.0004			
9	Coefficient	-12.262			-1.6194		4.1183		
	Uncertainty	0.0228			0.0235		0.0032		

BA595

Model Number	Cp	R^2	P	Number of Observations Used	Colinearities		C5	C6	C7	C8	ER	IGNTIM	OILT	DRYB	T10	VLRATIO	E70	RON	LEAD	SULPHUR
1	9.69	0.9993	10	87	T10 / E70	Coefficient	*16.5822*	*8.8513*	*15.8291*	*5.8241*			*-0.1614*	0.3278	0.3771	0.1318	0.2598			-46.618
						Uncertainty	*0.0576*	*0.3700*	*0.0684*	*0.5508*			*0.0597*	0.0004	0.0001	0.0001	0.0001			0.0001
2	9.30	0.9993	11	87	-	Coefficient	45.9817	36.7986	45.0208	36.7830	-23.675			0.2726	0.3988		0.2273	-0.1491	0.0072	-40.261
						Uncertainty	0.0060	0.0333	0.0067	0.0474	0.0467			0.0022	0.0001		0.0013	0.0361	0.0001	0.0014
3	10.04	0.9993	11	87	T10 / E70	Coefficient	28.0268	*21.4745*	29.8266	*16.3056*		*-0.5091*	-0.1710	0.3458	0.3676	0.1321	0.2492			-44.609
						Uncertainty	0.0257	*0.1243*	0.0336	*0.2005*		*0.2002*	0.0463	0.0002	0.0001	0.0001	0.0001			0.0002
4	10.11	0.9993	11	87	T10 / E70 / ER	Coefficient	33.9939	*27.1158*	33.0539	*25.6765*	*-14.410*		*-0.1581*	0.3298	0.3214	0.1300	0.2034			-40.218
						Uncertainty	0.0393	*0.1240*	0.0431	*0.1678*	*0.2096*		*0.0642*	0.0004	0.0001	0.0001	0.0033			0.0015

Z2BA298

Model Number	Cp	R^2	P	Number of Observations Used	Colinearities		C5	C6	C7	C8	A	O	P	OP	IGNTIM	OILT	EXHT
1	16.95	0.9983	16	81	A / T90 / DENS	Coefficient	343.41	355.98	379.41	322.27	*0.2111*				-7.4739	-0.8136	
						Uncertainty	0.0001	0.0001	0.0001	0.0002	*0.0747*				0.0001	0.0001	
2	17.01	0.9984	17	81	-	Coefficient	225.66	238.29	260.49	205.61					-7.2389	-0.8387	
						Uncertainty	0.0003	0.0002	0.0001	0.0011					0.0001	0.0001	
3	17.39	0.9983	17	81	VOLIND / E70 / VAPPRES	Coefficient	362.96	374.48	398.70	341.25					-7.4165	-0.7625	
						Uncertainty	0.0001	0.0001	0.0001	0.0001					0.0001	0.0002	
4	16.08	0.9984	18	81	T10 / E70 / ER	Coefficient	*33.0654*	*39.9597*	*68.4485*	*5.3577*		-1.4443	-1.0449	0.0269	-7.2738	-1.0697	*0.0430*
						Uncertainty	*0.4047*	*0.3362*	*0.1084*	*0.8919*		0.0002	0.0008	0.0002	0.0001	0.0012	*0.3391*

Model Number		IBP	T10	T30	T50	T70	T90	DENS	VAPPRES	E70	VOLIND	RON	SENS	LEAD	SULPHUR	OXYGEN
1	Coefficient	*-0.1475*	0.7121	0.4083		*0.0880*	-0.1866	-188.48		0.9368				0.0147	-131.47	
	Uncertainty	*0.1722*	0.0026	0.0036		*0.2863*	0.0163	0.0370		0.0001				0.0021	0.0010	
2	Coefficient	-0.2971	1.2652			0.3622	-0.2097	-123.14		1.3892	-0.2137	0.7333	-1.1958		-167.26	-1.9519
	Uncertainty	0.0164	0.0001			0.0010	0.0031	0.0649		0.0001	0.0132	0.0001	0.0102		0.0142	0.0319
3	Coefficient	-0.3443	0.7046		*0.1986*	0.3845	-0.2820	-237.27	1.6963	2.0479	-1.9367	0.5208	-1.4873			
	Uncertainty	0.0093	0.0175		*0.1827*	0.0020	0.0004	0.0001	0.0334	0.0002	0.0207	0.0080	0.0008			
4	Coefficient	-0.4982	0.9434	0.5893	0.3389					1.4799		2.0326	-4.1741	*-0.0200*		
	Uncertainty	0.0007	0.0006	0.0020	0.0053					0.0001		0.0004	0.0010	*0.0513*		

Equivalence Ratio

Model Number	Cp	R^2	P	Number of Observations Used	Colinearities		C1	C2	C3	C4	C5	C6	C7	C8	C9	C10	C11
1	22.56	0.9999	23	238	A/O/P/MANP FBP/E70	Coefficient	-0.01556	0.07458	0.09873	0.28629	-0.0743	0.04271	-0.08821	0.24934	-0.0997	0.14378	0.21557
						Uncertainty	0.1586	0.0001	0.001	0.0001	0.0001	0.0762	0.0001	0.0002	0.0001	0.0001	0.0002
3	22.38	0.9999	24	238	A/O/P/BARO	Coefficient	-0.01546	0.07473	0.09903	0.28694	-0.07431	0.04294	-0.08824	0.24998	-0.09986	0.14409	0.21615
						Uncertainty	0.1824	0.0001	0.0018	0.0001	0.0001	0.0899	0.0001	0.0003	0.0001	0.0001	0.0004
5	22.93	0.9999	24	206	A/O/P/MANP T10/FBP/E70	Coefficient	-0.00246	0.09408	0.13697	0.36873	-0.07009	0.07627	-0.08664	0.33469	-0.12208	0.18084	0.28723
						Uncertainty	0.8415	0.0001	0.0001	0.0001	0.0001	0.0044	0.0001	0.0001	0.0001	0.0001	0.0001
6	23.02	0.9999	24	233	A/O/P/MANP T10/FBP/E70	Coefficient	-0.01488	0.07556	0.10065	0.29052	-0.07327	0.04543	-0.08721	0.25418	-0.09838	0.14825	0.22217
						Uncertainty	0.1756	0.0001	0.0008	0.0001	0.0001	0.059	0.0001	0.0001	0.0001	0.0001	0.0001

Model Number		A	O	P	AO	MANP	BARO	DRYB	T10	T70	T90	FBP	E70	NITROGEN	OXYGEN	BENZENE
1	Coefficient	0.014008	0.014313	0.012991	-3.302E-05	-0.0029		0.001532	-0.001908	-0.000638	0.000647	-0.000542	-0.001485		-0.010102	
	Uncertainty	0.0001	0.0001	0.0001	0.0005	0.0286		0.0001	0.0001	0.0001	0.0001	0.0003	0.0001		0.0001	
3	Coefficient	0.013952	0.014256	0.012936	-3.298E-05	-0.002913	6.043E-06	0.001535	-0.001908	-0.000637	0.000646	-0.000541	-0.001485		-0.010098	
	Uncertainty	0.0001	0.0001	0.0001	0.0006	0.0372	0.9759	0.0001	0.0001	0.0001	0.0001	0.0003	0.0001		0.0001	
5	Coefficient	0.014878	0.01523	0.01363	-3.95E-05	-0.004576		0.002327	-0.001905	-0.000823	0.000766	-0.000545	-0.001562	-9.9338E-05	-0.009061	
	Uncertainty	0.0001	0.0001	0.0001	0.0001	0.0021		0.0001	0.0001	0.0001	0.0001	0.0002	0.0001	0.3323	0.0001	
6	Coefficient	0.013755	0.014038	0.012807	-3.006E-05	-0.002986		0.00131	-0.001632	-0.000715	0.000715	-0.000507	-0.001198		-0.011052	-0.001034
	Uncertainty	0.0001	0.0001	0.0001	0.0014	0.0237		0.0008	0.0002	0.0001	0.0001	0.0007	0.0008		0.0001	0.0118